15958-T-1548-MA-129T-003F

COMBUSTION PERFORMANCE AND HEAT TRANSFER CHARACTERIZATION OF LOX/HYDROCARBON TYPE PROPELLANTS

FINAL REPORT
Volume II

September 1983

Prepared For:

NATIONAL AERONAUTICS AND SPACE ADMINISTRATION

Lyndon B. Johnson Space Center
Contract NAS-9-15958

Prepared By:

AEROJET LIQUID ROCKET COMPANY

Report 15958T-1548-MA-129T-003F

September 1983

Combustion Performance and Heat Transfer Characterization of LOX/Hydrocarbon Type Propellants

Contract NAS 9-15958

FINAL REPORT

Volume II

Prepared For:

NASA-Lyndon B. Johnson Space Center
Houston, Texas

Prepared By:

L. Schoenman

L. Schoenman

Approved By:

R. W. Michel

R. W. Michel

Aerojet Liquid Rocket Company
P.O. Box 13222
Sacramento, California 95813

TABLE OF CONTENTS

TABLE OF CONTENTS (cont.)

LIST OF TABLES

LIST OF TABLES (cont.)

LIST OF FIGURES

LIST OF FIGURES (cont.)

LIST OF FIGURES (cont.)

LIST OF FIGURES (cont.)

LIST OF FIGURES (cont.)

LIST OF FIGURES (cont.)

LIST OF FIGURES (cont.)

LIST OF FIGURES (cont.)

E. TASKS II AND IV SUBSCALE INJECTOR CHARACTERIZATION

1. Introduction

The experimental subscale combustion investigation was designed to evaluate the performance, heat transfer and stability characteristics of typical hydrocarbon fuels such as propane and ethanol when used in conjunction with liquid and gas-phase oxygen as the oxidizer. The propellant selections, thrust level, operating pressures and mixture ratio, etc. were based on the results of cooling comparison studies of Task I and the system studies of Task III and Reference 1.

The nominal operating point (1000 lbF thrust at 300 psia chamber pressure) was selected to provide data applicable to an OMS regeneratively-cooled thrust chamber and a film-cooled RCS chamber. These data are believed to provide meaningful scaling relationships for thrust levels of 500 to 10,000 lbF.

2. Objectives

The objectives of this experimental program were to generate a data base which relates candidate design variables, such as injector type, acoustic cavity configuration, chamber length, fuel film-cooling, etc., to operational characteristics such as combustion efficiency, combustion stability, carbon deposition, and chamber gas-side heat flux.

3. Results, Conclusions, and Recommendations

a. Performance and Stability

(1) A 42 element like-on-like injector pattern was fired with LOX/propane in a heat-sink chamber and found to be low-performing (93%), as a result of both poor atomization and poor mixing. The combustion was bomb-stable.

(2) A 40-element OFO triplet injector was fired with both LOX/propane and LOX/ethanol in both heat-sink and water-cooled calorimeter chambers. In the calorimeter chamber it was tested with and without fuel film-cooling. Performance was very high (99%) with LOX/propane, for which the unit was designed, and slightly lower (97%) with LOX/ethanol due to non-optimum propellant momentum match. Combustion was stable with both propellant combinations.

Hot-fire mixing efficiency (E_m) analysis of the EDM'd OFO triplet element indicated that propane and ethanol have virtually identical E_m values as a function of the oxidizer-to-fuel momentum ratio. The E_m reaches its peak (100%) at about a momentum ratio of 2.3, which is greater than the 1.1 value for optimum momentum ratio determined from cold-flow data correlations. This increase in optimum momentum ratio may be due to the high volatility of LOX.

E, Tasks II and IV Subscale Injector Characterization (cont.)

The optimum mixing of OFO triplet LOX/HC elements requires higher momentum ratio for hot-fire than is indicated by correlations developed by cold-flow techniques.

(3) A 45-element preatomized platelet OFO triplet injector was tested with LOX/ethanol propellants. This design was able to provide 2% higher combustion efficiency than the EDM'd design tested while providing lower heat flux to the chamber wall. Combustion was stable in all tests.

(4) A 45-element preatomized platelet triplet injector was tested with GOX/ethanol propellants and was found to be equally high in performance (99%). The GOX/ethanol configuration was found to be less sensitive to mixture ratio variations and was stable over a wide MR, Pc and propellant temperature operating range. A 2% reduction in performance was observed when the propellant (fuel and oxidizer) temperature was reduced from +50°F to -130°F.

(5) The measured specific impulse values for the LOX propane as well as LOX and GOX/ethanol tests are displayed in Figures 1 and 2.

b. Thermal Results

(1) The most significant heat transfer result, apart from the carbon deposition observed with propane and discussed later, is the high throat heat fluxes observed with ethanol (Figure 3). Pipe-flow correlation coefficients (Cg) inferred from these heat fluxes (Figure 4) are approximately 70 percent higher than the accleration-induced coefficients typically observed with storable propellants and with oxygen/hydrogen systems. These high throat region correlation coefficients are of the same magnitude as those observed previously with LOX/RP-1 on Contract NAS 3-21030, High-Density Fuel Combustion and Cooling Investigation. Since these abnormal correlation coefficients occur only in the throat region, it is not clear if they are related to cracking of specific hydrocarbon fuels and delayed burning of the decomposition products.

(2) Normal Cg profiles, with lower values in the throat region relative to the barrel, were observed with the maximum propane heat fluxes, i.e., the fluxes in the 2-5 sec period prior to the significant decrease caused by carbon deposition. Ethanol correlation coefficients with the same EDM injector exhibited an extreme mixture ratio sensitivity, with Cg increasing with mixture ratio. In all cases Cg decreased from the barrel to the first segment of the convergent section, but then increased to the abnormal throat values noted above before decreasing in the nozzle. This throat spike is illustrated in Figure 4 and compared with the expected dip due to acceleration effects. For a mixture ratio of 1.8, approximately the value for optimum performance, barrel Cg values were essentially the same as the propane data.

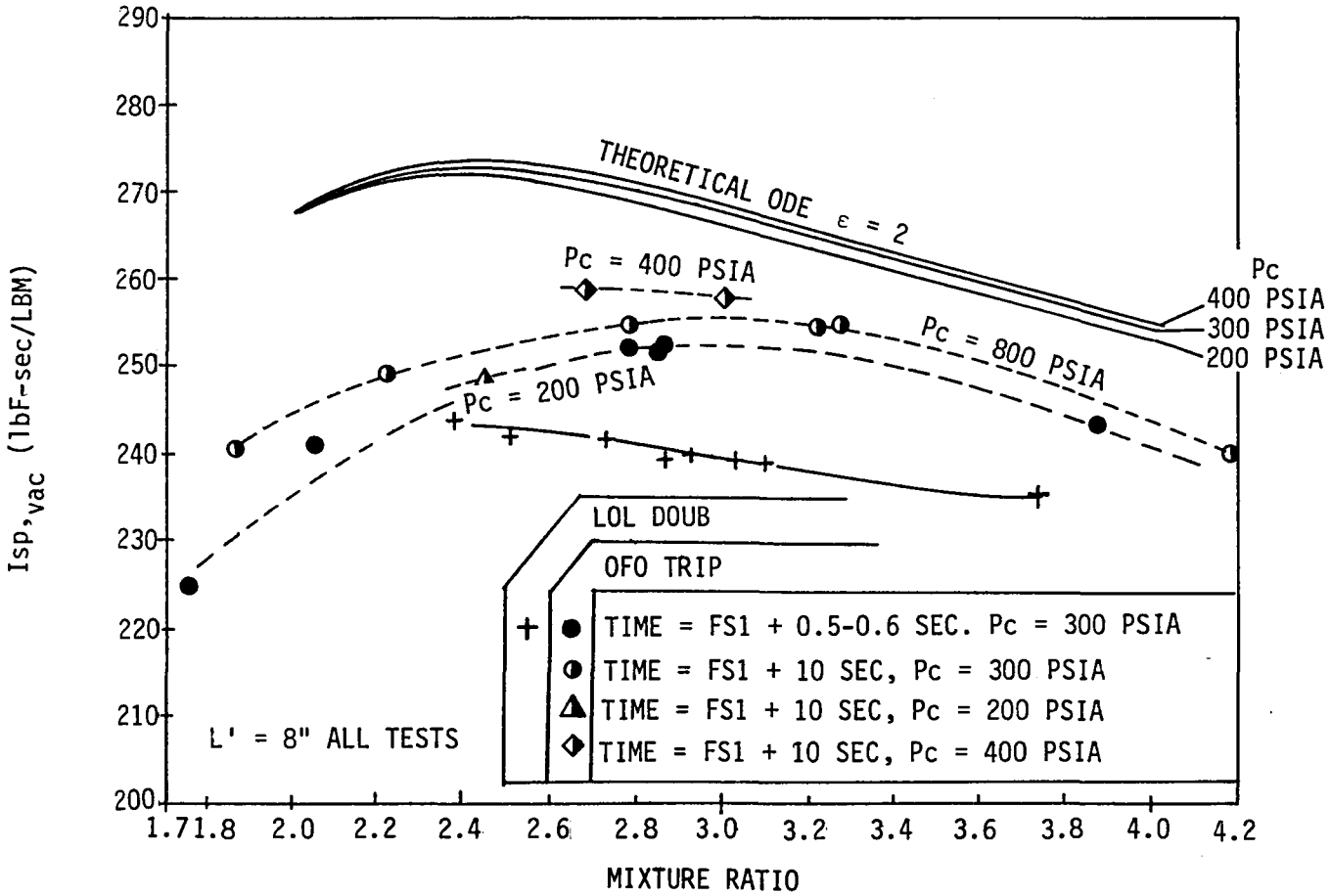

Figure 1. LOX/Propane Injector Element, MR, and Chamber Pressure Effects on Measured $Isp_{,vac}$

LOX/ETHANOL		GOX/ETHANOL
PLATELET PAT	EDM-OFO	PLATELET PAT
△ 0% FFC	⬡ 0% FFC	○ 0% FFC
▲ 17% FFC	⬢ 14% FFC	● 20% FFC
	◑ 7.5% FFC	

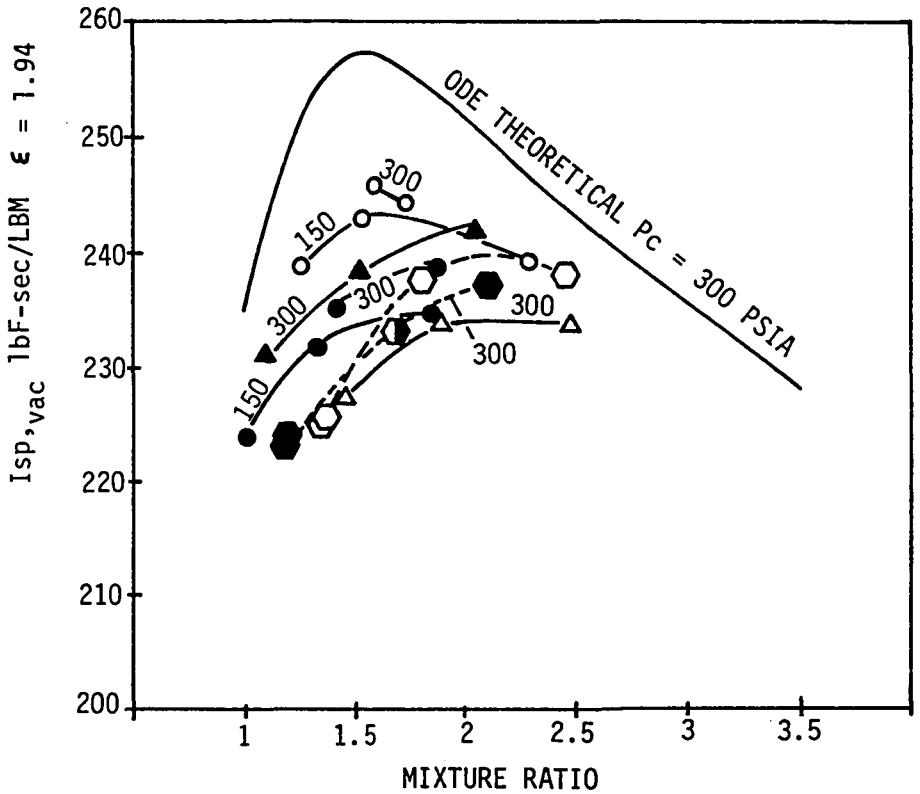

Figure 2. $Isp_{,vac}$ vs MR Relationship of GOX & LOX/Ethanol, With and Without FFC, In Water Cooled Chamber

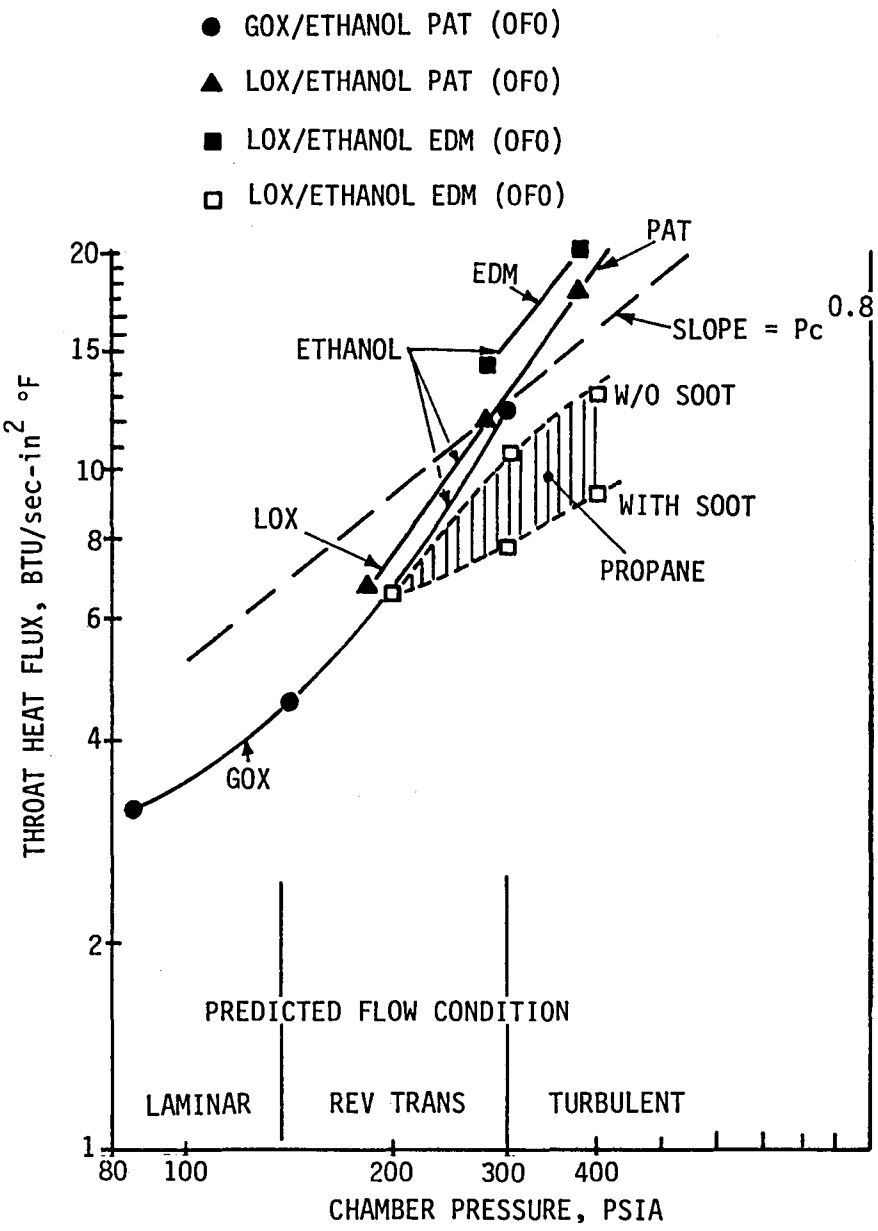

Figure 3. Maximum Thrust Heat Flux vs Chamber Pressure

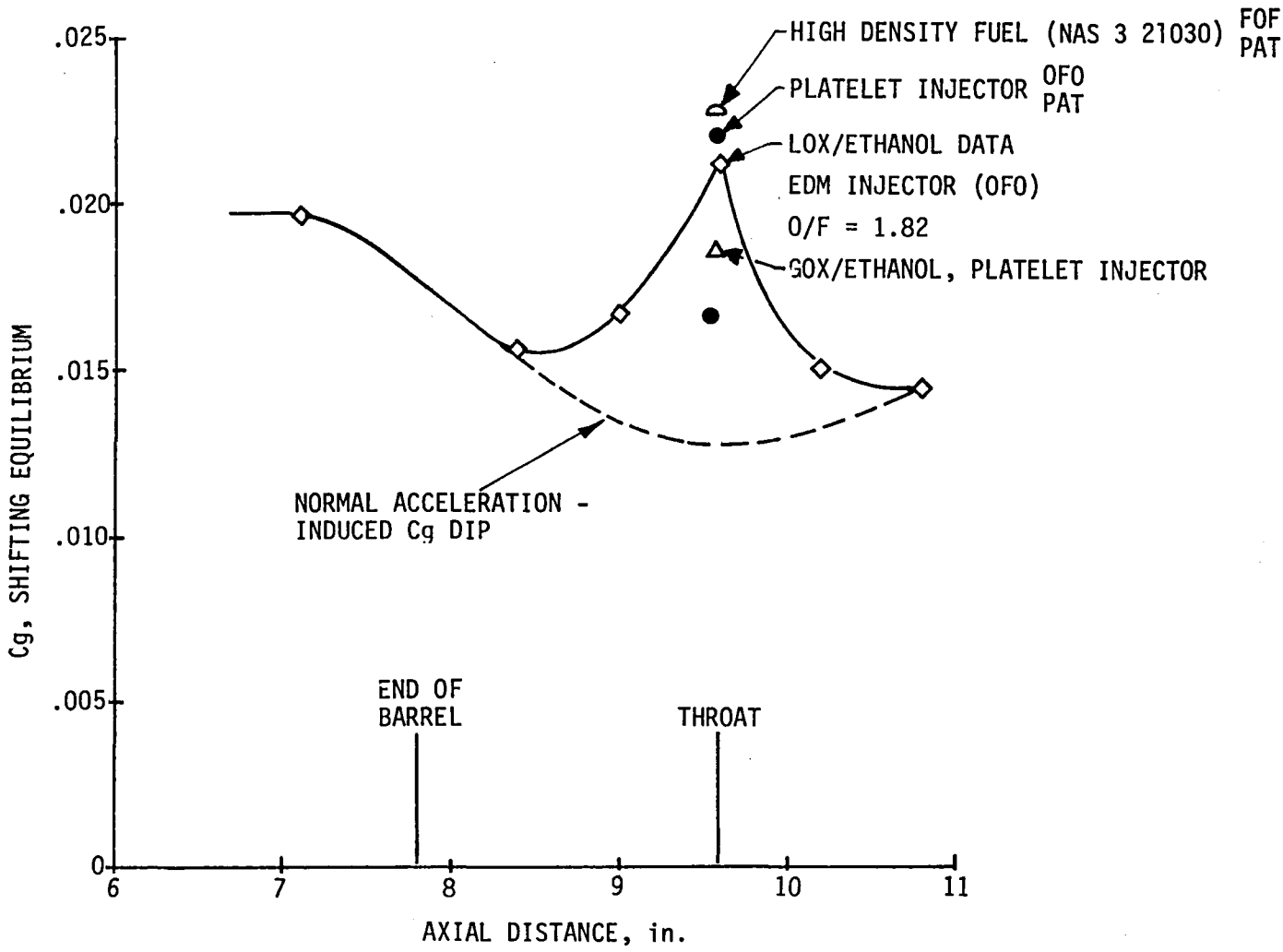

Figure 4. Throat Region Heat-Transfer Correlation Coefficient Characteristics

E, Tasks II and IV Subscale Injector Characterization (cont.)

(3) Ethanol testing was also conducted with two platelet injectors. It was apparent (Figure 5), from the low head-end heat flux measurements, that the LOX platelet injector was providing significant amounts of oxidizer film-cooling, presumably due to blowapart with the PAT O-F-O element. The addition of 8.7 percent fuel film-cooling increased heat fluxes throughout the chamber and resulted in a throat Cg in good agreement with the EDM injector value for the same mixture ratio; a higher fuel film-coolant flow resulted in lower heat fluxes. GOX platelet injector Cg data are lower than the EDM injector results in both the barrel and throat regions as shown in Figures 3 and 5.

(4) A comparison of throat correlation coefficients, based on the data of Figure 3 and shifting equilibrium compositions and assuming a Lewis number of unity, is shown in Figure 6 as a function of chamber pressure. The data confirm the prediction that the boundary layer at the throat is not turbulent under all test conditions. The GOX/ethanol data indicate a turbulent boundary layer above 250 psia, and the propane data show the same above 300 psia. A comparison of barrel correlation coefficients is shown in Figure 7 also as a function of chamber pressure in order to look for blowapart effects. The propane data exhibits a continuous decrease with Pc, and the oxidizer film-cooling interaction with the LOX/ethanol platelet injector is clearly evident.

c. Other Results

(1) Carbon deposition in the acoustic cavities with LOX/propane was extensive to the point that acoustic damping capabilities could be lost. Film-coolant injection from the forward end of the cavity reduced the amount of carbon deposition within the cavities.

(2) With LOX/ethanol, carbon deposition on the chamber wall was non-existent; with propane it was largely lost during start and shutdown transient. Engine restart was marked by a return to clean-wall heat flux conditions, followed by a progressive decay as the deposition layer increased. As a result, the thermal resistance of the deposition layer cannot be assumed for design purposes to limit gas-side wall temperatures to less than clean-wall values.

(3) Testing at higher pressures produced greater heat flux reductions; this was not expected.

d. Recommendations

A number of significant deviations from the perceived data base for LOX/hydrocarbon propellants have been uncovered in this test program; namely (1) the requirement for higher oxidizer-to-fuel momentum ratios for optimum performance under hot fire conditions than in cold-flow, (2) unexplainably

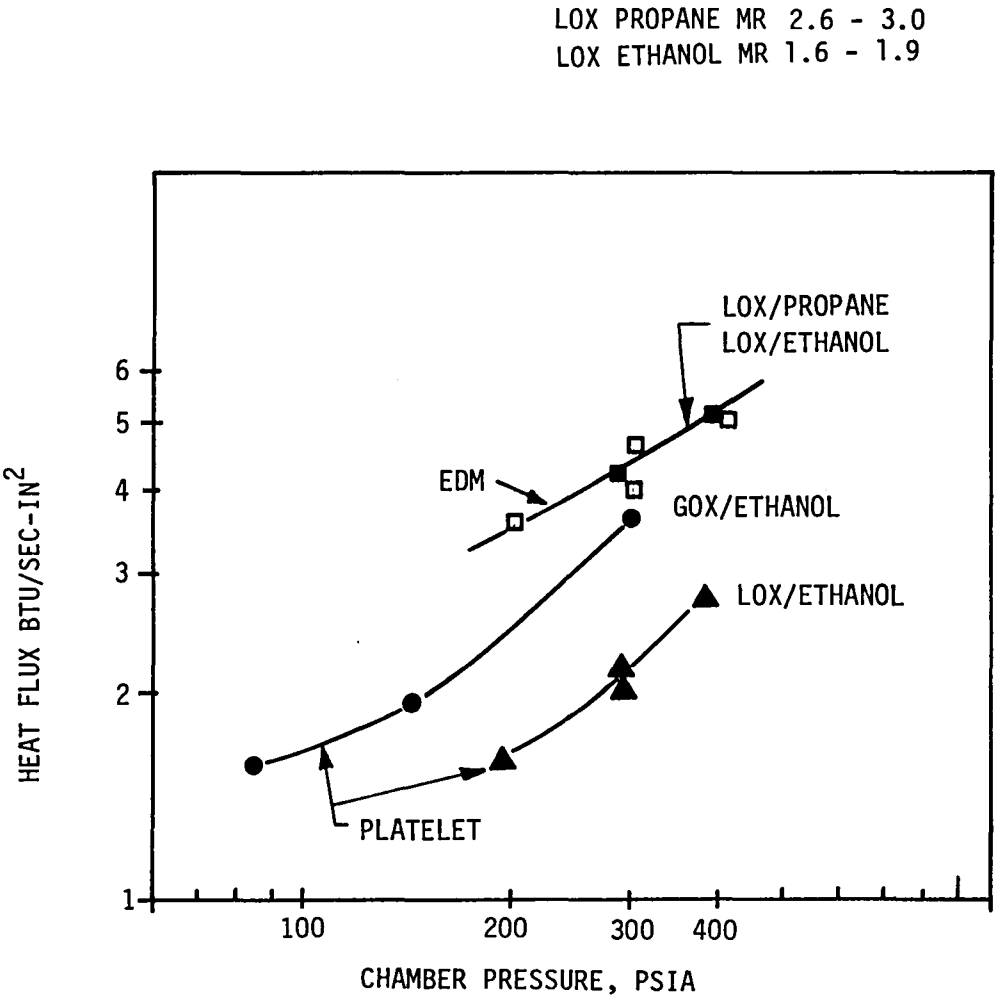

Figure 5. Maximum Mid Chamber Region Heat Flux vs Chamber Pressure

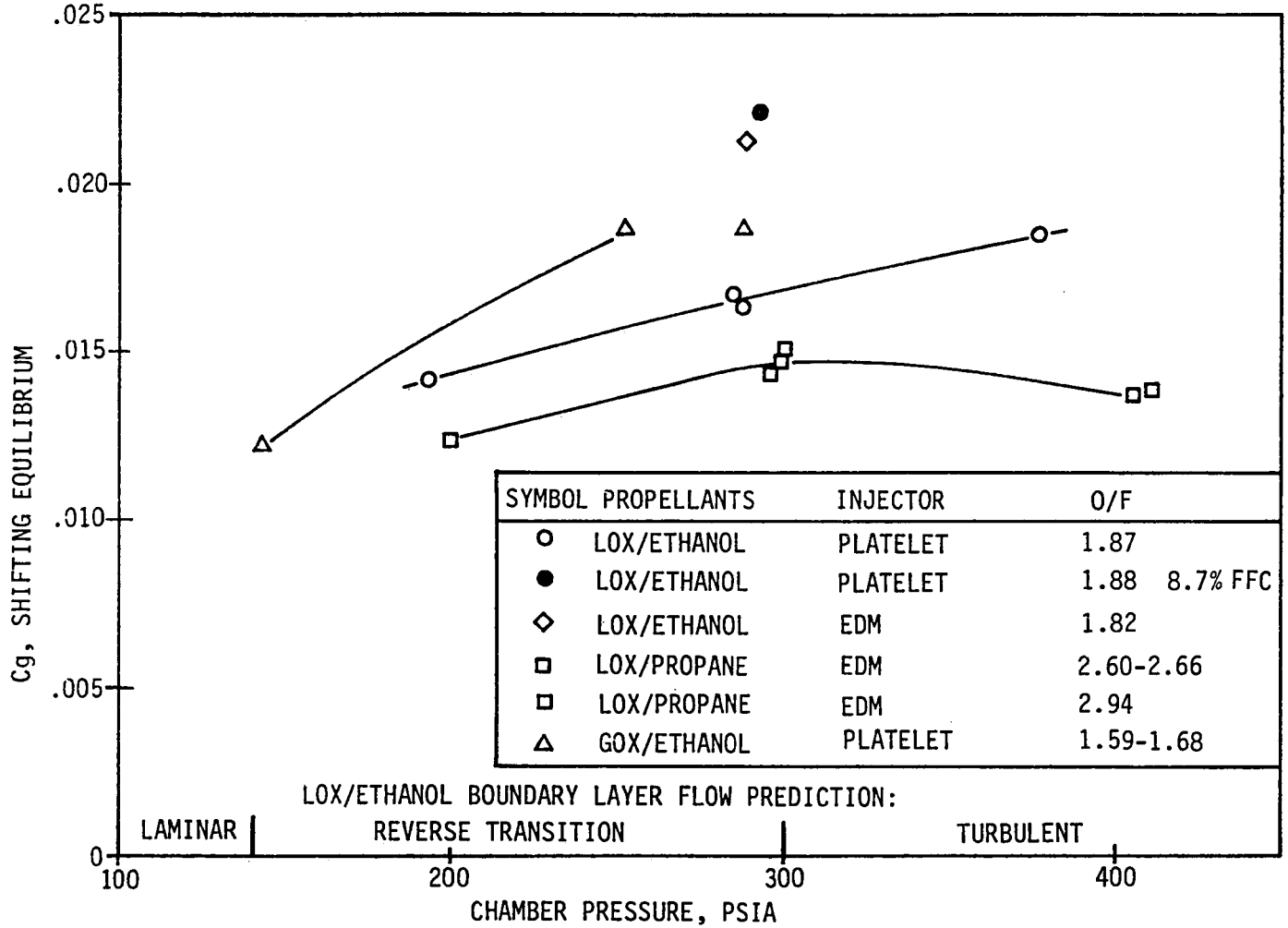

Figure 6. Comparison of Throat Heat Transfer Correlation Coefficients

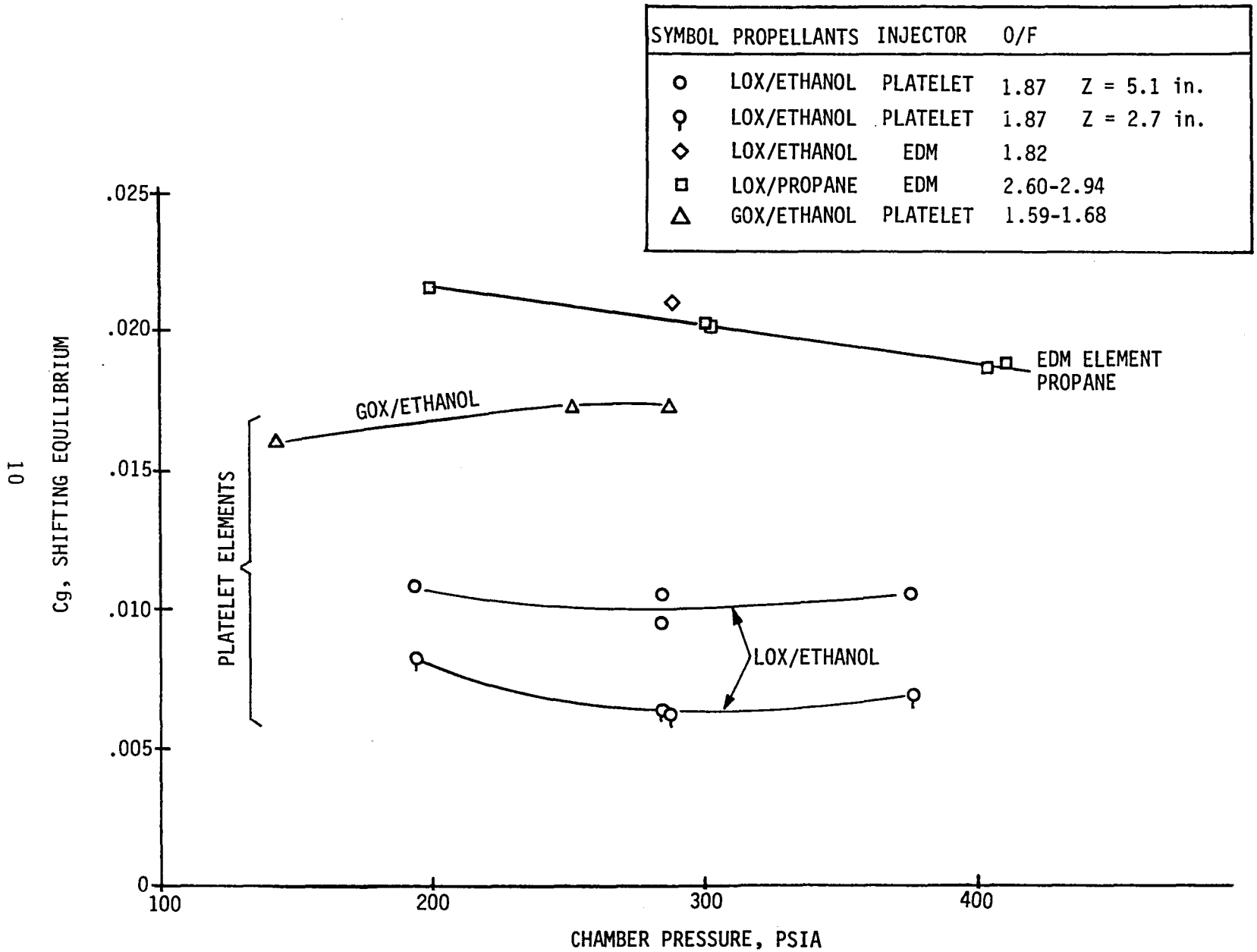

Figure 7. Comparison of Barrel Heat Transfer Correlation Coefficients

high throat heat fluxes with ethanol, (3) increased carbon deposition effects at higher mass flux, (4) carbon buildup in acoustic resonator cavities and (5) changes in injector hydraulics with time due to thermal effects within the injector manifolding.

This program was not designed to cope with these deviations, only to identify and quantify the effects; this was accomplished. Future work must be directed towards first developing an understanding of the mechanisms which control these events and second, the creation of the analytical tools and design procedures required for future LOX/hydrocarbon fuel development programs.

A follow-on data analysis effort which tests and correlates the data provided in this data dump against existing and new theory is recommended as the next logical event in improving the technology.

4. Summary of Hot Fire Testing

Seven different test series were conducted as part of the hot fire test program. The major test variables were as follows:

- Two propellant combinations: oxygen/propane and oxygen/ethanol.
- Four injector designs: conventional drilled orifice like-on-like and OFO triplet patterns, and unconventional platelet injectors with preatomized triplet (PAT) patterns utilizing vortex and splash splate elements.
- Two chamber types: 4 inch and 8 inch heat sink chambers, and a water-cooled calorimeter chamber.
- Other test variables included: oxygen state, film-cooling percentage, propellant temperature, chamber pressure, and mixture ratio.

Table I identifies the hardware combinations employed for each of the test series.

LOX/propane Test Series I involved 18 hot-fire tests of a 42 element quadlet (2 sets of like-on-like doublets) injector in 4 inch and 8 inch long heat sink chambers. The test durations of 0.5 to 1.5 sec covered chamber pressures of 100 to 400 psia, mixture ratios of 2 to 4 and fuel inlet temperatures of 27 to 127°F.

Ignition on all tests was reliable and smooth. Stability evaluation bombs produced chamber pressure overpressures of 100% which were damped in less than .004 sec with the aid of axial resonator cavities. This injector was found to be stable and compatible but low in performance having a C* efficiency of 85% in a 4 inch long chamber and 93% C* in an 8 inch long chamber.

TABLE I

SUMMARY OF TEST CONFIGURATIONS

Test Series	Injector	Propellant	Chamber	Film Coolant	Test Identification
1	EDM Like-On-Like	LOX-Propane	4 & 8 in. L' Heat Sink	No	LPB6797-101 to 118
2	EDM OFO	LOX-Propane	8 in. L' Heat Sink	No	119 to 132
3	EDM OFO	LOX-Propane	8 in. L' Water Cooled	No	133 to 143
4	EDM OFO	LOX-Propane	8.7 in. L' Water Cooled	Yes & No	144 to 152
5	EDM OFO	LOX-Ethanol	8.7 in. L' Water Cooled	Yes & No	153 to 160
6	Platelet PAT	LOX-Ethanol	8.7 in. L' Water Cooled	Yes & No	161 to 169
7	EDM/ Platelet	GOX-Ethanol Ambient Temp Cold - 130°F	8.7 in. L' Water Cooled	Yes & No	101 - 111 112 -

E, Tasks II and IV Subscale Injector Characterization (cont.)

In LOX/propane Test Series II, eleven short (0.5 to 1.2 sec) hot-fire heat sink chamber tests were conducted with an unlike impinging element injector with an electrical-discharge-machined (EDM) OFO triplet injection pattern. The engine was found to be stable at chamber pressures of 200 to 400 psia and mixture ratios of 2 to 4 when bombed with 2 and 6.5 grain (gr) bombs at a resonator cavity depth of 0.7 inches. The engine could be bombed into an unstable condition when the cavity was eliminated. The C* performance and thrust-based energy release efficiency (ERE) data ranged from 95 to 99% in an 8 inch long chamber. The unlike-element injector was 4.5% more efficient than the like-on-like design at the nominal design point (97.5 vs 93.0) based on test durations of 1 second.

In Test Series III, eleven additional long-duration tests were conducted with the same injector and a water-cooled calorimeter chamber. A total of 600 seconds of burn time was achieved with a maximum single burn of 80 seconds. Firing durations of 20 to 60 seconds were required before the full heat flux reduction due to carbon deposition was realized. No major cumulative test-to-test heat flux reductions due to carbon were observed; the shutdown and startup transients removed most of the heat-resisting deposits. The highest heat fluxes were recorded at the low mixture ratio conditions while the highest carbon buildup rates were observed at the highest mixture ratios. The increased carbon deposition at high mixture ratio is believed to be a unique result of the OFO injector element which produces a fuel-rich wall environment when the oxidizer/fuel momentum ratio is high. The performance results (C* and ERE) from these longer duration tests were slightly higher (1.5% at nominal design chamber pressure and mixture ratio) and more internally consistent than those of the previous shorter tests. The 40 element OFO triplet injector is rated at 99% ERE at all mixture ratios over 2.7 but performance degrades very rapidly at mixture ratios less than 2.6. The nominal design mixture ratio for propane is approximately 3.0.

Inspection of the hardware after testing indicated that the resonator cavities contained a significant amount of solid carbon, to the extent that they could become detuned. This is not compatible with a low-maintenance, long life, design approach.

In Test Series IV, a preatomized film-cooling injector which sprayed fuel into the resonator cavity was added to the test setup. A separate film-coolant valve and flow-measuring instrumentation was provided. The chamber length was increased to 8.7 in. by the added hardware.

Nine long hot-firing tests were conducted. Performance and heat transfer data were obtained at 0, 9, and 14% fuel (propane) film-cooling and at the same wide range of mixture ratio and chamber pressure conditions as Series III. Postfire inspection of the resonator showed the cavities to be considerably cleaner than after the previous test series without film-cooling. The total firing duration on this series was approximately 400 sec, and the

E, Tasks II and IV Subscale Injector Characterization (cont.)

longest single burn was 70 seconds. The fuel film-cooling did not appear to affect the combustion stability although no bomb tests were conducted. Significant reductions (approximately 50%) in both chamber and throat heat fluxes were recorded with 15% fuel film-cooling. In the last 5 seconds of each test the fuel film-cooling valve was closed and the rise in heat flux was observed. The wall heat flux gradually returned to the value measured without film-cooling in Series IV, indicating that any additional soot deposited by the extra fuel was slowly removed by the hot gas.

In Test Series V, the same 40 element OFO triplet injector, preatomized fuel film-cooling injector, and water-cooled chamber that had been used for the propane testing were tested with LOX/ethanol. Seven tests in total were conducted. The test parameters included mixture ratio variations of 1.3 to 2.5, chamber pressures of 300 and 400 psia, and fuel film-cooling flows of 0, 8, and 14%. The duration of each test was 30 seconds. On each test, the fuel film-cooling valve was closed for the last 5 seconds to provide data without film-cooling. In contrast to the testing with propane which revealed sooting of the combustion chamber, the tests with ethanol produced a clean chamber and injector and a clear exhaust plume. The same resonator cavity depth as in the propane testing was used with no incidence of combustion instability. The throat heat flux for the ethanol was considerably higher (20%) than the peak values for propane and 60% higher than steady-state values when full propane-induced soot buildup was reached. The heat flux with LOX/ethanol propellants showed no reduction with time. The effectiveness of the ethanol film-cooling at the throat station was very small compared to the significant heat flux reductions experienced with propane film-cooling. It was reasoned that a portion of the loss of film-cooling effectiveness with ethanol could be due to the non-optimum propellant injection momentum ratios; however, most of the loss in cooling is probably due to the absence of the soot layer that develops when propane is added as film coolant.

The performance of the OFO injector with ethanol ranged from 92% ERE at low mixture to approximately 100% at high mixture ratio. Performance results were roughly 1.5% lower at the nominal mixture ratio with ethanol as compared to propane. With a 1.94 nozzle expansion, the test data at 300 psia, showed a maximum Isp of 259 lbF-sec/lbM for propane at a mixture ratio of 2.6 and 238 lbF-sec/lbM for ethanol at a mixture ratio of 1.75.

Recent data (Ref. 2) indicated hydrocarbon propellants could produce higher throat heat fluxes than predicted by normal analytical methods when the chamber walls are clean. The present test series confirmed these findings. The heat transfer correlating coefficient (Cg) profiles for propane and ethanol combustion with and without film-cooling were found to be in reasonable agreement with the higher-than-normal values of Reference 2 which were employed in the Task III design feasibility studies for propane. However,

for ethanol, the OFO triplet pattern must be augmented with approximately 15% fuel film-cooling to reduce the head-end heat load to match the design values.

In Test Series VI, the injector was replaced by a a photo-etched unit containing 45 preatomized triplet (PAT) OFO element sets (two oxidizer splash-plates on one central vortex fuel). Nine hot-fire tests were conducted with LOX/ethanol. Test parameters included Pc variation (200 to 400 psia), mixture ratio variation (1.24 to 2.45), and film-cooling flows of 0, 9, and 17%. All tests were stable, using the same resonator cavities as employed in previous tests with the 8.7-in. water-cooled chamber. The head-end chamber wall heat-flux for this injector design was considerably lower than that for the EDM OFO triplet, whereas the performance was approximately the same for both. The EDM injector showed 1.6% higher specific impulse than the PAT without film-cooling; with the introduction of fuel film-cooling the PAT injector showed a 2% higher specific impulse than the EDM injector.

The net result is that the PAT platelet injector was found to provide higher performance and lower chamber heat flux than the conventional EDM triplet design.

The presence of PAT element "blowapart" was identified by the decrease in specific impulse with increased chamber pressure. This occurs because as chamber pressure increases, the combustion intensity increases at the interface between the oxidizer and fuel streams which inhibits the mixing process. Futher evidence of blowapart was obtained by very low (approximately zero) head-end heat flux without fuel film-cooling. The increase of both performance and head-end heat flux with the addition of small amounts of fuel film-cooling proved that the core element propellant being directed towards the chamber wall was oxygen. Of even further significance was the observed lower throat region heat flux for the oxidizer-rich wall condition.

In Test Series VII, the liquid oxygen (LOX) was replaced by gaseous oxygen (GOX) which represented the selected RCS engine propellant state. Another PAT element injector was tested. This design utilized the same vortex fuel element as Series VI and an EDM oxidizer element similar to the OFO triplet, enlarged to accommodate gas-phase oxidizer.

Eleven tests each up to 20 seconds in duration, were conducted with nominal 50 $\pm$ 20°F propellants; two additional tests were conducted with -130 $\pm$15°F propellants. As before, tests provided performance, thermal, and stability data with 10 to 15% film-cooling at the start of each test and no film-cooling for the final 5 seconds of each test.

The injector was found to be stable at all test conditions: chamber pressure ranged from 95 to 400 psia, and mixture ratio from 1.3 to 2.7. The gas/liquid PAT element did not exhibit the blowapart characteristics of the

liquid/liquid element. Isp improved with increasing pressure and degraded with the addition of fuel film-cooling. The maximum GOX/ethanol performance was slightly higher than LOX/ethanol data of Series VI (245 versus 242 lbF-sec/lbM). Cold propellants resulted in a reduction of 2% in energy release efficiency, i.e., 97% versus 99%.

5. Test Series Description

The details of each of the seven test series are presented chronologically in the following sections. The format used for each series is as follows: the test objectives are stated, the test facility is described, followed by the design details of the test hardware. Checkout or cold flow tests of injectors are documented by pressure drop and photographic data. A narrative of the tests and/or tabular data defining the test conditions for each series is provided, followed by presentation of the test results. The results include specific impulse, C*, and heat flux profiles versus time. Data analyses and comparisons of test results are provided in Sections 6 and 7. This includes calculation of combustion efficiencies, loss analyses, and comparison of experimental-to-predicted heat flux ratios (Cg profiles), etc.

a. Test Series I - LOX/Propane, LOL-EDM Injector, Heat Sink Chamber

(1) Objective

Previous experimental history has shown that matched pairs of like-on-like impinging (LOL) doublet elements (also known as quadlets) provide good combustion stability, low chamber wall heat flux, and modestly good combustion efficiency. The existing data base was confined mainly to the LOX/RP-1 propellant combination and N_2O_4/MMH propellants utilized on the Space Shuttle OMS engines. The first phase of this program was to extend this data base to include propane fuel.

The sensitivity of performance and stability to operating pressure (100-400 psia), fuel temperature (34 to 127°F), mixture ratio (2 to 4), and chamber length (4 inches and 8 inches), were to be experimentally evaluated using a 42 element LOL doublet pattern.

(2) Test Facility

The subscale hot fire testing was conducted in Bay 6 of the ALRC Research Physics Laboratory. The setup consisted of the fuel and oxidizer feed systems, a thrust stand, the test hardware, the igniter and its feed system, and instrumentation.

(a) Propellant Feed System

A schematic of the propellant feed system is shown in Figure 8. The propellants were supplied to the engine from gaseous helium-pressurized tankage. The fuel system contained a jacketed portion of the feed line which provided temperature conditioning capability.

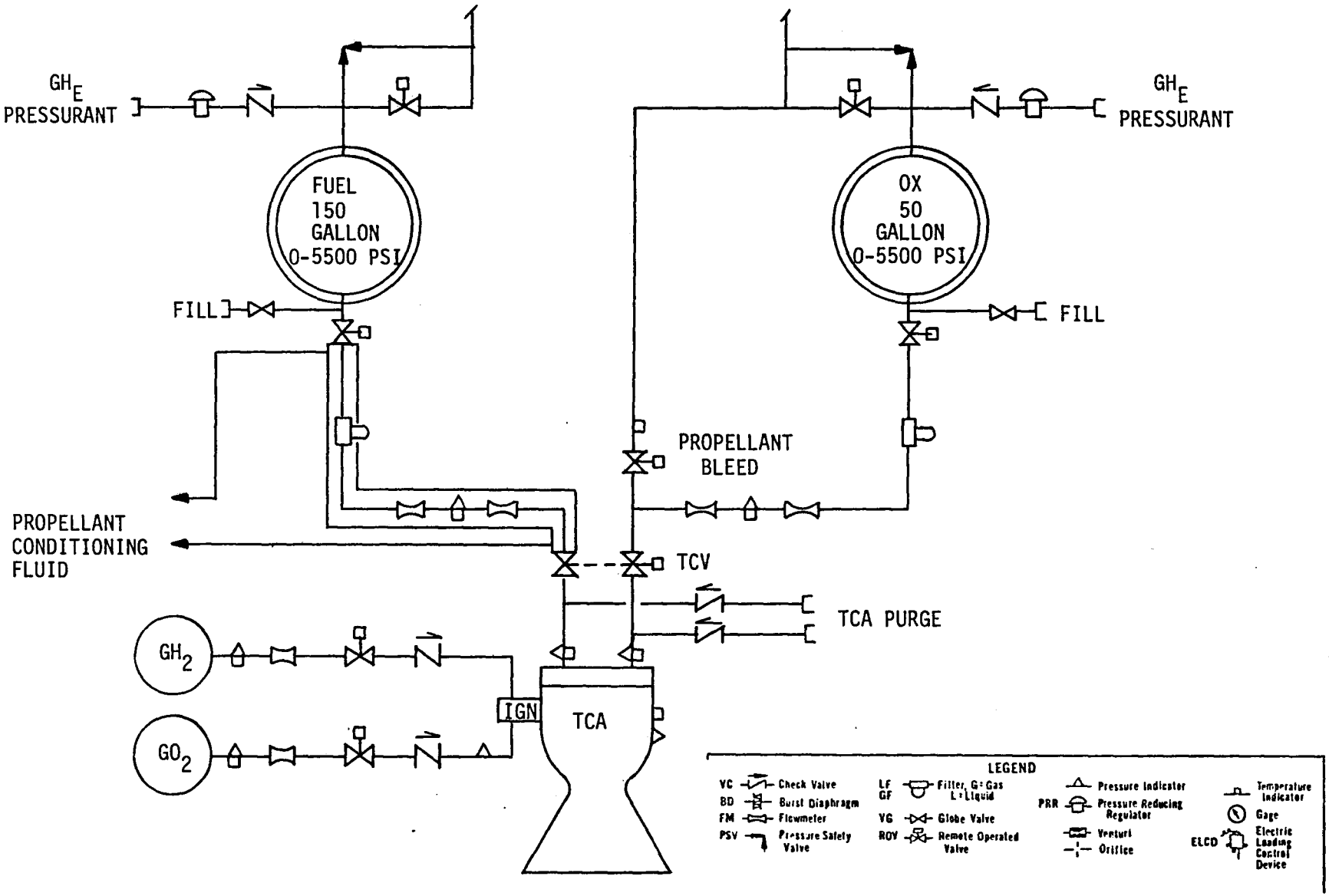

Figure 8. Propellant Feed System

E, Tasks II and IV Subscale Injector Characterization (cont.)

The GO_2/GH_2 igniter was fed from high pressure 'K' bottles. Sonic venturis were used to control and measure the flowrates. A GLA power supply provided the required energy for ignition.

(b) Thrust Stand

The engine was mounted on a thrust measurement stand to permit performance evaluation. The thrust stand is of the compression leaf flexure design and permits accurate measurements over a range of 500 to 5000 lbF.

(c) Instrumentation

The feed system and test hardware were instrumented, as shown in Figures 8 and 9, to measure the performance, stability and thermal parameters. The measured parameter nomenclature, instrument type, and accuracy are listed in Table II. The measured parameters were recorded on both a digital data acquisition system and on an analog oscillograph.

(3) Test Hardware

The hardware tested is shown schematically in Figure 10 and pictorially in Figure 11. It consisted of the injector, chamber segments containing acoustic cavity resonator with blocks to allow depth (tune) adjustment, L' sections, a nozzle and igniter.

The injector design was a 7 concentric ring manifold configuration which contained 42 EDM LOL elements. Each oxidizer orifice was .033 in. and each fuel orifice size was .023 inch. Details of the element impingement are shown in Figure 12. Fabrication drawings and a photograph of the face are shown in Figures 13 and 14.

Ignition of the LOX/propane propellant combination was accomplished with a chamber-mounted GH_2/GO_2 spark igniter which could be turned off following engine ignition.

The L' sections provided instrumentation ports for both high and low frequency transducers and brazed in place gas-side thermocouples spaced axially at two circumferential locations. The copper nozzle contained additional circumferential thermocouples at the throat plane.

The L' and nozzle sections were clamped between injector and aft retainer ring with six 3/8-in. dia x 24-in. length studs and were sealed with teflon 'O' rings. Four threaded holes were provided in the aft ring for attachment of a leak-check fixture.

(4) Cold-Flow Testing

Tests of the injector were conducted to verify the pressure drop and impingement pattern. Photographs of the spray are shown in Figure 15.

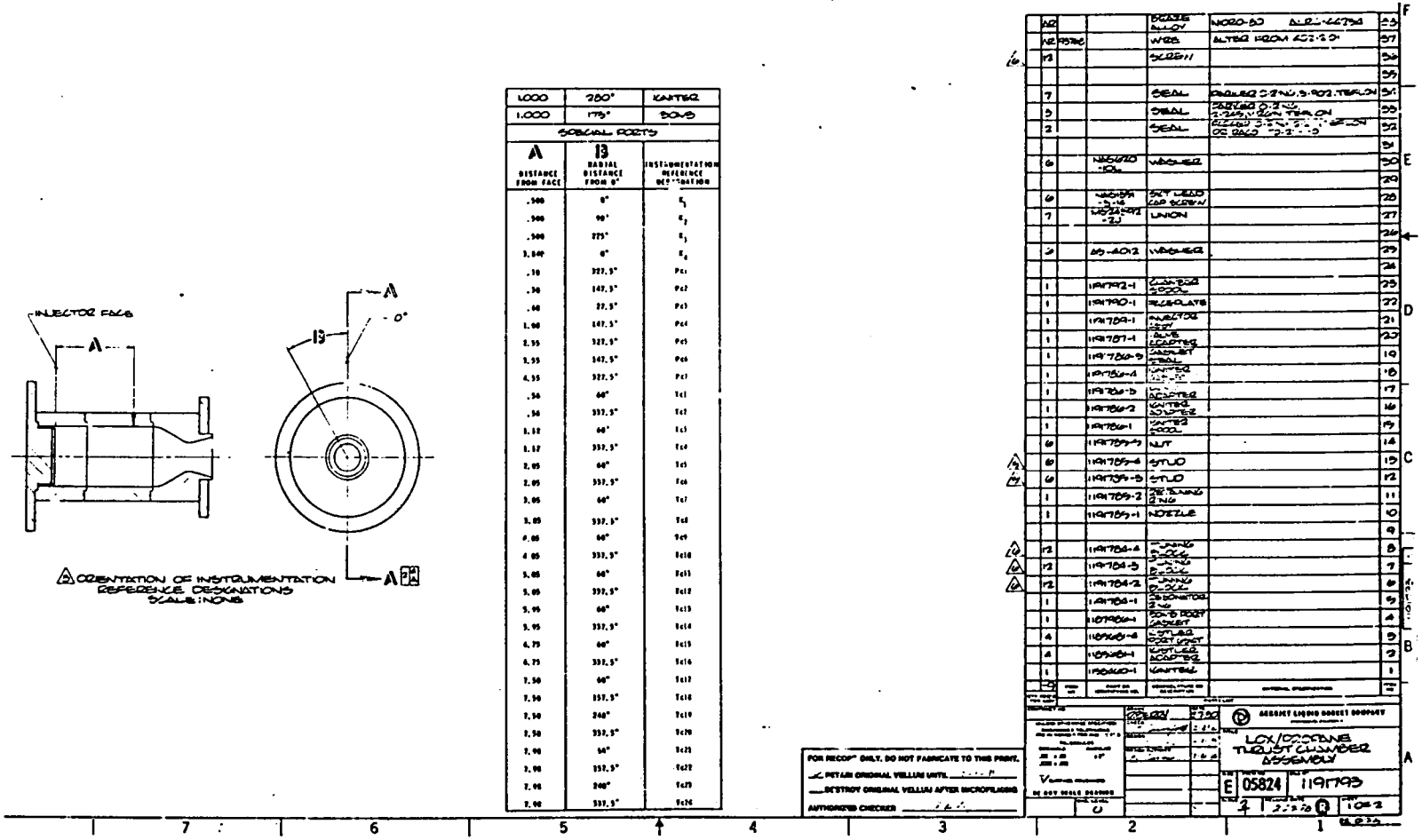

Figure 9. Test Hardware Instrumentation

TABLE II

COMBUSTION TESTING INSTRUMENTATION LIST

PARAMETER	SYMBOL	TRANSDUCER TYPE	RANGE	ACCURACY ± % READING	RECORDING DEVICE TAPE	VISUAL	GRAPH	DISC	MALFUNCTION DETECTION
Oxidizer Tank Pressure	POT	Strain Gauge	0-1000 psi	.25		X		X	
Oxidizer Flowmeter Pressure	POFM	" "	0-1000 psi	.25		X		X	
Oxidizer Injection Pressure	POJ	" "	0-1000 psi	.25			X	X	
Oxidizer Flowmeter Temperature	TOFM	Thermocouple	-200-(-)300°F	.5		X	X	X	
Oxidizer Injection Temperature	TOJ	"	" "	.5			X	X	
Oxidizer Flowrate	WO-1	Turbine	0-4#/sec	.5			X	X	
Oxidizer Flowrate	WO-2	"	0-4#/sec	.5				X	
Fuel Tank Pressure	PFT	Strain Gauge	0-1000 psi	.25		X		X	
Fuel Flowmeter Pressure	PFFM	" "	0-1000 psi	.25		X		X	
Fuel Injection Pressure	PFJ	" "	0-1000 psi	.25			X	X	
Fuel Flowmeter Temperature	TFFM	Thermocouple	-44-170°F	.5		X	X	X	
Fuel Injection Temperature	TOJ	"	" "	.5			X	X	
Fuel Flowrate	WF-1	Turbine	0-1.5#/sec	.5			X	X	
Fuel Flowrate	WF-2	"	0-1.5#/sec	.5				X	
Chamber Pressure	PC-1 thru PC-7	Strain Gauge	0-500 psi	.25			X	X	<80% Pc
High Frequency Pc	K-1 thru K4	Piezioelectric	50 p-p psi	5.0	X				>15% Pc P-P
Thrust	FA	Strain Gauge	0-2000 lbF	0.25		X	X	X	
Thrust	FB	" "	0-2000 lbF	0.25				X	
Thrust Cal	FCALA	" "	0-2000 lbF	0.25		X		X	
Thrust Cal	FCALB	" "	0-2000 lbF	0.25				X	
Chamber Wall Temperature	TC1 - TC 24	Thermocouple	0-1500°F	0.5			X	X	>1000°F
TCV Linear Trace	LTTCV	Potentiometer	0-100%	1.0			X	X	
TCV Signal	VITCV	Voltage	---	---	X		X	X	
Igniter Valve Signal	VTIGN	"	---	---	X		X	X	
Igniter Chamber Pressure	PIGN	Strain Gauge	0-500 psi	.25			X	X	<200 psi
Igniter Oxidizer Pressure	POIGN	" "	0-1000 psi	.25		X		X	
Igniter Fuel Pressure	PFIGN	" "	0-1000 psi	.25		X		X	

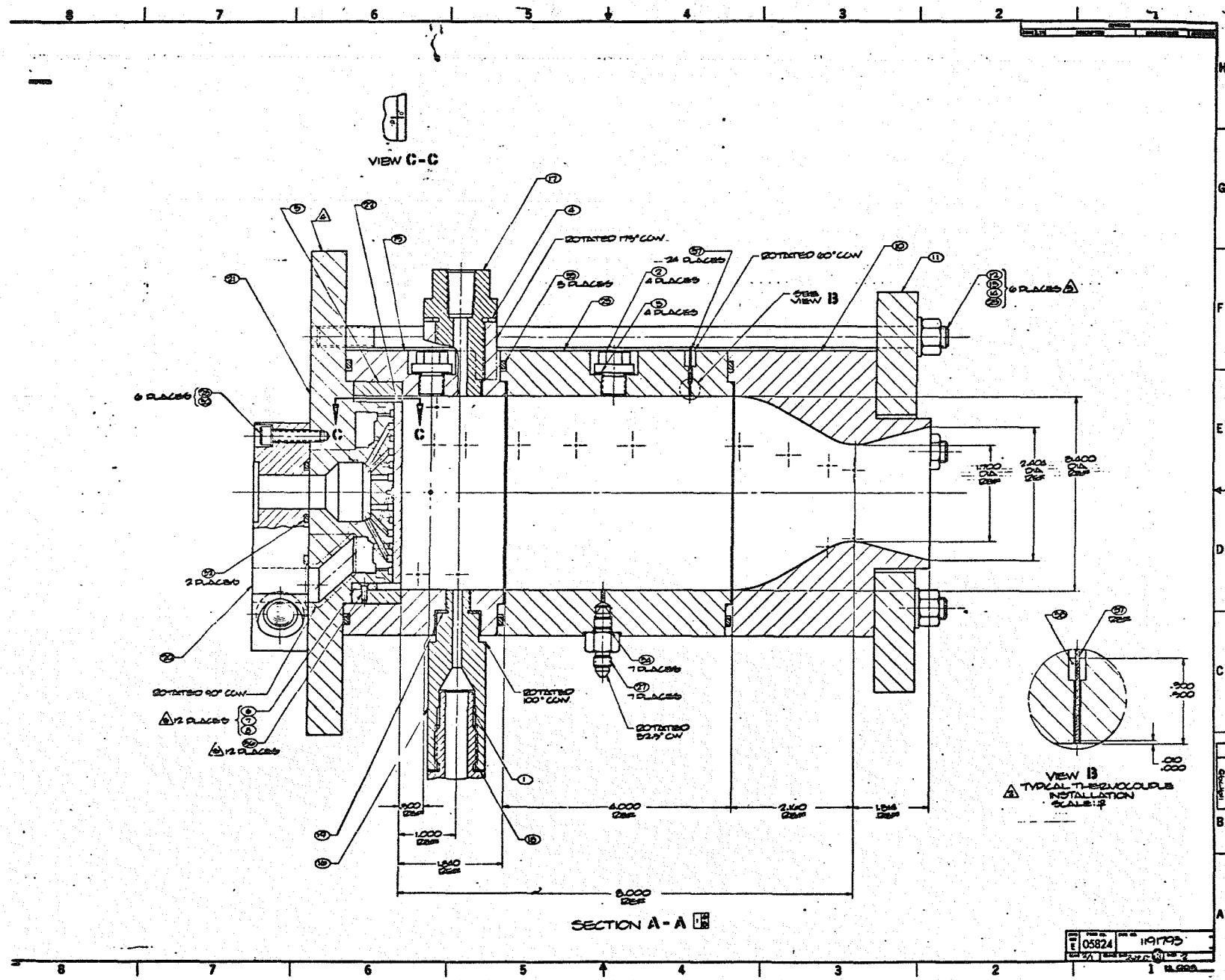

Figure 10. LOX/Propane Thrust Chamber Assembly

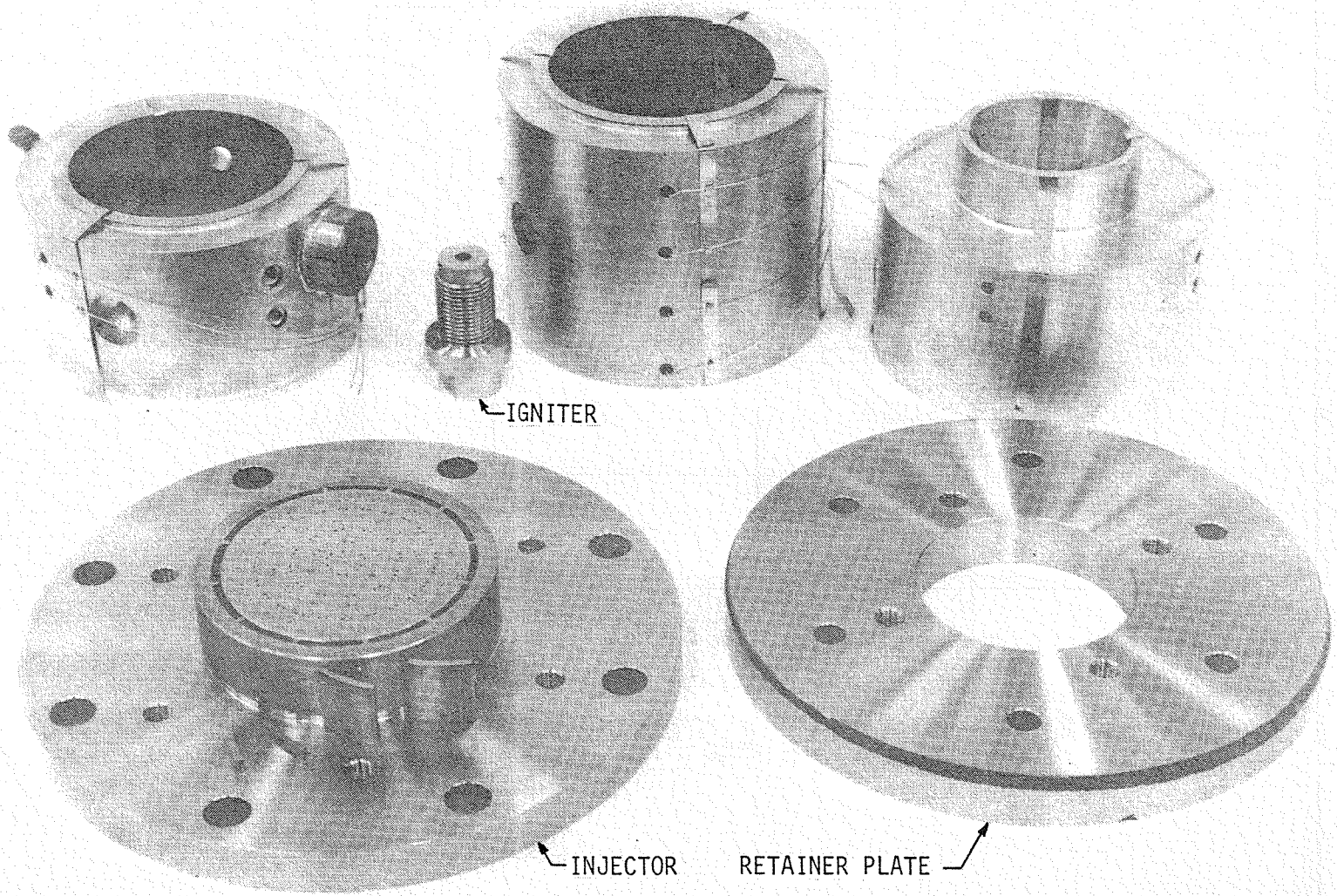

Figure 11. LOX/Propane Thrust Chamber Assembly (Pictorial View)

PARAMETERS	
CR	4.0
Injector Diameter (in.)	3.20
Cavity Width (in.)	0.10
D_c (in.)	3.40
D_t (in.)	1.70
C_{D_o}	0.75
C_{D_f}	0.75
No. LOL Pairs, o	42
No. LOL Pairs, f	43
d_o (in.)	0.033
d_f (in.)	0.023
Nominal Condition:	
Pc (psia)	300
MR	3.0
T_o (°F)	-297
T_f (°F)	70
C* (ft/sec)	5870
$\dot{W}_o$ (lbm/sec)	2.85
$\dot{W}_f$ (lbm/sec)	0.95
$\Delta P_{o,\ face}$ (psi)	87.0
$\Delta P_{f,\ face}$ (psi)	90.7

			Ox	Fuel
IMPINGEMENT ANGLE	θ	=	30°	25°
LIKE IMPINGEMENT HEIGHT	H_L	=	0.10"	0.10"
CANT ANGLE	ϕ		10°	22°
FACE THICKNESS	T	=	0.125"	0.125"
FAN OFFSET	S	=	0.0	0.0

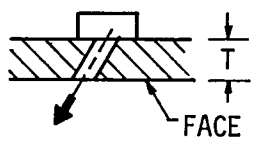

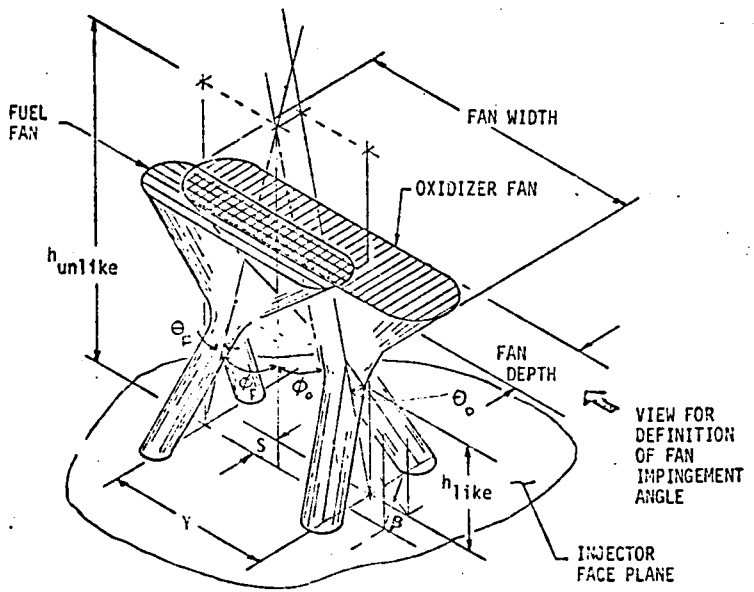

Figure 12. Injector Element Design Summary

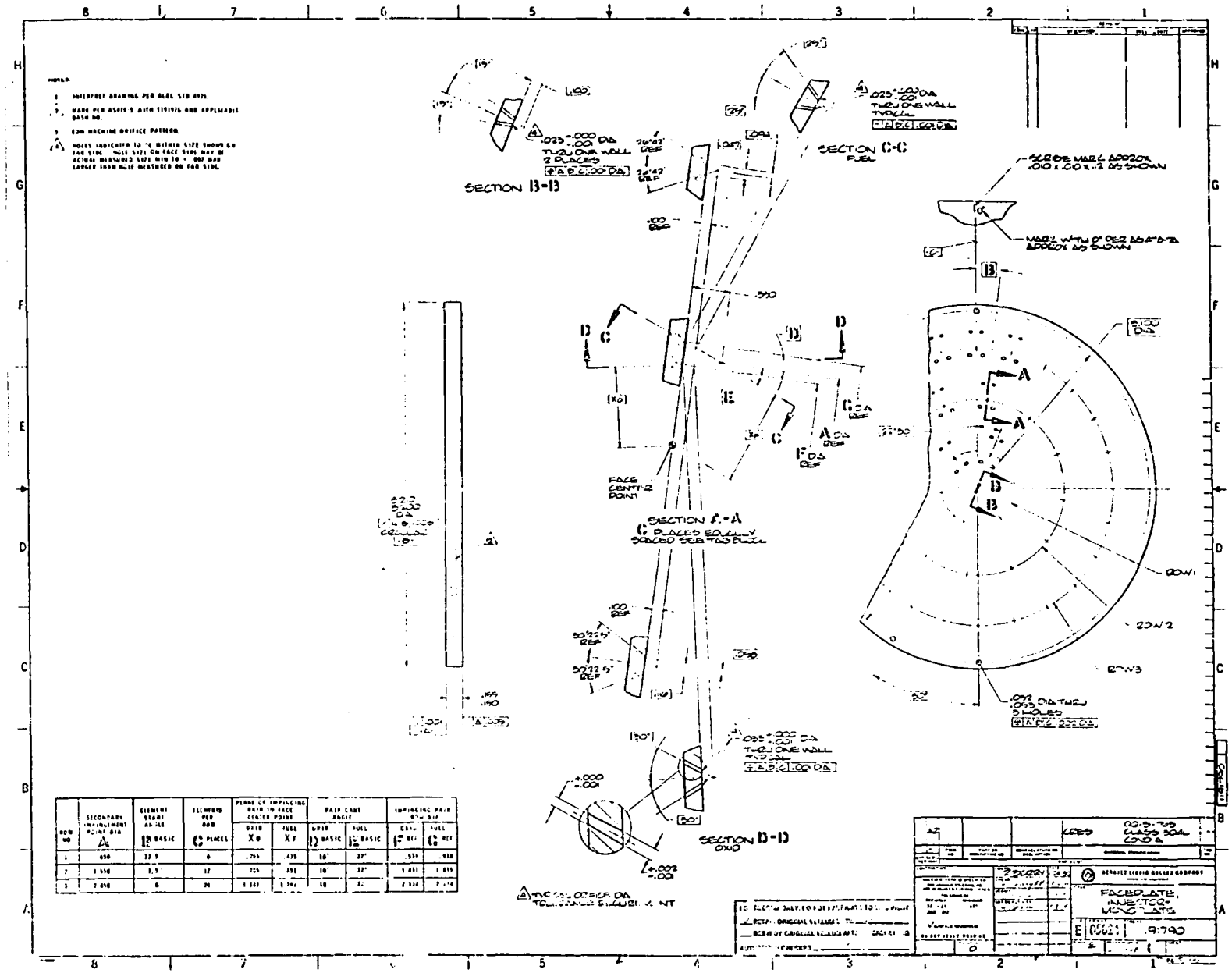

Figure 13. Like-On-Like Doublet Injector Pattern

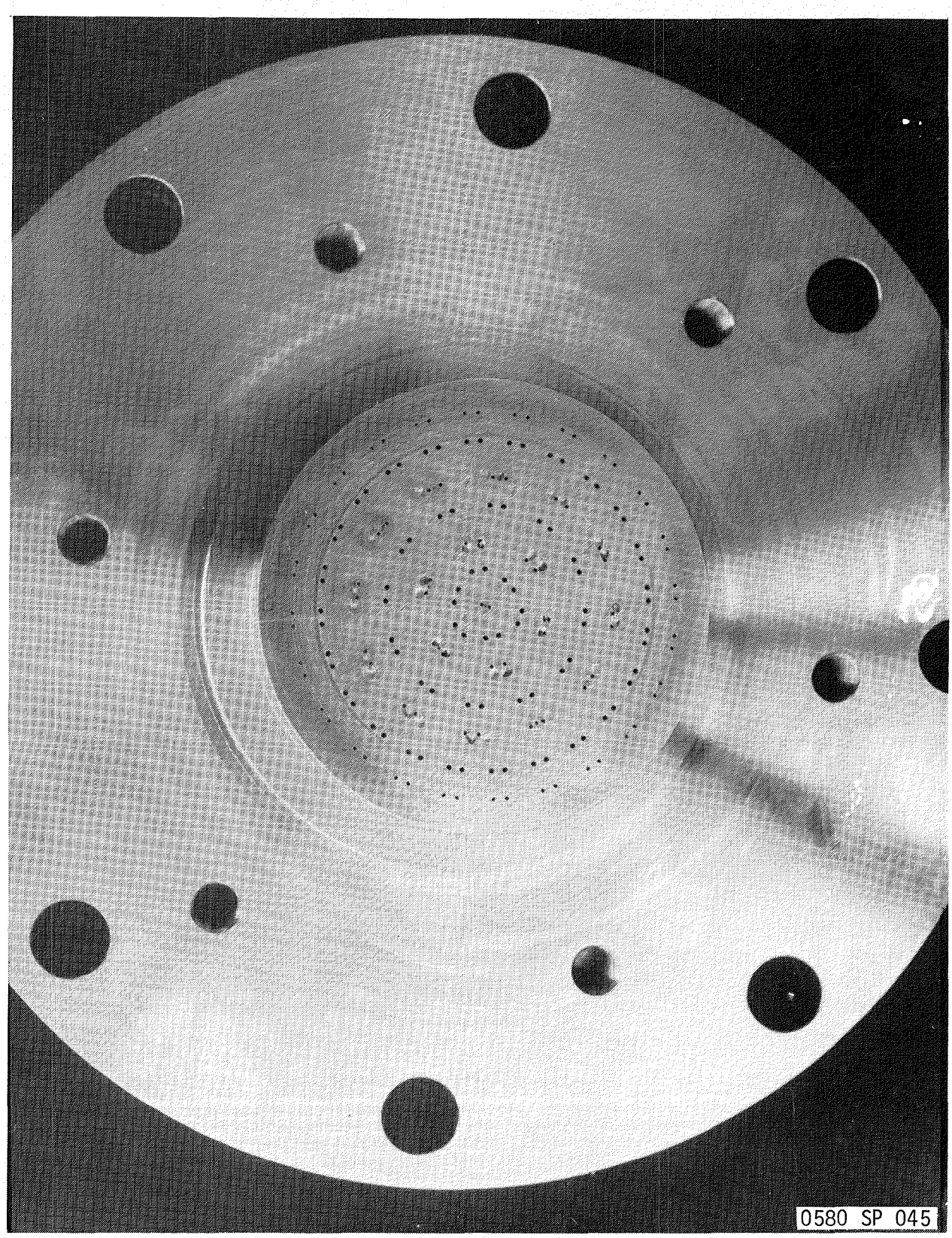

Figure 14. Like-On-Like EDM Injector Pretest

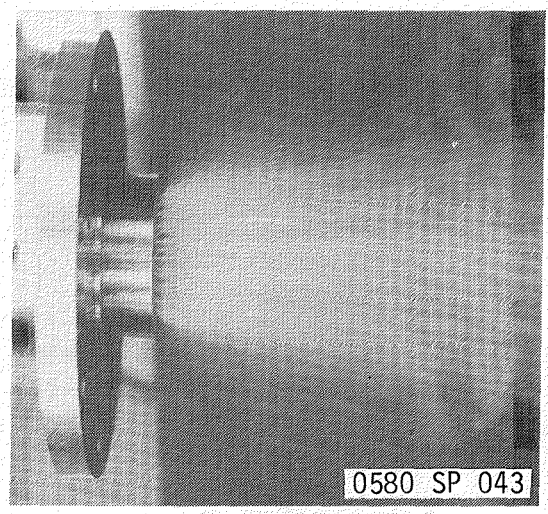

OXIDIZER CIRCUIT

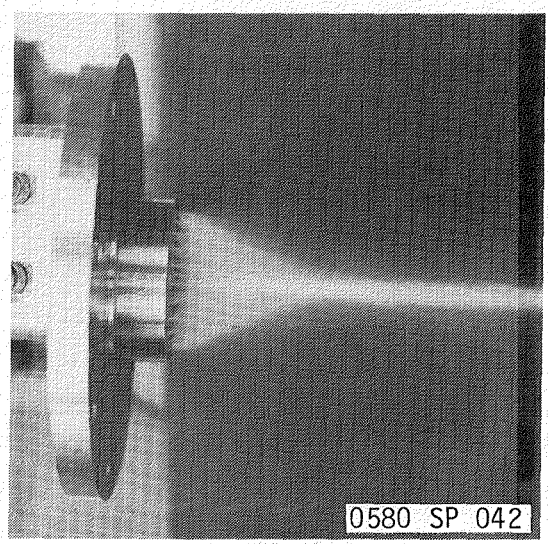

FUEL CIRCUIT

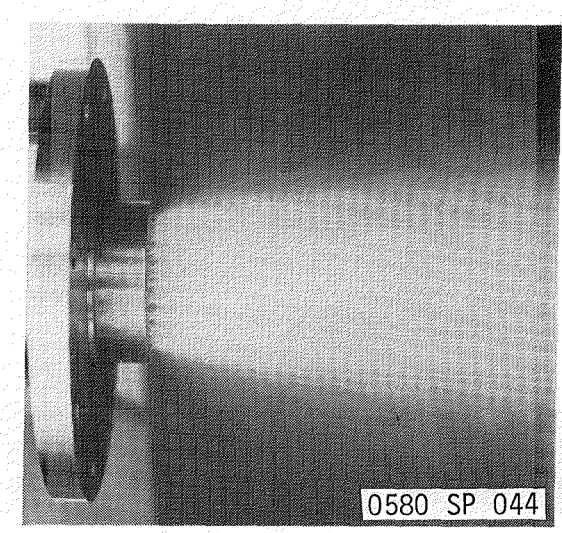

OXIDIZER AND FUEL CIRCUIT

Figure 15. Spray Patterns for Fuel, Oxidizer, and Oxidizer and Fuel Circuits

E, Tasks II and IV Subscale Injector Characterization (cont.)

(5) Hot-Fire Testing

Tables III, IV, and V summarize the test conditions and results. In Tests 101 through 110, variations included chamber length (4 and 8 inch), mixture ratio (2 to 4), and fuel temperature (70 to 127°F). In Tests 111 to 118, chamber pressure was added as a test variable and cold fuel (30°F) tests were conducted. Although no metal removal was noted, the injector face appears to have been hot as shown in Figure 16.

Ignition on all tests was reliable and smooth. Stability verification bombs caused chamber pressure increases of over 100%, which were all damped in less than 4 msec. Testing was terminated with this injector following Test 118 because the combustion efficiency was much lower than expected. The C* and thrust-based energy efficiency was near 85% for the 4-in. long chamber and near 93% for the 8-in. L' chamber. The low efficiency was attributed to both poor atomization and poor mixing. Analysis of the test results are presented in subsequent Sections. The data correlation indicated a 4% deficiency in performance caused by incomplete propellant vaporization and an additional loss of up to 4% due to poor mixing
(E_m = 0.7) as shown in Figure 17.

b. Test Series II - LOX/Propane OFO EDM Orifice Triplet Injector, Heat Sink Chamber

(1) Objectives

The objective of this series was to determine if an unlike-element (OFO triplet) injector would provide improved performance, and if injector face cooling and combustion stability would present operational limitations. Comparison of the chamber wall heating rates would also be made.

(2) Test Facility

Minor changes in the test facility were made to accommodate a through-the-injector face igniter port and to reposition the valves for the new injector.

(3) Test Hardware Design

Testing was conducted in the same 8-in. L' heat sink copper chamber. Instrumentation included three Kistler transducers, twenty thermocouples, two chamber pressure measurement ports, and a bomb port. A new injector design was prepared in order to improve the combustion efficiency.

TABLE III

TASK II INJECTOR TESTING SUMMARY OF TEST CONDITIONS (L' & MR VARIATION)

Test Number	Date	Data Pt. Time Summary - Sec	Hardware Description			Test Conditions					Test Objectives
			Injector	Resonator Depth in.	L' in.	Pc (Face) psia	MR	Fuel Temp °F	Bomb	Test Duration-sec	
LPB6-797-101	5/27/80	-	EDM LOL	.7	4	-	-	-	-	-	Igniter-sequence checkout
102		.3-.63				269	2.03	70	No	.5	Main stage ignition characteristic
103						281	2.76	72	No	.5	Balance and performance
104	5/28/80				8	291	2.72	72	Yes	.5	Improve performance - increase L' - check stability
105	5/29/80					290	2.79	69	Yes	.5	Improve high frequency measurement technique - transducers saturating on start
106	5/30/80	.3-.59				301	2.83	72	No	.5	Increase duration - performance (bad Tc caused premature shutdown)
107		.3-.63 .63-1.13				307 305	3.05 3.17	72 72	No	1	Rpt. 106
108		.3-.63				297	2.38	73	Yes	1	Low MR - performance/ stability
		.63-1.13				294	2.48	73			
109		.3-.63				308	3.59	72	Yes	1	High MR - performance/ stability
		.63-1.13				305	3.74	72			
110		.3-.63				304	2.93	126	Yes	1	Increase fuel temperature - performance/stability
		.63-1.13				300	3.10	127			

TABLE IV

INJECTOR TEST SUMMARY

(L', Chamber Pressure, and Mixture Ratio Variation)

Test Number	Date	Hardware Description			Test Conditions					Test Objectives
		Injector	Resonator Depth in.	L' in.	Pc (Face) psia	MR	Fuel Temp °F	Bomb	Test Duration-Sec	
111	6-18-80	EDM LOL	.7	8	398	2.9	73	Yes	1.0	Pc Influence
112	↓	↓	↓	↓	399	3.0	27	Yes	1.0	Pc Influence Temperature Influence
113	↓	↓	↓	↓	199	2.9	77	Yes	1.0	Pc Influence
114	↓	↓	↓	↓	148	4.0	77	No	1.0	Pc Influence
115	6-19-80	↓	↓	4	193	2.9	58	No	1.0	Pc Influence - Chug Limit -
116	↓	↓	↓	↓	144	3.14	61	No	1.0	"
117	↓	↓	↓	↓	129	2.5	34	No	1.5	"
118	↓	↓	↓	↓	99	2.9	37	No	1.5	"

TABLE V

EDM LOL INJECTOR TEST RESULTS

Test Number	Date	Data Pt Summary Time	Test Conditions								Calculated Data					
			L' in.	W_o lb/sec	W_F lb/sec	MR	Pc Freq psia	$F_{S.L.}$ k lb	Fuel Temp °F	Duration sec*	Kw_{ox}	KN_f	C* ODE	% Corr.	Isp sec	ERE %
LPB6-717-102		.3-.63	4.0	-	-	-	-	-								
103	5/27/80	.3-.63	4.0	2.907	1.051	2.765	280.5	.9828	72°F	.5	.259	.129	5940	85.5	223	85.7
104	5/28/80	.3-.63	8.0	2.772	1.018	2.721	291.3	.9862	72	.5	.257	.129	5950	92.9	242	92.9
105	5/29/80	.3-63	8.0	2.783	.9936	2.792	290.1	.9862	69°F	.5	.255	.123	5934	92.9	242	93.1
106	5/30/80	.3-.57	8.0	2.940	.103	2.830	301.1	.9862	72	.5	.257	.150	5934	91.81	239	92.1
107	5/30/80	.3-.63	8.0	3.057	.1001	3.055	307.0	.9862	72	1.0	.256	.129	5858	72.81	239	93.1
	5/30/80	.63-1.13	8.0	3.075	.9684	3.175	304.8	.9862	72	1.0	.255	.126	5821	93.18	239	93.6
108	5/30/80	.3-.63	8.0	2.698	1.134	2.38	297.0	.9856	73	1.0	.253	.128	6002	92.71	244	93.2
	5/30/80	.63-1.13	8.0	2.728	.1100	2.781	293.9	.9856	73	1.0	.252	.125	5117	92.0	242	92.3
109	5/30/80	.2-.65	8.0	3.215	.8947	3.592	307.6	.9862	72	1.0	.253	.125	5692	94.7	236	94.5
109	5/30/82	.63-1.13	8.0	3.237	.8649	3.743	305.3	.9862	72	1.0	.254	.126	5818	94.7	235	94.8
110	5/30/80	.3-.63	8.0	2.981	.1016	2.935	304.0	.9862	126	1.0	.255	.130	5843	92.9	240	92.9
	5/30/80	.63-1.13	8.0	2.999	.7673	3.100	300.2	.9862	127	1.0	.252	.123	5843	93.0	239	94.2

* = Bomb

D_T = 1.700 in.

Exp Ratio 1.98

Desonator depth 0.7 in.

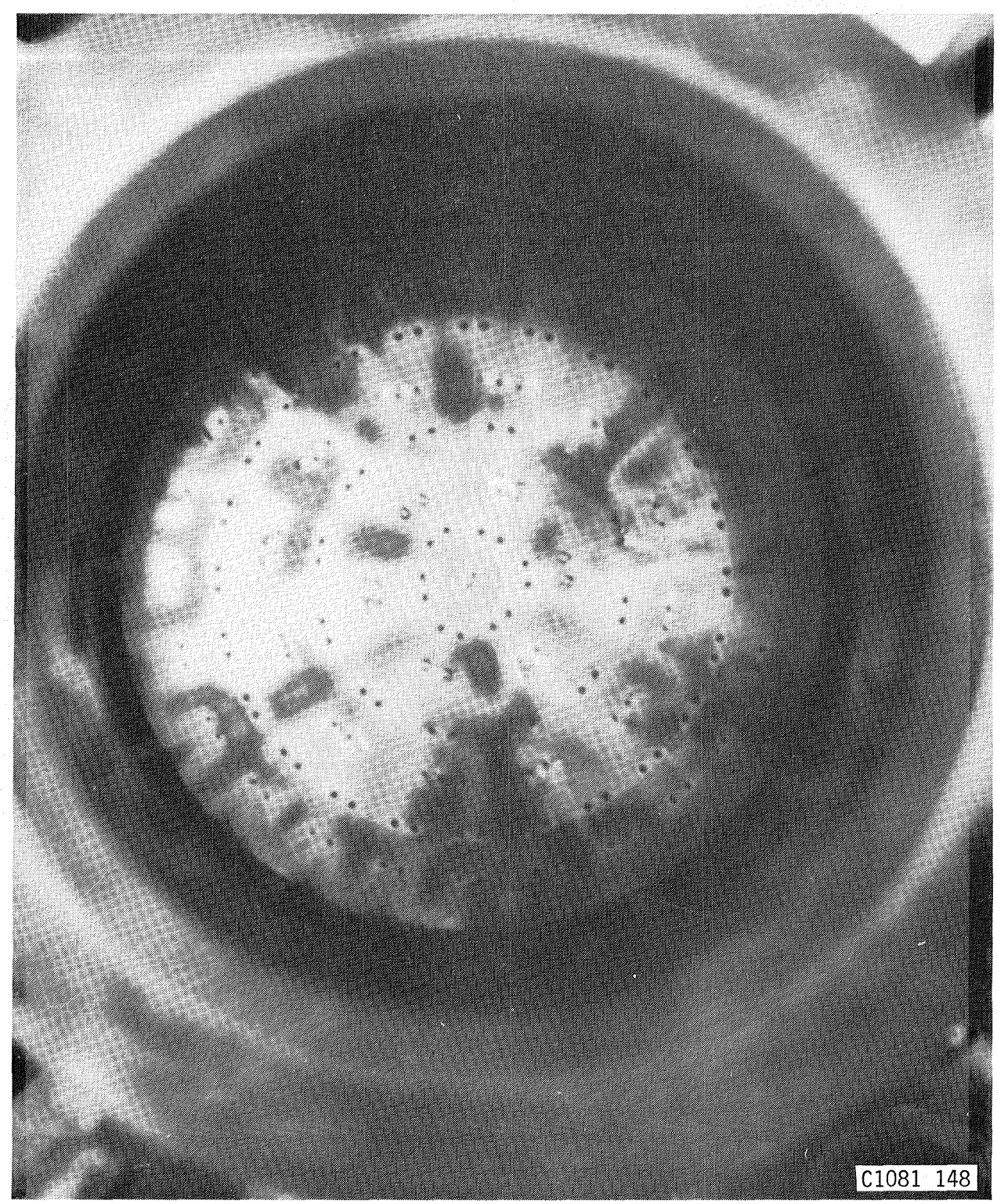

Figure 16. Injector #1 LOL Pattern After Test

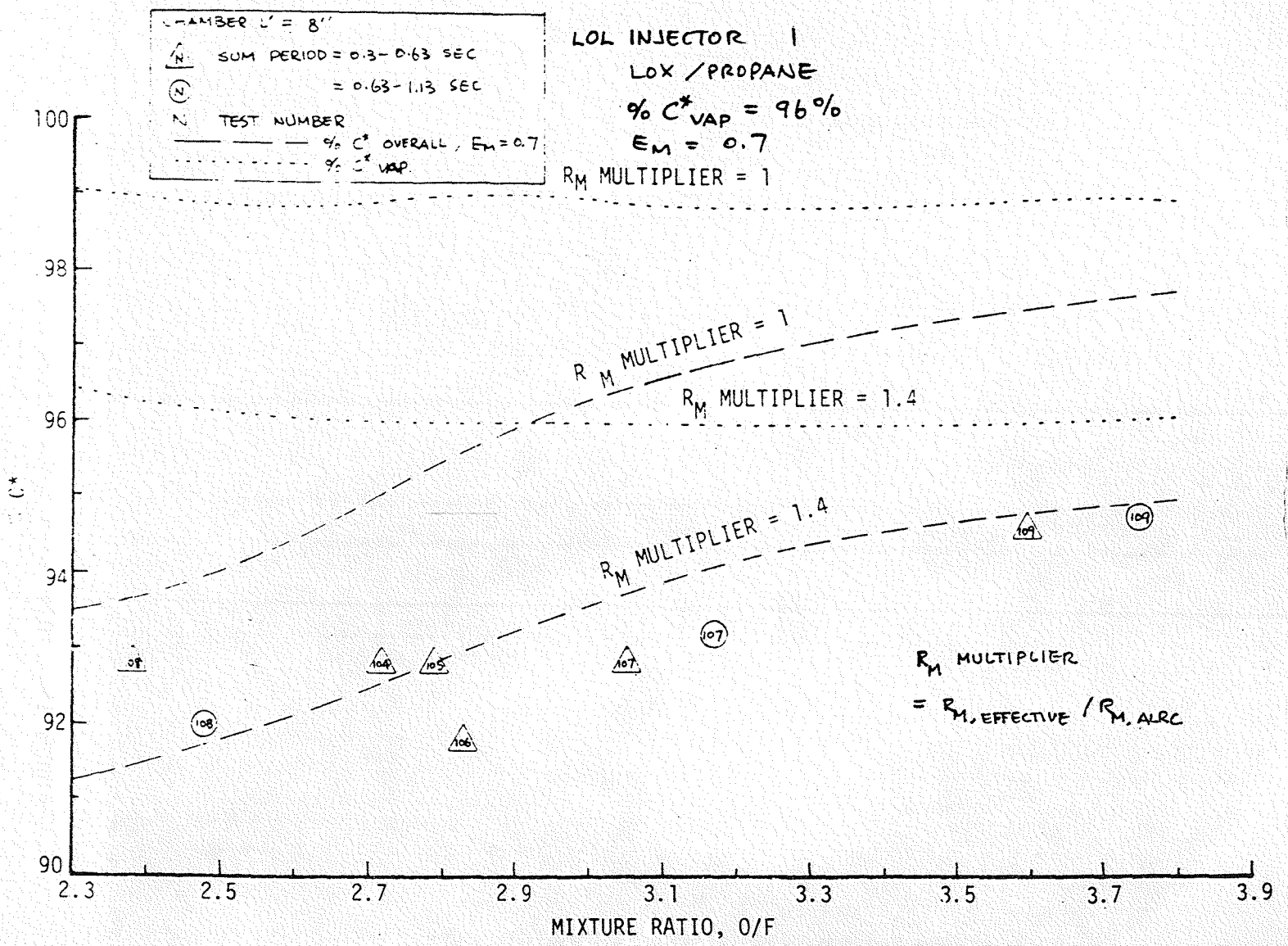

Figure 17. C* Efficiency Versus Mixture Ratio

E, Tasks II and IV Subscale Injector Characterization (cont.)

(a) Injector

In order to improve the injector performance, using the existing 7-ring manifold, a 3-row, 40-element OFO triplet pattern was designed as shown in Figure 18. The adoption of the triplet pattern was based on both anticipated high performance and on mixture ratio-independent resultant stream direction. Equal fuel and oxidizer injector orifice diameter was specified for good jet-stream match-up. During fabrication of this injector, a weld failure was discovered during an intermanifold leak check procedure. Leakage was observed between adjacent ring channels at the center and at the periphery of the injector. As a result, this second injector assembly was scrapped and eliminated from the program.

A decision was made to redesign the manifold as well as the injector in order to simplify fabrication and allow for future testing of gas propellants in a water cooled chamber. The design criteria were: (1) either circuit of the manifold be suitable for GCH_4; (2) an igniter port be provided at the center of the injector; and (3) the injector pattern be an O-F-O triplet. As a result, a 5 concentric ring channel manifold was designed. Figures 19 and 20 document the detailed drawings and photographs of the manifold design. The design highlights are listed as follows:

(a) Concentric Ring - 5 Channels

- Nominal channel width = .180 in.
- Nominal land width = .100 in.
- Nominal depth to accommodate desired channel cross velocity.

(b) Center-Mounted Igniter Port

- 0.2 inch diameter
- Compatible with existing H_2/O_2 torch igniter

(c) Provision for face pattern rework

(d) Plenums and downcomers sized for gaseous methane at a nominal Pc of 800 psia (both circuits)

A 2-row, 40-element OFO triplet injector face pattern was designed to match this manifold; the pattern layout and photograph view of the injector are provided in Figure 21. The injector configuration was as follows:

Oxidizer Orifice Dia.	= 0.033 in.
Fuel Orifice Dia.	= 0.033 in.
Number of Elements	= 40
Spacing (2 Rows)	= 30 outside row, 10 inside row

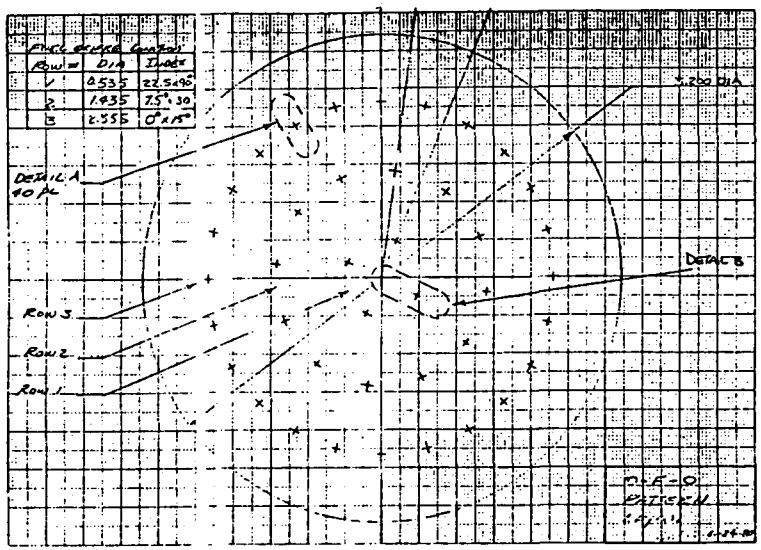

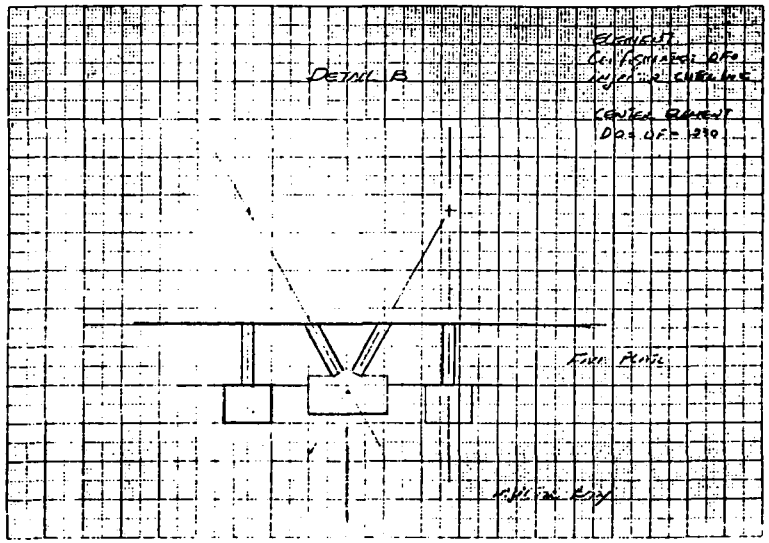

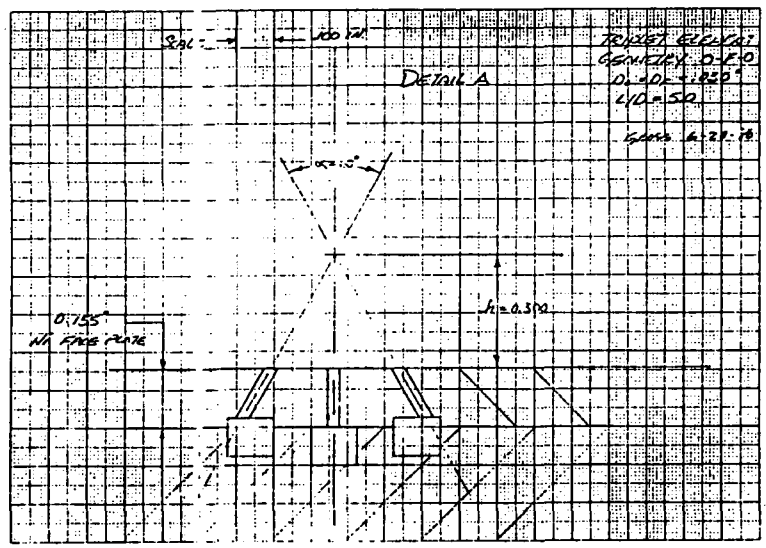

OFO TRIPLET

40 ELEMENTS

7 CONCENTRIC RING CHANNELS

$\Delta P_o = \Delta P_F = 90$ PSI

$P_c = 300$ PSIA

MR = 3

$D_o = D_F = 0.030"$

Figure 18. OFO Triplet Pattern Layout for 7-Ring Injector

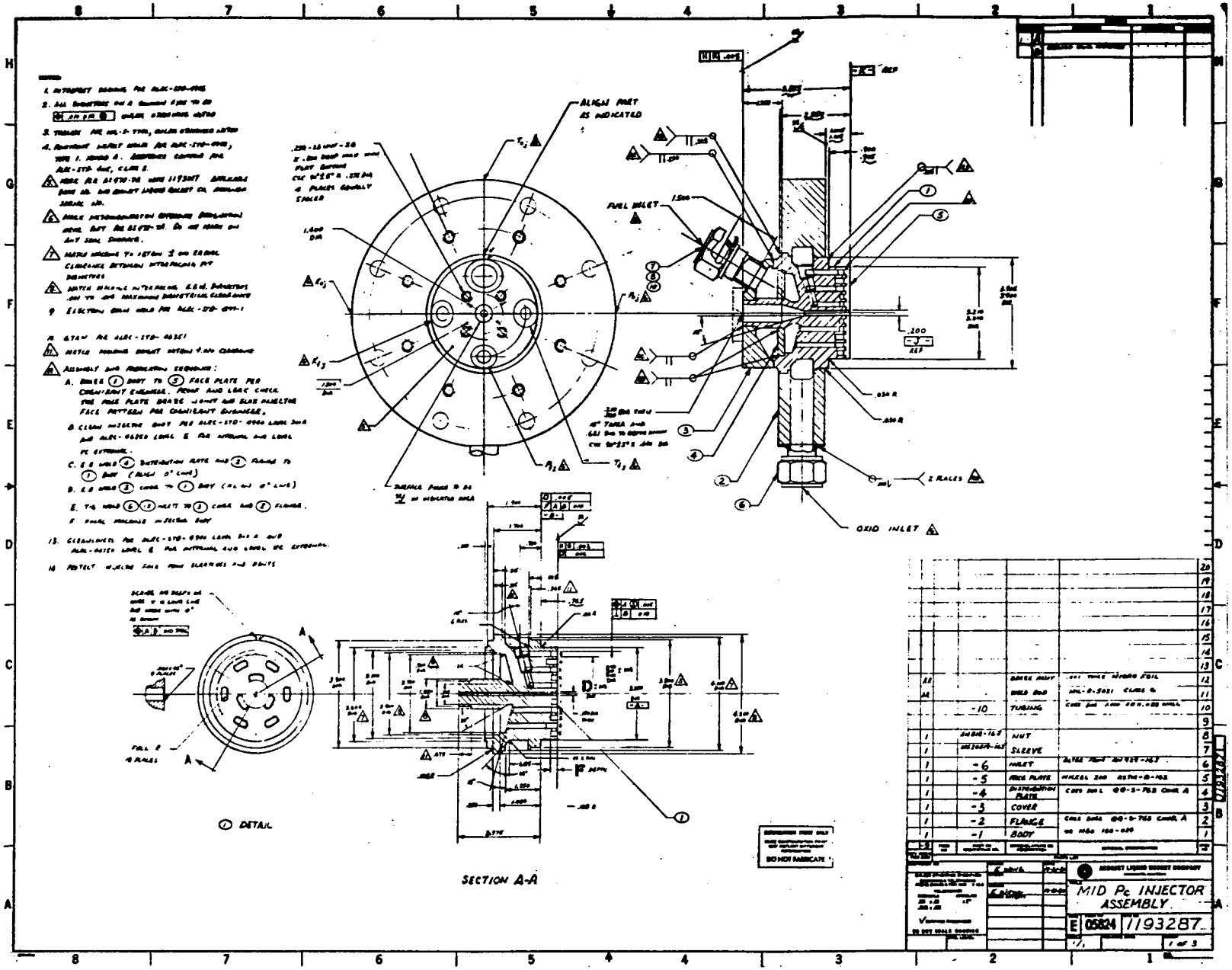

Figure 19. Injector Assembly Engineering Drawing (1 of 3)

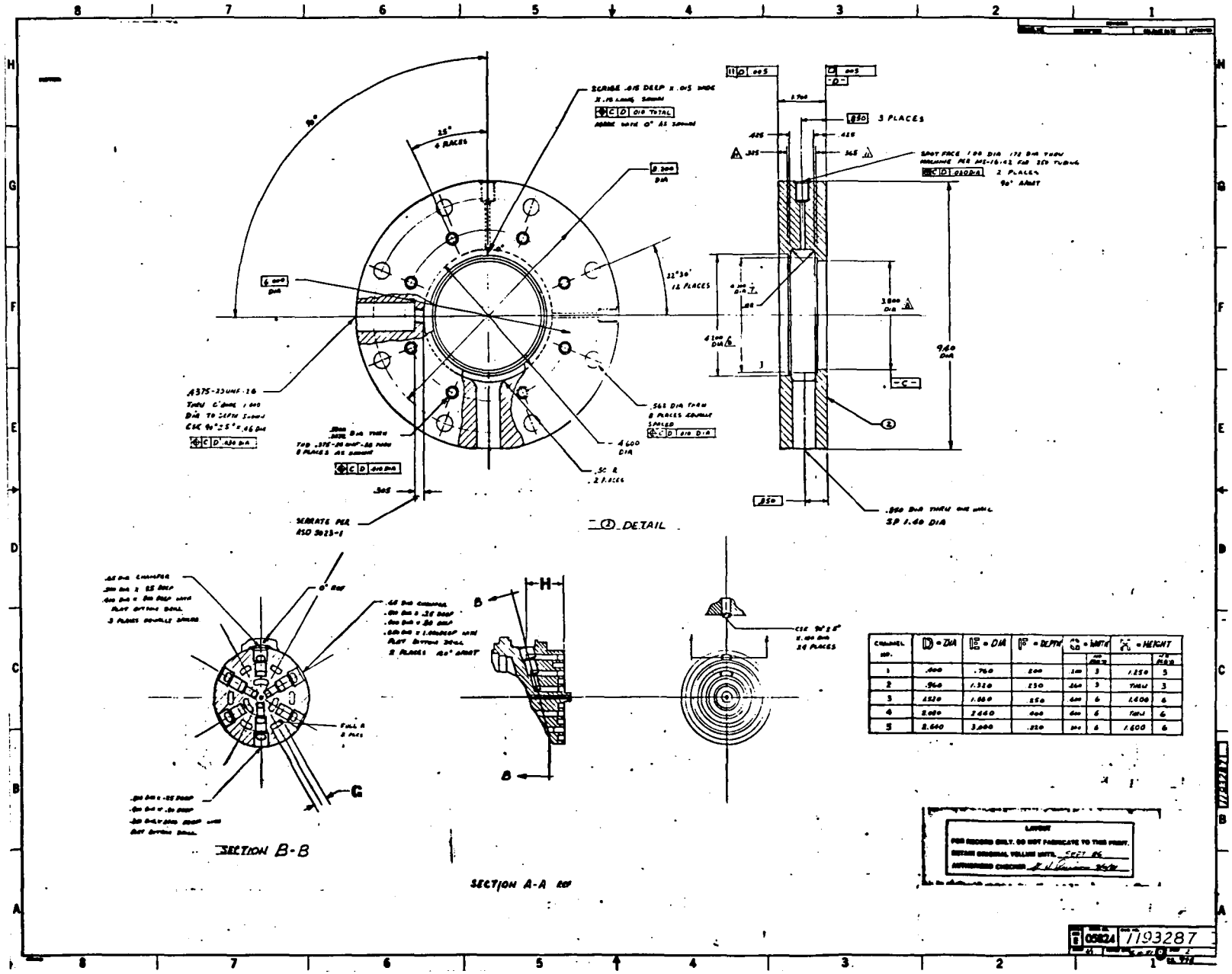

Figure 19. Injector Assembly Engineering Drawing (2 of 3)

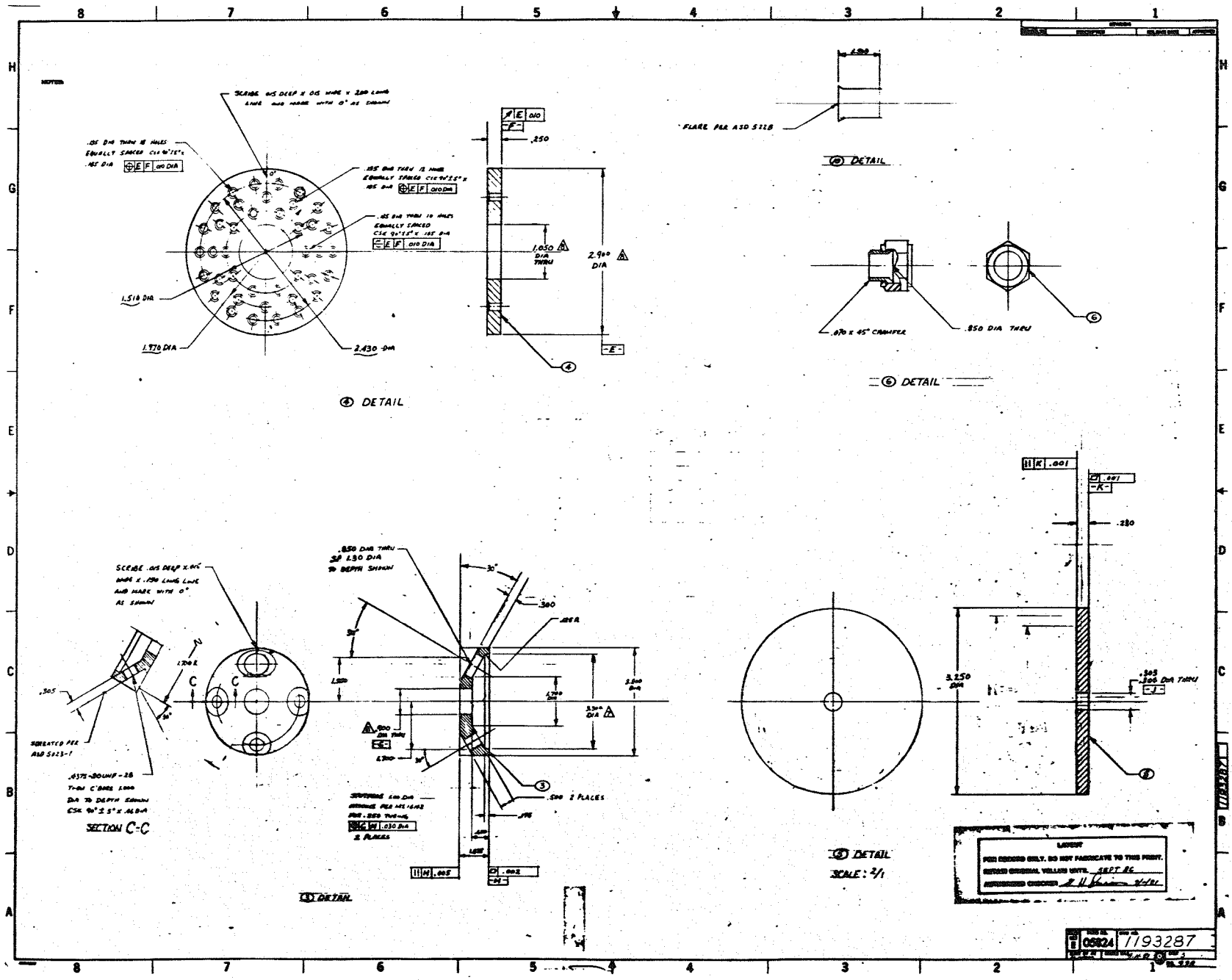

Figure 19. Injector Assembly Engineering Drawing (3 of 3)

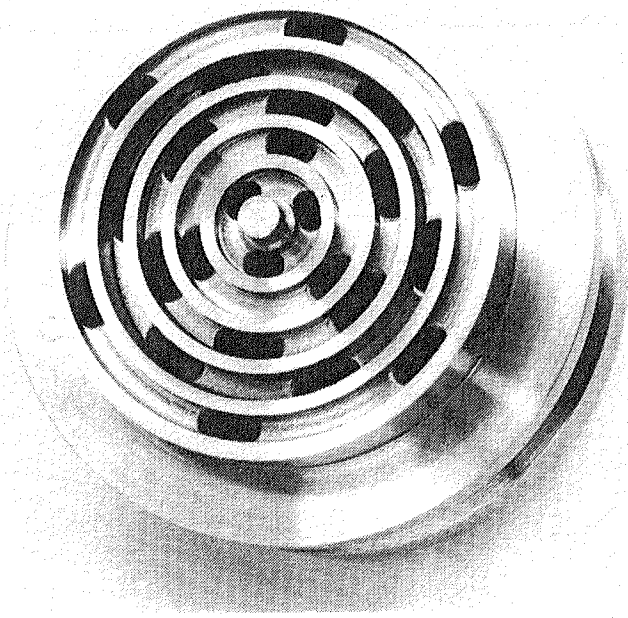

0581 SP 051

MANIFOLD

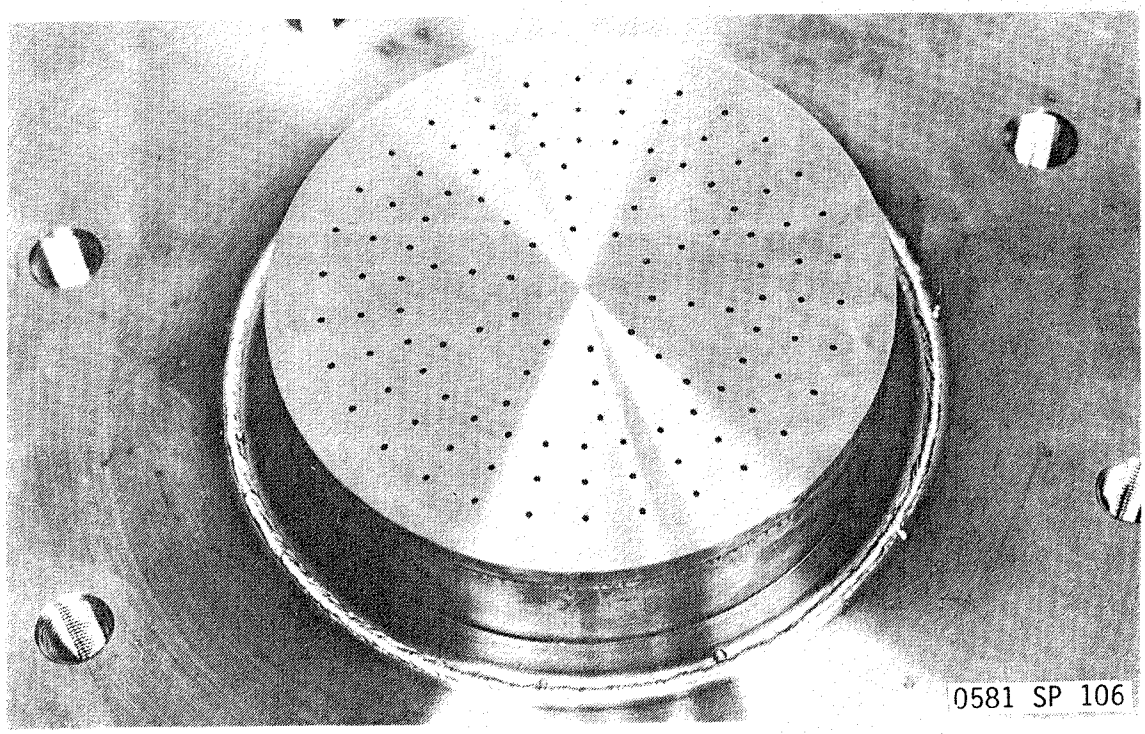

0581 SP 106

FACE

Figure 20. 40-Element OFO EDM-Triplet Injector

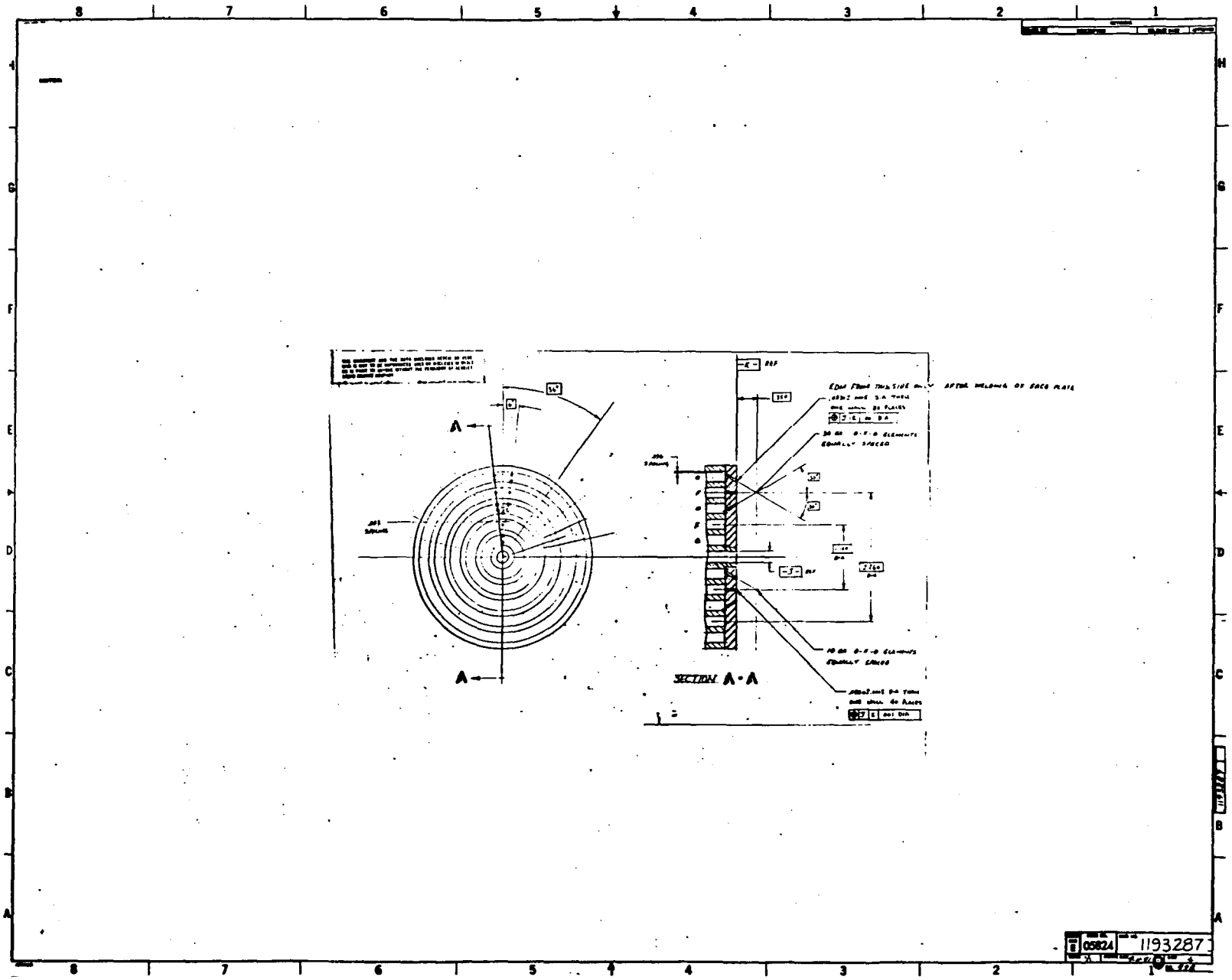

Figure 21. OFO Triplet Pattern Layout for 5-Ring Injector

E, Tasks II and IV Subscale Injector Characterization (cont.)

Impingement Half Angle	= 30°
Impingement Height	= 0.35 in.
Oxidizer Orifice L/D	= 7.0
Fuel Orifice L/D	= 6.1
Oxidizer Free Jet L/D	= 12.3
Fuel Free Jet L/D	= 10.6

The selection of the above injector design resulted from the analyses presented below.

1. Nominal Injector/Chamber Operating Condition

The following operating condition was assumed for both the injector hydraulic analysis and the combustion performance analysis:

Propellants	= LOX/Propane
Pc	= 300 psia
MR	= 3.0 (LOX/C_3H_8)
W_T	= 3.8 lbM/sec
T_O	= -297°F (ρ_O = 72 lbM/ft^3)
T_f	= 70°F (ρ_f = 31 lbM/ft^3)

A sketch of the combustion chamber internal geometry is provided in Figure 22.

2. Selection of Injector Orifice Size and Pressure Drop

Based on the Elverum-Morey triplet element correlation (Ref. 3), as discussed in Reference 4, the propane orifice pressure drop required for the operation at a nominal O/F of 3.0 is almost twice as large as the oxidizer injector pressure drop if the mixing efficiency is to be at its predicted optimum value. These large differences in pressure drops are not only undesirable from the viewpoint of the system pressure schedule, but also result in a severe fuel vaporization inefficiency. Moreover, the mismatch of oxidizer and fuel jet diameters will result in poor propellant mixing. As a result, a design having equal injector orifice size was selected. The derivation of the optimum mixing equations based on continuity, orifice pressure drop considerations, and the data from References 3 and 4 is shown on Figure 23 along with the plotted results. Both the anticipated element E_m (based on the cold-flow mixing data of Ref. 4) and the injector pressure drop ratio as a function of the propellant mixture ratio are shown in Figure 24. The values of E_m are above 0.8 over the expected operating mixture ratio range and the injector pressure drops of the oxidizer and fuel circuits become nearly equal at the nominal mixture ratio value of 3.0.

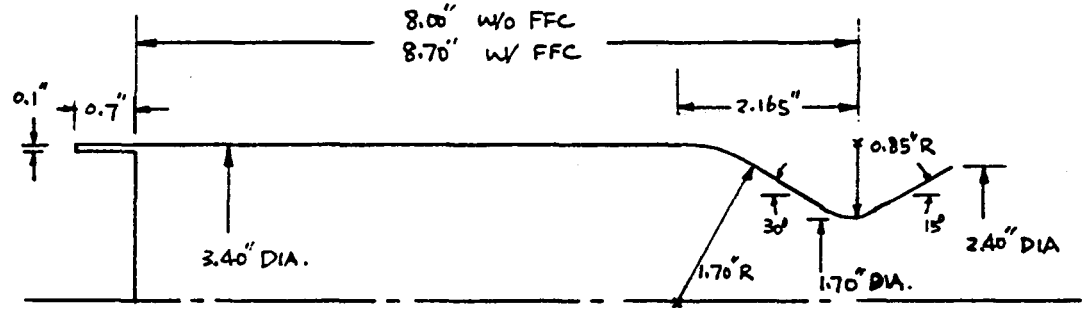

Figure 22. Mid-Pc Combustion Chamber Contour

A. Centerline Momentum Ratio

$$\mathscr{J} = 2 \frac{\rho_o}{\rho_f} \left(\frac{V_o}{V_f} \right)^2 \frac{d_o}{d_f}$$

B. Continuity - Mixture Ratio

$$MR = 2 \left(\frac{d_o}{d_f} \right)^2 \frac{V_o}{V_f} \frac{\rho_o}{\rho_f}$$

C. Orifice Hydraulics

$$V = (2 \Delta P/\rho)^{1/2}$$

D. Pressure Drop Ratio (A, B, C)

$$\frac{\Delta P_f}{\Delta P_o} = \left(\frac{MR}{\mathscr{J}} \right)^2 \frac{\rho_f}{\rho_o} \left(\frac{d_f}{d_o} \right)^2$$

E. Optimum Mixing (Refs. 4 & 5)

$$\mathscr{J}_{op} = 1.11 \left(\frac{d_o}{d_f} \right)^{1/2}$$

F. Pressure Drop Ratio at Optimum Mixing (D, E)

$$\frac{\Delta P_f}{\Delta P_o} = \left(\frac{MR}{1.11} \right)^2 \frac{\rho_f}{\rho_o} \left(\frac{d_f}{d_o} \right)^3$$

Figure 23. Injector Orifice Size and Pressure Drop Requirement for Optimum OFO Triplet Mixing (1 of 2)

G. Pressure Drop Ratio vs Hole Diameter Ratio at Optimum Mixing (A,C,E)

$$\frac{\Delta P_f}{\Delta P_o} = \frac{2}{1.11} \left(\frac{d_o}{d_f} \right)^{1/2}$$

H. Pressure Drop and Hole Diameter Ratio vs Mixture Ratio at Optimum Mixing (F, G)

$$\frac{\Delta P_f}{\Delta P_o} = 1.608 \left(\frac{\rho_f}{\rho_o} \right)^{1/7} MR^{2/7}$$

$$\frac{d_f}{d_o} = 1.253 \left(\frac{\rho_o}{\rho_f} \right)^{2/7} \Big/ MR^{4/7}$$

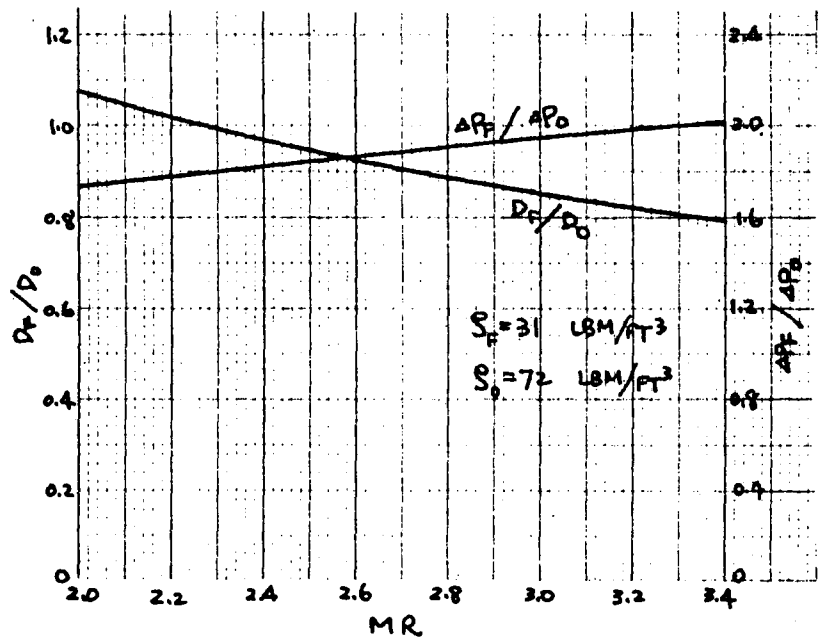

Figure 23. Injector Orifice Size and Pressure Drop Requirement for Optimum OFO Triplet Mixing (2 of 2)

A. Centerline Momentum Ratio

$$\phi = 2 \frac{\rho_o}{\rho_f} \left(\frac{V_o}{V_f}\right)^2 \frac{d_o}{d_f}$$

B. Continuity - Mixture Ratio

$$MR = 2 \left(\frac{d_o}{d_f}\right)^2 \frac{V_o}{V_f} \frac{\rho_o}{\rho_f}$$

C. Centerline Momentum Ratio vs Mixture Ratio and Hole Diameter Ratio (A,B)

$$\phi = 1/2 \frac{\rho_f}{\rho_o} MR^2 \left(\frac{d_f}{d_o}\right)^3$$

D. Orifice Hydraulics

$$V = (2 \Delta P/\rho)^{1/2}$$

E. Injector Pressure Drop Ratio (B, D)

$$\frac{\Delta P_f}{\Delta P_o} = 4 \frac{\rho_o}{\rho_f} \frac{1}{MR^2} \left(\frac{d_o}{d_f}\right)^4$$

F. E_m vs ϕ Relationship (Ref. 4)

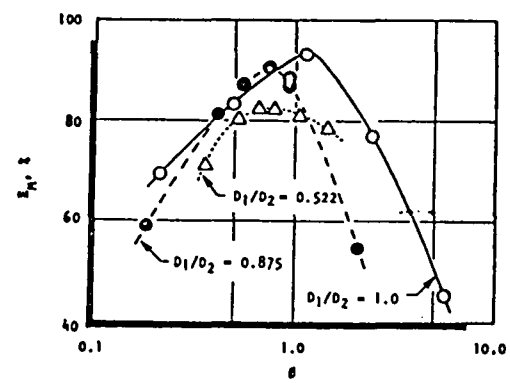

Figure 24. Analysis of Selection of Equal Injector Hole Size and Pressure Drop (1 of 2)

G. Maximum E_m vs d_o/d_f Relationship (Ref. 4)

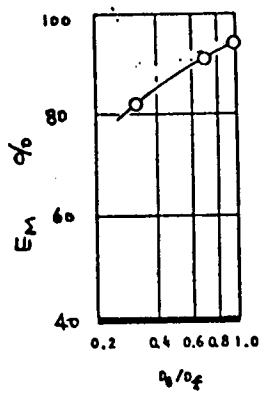

H. E_m and $\Delta P_o/\Delta P_f$ for Equal Hole Size

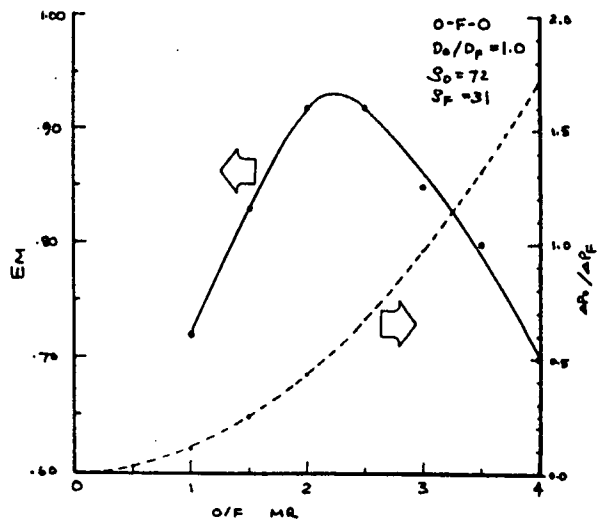

Figure 24. Analysis of Selection of Equal Injector Hole Size and Pressure Drop (2 of 2)

E, Tasks II and IV Subscale Injector Characterization (cont.)

3. Combustion Performance Prediction

The analysis of combustion performance for the LOX/C_3H_8 propellants consisted of two tasks; namely, characterization of droplet vaporization and vapor mixing. The vaporization analysis was made utilizing the Priem-Heidmann vaporization model. Using this model propellant vaporization was correlated to a generalized chamber length, L_{GEN}, which accounted for propellant properties, injector geometry, operating conditions, and chamber geometry. The mass median propellant drop size resulting from the injection process is a critical parameter in defining vaporization performance. The mixing effect on performance was accounted for by an analysis which assumes the entire reactive flow field is divided into two stream tubes. The two stream tubes have mixture ratios defined by the nominal vapor mixture ratio multiplied or divided by the E_m value. Figure 25 summarizes the performance calculation, including the predicted vaporization and C* efficiency, based on the E_m values shown on Figure 24. Propellant mass median drop sizes were calculated using three different approaches which resulted in three different predicted vaporization efficiencies. The first two approaches (Priem correlation and ALRC analytical model) have been used extensively at ALRC in the past with satisfactory results and good agreement with each other. However, in the present case, the latter predicts drop sizes about three times as large as the former does. For the EDM LOL injector, the drop sizes calculated using the ALRC analytical model were multipled by a factor of 1.4 in order to correlate with the hot-fire data. This modification (the third approach) yields drop sizes about four times as large as the Priem correlation. However, the unusually large apparent drop size implied by the poor vaporization efficiency in the EDM LOL injector is believed to be partially caused by poor mixing. Since the present triplet injector was expected to have better mixing efficiency, the apparent hot fire drop size was expected to be bounded by the Priem and ALRC correlations. The C* efficiencies predicted by these three different drop size approaches are all insensitive to the mixture ratio, and are approximately equal to 99.5%, 99% and 97%, respectively.

(4) Injector Cold Flow Data

The injector was cold-flow tested using water to determine its hydraulic characteristics under atmospheric conditions. Figure 26 documents the injector flow coefficient (Kw) and orifice C_D values at various injector pressure drops and also includes the photographs of the injector pattern check. The cold-flow C_D's are smaller than the assumed value of 0.8. This is because the high cold-flow injector pressure drops cause cavitation at the vena contracta. This subject will be further discussed in the following hot-fire data analysis.

		Oxidizer	Fuel
Propellant Properties			
Propellant		LO_2	C_3H_8
T	°F	-297	70
ρ	lbm/ft^3	72	31
μ	lbm/ft-sec	0.000135	0.00006
σ	lbf/ft	0.0009	0.00069
T_{cr}	°R	278	665
ΔH_v	Btu/lbm	91.6	183
MW		32	44
Chamber Geometry			
D_c	in	3.40	
CR		4.0	
D_t	in	1.70	
L_N	in	2.55	
θ_N	deg	30	
L'	in	8.0	
W_{cav}	in	0.1	
L_{cav}	in	0.7	
Nominal Operating Condition			
Pc	psia	300	
MR		3.0	
C^*_{del}, assumed 98% C^*_{ODE}		5765	
$\dot{W}_T$	lbm/sec	3.80	

Figure 25. LOX/Propane Performance Prediction of Injector #3 (1 of 3)

		Oxidizer	Fuel
Injector Element Configuration			
d	in	0.033	0.033
No. Holes		80	40
FFC	%	0	0
C_D		0.8	0.8
$\dot{W}$	lbm/sec	2.85	0.95
ΔP	psi	82	87
θ	deg	30	0
H_i	in	0.35	0.35
Atomization			
α	deg	35	28
λ_{atom}	in	0.34	0.42
r_m	in		
	Priem	0.349×10^{-3}	0.330×10^{-3}
	ALRC (Ito)	0.878×10^{-3}	0.962×10^{-3}
	Mod ALRC (x 1.4)	1.229×10^{-3}	1.347×10^{-3}
Vaporization & C* Efficiency			
Attached Figures			

Figure 25. LOX/Propane Performance Prediction of Injector #3 (2 of 3)

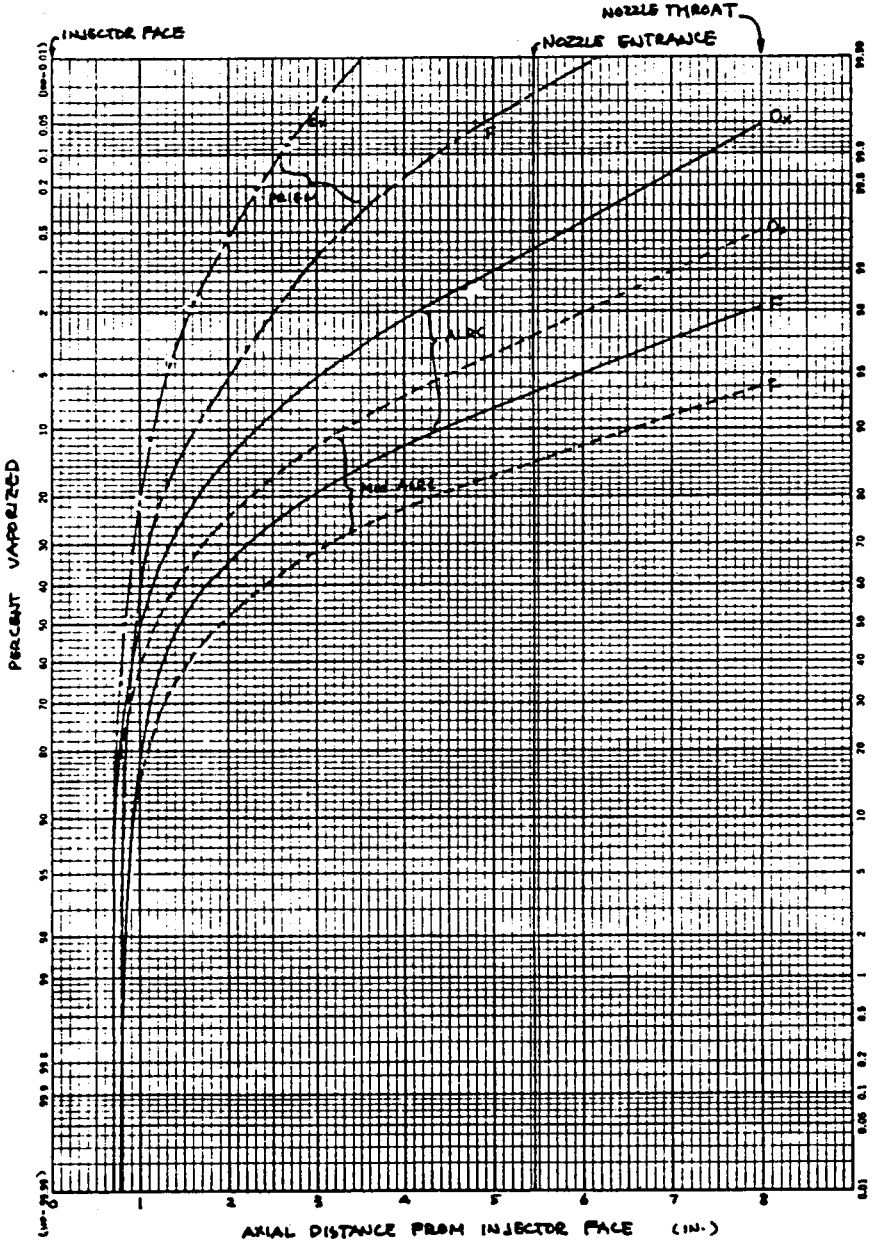

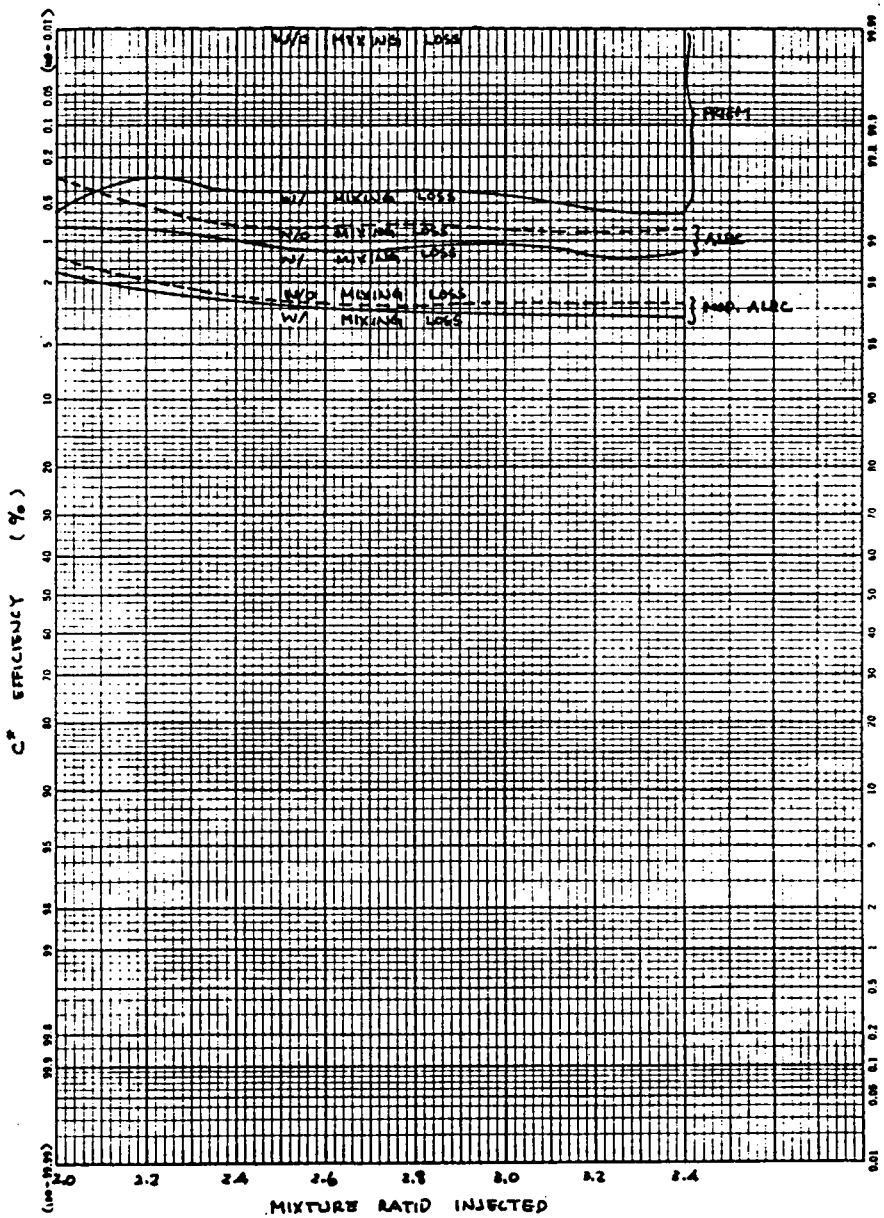

Figure 25. LOX/Propane Performance Prediction of Injector #3
(3 of 3)

ΔP (psi)	$\dot{W}_o$ (lbm/sec)	$\dot{W}_f$ (lbm/sec)	K_{wo} (lbm/sec-psi$^{1/2}$)	K_{wf} (lbm/sec-psi$^{1/2}$)	C_{D_o}	C_{D_f}
30	1.52	0.70	0.2775	0.1278	0.768	0.707
45	1.82	0.82	0.2713	0.1222	0.751	0.677
60	2.02	0.92	0.2608	0.1190	0.722	0.657
80	2.20	1.07	0.2627	0.1196	0.727	0.662
100	2.45	1.22	0.2450	0.1220	0.678	0.675

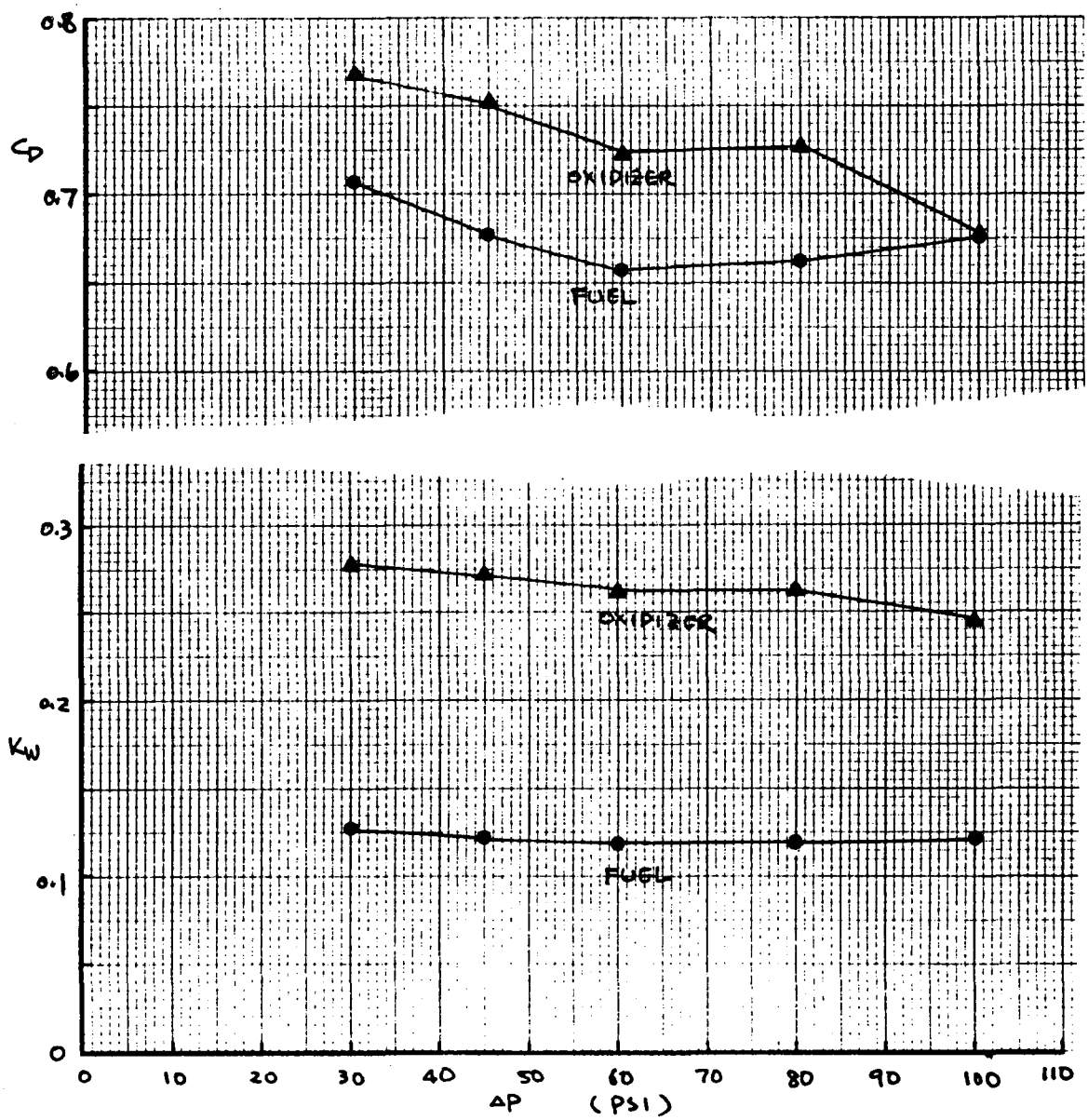

Figure 26. Water Cold-Flow Data of Injector #3 (1 of 2)

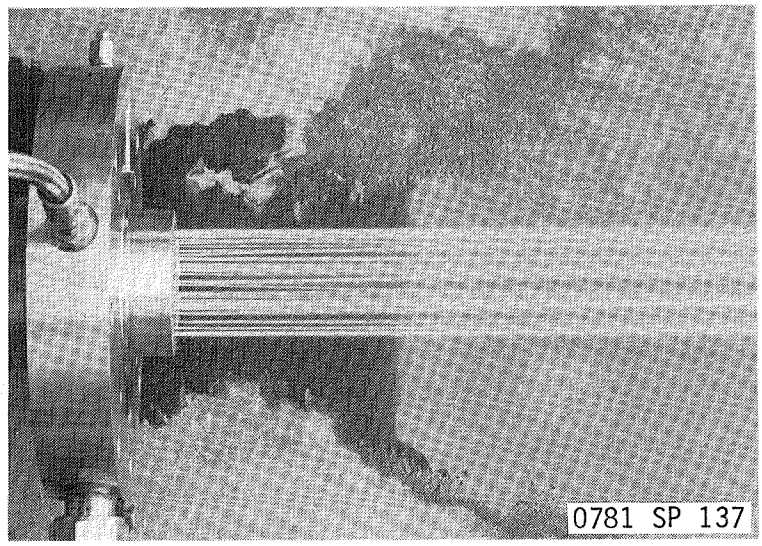

FUEL ONLY

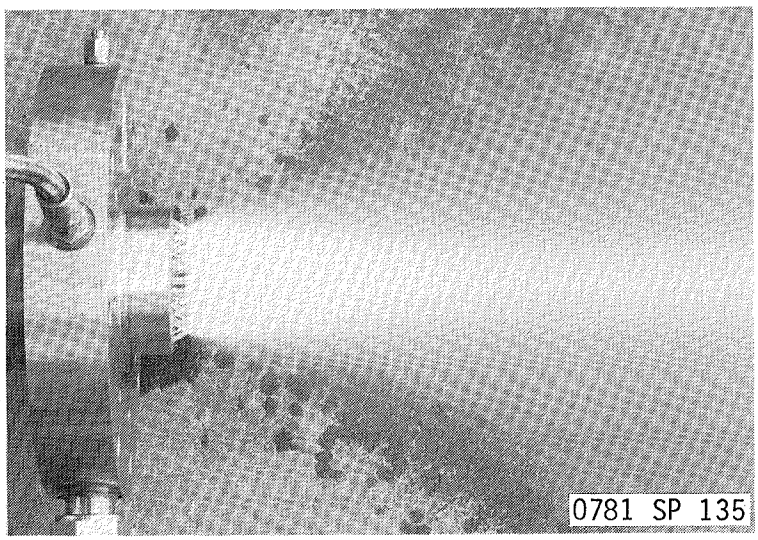

OXIDIZER ONLY

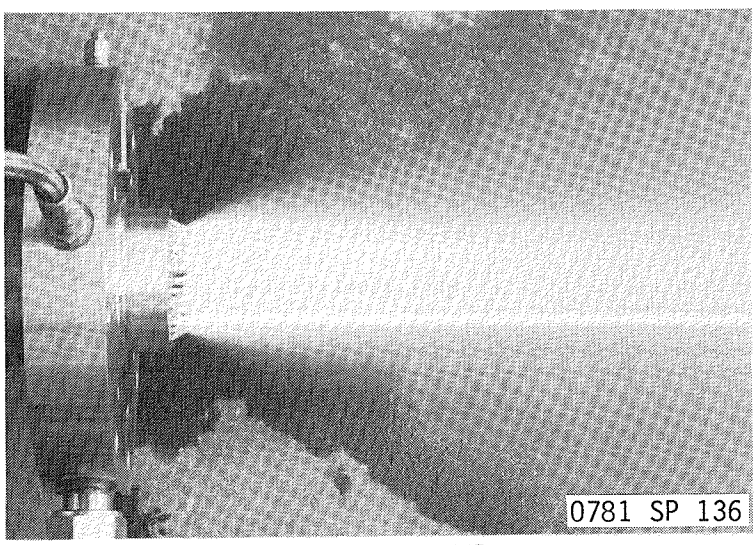

FUEL & OXIDIZER

Figure 26. Water Cold-Flow Data of Injector #3 (2 of 2)

E, Tasks II and IV Subscale Injector Characterization (cont.)

(5) Checkout and Hot Fire Test Events

The initial series of tests involved igniter cold flow, igniter hot-fire checkout, main valve response times, injector cold-flow fill time evaluation, and valve sequence and ignition characterization. These were followed by a series of eleven hot-fire tests in which MR, Pc, bomb size, and resonator cavity blocks were systematically varied. The range of test conditions is summarized below.

	Min.	Max.
MR	2	4
Pc (psia)	200	400
Cavity Depth (in.)	0	0.7
Bomb Size (gr)	2	6.5

The resonator cavity depth was changed from 0.7 in. to 0.0 in. after Test 128. A detailed description of the individual tests and their results follows. The test conditions and results are summarized in Tables VI and VII.

Test 001 was an igniter cold-flow test to determine the igniter chamber pressure under a no-light condition. Both igniter valves open together; however, the fuel valve closing was delayed by 0.03 sec to prevent an oxidizer-rich shutdown. In addition, a small GN_2 purge flow was introduced through a 0.03-in. diameter orifice in the oxidizer circuit when the oxidizer valve closed. This was to prevent backflow of the hot main chamber combustion gases into the igniter cavity in the event of an instability. The peak propellant cold-flow pressure recorded was 120 psia. The cold-flow pressure of the GN_2 following valve closure was 60 psia. The purge flow was reduced on subsequent tests.

Test 002 was a repeat cold-flow test to check out the non-ignition shutdown logic.

Test 003 was a 0.3-sec duration igniter hot test at MR = 1.5. The hot-fire igniter pressure was 187 psia.

Tests 004 and 005 were fuel valve functional and manifold fill-rate tests. The fuel and oxidizer manifold purges were set to check valve off at 200 psia. The rapid manifold fill resulted in the overpressure shown in Figure 27. This condition was considered acceptable.

Tests 006 and 007 were oxidizer valve response and manifold fill tests. A similar manifold overpressure on fill was noted on Poj, as shown in Figure 27. The desired 0.010-sec oxidizer lead was verified by the results of Tests 004 through 007.

TABLE VI

OFO TRIPLET INJECTOR (INJECTOR #3) STABILITY DATA SUMMARY OF
TEST SERIES #II - HEAT SINK CHAMBER, NO FFC, LOX/PROPANE

								Spontaneous Effects				Bomb Effects							
Test No.	Date	Duration sec	Resonator (in.)	T_{oj} (°F)	T_{fj} (°F)	Pc-1 (psia)	MR	Max Amp. S.S. (psi p-p)	Freq. (Hz)	Dur. (ms)	Status	Size (Grain)	Poj Spike/Amp (psi)	Chamber Over Pressure (psi)	Amp at CPIA Time (psi p-p)	Freq. (Hz)	Recovery Time (ms)	Status	Mode
122	8/26/81	0.5	12 @ 0.7	-273*	83	299	2.108	24	Random	17	Stable	None	-	-	Normal	-	-	-	
123	"	0.75	↓	-280*	82	304	2.563	24	"	14	Stable	None	-	-	"	-	-	-	
124	8/27/81	0.75	↓	-232	78	305	2.909	10	"	560	Stable	2.5	58	100	"	-	5	Stable	
125	"	↓	↓	-202	84	201	3.013	9	"	25	Stable	2.5	56	93	"	-	9	Stable	
126	"	↓	↓	-239	83	406	3.123	17	"	540	Stable	6.5	81	90	"	-	8	Stable	
127	"	1.2	↓	-256	84	305	3.133	10	"	1010	Stable	None	-	-	"	-	-	-	
128	"	0.75	↓	-234	84	302	4.089	11	20,580	550	Stable	6.5	81	211	"	-	-	Stable	
129	8/28/81	0.5	None	-287*	91	308	2.768	10	Random	260	Stable	"	72	213	270	7,981	≈150	Unstable	1-T
130	"	↓	↓	-296*	95			-	Random	-	Stable	None	-	-	-	-	-	-	-
131	"	↓	↓	-294*	91	199	3.821	-	590	26	Stable	6.5	73	112	13	572	80	Stable	Chug
132	"	↓	↓	-299*	91	200	2.307	-	Random	-	Stable	"	66	109	4	494	40	Stable	Chug

Chamber L' = 8" *T_{oj} Based on TOFM SS = Steady State CPIA Amp. = at Time = $\frac{1250}{\sqrt{Freq}}$ (ms)

TABLE VII

OFO TRIPLET PERFORMANCE DATA SUMMARY

Test No.	Date	T_{oj} (°F)	T_{fj} (°F)	Pc-1 (psia)	MR	Test Dur. (sec)	$\dot{w}_o$	$\dot{w}_f$	P_{N_2} (psia)	C^*_{Pc-1}	C*corr	C*ODE	% C*	P_{oj}	P_{fj}	FA (Vac)	Isp (Vac)	ΔP_{oj} (psi)	ΔP_{fj} (psi)	η_{Isp} %	η_{ER} Based on η_{Isp} %
122	8/26/81	-273	83	299	2.108	0.49	2.531	1.201	800	5824.2	5743	5955	96.44	393	435	945	253.32	94	136	93.79	97.68
123	"	-280	82	304	2.563	0.79	2.767	1.079	"	5744.6	5664	5985	94.64	410	415	962	249.9	106	111	91.76	95.45
124	8/27/81	-232	78	305	2.909	0.79	2.837	0.975	500	5823.6	5742	5900	97.32	419	396	967	253.4	114	91	94.45	98.14
125	"	-202	84	201	3.013	0.80	1.922	0.638	350	5711.5	5632	5844	96.37	250	241	636	248.5	49	40	93.32	97.11
126	"	-239	83	406	3.123	0.79	3.789	1.213	550	5905.1	5822	5840	99.69	613	544	1279	255.1	207	138	95.65	99.29
127	"	-256	84	305	3.133	1.25	2.910	0.929	500	5771.7	5691	5838	97.48	419	387	966	250.9	114	82	94.39	98.02
128	"	-234	84	302	4.089	0.80	3.204	0.784	"	5506.9	5430	5521	98.35	448	360	956	239.4	146	58	94.62	98.19
129	8/28/81	-287 *	91	308	2.768	0.49	2.823	1.020	800	5819	5738	5940	96.60	417	405	973	253.13	109	97	93.58	97.29
130	"	-296 *	95	NO DATA																	
131	"	-294 *	91	199	3.821	0.50	2.140	0.560	"	5639	5294	5581	94.86	259	228	631	233.6	60	29	91.55	95.19
132	"	-299 *	91	200	2.307	0.52	1.813	0.786	"	5582	5504	5987	91.93	240	263	629	242.11	40	63	89.09	92.90

*Oxidizer temperature in manifold assumed equal to temp at ox flow meter

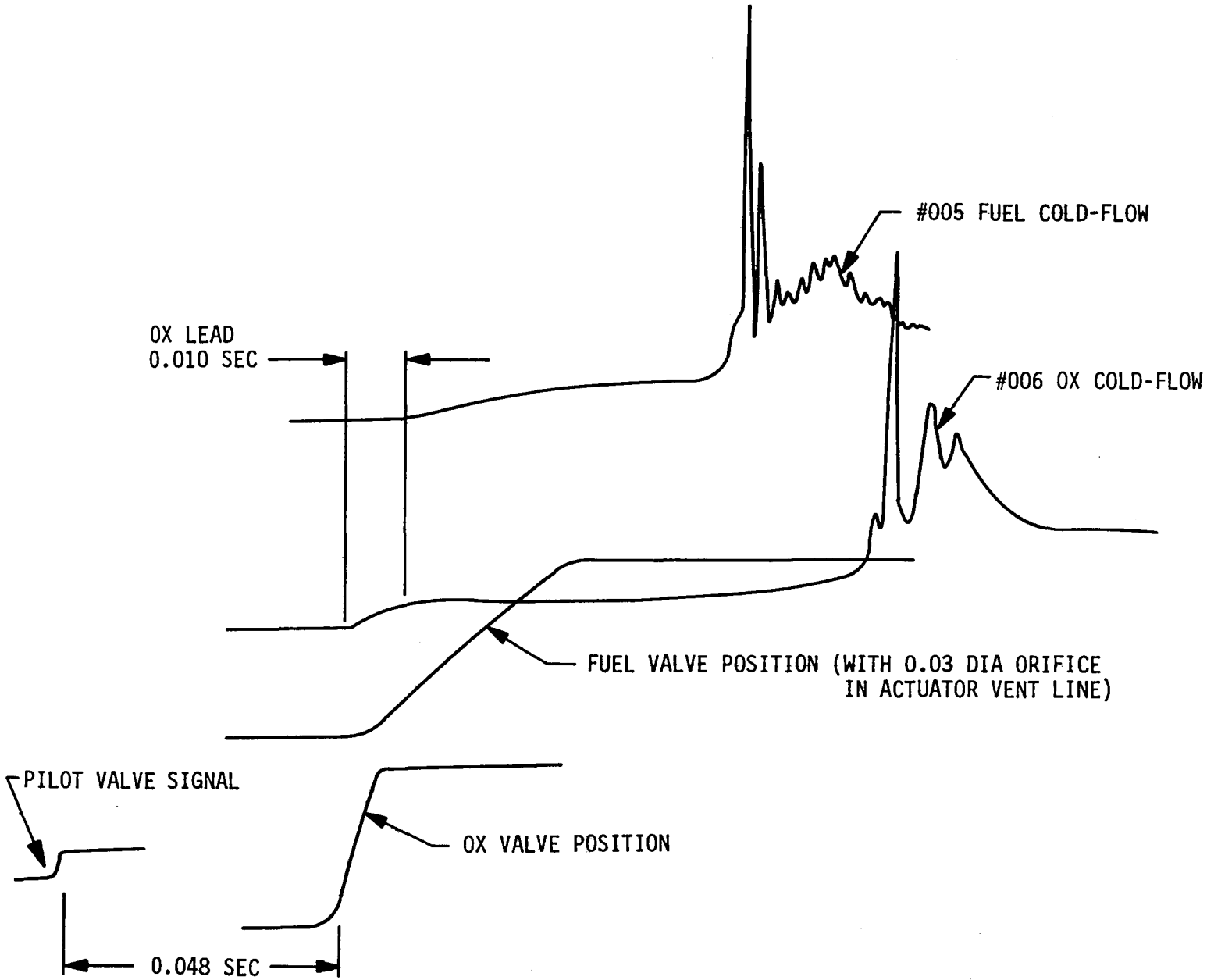

Figure 27. Propellant Fill and Line Dynamics Evaluation

E, Tasks II and IV Subscale Injector Characterization (cont.)

Test 119 was the first scheduled hot-fire test. This test, as well as Tests 120 and 121, were terminated by a low igniter chamber pressure kill. The main valves did not receive a signal to open even though the igniter had performed satisfactorily on each test. The problem was due to filtration of the electrical signal which delayed the pressure (PojI) rise rate seen by the computer. Following the correction of the kill logic, successful chamber ignition was attained on all eleven hot-fire tests.

Test 122 was the first hot-fire test to verify the start and shutdown sequence and balance the engine for proper MR and Pc. The test MR, duration, and pressure are defined in Table VI. The nominal operating point for this design is MR = 3.0, Pc = 300 psia. A Pc of 299 psia and a MR of 2.1 was attained in the first 0.5-sec test. No stability problems were noted; however, the increased magnitude and nature of the manifold water hammer indicated by Poj (the oxidizer manifold pressure) were of some concern. Review of the high frequency pressure measurements including Koj (the Kistler transducers) in the oxidizer manifold indicated no evidence of overpressures. It was concluded that the overpressure was confined to the oxidizer line/transducer diaphragm flow dynamics and was not a significant event for this test series. Figure 28 shows the full engine start transient.

On Test 123, the duration was increased to 0.75 sec from 0.5 sec in the previous test, and the set pressures were adjusted to increase mixture ratio. The actual MR was 2.5, and the Pc was 304. No instabilities or heat marks were observed.

On Test 124, a 2-gr bomb was installed and set to go off shortly before the end of the 0.75-sec test. Approximately 0.1 sec of data was attained after the bomb. The engine recovered rapidly from the bomb overpressure at MR = 2.9 and Pc = 305 psia.

Test 125 was a low pressure test with a 2-gr bomb. The injector manifold purge pressures were reduced to 100 psia, and the igniter purge supply pressure was reduced to 350 psia, compared to 500 psia used in previous tests. Recovery of the engine from the bomb was rapid (CPIA stable) at a MR of 3.0 and Pc of 201 psia.

Test 126 was a high-pressure test with a 6.5-gr bomb. The engine recovered rapidly from the larger bomb at a MR of 3.1 and Pc of 406 psia.

Test 127 was a repeat of Test 124 for a longer duration (1.20 sec) without a bomb. The objective was to determine if the relatively large bomb cross section in the chamber altered the mixing rates and thus influenced the performance. The C* efficiency on these two tests was 98.6 and 98.7%, respectively; i.e., the bomb had no measurable influence on performance.

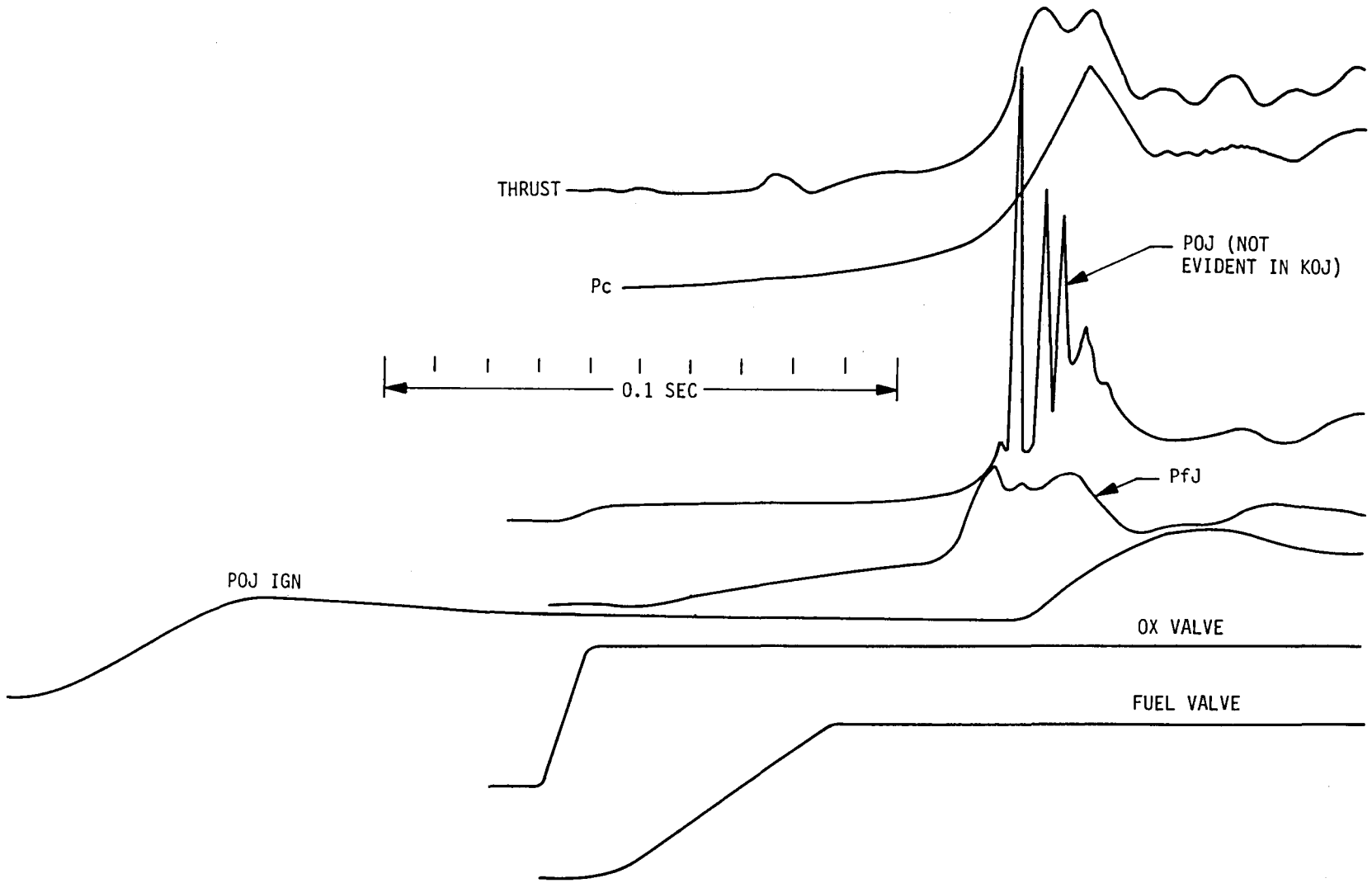

Figure 28. Start Transient, Test 122

Test 126 was a high-pressure test with a 6.5-gr bomb. The engine recovered rapidly from the larger bomb at a MR of 3.1 and Pc of 406 psia.

Test 127 was a repeat of Test 124 for a longer duration (1.20 sec) without a bomb. The objective was to determine if the relatively large bomb cross section in the chamber altered the mixing rates and thus influenced the performance. The C* efficiency on these two tests was 98.6 and 98.7%, respectively; i.e., the bomb had no measurable influence on performance.

Test 128 returned the duration to 0.75 sec and utilized a 6.5-gr bomb at high mixture ratio. The engine recovered rapidly from the bomb at a MR of 4.08 and a Pc of 302 psia.

For Tests 129 through 132, resonator cavities were filled with copper blocks prior to testing to determine if cavities were required for stable operation. The engine was stable at a MR of 2.73 and 308 psia until the bomb went off near the end of the test. The 6.5-gr bomb set off a 1-T instability mode, and the engine did not recover, thus demonstrating the need for the cavities.

Test 130 was a low Pc, low MR test with a 6.5-gr bomb. The test was terminated early in the burn due to a low Pc cutoff kill which was similar to that of Tests 119, 120, and 121. This test condition was repeated later.

Test 131 was a high MR, low Pc condition using the same bomb as used in Test 130. The engine was stable prior to the bomb but appeared to develop a low amplitude chug mode following the bomb. Actual test conditions were MR = 3.8 and Pc = 199 psia.

E, Tasks II and IV Subscale Injector Characterization (cont.)

Test 128 returned the duration to 0.75 sec and utilized a 6.5-gr bomb at high mixture ratio. The engine recovered rapidly from the bomb at a MR of 4.08 and a Pc of 302 psia.

For Tests 129 through 132, resonator cavities were filled with copper blocks prior to testing to determine if cavities were required for stable operation. The engine was stable at a MR of 2.73 and 308 psia until the bomb went off near the end of the test. The 6.5-gr bomb set off a 1-T instability mode, and the engine did not recover, thus demonstrating the need for the cavities.

Test 130 was a low Pc, low MR test with a 6.5-gr bomb. The test was terminated early in the burn due to a low Pc cutoff kill which was similar to that of Tests 119, 120, and 121. This test condition was repeated later.

Test 131 was a high MR, low Pc condition using the same bomb as used in Test 130. The engine was stable prior to the bomb but appeared to develop a low amplitude chug mode following the bomb. Actual test conditions were MR = 3.8 and Pc = 199 psia.

Test 132 was a repeat of Test 130 conditions, with the results being similar to those of Test 131. The actual MR and Pc were 2.3 and 200 psia, respectively. The condition of the injector face following Test 132 is shown in Figure 29.

Analysis of the data (Figure 30) shows significantly improved combustion efficiencies (approximately 97%) as compared to 93% for the LOL element. Detailed analyses are provided in Section 5.

Figure 31 provides a comparison of the chamber wall heating rates for the OFO element versus the LOL pattern tested earlier. The OFO element heating rates are considerably faster, indicating a higher heat flux on the same thermocouples under similar operating conditions.

c. Test Series III - LOX/Propane OFO-EDM Orifice Triplet Injector, 8-Inch L' Water-Cooled Calorimeter Chamber

(1) Objective

The objective of this series was to obtain detailed thermal data for the design of regeneratively-cooled chambers including the effect of gas-side sooting on the heat flux as a function of chamber pressure and mixture ratio. Injector durability would also be assessed in tests of longer duration.

(2) Facility Modification

The facility was modified to provide cooling water for the calorimeter chamber as shown in the flow schematic of Figure 32 and the photograph of Figure 33. No changes to the igniter, injector, or propellant and valve sequences were made.

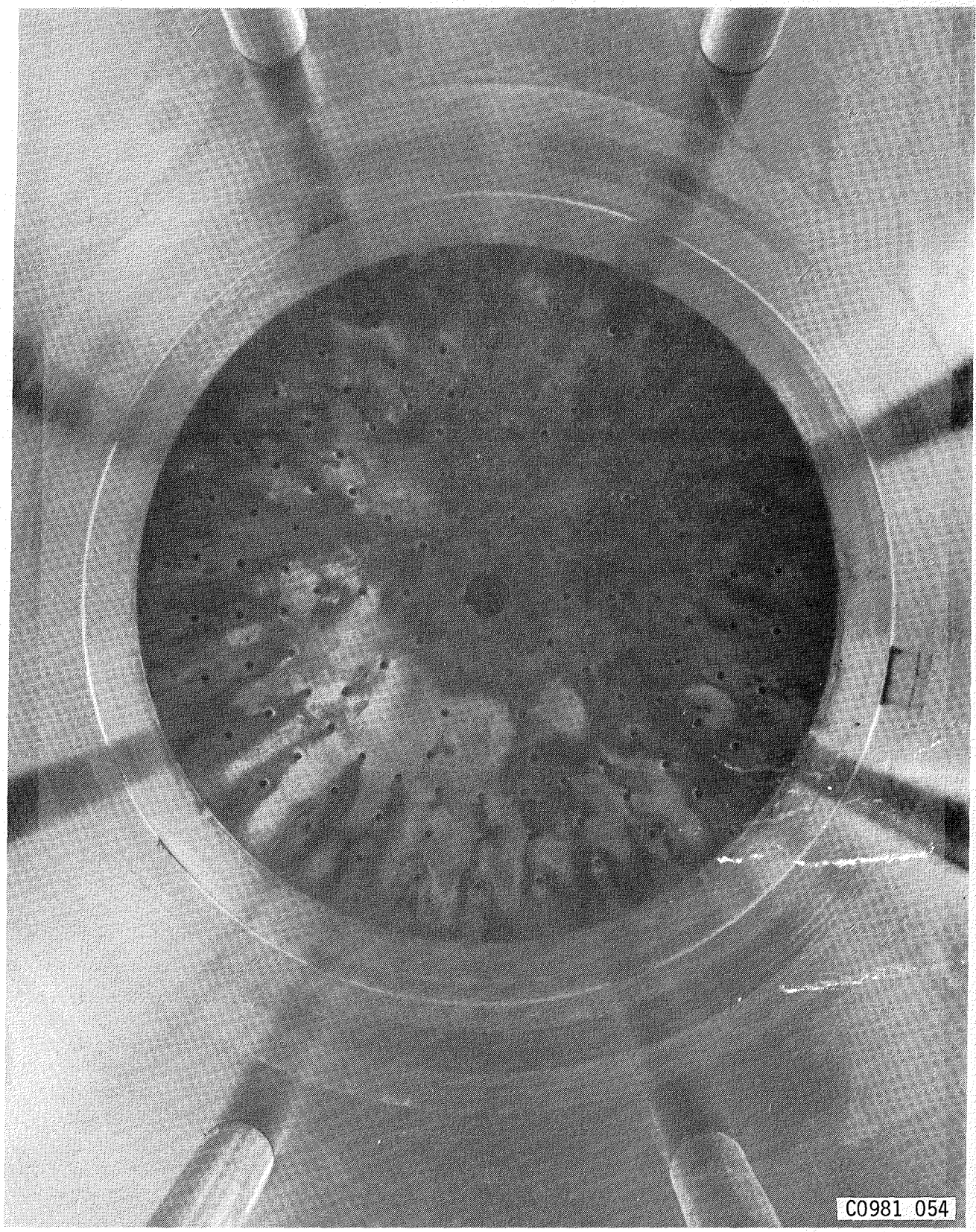

Figure 29. OFO Triplet After Testing in Heat Sink Chamber Test 132

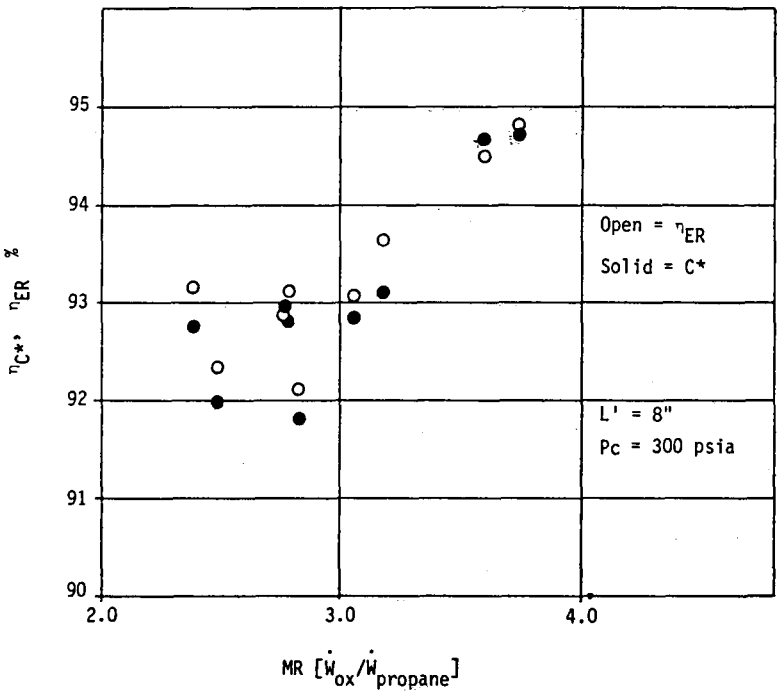

C* and Energy Release Efficiency for LOL Pattern

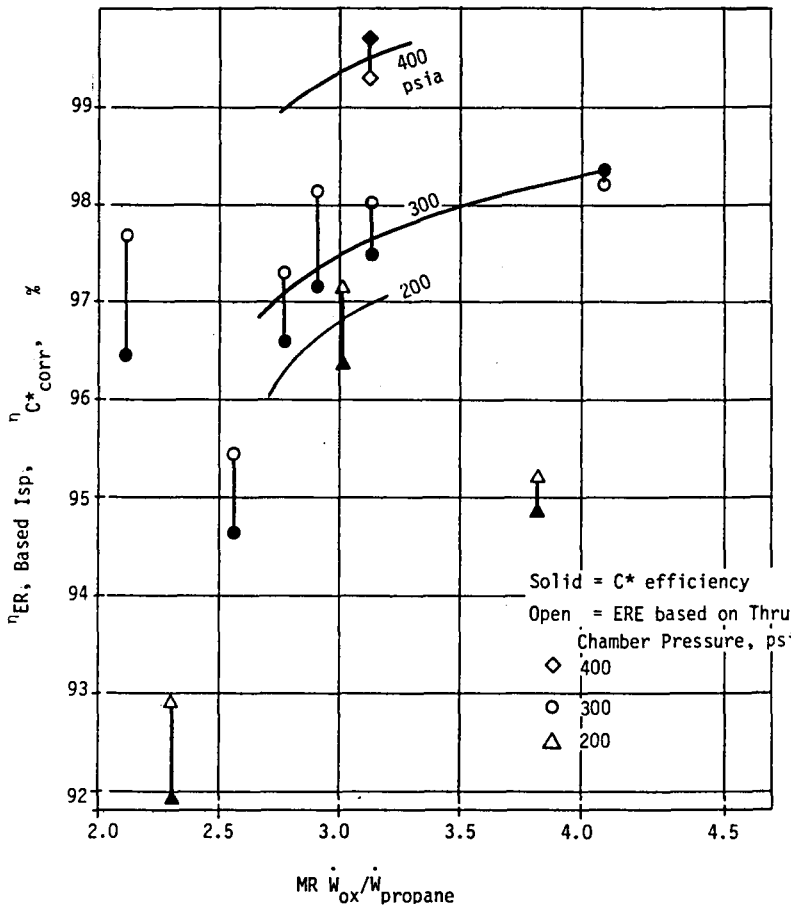

C* and Energy Release Efficiency for OFO Triplet in 8-inch L' Chamber

Figure 30. Comparison of Efficiencies of LOL Doublet and Unlike OFO Triplet Injectors for LOX/Propane Propellants, Chamber L' = 8"

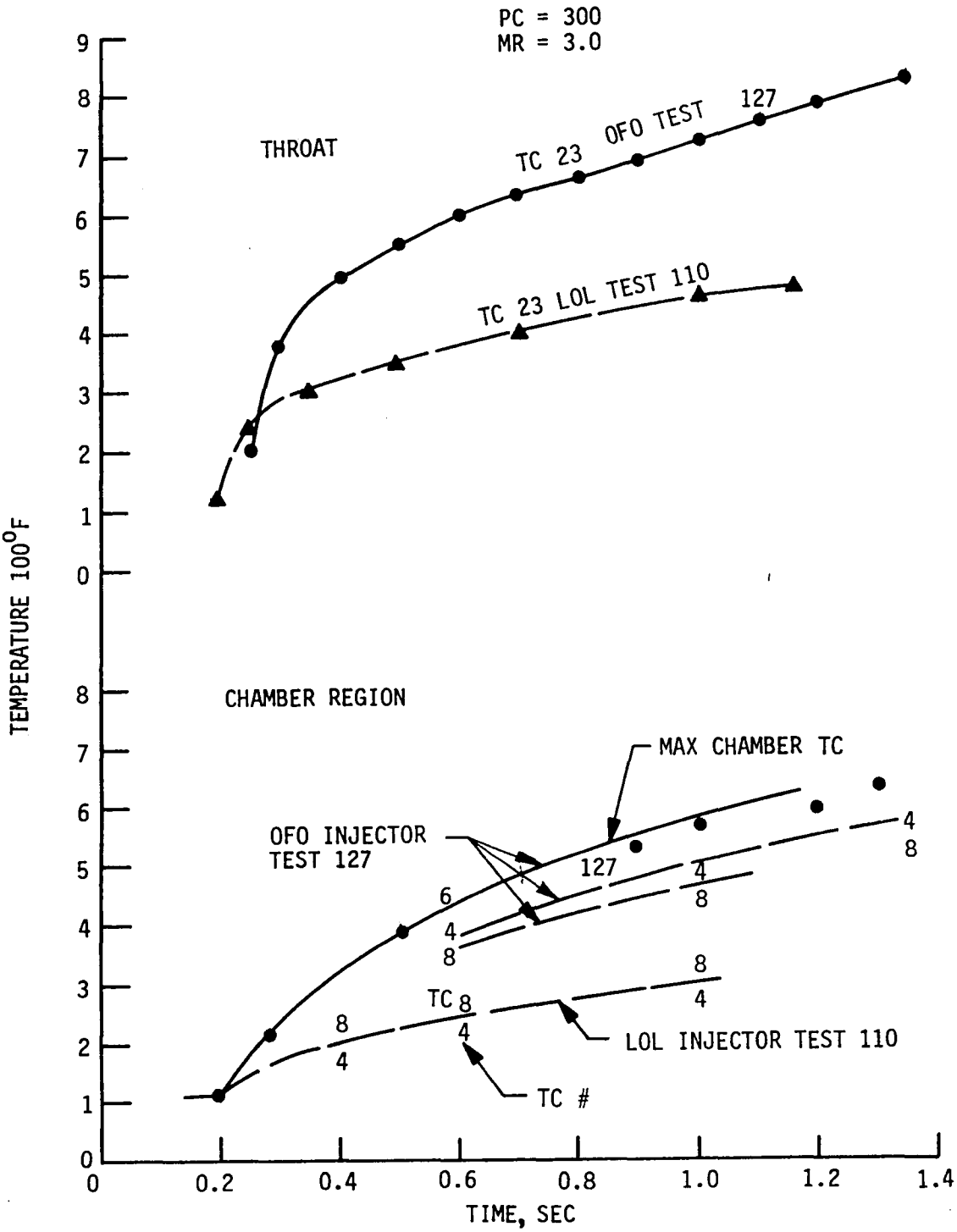

Figure 31. Comparison of Chamber Wall Heating Rates, OFO Versus LOL Injector

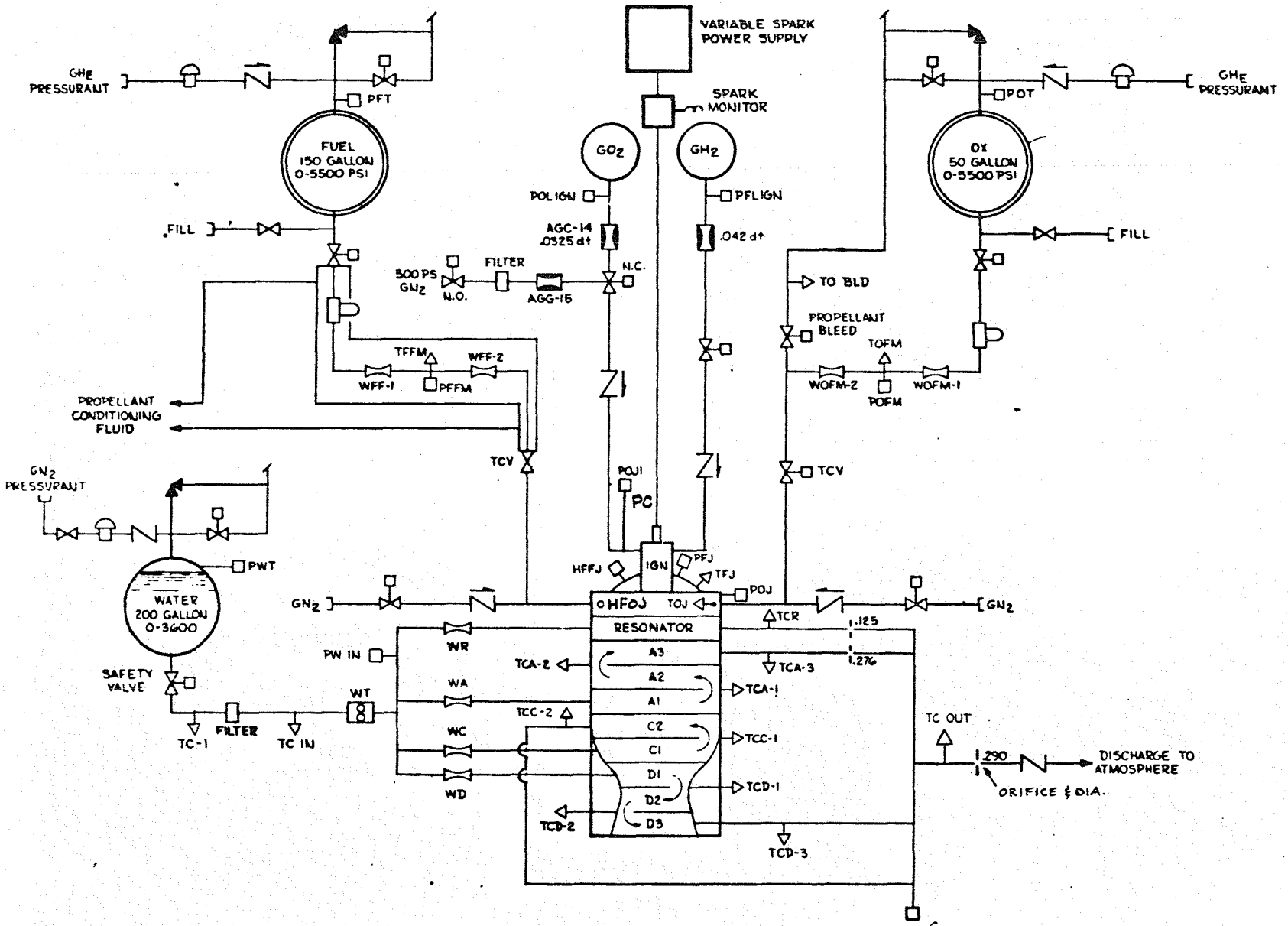

Figure 32. Bay 6 Test Facility Flow and Instrumentation Schematic

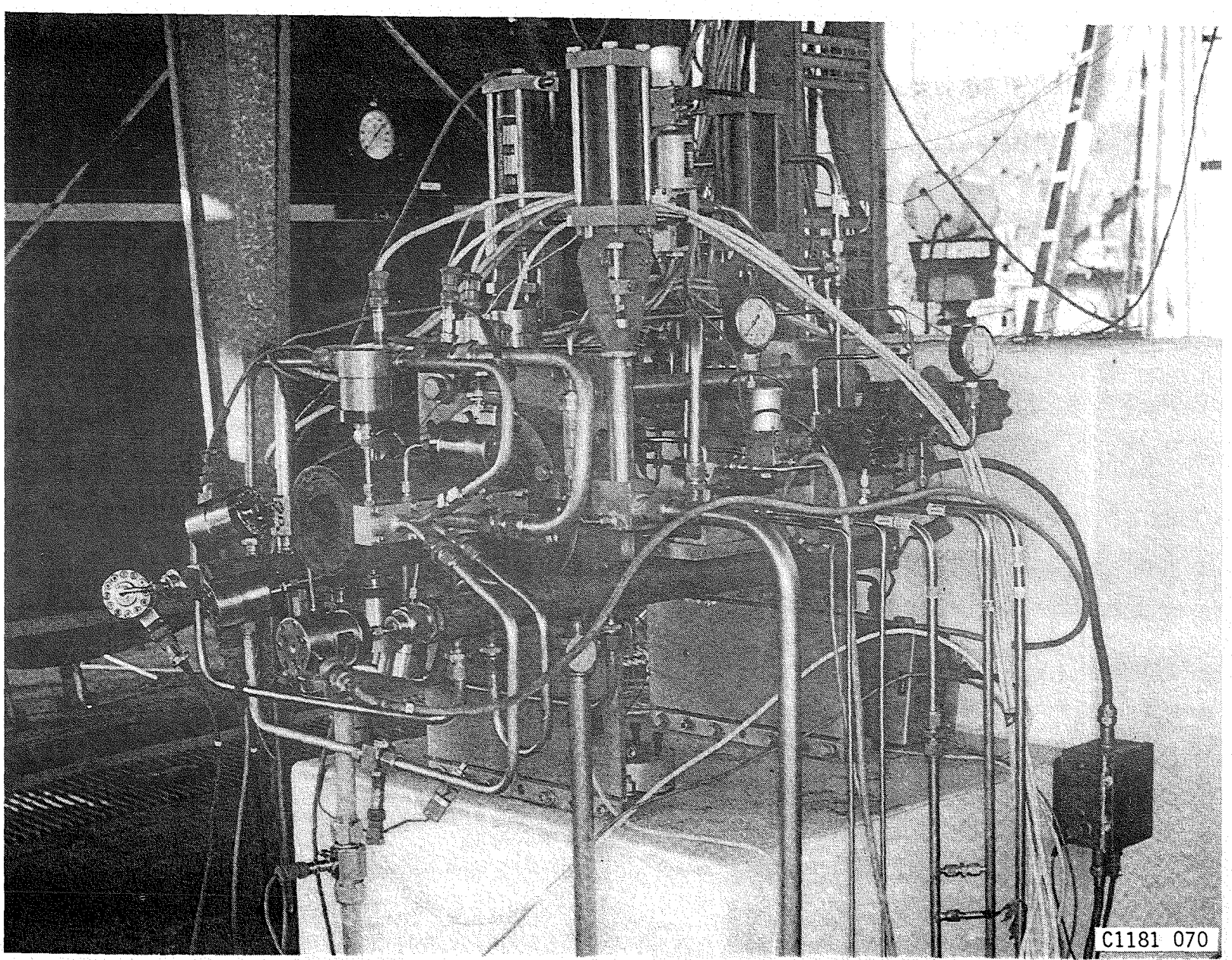

Figure 33. Bay 6 Test Facility with Water-Cooled Chamber In Place

E, Tasks II and IV Subscale Injector Characterization (cont.)

(3) Hardware, Instrumentation, and Measurements

Detailed drawings of the calorimeter chamber are provided in Figure 34. A photograph of the copper liner prior to braze assembly is provided in Figure 35. The final chamber assembly is shown in Figure 36 and also on the test stand in Figure 33.

As can be noted in Figure 32, the chamber is divided into nine hydraulically separated compartments. Four separately metered water lines are employed to supply the nine compartments. The heat flux for each compartment is determined by the measured water flowrate and the water temperature rise. The measured flow to each of four sections (resonators, A, C, and D) is cross-checked by comparing the sum of the individual flows with an independent total water flow measurement. In order to avoid water temperature measurement errors resulting from comparing two different thermocouples, and to account for possible changes in water inlet temperature with time during the test, the computational procedures listed in Figure 37 were employed. This procedure compares the prefire (water flowing) measurement with the firing value and corrects for changes in supply temperatures by using the average of two thermocouples located in the supply line. Chamber pressure is measured through the injector face using the igniter port and igniter oxidizer manifold pressure transducer. There is no propellant flow or purge flow through the igniter port at the time the measurements for C* calculations are made.

(4) Cold-Flow Tests

The following cold-flow tests were conducted prior to the hot-fire testing:

(1) Proof- and leak-test at 1200 psi
(2) Water-flow without orifices
(3) Water-flow after installing flow balancing and back-pressure orifices
(4) Sequence checkout to verify no-flow, no-ignition kills
(5) 60-sec water flow test to verify capability of water supply to maintain pressure and flowrate

No additional injector cold-flow tests were conducted.

(5) Hot-Fire Tests

Eleven LOX/propane hot-fire tests with the OFO triplet injector were conducted in this series.

Test No. 133 was a 3 second checkout test at nominal conditions (MR = 3; Pc = 300 psia).

Test 134 was a repeat of Test 133 for a duration of 40 seconds. The chamber total heat load peaked at 2 to 5 seconds and then continued to drop with time until the end of the test.

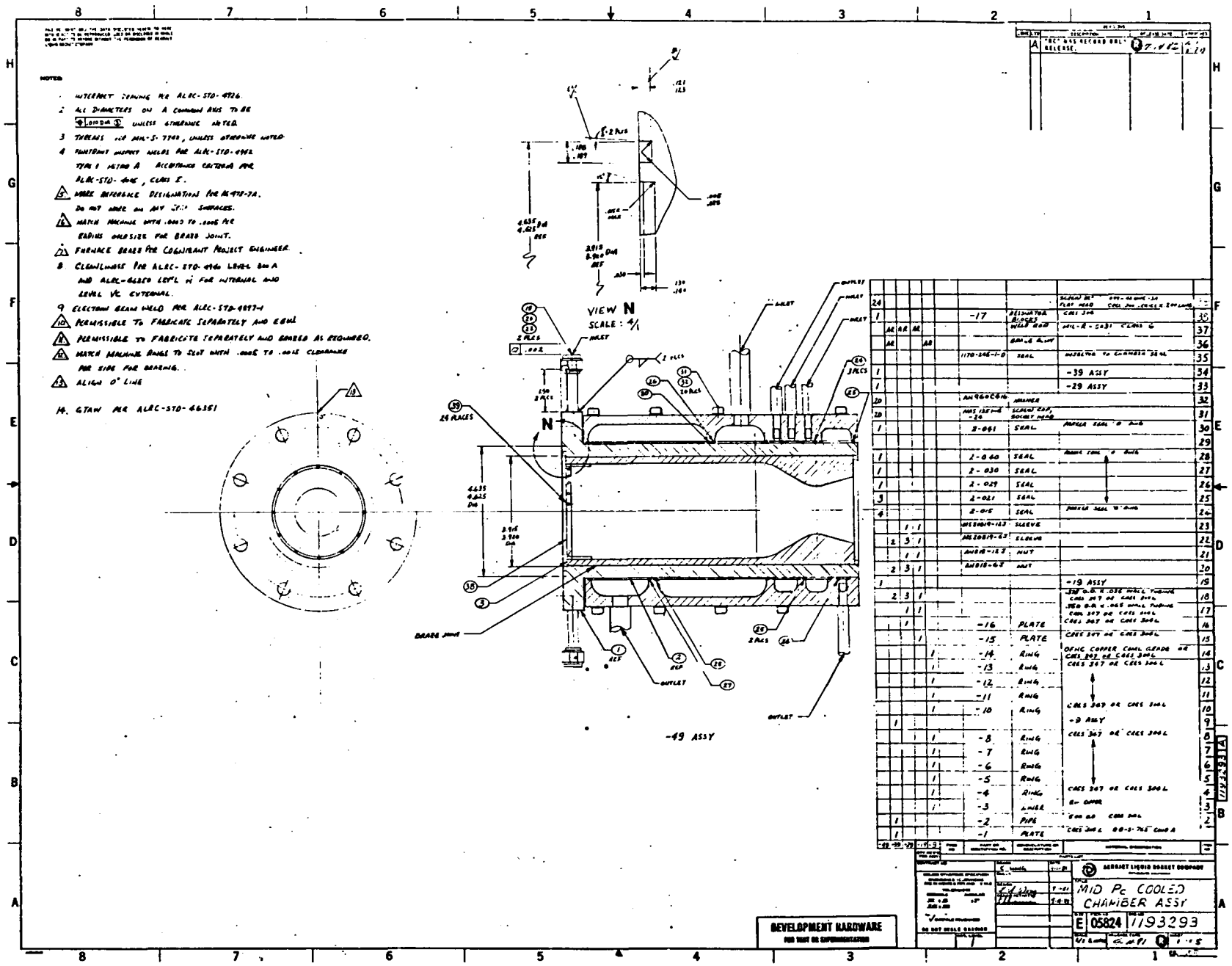

Figure 34. Cooled Chamber Assembly Engineering Drawing (1 of 5)

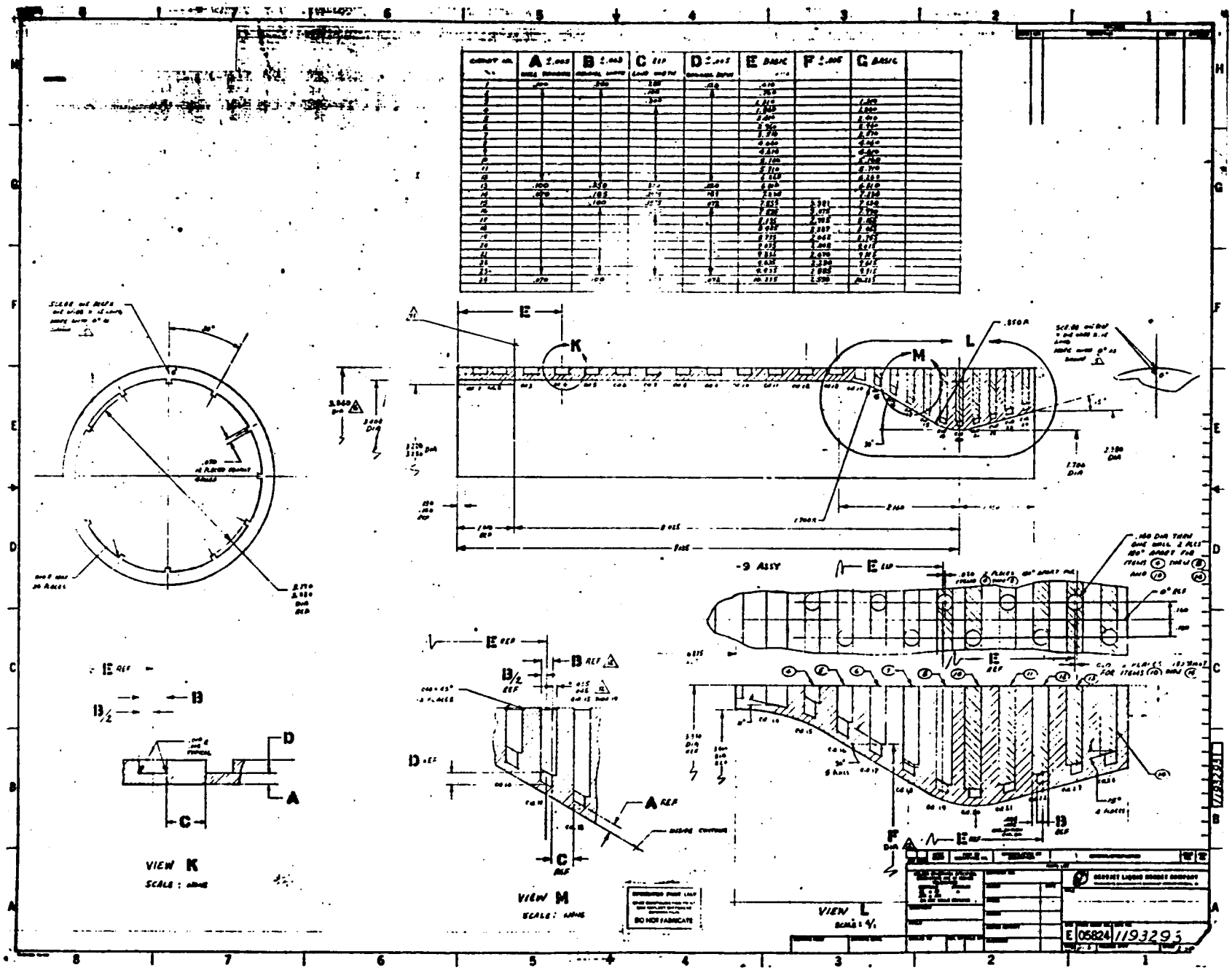

Figure 34. Cooled Chamber Assembly Engineering Drawing (2 of 5)

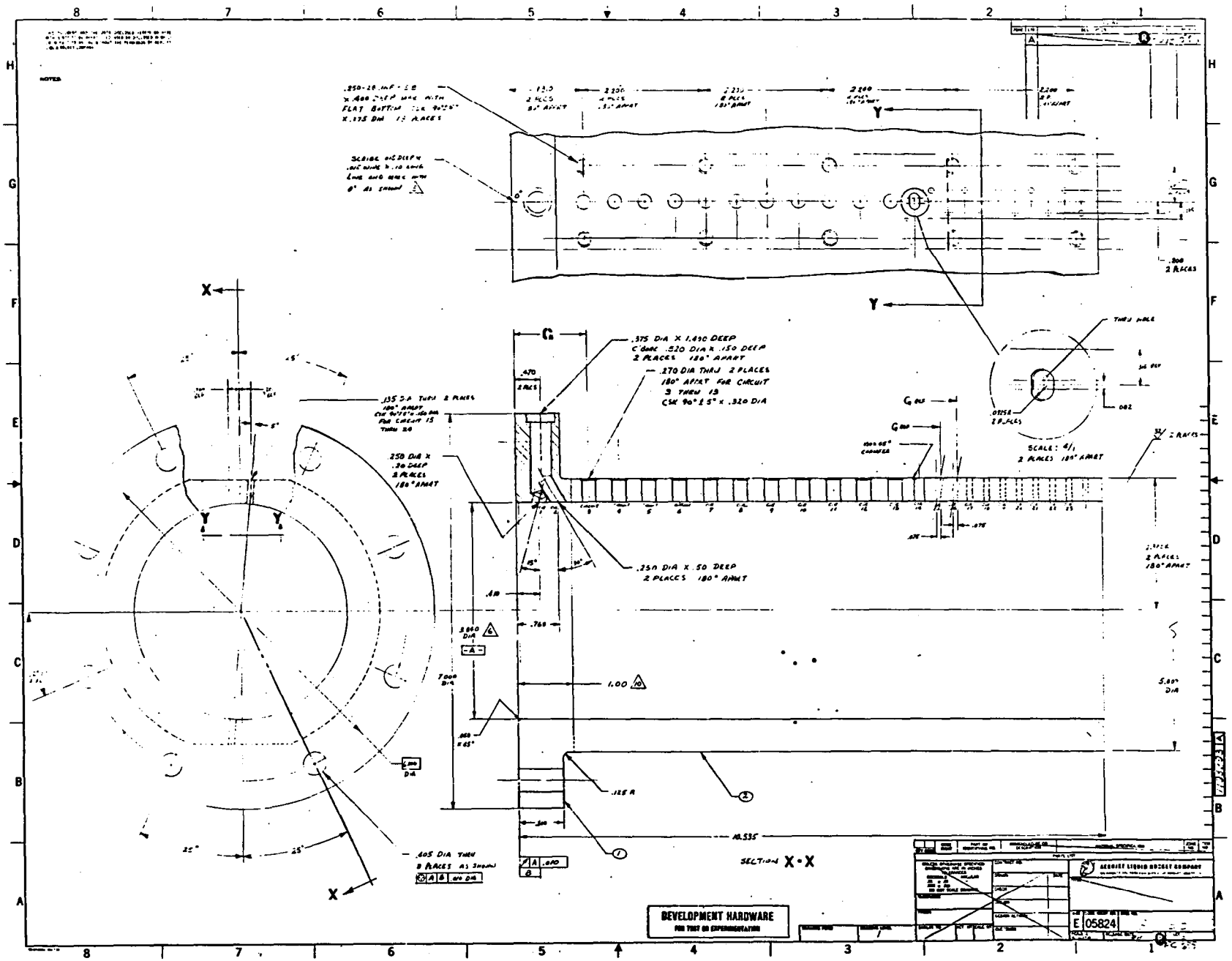

Figure 34. Cooled Chamber Assembly Engineering Drawing (3 of 5)

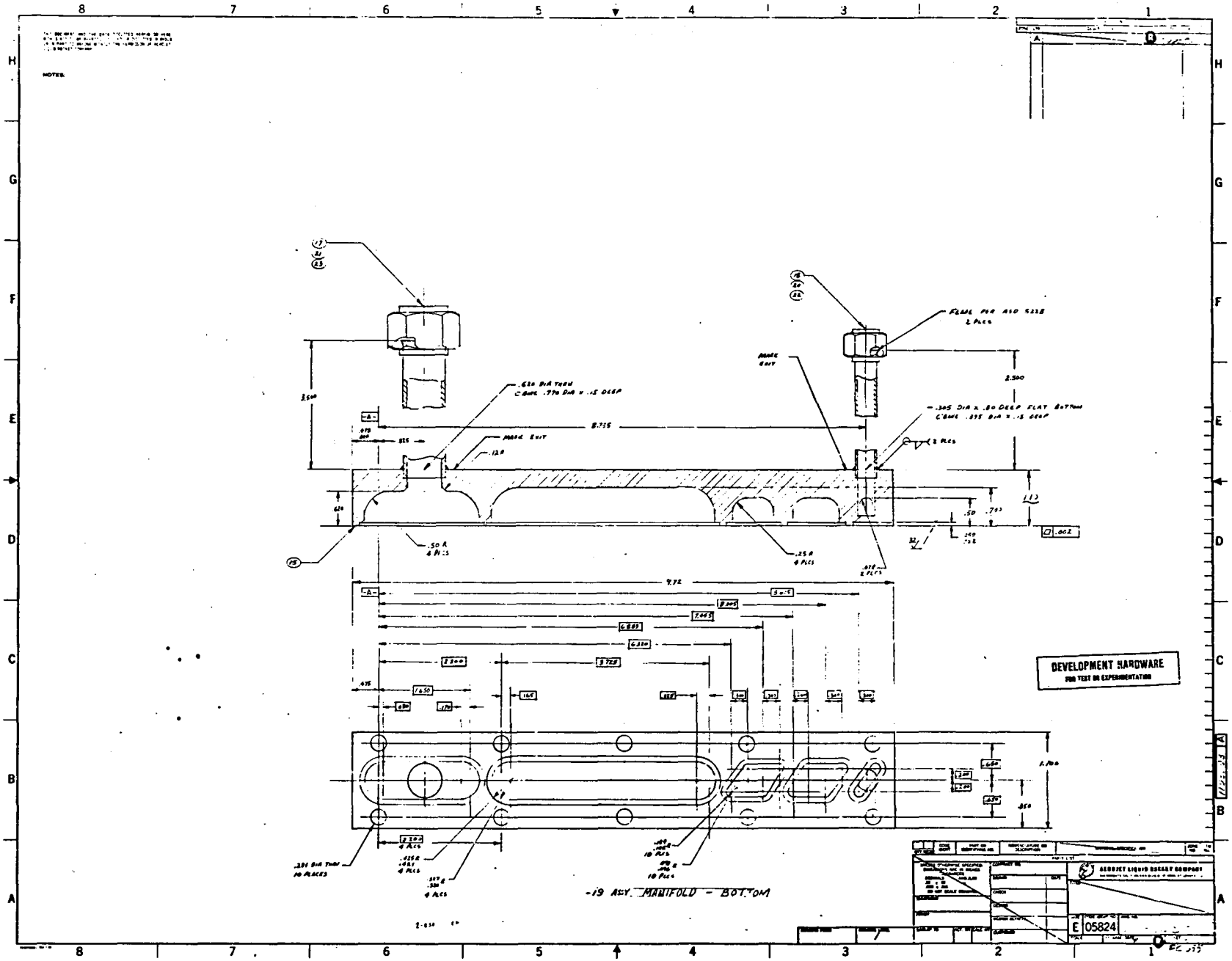

Figure 34. Cooled Chamber Assembly Engineering Drawing (4 of 5)

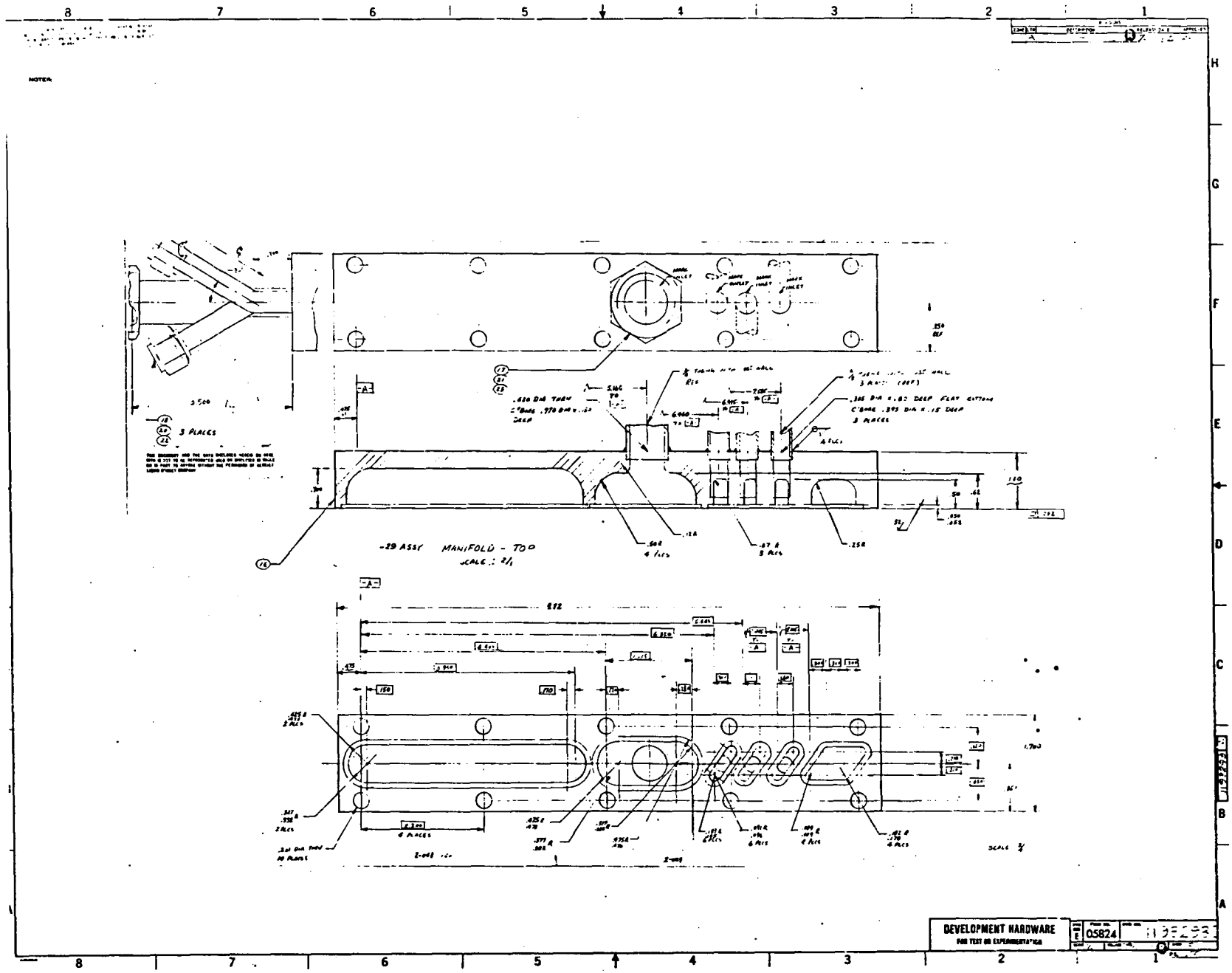

Figure 34. Cooled Chamber Assembly Engineering Drawing (5 of 5)

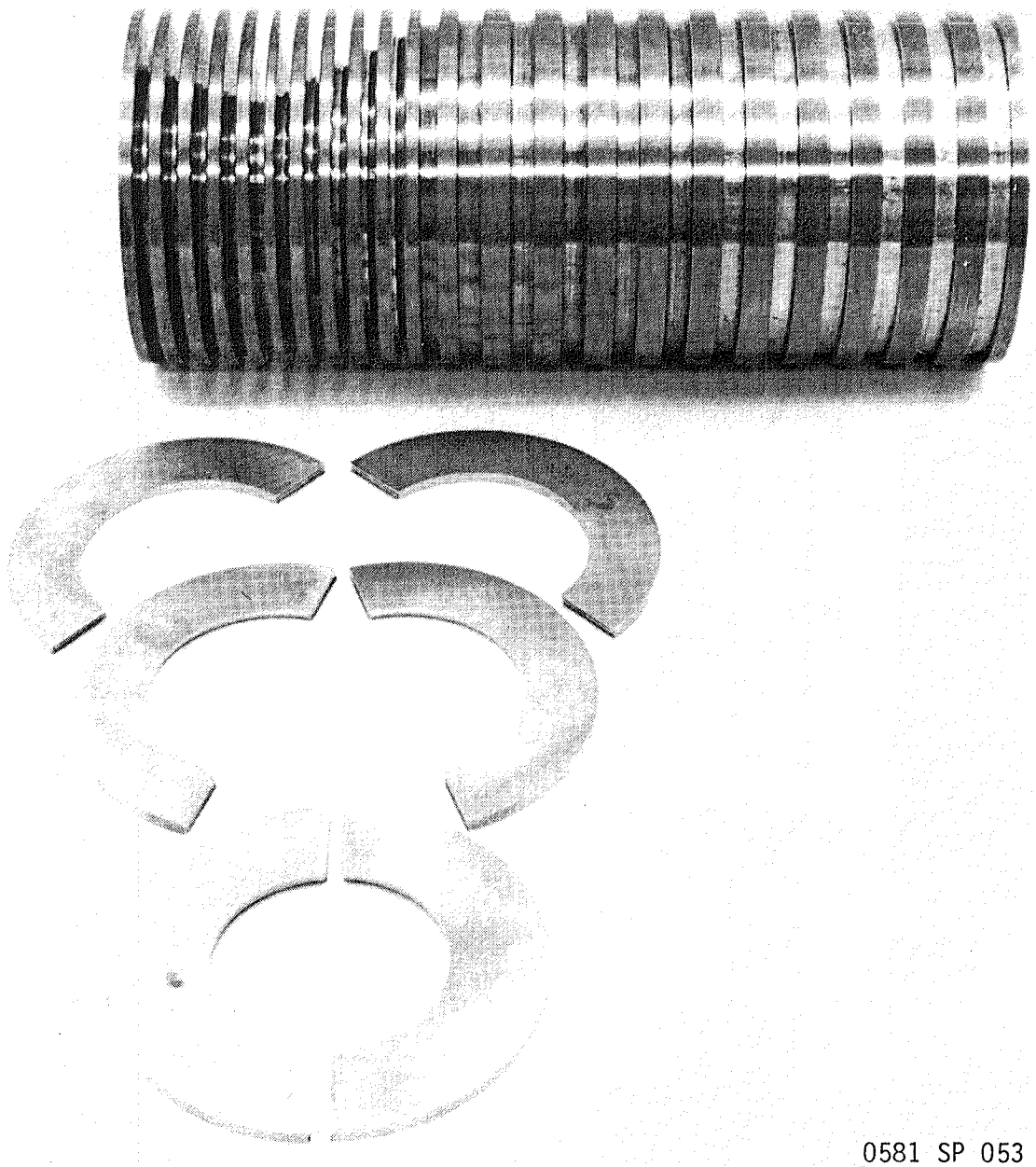

0581 SP 053

Figure 35. Copper Liner Prior to Braze Assembly

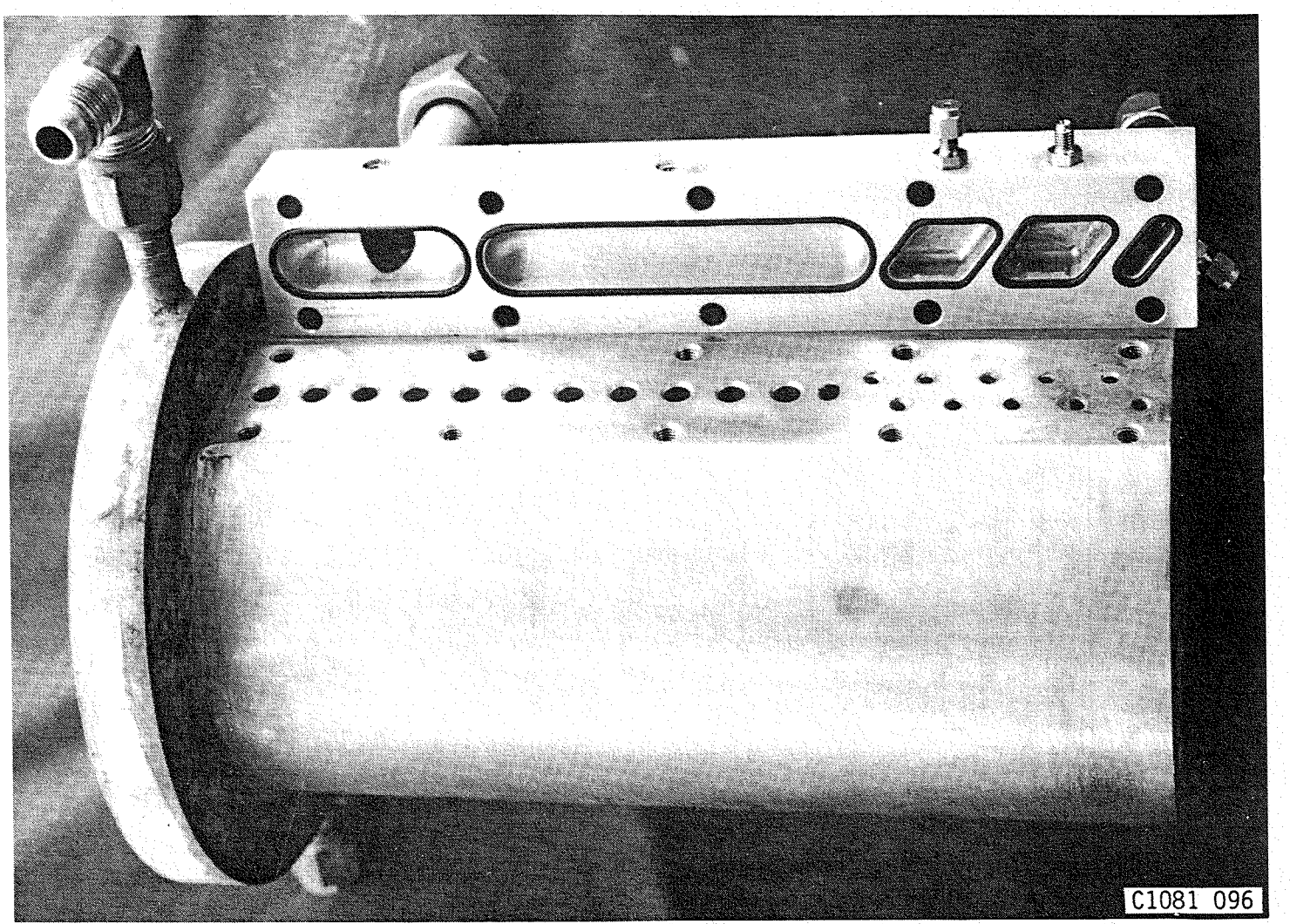

Figure 36. Final Chamber Assembly

$$\left(\frac{Q}{A}\right)_{A1} = \frac{\dot{w}_A(\Delta T_c A1 - \overline{\Delta T_{in}})}{21.1^{(**)}}$$

$$\left(\frac{Q}{A}\right)_{A2} = \frac{\dot{w}_A(\Delta T_c A2 - \Delta T_c A1) - \overline{\Delta T_{in}}}{23.5}$$

$$\left(\frac{Q}{A}\right)_{A3} = \frac{\dot{w}_A\ (\Delta T_c A3 - \Delta T_c A2) - \overline{\Delta T_{in}}}{23.5}$$

$$\left(\frac{Q}{A}\right)_{C1} = \frac{\dot{w}_c\ (\Delta T_c C1 - \overline{\Delta T_{in}})}{5.06}$$

$$\left(\frac{Q}{A}\right)_{C2} = \frac{\dot{w}_c\ (\Delta T_c C2 - \overline{\Delta T_c C1}) - \Delta T_{cin}}{6.45}$$

$$\left(\frac{Q}{A}\right)_{D1} = \frac{\dot{w}_D\ (\Delta T_c D1 - \overline{\Delta T_{in}})}{3.28}$$

$$\left(\frac{Q}{A}\right)_{D2} = \frac{\dot{w}_D\ (\Delta T_c D2 - \Delta T_c D1) - \overline{\Delta T_{in}}}{3.66}$$

$$\left(\frac{Q}{A}\right)_{D3} = \frac{\dot{w}_D\ (\Delta T_c D3 - \Delta T_c D2) - \overline{\Delta T_{in}}}{4.44}$$

$$\left(\frac{Q}{A}\right)_{R} = \dot{w}_R \frac{(DT_c R - \overline{\Delta T_{in}})}{7.48}$$

where: $\overline{\Delta T}_{inlet} = \left[\frac{T_{in\ 1} + T_{in\ 2}}{2}\right]_{\text{Time = X}} - \left[\frac{T_{in\ 1} - T_{in\ 2}}{2}\right]_{\text{Prefire}}$

and $\Delta T_c\ (A, C, D \text{ or } R) = \left[TC(A, C, D \text{ or } R - \text{Prefire Value}\right]$

Q/A = heat flux Btu/sec in.^{2}

** = exposed surface or gas-side of chamber

Figure 37. Procedure for Calculating Heat Flux

E, Tasks II and IV Subscale Injector Characterization (cont.)

Test 135 was a repetition of the same conditions, with the duration extended to 80 seconds. The heat load continued to decrease until about 60 seconds and then stabilized. Plots of the measured heat flux versus time data are provided in Figures 38 through 47. All subsequent tests were for a duration of 65 seconds.

A comparison of the total heat loads (Q, Btu/sec) for these three tests yielded the following data:

Test No.	Q at 3 Sec	Q at 5 Sec	Q at End of Test	Chamber Condition
133	418	-	-	New, clean
134	410	412	314	2nd firing
135	393	402	295	3rd firing

The small test-to-test heat load reduction of 6% (Test 135 vs Test 133) indicates that the carbon buildup occurring during a test is essentially cleaned out by the shutdown and startup transients. No attempt to physically clean the chamber between tests was made. The total heat reductions during the 40 and 80 second tests were 24 and 27%, respectively.

Test 136 was a 65 second high mixture ratio (4.3) test at nominal pressure. Contrary to what was expected, the carbon buildup rate was much faster and equally extensive at higher mixture ratios. Thermal equilibrium conditions, measured by total Q, were attained after only 20 seconds of burn time compared to 60 seconds at a mixture ratio of 3. The maximum Q of 337 Btu/sec occurred at 3 sec, and the steady-state value of 250 after 20 seconds represented a 26% reduction from the peak value.

Test 137 was a low mixture ratio test (MR = 2) at nominal pressure. Higher heat fluxes and little drop-off with time were observed at this condition. The maximum Q of 440 Btu/sec occurred at 6 seconds, and this dropped to 412 Btu/sec at 65 seconds, a reduction of only 6%.

Test 138 was a nominal mixture ratio test (MR = 3) at a Pc of 400 psia. The trends were similar to those of Tests 134 and 135 but with higher total heat loads. The max Q of 467 Btu/sec at 4 seconds dropped to 337 at 50 seconds and to 319 at 65 seconds.

Test 139 was a 300 psi test at a MR of 2.7. The maximum Q and end-of-test Q values were 410 and 346 Btu/sec, respectively, for a 16% reduction.

Test 140 was a high-pressure (408 psi) test at the same mixture ratio as Test 139 (MR = 2.7). The max Q and end-of-test Q values were 469 and 396 Btu/sec, respectively, for a 16% reduction. The trend toward diminished carbon deposition effects at lower MR continued to hold.

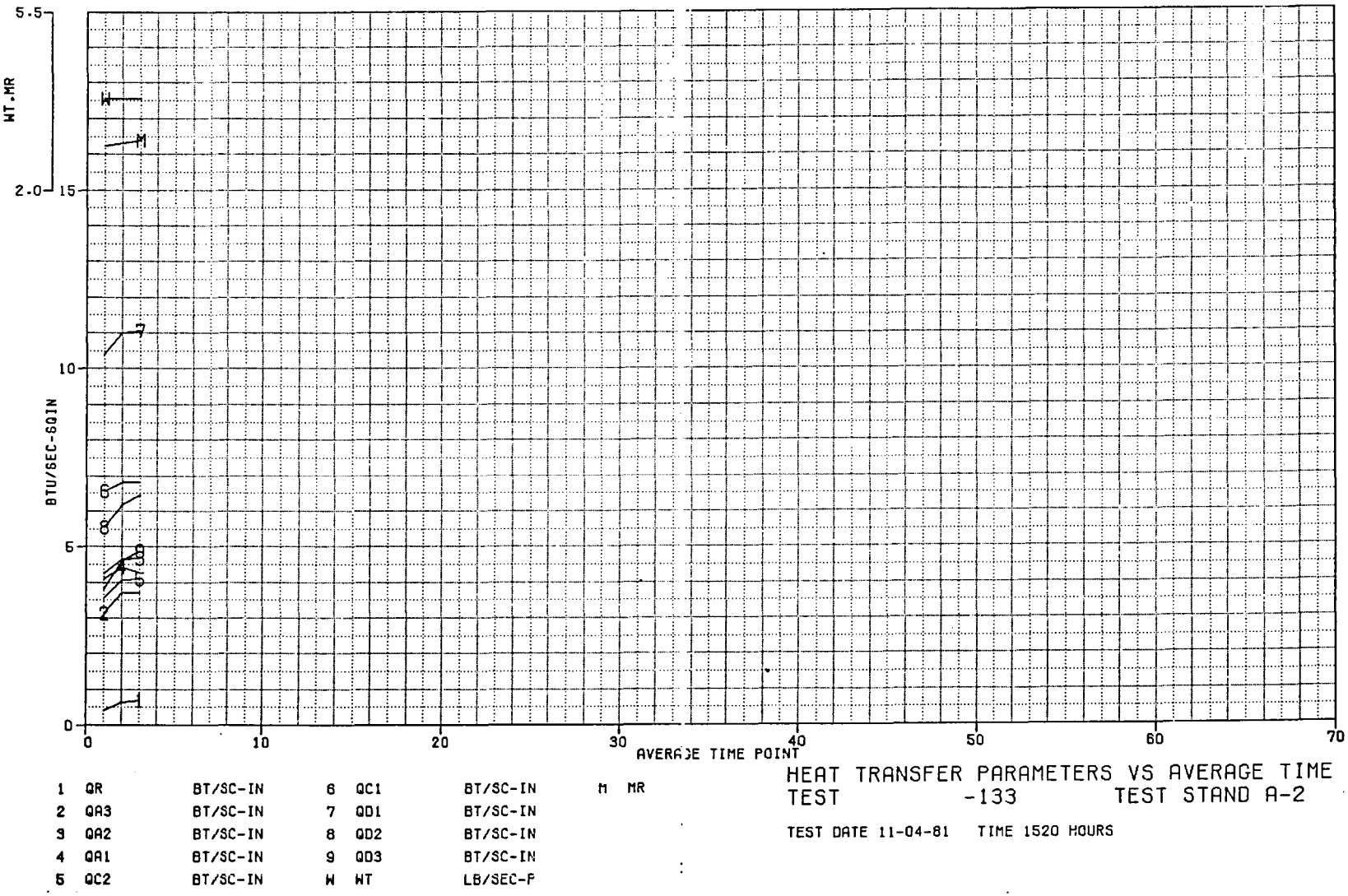

Figure 38. Heat Transfer Parameters Versus Average Time, Test -133

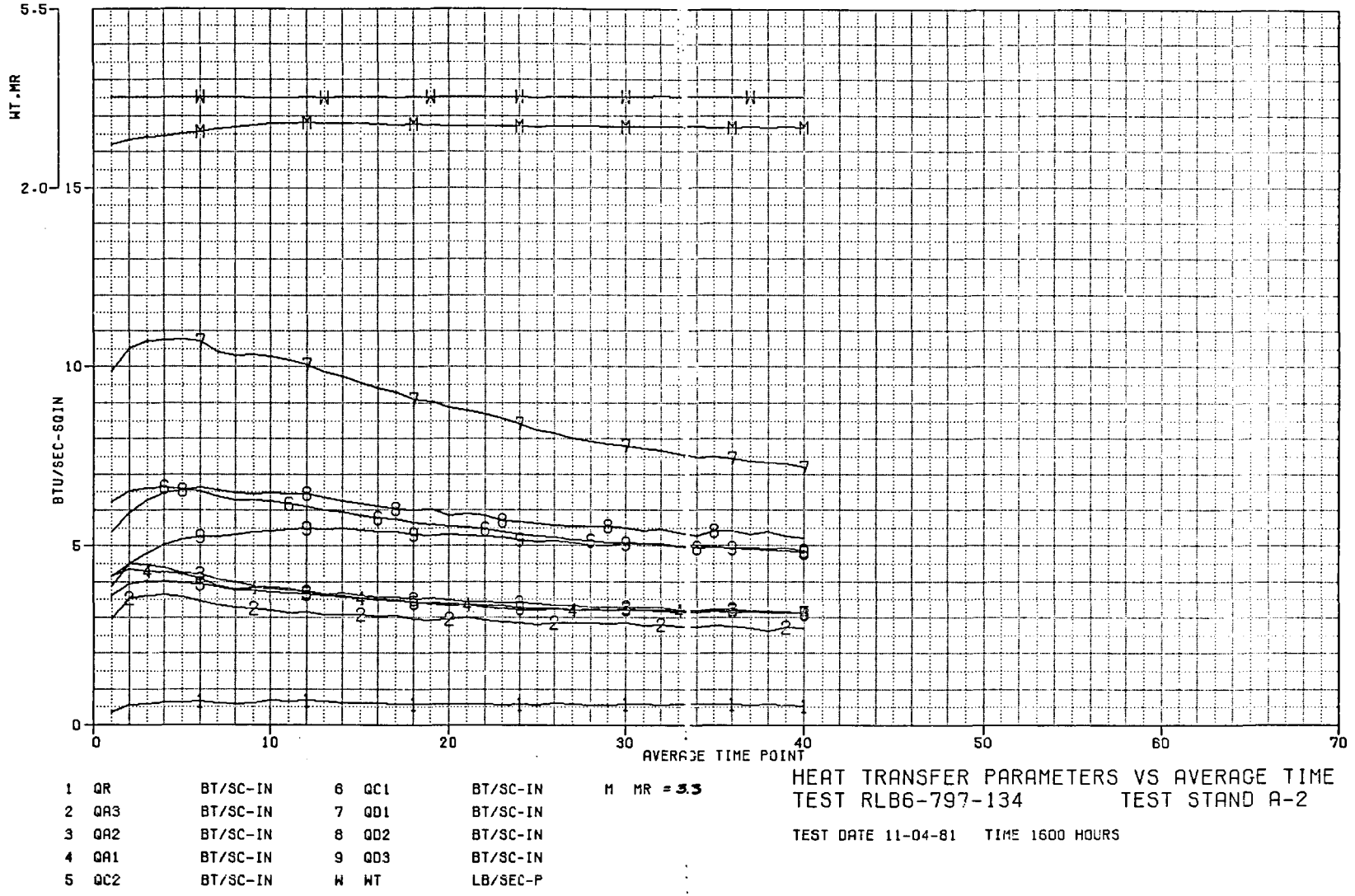

Figure 39. Heat Transfer Parameters Versus Average Time, Test -134

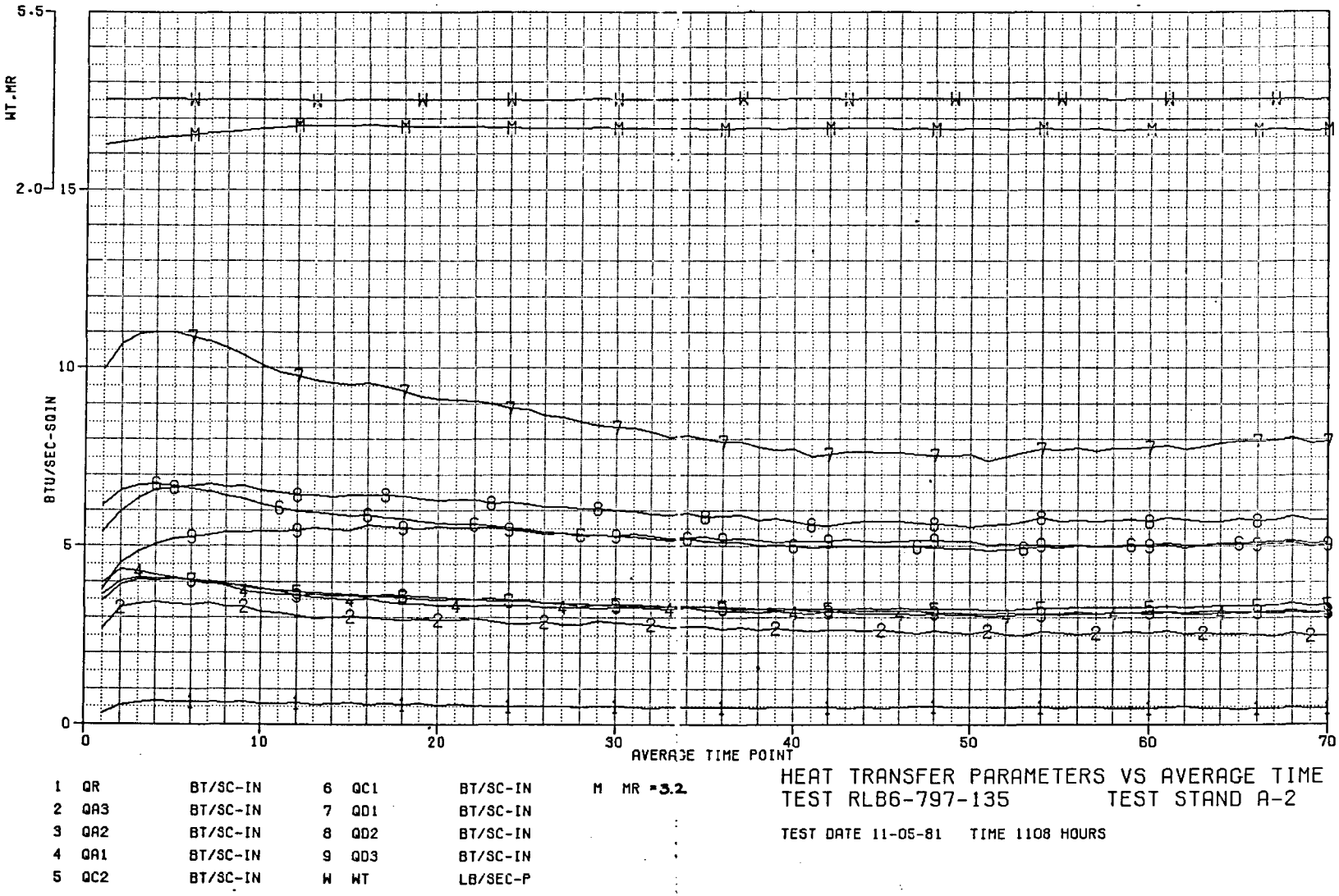

Figure 40. Heat Transfer Parameters Versus Average Time, Test -135

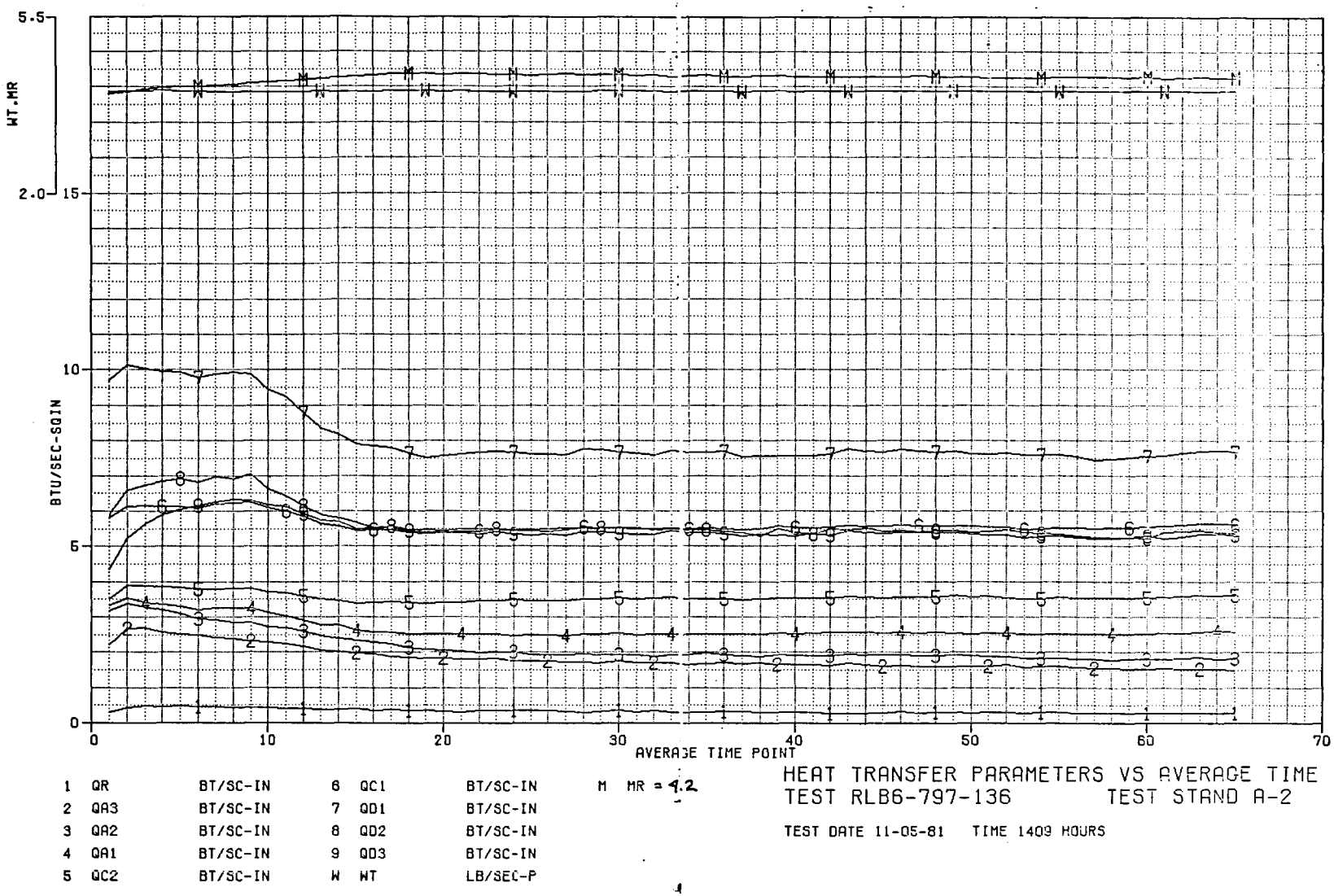

Figure 41. Heat Transfer Parameters Versus Average Time, Test -136

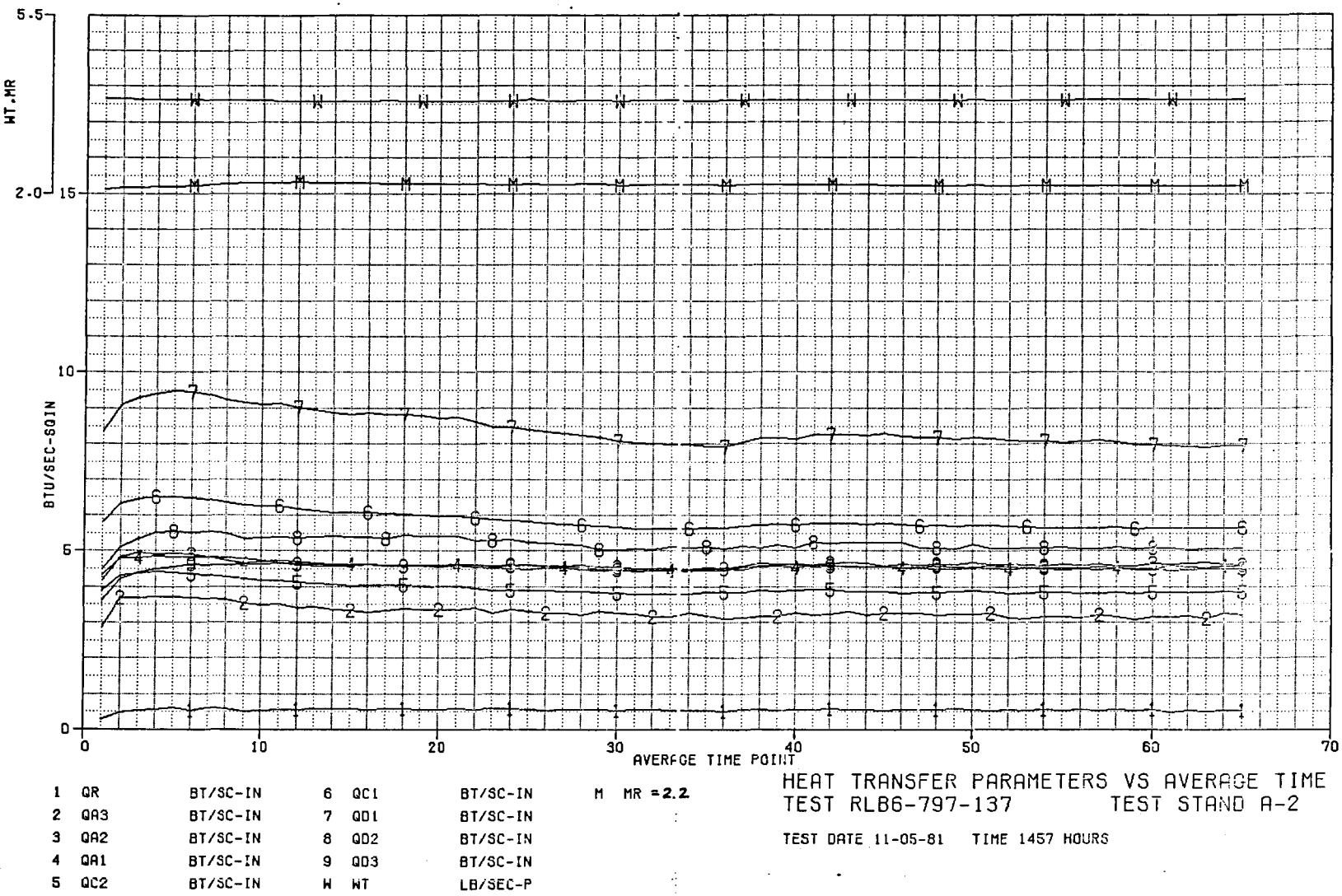

Figure 42. Heat Transfer Parameters Versus Average Time, Test -137

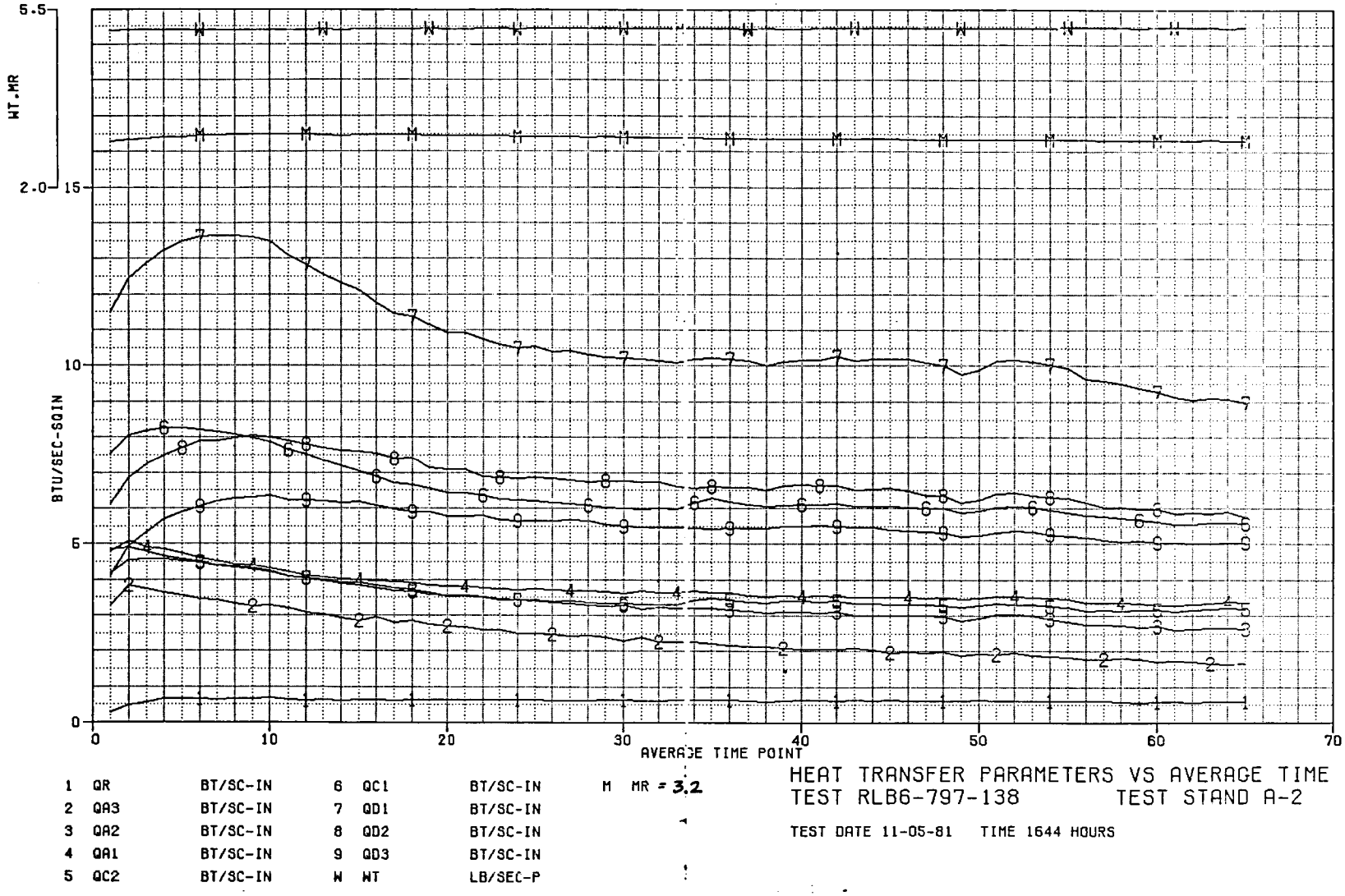

Figure 43. Heat Transfer Parameters Versus Average Time, Test -138

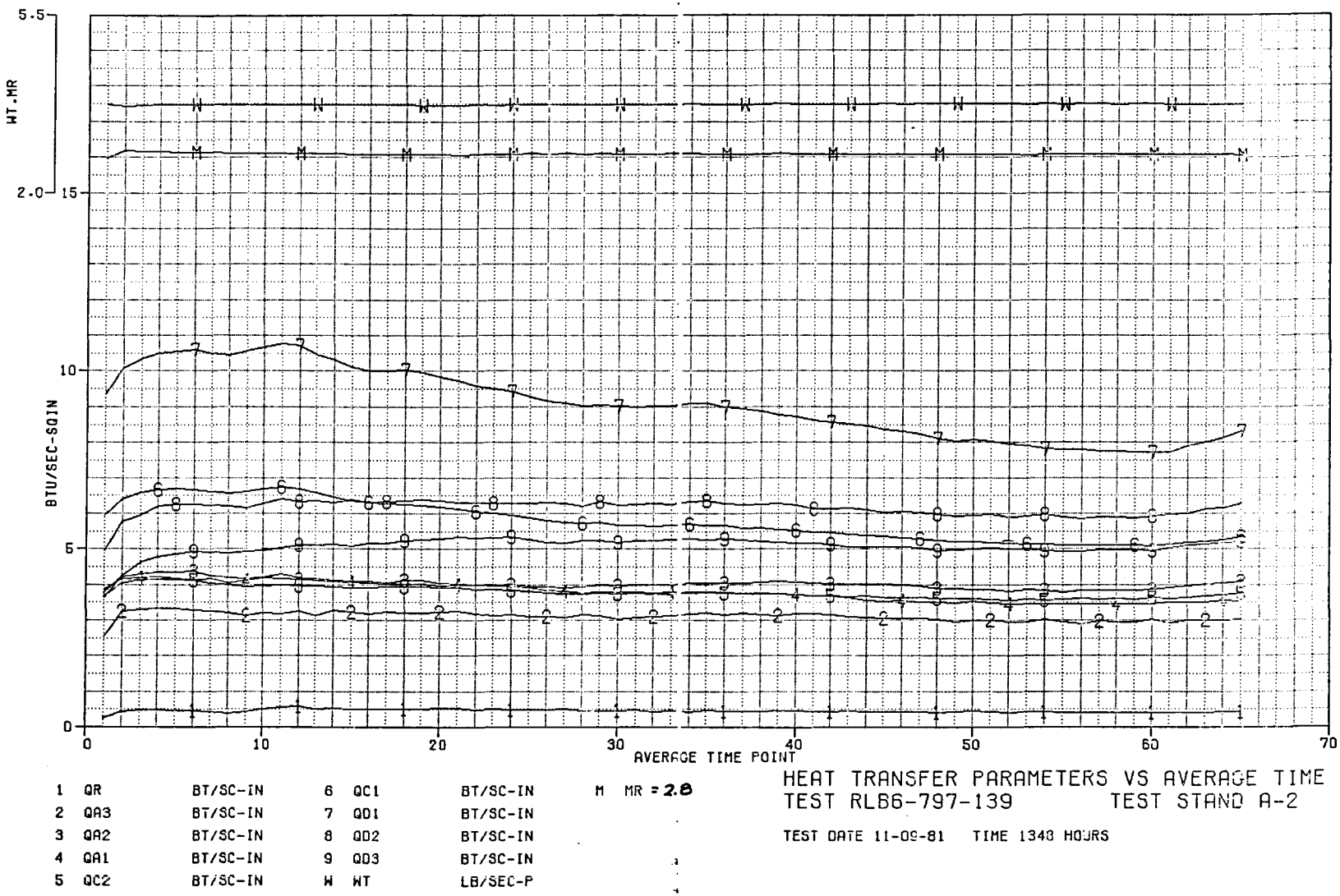

Figure 44. Heat Transfer Parameters Versus Average Time, Test -139

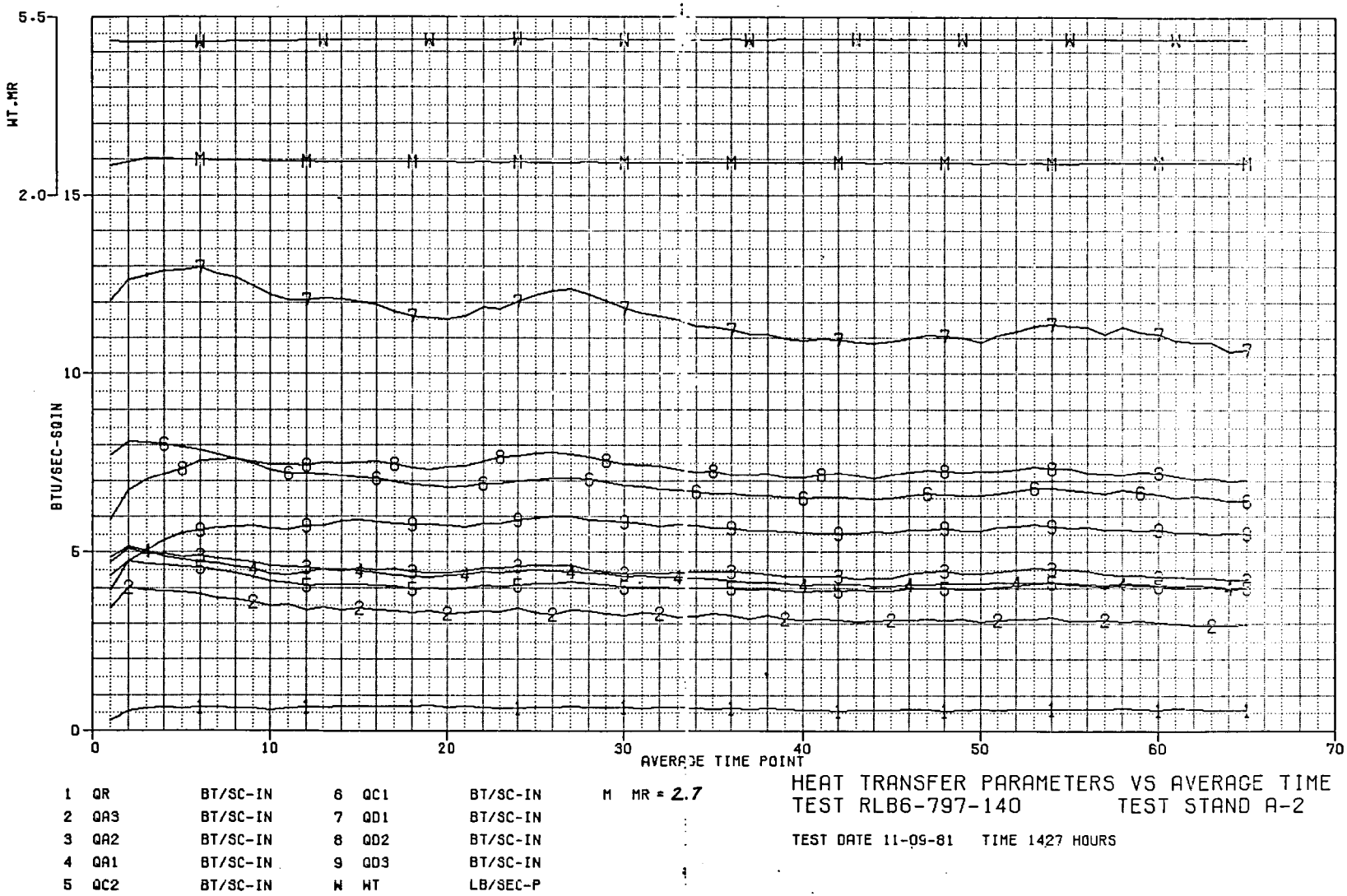

Figure 45. Heat Transfer Parameters Versus Average Time, Test -140

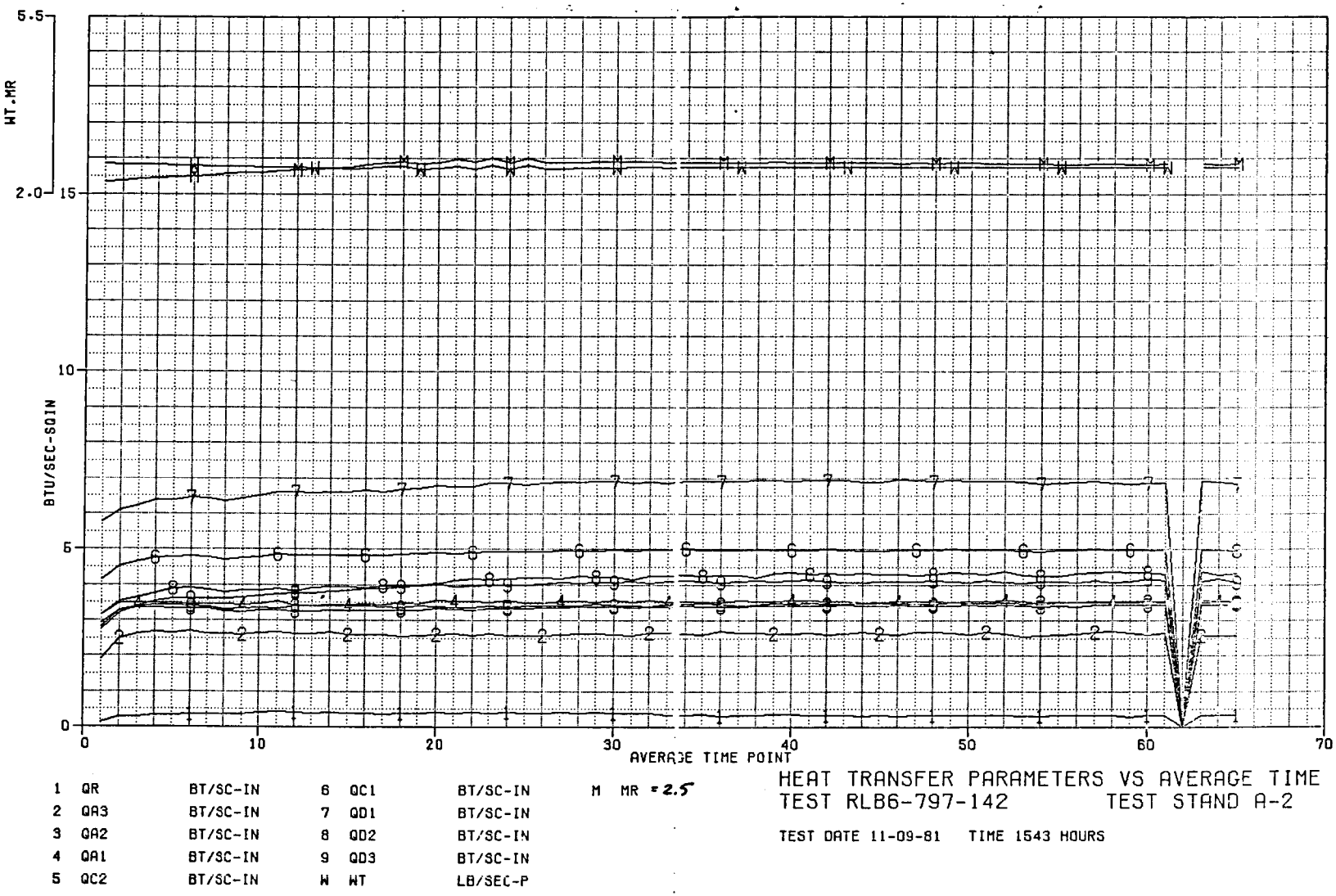

Figure 46. Heat Transfer Parameters Versus Average Time, Test -142

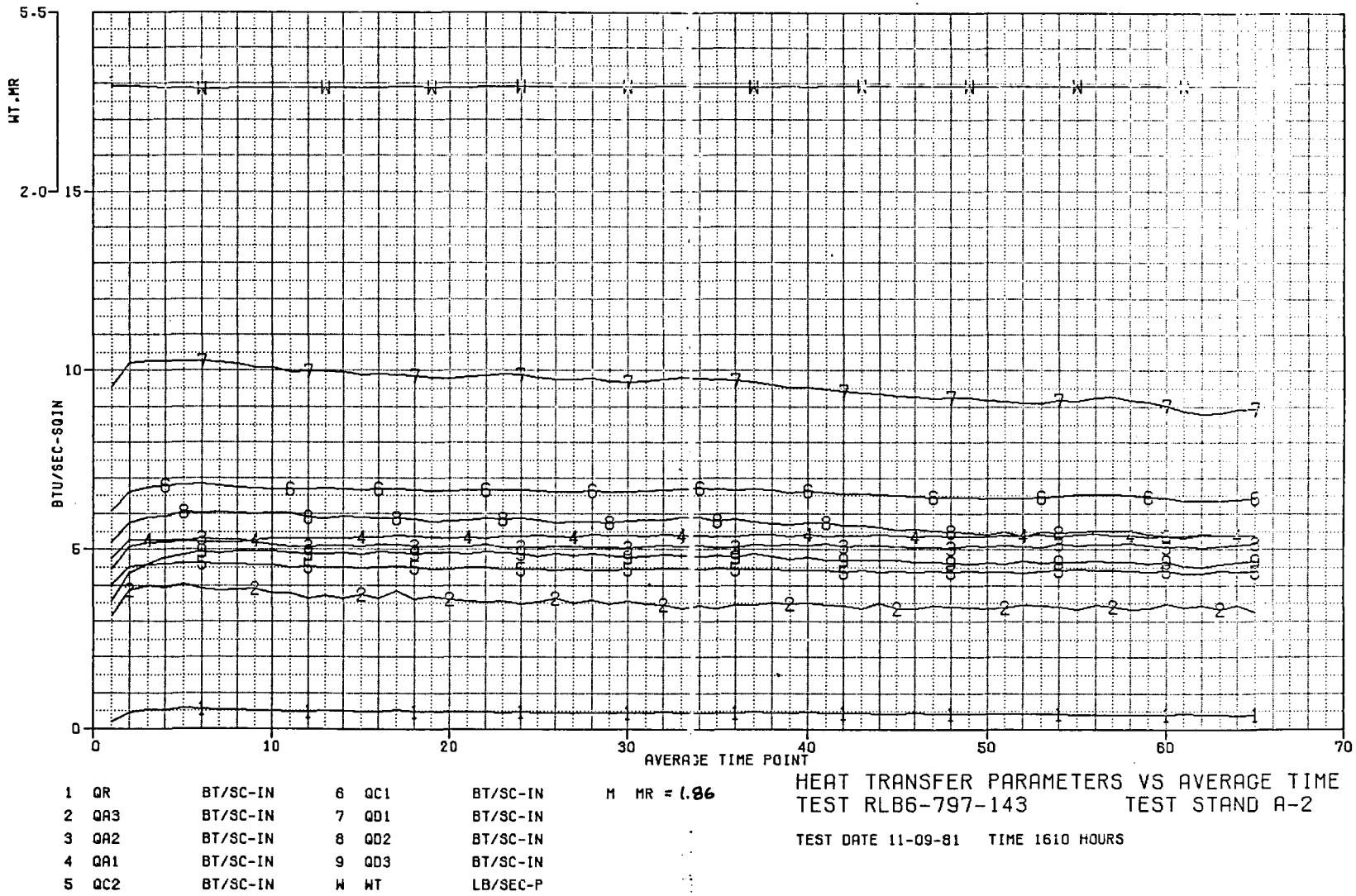

Figure 47. Heat Transfer Parameters Versus Average Time, Test -143

E, Tasks II and IV Subscale Injector Characterization (cont.)

Test 141 was a low pressure (200 psi) test at the same MR as that of Test 140. The test was terminated shortly after successful ignition by a faulty nonignition kill indication. No data were obtained in this test.

Test 142 was a repeat of the Test 141 conditions for a successful 65 second burn at a MR of 2.6. The maximum Q of 323 Btu/sec was not attained until 37 seconds into the test and remained at that level for 65 seconds. The carbon build-up phenomena was significantly different from the higher pressure tests.

Test 143 was an extra-low (1.82) MR test at the nominal 300 psi condition to determine if the trends of higher Q and lower carbon deposits would continue at reduced mixture ratios. A maximum Q of 472 Btu/sec was reached at 8 seconds, and the heat load remained between 462 and 468 Btu/sec for the entire 65 second test, for a reduction of only 1%.

The peak heat loads at mixture ratios 1.8, 3.0 and 4.3 were 472, 412, and 373 Btu/second. These data led to the conclusion of a propellant flow inversion at high oxidizer to fuel momentum ratios.

Figure 48 shows two posttest views of the injector face coated with carbon as a result of the testing. Figure 49 shows the head-end and throat of the chamber. The heavy carbon buildup in the resonator cavity is visible in the original color photo but cannot be seen clearly in the black and white reproduction. The heavy carbon deposits in the resonator cavity indicate that these are becoming plugged over a long period of operation and eventually could lead to reduced stability margin or even unstable operation, since it was proven that the cavities were required to assure stable combustion. Evaluation of designs which would keep these cavities clean was recommended and evaluated in subsequent testing.

The chamber barrel was found to be relatively clean. A darkening observed at the start of convergence continued through the throat to the exit plane. These observations support the subsequent thermal data analyses which indicate an oxidizer-rich environment in the cylindrical section changing to a fuel-rich wall environment at the start of convergence.

Table VIII provides a summary of the test conditions and the resulting overall thermal data. Figures 38 through 47 are plots of the propellant flowrate, mixture ratio and resulting heat flux measurements for each compartment.

(a) Thermal Results

Figure 50 provides a map of the measured axial heat flux profiles at 300 psi and 5 different mixture ratios. Two time periods are shown. The first plot shows the maximum value observed early in the test. In this plot, each data

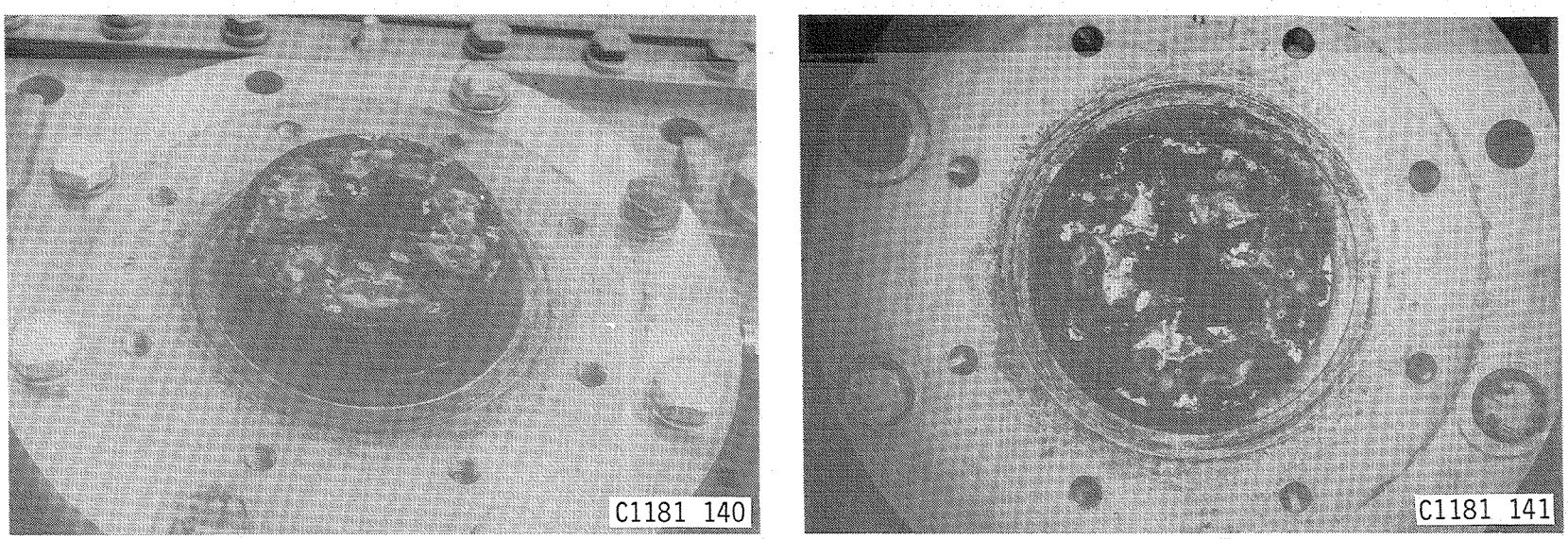

Figure 48. Views of OFO Injector Face Coated with Carbon Following LOX/Propane Testing

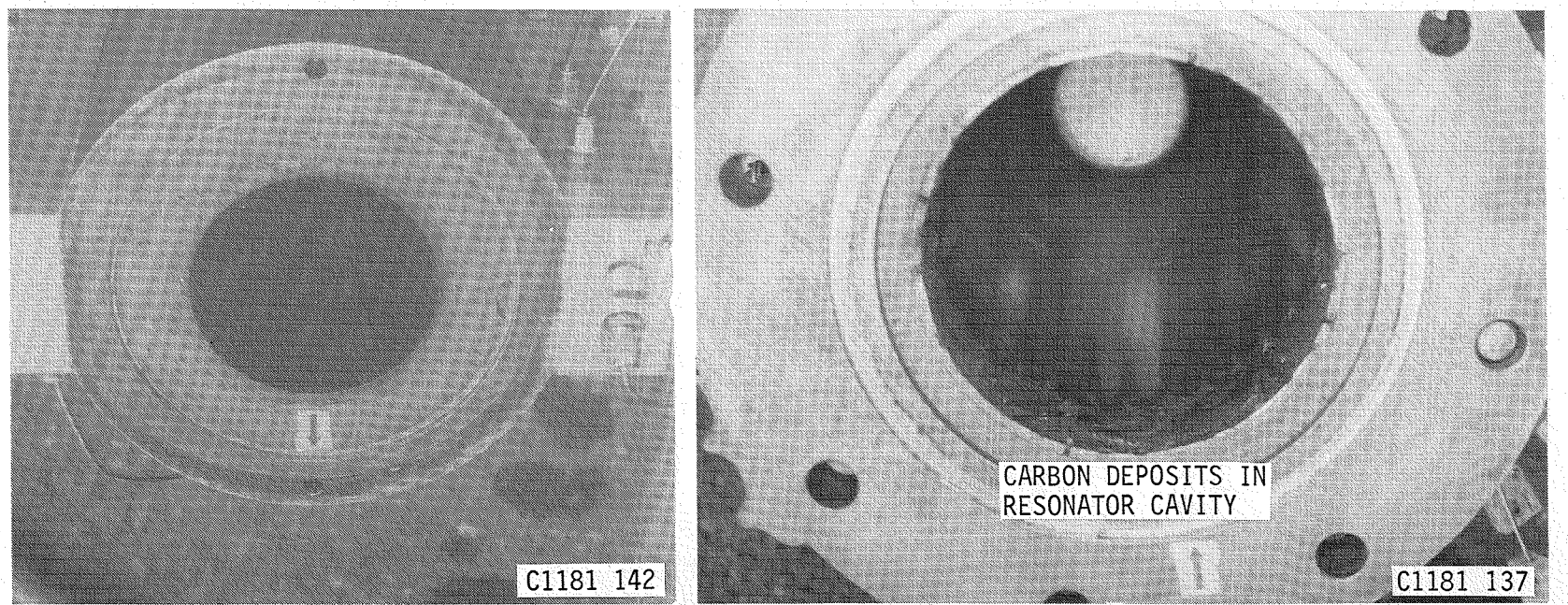

Figure 49. Water-Cooled Chamber Following Test 143 at 630 Seconds of Accumulated Burn Time with LOX/Propane

TABLE VIII

HOT-FIRE TEST SUMMARY - OFO INJECTOR AND CALORIMETER CHAMBER

Test	Date	O/F (-)	Pc (psia)	Duration (sec)	Max. Throat Heat Flux (Btu/sec-in.^{2})	Max. Total Heat Load (Btu/sec)	Total Heat Load at 60 sec (Btu/sec)
133	4 Nov	2.9	300	3	11	417	
134	4 Nov	3.1	300	40	10.7	412	314 (at 40 sec)
135	5 Nov	3.18	301	80	11.0	402	313
136	5 Nov	4.3	304	65	10.0	337	244
137	5 Nov	2.1	296	65	9.4	440	412 (at 65 sec)
138	5 Nov	3.0	400	65	13.6	467	337
139	9 Nov	2.75	300	65	10.7	410	346
140	9 Nov	2.6	408	65	12.9	469	396
142	9 Nov	2.58	200	65	6.3	323	323
143	9 Nov	1.82	300	65	10.2	472	462-468

L' = 8 in.

Fuel = Propane

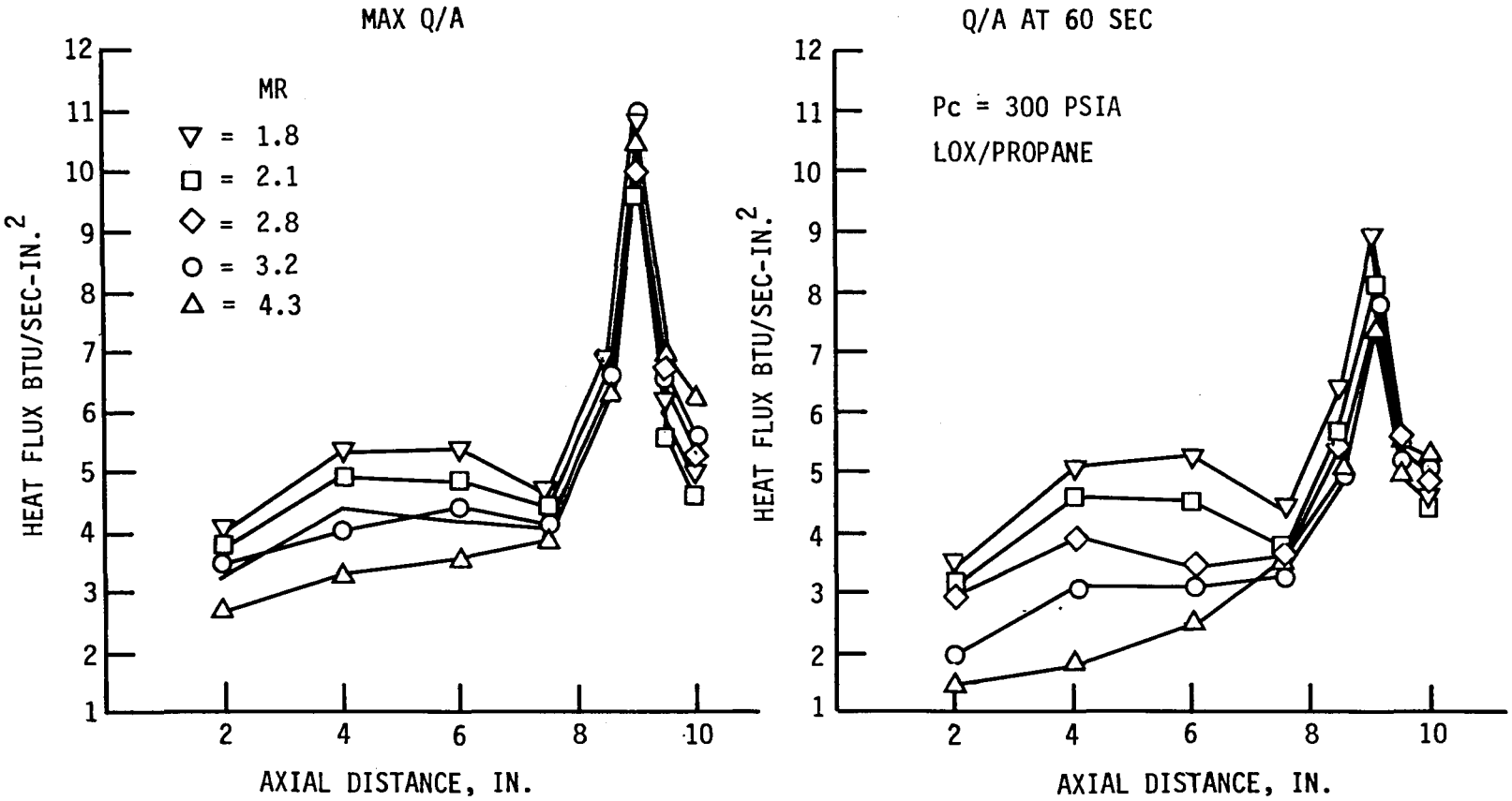

Figure 50. Effect of Mixture Ratio on Heat Flux Profiles at the Time of Maximum Flux and at 60 Seconds

point may represent a slightly different time. The second profile to the right provides the flux 60 seconds into the burn, when near-equilibrium carbon deposition conditions exist. The chamber region shows significant flux reductions at higher mixture ratios and with increasing time whereas the supersonic region indicates a lesser influence of both MR and time. The lower heat flux at the 2-in. station is highly influenced by the injector.

Figure 51 provides similar data, showing the influence of chamber pressure at a constant MR value of approximately 2.6. The fact that the greatest flux reductions, due to carbon deposition, take place at high flowrates (400 Pc) and that little or no reductions are noted at lower flowrates (200 Pc) is inconsistent with previous data and needs to be studied further. The internal consistency of all data suggests that these effects are real.

Figure 52 provides a cross-plot of the throat station heat flux versus mixture ratio as a function of time, at a constant chamber pressure of 300 psia. The heat flux reduction with time is expressed by the ratio of the 60 second flux to the maximum flux in the upper curve. The trend toward less carbon deposition at lower MR at the throat station is consistent with the total heat load data presented in the previous section. Mixture ratios between 2.0 and 4.3 appear to have little influence on the heat flux at the 60 second time slice.

The 60 second data of Figure 51 show that chamber pressure has little influence on the chamber region heat flux. The rise in heat flux at low MR at the throat station is consistent with other stations and suggests that this particular element should not be selected to operate at a fuel-rich condition near the wall when low heat flux is desired.

Figure 53 provides a complete heat flux versus mixture ratio map for each of the eight compartments at a chamber presure of 300 psia. All data represent the maximum flux values which are assumed to correspond to a relatively clean wall condition. With very few exceptions, these data provide smooth, continuous curves and are internally consistent, an indication that the trends are real.

The cylindrical chamber section in the first column shows a reduction in heat flux as the mixture ratio increases from 1.8 to 4.3. Theoretical predictions indicate that the maximum convective heat flux occurs at a mixture ratio of 2.2 and falls off at both higher and lower MR values. The convergent nozzle shows less of a MR-dependency in Section C-2 and becomes almost flat in Section C-1 just upstream of the throat. The flux versus MR trend reverses starting in the throat station and produces an increasing flux versus MR downstream. It is suspected that unvaporized fuel droplets are impinging on the convergent nozzle and significantly reducing the local mixture ratio in the wall film. Overall engine MR was employed in preparing the plots. This MR dependency would be expected to be a strong function of injector pattern and chamber length.

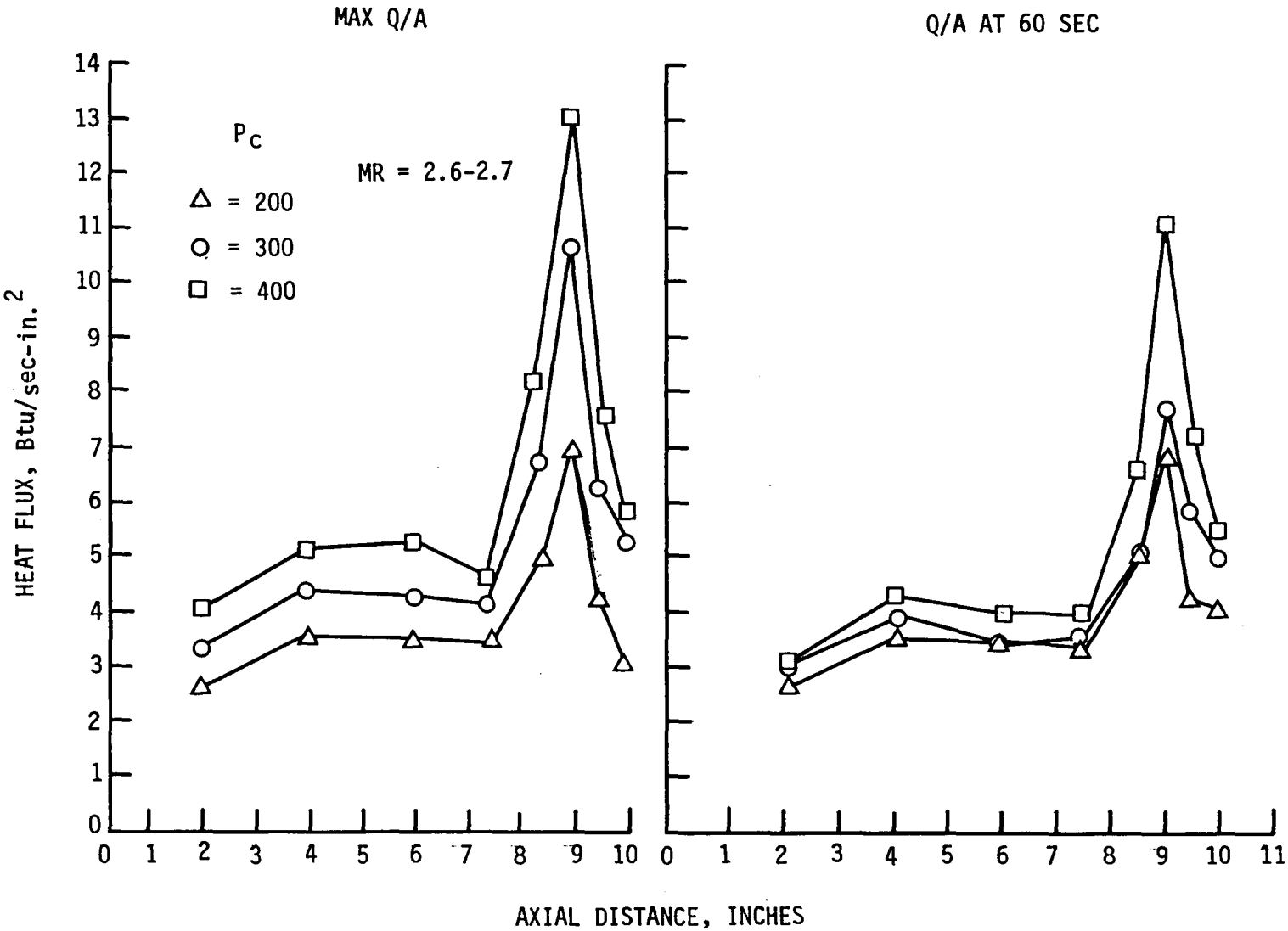

Figure 51. Effect of Chamber Pressure on Maximum Heat Flux and at 60 Seconds

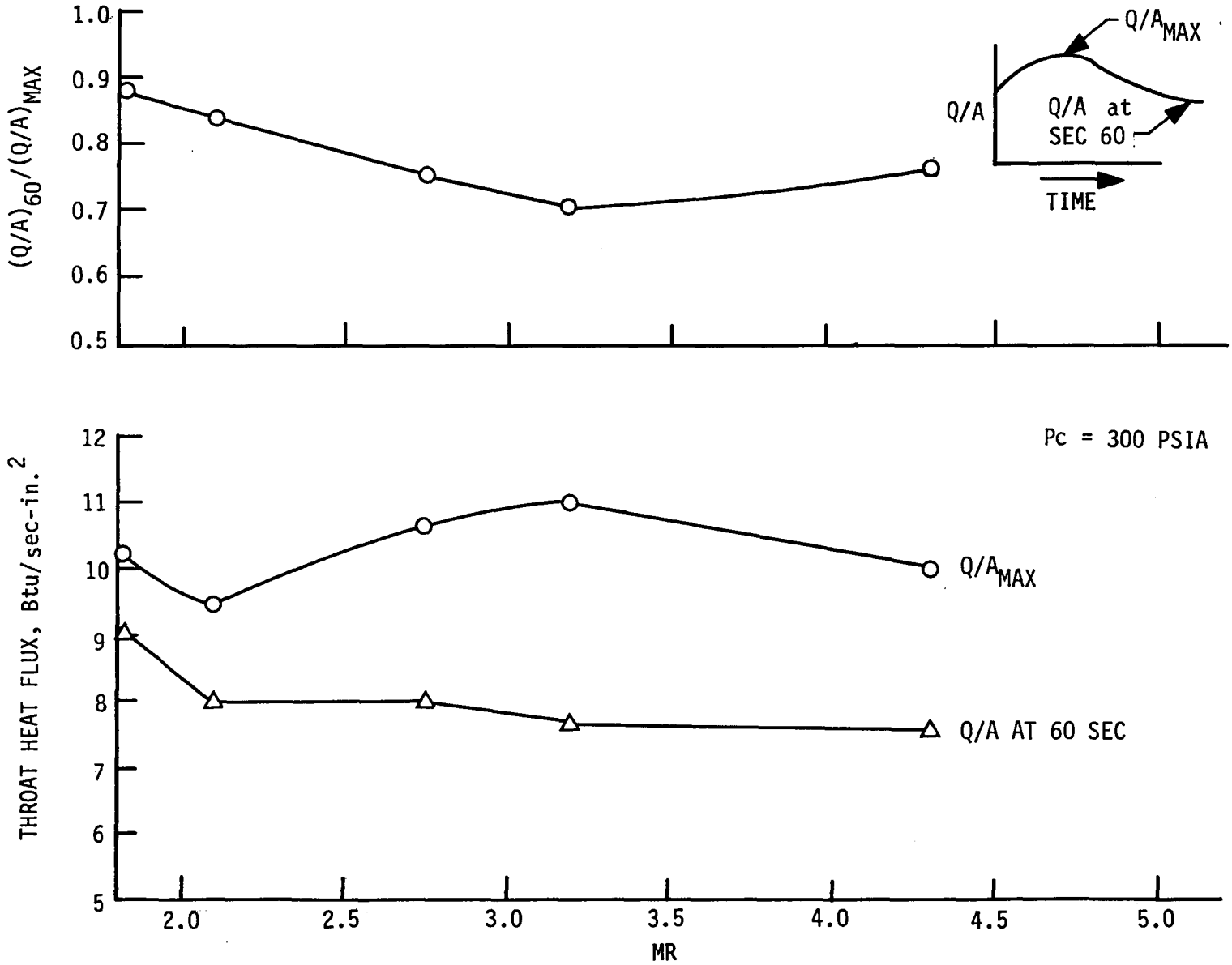

Figure 52. Throat Station (D-1) Heat Flux Versus MR and Time

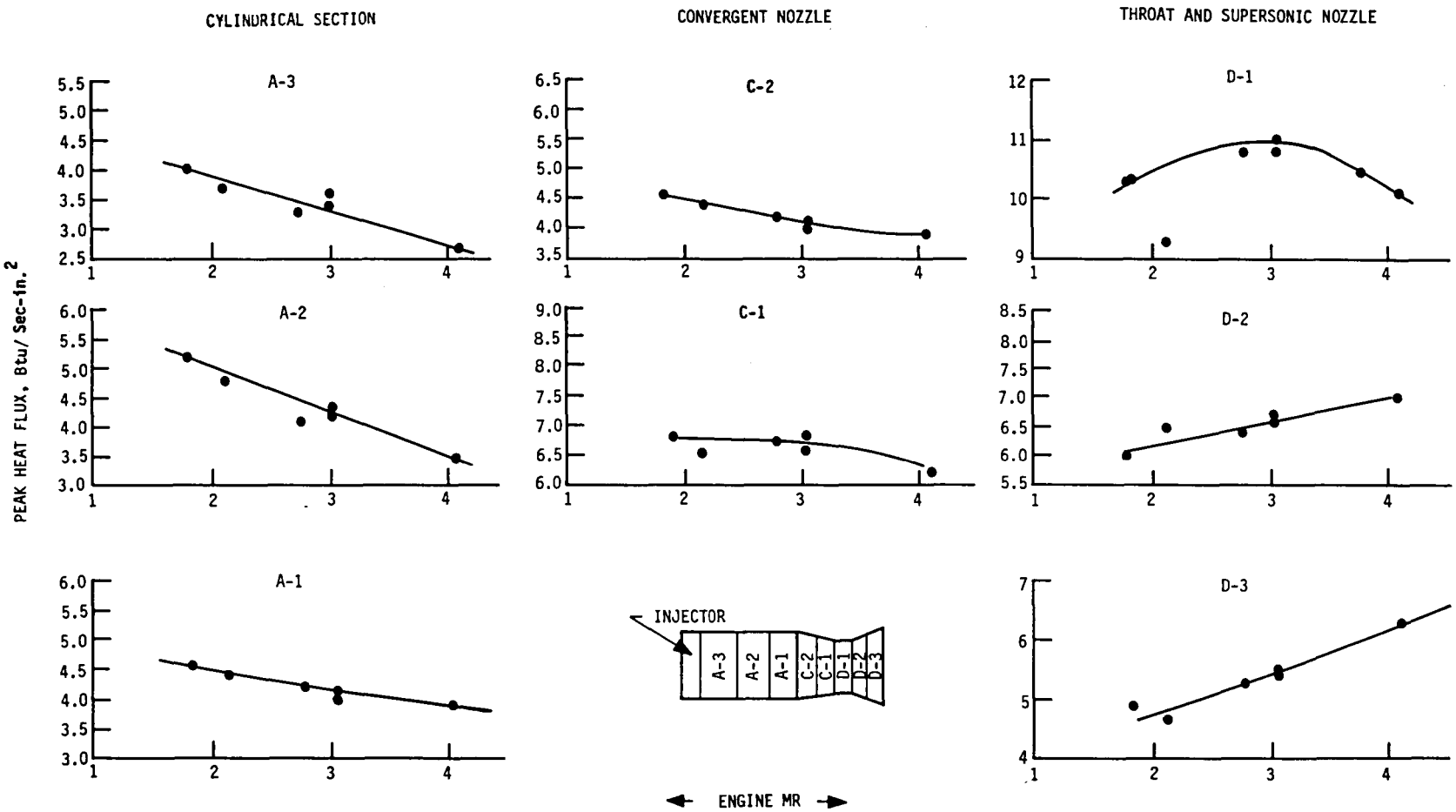

Figure 53. Maximum Heat Flux Versus Engine MR for a Chamber Pressure of 300 psia

E, Tasks II and IV Subscale Injector Characterization (cont.)

(b) Performance Results

A summary of the test conditions and performance parameters is shown in Table IX. Data in this table are presented at three firing-time summary periods of 1, 5, and 10 sec, respectively. Figure 54 provides a comparison of the thrust-based specific impulse data from the water-cooled calorimeter chamber with that from the heat sink chamber at a data summary time of 0.5 to 0.6 seconds. The consistency of these data indicates that the addition of the water-cooling lines did not influence the thrust measurement and thrust calibration system.

Figure 55 shows the vacuum specific impulse for the 8-in. L', 1.94 area ratio chamber as a function of mixture ratio, chamber pressure, and burn duration. Some improvement in Isp and a significant reduction in data scatter are noted for the 10 second as opposed to the 0.5 second data summary period. The 10 second data are considered to be more accurate.

Figure 56 provides the energy release efficiency (ERE) calculated from the Isp measurement. The influence of MR and Pc on these data is internally very consistent. The large fall-off of ERE at low MR is due to the increase of the fuel-to-oxidizer momentum ratio in the OFO element. The energy release efficiency shown in the figure is based on the 10 second data summary period and is slightly higher than the data reported earlier in the short duration heat sink chamber tests.

Uncorrected C* data are provided in Table IX. No comparison with previous data was made because of the change in Pc measurement location from a through-the-chamber-wall measurement to a through-the-injector-face-igniter-port (P_{oji}) measurement. Further discussion of these test results is presented at the end of Section 5,d.

d. Test Series IV - LOX/Propane and Propane Film-Cooling, OFO Triplet Injector, 8.7-in. L' Water Cooled Calorimeter Chamber

(1) Test Objectives

The objectives of this test series were to define the changes in heat flux and performance loss resulting from the use of propane film-cooling and to determine if the method of coolant injection would prevent carbon buildup in the resonator cavities.

(2) Facility Changes

The fuel feed system was modified to provide a separate valve and flow meter for the film-cooling injector as shown in the facility flow schematic of Figure 57. The bleed for the coolant was obtained downstream of the main flow measurement such that the core flow rate is the difference between total flow and coolant flow for the portion of each test where coolant is utilized.

TABLE IX

DATA SUMMARY FOR OFO TRIPLET WITH LOX/PROPANE PROPELLANT

Test No.	Date	Data Summary (sec)	T_{oj} (°F)	T_{fj} (°F)	P_{oji} (Pc) (psia)	MR	Test Duration (sec)	Prop-flow $\dot{W}_o$ (lb/sec)	Prop-flow $\dot{W}_f$ (lb/sec)	Prop-flow C^*P_{oji} (vac)	P_{oj}	P_{fj}	F_{vac}	Ispvac	ΔP_{oj}	ΔP_{fj}	ηIsp	ηERE	Kw_{oj}	Kw_{fj}
133	11-04-81	1.5-1.8	-264	69	301.6	2.882	3.37	2.815	0.977	5661	417.6	393	970	256.0	116.0	91.4			0.2490	0.1445
134	11-04-81	1.4-1.85	-262	68	300.2	2.897	40.39	2.803	0.968	5664	415.5	388.7	965	256.0	115.3	88.5			0.2493	0.1452
134	11-04-81	5.4-5.85	-267	67	298.4	3.077	40.39	2.844	0.924	5635	415.9	377.4	965	256.1	117.5	79.0			0.2507	0.1467
134	11-04-81	10.4-10.85	-267	66	296.1	3.264	40.39	2.880	0.883	5599	415.4	366.8	959	254.9	119.3	70.7	0.96	1.003	0.2523	0.1480
135	11-05-81	1.4-1.85	-261	68	300.3	2.914	80.35	2.810	0.964	5663	415.5	387.6	966	256.1	115.2	87.3			0.2499	0.1457
135	11-05-81	5.4-5.85	-266	64	299.0	3.057	80.35	2.850	0.932	5625	415.6	378.6	967	255.7	116.6	79.6			0.2519	0.1471
135	11-05-81	10.4-10.85	-268	63	297.1	3.218	80.35	2.882	0.895	5597	416.3	368.4	962	254.6	119.2	71.3	0.962	0.999	0.2519	0.1491
136	11-05-81	1.40-1.85	-267	68	302.8	3.997	65.36	3.211	0.804	5366	448.3	362.0	970	241.5	145.5	59.2			0.2514	0.1472
136	11-05-81	5.40-5.85	-273	67	301.4	4.107	65.36	3.237	0.788	5327	449.2	356.5	968	240.5	147.8	55.1			0.2515	0.1496
136	11-05-81	10.4-10.85	-275	64	298.8	4.187	65.36	3.231	0.772	5311	448.7	350.4	961	240.0	149.9	51.6	0.953	0.989	0.2494	0.1510
137	11-05-81	1.40-1.85	-262	67	294.3	2.087	65.36	2.609	1.250	5426	393.6	442.4	943	244.2	99.3	148.1			0.2494	0.1448
137	11-05-81	5.40-5.85	-267	64	294.5	2.150	65.36	2.623	1.220	5453	395.6	433.3	948	246.7	101.1	138.8			0.2487	0.1456
137	11-05-81	10.40-10.85	-268	65	295.3	2.217	65.36	2.632	1.187	5503	396.3	424.4	952	249.3	101.0	129.1	0.917	0.955	0.2498	0.1469
138	11-05-81	1.4-1.85	-259	69	408.1	2.920	65.36	3.785	1.296	5715	620.0	563.9	1310	257.8	211.9	155.8			0.2485	0.1466
138	11-05-81	5.4-5.85	-263	65	408.5	3.004	65.36	3.823	1.273	5704	620.3	554.0	1316	258.3	211.8	145.5			0.2515	0.1485
138	11-05-81	10.4-10.85	-263	67	407.1	3.040	65.36	3.833	1.261	5687	619.6	547.2	1313	257.8	212.5	140.1	0.962	0.999	0.2523	0.1501
139	11-09-81	1.4-1.85	-257	69	294.8	2.777	65.36	2.730	0.983	5650	403.4	385.7	937	252.5	108.6	90.9			0.2497	0.1456
139	11-09-81	5.4-5.85	-265	67	296.2	2.792	65.36	2.749	0.985	5646	405.5	385.8	947	253.6	109.3	89.6			0.2507	0.1467
139	11-09-81	10.4-10.85	-266	66	297.3	2.778	65.36	2.744	0.988	5669	406.3	386.0	951	254.8	109.0	88.7	0.943	0.980	0.2503	0.1477
140	11-09-81	1.4-1.85	-258	69	402.2	2.624	65.36	3.626	1.382	5714	598.2	581.8	1288	257.2	196.0	179.6			0.2474	0.1457
140	11-09-81	5.4-5.85	-263	66	403.8	2.697	65.36	3.652	1.354	5739	598.8	571.3	1298	259.3	195.0	167.5			0.2499	0.1475
140	11-09-81	10.4-10.85	-264	64	404.8	2.671	65.36	3.656	1.369	5732	599.0	572.9	1302	259.1	194.2	168.1	0.952	0.989	0.2507	0.1485
141																				
142	11-09-81	1.4-1.85	-255	68	197.3	2.249	65.3	1.795	0.798	5414	242.2	257.4	628	242.3	44.9	60.1			0.2564	0.1453
142	11-09-81	5.4-5.85	-260	67	197.3	2.348	65.3	1.800	0.767	5471	244.1	252.4	632	246.2	46.8	55.1			0.2519	0.1456
142	11-09-81	10.4-10.85	-260	65	196.8	2.448	65.3	1.800	0.735	5521	244.4	247.3	632	259.2	47.6	50.5	0.917	0.956	0.2498	0.1457
143	11-10-81	1.4-1.85	-259	68	299.8	1.795	65.4	2.605	1.452	5258	400.5	502.9	958	236.1	100.7	203.1			0.2477	0.1438
143	11-10-81	5.4-5.85	-265	64	300.2	1.865	65.4	2.613	1.401	5320	402.2	488.3	963	240.0	102.2	188.1			0.2467	0.1438
143	11-10-81	10.4-10.85	-267	63	300.9	1.855	65.4	2.611	1.408	5328	401.9	487.7	966	240.5	101.0	186.8	0.909	0.945	0.2479	0.1448

TABLE IX (cont.)

Test Run	Time sec	MR	Pc psia	$\dot{W}_t$ lb/sec	Compartment Q/A-A_1 Btu/sec-in.2	Compartment Q/A-A_2 Btu/sec-in.2	Compartment Q/A-A_3 Btu/sec-in.2	T_c °R	T_f °R	ΔT °R	DB_f	Cp_s/Cp_f	Cg_s (Shifting Equilibrium) A_1	Cg_s (Shifting Equilibrium) A_2	Cg_s (Shifting Equilibrium) A_3	Cg_f (Frozen Equilibrium) A_1	Cg_f (Frozen Equilibrium) A_2	Cg_f (Frozen Equilibrium) A_3
134	2	2.94	300	3.78	4.347	4.502	3.542	6150	3630	5040	0.00162	1.395	0.0203	0.0211	0.0166	0.0283	0.0294	0.0232
	4	3.01		3.76	4.260	4.397	3.639	6160	3635	5050	0.00162	1.390	0.0200	0.0207	0.0171	0.0279	0.0287	0.0238
	40	3.16		3.76	3.119	3.110	2.684	6165	3638	5055	0.00158	1.380	0.0151	0.0151	0.0130	0.0209	0.0208	0.0180
135	2	2.94	301	3.78	4.347	3.925	3.273	6150	3630	5040	0.00162	1.395	0.0203	0.0184	0.0153	0.0284	0.0256	0.0214
	4	3.02		3.79	4.205	4.051	3.441	6160	3635	5050	0.00162	1.390	0.0197	0.0189	0.0161	0.0273	0.0263	0.0224
	5	3.04		3.78	4.127	4.083	3.370	6160	3635	5050	0.00162	1.388	0.0194	0.0191	0.0158	0.0269	0.0266	0.0219
	60	3.18		3.78	3.113	3.145	2.567	6165	3638	5055	0.00158	1.380	0.0150	0.0152	0.0124	0.0208	0.0210	0.0171
136	2	4.01	304	4.01	3.545	3.371	2.679	6110	3610	5000	0.00144	1.332	0.0188	0.0179	0.0142	0.0250	0.0238	0.0189
	60	4.30		4.02	2.520	1.801	1.521	6070	3590	4960	0.00139	1.315	0.0141	0.0101	0.0085	0.0186	0.0133	0.0112
137	2	2.11	296	3.86	4.796	4.832	3.698	5640	3375	4530	0.00187	1.48	0.0203	0.0204	0.0156	0.0300	0.0302	0.0231
	3	2.12		3.85	4.808	4.951	3.696	5660	3385	4550	0.00187	1.48	0.0203	0.0209	0.0156	0.0300	0.0309	0.0230
	60	2.15		3.84	4.477	4.664	3.161	5700	3405	4590	0.00186	1.475	0.0189	0.0197	0.0133	0.0279	0.0290	0.0197
138	2	2.94	411	5.08	5.082	4.898	3.846	6150	3630	5040	0.00162	1.395	0.0188	0.0181	0.0142	0.0262	0.0252	0.0198
	60	2.92		5.14	3.288	2.688	1.717	6145	3628	5035	0.00162	1.398	0.0120	0.0098	0.0063	0.0168	0.0137	0.0088
139	4	2.81	297	3.73	4.212	4.339	3.325	6125	3618	5015	0.00165	1.405	0.0195	0.0201	0.0154	0.0274	0.0282	0.0216
	6	2.79		3.73	4.120	4.372	3.289	6120	3615	5010	0.00166	1.407	0.0190	0.0201	0.0151	0.0267	0.0283	0.0213
	60	2.76		3.75	3.462	3.863	3.014	6110	3613	5000	0.00167	1.410	0.0158	0.0176	0.0137	0.0223	0.0248	0.0194
140	2	2.66	405	4.99	5.147	5.099	4.006	6080	3595	4970	0.00168	1.418	0.0186	0.0184	0.0145	0.0263	0.0261	0.0205
	60	2.63		5.06	4.063	4.299	3.036	6070	3590	4960	0.00169	1.420	0.0144	0.0153	0.0108	0.0205	0.0217	0.0153
142	4	2.26	200	2.59	3.488	3.285	2.481	5830	3470	4720	0.00180	1.458	0.0204	0.0192	0.0145	0.0298	0.0281	0.0212
	6	2.35		2.56	3.453	3.415	2.685	5910	3510	4800	0.00175	1.448	0.0208	0.0205	0.0161	0.0301	0.0297	0.0234
	60	2.58		2.52	3.545	3.525	2.586	6055	3583	4975	0.00173	1.426	0.0215	0.0213	0.0157	0.0306	0.0304	0.0223
143	5	1.86	302	4.02	5.274	5.245	4.055	5170	3140	4060	0.00195	1.555	0.0222	0.0221	0.0171	0.0346	0.0344	0.0266
	6	1.87		4.01	5.223	5.320	3.917	5200	3155	4090	0.00196	1.553	0.0218	0.0222	0.0163	0.0338	0.0345	0.0254
	60	1.82		4.06	5.353	5.070	3.473	5080	3095	3970	0.00195	1.580	0.0226	0.0214	0.0147	0.0357	0.0338	0.0231

T_{wg} = 1110°R

Chamber Diameter = 3.40 in.

TABLE IX (cont.)

Test Run	Time sec	MR	Pc psia	Compartment Q/A-C_2	Q/A-C_1	Q/A-D_1	Q/A-D_2	Q/A-D_3	Cg_f (Frozen Equilibrium) C_2	C_1	D_1	D_2	D_3	Cg_s (Shifting Equilibrium) C_2	C_1	D_1	D_2	D_3
				Btu/sec-in^2														
134	2	2.94	300	3.929	6.523	10.53	5.920	4.506	0.0204	0.0210	0.0206	0.0133	0.0135	0.0146	0.0150	0.0147	0.00951	0.00967
	40	3.16	"	3.139	4.798	7.182	5.204	4.867										
	*	3.01-3.50		4.020	6.631	10.77	6.635	5.496	0.0211	0.0215	0.0192	0.0136	0.0152	0.0148	0.0151	0.0135	0.0096	0.0107
135	2	2.94	301	4.016	6.564	10.68	5.975	4.533	0.0209	0.0211	0.0209	0.0134	0.0136	0.0150	0.0151	0.0150	0.0096	0.00973
	60	3.18		3.286	5.025	7.788	5.682	5.026										
	*	2.98-3.27		4.100	6.730	11.01	6.731	5.581	0.0213	0.0217	0.0216	0.0153	0.0191	0.0150	0.0152	0.0152	0.0108	0.0135
136	2	4.01	304	3.879	6.132	10.13	6.581	5.228	0.0218	0.0213	0.0214	0.0160	0.0169	0.0164	0.0160	0.0161	0.0120	0.0127
	60	4.25		3.546	5.534	7.550	5.206	5.293										
	*	4.01-4.18		3.886	6.259	10.13	7.034	6.320	0.0218	0.0219	0.0215	0.0173	0.0207	0.0160	0.0162	0.0158	0.0128	0.0154
137	3	2.12	296	4.378	6.455	9.307	5.329	4.403	0.0218	0.0198	0.0174	0.0114	0.0126	0.0147	0.0134	0.0117	0.00771	0.00852
	60	2.15		3.839	5.646	7.967	5.076	4.489										
	*	2.13-2.21		4.417	6.511	9.478	5.552	4.642	0.0220	0.0200	0.0177	0.0120	0.0134	0.0137	0.0125	0.0111	0.0075	0.0085
138	2	2.94	411	4.546	8.052	12.46	6.852	4.958	0.0187	0.0204	0.0192	0.0121	0.0117	0.0134	0.0146	0.0138	0.00869	0.00840
	60	2.92		3.148	5.615	9.264	5.963	5.032										
	*	2.96-3.05		4.576	8.257	13.66	8.001	6.358	0.0188	0.0210	0.0211	0.0143	0.0150	0.0118	0.0131	0.0132	0.0089	0.0094
139	4	2.81	297	4.138	6.666	10.50	6.202	4.771	0.0214	0.0214	0.0205	0.0139	0.0142	0.0153	0.0152	0.0146	0.00987	0.0101
	60	2.76		3.628	5.089	7.726	5.913	4.969										
	*	2.76-2.80		3.327	6.738	10.78	6.402	5.328	0.0173	0.0216	0.0210	0.0143	0.0159	0.0120	0.0150	0.0146	0.0099	0.0111
140	2	2.66	405	4.745	8.113	12.63	6.729	4.774	0.0193	0.0204	0.0193	0.0118	0.0111	0.0136	0.0144	0.0136	0.00834	0.00786
	60	2.63		4.040	6.608	11.09	7.216	5.629										
	*	2.64-2.70		4.745	8.113	12.99	7.802	5.993	0.0189	0.0199	0.0194	0.0133	0.0136	0.0129	0.0133	0.0133	0.0091	0.0093
142	6	2.35	200	3.339	4.804	6.451	3.917	3.604	0.0143	0.0206	0.0168	0.0117	0.0144	0.0101	0.0145	0.0119	0.00826	0.0101
	60	2.58		3.426	4.990	6.868	4.349	4.159										
	*	2.60		3.463	5.003	6.959	4.382	4.168	0.0239	0.0213	0.0180	0.0130	0.0165	0.0163	0.0146	0.0123	0.0089	0.0113
143	5	1.86	302	4.637	6.810	10.26	6.055	4.853	0.0242	0.0220	0.0201	0.0134	0.0146	0.0164	0.0141	0.0129	0.0092	0.00939
	60	1.82		4.386	6.429	9.031	5.374	4.648										
	*	1.87		4.637	6.826	10.27	6.055	4.963	0.0240	0.0218	0.0199	0.0134	0.0148	0.0164	0.0149	0.0136	0.0092	0.0101

Diameter at C_2 = 2.998 in.
Diameter at C_1 = 2.294 in.

Diameter at D_1 = 1.740 in. (Throat)
Diameter at D_2 = 1.878 in.
Diameter at D_3 = 2.206 in.

*Maximum Observed Value For Each Compartment

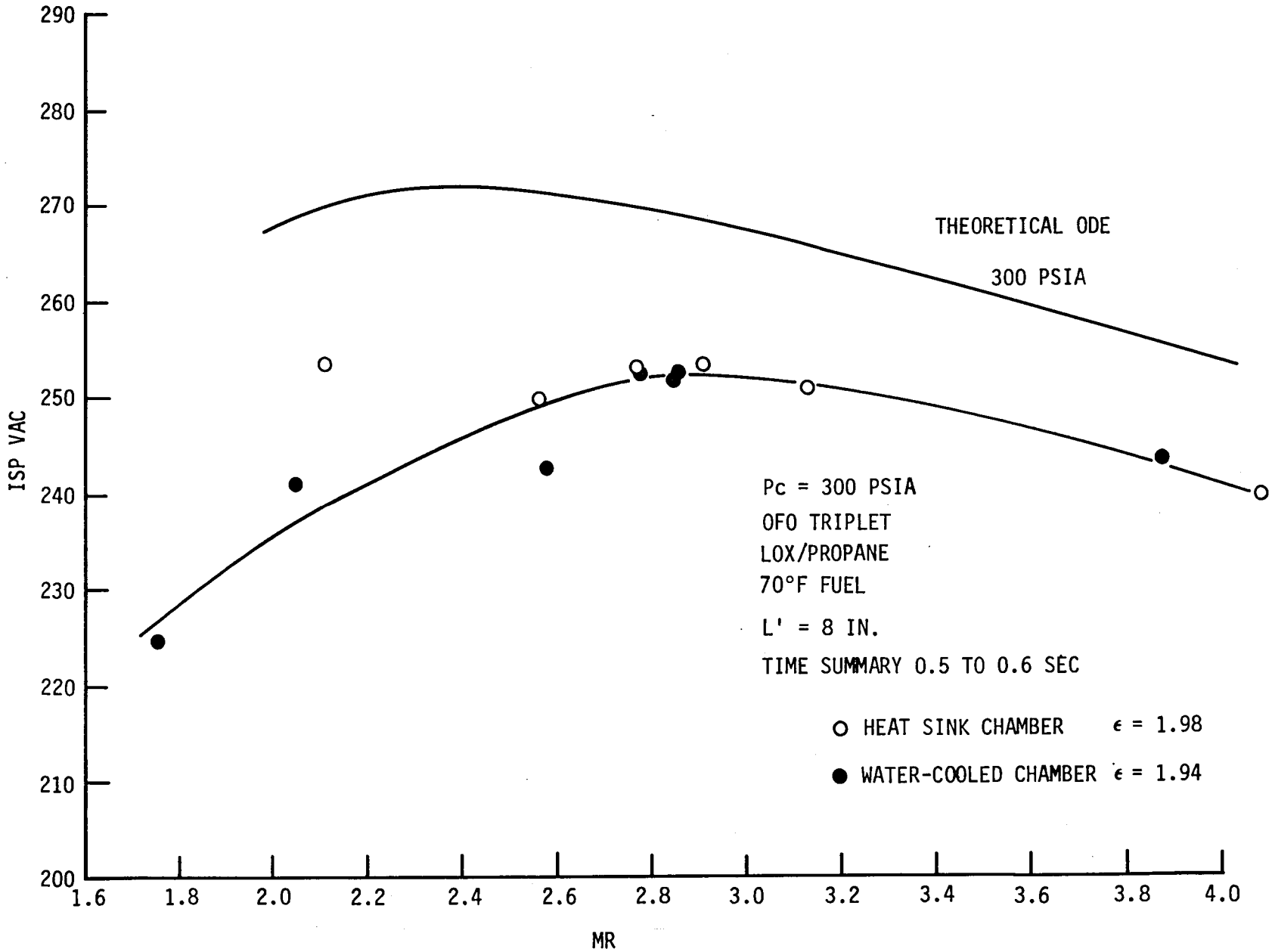

Figure 54. Comparison of Isp Measurements of Heat Sink Chamber and Water-Cooled Chamber

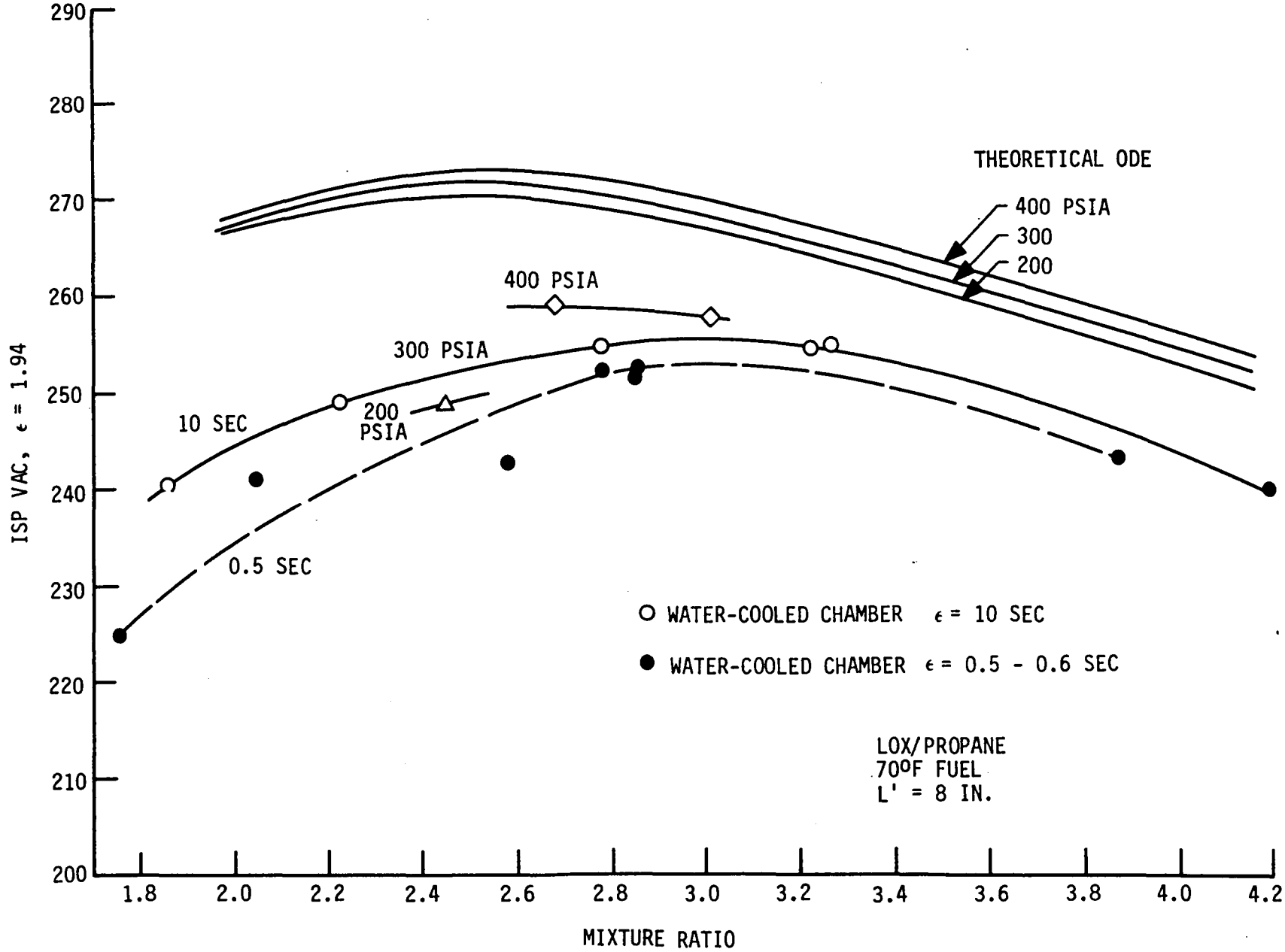

Figure 55. Effect of MR, Pc, and Duration on Isp of OFO Triplet

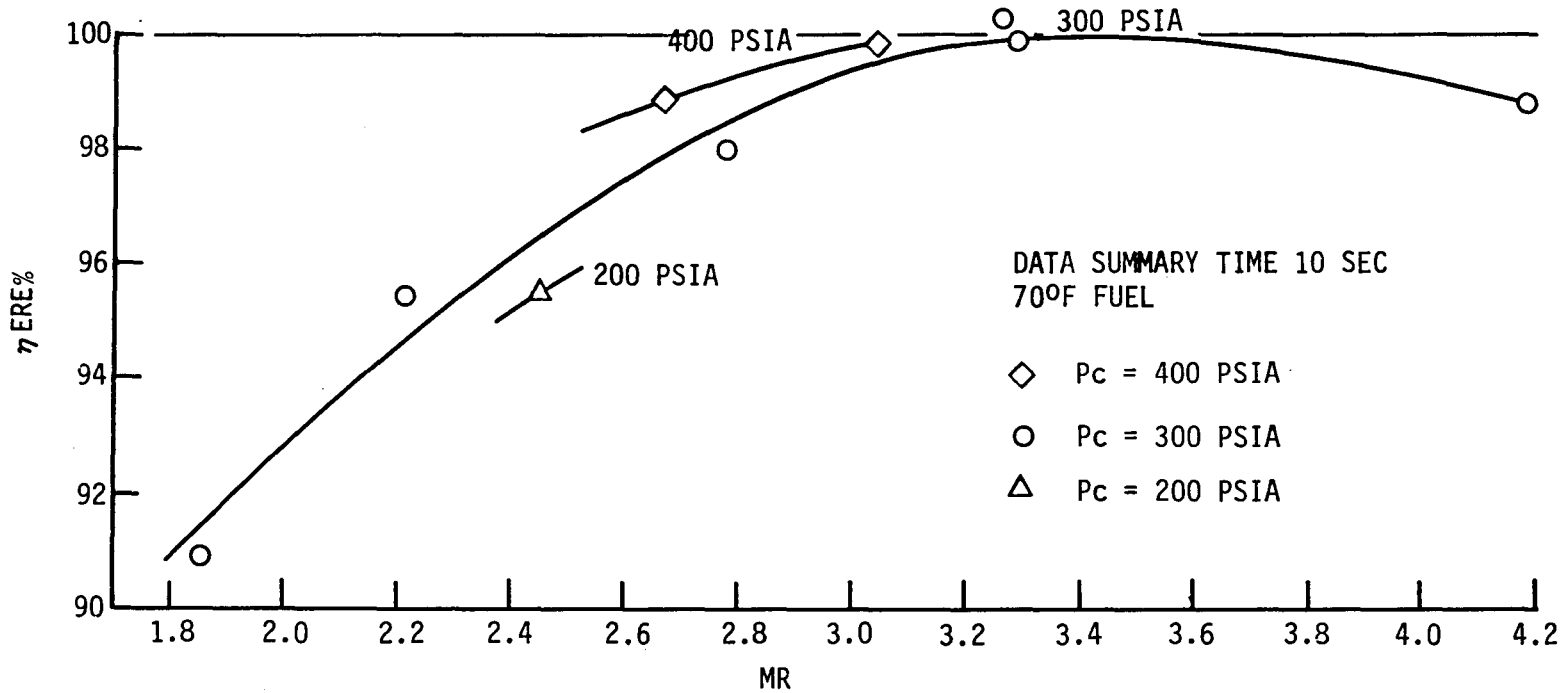

Figure 56. LOX/Propane Energy Release for OFO Triplet Injector in 8-in. L' Chamber

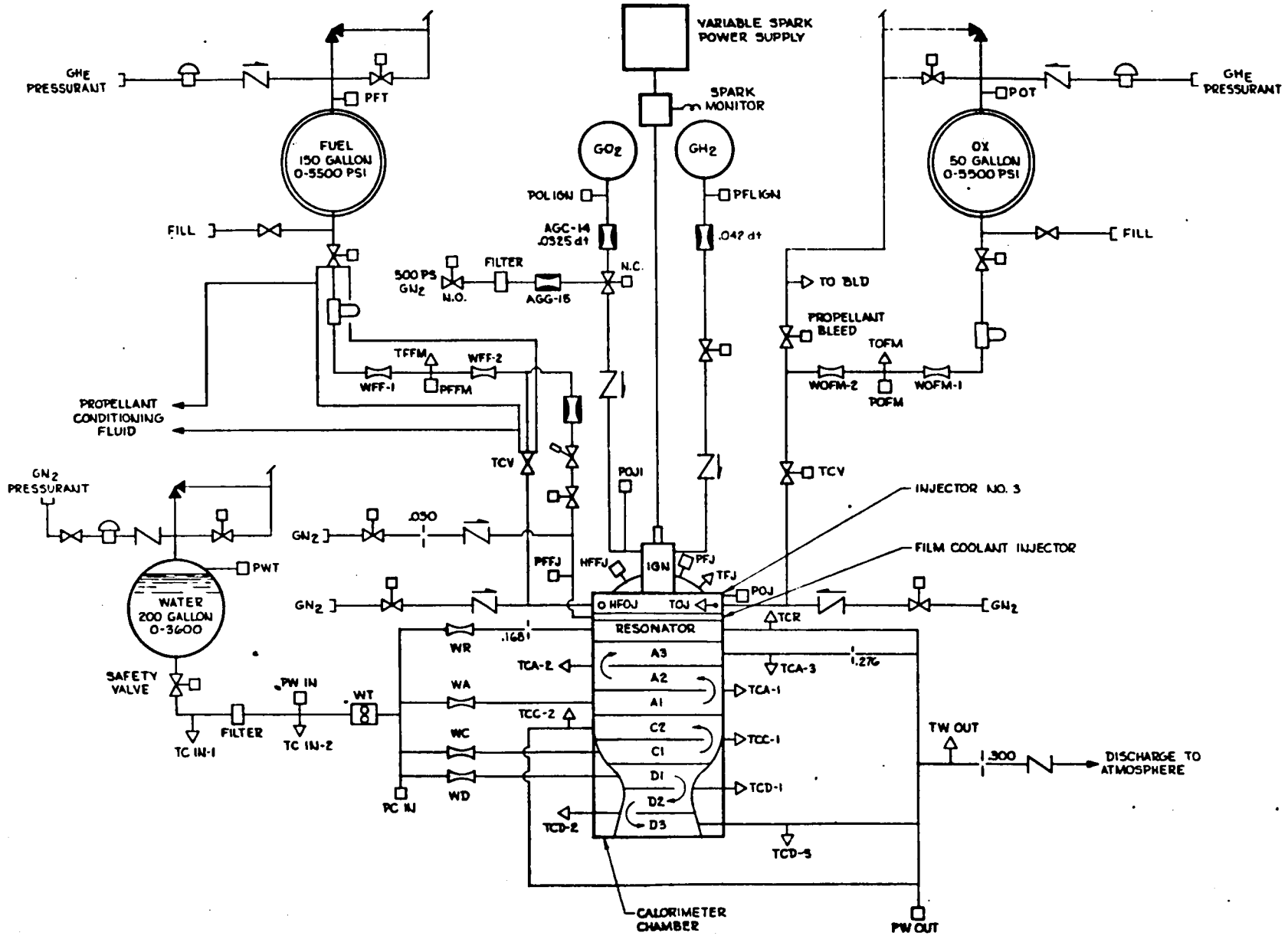

Figure 57. Bay 6 Flow and Instrumentation Schematic for Water-Cooled Chamber with Fuel Film-Cooling

E, Tasks II and IV Subscale Injector Characterization (cont.)

(3) Hardware

This test series utilized the same 40-element OFO triplet injector (Figure 58, Posttest 148), a new film-cooling injector (Figure 59) and the same water-cooled calorimeter chamber. The chamber L' (injector face to throat distance) was increased to 8.7 inches by the addition of the film-cooling injector. The throat area remained at 2.20 in. and the contraction ratio at 4.0. The mating of the film-cooling injector and OFO triplet injector produced a fuel-cooled resonator 0.7 in. deep and 0.085 in. wide. The resonator was an annular cavity without partitions (previous tests employed twelve cavity partitions).

Operation of the preatomized film-cooling injector is illustrated in Figure 60. The liquid streams from thirty-six .015/.016 in. diameter orifices impinge on the outer rim of the main injector, producing a continuous ring of fuel droplets which flow from the resonator cavity parallel to the chamber wall. Figure 60 shows the ring flowing without the injector impingement rim and Figure 61 shows the ring flowing with the splash-rim and 15% of the total flow in the cooling circuit.

The following changes in the water-cooling circuits were made to accommodate the 0.7-in. long film-cooling ring.

° The water flow in the former resonator channels was increased from 0.74 lb/sec to 1.20 lb/sec by increasing the orifice diameter to 0.168 inches. This allows these channels to accept a maximum heat flux of 9 Btu/sec-in.^{2}. This change was required because these channels moved to a higher heat flux position downstream of the injector face when the film-cooling injector was inserted between the injector and chamber. The resonator circuit orifice was also moved from the discharge side of the cooling passage to the inlet side. This reduced the pressure on a repaired braze joint from 1065 psia to 750 psia.

° The discharge orifice on the total water circuit was increased from 0.290 to 0.300 in. to accommodate the higher overall flowrate, 6.28 versus 5.8 lb/sec.

(4) Cold-Flow

Photographs showing the operation of the film-cooling injector are provided in Figures 60 and 61.

(5) Summary of Hot-Fire Film-Cooling Tests With LOX/Propane

Tables X and XI provide documentation of the test parameters, measured performance, and thermal data. The following paragraphs provide a narrative of the individual tests.

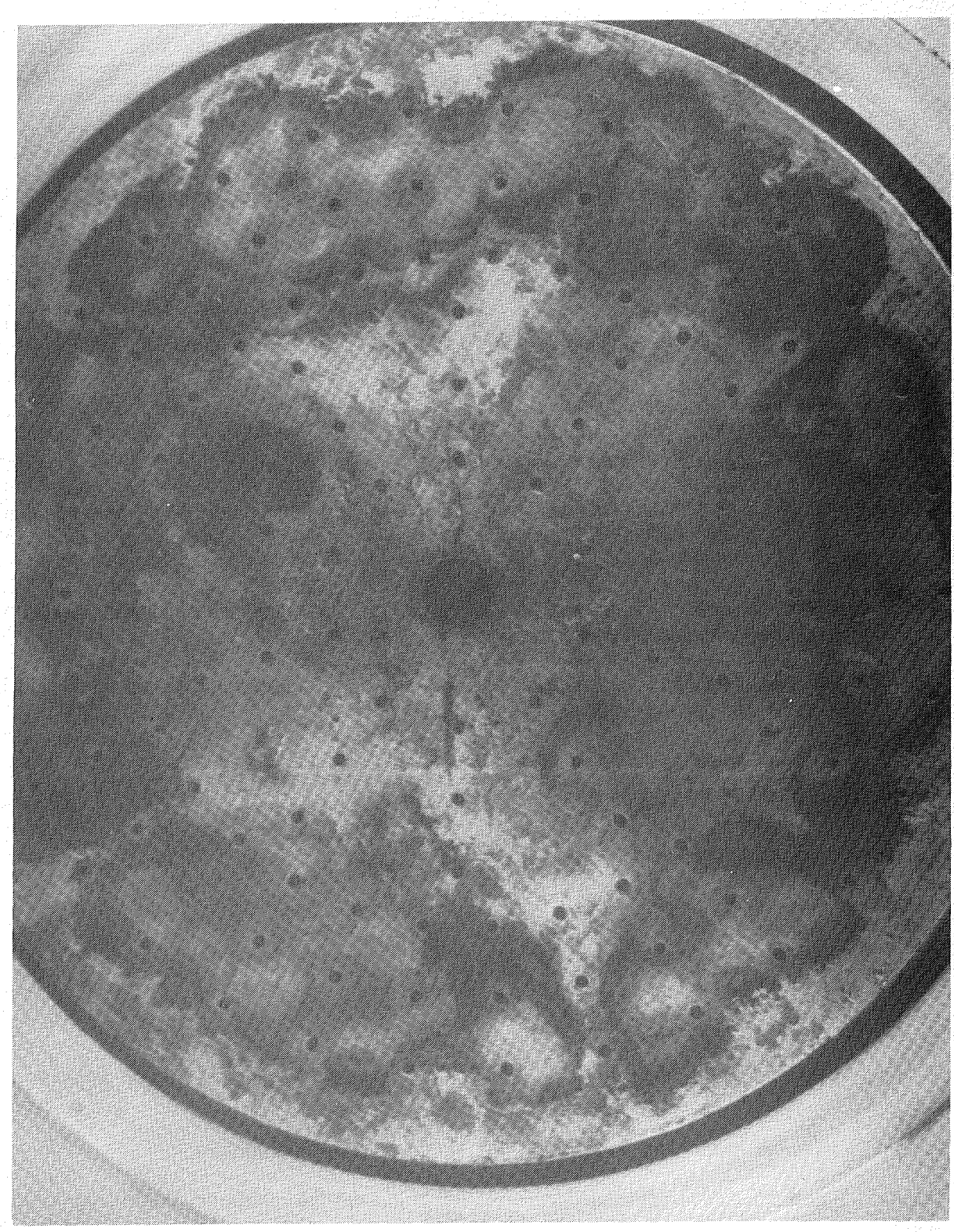

Figure 58. 40-Element OFO Triplet Injector, P/N 1193287, at the Start of Test Series 4

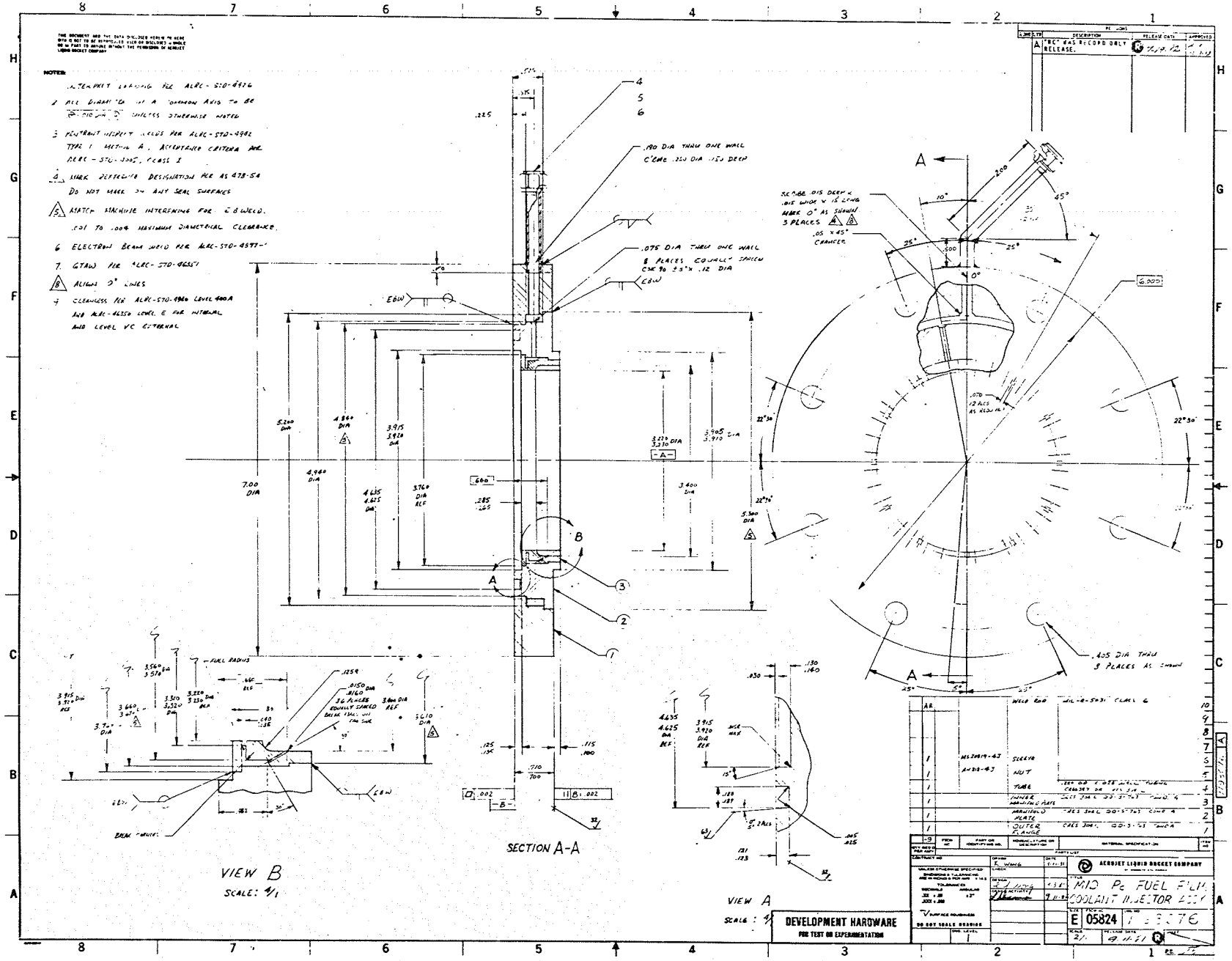

Figure 59. Mid Pc Fuel Film Coolant Injector Assembly

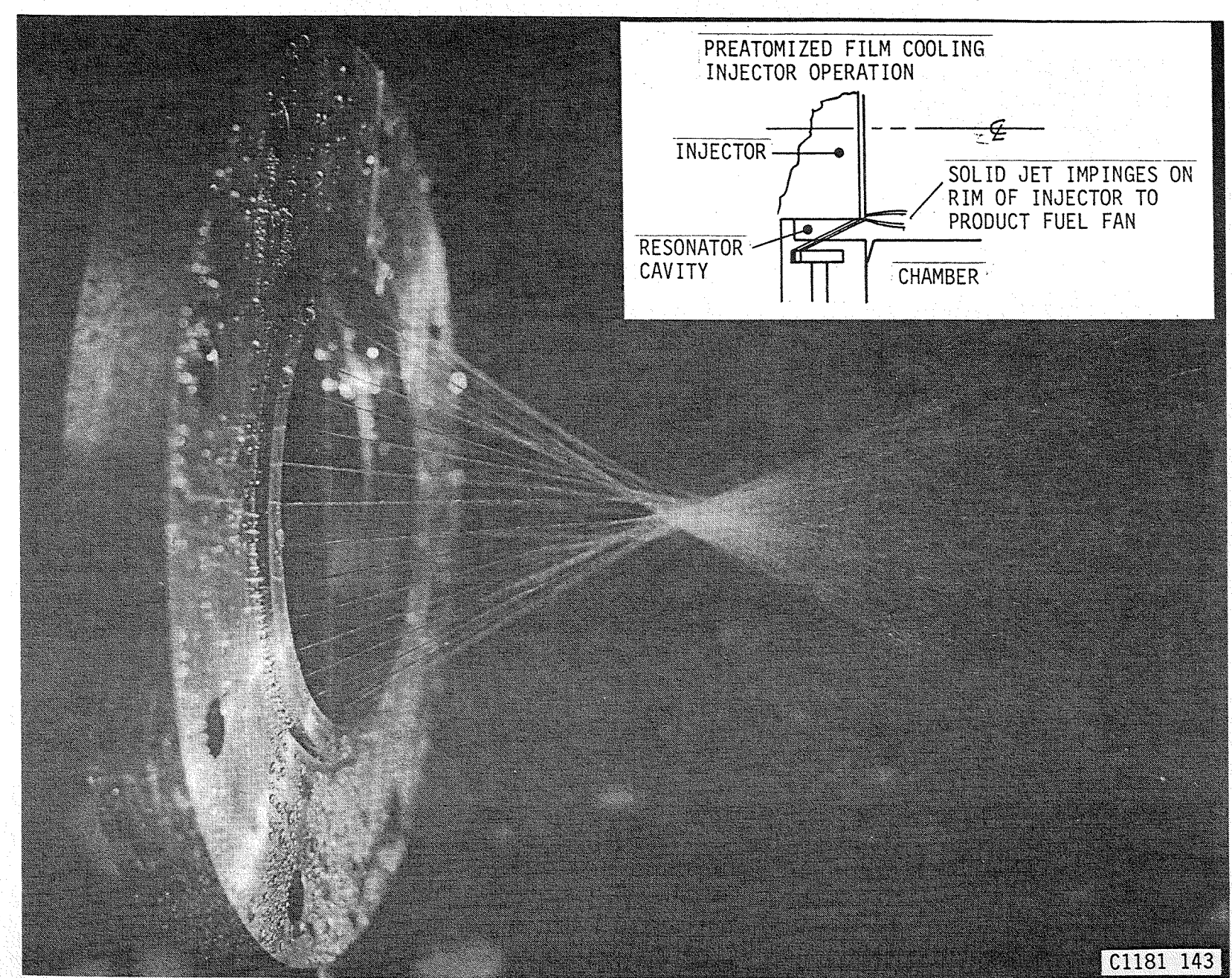

Figure 60. Cold Flow of 36-Orifice FFC Ring

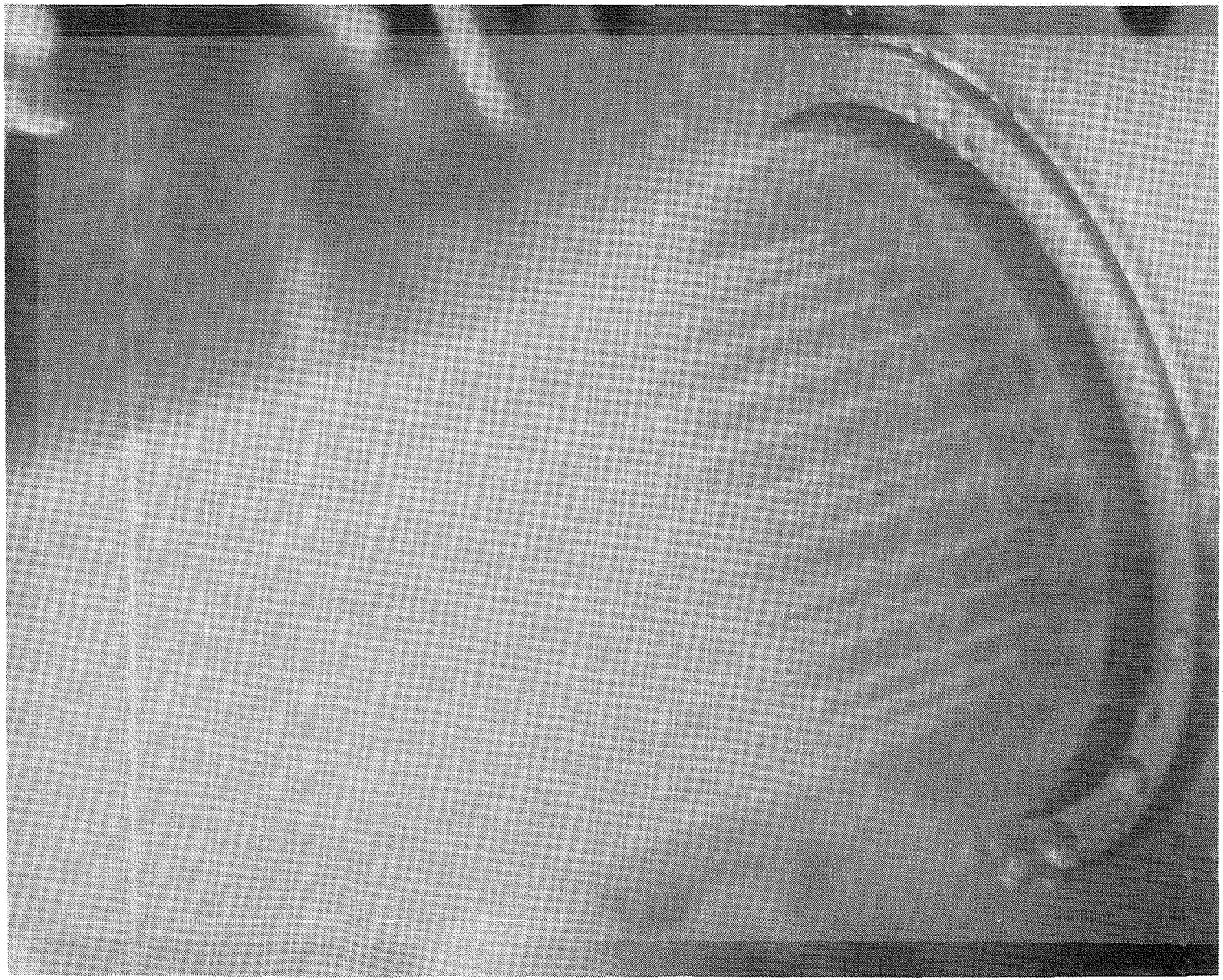

Figure 61. OFO Triplet Injector and Film-Cooling Injector, P/N 1193676, with Fuel Flowing

TABLE X

OFO TRIPLET INJECTOR (INJECTOR #3) PERFORMANCE DATA SUMMARY OF TEST SERIES #3 - WATER-COOLED CALORIMETER CHAMBER, WITH FFC (INJECTOR #4), LOX/PROPANE

Test No.	Date	Data Summary Period (sec)	Propellant Flow ToJ (°F)	TfJ (°F)	PoJi (Pc) (psia)	MR Eng	MR_c	$\dot{W}_o$ (lb/sec)	$\dot{W}_{f_T}$ (lb/sec)	$\dot{W}_{FFC}$ (lb/sec)	$\dot{W}_{FC}/\dot{W}_{ft}$	PoJ (psia)	PfJ (psia)	ΔPoJ (psi)	ΔPfJ (psi)	F_{VAC} (lbF)	C*	Isp_{vac}	ERE	Kw_{oj}	Kw_{fj}	Kw_{FFC}
144	1-13-82	1.40-1.85	-239.3	54.5	192.11	-		1.617	-	0.239	-	433.69	366.86	241.58	174.75	611.56	-	-	-	0.0986	-	0.0313
		3.30-5.30	-266.8	51.4	254.45	1.553	1.854	2.164	1.393	0.204	0.146	420.48	381.61	166.03	127.16	800.31	5066	225.04	.9211	0.1568	0.1468	0.0314
145	1-14-82	1.40-1.85	-267.0	45.1	302.88	2.284	2.674	2.743	1.201	0.175	0.146	407.28	397.10	104.40	94.2	964.66	5438	244.61	.9341	0.2522	0.1465	-
		3.30-5.30	-274.2	43.6	307.58	2.275	2.664	2.752	1.210	0.176	0.146	409.49	400.19	101.69	92.61	975.09	5497	246.10	.9405	0.2561	0.1488	0.0310
146	1-14-82	1.30-1.85	-256.4	47.0	300.03	2.270	2.748	2.706	1.192	0.174	0.146	407.06	393.85	107.03	93.82	955.96	5452	245.29	.9377	0.2500	0.1459	-
		5.30-5.85	-263.9	44.0	303.15	2.255	2.733	2.718	1.205	0.175	0.145	409.08	396.75	105.93	93.60	967.75	5472	246.67	.9433	0.2522	0.1476	0.0307
		10.30-10.85	-266.2	44.3	304.34	2.252	2.726	2.717	1.207	0.174	0.144	409.37	396.82	105.03	92.48	971.33	5492	247.55	.9467	0.2531	0.1489	0.0305
		20.30-20.85	-267.4	44.7	306.75	2.241	2.710	2.715	1.212	0.173	0.143	409.29	396.34	102.54	89.59	971.78	5532	247.49	.9458	0.2560	0.1522	0.0306
		68.31-70.31	-270.6	45.2	306.26	2.559	2.559	2.737	1.070	-	-	410.00	399.41	103.74	93.15	974.26	5697	255.94	.9773	0.2565	0.1537	-
147	1-14-82	1.30-1.85	-261.7	47.7	306.23	1.585	1.856	2.648	1.671	0.244	0.146	405.10	486.70	98.87	180.47	975.26	5020	225.81	.9192	0.2526	-	-
		5.30-5.85	-276.7	44.6	311.89	1.571	1.840	2.614	1.664	0.243	0.146	410.00	489.32	98.11	177.43	993.34	5162	232.20	.9489	0.2496	-	0.0309
		10.30-10.85	-277.3	44.2	311.82	1.547	1.811	2.606	1.685	0.246	0.146	409.60	492.61	97.78	180.79	995.89	5145	232.09	.9503	0.2496	-	0.0316
		20.3-20.85	-277.7	44.0	314.79	1.531	1.793	2.601	1.699	0.248	0.146	409.11	495.14	94.32	180.35	995.42	5182	231.49	.9490	0.2538	-	0.0315
		53.32-55.32	-277.3	44.1	312.41	1.779	1.779	2.632	1.479	-	-	409.69	499.95	97.28	187.54	995.46	5359	242.17	.9599	0.2533	0.1497	-
148	1-14-82	1.30-1.85	-259.9	50.1	304.18	3.572	4.163	3.176	0.889	0.127	0.142	443.60	333.58	139.42	29.40	973.43	5298	239.45	.9559	0.2568	0.1956	-
		5.30-5.85	-267.9	47.5	303.18	3.802	4.426	3.219	0.847	0.120	0.141	444.65	325.14	141.47	21.96	969.18	5281	238.40	.9629	0.2584	0.2155	0.0286
		10.30-10.85	-267.0	44.8	302.09	3.755	4.419	3.199	0.852	0.120	0.141	442.13	325.46	140.04	23.37	968.87	5281	239.19	.9642	0.2581	0.2100	0.0307
		20.30-20.85	-267.9	44.8	309.19	3.634	4.226	3.189	0.878	0.123	0.140	447.39	331.89	138.20	22.70	982.48	5384	241.60	.9683	0.2591	0.2196	0.0309
		43.31-45.31	-268.7	44.1	306.66	4.038	4.038	3.209	0.795	-	-	446.09	335.27	139.43	28.61	976.36	5423	243.84	.9979	0.2597	0.2060	-
149	1-14-82	1.30-1.85	-253.3	50.1	302.50	2.361	2.580	2.766	1.172	0.0994	0.085	403.03	382.62	100.53	80.12	964.87	5439	245.01	.9348	0.2628	0.1668	-
		5.30-5.85	-270.1	45.9	306.21	2.497	2.726	2.759	1.105	0.0933	0.084	408.08	372.39	101.87	66.18	980.43	5611	253.70	.9684	0.2598	0.1728	0.0274
		10.30-10.85	271.1	45.9	305.43	2.499	2.728	2.757	1.103	0.0922	0.084	408.08	370.17	102.65	64.74	978.72	5602	253.51	.9677	0.2589	0.1746	0.0293
		20.30-20.85	-272.0	44.8	309.13	2.471	2.695	2.750	1.113	0.0924	0.083	408.50	372.49	99.37	66.36	982.77	5667	254.44	.9705	0.2627	0.1778	0.0292
		43.31-45.31	-272.0	43.7	308.06	2.622	2.622	2.749	1.048	-	-	407.59	374.67	99.53	66.61	981.67	5745	258.55	.9893	0.2627	0.1781	-
150	1-14-82	No Data																				
151	1-14-82	1.30-1.85	-253.8	49.2	203.94	1.913	2.243	1.823	0.953	0.140	0.147	244.23	252.27	40.29	48.33	648.66	5202	233.66	.9201	0.2746	0.1628	-
		5.30-5.85	-267.9	47.1	205.56	1.987	2.329	1.810	0.911	0.134	0.147	245.07	246.37	39.51	40.81	648.77	5349	238.40	.9324	0.2730	0.1690	0.0294
		10.30-10.85	-272.4	45.9	203.94	2.097	2.456	1.834	0.875	0.127	0.146	246.22	242.15	42.28	38.21	651.21	5330	240.35	.9317	0.2674	0.1679	0.0300
		20.30-20.85	-272.1	44.1	206.29	2.112	2.470	1.805	0.855	0.124	0.145	246.64	238.78	40.35	32.49	651.43	5493	244.94	.9488	0.2697	0.1779	0.0302
		48.32-50.32	-274.7	43.1	205.31	2.401	2.401	1.844	0.768	-	-	246.54	242.19	41.23	36.88	653.05	5566	250.04	.9583	0.2727	0.1753	-
152	1-14-82	1.30-1.85	-263.7	50.3	408.10	2.156	2.555	3.611	1.674	0.261	0.156	582.82	553.91	174.72	145.00	1299.2	5468	245.83	.9432	0.2589	0.1629	-
		5.30-5.85	-273.9	47.2	414.42	2.187	2.588	3.598	1.645	0.255	0.155	589.96	549.69	175.54	135.27	1319.3	5598	251.65	.9638	0.2574	0.1658	0.0341
		10.30-10.85	-275.0	47.2	413.17	2.156	2.548	3.591	1.666	0.257	0.154	588.28	552.22	175.11	139.05	1318.3	5566	250.35	.9606	0.2575	0.1658	0.0352
		20.30-20.85	-273.9	46.1	416.46	2.107	2.488	3.584	1.701	0.260	0.153	589.96	560.66	173.50	144.20	1324.95	5579	250.68	.9651	0.2585	0.1664	0.0351
		43.31-45.31	-275.2	45.7	413.24	2.429	2.429	3.599	1.482	-	-	589.44	565.87	176.20	152.63	1318.25	5759	259.45	.9859	0.2579	0.1663	-

TABLE XI

LOCAL HEAT FLUX DATA FOR OFO TRIPLET INJECTOR

Axial Distance:					0.5	2	4	6	7.5	8.5	9	9.5	10				
					Heat Flux Btu/sec in.^{2}												
Test Run	Start Time	Eng. MR	Pc	Wt	QR	QA-3	QA-2	QA-1	QC-2	QC-1	QD-1	QD-2	QD-3	Total Q Btu/sec	Core MR	%FFC	WFC
146	2.0	2.26	300	3.89901	1.09	3.15	3.06	2.43	2.29	3.16	4.18	2.72	1.96	258		.146	.174257
	10	2.25	304	3.92201	1.27	2.81	2.13	1.54	1.33	2.15	4.11	2.54	2.01	215	2.63	.144	.173763
	20	2.24	306	3.92815	1.18	2.06	1.20	1.26	1.28	2.52	4.03	1.67	1.57	189	2.61	.142	.172848
	FS-2	2.55	306	3.80825	2.81	2.81	2.30	3.17	2.73	5.02	6.92	3.71	2.56	337		0	0
147	2.0	1.59	306	2.64876	0.71	2.52	2.47	2.28	2.20	2.84	4.14	2.52	1.82	215		14.6	.244062
	10	1.54	311	2.60488	0.79	2.34	1.79	1.52	1.48	1.90	3.53	2.12	1.85	186	1.8*	14.6	.246013
	20	1.53	314	2.60240	0.87	2.09	1.44	1.26	1.61	1.79	3.15	1.95	1.79	164	1.8*	14.6	.247895
	FS-2	1.78	312	4.11402	3.13	4.82	4.90	4.45	3.72	5.34	8.13	5.21	3.52	455		0	0
148	2.0	3.62	304	4.06126	0.77	2.51	2.88	2.50	2.27	3.14	4.99	3.77	2.67	244		.142	.126656
	10	3.75	302	4.05066	0.82	1.93	1.78	1.65	1.82	2.85	4.88	4.25	3.34	201	4.37	.141	.120153
	20	3.63	309	4.06661	0.71	1.63	.98	1.45	1.70	2.75	4.15	3.64	3.14	172	4.23	.140	.123237
	FS-2	4.04	306	4.00331	1.40	1.95	1.69	2.69	3.29	5.45	9.32	7.43	5.39	282		0	0
149	2.0	2.41	302	3.92563	1.36	3.44	2.99	2.86	2.90	4.07	5.87	3.89	2.69	287		.084	.099361
	10	2.50	305	3.86073	1.42	3.28	2.57	2.30	2.23	3.13	4.93	4.00	2.66	269	2.73	.083	.092214
	20	2.47	309	3.86248	1.52	2.82	2.13	2.21	2.01	3.02	4.57	3.35	2.70	250	2.70	.083	.092403
	FS-2	2.61	308	3.79591	2.48	3.38	3.17	3.28	2.87	4.41	6.09	4.89	3.91	339		0	0
151	2.0	1.94	203	2.78965	0.54	1.94	2.02	1.99	1.89	2.60	3.44	2.15	1.59	177		.147	.140218
	10	2.09	203	2.70938	0.69	2.05	2.01	1.85	1.75	2.27	2.82	1.85	1.62	188	2.45	.145	.127426
	20	2.11	206	2.65952	0.58	1.94	1.84	1.35	1.62	1.87	2.91	1.56	1.41	172	2.47	.144	.123691
	FS-2	2.39	205	2.61055	2.81	3.18	3.28	3.25	2.84	4.06	5.14	3.65	3.67	321	-	0	0
152	2.0	2.17	408	5.25099	1.24	3.68	3.00	2.62	2.06	3.20	5.65	3.47	2.41	283		.155	.260970
	10	2.15	413	5.25659	1.33	3.02	1.93	1.76	2.23	3.31	6.16	3.67	2.80	237	2.55	.154	.256975
	20	2.10	416	5.28544	1.14	2.72	1.55	1.72	2.54	3.85	6.01	3.57	2.40	226	2.49	.152	.260055
	FS-2	2.42	413	5.07460	3.15	5.10	5.07	4.36	4.15	6.93	10.36	5.85	4.26	495	-	0	0

*Estimated

Wt = Total propellant flowrate

E, Tasks II and IV Subscale Injector Characterization (cont.)

Test 144

The series started with Test No. 144. This was a 5 second checkout test with the engine balanced to provide a chamber pressure of 300 psia and a core mixture ratio of 2.8 plus 14% fuel film- cooling. The actual engine core MR was 1.55 rather than the anticipated value of 2.8 and the Pc was 254 rather than 300 psia. The percent fuel cooling was 14.6% as expected. Data analyses indicated that low oxygen flow, due to a high resistance in the oxygen circuit of the injector, was responsible for the low MR. The chamber pressure was only 85% of the expected value. Postfire inspection of the injector indicated the presence of moisture in the oxidizer manifold. A period of heavy rain and high humidity had preceded the test series, and apparently the moisture froze on contact with the LOX, thereby blocking some of the injector orifices.

Test 145

A hot GN_2 purge of the oxygen manifold was applied prior to this test which employed the same tank pressure settings as the previous test. The resulting core MR was 2.6 (engine MR = 2.2) and the oxidizer flow resistance returned to the original value. Posttest engine inspection showed only a light oily soot film on the chamber wall rather than the expected heavy carbon deposits.

Test 146

This test was a repetition of Tests 144 and 145 with tank pressure settings for a duration of 70 seconds. At 61 seconds into the test, the film-cooling valve was closed. This allowed an additional 9 second data sample for direct comparison of Isp and heat flux with and without film-cooling. Posttest data evaluation indicated that steady-state water temperatures were attained in 40 seconds with the film-cooling flowing. The duration of the subsequent tests was reset to 50 seconds with film- cooling and a 5 seconds period without film-cooling.

Test 147

This test was a 50 + 5 second duration test at 14% FFC and a low core MR (1.8). The tank pressure settings are provided in Tables X and XI. The fuel flowmeter was off-scale for the first 50 seconds in this test and flow values were estimated using the injector flow resistance. Flow data for the last 5 second period were valid; Pc was 312 psia.

Test 148

This test was a 40 + 5 second test at a core mixture of 4.4 (engine MR = 3.6) with 14% fuel film-cooling; Pc was 309 psia. The duration was reduced in order to allow completion of the series without refilling the fuel tank.

E, Tasks II and IV Subscale Injector Characterization (cont.)

The thickness of the carbon deposited on the injector face and chamber wall appeared much greater and more dense after this high MR test. Previous analyses of the deposits removed after a high MR (no film-cooling) test indicated the material to be more than 99+ percent carbon and included traces of copper and nickel. The fuel manifold pressure (PfJ) was invalid on this test.

Test 149

This was a 40 + 5 second, 305 psia test at a core MR of 2.7 and an engine MR of 2.5. The fuel film-cooling was 8.4%.

Test 150

This was a low Pc test which was terminated automatically (prior to ignition) by the computer because of a delayed opening of the water cooling valve.

Test 151

This was a repeat firing for 40 + 10 seconds at a Pc of 204 psia. The core MR was 2.5 and the engine MR was 2.0. The fuel film-cooling percentage during the first 40 seconds was 14.5. There was no film-cooling for the final 10 seconds of this test.

Test 152

This was a high pressure (410 psia) test at a core MR of 2.6 and an engine MR of 2.2 with 15.4 percent film-cooling. The test duration was 40 seconds with film-cooling and 5 seconds without.

Posttest inspection of the engine after the last test showed clean areas around each fuel orifice and heavy buildup around the inner row oxidizer elements, especially at the bottom of the manifold. The resonator cavity was significantly cleaner, in terms of carbon, compared to the previous test series without film-cooling. It is possible that all the carbon observed resulted from the last 5 seconds of operation in Test -152 where the film-cooling was off.

Posttest inspection of the engine showed all seals and joints to be leak free and all components in good condition. The chamber was cleaned with copper cleaner after the test series was completed. The resulting surface had a silver grey color, possibly indicating exposure of the nickel sublayer of the laminated chamber I.D. The chamber I.D. did not have the copper color which would normally be expected. No dimensional changes at the throat were indicated by the posttest measurements (<.001 in.).

E, Tasks II and IV Subscale Injector Characterization (cont.)

(6) Thermal Results

(a) Calculated Time-Dependent Heat Flux

The measured heat flux versus time values for each test (Tests 144 through 152) are provided in Figures 62 through 69. Table XI summarizes the data at selected time periods. The last data summary period (FS-2) for each test corresponds to the last one second of burn; i.e., no film-cooling.

(b) Axial Flux Profiles

The data from Table XI are cross-plotted as heat flux versus axial distance in Figures 70 through 75. Each figure represents a different test condition, i.e., Pc, MR or % film-cooling. Four curves are shown on each plot. The lowest heat flux curve corresponds to the profile with the indicated fuel film-cooling flow 20 seconds into the burn. This represents a steady-state condition for most parameters. The curve labeled FS-2 provides the profile 5 seconds after the film-cooling flow is terminated (10 seconds in the case of Test 151.) As noted in the previous figures, this higher flux may not be a steady-state value. These data show that any carbon buildup on the wall from the film-cooling is quickly removed when the cooling is terminated.

The highest heat flux profile labeled "Max, no FFC" in these same figures is obtained from the previous test series (133-144) where the engine (8-in. L' chamber) was operated without film- cooling and peak values were reached early in the test before the carbon deposits could build up. The fourth curve, labeled "SS, no FFC" provides the steady state heat flux profiles from previous tests without fuel film-cooling after firing durations of approximately 60 seconds. The latter two curves for the no film-cooling tests were generated from the data shown in Figure 76 for 300 psia operation and in Figure 77 for other pressures. Constant core mixture ratio was selected for the thermal comparisons in Figures 70 through 75.

(c) Peak Heat Flux Values

The cycle life and cooling requirements for a regeneratively cooled chamber are controlled by the peak throat heat flux. Throat heat flux values for a typical 300 psia operating pressure and core mixture ratio of 2.6 $\pm$ 0.1 are as follows:

Maximum at startup without film-cooling	10.8 Btu/sec-in.^{2}
Steady-state without film-cooling	7.5 Btu/sec-in.^{2}
Maximum/steady-state with 8.4% film-cooling	7.0/4.2 Btu/sec-in.^{2}
Maximum/steady-state with 14.4% film-cooling	4.5/4.0 Btu/sec-in.^{2}

The use of 8.4% film-cooling would reduce the peak operating flux from 10.8 to 7.0 Btu/sec, or 35%, while 14.4% would reduce the flux by 58%.

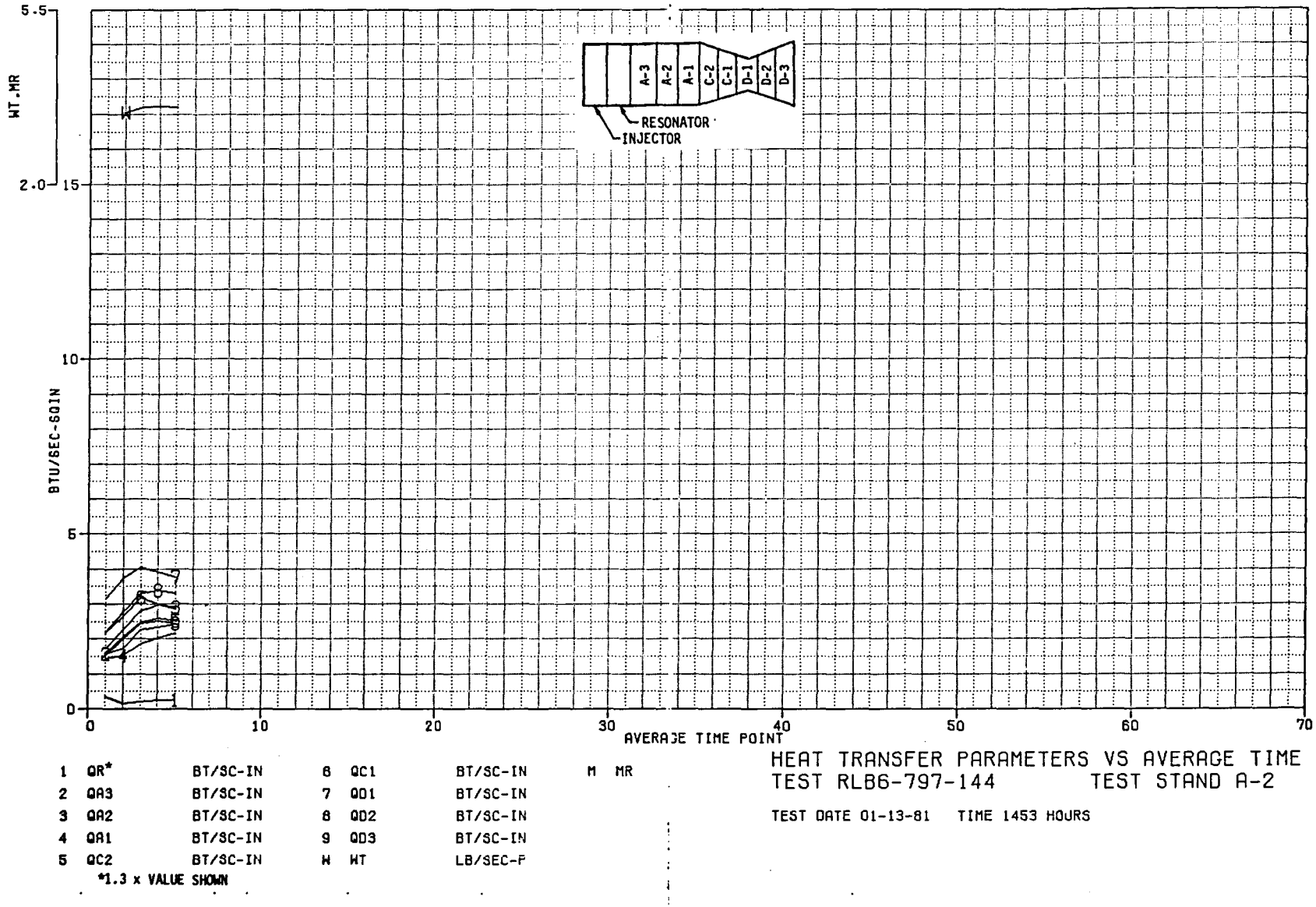

Figure 62. Heat Transfer Parameters Versus Average Time, Test -144

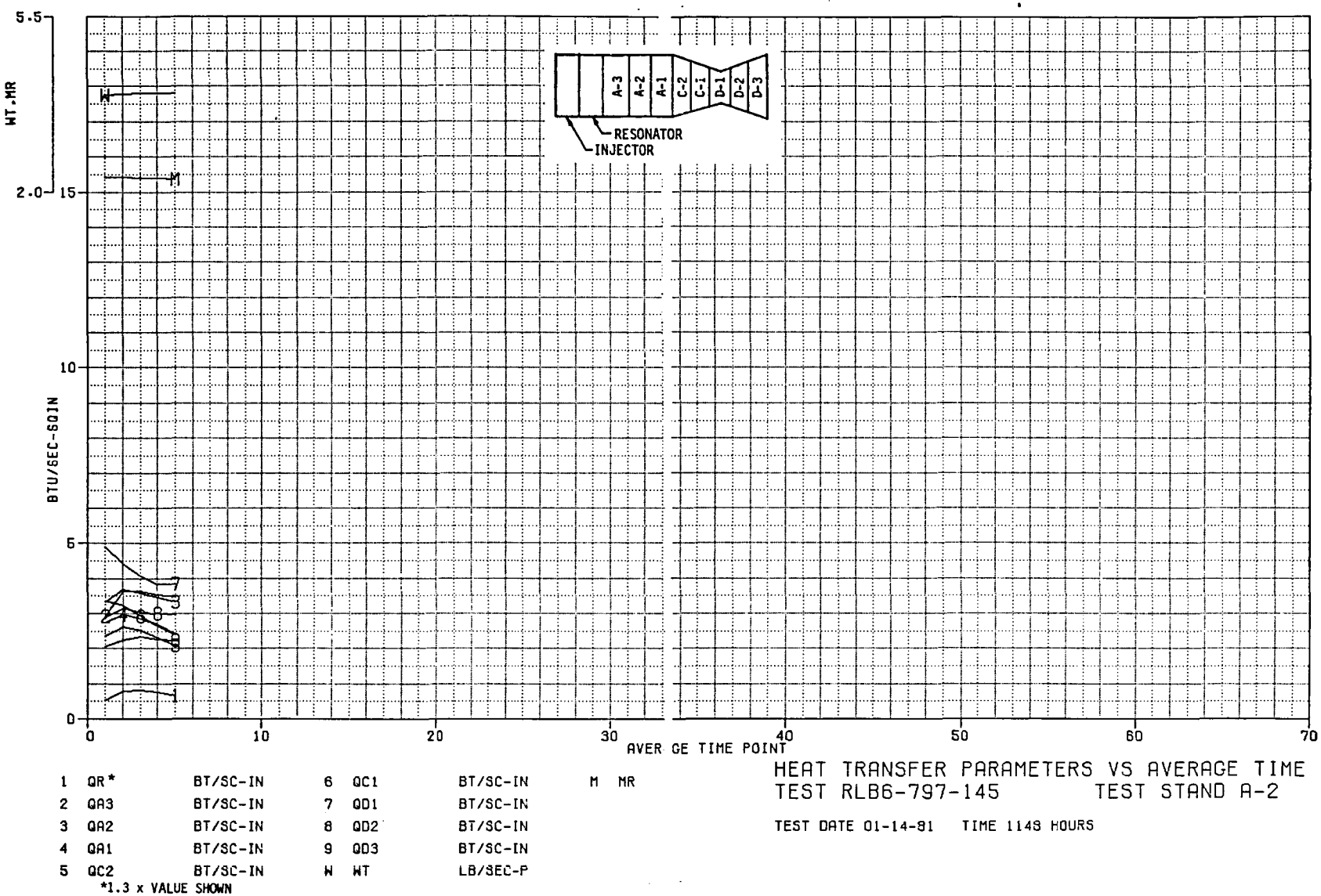

Figure 63. Heat Transfer Parameters Versus Average Time, Test -145

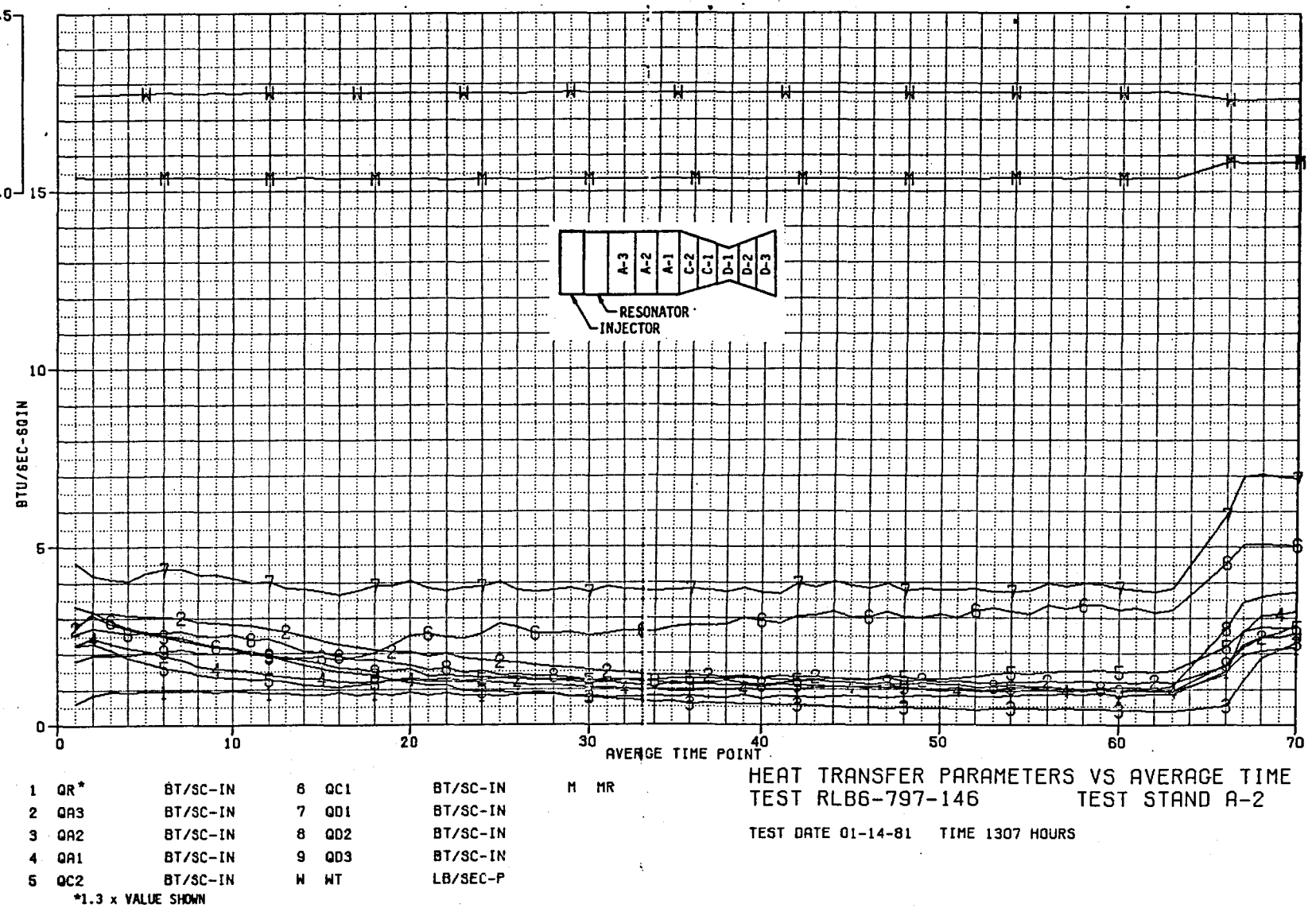

Figure 64. Heat Transfer Parameters Versus Average Time, Test -146

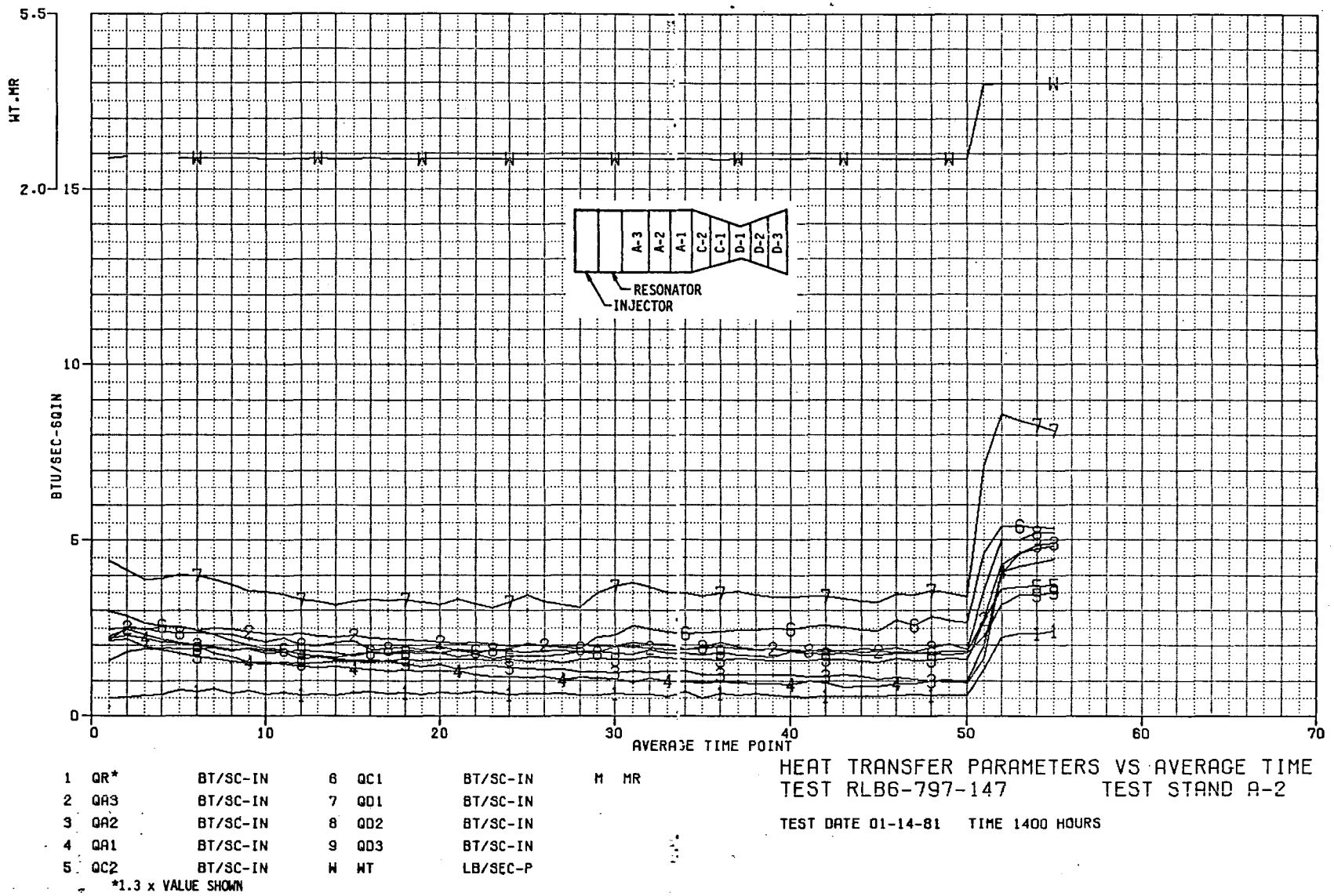

Figure 65. Heat Transfer Parameters Versus Average Time, Test -147

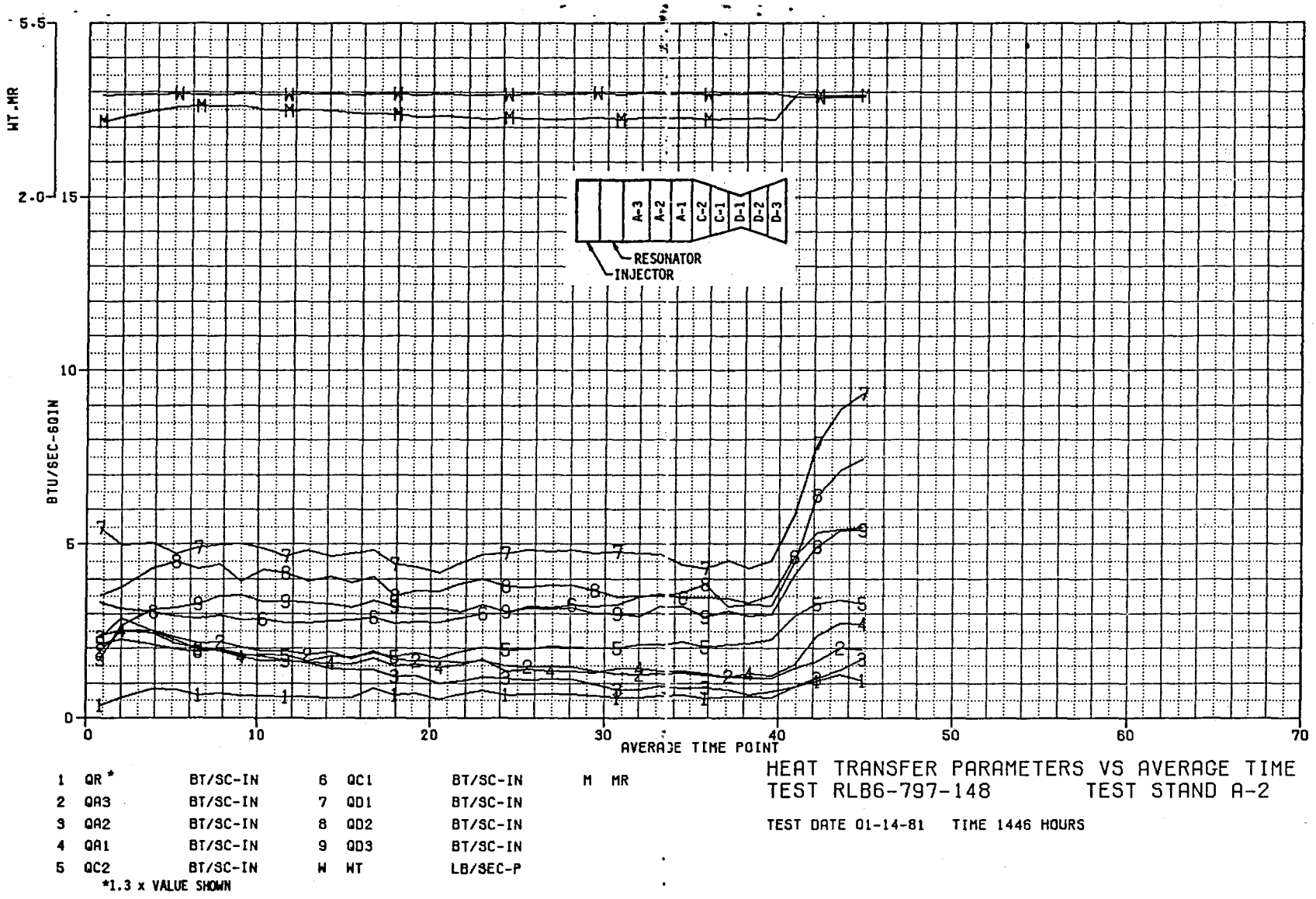

Figure 66. Heat Transfer Parameters Versus Average Time, Test -148

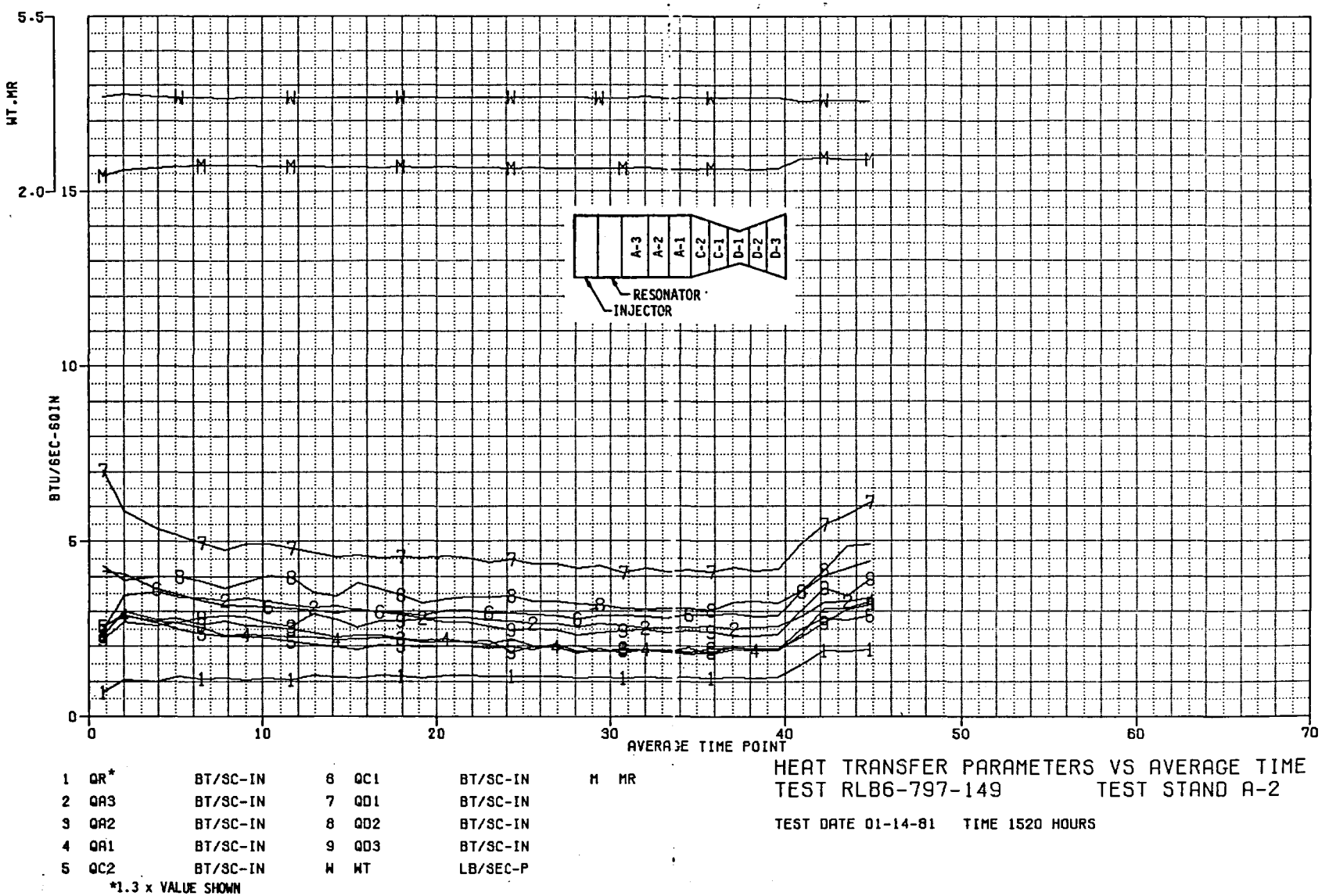

Figure 67. Heat Transfer Parameters Versus Average Time, Test -149

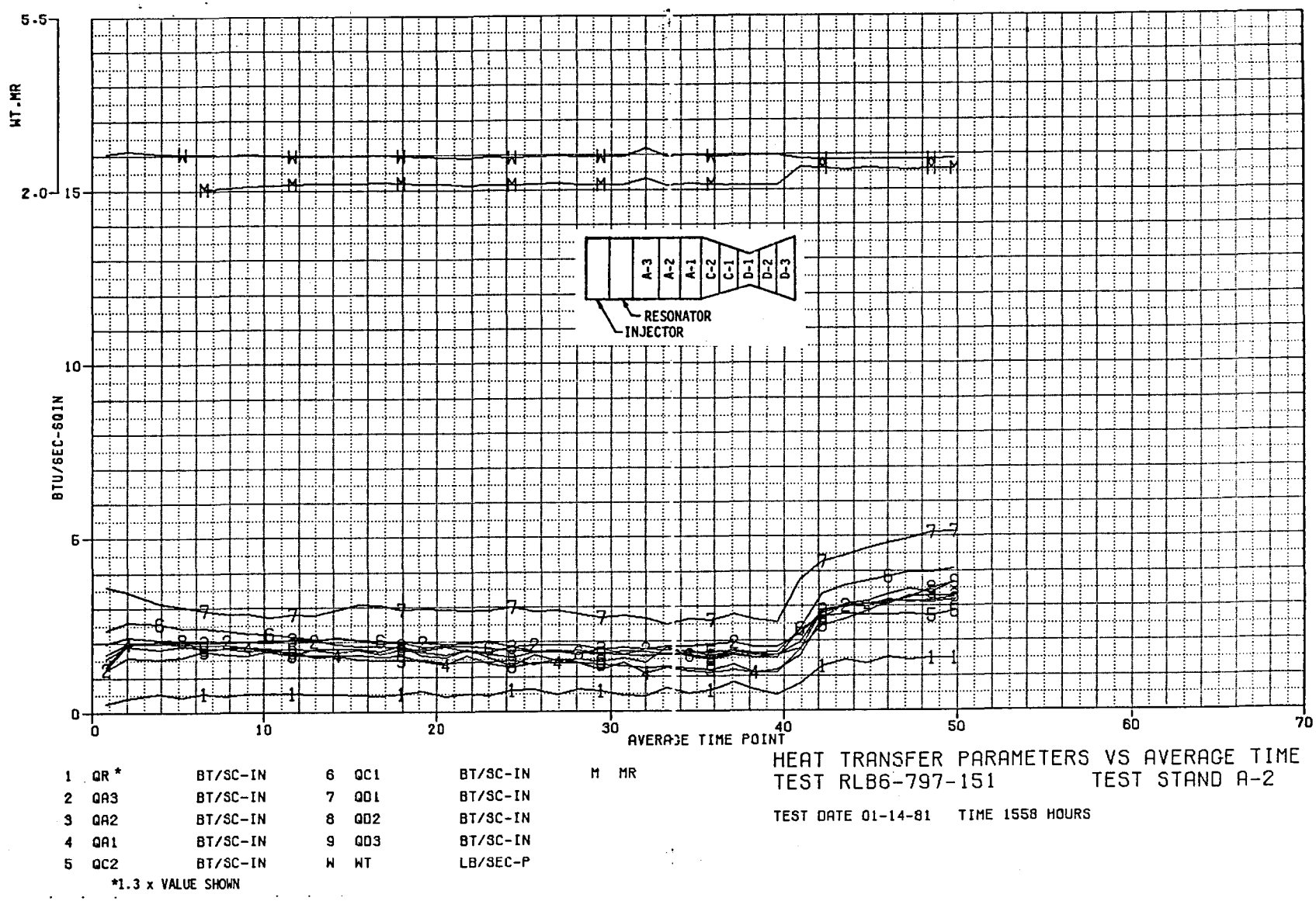

Figure 68. Heat Transfer Parameters Versus Average Time, Test -151

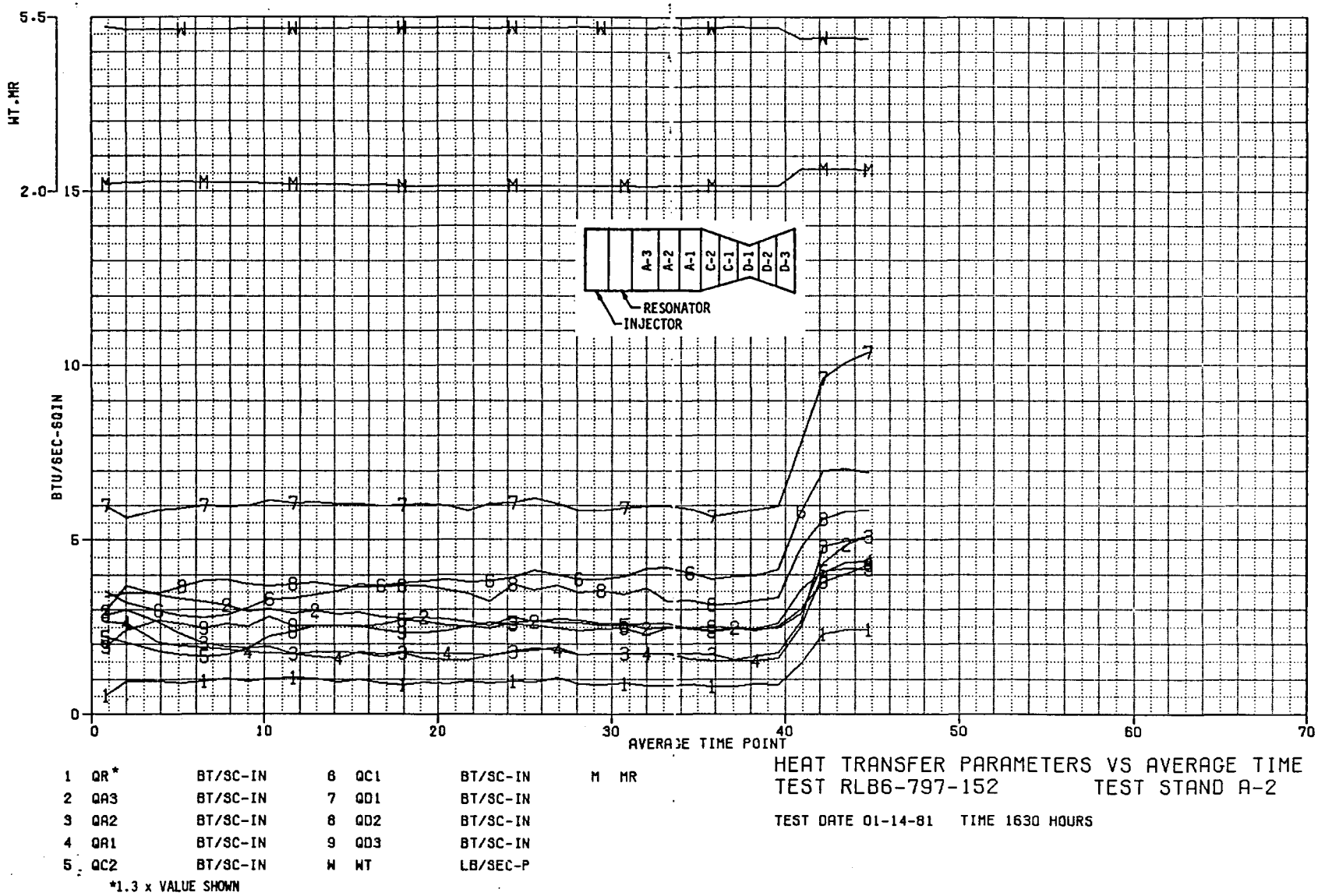

Figure 69. Heat Transfer Parameters Versus Average Time, Test -152

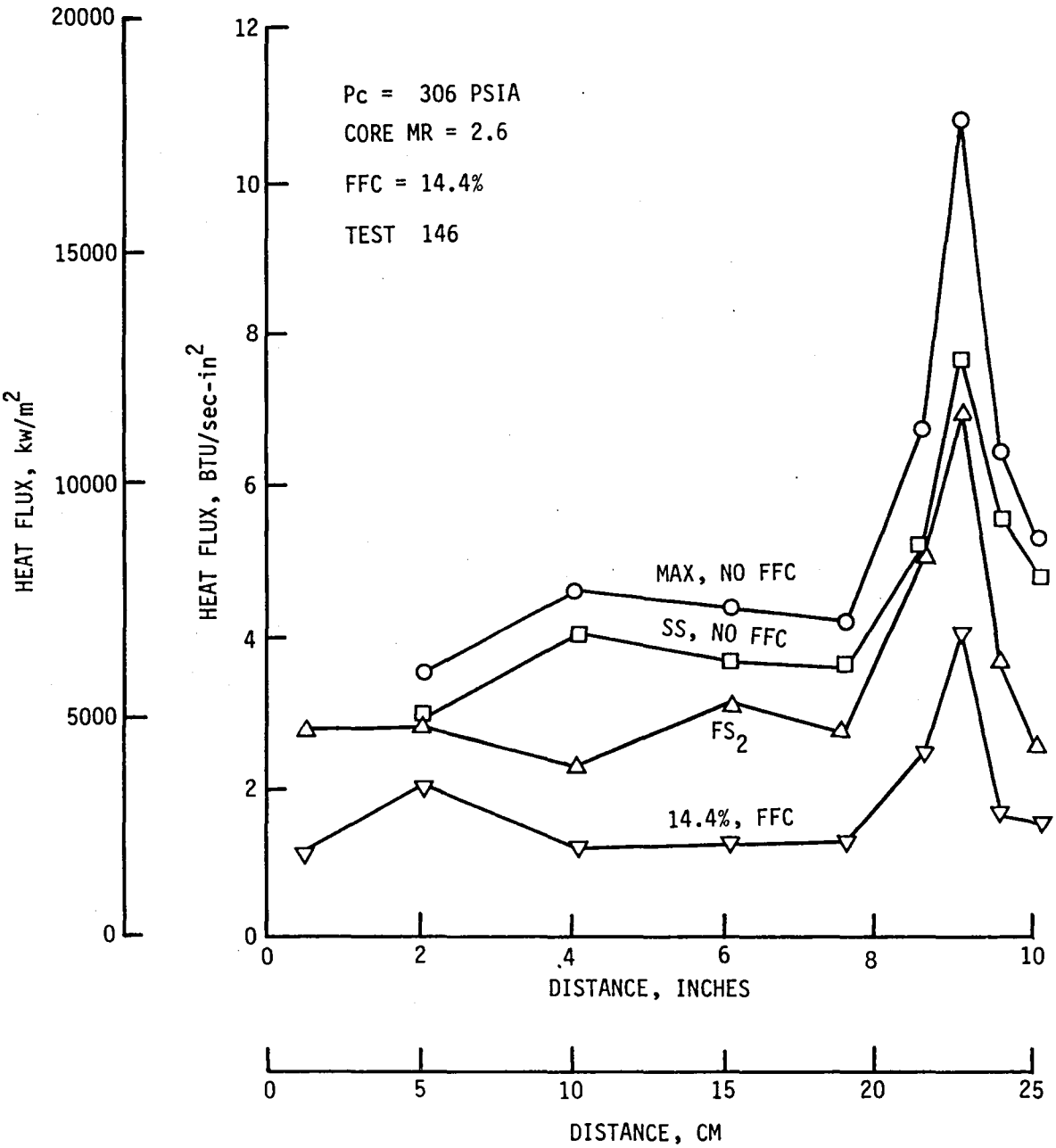

Figure 70. Heat Flux Versus Distance, Test -146

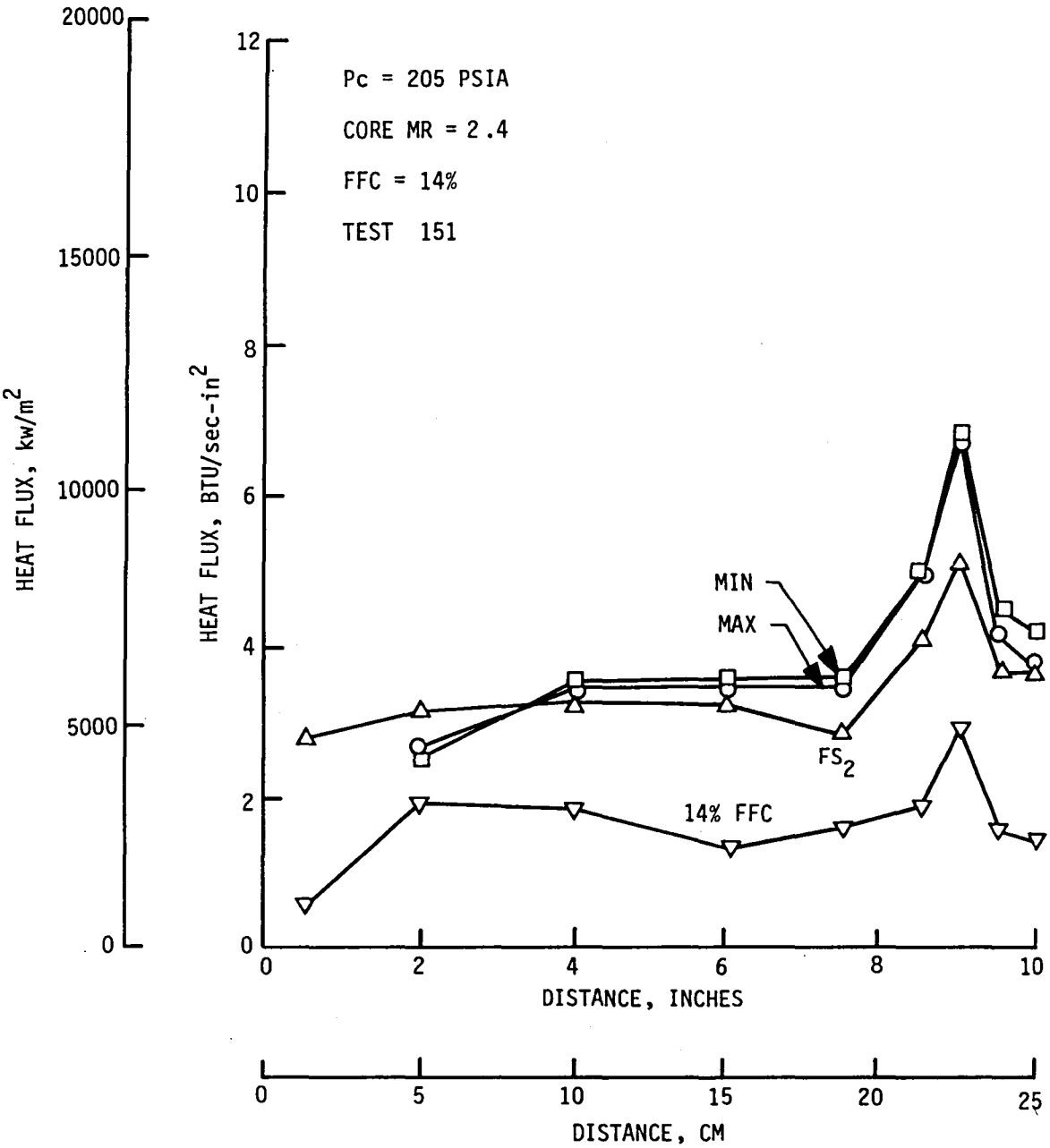

Figure 71. Heat Flux Versus Distance, Test -151

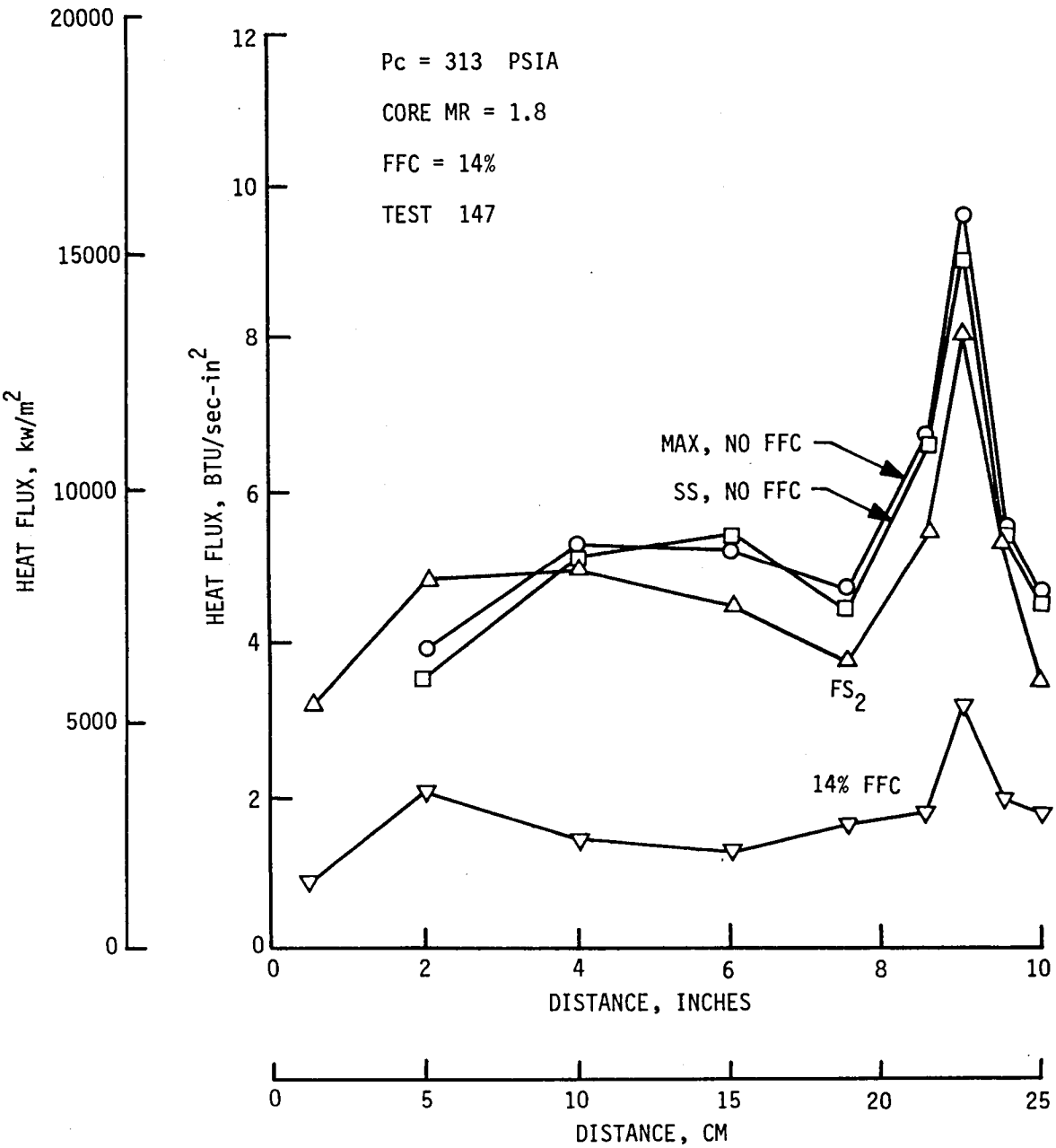

Figure 72. Heat Flux Versus Distance, Test -147

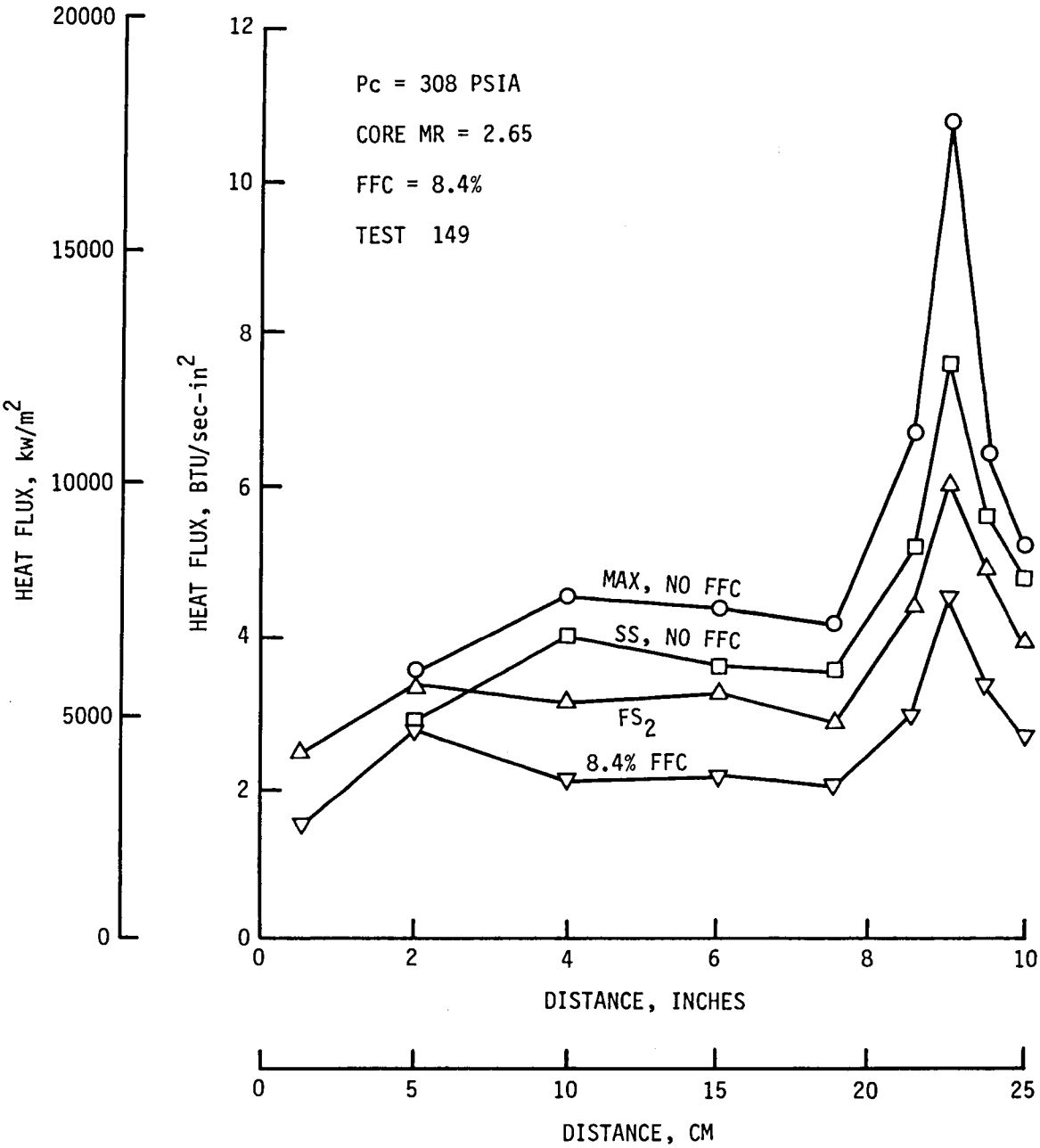

Figure 73. Heat Flux Versus Distance, Test -149

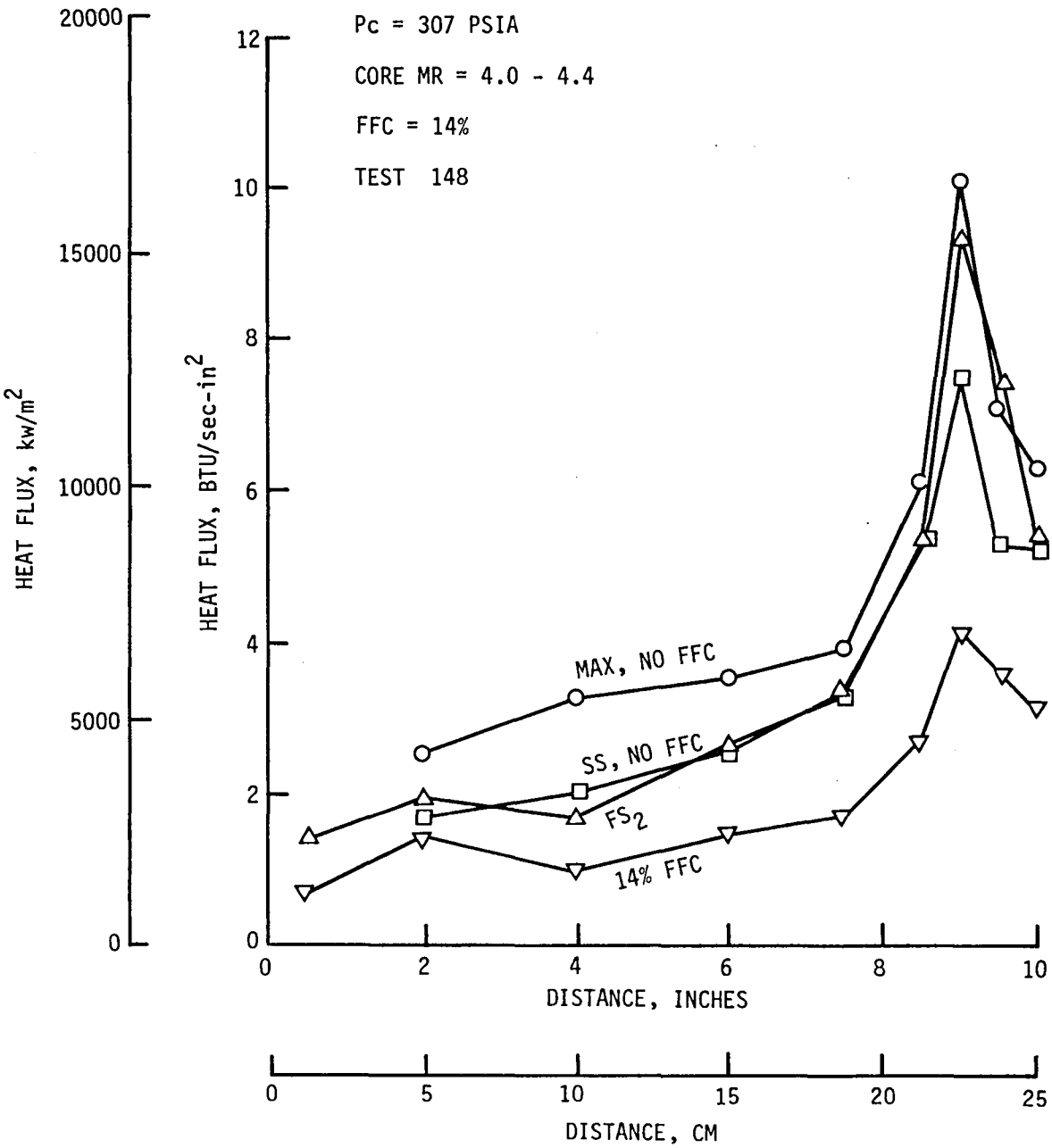

Figure 74. Heat Flux Versus Distance, Test -148

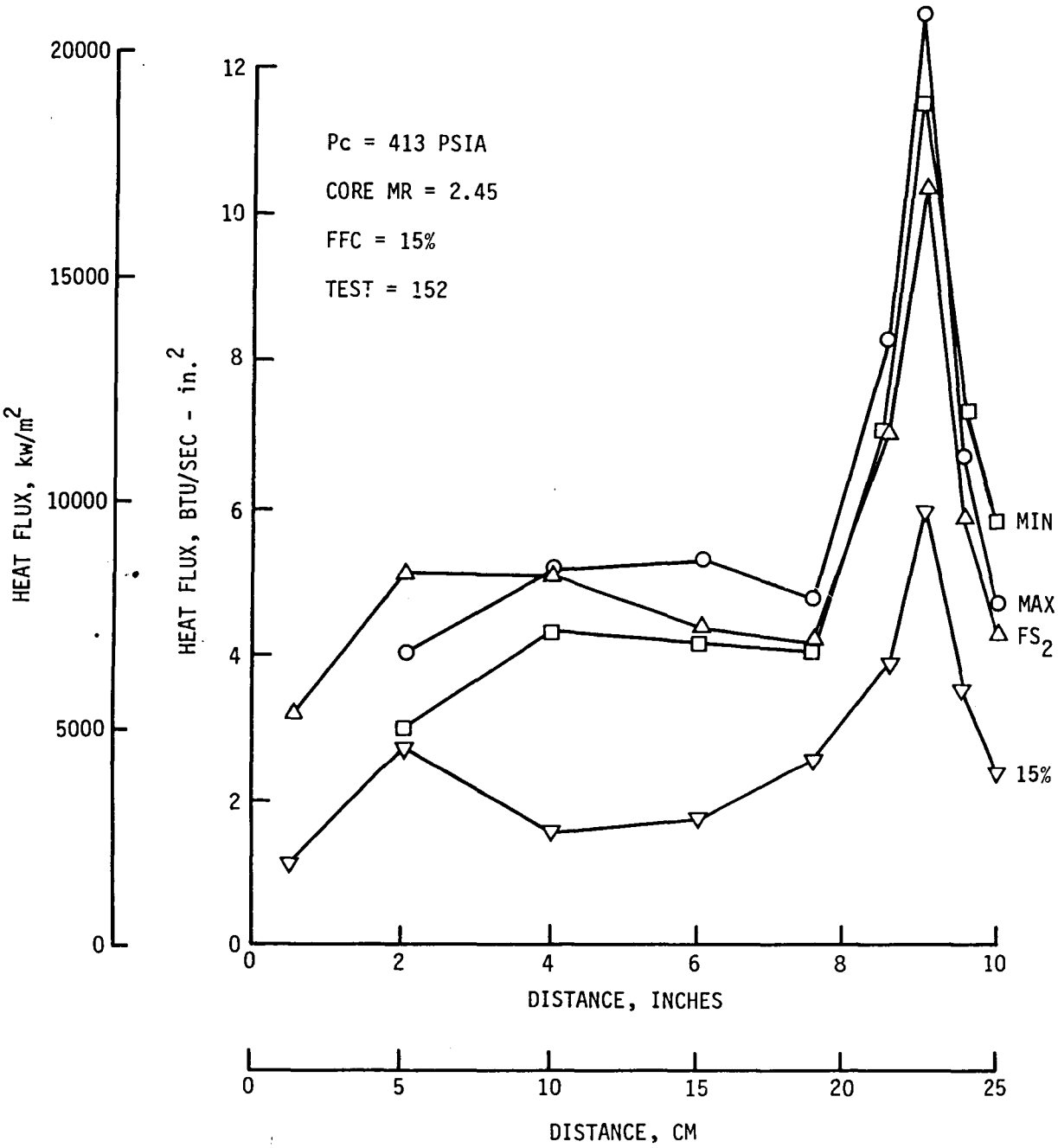

Figure 75. Heat Flux Versus Distance, Test -152

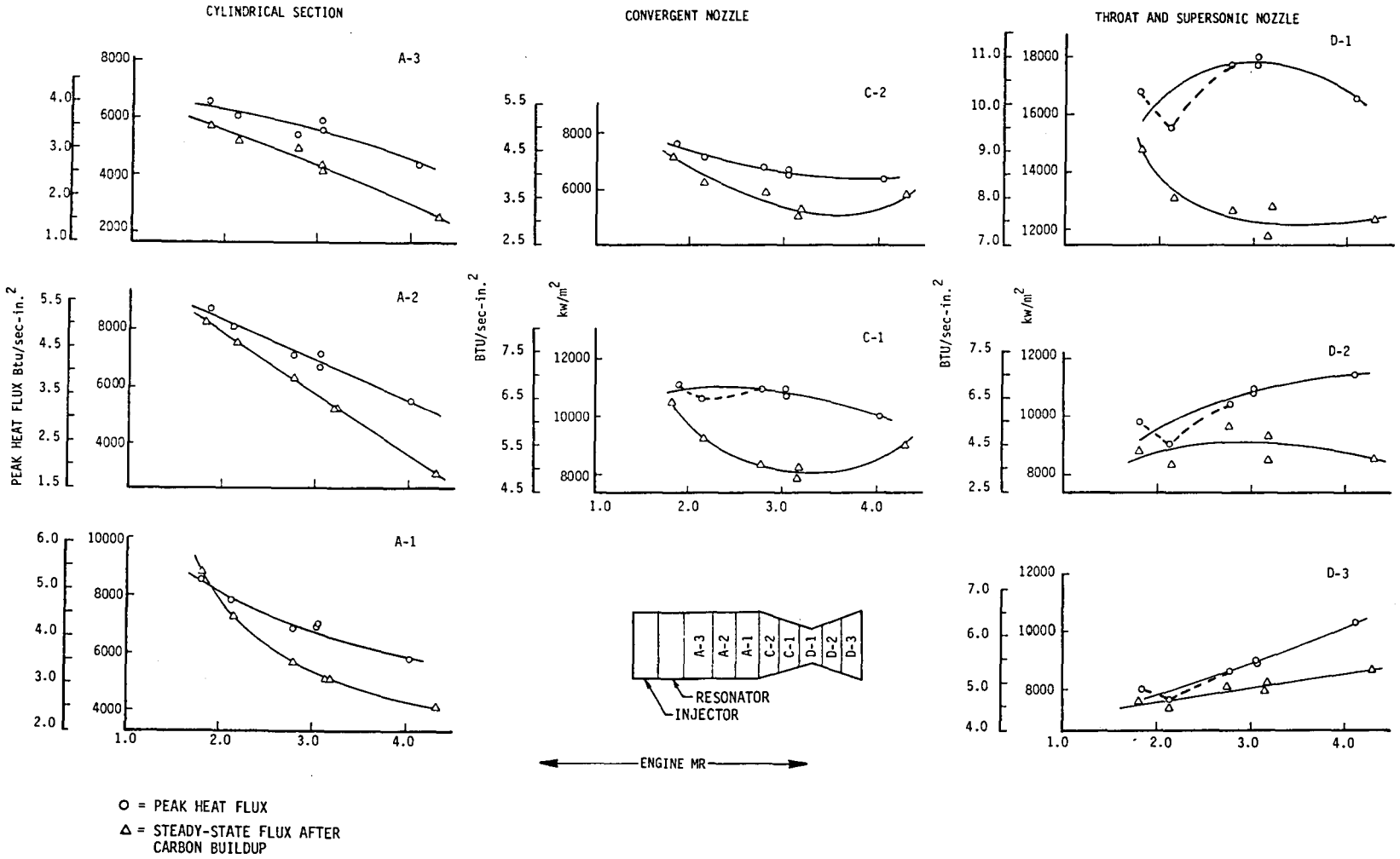

Figure 76. Maximum and Steady-State Heat, Flux Versus Engine MR for a Chamber Pressure of 300 psia (LOX/Propane, No Fuel Film Cooling)

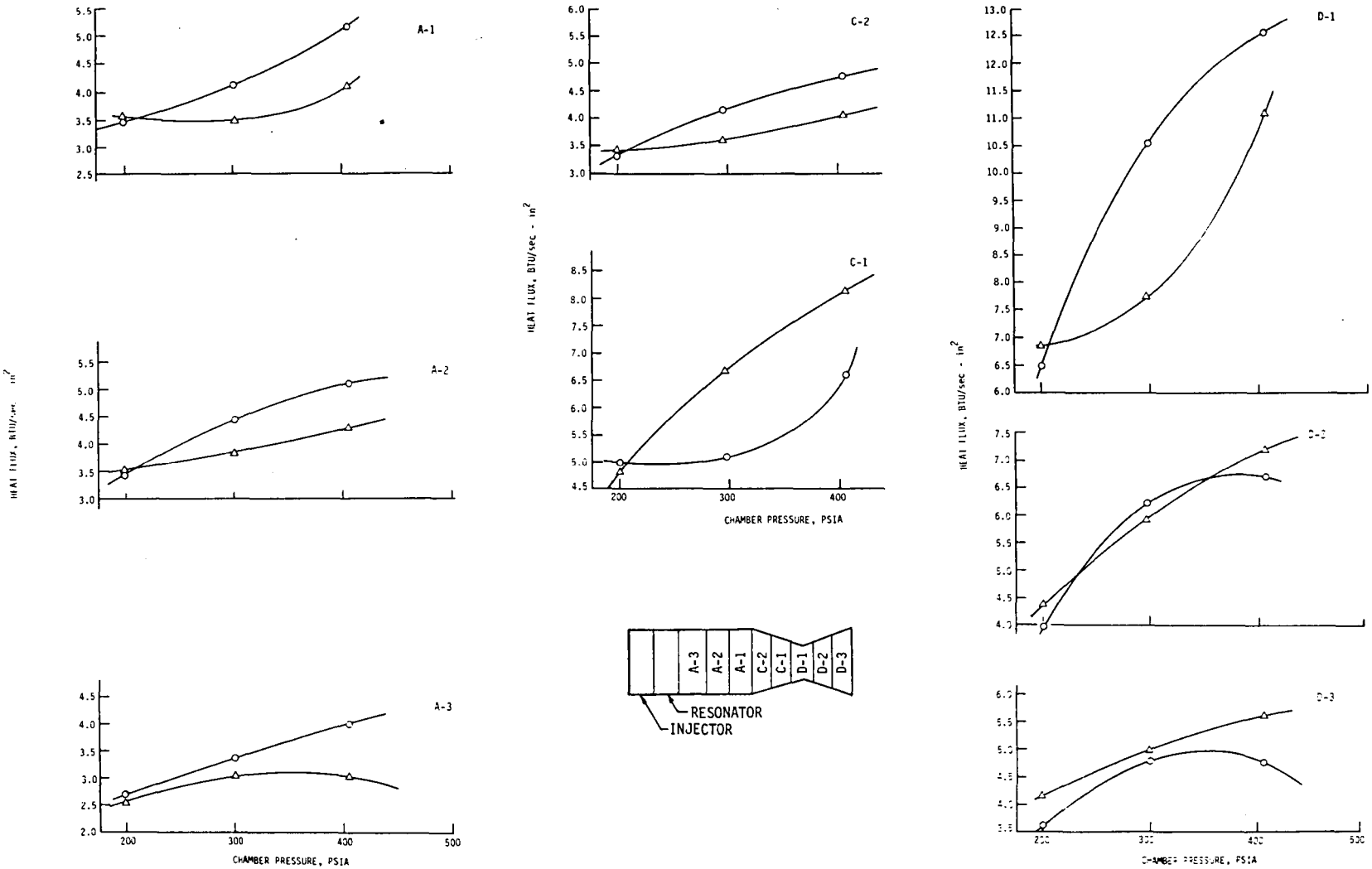

Figure 77. Effect of Chamber Pressure on Maximum and Steady State Heat Flux (LOX/Propane, No Fuel Film Cooling)

Reductions in peak heat flux during the firing do not aid in the cooling system design and cyclic life, since the chamber must be designed for the peak values. The reduction of total cooling heat load with time will, however, influence the regenerative propellant supply temperature to the injector and possibly influence both performance and stability.

(d) Total Heat Load

The total heat load to the coolant in the calorimeter chamber provides insight into both the carbon deposition process and the effectiveness of film coolant in reducing the heat flux. Table XII and Figure 78 show the total heat load as a function of the core mixture ratio for five different conditions. The data of the uppermost curve were obtained very early in the tests with no film-cooling and should be representative of operation with little or no carbon deposits on the chamber wall. A lower heat load value curve (labeled "0% FFC end of no FFC test") is obtained near the end of the tests with no film-cooling. These data points represent steady-state values obtained after the carbon deposition process had occurred. The difference between these two curves shows the heat flux reduction due to carbon deposition. What is particularly interesting is that the effect of carbon deposition is substantial at high mixture ratios and small at low mixture ratios. This was not anticipated as there is much more carbon available at the lower mixture ratios.

The two lower curves are similar to those just described except they were obtained with 14.5% fuel film-coolant. The curve, obtained two seconds into the film-cooling tests, presumably shows the effect of the film-cooling in reducing the heat flux with little or no carbon deposition. The 40 second data show the combined effect of film-cooling and carbon deposition. With 14.5% film-cooling, the carbon deposition shows almost no mixture ratio-dependence. This is substantially different from the strong mixture ratio-dependence encountered with no film-cooling.

On the film-cooling tests, the film coolant was turned off 5 seconds before the end of the firing. The remaining curve in Figure 68 shows the heat load immediately before the end of these tests (5 seconds after the film-cooling was shut off). This curve is nearly identical to that obtained near the end of the tests with no film-cooling. This is significant in that it indicates the carbon deposit effect depends on the current operating condition and not previous operating conditions, i.e., there is very little hysterisis in the process. Thus, the concept of initially operating a hydrocarbon engine in a heavy sooting condition to place a thermal barrier on the chamber walls, and then shifting to a higher performing but more thermally severe operating conditions, does not appear to be valid based on these results. The removal of the carbon barrier after the film-cooling was shut off is clearly evident at the low mixture ratios.

TABLE XII

COMPARISON OF TOTAL ENGINE HEAT LOADS

Test No.	Pc @ 20 sec psia	MR Core/Eng	% FFC	Heat Load BTU/sec: With Film Cooling 2 sec.	With Film Cooling Final	Without Film Cooling Final	Previous Data Peak	No FFC SS
145	307	2.6/2.3	14.6	143	228	-	425	340
146	306	2.6/2.2	14.4	259	164	337	425	340
147	314	1.8/1.5	14.6	215	147	455	480	470
148	309	4.0/3.2	14.1	244	157	282	355	257
149	309	2.6/2.5	8.4	287	222	339	425	340
151	205	2.4/2.1	14.6	177	156	321	320	320
152	415	2.4/2.1	15.3	284	221	495	465	420

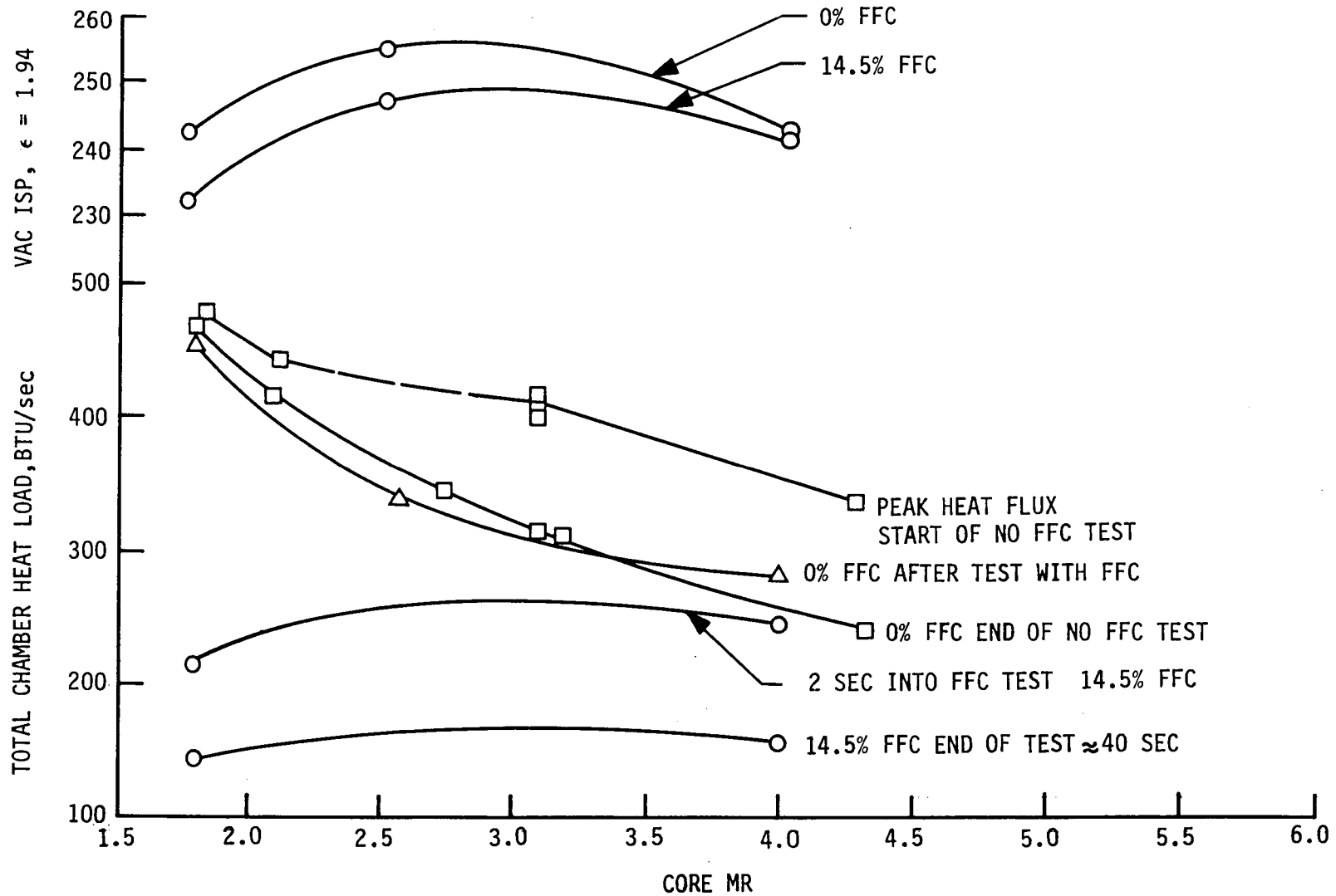

Figure 78. Effect of Core MR and Propane Film Cooling on Isp and Heat Load Reduction

E, Tasks II and IV Subscale Injector Characterization (cont.)

The effectiveness of the film-cooling in reducing the total heat load at pressures of 200, 300, and 400 psia both with and without the accumulation of carbon deposits is illustrated in Figure 79. These results show the same general film-cooling influence characteristics.

(7) Propane Hot-Fire Performance and Stability Test Results

This section summarizes the performance and stability data analyses for Test Series II, III, and IV. The injector was hot-fire tested with propane as the fuel with the following different hardware configurations: (1) heat sink chamber tests used for the injector checkout and stability tests (Test Series #2), (2) water-cooled calorimeter chamber tests with 0% FFC used to obtain heat transfer data (Test Series #3), and (3) water-cooled calorimeter chamber tests with a pre-atomized fuel film- cooling injector (Test Series #4).

(a) Heat Sink Chamber Tests

Table VI summarizes the stability data of the eleven heat sink chamber tests (Test Series #2). The stabilization effectiveness of the 0.7 in. deep resonator is apparent from the data on Table VI. In Test Series #2, the only incidence of instability per CPIA criteria occurred on Test 129 after bombing with no acoustic cavities. The instability was in the first tangential (1T) acoustic mode of the combustion chamber. At a chamber pressure of 200 psia, chugging oscillations were observed at both high and low mixture ratios (Tests 131 and 132). The amplitudes were small and the tests were classified as stable per CPIA criteria.

Table VII, Test Series #2, summarizes the performance data of the heat sink chamber tests. The specific impulse values and energy release efficiencies (calculated using both the C* data and the Isp data) are presented graphically in Figure 80. The calculated results using these two methods agree quite well, with an approximate 1% maximum data dispersion. The performance appears to increase as the chamber pressure increases. Although the measured ERE level of the 300 psia chamber pressure tests appears to agree with the predicted values using the modified ALRC vaporization approach (Figure 25), subsequent results from longer duration tests indicate a measurable influence of test duration on ERE, apparently due to nonsteady-state conditions within the injector. Further analysis was not pursued due to the short test durations.

(b) Water-Cooled Chamber Tests Without Fuel Film-Cooling Ring

Table IX is a summary of the performance data from the water-cooled calorimeter chamber tests (Test Series #III). All the tests in this series had test durations of 40 to 80 seconds, except for Test #133, which was a 3 second test duration. Engine specific impulse and mixture ratio varied as a function of time from FS1 as is shown on Figure 81. This mixture ratio and

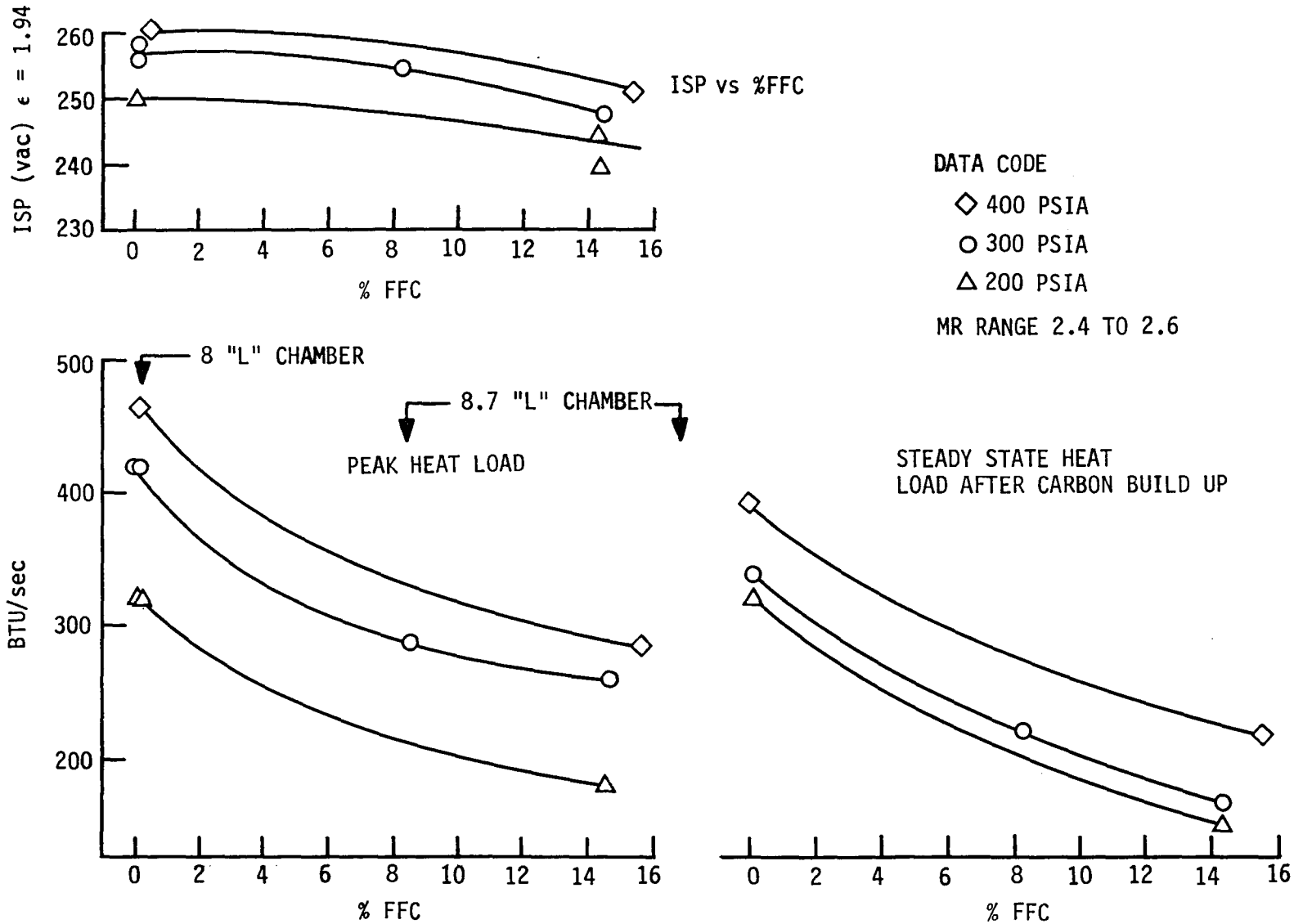

Figure 79. Effect of Propane Film Cooling on Isp and Total Heat Load

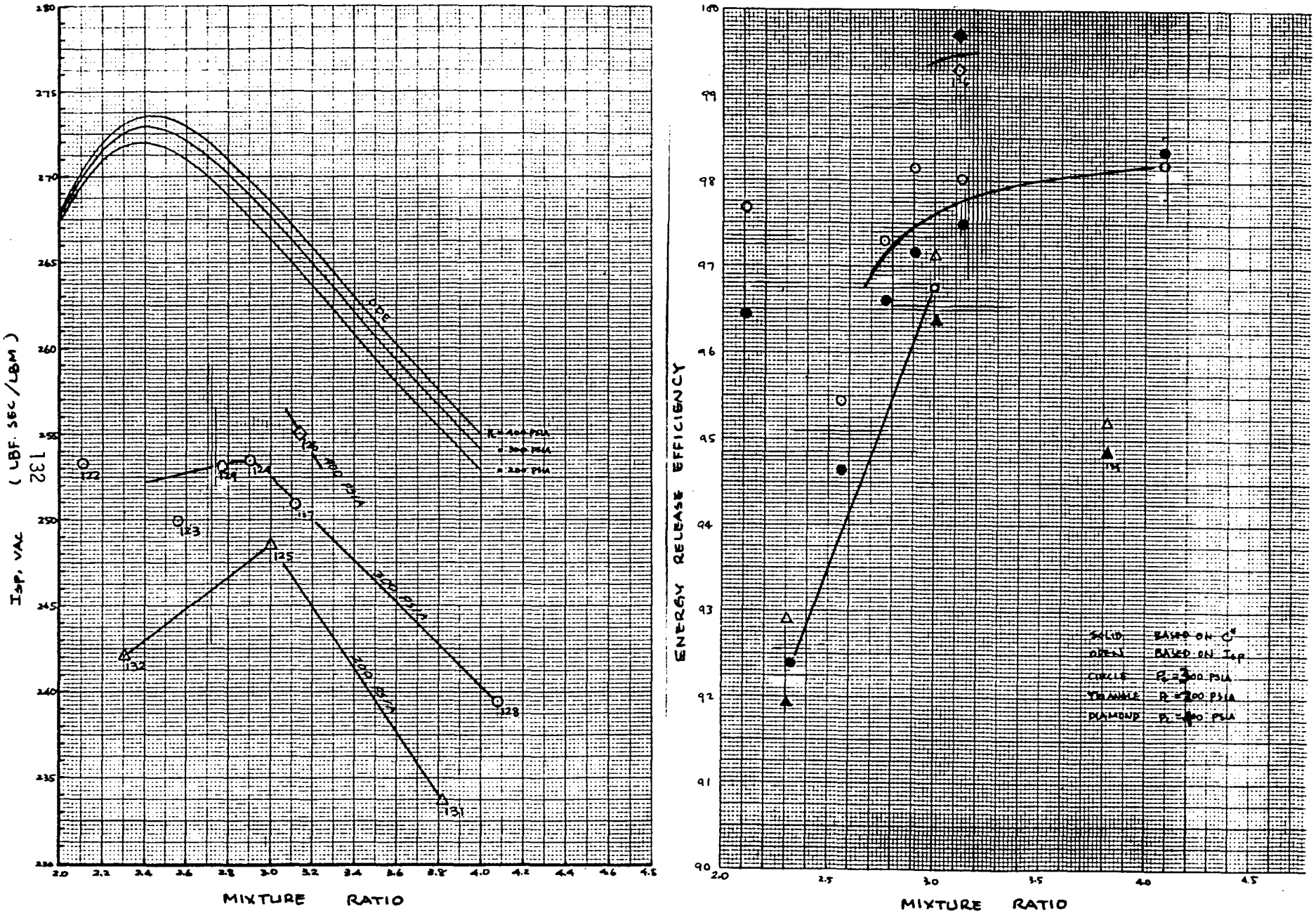

Figure 80. Performance of Injector #3, Test Series #2, LOX/Propane, Heat Sink Chamber, No FFC

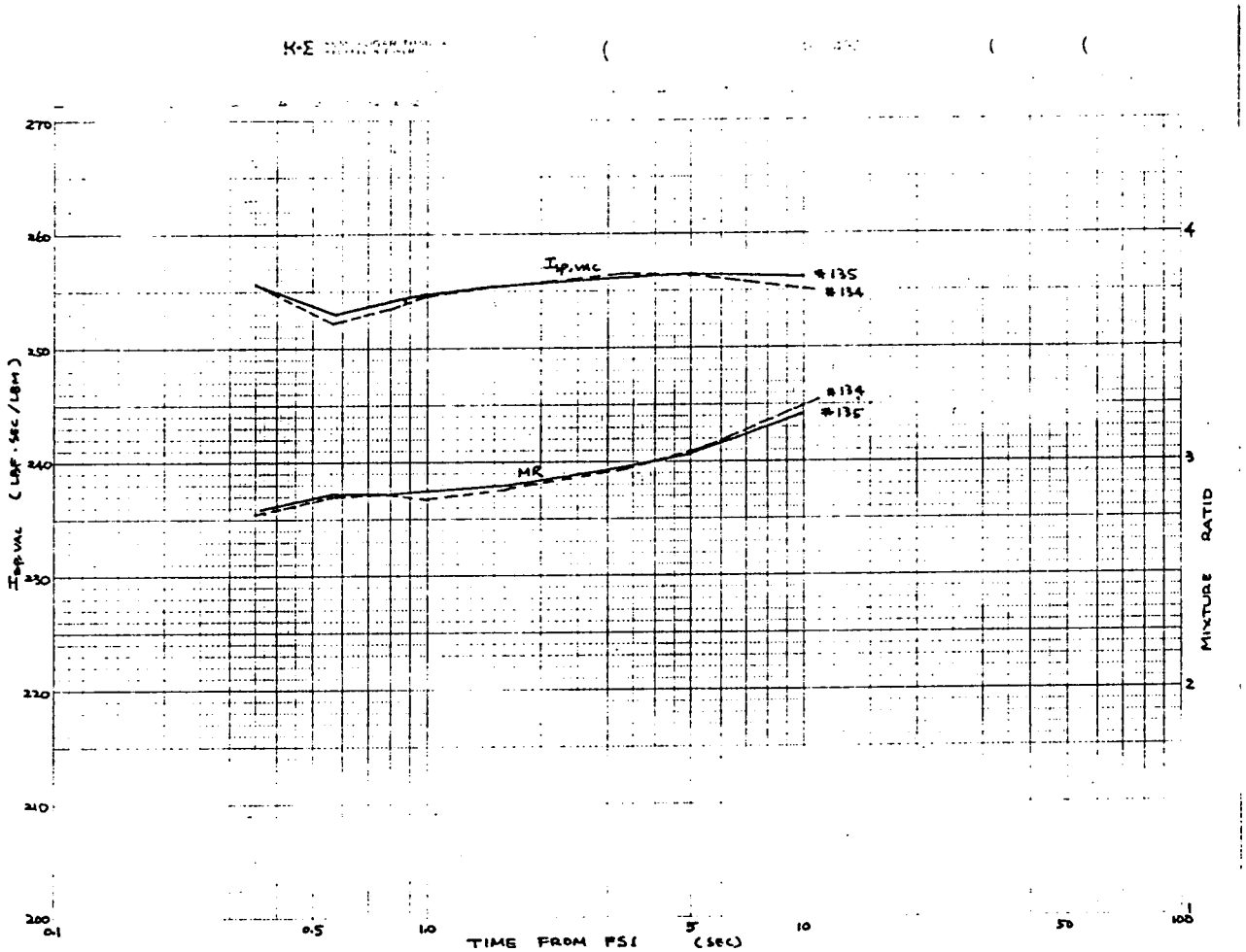

Figure 81. Representative Time Histories of Isp, Vac and MR of Test Series #3, Injector #3, Water-Cooled Chamber, No FFC, LOX/Propane

E, Tasks II and IV Subscale Injector Characterization (cont.)

Isp time history is typical of that observed on all tests. The Isp decays to a minimum value at approximately 0.6 second from FS1 and then gradually increases with time until the steady-state mixture ratio is achieved. The Isp dip is probably due to transient LOX manifold chilldown and propellant accumulation between the LOX flowmeter and injector face during this time period.

The time interval from FS1 to the minimum Isp point (approximately 0.6 seconds) is nearly equal to the heat sink chamber test durations. Figure 54 shows good agreement of Isp data between the heat sink chamber tests and the water cooled chamber tests at FS1 + 0.6 sec. The variation of Isp with both mixture ratio and firing duration is shown on Figure 55. The steady-state values taken at FS1 + 10 sec. are at least 3 lbF-sec/lbM greater than their corresponding values at FS1 + 0.6 sec. for the 300 psia Pc case. The Isp peaks at a mixture ratio of approximately 3.0. The energy release efficiencies, using the definition given below, based on the steady-state Isp, are shown in Figure 82.

$$ERE = \frac{I_{sp,\ measured}/\eta_D\ \eta_B\ \eta_K}{I_{sp,\ ODE,\ MR\ engine}} = I_{sp}/\eta_D\ \eta_B\ \eta_K$$

where:

I_{sp} = $\frac{I_{sp,\ measured}}{I_{sp,\ ODE,\ MR\ engine}}$

η_D = divergence efficiency for 15° cone nozzle

η_B = boundary layer efficiency for 0.2 wall to stagnation temperature ratio

η_K = kinetic efficiency at uniform engine mixture ratio

For the 300 psia chamber pressure tests, the ERE increases with increasing mixture ratio and is 100% at a mixture ratio of approximately 3.2. The chamber pressure was a varied parameter during low mixture ratio testing. These data indicate that the ERE increases as the chamber pressure is increased. The substantial influence of mixture ratio on ERE indicates the importance of triplet momentum ratio on the propellant mixing process.

The hot-fire fuel injector Kw data are shown in Table IX. These data are plotted on Figure 83 and show a significant (3-7%) increase in Kw with time. The same phenomenon was observed in the testing of the like-on-like injector. The fuel Kw also increases as the mixture ratio is increased as shown on Figure 84. This increase of fuel Kw is probably caused by a fuel density increase due to fuel/oxidizer heat exchange within the injector. The insert in Figure 83 shows the calculated fuel Kw as a function of temperature assuming a Kw of 0.145 at 65°F. Operational engines must account for this effect in both design and operations.

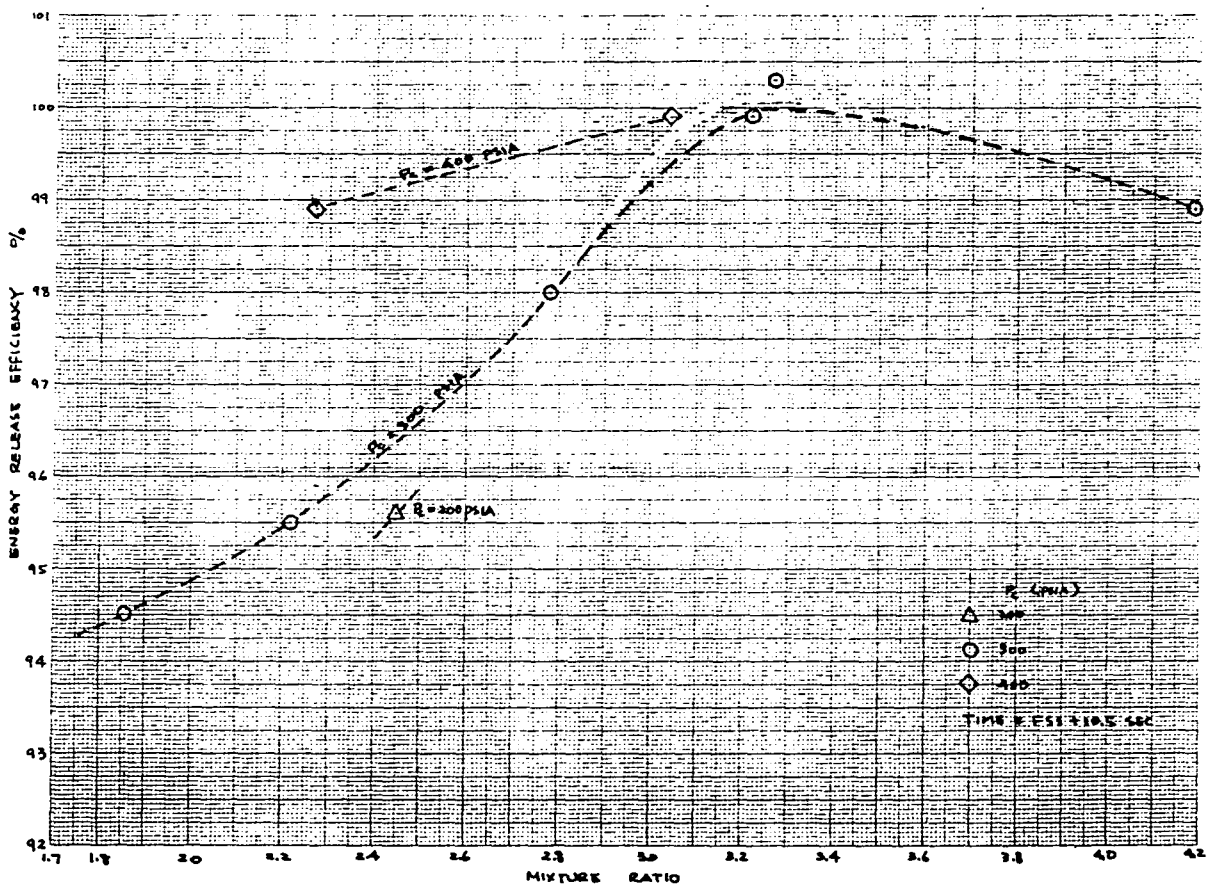

Figure 82. Energy Release Efficiency of Test Series #3, Injector #3, No FFC, Water-Cooled Chamber, LOX/Propane

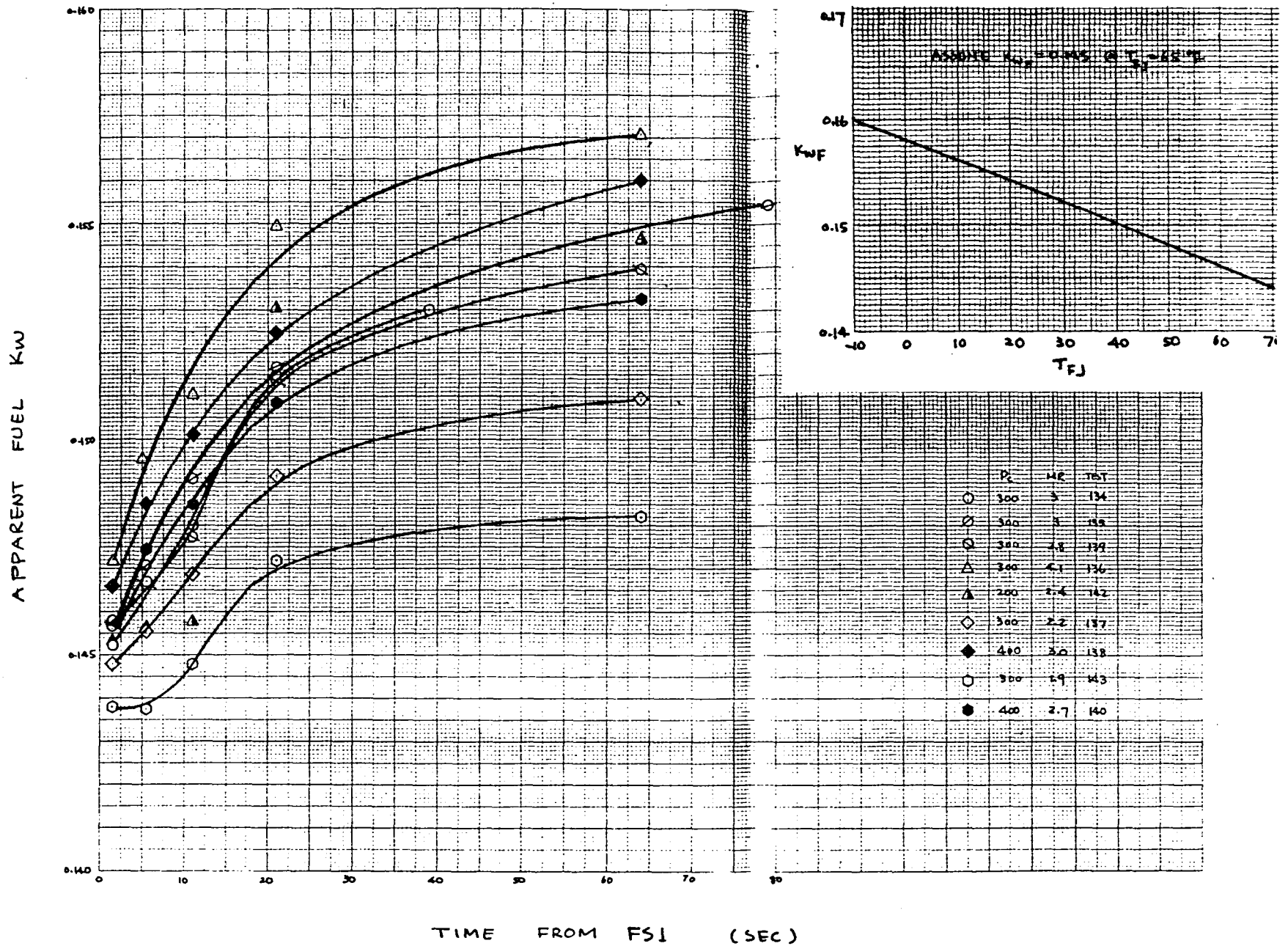

Figure 83. Time History of Apparent Fuel Injector Kw of Injector #3, Test Series #3, LOX/Propane, No FFC, Water-Cooled Chamber

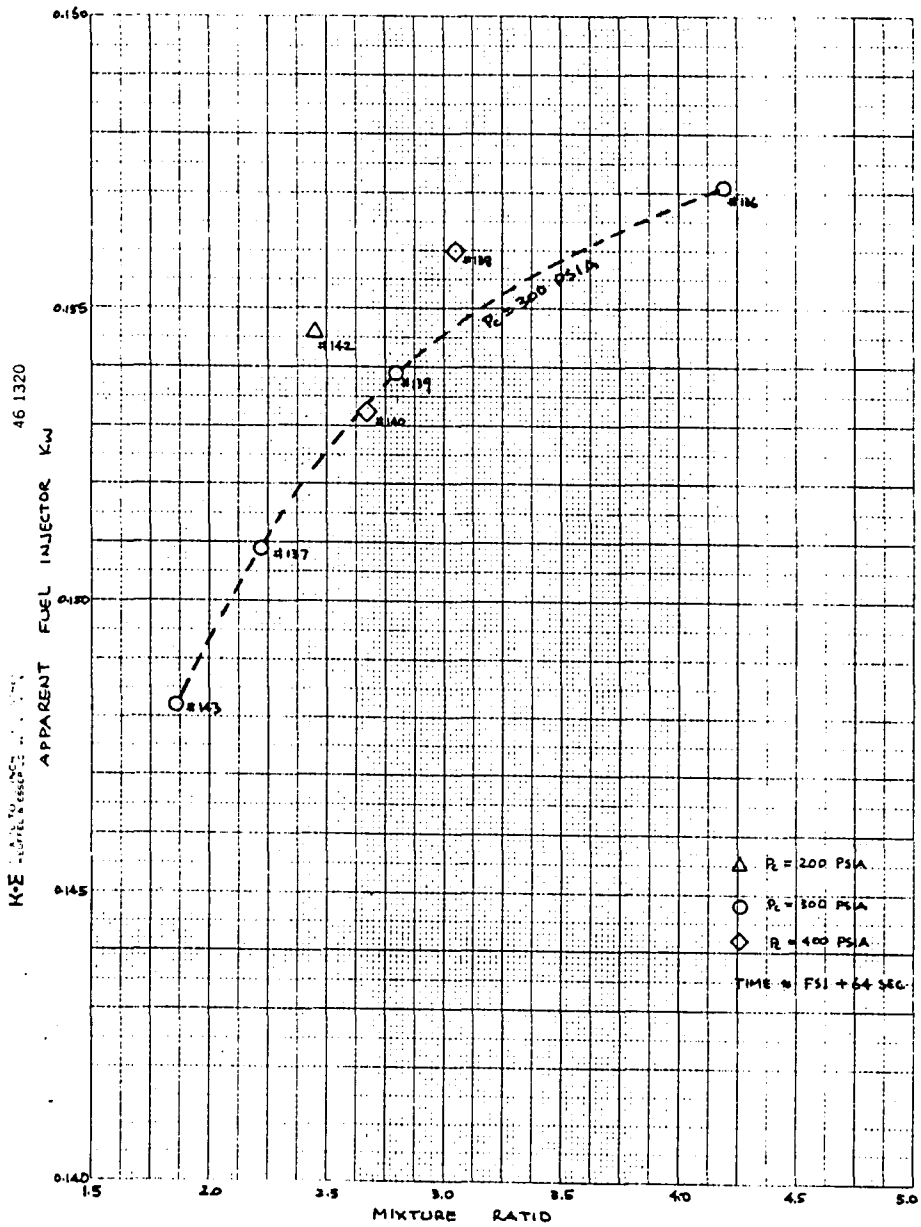

Figure 84. Effect of Mixture Ratio on Apparent Fuel Injector Kw of Injector #3, Test Series #2, LOX/Propane, No FFC, Water-Cooled Chamber

E, Tasks II and IV Subscale Injector Characterization (cont.)

(c) Water-Cooled Chamber Tests with Fuel Film-Cooling Ring

The performance data of nine tests (Test Series #4) conducted with the FFC ring (designated as Injector #4) are summarized on Table X. During each test the FFC was shutoff near the end of the firing to give a direct comparison of performance with and without FFC. The 0% FFC ERE data from test Series #4 are shown on Figure 85 along with the data generated during test Series #3. Both sets of data appear to have the same trend, however the Series #4 data show substantially higher ERE values for the 300 psia chamber pressure tests at low mixture ratio than do the Series #2 data. These apparent differences in ERE are probably due to lack of propellant thermal/flow stabilization at the FS1 + 10 second sample period of Test Series #2 as indicated by the Kw data of Figure 83. These two tests series would probably have the same apparent ERE if the data sample times were the same. The impact of test sample time on apparent ERE is illustrated by the data on Figure 86. These data show a 1% increase in apparent ERE for the FS1 + 10.4 to 10.9 second sample period compared to the FS1 + 1.4 to 1.9 second sample period. Based on the Kw data of Figure 82, a similar or even greater increase in apparent ERE is possible when comparing the FS1 + 10 sec- ond to the FS1 + 40 or 60 second sample period.

Combustion efficiency data are plotted on Figure 87 for the Test Series #3 data at 300 psia chamber pressure with and without fuel film-cooling. The data from Test Series #2 are also included for the comparison to the non-FFC data (Series #2) and the film cooled data (Series #3) at the same test duration (FS1 + 10 seconds). The figure shows the following: (1) the expected increase in apparent combustion efficiency with test duration; (2) a higher combustion efficiency with fuel film-cooling at low mixture ratios (2.0); (3) a significant reduction in combustion efficiency due to film-cooling as mixture ratio is increased. These data are also plotted on Figure 88 as a function of core mixture ratio. The higher combustion efficiency with FFC than without FFC at low MR (below approximately 2.0) suggests the existence of an oxidizer-rich core boundary. In the oxidizer-rich environment, addition of fuel film-cooling provides a more uniform MR distribution and reduces the mixing loss. On the other hand, the lower efficiency with FFC than without FFC at high MR implies the lack of an oxidizer-rich core boundary. At the higher mixture ratio, the addition of film-cooling causes a MR maldistribution which decreases the combustion efficiency. The existence of an oxidizer-rich environment at the chamber wall may be caused by two possible mechanisms:

1. Without the combustion effects, a triplet injector element has mixing characteristics as described in Appendix A. For an OFO triplet element, the fuel fan angle can be greater than or less than the oxidizer fan angle depending on whether the momentum ratio (or the mixture ratio) is high or low. Consequently, at high mixture ratios the fuel fans can overspread the oxidizer fans and form a fuel-rich zone at or near the chamber walls. Conversely, at low mixture ratios, the fuel fans underspread and an oxidizer-rich zone is formed near the walls.

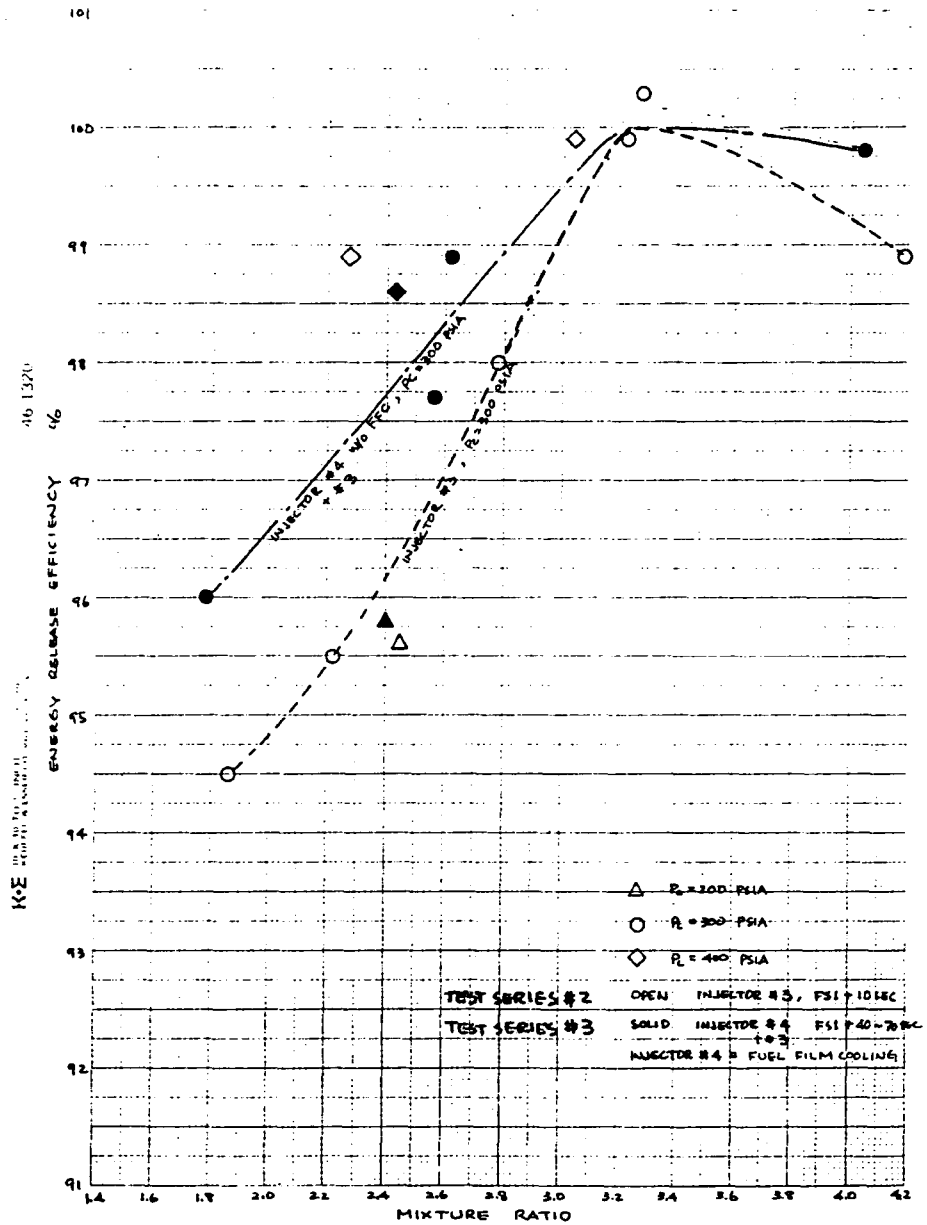

Figure 85. Energy Release Efficiency Comparison of Non-Fuel Film Cooled Tests, Test Series #3, and #4, LOX/Propane, Injector #3

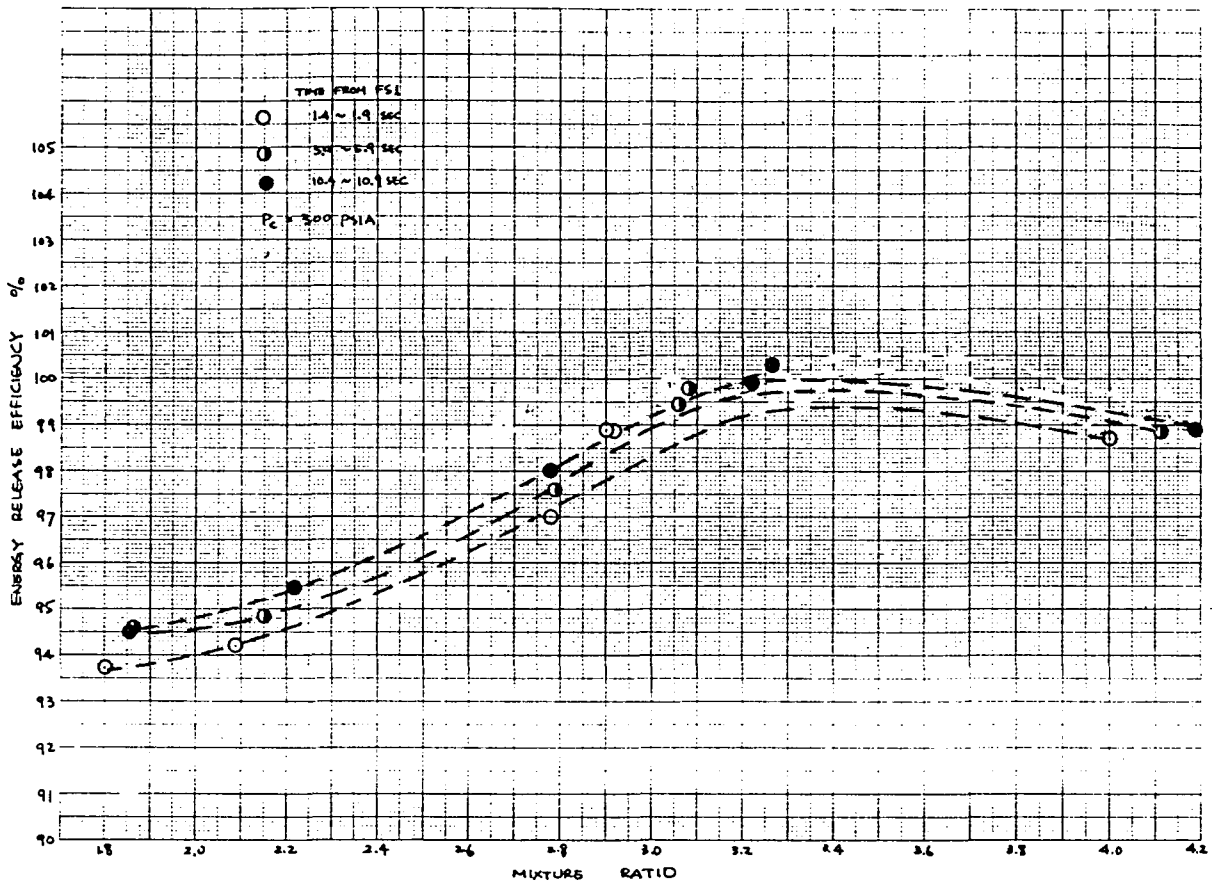

Figure 86. Energy Release Efficiency Variation with Time, Test Series #3, Injector #3, No FFC, LOX/Propane, Water-Cooled Chamber

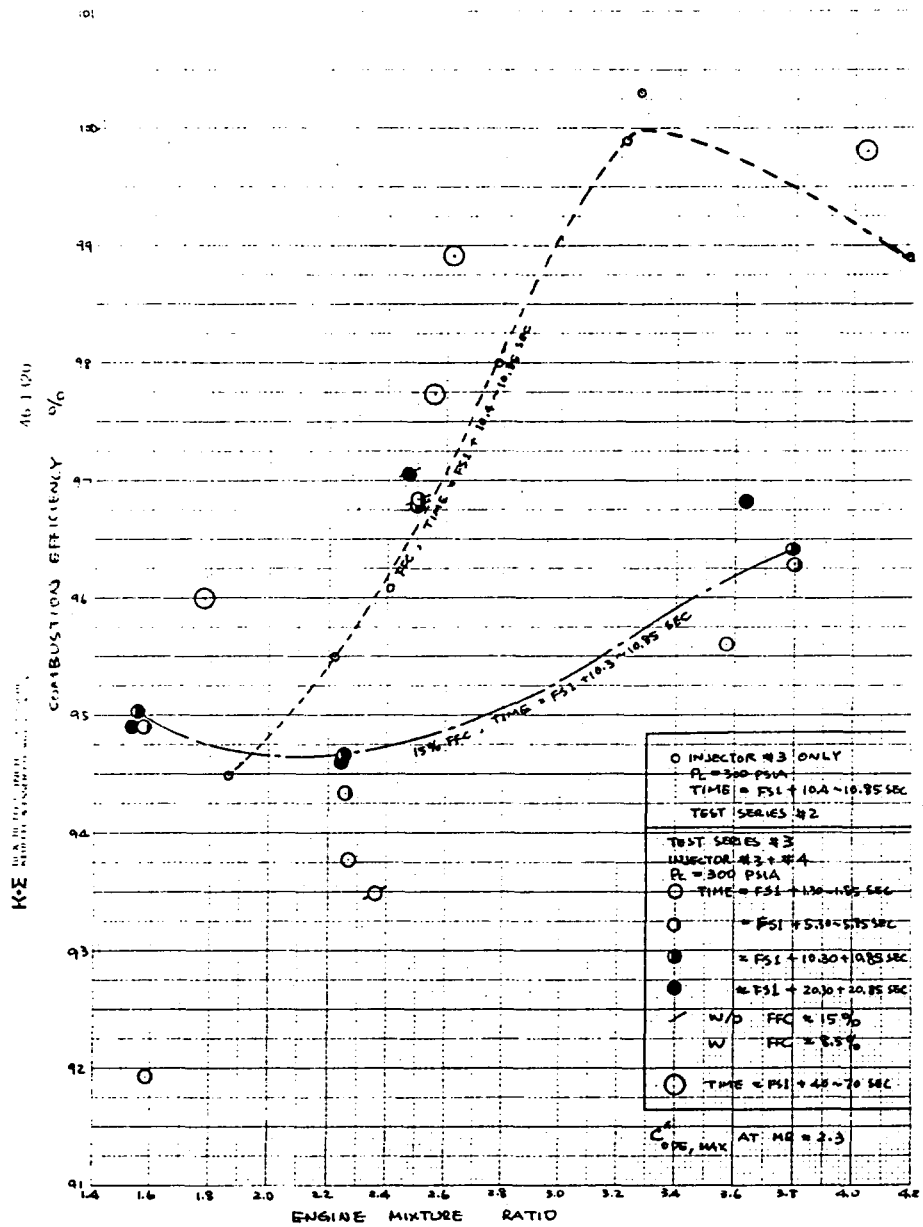

Figure 87. Combustion Efficiency Comparison of LOX/Propane with (Series #4) and without (Series #3 & #4) FFC, Injector #3, Water-Cooled Chamber, Pc = 300 psia

2. The element radial mixing is another possible cause. At low MR operation the oxidizer streams may not have sufficient radial impingement momentum to penetrate the fuel stream resulting in an oxidizer-rich periphery. At high MR operation, oxidizer momentum is high enough to have deep penetration of the fuel stream preventing the oxidizer rich zone from forming at the periphery.

Both these mechanisms lead to the existence of an oxidizer-rich environment at the chamber walls at low mixture ratio. As the mixture ratio increases, the oxidizer-rich environment decreases. As previously stated, when an appropriate amount of fuel is added by virtue of fuel film-cooling the near-wall zone at low engine mixture ratio, the unreacted oxidizer is consumed stoichiometrically and consequently the overall combustion efficiency is improved. At higher mixture ratios, however, the oxidizer-rich environment does not exist and therefore fuel film-cooling will lower the overall combustion efficiency. The heat transfer data analysis (Section 6) also indicates the existence of an oxidizer-rich environment at the walls based on the wall heat flux data trends.

In summary, Figures 82, 85, 87 and 88 all show that 100% of combustion efficiency is obtainable with the OFO triplet and the LOX/propane propellant combination, at certain optimum mixture ratios. This indicates the occurrence of uniform atomization and complete vaporization efficiency at the optimum MR. The reduction in efficiency as the mixture ratio decreases can be due to the deterioration of both momentum ratio-dependent atomization efficiency and mixing efficiency. Also, data contained on Figures 81, 55, 83, 84, 85, 86, and 87 indicate the significant influence data sample time has on injector flow stabilization and apparent combustion efficiency for this injector using LOX/propane. Only the long duration tests ($\geq$ 40 seconds) will yield reliable efficiencies.

e. Test Series V - LOX-Ethanol, Ethanol Film-Cooling, 8.7-in. Water-Cooled Calorimeter Chamber, OFO Triplet Injector

(1) Test Objectives

The objectives of this test series were to compare the performance, heat transfer, and stability characteristics of the 40-element OFO triplet injector utilizing LOX/ethanol propellants with data obtained from the same hardware utilizing LOX/propane. Heat transfer parameters included the effects of carbon deposition and fuel film-cooling on the heat flux profiles.

(2) Facilities and Hardware

The facility and hardware were the same as that employed in Test Series #4. The carbon was cleaned off the injector face and the calorimeter chamber with

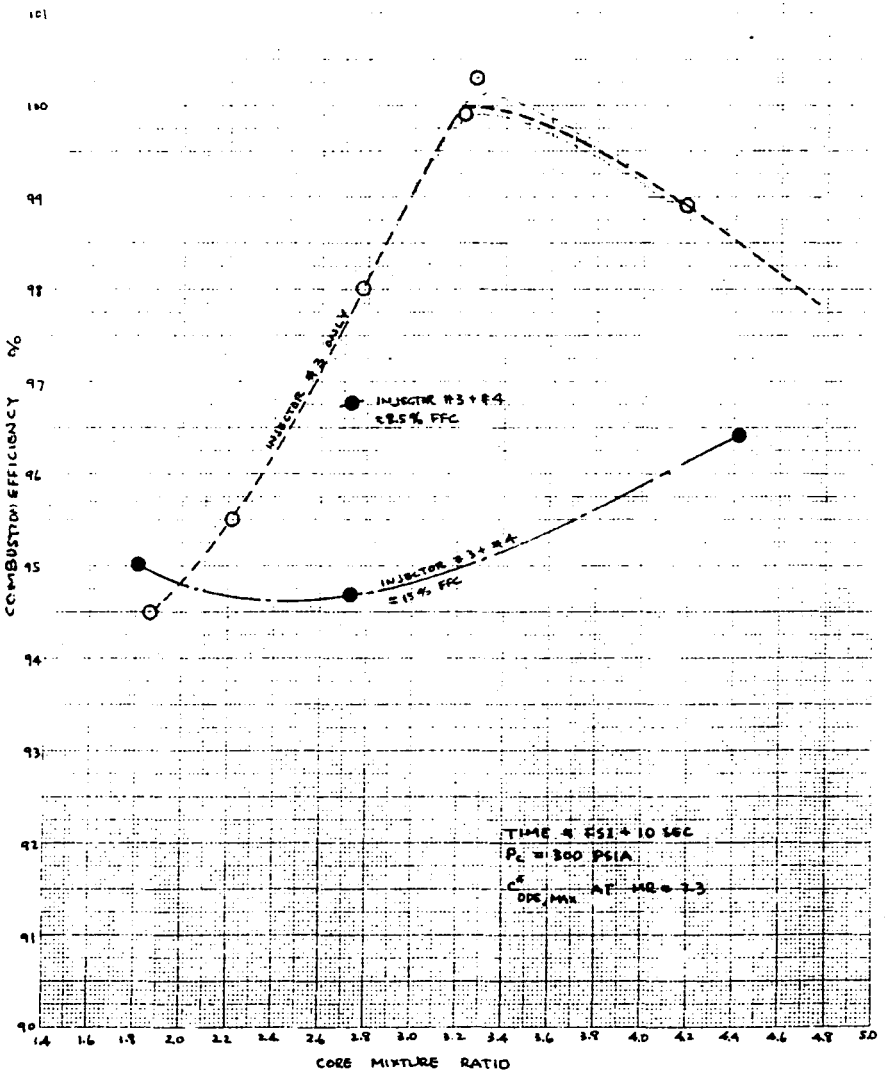

Figure 88. Combustion Efficiency Versus Mixture Ratio of LOX/Propane, Injector #3, Test Series #3, (without FFC) and Test Series #8 (with FFC), Pc = 300 psia

copper cleaner and fine abrasive at the start of this test series. The fuel tank was drained and refilled with ethanol. The measured water content was less than 0.1%.

(3) Summary of Testing with LOX/Ethanol

Tables XIII and XIV provide documentation of the test parameters and measured performance and thermal data. The following paragraphs provide a narrative of the individual tests. Figures 89 through 95 are graphic presentations showing the propellant flowrates and heat flux versus time for each test.

Test 153 - This series started with a 2 second checkout test at 300 psia at nominal MR (1.7) with 14% fuel film-cooling. The injector and chamber appeared clean and free of carbon following this test. The exhaust plume exhibited clearly visible shock diamonds which was in contrast with the brilliant white flame noted with propane (see Figure 96). No indication of combustion instability was noted.

Test 154 - This was a repeat test for longer duration. The test was terminated prior to ignition due to low water flow (approximately 13% low) in the resonator cooling circuit. There is no explanation for the low flow measurement. A determination was made that the cooling margin was adequate to proceed with testing as planned.

Test 155 - This test was a repeat of Test 154 conditions with the low water flowrate kill for the resonator reduced to 1 lb/sec. The test was terminated after 5 seconds by a computer time problem. The 5 second test was long enough to obtain steady-state performance data and approach steady-state thermal conditions.

Test 156 - This test was a 300 psia low MR (1.4 core) test for a duration of 30 seconds with 14% fuel film-cooling. The last 5 seconds was with the film cooling valve closed to provide data with no film-cooling.

Test 157 - Test 157 repeated the Test 156 conditions for the same duration. Inspection of the heat flux for tests 156 and 157 (Figures 91 and 92) shows highly repeatable chamber heat flux values.

Test 158 - This was a 30 second nominal MR test (1.7 core) at 300 psia with the film cooling reduced to 7.6%. In this test, the throat heat flux dropped when the film coolant was turned off at 25 seconds. Posttest inspection showed a light dusting of carbon in the throat and exit cone.

Test 159 - Test 159 was a 30 second duration, 300 psia, oxidizer-rich test (MR core 2.5), with 14% fuel-film cooling for 25 seconds and 0% film-cooling for the last 5 seconds. A significant increase in the throat heat flux was observed when the film coolant was terminated. Posttest inspection showed the injector face to be darker and more carbon-coated than in previous tests while the throat had bright clean copper-colored streaks.

TABLE XIII

OFO TRIPLET INJECTOR (INJECTOR #3) PERFORMANCE DATA SUMMARY OF TEST SERIES #4 - WATER-COOLED CALORIMETER CHAMBER, WITH FFC (INJECTOR #4), LOX/ETHANOL

Test No.	Time (sec)	MR_{ENG}	MR_{CORE}	P_{oj} (Pc) (psia)	$\dot{W}_T$ (lbm/sec)	% FFC (% Fuel)	Isp,vac	ηIsp	ERE
153	1.5	1.54	1.79	201	3.95	14.2	231.5	0.8990	0.9352
155	1.5	1.46	1.71	291	3.97	14.2	231.6	0.9019	0.9382
	4.0	1.46	1.71	294	3.97	14.2	232.9	0.9069	0.9434
156	1.5	1.20	1.41	276	3.91	14.3	221.8	0.8918	0.9277
	5.5	1.19	1.39	276	3.90	14.4	222.9	0.8988	0.9350
	10.5	1.18	1.38	278	3.93	14.4	222.5	0.8994	0.9356
	20.5	1.18	1.38	279	3.92	14.3	223.5	0.8994	0.9356
	29	1.36	1.36	272	3.79	0	225.1	0.8827	0.9182
157	7.5	1.21	1.41	279	1.21	14.3	222.4	0.8932	0.9292
	5.5	1.20	1.40	280	3.96	14.4	223.3	0.8979	0.9340
	20.0	1.18	1.38	283	3.98	14.4	223.6	0.8994	0.9356
	29	1.37	1.37	276	3.86	0	225.4	0.8829	0.9184
158	1.5	1.74	1.88	288	3.84	7.2	235.6	0.9207	0.9578
	5.5	1.72	1.86	289	3.86	7.6	236.9	0.9247	0.9619
	20.5	1.69	1.83	293	3.88	7.8	238.1	0.9279	0.9653
	29	1.82	1.82	289	3.84	0	237.5	0.9325	0.9700
159	1.5	2.13	2.48	291	3.92	13.9	234.2	0.9391	0.9769
	5.5	2.13	2.47	292	3.93	14.0	235.9	0.9459	0.9840
	20.5	2.09	2.44	296	3.95	14.0	236.9	0.9472	0.9853
	29	2.35	2.35	292	3.88	0	237.8	0.9686	1.008
160	1.5	1.67	1.95	384	5.11	14.5	236.1	0.9133	0.9495
	5.5	1.66	1.94	388	5.13	14.6	239.5	0.9265	0.9632
	20.5	1.65	1.93	391	5.16	14.6	239.4	0.9261	0.9628
	24	1.67	1.93	390	5.14	13.1	240.4	0.9300	0.9668

TABLE XIV

THERMAL PARAMETERS FOR LOX/ETHANOL WITH OFO TRIPLET IN 8.7 IN. L' CHAMBER

Test Run	Time (sec)	MR_{Eng}	MR_{core}	Pc (psia)	$\dot{W}_T$ (lbm/sec)	% FFC (% Fuel)	$\dot{W}_{FFC}$ (lbm/sec)	% FFC (% Total)	$\dot{Q}_{Total}$ (BTU/sec)	Heat Flux $\dot{Q}/A$ (BTU/in.^{2}-sec) 0.5 R	2 A-3	4 A-2	6 A-1	7.5 C-2	8.5 C-1	9 D-1	9.5 D-2	10 D-3
153	2.0	1.54	1.79	291	3.95	14.2	.222	5.62	329.5	1.05	2.53	3.97	3.77	3.44	5.51	10.38	6.30	4.28
155	2.0	1.46	1.71	291	3.97	14.2	.228		334.4	1.09	2.34	3.97	3.85	3.35	5.64	10.5	6.39	4.24
	5.0	1.46	1.71	294	3.97	14.2	.229	5.76	371.3	1.10	2.54	4.14	3.82	3.56	6.06	11.3	7.00	4.84
									380	1.1	2.7	4.3	3.95	3.95	6.35	11.65	7.3	5.10
156	2.0	1.20	1.41	276	3.91	14.3	.252		282.5	0.92	1.75	3.17	3.43	3.15	5.03	9.52	5.64	3.79
	5.0	1.19	1.39	276	3.90	14.4	.256		320.0	1.02	1.83	3.32	3.49	3.26	5.44	10.22	6.04	4.26
	10.0	1.18	1.38	277	3.93	14.4	.259		325.4	1.06	1.84	3.32	3.39	3.32	5.51	10.42	6.21	4.39
	20.0	1.18	1.38	279	3.92	14.3	.257	6.55	328.9	0.90	1.85	3.35	3.37	3.36	5.64	10.58	6.26	4.48
	FS-2/30	1.36	1.36	272	3.79	0	0		388.2	3.54	3.44	3.21	3.35	3.55	6.08	11.30	7.33	5.30
157	2.0	1.21	1.41	279	3.94	14.3	.255											
	5.0	1.20	1.40	280	3.96	14.4	.259											
	20.0	1.18	1.38	283	3.97	14.4	.262	6.60	338.3	0.98	1.87	3.44	3.38	3.39	6.31	11.21	6.21	4.43
	FS-2/30	1.37	1.37	276	3.85	0	0		395.0	3.54	3.47	3.28	3.26	3.50	6.23	11.67	7.45	5.20
158	2.0	1.74	1.88	288	3.84	7.2	.101											
	5.0	1.72	1.86	289	3.86	7.6	.108											
	20.0	1.69	1.83	293	3.88	7.8	.113	2.90	459.6	1.31	3.46	4.49	4.36	4.16	7.31	14.58	8.33	5.81
	FS-2/30	1.82	1.82	289	3.84	0	0		483.9	3.27	4.48	4.36	4.18	4.16	7.18	14.43	8.54	5.92
159	2.0	2.13	2.48	291	3.92	13.9	.174											
	5.0	2.13	2.47	292	3.93	14.0	.175											
	20.0	2.09	2.44	296	3.95	14.0	.178	4.52	409.3	1.28	3.00	4.04	3.70	3.54	7.06	13.91	7.25	5.26
	FS-2/30	2.35	2.35	292	3.88	0	0		504.1	2.80	4.45	4.80	4.37	4.20	7.43	15.68	8.95	6.02
160	2.0	1.67	1.95	384	5.11	14.5	.280	5.44	441.4	1.21	3.80	5.09	4.44	4.11	8.55	15.80	7.64	4.94
	5.0	1.66	1.94	388	5.13	14.6	.282		505.5	1.38	4.03	5.25	4.66	4.37	9.32	16.91	8.49	5.75
	20.0	1.65	1.93	391	5.16	14.6	.283	5.51	528.5	1.55	4.05	5.36	4.70	4.49	9.65	17.5	8.80	6.04

TABLE XIV (cont.)

Run	Pc	MR	WT.	Section	Heat Flux ϕ	Cg_f	Cg_s
156	272	1.36	3.79	R	3.54	0.0241	0.0181
No Film-Cooling				A-3	3.44	0.0234	0.0176
				A-2	3.21	0.0219	0.0164
				A-1	3.35	0.0228	0.0171
				C-2	3.55	0.0193	0.0145
				C-1	6.08	0.0206	0.0155
				D-1	11.30	0.0245	0.0184
				D-2	7.33	0.0194	0.0145
				D-3	5.30	0.0204	0.0153
157	276	1.37	3.85	R	3.54	0.0238	0.0179
No Film-Cooling				A-3	3.47	0.0233	0.0175
				A-2	3.28	0.0221	0.0166
				A-1	3.26	0.0219	0.0164
				C-2	3.50	0.0188	0.0141
				C-1	6.23	0.0208	0.0156
				D-1	11.67	0.0249	0.0187
				D-2	7.45	0.0195	0.0146
				D-3	5.20	0.0198	0.0148
158	289	1.82	3.84	R	3.27	0.0220	0.0153
No Film-Cooling				A-3	4.48	0.0302	0.0210
				A-2	4.36	0.0294	0.0205
				A-1	4.18	0.0282	0.0197
				C-2	4.16	0.0224	0.0156
				C-1	7.18	0.0240	0.0167
				D-1	14.43	0.0305	0.0212
				D-2	8.54	0.0215	0.0150
				D-3	5.92	0.0207	0.0144
159	292	2.35	3.88	R	2.80	0.0205	0.0140
No Film-Cooling				A-3	4.45	0.0326	0.0222
				A-2	4.80	0.0352	0.0240
				A-1	4.37	0.0320	0.0218
				C-2	4.20	0.0246	0.0168
				C-1	7.43	0.0270	0.0184
				D-1	15.68	0.0358	0.0244
				D-2	8.95	0.0243	0.0165
				D-3	6.02	0.0227	0.0154
		1.69 Engine					
158	293	1.83 Core	3.88	R	1.31	0.0088	0.0063
7.8% Fuel Film-Cooling				A-3	3.46	0.0231	0.0164
				A-2	4.49	0.0300	0.0213
				A-1	4.36	0.0292	0.0208
				C-2	4.16	0.0222	0.0158
				C-1	7.31	0.0242	0.0172
				D-1	14.58	0.0303	0.0215
				D-2	8.33	0.0206	0.0146
				D-3	5.81	0.0200	0.0142

Local Diameter Versus Station

R = A-1, A-2, A-3 = 3.40" dia.

C_2 = 2.998", C_1 = 2.294"

D_1 = 1.740", D_2 = 1.878", D_3 = 2.206"

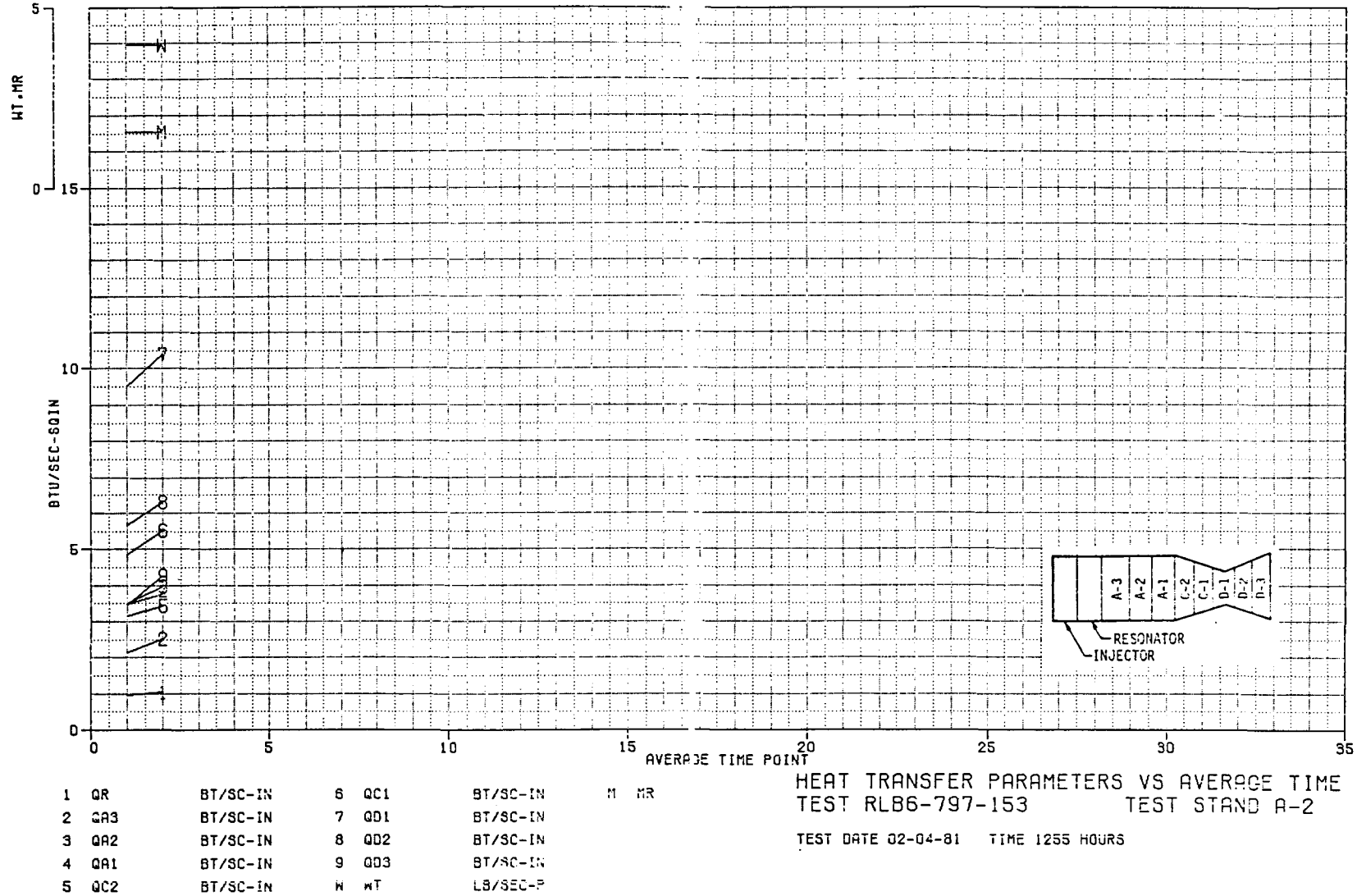

Figure 89. Heat Transfer Parameters Versus Average Time, Test -153

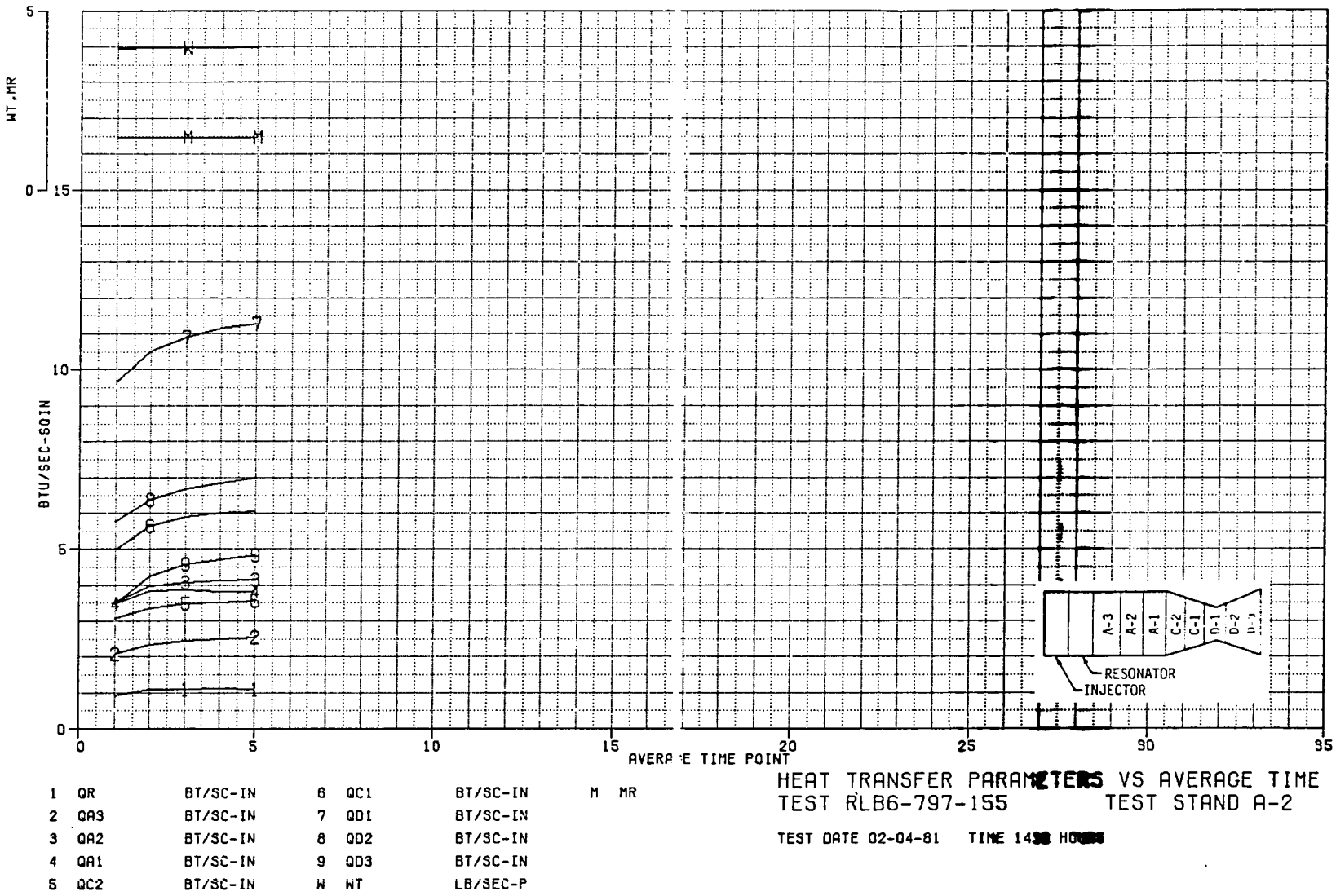

Figure 90. Heat Transfer Parameters Versus Average Time, Test -155

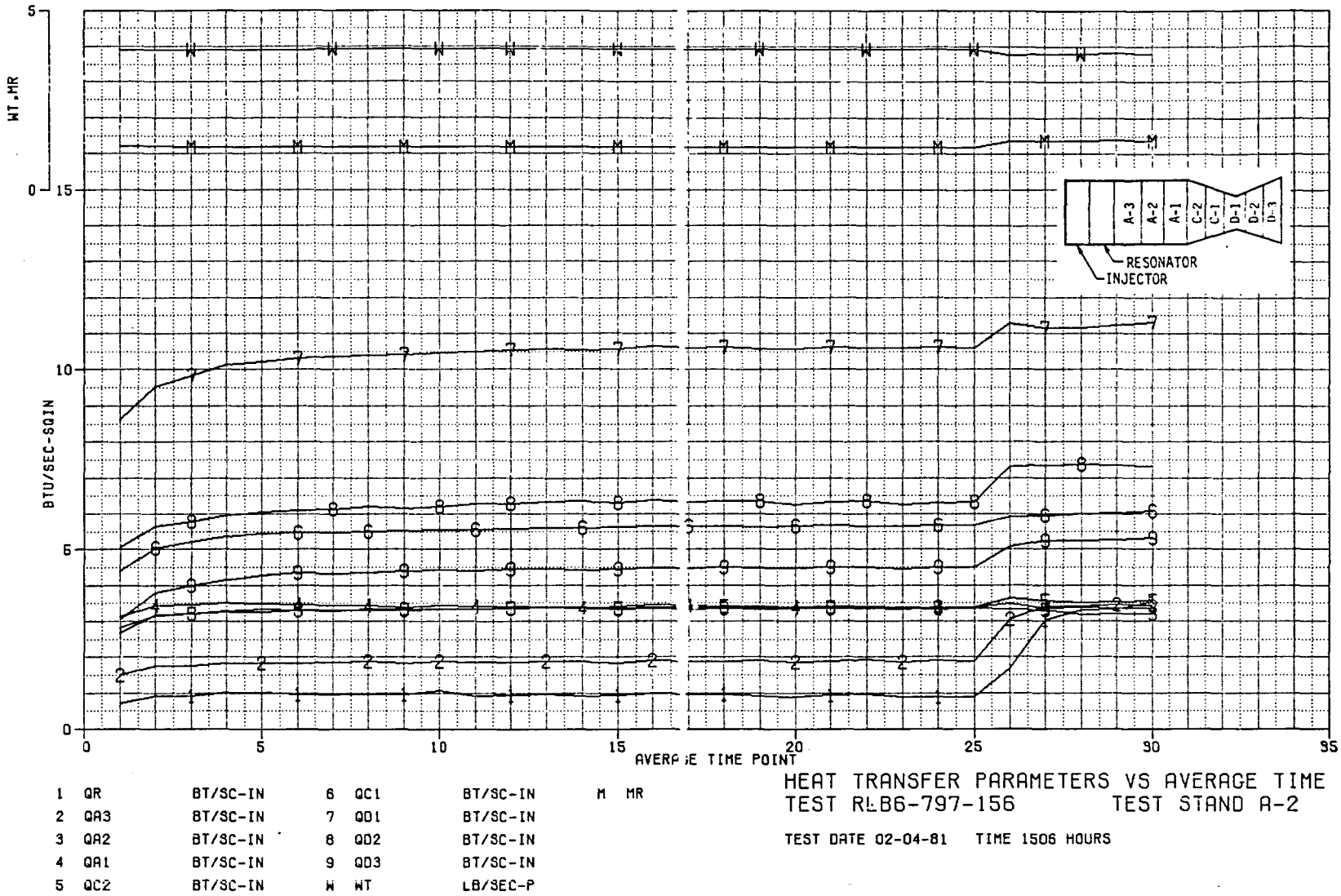

Figure 91. Heat Transfer Parameters Versus Average Time, Test -156

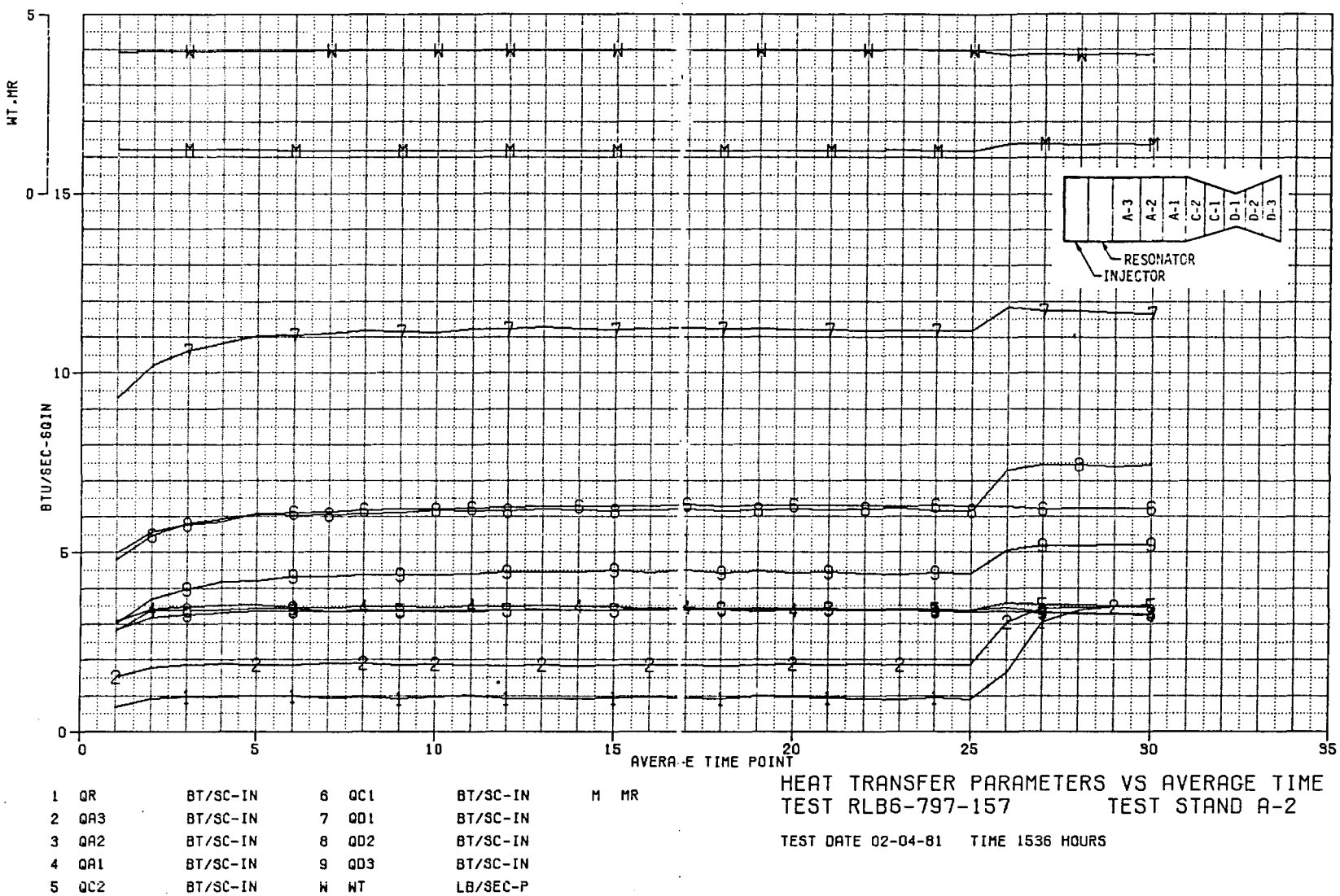

Figure 92. Heat Transfer Parameters Versus Average Time, Test -157

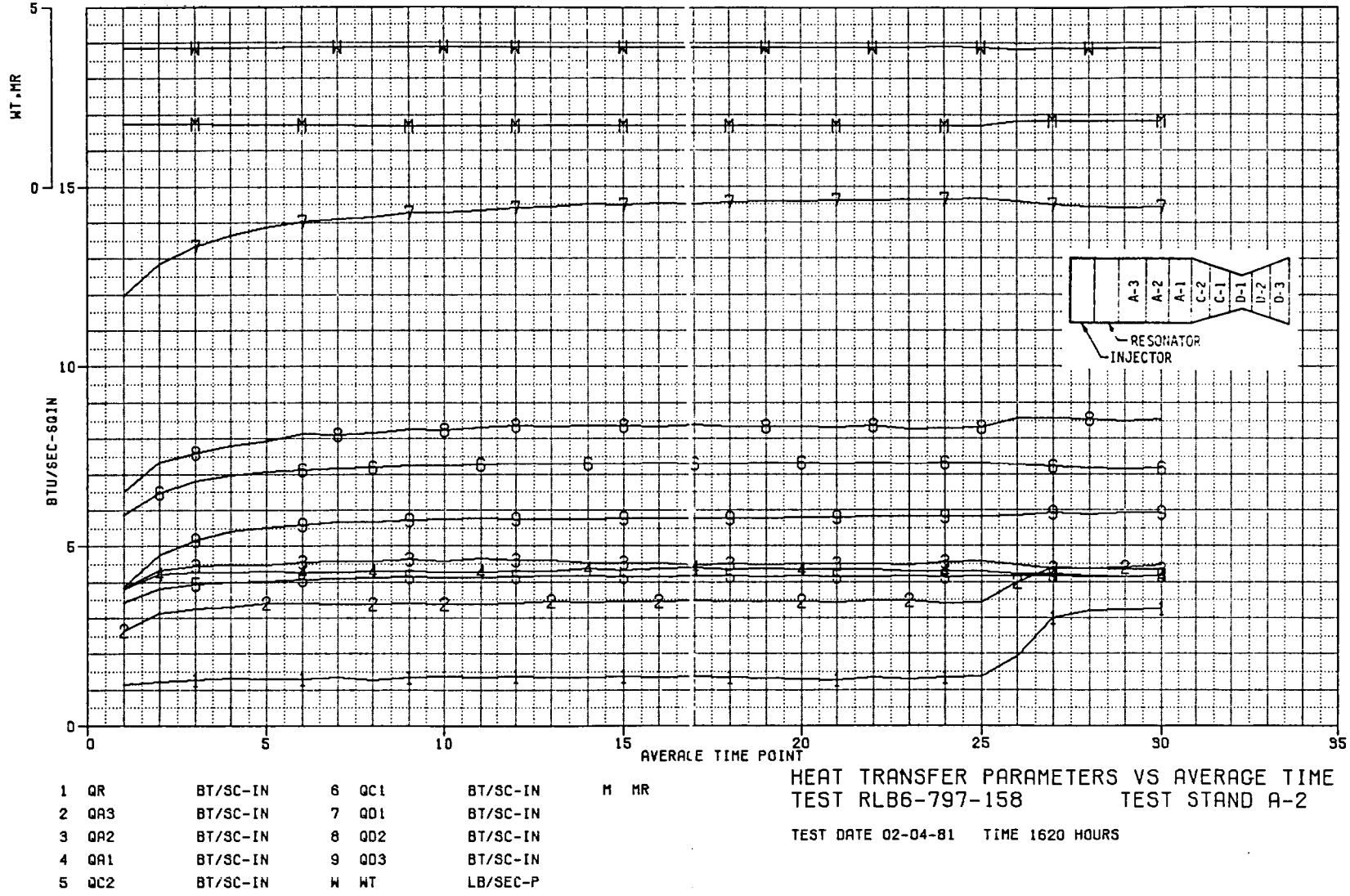

Figure 93. Heat Transfer Parameters Versus Average Time, Test -158

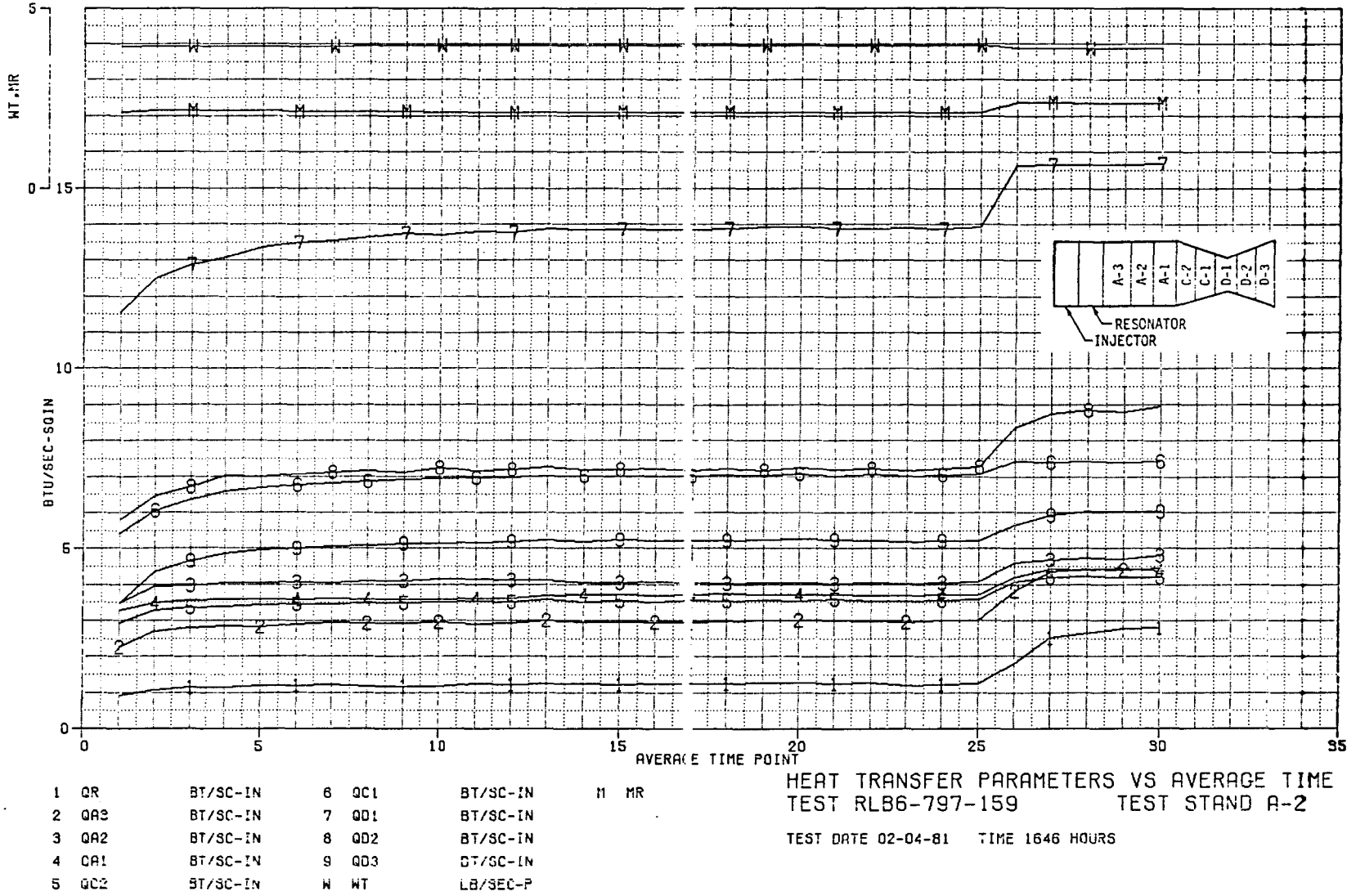

Figure 94. Heat Transfer Parameters Versus Average Time, Test -159

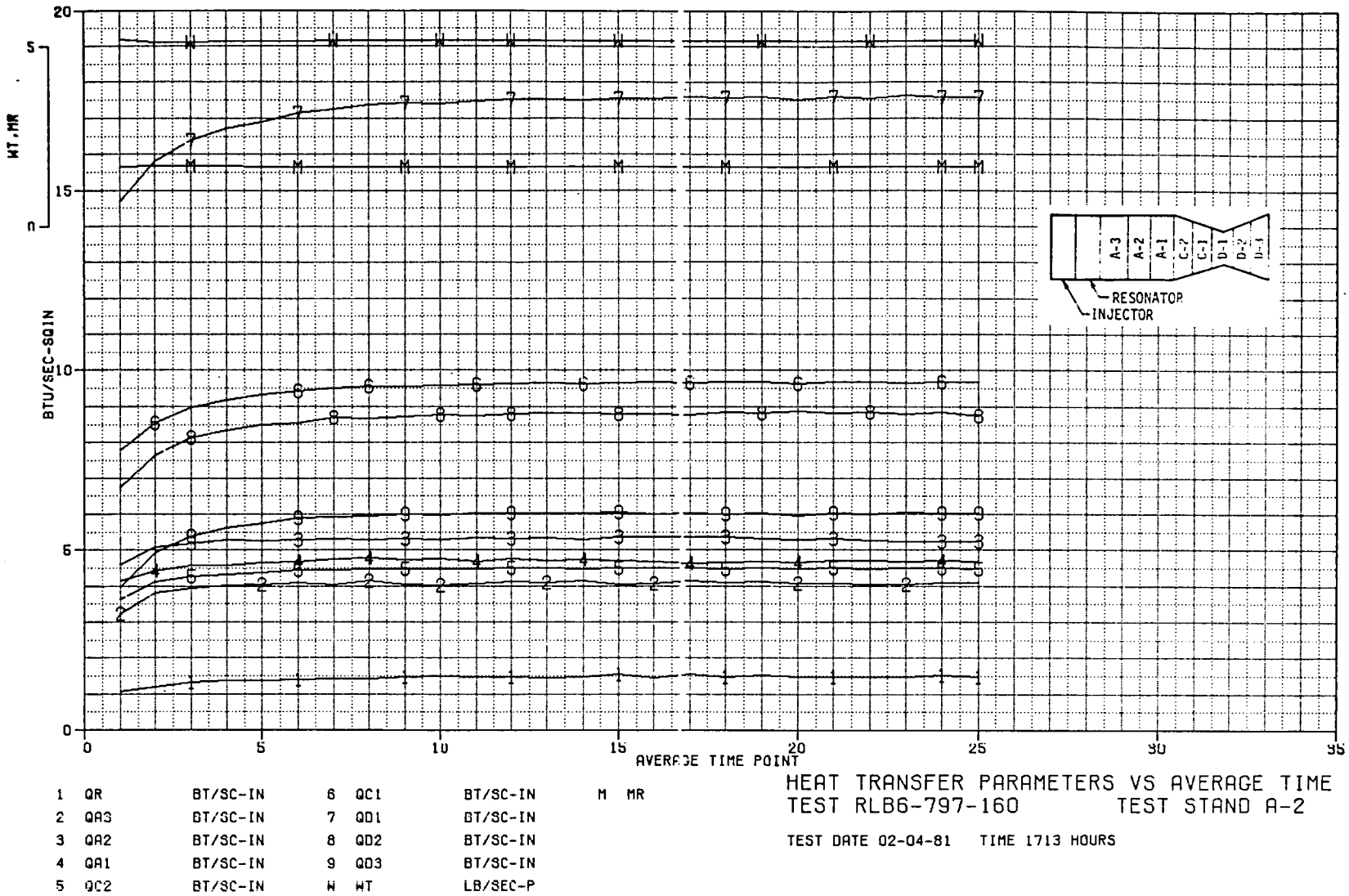

Figure 95. Heat Transfer Parameters Versus Average Time, Test -160

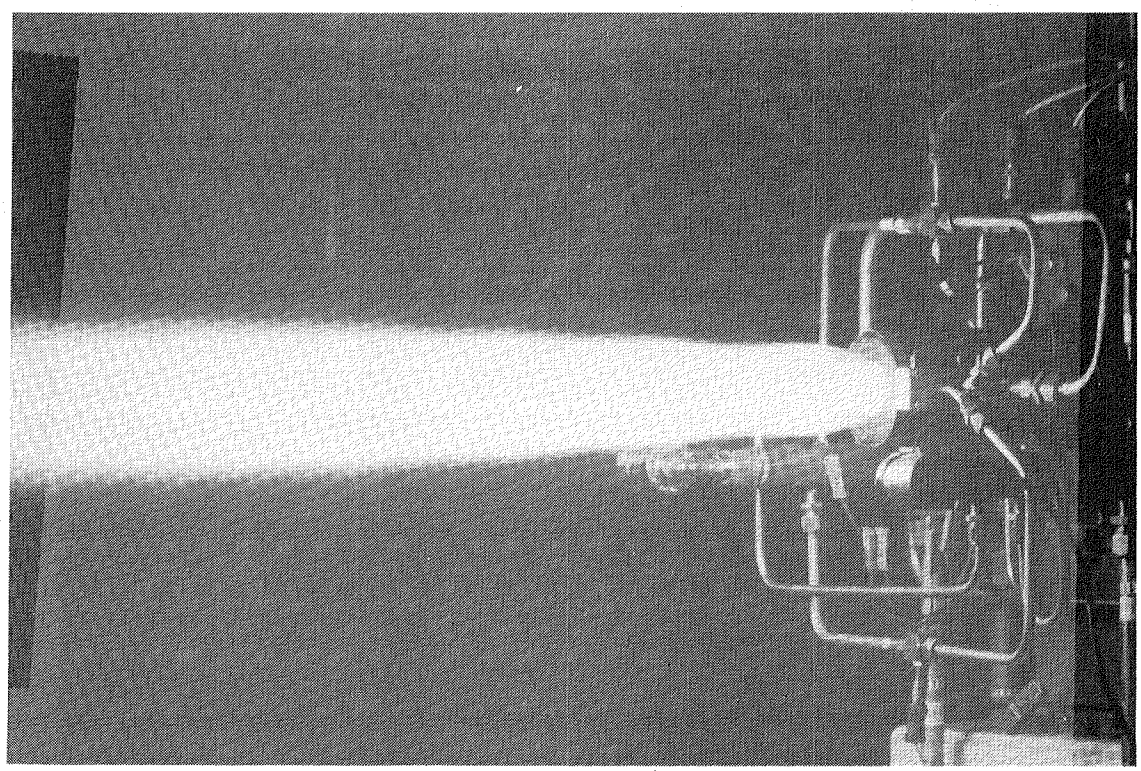

PROPANE EXHAUST PLUME

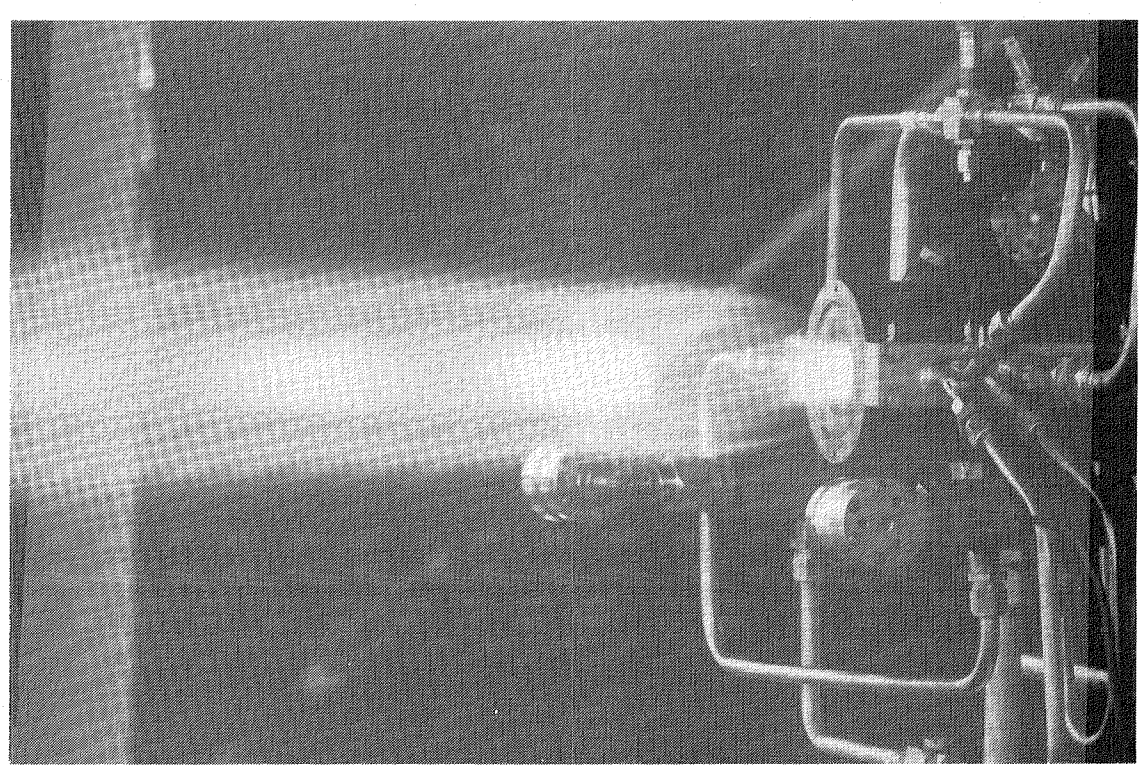

ETHANOL EXHAUST PLUME TEST 157

Figure 96. Comparison of Exhaust Plumes for Propane and Ethanol

E, Tasks II and IV Subscale Injector Characterization (cont.)

Test 160 - This was a 30 second scheduled test at nominal MR (1.7) and 400 psia with 14%/0% FFC. The testing was terminated at approximately 26 seconds (one second following the closing of the film- cooling valve) due to high water temperature leaving the throat section. The throat heat flux of 17.6 Btu/sec-in.^{2} at 25 seconds jumped to 20.9 Btu/sec-in.^{2} at 26 seconds and was still rising when the water rise temperature limit was reached. No hardware damage was noted.

(4) Thermal Results

Axial heat flux profiles for each test of 5 seconds or more duration are provided in Figures 97 through 101. Figure 97 shows the superposition of the nominal test conditions using data from Test 155 with 14.2% FFC and the end of Test 158 with 0% FFC. The coolant is noted to be effective in reducing the head-end temperatures and also the throat temperatures. The throat flux reduction of 19% with 14% ethanol film-cooling compares to a 58% flux reduction with the same percentage of propane film- cooling. When the fuel coolant is expressed as a percentage of total propellant flow, there is a lesser quantity of propane than ethanol.

The data suggest that the film-cooled head end is fuel-rich, that the fuel coolant burns off at the end of 4 inches and that uncombusted fuel droplets deposit on the convergent section to reduce the throat flux.

Figure 98 shows the same type data for fuel-rich Tests 156 and 157. Low MR results in lower overall heat loads for ethanol compared to higher heat loads with propane. The repeat firing of Test 156 conditions in Test 157 provided data showing consistency of the flux measurements and absence of test-to-test variations (within approximately 5%). Coolant burn-off appears to take place within the first 4 inches of the chamber and does little to reduce the throat heat flux at low MR.

Figure 99 provides the heat flux profiles for Test 158 which had approximately 8% and 0% FFC. The rapid consumption of the coolant in the first 3 inches of chamber length, the higher flux with coolant at 4 and 6 inches, and the loss of effectiveness at the throat suggest that there is an oxidizer-rich condition at the head-end wall resulting in a reaction with the coolant. The performance with 8% coolant was found to be higher than with 0% coolant, thus supporting the coolant burnoff theory.

An improvement of film-coolant effectiveness length at high MR is indicated by the data in Figure 100. Under ideal conditions a high MR core should result in more rapid coolant burnoff. Since this is not the case, it must be concluded that the OFO triplet element is less oxidizer-rich near the wall at high MR than at low MR. This conclusion is consistent with the propane test observations where higher wall carbon deposits were observed at high mixture ratio.

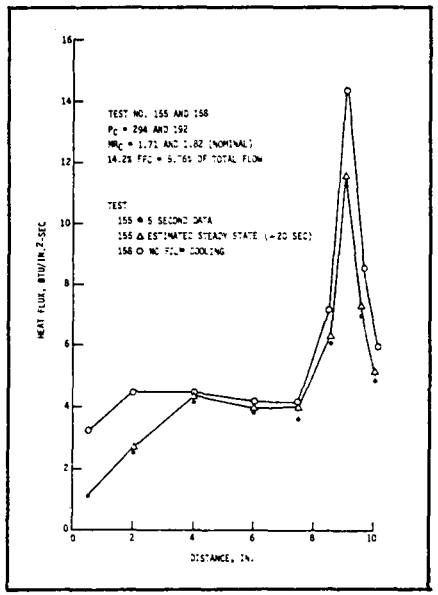

Figure 97. Heat Flux Versus Distance, Tests -155 and -158

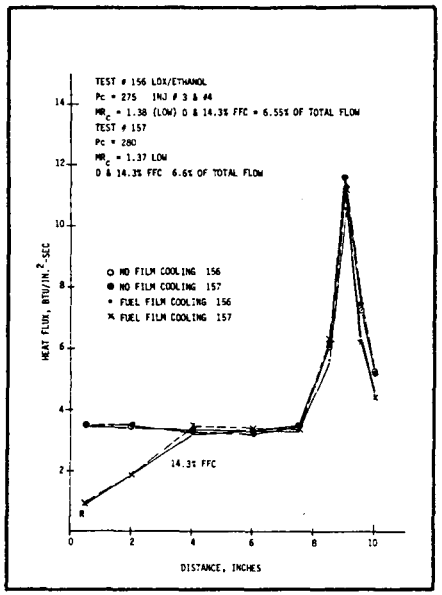

Figure 98. Heat Flux Versus Distance, Tests -156 and -157

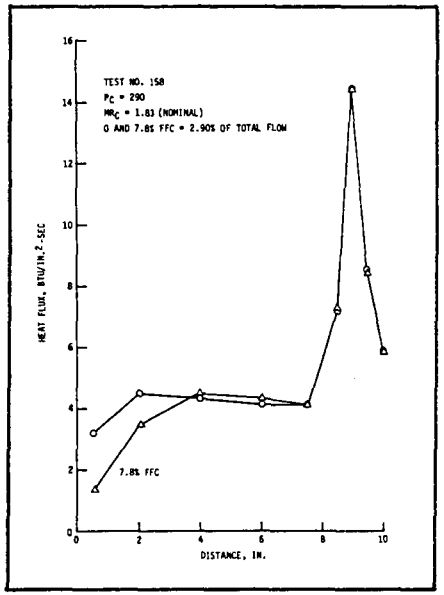

Figure 99. Heat Flux Versus Distance, Test -158

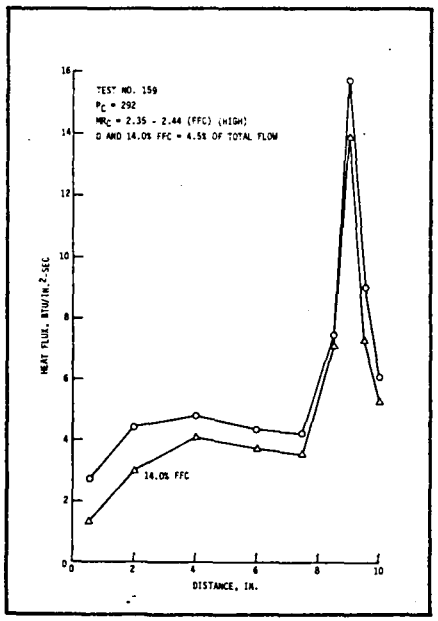

Figure 100. Heat Flux Versus Distance, Test -159

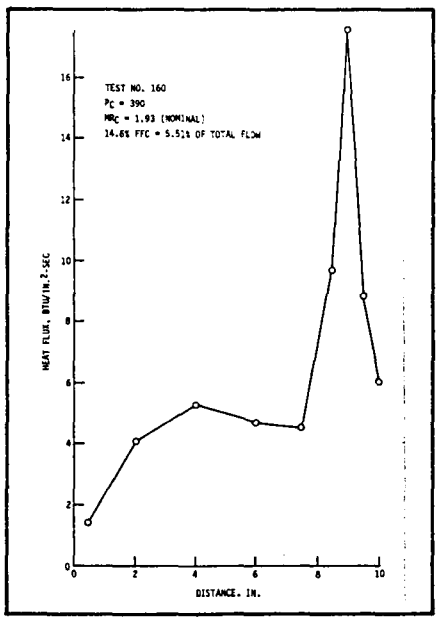

Figure 101. Heat Flux Versus Distance, Test -160

Figure 101 shows the heat flux profile for operation at 400 psia with 14.6% coolant. The estimated throat flux exceeded 21 Btu/sec-in.^{2} when the film-coolant flow was terminated.

Figure 102 provides a comparison of the steady- state heat flux profiles versus mixture ratio for each chamber station and compares the ethanol data to the propane test results. The upper propane flux curves correspond to early times in the test while the lower curves show the fluxes after a steady-state carbon deposit is attained. The heat flux profiles with ethanol do not decay with time and thus indicate no measurable carbon buildup.

The increase of heat flux with increasing MR for ethanol in the chamber region is in contrast to the propane which decreases with increasing MR. The higher oxidizer-to-fuel momentum ratio with the OFO element and propane fuel is believed to result in a fuel-rich condition near the wall when the oxidizer flow is increased even though the engine is oxidizer-rich overall. Conversely, operating at an increased fuel (propane) flow (low MR) results in an oxidizer-rich condition near the chamber head- end. This could explain why there are no carbon deposit effects at the chamber head end at low MR and a large carbon effect at high MR.

The ethanol test data are believed to also indicate a more oxidizer-rich condition near the wall at all operating MR's without fuel film cooling. The wall MR moves to a more optimal mixed condition as the oxidizer-to-fuel momentum ratio increases and thus results in high heat fluxes throughout the chamber, even though in theory the flux should drop at MR values greater than approximately 2.0. These conclusions are consistent with the poor film-cooling effectiveness with ethanol and the improvement in Isp and combustion efficiency as the MR is increased.

Figure 103 provides a comparison of the total heat loads versus core MR for the two fuels . In contrast, the theoretical heat flux for propane is higher than ethanol for an assumed clean-wall condition. The experimental total heat load for ethanol is higher than for propane at the nominal design points (475 Btu/sec for ethanol versus 410 Btu/sec for propane). These data are believed to be highly dependent on the injector design and suggest some carbon deposition effects in the early time heat flux data. The significant differences in the effect of MR and fuel film coolant should also be noted.

(5) Performance results

The measured values of specific impulse relative to the theoretical ODE values are plotted in Figure 104. The peak Isp appears to occur at MR near 2.1. Fuel film-cooling increases the Isp at low MR and reduces the Isp at high MR. The combustion efficiencies with and without FFC are compared on Figure 105, assuming that the product of divergence, boundary layer and kinetic efficiencies of the LOX/ethanol propellant combination is

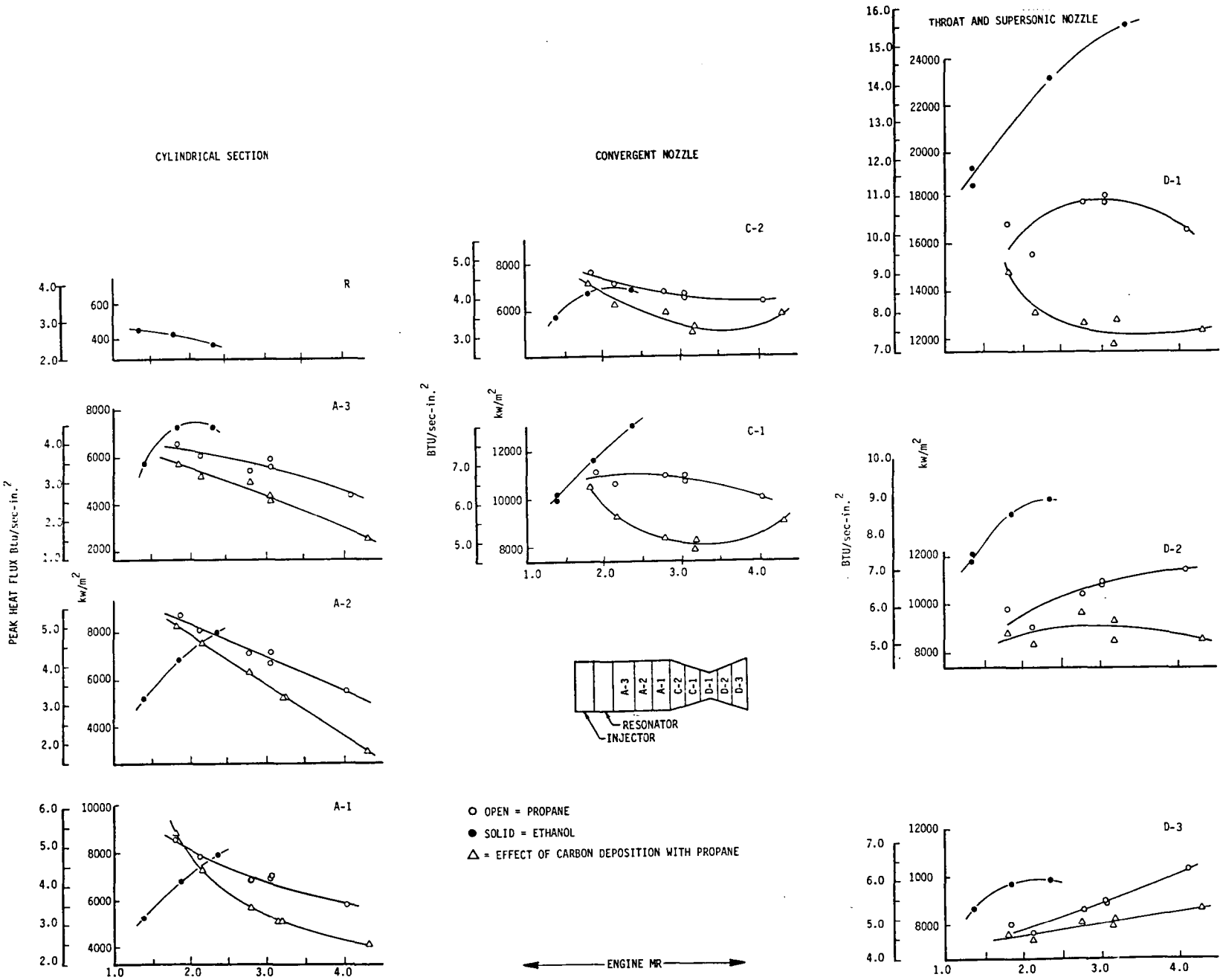

Figure 102. Maximum and Steady-State Heat Flux Versus Engine MR for a Chamber Pressure of 300 psia, No Fuel Film Cooling

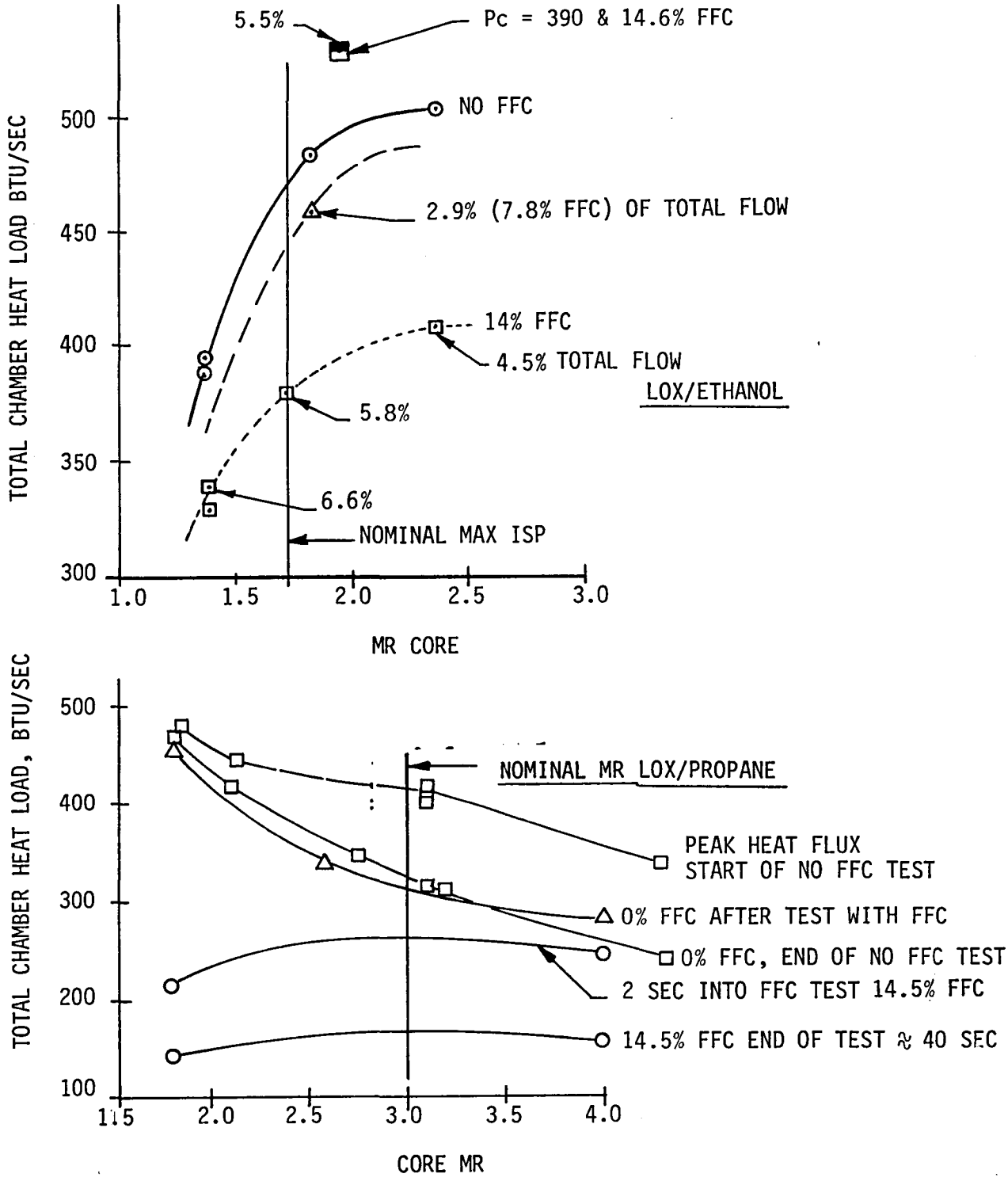

Figure 103. Effect of Core MR and Film Cooling on Heat Load for Propane and Ethanol

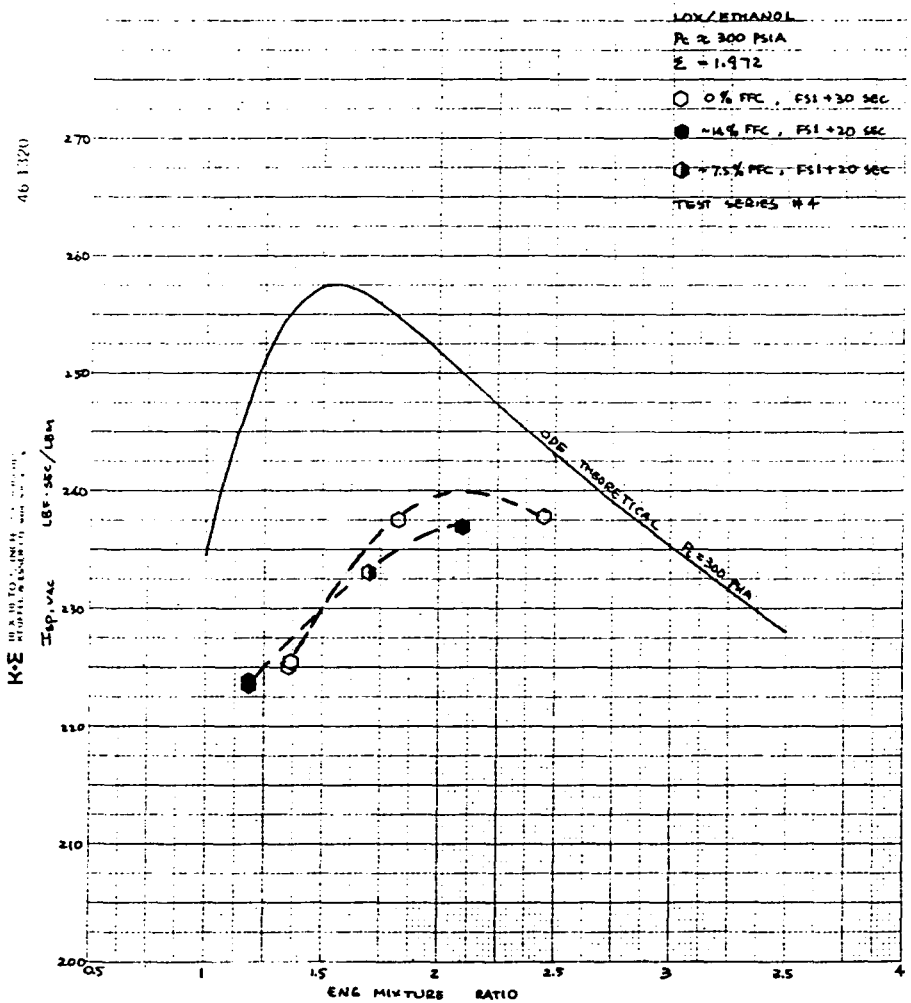

Figure 104. Isp, Vac Versus MR Relationship of LOX/Ethanol, Injector #3, With and Without FFC, Water-Cooled Chamber, Pc = 300 psia, Test Series #5

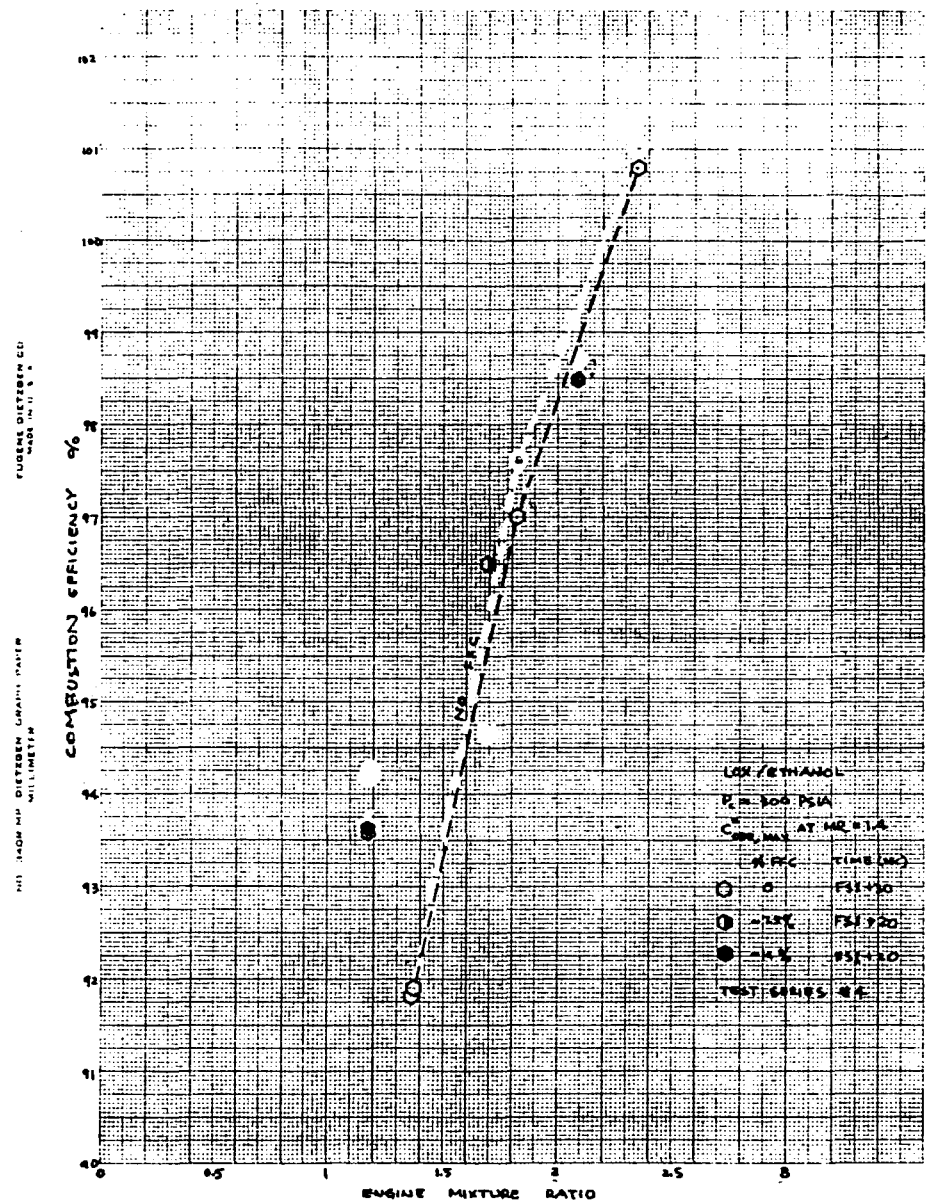

Figure 105. Combustion Efficiency Versus Mixture Ratio of LOX/Ethanol With and Without FFC, Injector #3, Test Series #5, Water-Cooled Chamber

approximately equal to that of LOX/propane combination. The efficiency increases with the addition of FFC at low MR and is decreased by the addition of FFC at high MR. This trend and its causes are similar to those of the propane tests (Figure 87 and 88).

Comparison of Propane and Ethanol Data

Both propane and ethanol have exhibited a strong dependency of performance on mixture ratio. 100% combustion efficiency has been demonstrated at certain mixture ratios. This indicates the existence of uniform atomization, complete vaporization, and high mixing efficiency at the optimum injection momentum ratio for the OFO triplet. Figure 106 shows the graphical relationship of ERE versus momentum ratio for non-film-cooled tests using both propane and ethanol as fuel. The similarity of the ERE-momentum ratio dependency between propane and ethanol is significant. Operation of this injector at a momentum ratio between 2 to 3 will result in the highest ERE. In future designs, the oxidizer injector ΔP should be increased relative to the fuel ΔP in order to achieve optimum efficiency at the mixture ratio corresponding to peak Isp.

Injector Orifice C_D

The injector orifice C_D values determined from the cold flow tests (Figure 26) and the Series #3 hot fire tests (Table VIII) are plotted in Figure 107 as a function of $[(P_j-P_v)/(P_j-P_c)]^{1/2}$, where P_j, P_v, and P_c are manifold, vapor, and chamber pressures, respectively. A discussion of this parameter for correlating orifice cavitation data is provided in Appendix B.

Figure 107 shows that the cold-flow tests were conducted in a cavitating regime, while the hot-fire tests were noncavitating. Both cold-flow and hot-fire fuel data agree well with the theoretical models and indicate that the inception of cavitation is at $[(P_{fj}-P_{fv})/(P_{fj}-P_c)]^{1/2} = 1.3$. The oxidizer hot-fire C_D data are low for noncavitating flow. This is believed to be due to an oxidizer density reduction caused by heat exchange with the fuel in the manifold.

E_m Correlation

The energy release efficiency data presented in Figure 106 were used to infer a hot-fire E_m, assuming a 100% vaporization efficiency for both the oxidizer and the fuel. This hot-fire E_m analysis, shown on Figure 108, indicates that propane and ethanol have virtually identical E_m values as a function of the oxidizer-to-fuel momentum ratio. The E_m reaches its peak (100%) at about a momentum ratio of 2.3, which is greater than the 1.1 value for optimum momentum ratio determined from cold-flow data correlations (Appendix A). This increase in optimum momentum ratio may be due to the high volatility of LOX. The cold-flow mixing is strictly a liquid-phase momentum

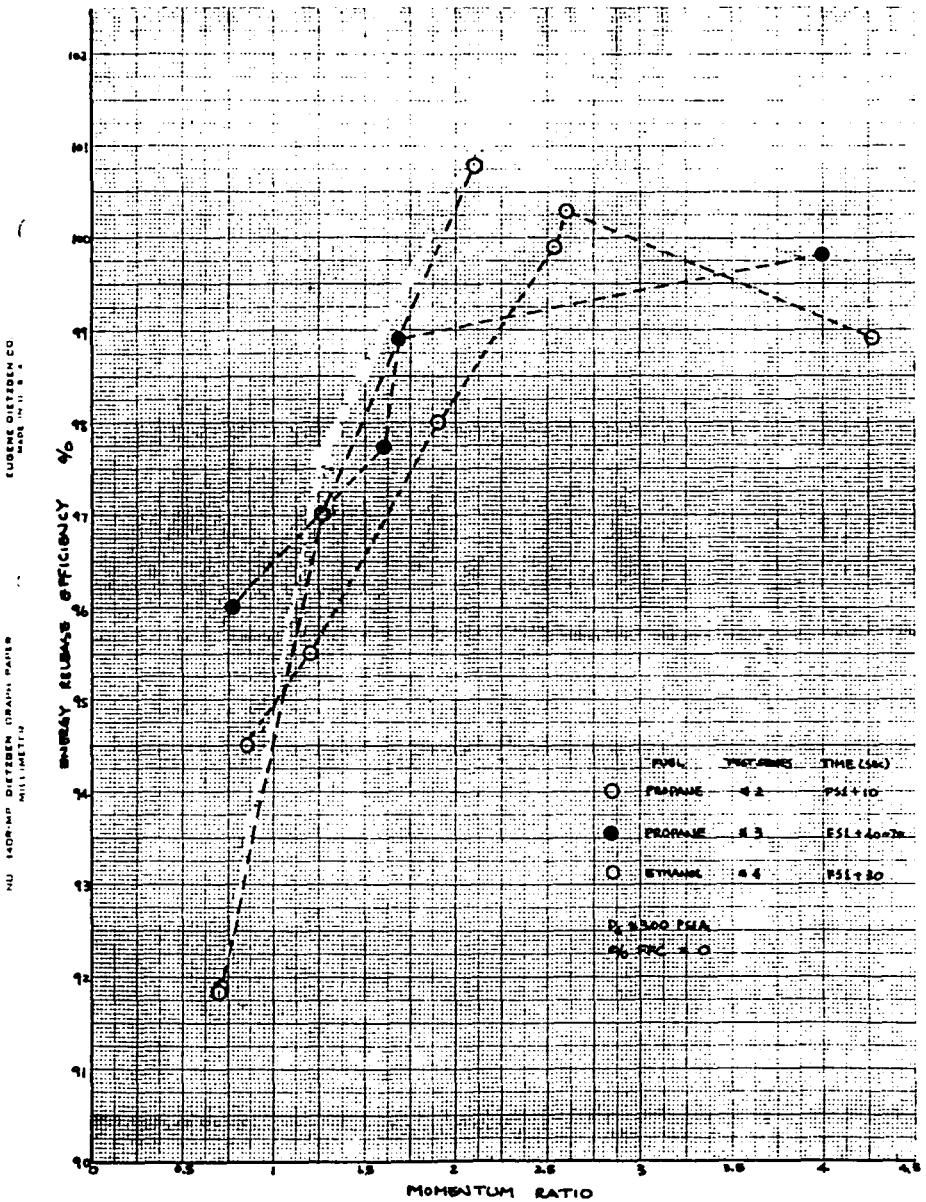

Figure 106. Energy Release Efficiency Comparison of LOX/Propane and LOX/Ethanol Without FFC, Injector #3, Water-Cooled Chamber, Pc = 300 psia

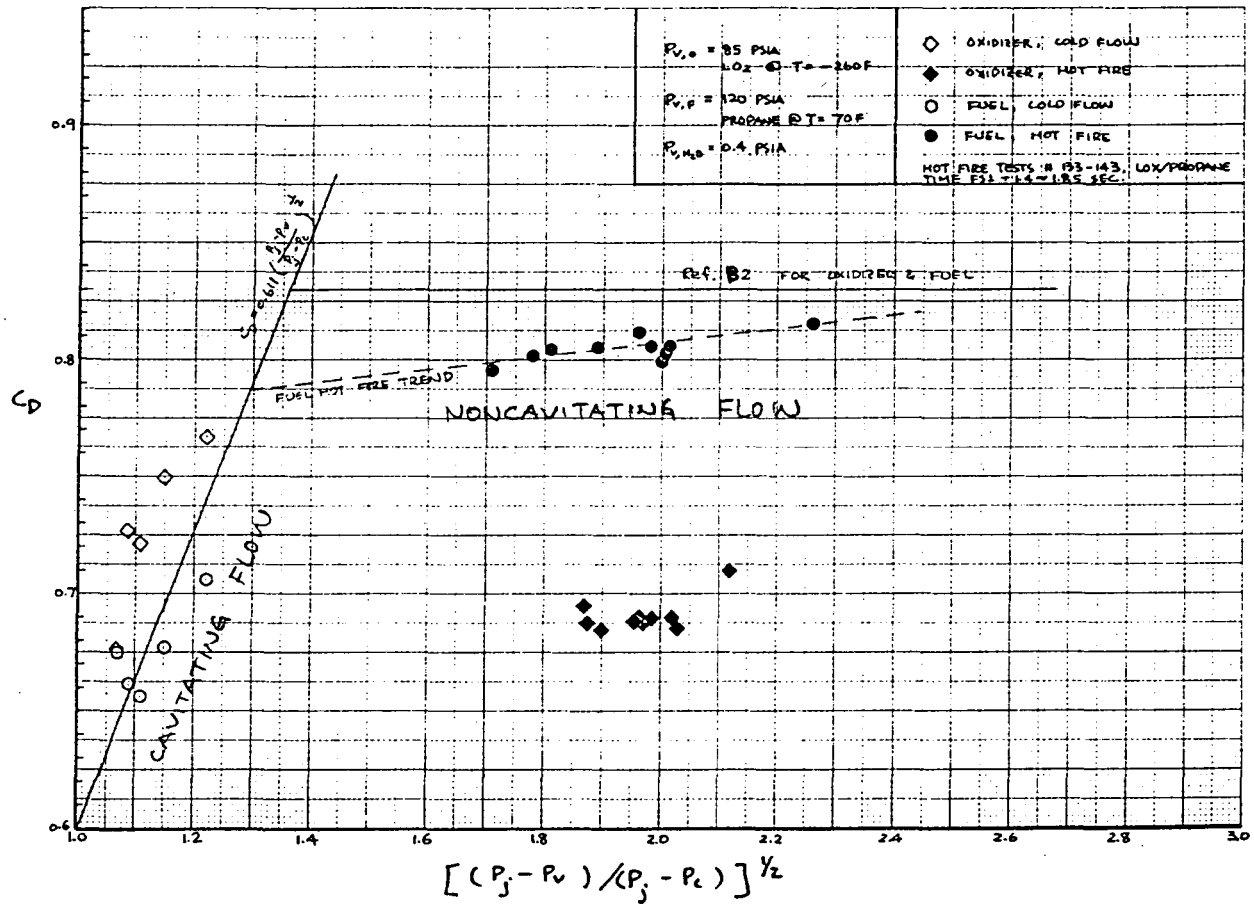

Figure 107. Injector Orifice C_D Data Correlation

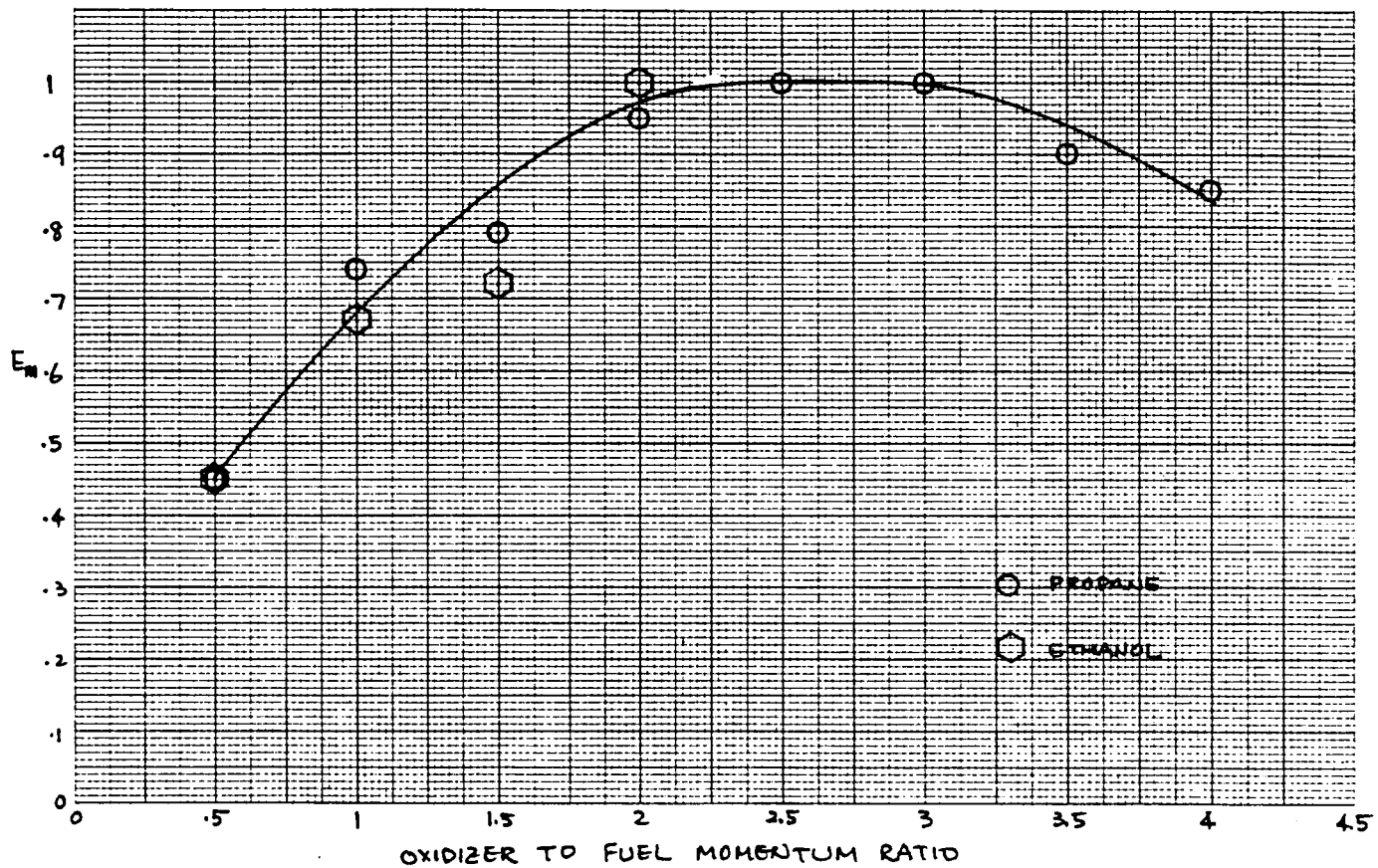

Figure 108. Correlated E_M for Both LOX/Propane and LOX/Ethanol Based on Data Presented in Figure 98 and Assuming 100% Oxidizer and Fuel Vaporization Efficiency

mixing phenomenon without involving the vaporization process. Under hot-fire conditions, however, high LOX volatility can cause a mixing problem that does not exist under cold-flow conditions. The faster vaporizing LOX spray fans produce oxidizer-rich zones surrounding the slower vaporizing fuel core. This not only causes mixing nonuniformity in the radial direction because of the slow diffusion mixing process, but also creates mixture ratio maldistributions in the axial direction. If the hot-fire momentum ratio is increased, a wider fuel fan formation will provide both wider distributed and smaller (faster vaporizing) liquid fuel droplets. Both these two phenomena will improve the propellant mixing. Therefore, optimum mixing of OFO triplet LOX/HC elements requires higher momentum ratio for hot-fire than for cold-flow.

(6) Engine Application Consideration

The results of the test data analysis have shown that the performance of the OFO triplet injector for both propane and ethanol is controlled by the element's oxidizer-to-fuel momentum ratio. The maximum combustion efficiency occured at a momentum ratio range corresponding to a mixture ratio greater than the value selected for maximum specific impulse. To lower the mixture ratio at which the ERE is at its maximum, and thus obtain maximum ERE at maximum Isp, the following two element design modifications should be considered for future applications:

1. Increase the oxidizer-to-fuel momentum ratio by either increasing the oxidizer momentum or reducing the fuel momentum. To increase the oxidizer momentum, the oxidizer orifice area must be reduced while its injector pressure drop is increased. Increasing the fuel orifice area and reducing the fuel injector pressure drop is required for reducing the fuel momentum. Making either or both of the two modifications will result in an impingement stream diameter mismatch (smaller d_{ox}/d_f ratio) if the element is limited to circular orifices. This can be avoided by the use of non-circular EDM orifices having matched impingement element widths in addition to the optimum momentum ratio, or by replacing each existing fuel orifice with two parallel fuel orifices to form a O-F-F-O pattern. The atomization and mixing mechanism of the latter pattern may somewhat deviate from the OFO triplet pattern tested.

2. Increase the oxidizer impingement angle in order to increase the radial component of the oxidizer momentum.

f. Test Series VI - LOX/Ethanol, Ethanol Film-Cooling, PAT (OFO) Platelet Injector, 8.7-in. L', Water-Cooled Chamber

(1) Objectives

The test objectives were to: (1) determine if further improvements in performance could be obtained by using a preatomized OFO triplet, as compared

to the solid stream impinging triplet, 2) to compare the influence of element type and film cooling on the chamber heat flux profiles, and 3) to observe combustion stability characteristics.

(2) Facility

No changes in the facility were made between Series #5 and #6.

(3) Hardware

A new 45-element preatomized triplet injector was designed for LOX/ethanol. Detailed drawings of a new platelet faceplate are shown in Figure 109. The new injector was created by machining off the EDM-OFO pattern and welding the new photoetched platelet faceplate on the same body. Figure 110 shows a photograph of the injector at the conclusion of this test series. Some heat marks are noted on the film-cooling ring in this picture. The injector face however is clean (carbon free) and shows no indication of heat marks.

(4) Cold-Flow

Figure 111 shows the PAT element injector during water cold flow testing. The top picture shows the self-atomization of the oxidizer by the splash plate doublets. The center picture shows the fuel spray cones coming from the swirler elements and the bottom picture shows both circuits flowing simultaneously. The flow coefficients (Kw) were 0.18 for the oxidizer circuit and 0.083 to 0.088 for the fuel circuit. The predicted Kw values were 0.21 for the oxidizer and 0.13 for the fuel. The large difference between the predicted and measured values in the fuel circuit could not be fully explained. A second injector employing the same fuel circuit design provided an experimental Kw value of 0.10; thus one must conclude that at least a portion of the difference is a result of the fabrication process.

(5) Hot-Fire Tests

Nine hot-fire tests were conducted with the platelet OFO PAT injector in the 8.7-in. L' water-cooled calorimeter chamber. The test conditions are summarized in Table XV. The nominal test duration was 30 seconds. Fuel film-cooling was utilized for the first 25 seconds of each test, and the last 5 seconds were completed without film-cooling. Figures 112 through 120 document the propellant flowrate, MR, and local chamber heat flux measurements. Tables XVI and XVII document the heat flux without and with film-cooling, respectively. The events accompanying each test were as follows:

Test 161 was a checkout test at 300 psia for a duration of 1.8 seconds. Nominal Pc and MR were attained; however the fuel film-cooling flowrate was too high, i.e., 22.6% versus the 16% desired.

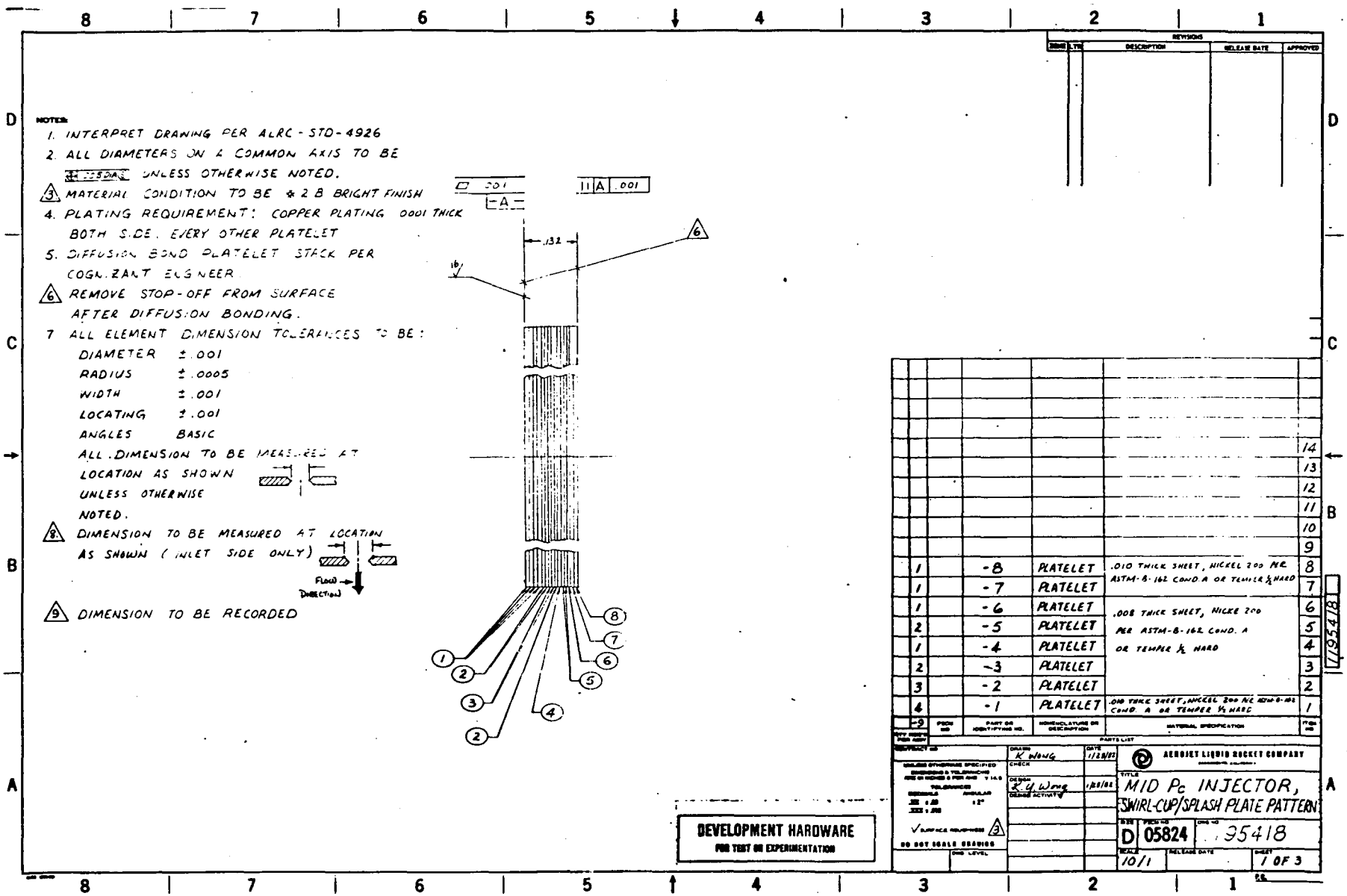

Figure 109. LOX/Ethanol Platelet Injector (1 of 3)

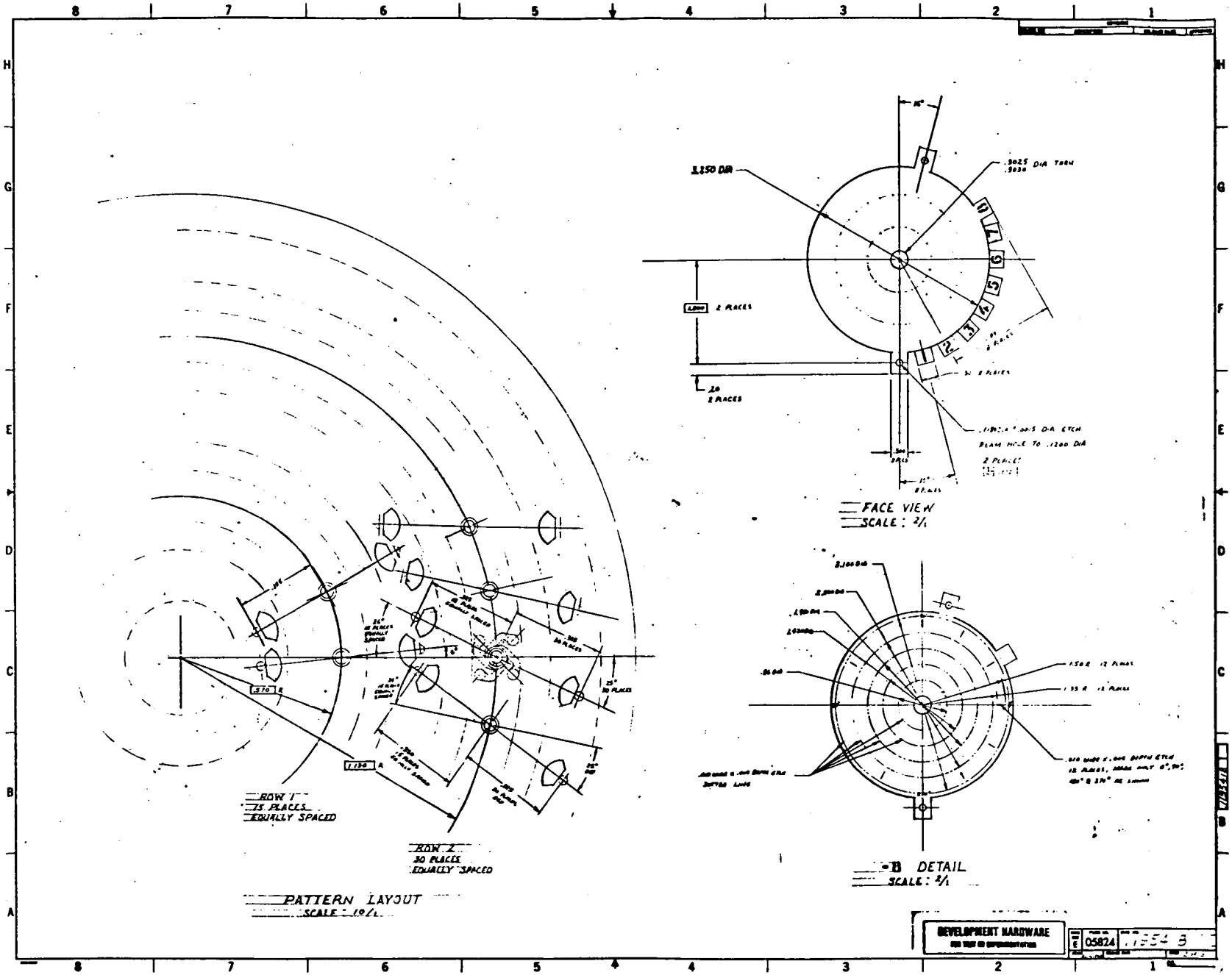

Figure 109. LOX/Ethanol Platelet Injector (2 of 3)

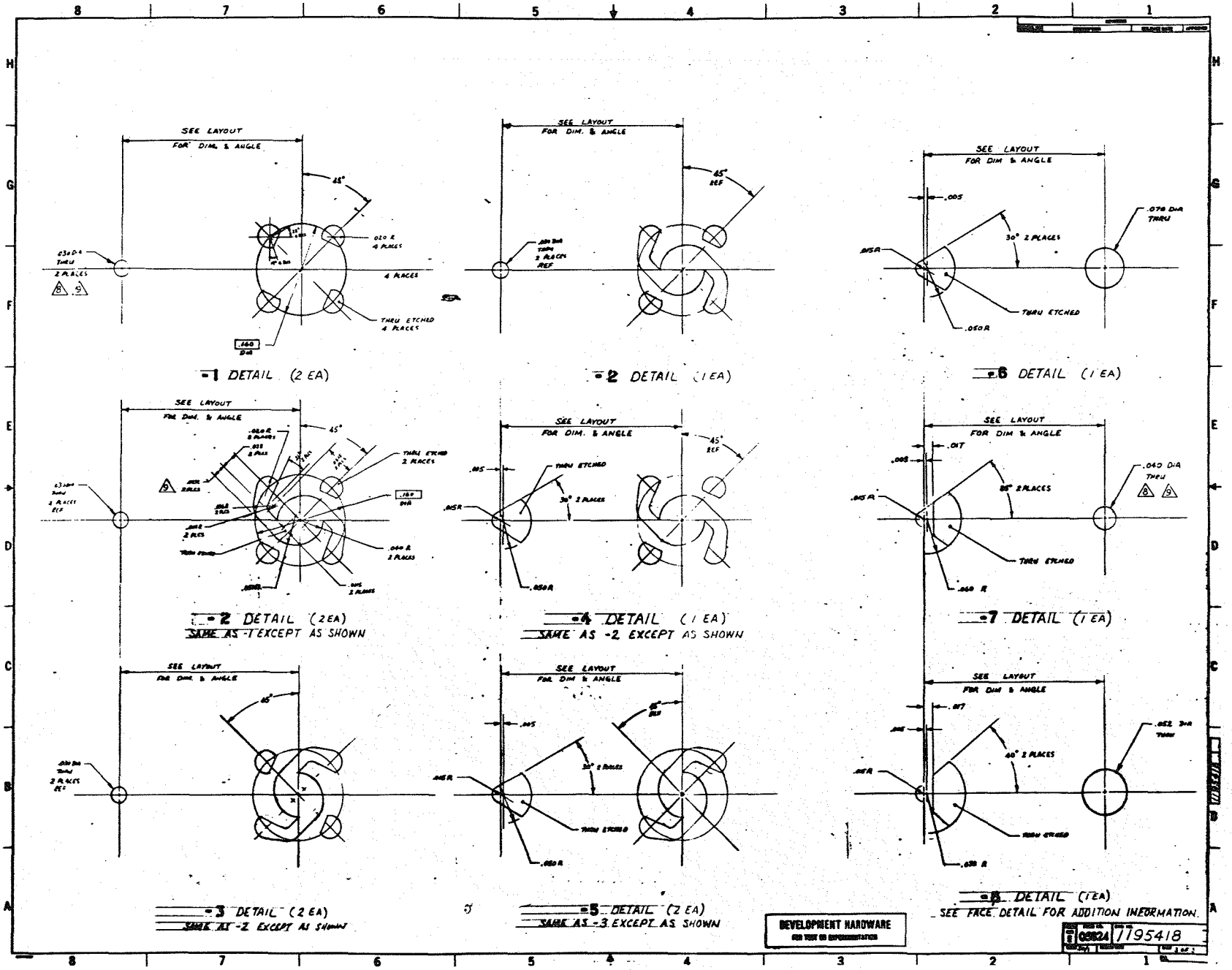

Figure 109. LOX/Ethanol Platelet Injector (3 of 3)

Figure 110. OFO PAT After Test -169

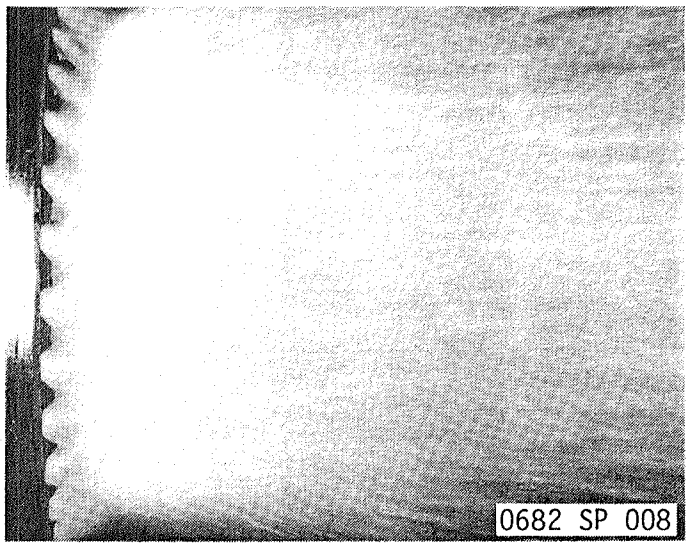

OX SPLASH PLATE ONLY

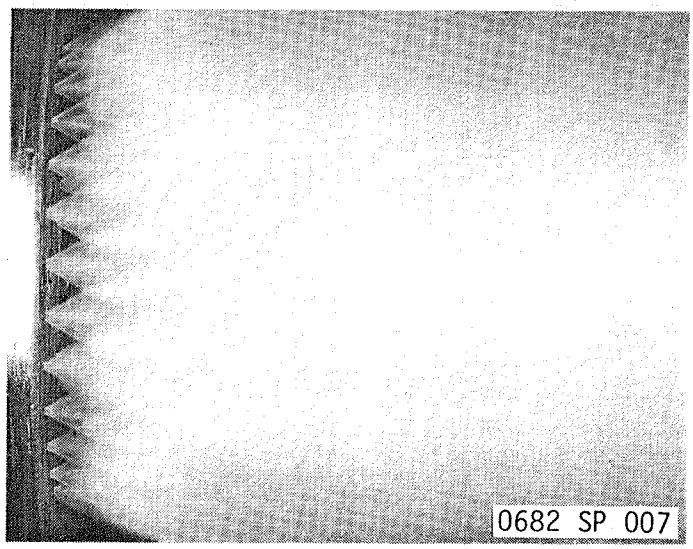

FUEL SWIRLER ONLY

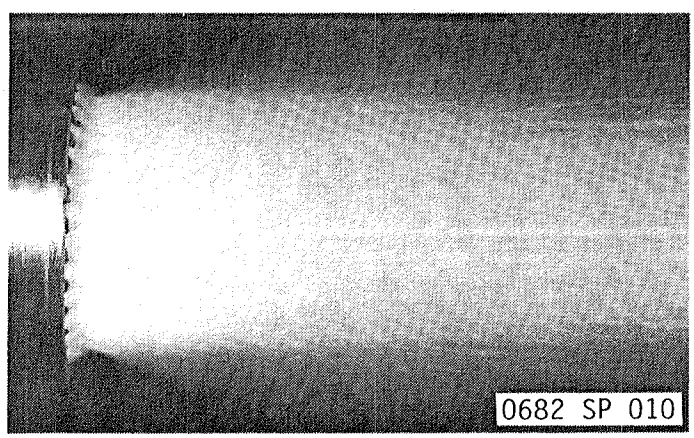

FUEL AND OX

Figure 111. Preatomized Triplet (PAT) Injector Cold Flow

TABLE XV

LOX/ETHANOL TEST SUMMARY OF PAT (OFO) PLATELET INJECTOR

Test	Time Sec	Pc	MR_{core}/MR_{eng}	%FFC	C*	Isp	Comments
161	1.85	283	1.61/1.24	22.6	5216	230.8	Checkout, FFC Too High
162	≈1.0						High FFC Kill
163	20.8	298	1.86/1.54	16.8	5346	238.7	Normal Test
	30.3	285	1.87/1.87	0	5258	233.7	
164	1.85	299	2.40/1.99	16.9	5368	239.8	Kill High Water Temp
165	20.8	296	2.49/2.07	16.9	5413	241.7	Normal Test
	30.3	283	2.45/2.45	0	5266	233.7	Normal Test
166	20.8	295	1.41/1.16	17.2	5180	230.7	Normal Test
	30.3	281	1.43/1.43	0	5123	227.3	Normal Test
167	20.8	201	1.85/1.55	16.5	5369	238.8	Normal Test
	30.3	194	1.87/1.87	0	5288	233.9	Normal Test
168	20.8	396	1.89/1.56	17.3	5301	236.2	Normal Test
	30.3	377	1.88/1.88	0	5252	232.9	Normal Test
169	20.8	292	1.87/1.70	8.7	5323	237.3	Normal Test
	30.3	288	1.87/1.87	0	5303	234.9	Normal Test

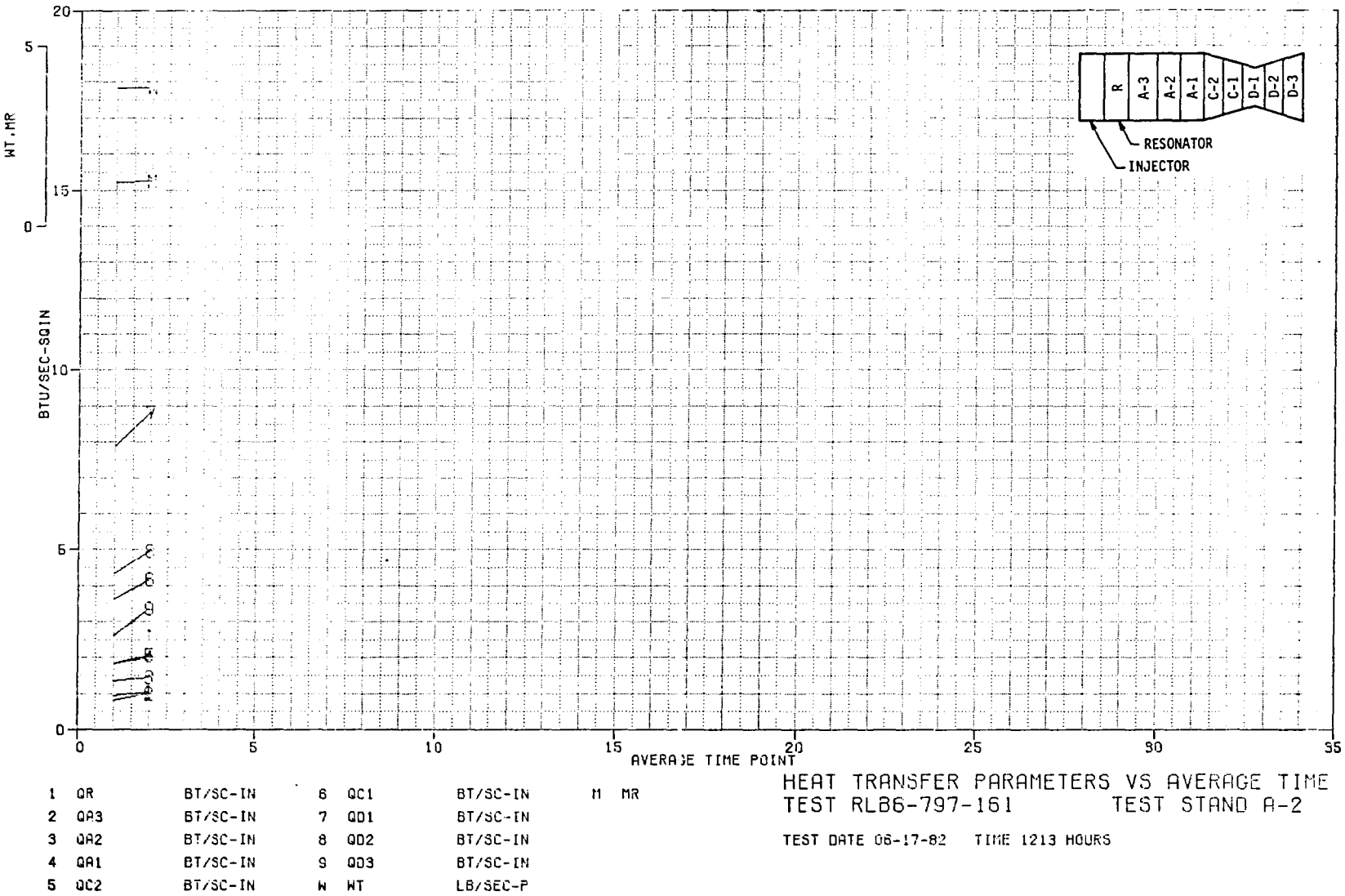

Figure 112. Heat Transfer Parameters Versus Average Time, Test RLB6-797-161

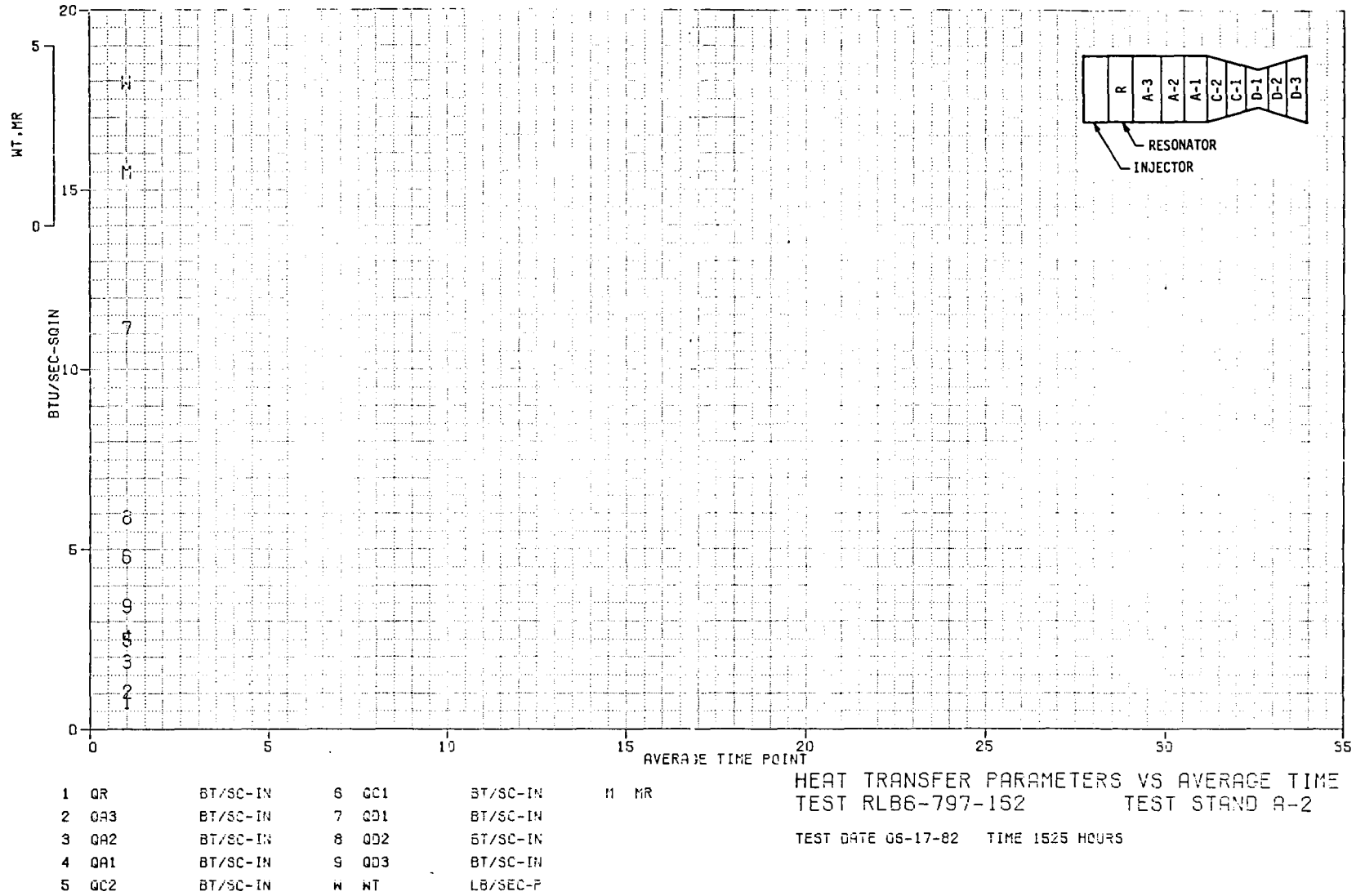

Figure 113. Heat Transfer Parameters Versus Average Time, Test RLB6-797-162

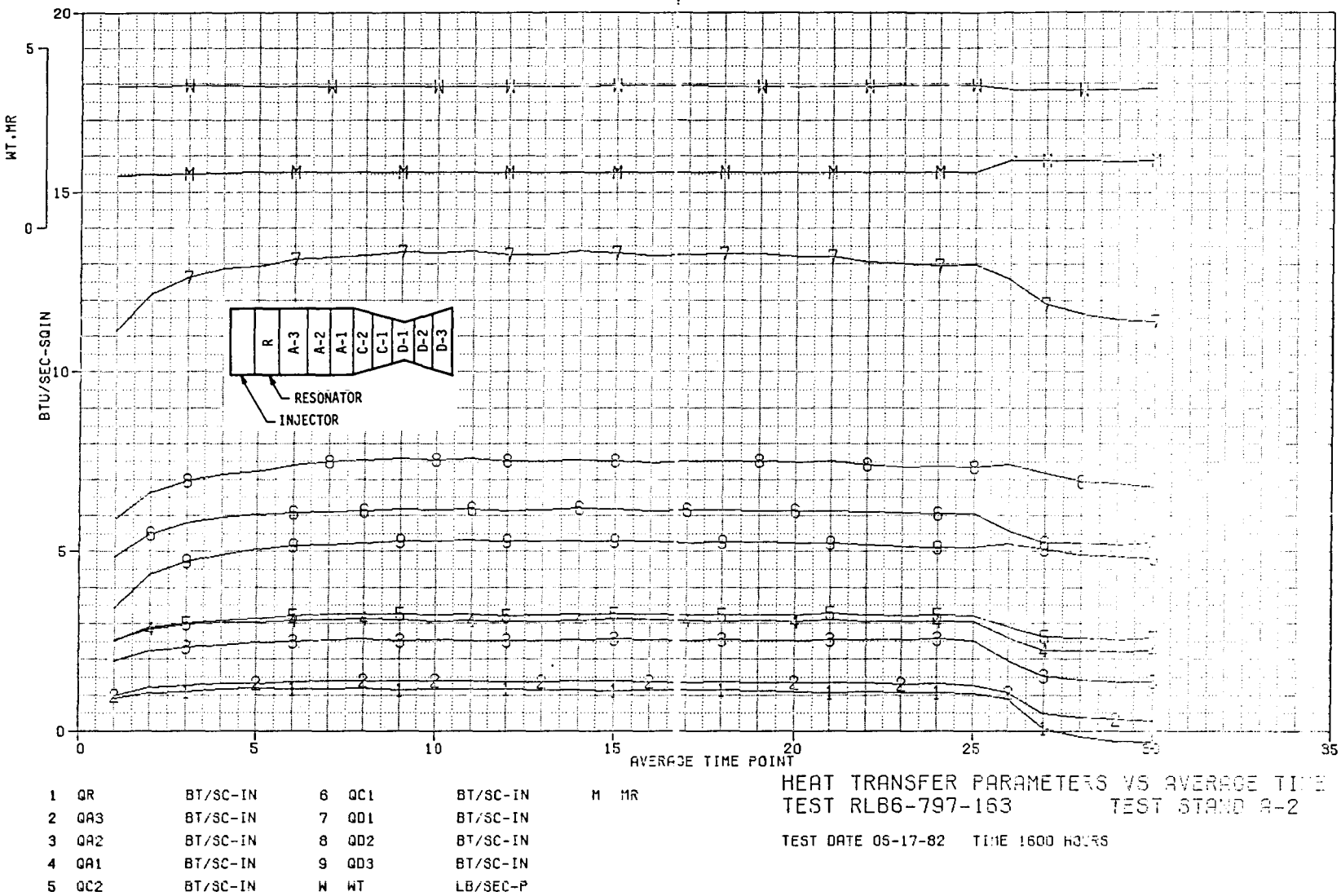

Figure 114. Heat Transfer Parameters Versus Average Time, Test RLB6-797-163

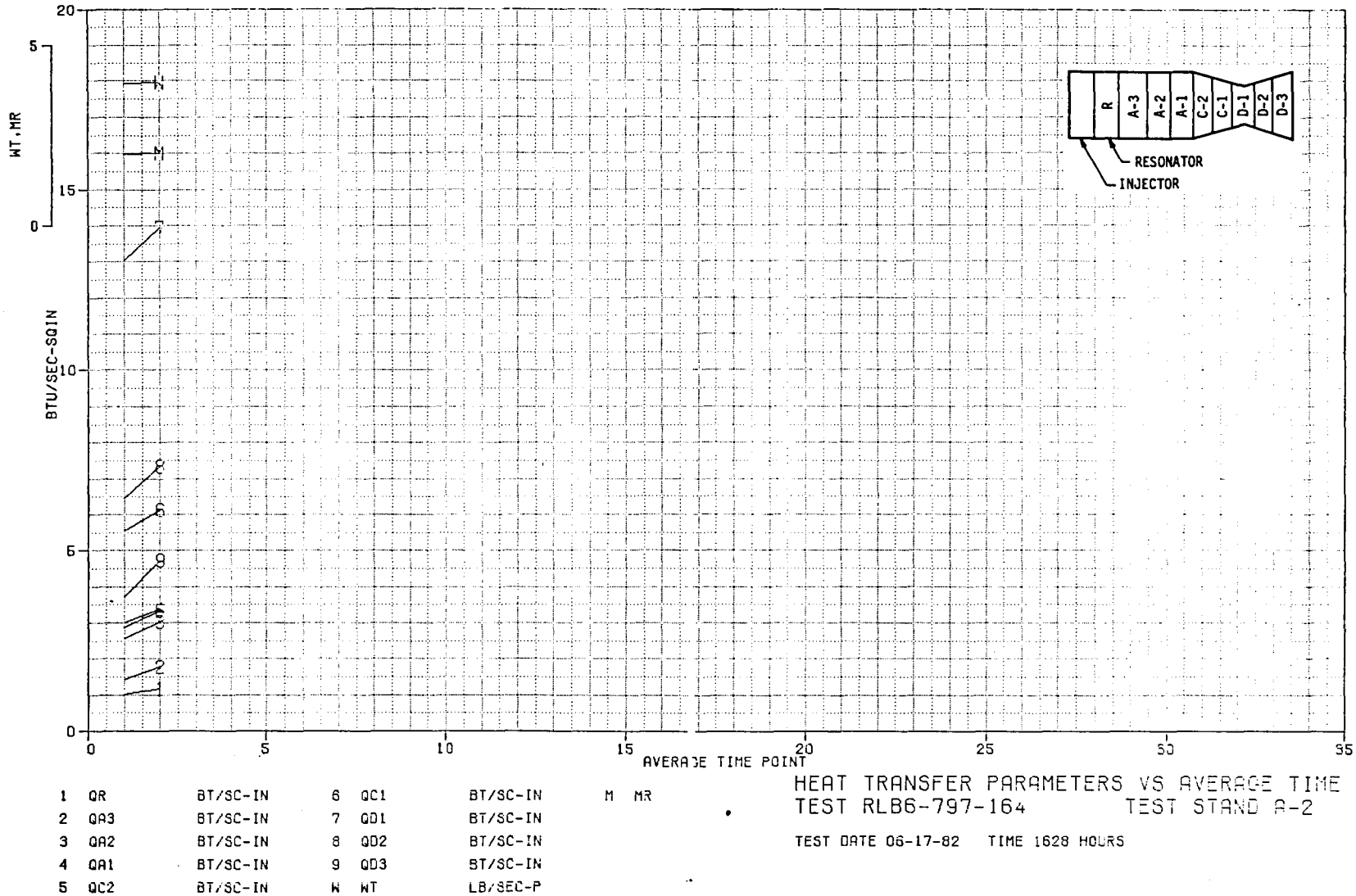

Figure 115. Heat Transfer Parameters Versus Average Time, Test RLB6-797-164

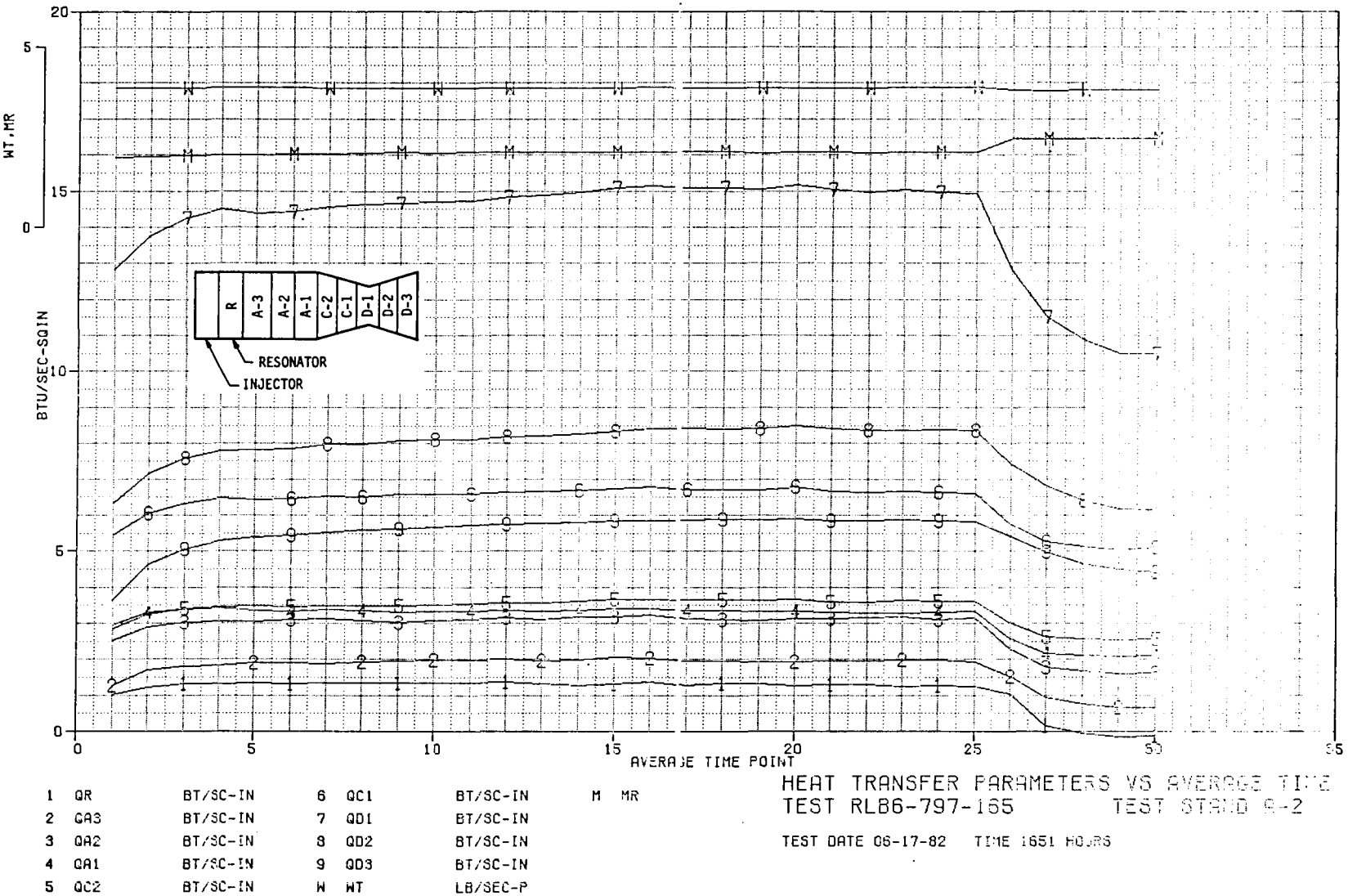

Figure 116. Heat Transfer Parameters Versus Average Time, Test RLB6-797-165

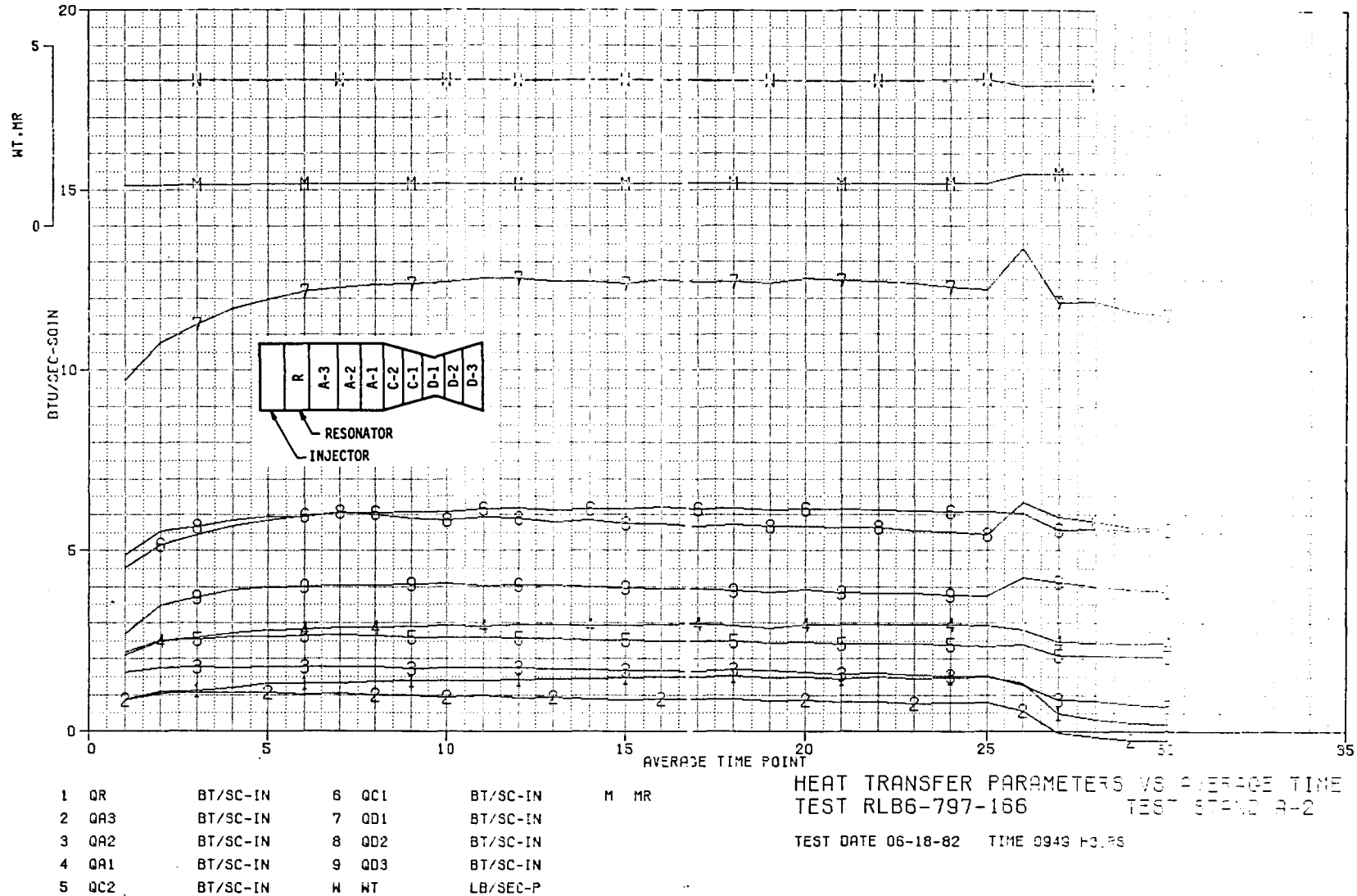

Figure 117. Heat Transfer Parameters Versus Average Time, Test RLB6-797-166

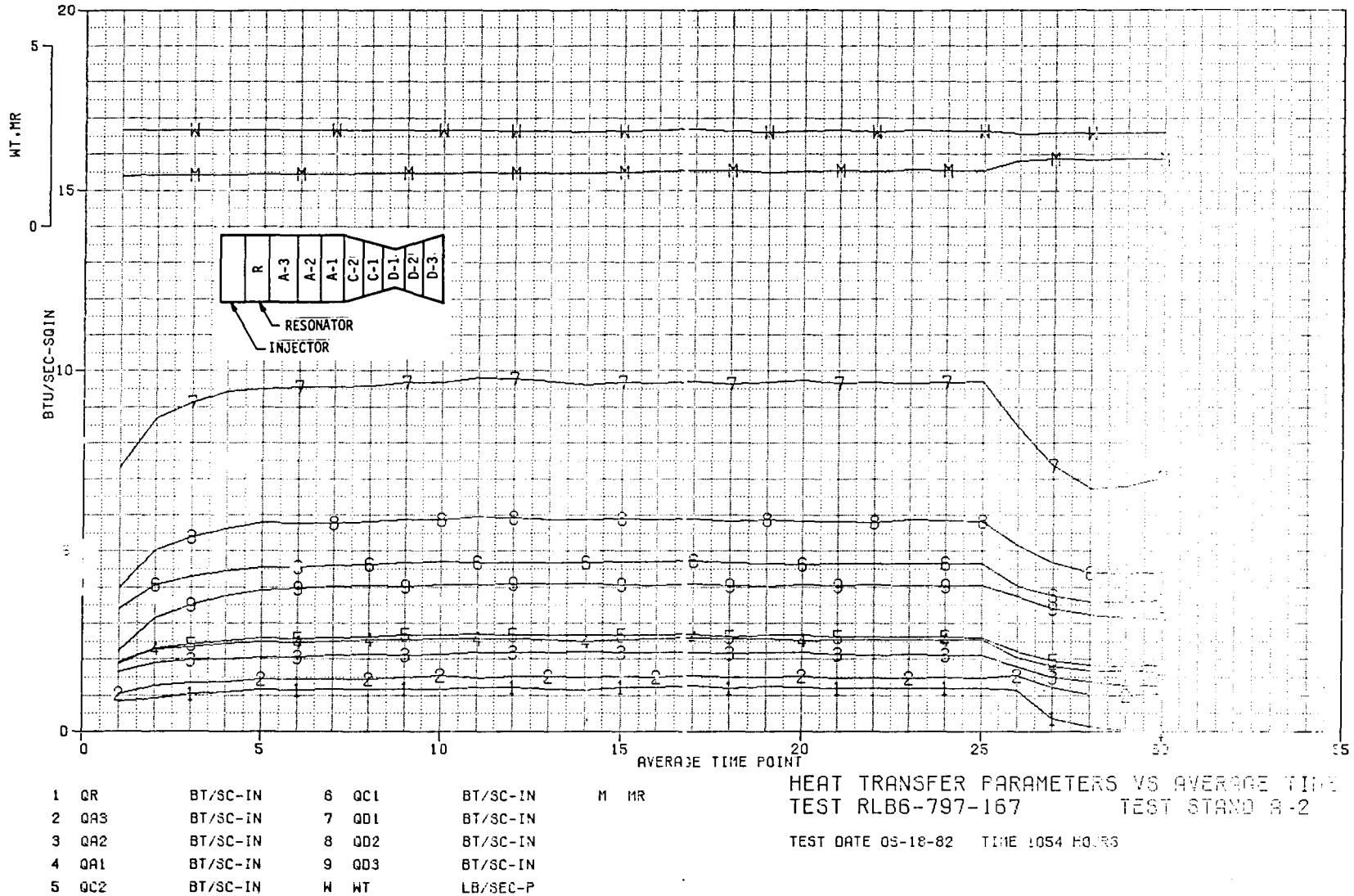

Figure 118. Heat Transfer Parameters Versus Average Time, Test RLB6-797-167

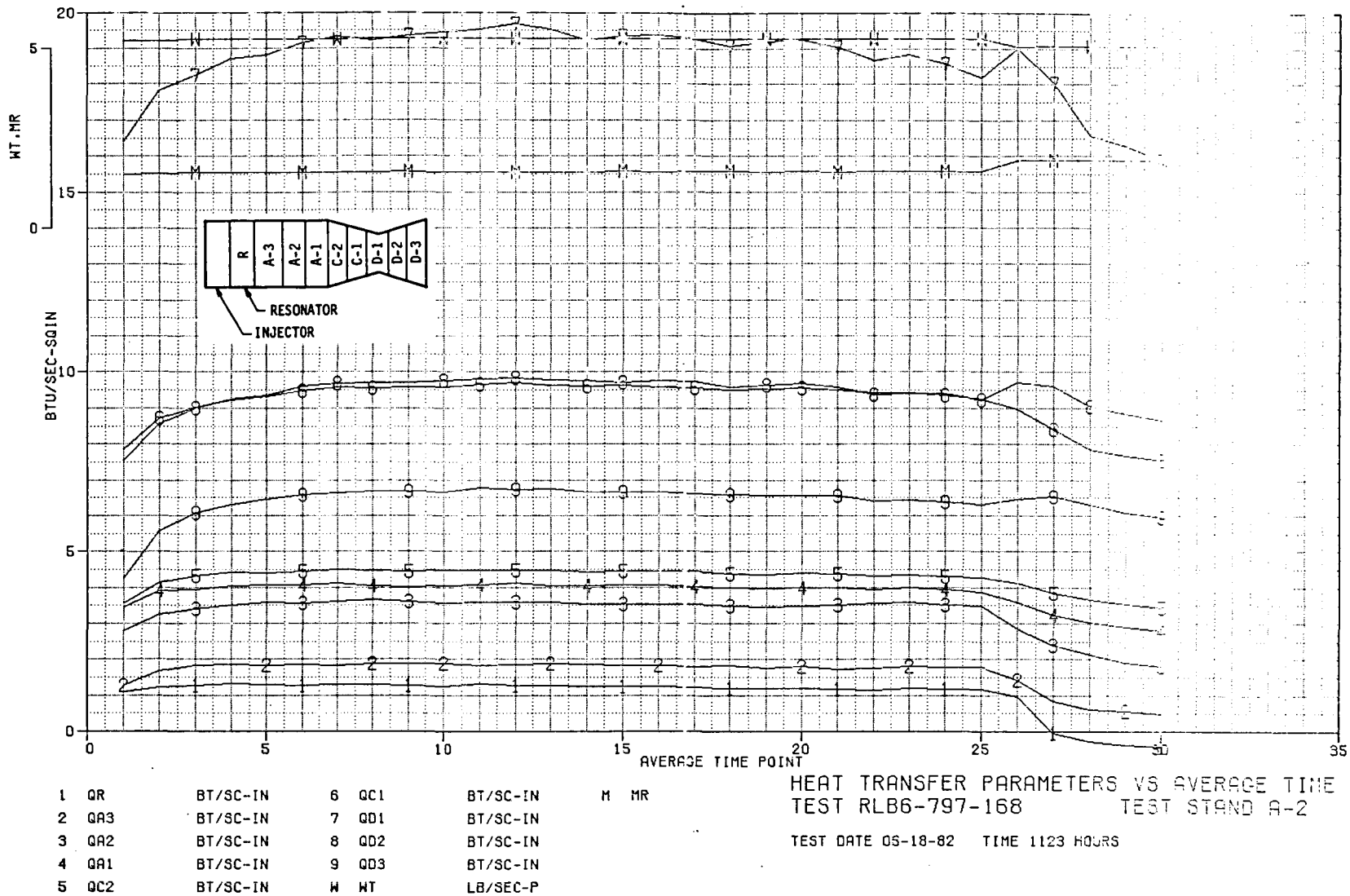

Figure 119. Heat Transfer Parameters Versus Average Time, Test RLB6-797-168

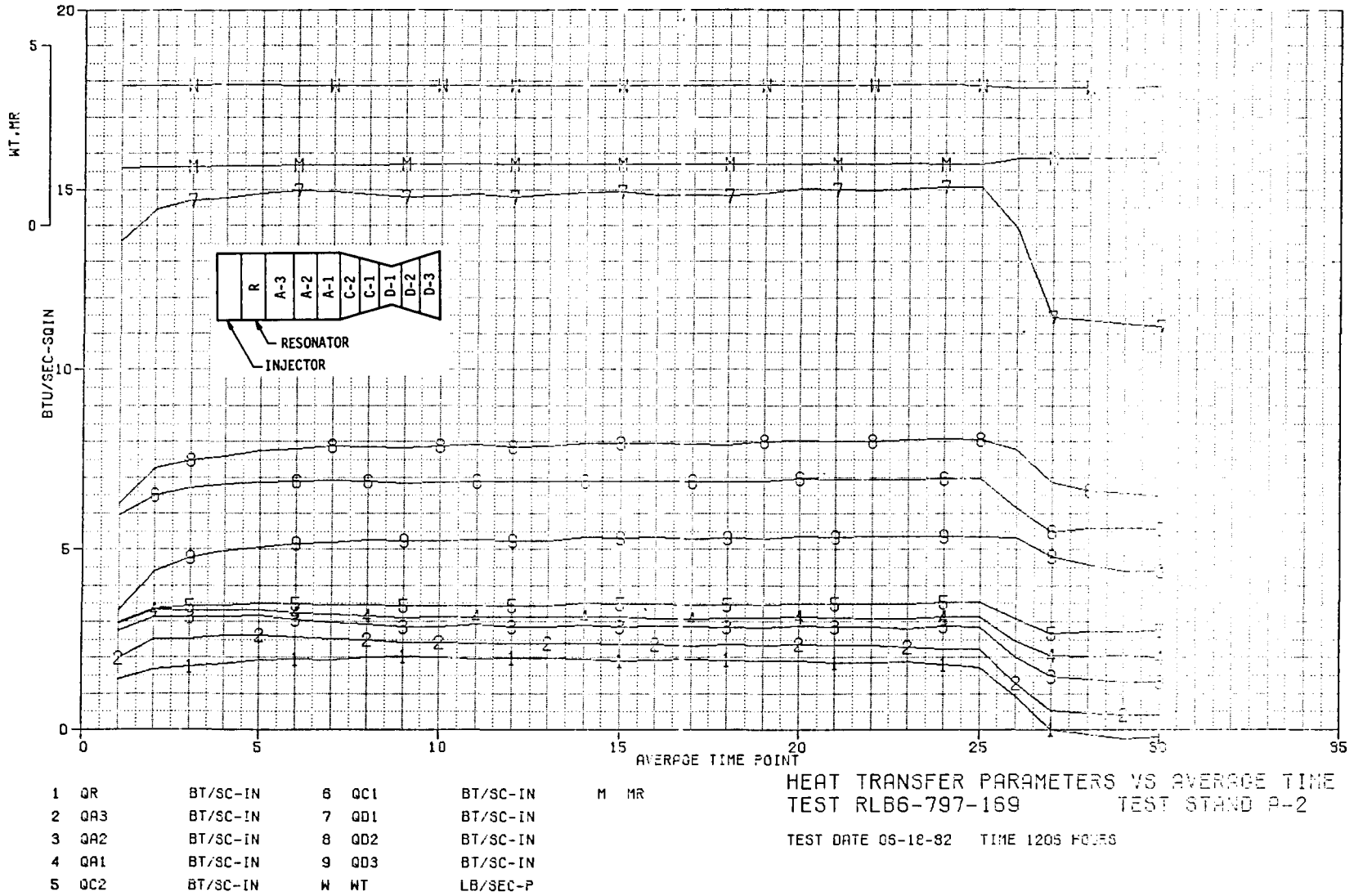

Figure 120. Heat Transfer Parameters Versus Average Time, Test RLB6-797-169

TABLE XVI

LOX/ETHANOL HEAT FLUX AND Cg VALUES FOR AN OFO TRIPLET
(PLATELET INJECTOR)

Run	Pc	MR	WT	Section	Heat Flux	Cg_f	Cg_s
163	285	1.87	3.85	R	-.31	-.0021	-.0014
No Film Cooling				A-3	.28	.0019	.0013
				A-2	1.36	.0092	.0063
				A-1	2.23	.0152	.0104
				C-2	2.60	.0141	.0097
				C-1	5.24	.0176	.0121
				D-1	11.40	.0242	.0166
				D-2	6.78	.0171	.0117
				D-3	4.79	.0169	.0116
165	283	2.46	3.81	R	-.11	-.0008	-.0006
No Film Cooling				A-3	.66	.0050	.0035
				A-2	1.62	.0122	.0085
				A-1	2.12	.0160	.0111
				C-2	2.56	.0154	.0107
				C-1	5.10	.0191	.0133
				D-1	10.51	.0247	.0172
				D-2	6.14	.0172	.0119
				D-3	4.42	.0173	.0120
166	281	1.43	3.89	R	.22	.0014	.0011
No Film Cooling				A-3	-.25	-.0016	-.0012
				A-2	.69	.0045	.0034
				A-1	2.43	.0159	.0120
				C-2	2.07	.0108	.0081
				C-1	5.56	.0181	.0136
				D-1	11.52	.0239	.0179
				D-2	5.60	.0141	.0106
				D-3	3.86	.0140	.0105
167	194	1.87	2.59	R	.03	.0003	.0002
No Film Cooling				A-3	1.04	.0099	.0067
				A-2	1.28	.0122	.0082
				A-1	1.66	.0158	.0107
				C-2	1.83	.0139	.0094
				C-1	3.63	.0172	.0115
				D-1	7.04	.0209	.0141
				D-2	4.43	.0157	.0105
				D-3	3.12	.0154	.0103
168	377	1.88	5.09	R	-.42	-.0022	-.0016
No Film Cooling				A-3	.47	.0025	.0017
				A-2	1.82	.0097	.0068
				A-1	2.81	.0150	.0104
				C-2	3.43	.0146	.0102
				C-1	7.54	.0200	.0139
				D-1	15.88	.0265	.0184
				D-2	8.68	.0173	.0120
				D-3	5.94	.0165	.0114
169	288	1.88	3.85	R	-.20	-.0014	-.0009
No Film Cooling				A-3	.41	.0028	.0019
				A-2	1.32	.0090	.0061
				A-1	2.01	.0136	.0094
				C-2	2.75	.0149	.0102
				C-1	5.58	.0188	.0129
				D-1	11.20	.0237	.0162
				D-2	6.48	.0163	.0112
				D-3	4.40	.0155	.0106
169	293	1.71 Eng.	3.90	R	2.03	.0133	.0095
8.7% Fuel Film Cooling		1.88 Core		A-3	2.63	.0172	.0124
				A-2	3.14	.0206	.0148
				A-1	3.31	.0217	.0156
				C-2	3.53	.0185	.0132
				C-1	6.97	.0226	.0162
				D-1	15.06	.0308	.0221
				D-2	8.08	.0198	.0142
				D-3	5.37	.0184	.0132
163	297	1.55 Eng.	3.95	R	1.19	.0076	.0057
16.8% Fuel Film Cooling		1.87 Core		A-3	1.41	.0090	.0067
				A-2	2.57	.0165	.0122
				A-1	3.12	.0200	.0148
				C-2	3.27	.0167	.0124
				C-1	6.19	.0197	.0146
				D-1	13.38	.0269	.0200
				D-2	7.60	.0184	.0136
				D-3	5.32	.0182	.0135

TABLE XVII

HEAT FLUX DATA OF PAT (OFO) PLATELET INJECTOR IN 8.7-IN. CHAMBER WITH FILM-COOLING

Test	Pc psia	MR_{CORE}/MR_{ENG}	%FFC	R	Heat Flux Btu/sec-in.^{2} A_3	A_2	A_1	C_2	C_1	D_1	D_2	D_3
163	298	1.86/1.54	16.8	1.2	1.4	2.6	3.1	3.3	6.2	13.3	7.5	5.3
165	296	2.49/2.07	16.9	1.3	2.0	3.2	3.4	3.7	6.7	15.0	8.4	5.8
166	295	1.41/1.16	17.2	1.5	0.8	1.7	2.9	2.5	6.2	12.5	5.7	3.9
167	201	1.85/1.55	16.5	1.2	2.0	2.2	3.0	3.2	4.6	9.7	5.8	4.1
168	396	1.89/1.56	17.3	1.3	1.8	3.5	4.0	4.5	9.6	19.0	9.7	6.6
169	292	1.87/1.70	8.7	2.0	2.4	2.8	3.1	3.5	6.9	15.0	8.0	5.3

E, Tasks II and IV Subscale Injector Characterization (cont.)

Test 162 was a repeat test with the film-cooling flow control needle valve reset. A computer kill terminated this test at approximately 1 second based on an indicated high film coolant flowrate. The indicated high flowrate was in error.

Posttest hardware inspection showed a water leak from the resonator cooling circuit in the chamber. The leak was at a previously repaired braze joint and at the lowest point in the chamber. Low water flow in the resonator cooling circuit in Test 162 (1.09 lb/sec versus 1.3 for all other tests) indicates that partial freezing of water may have caused the joint failure.

Measurements of the water leak rate at operating pressure conditions (Pwater - Pc = 450 psi) indicated a leak rate of 0.026 lb/sec compared to a propellant flowrate of over 3 lb/sec. Testing continued without repair of the leak on the basis that: 1) the addition of the small amount of water to the combustion process would not impact the measured performance by more than 0.5%; 2) the water flow data indicated that heating of the copper liner during the firing caused the leak to diminish or stop.

Test 163 was a 30 second duration test at nominal conditions. The final 5 seconds provided data with the film-cooling valve closed.

Test 164 and 165 were 300 psia tests at high MR (2.4). Test 164 had a thermal shutdown at 1.85 seconds due to high water temperature in section D.3. Review of the test data indicated an increase in water supply temperature, rather than very high heat flux, was responsible. Test 165 was a 30 second repeat with the kill level moved up slightly.

Test 167 was a normal 30 second test at low Pc (200 psia) and nominal MR.

Test 168 was a 30 second test conducted at 400 psia and nominal MR.

Test 169 repeated Test 163 conditions with the exception that the fuel film-coolant was reduced to 8.7% for the first 25 seconds of this 30 second test.

All of the above tests were stable and no hardware damage other than the small water leak was noted.

Posttest check of the water leak rate indicated the leakage increased to 0.044 lbM/sec in the cold chamber condition. Comparison of the chamber heat flux profile for the final 5 seconds of test 163 and 169, which had the same operating conditions, showed no measurable change. This supports the earlier conclusion that the water leak rate was small and did not measurably influence the test results.

The leak was braze-repaired following Test 169 in preparation for test series 7

E, Tasks II and IV Subscale Injector Characterization (cont.)

(6) Heat Transfer Test Results

A photograph of the injector at the conclusion of this test series is shown in Figure 110. The face was clean and showed no signs of being overheated. Heat marks were noted on the film cooling ring. These may have developed during the transients when the cooling flow was terminated. No change in flow or operating characteristics was noted for the film cooling injector.

Figure 121 provides a comparison of the exhaust plumes of the two injectors tested with LOX/ethanol. The platelet injector plume is more uniform and somewhat clearer than the EDM'd orifice design.

Figure 122 provides a graphical display of the heat flux (0% FFC) versus mixture ratio at each station in the chamber. Comparisons with the EDM orifice injector show the platelet injector to have lower heat flux at all stations and test conditions. The chamber head-end heat flux with the platelet injector is significantly lower, at the nominal operating conditions (MR = 1.8; Pc = 300) as shown in Figure 123.

Figure 124 presents a comparative plot of the effect of fuel film-cooling on the heat flux at nominal test mixture ratio and operating pressure. Small amounts of fuel (8.7%) added around the injector periphery cause an increase in heat flux, indicating that the environment near the chamber wall is oxidizer-rich without film-cooling. When the coolant flow is increased to 16.8%, the increase in heat flux is not as great, indicating that the wall environment is fuel-rich.

(7) Performance, Test Results

The performance data from this test series (Table XVIII) indicate combustion efficiencies in the range of 94% to 100%, dependent on engine mixture ratio and percent fuel film-cooling. The data indicate the following trends:

- Percent specific impulse and combustion efficiency increase with the addition of fuel film-coolant.
- Performance is a strong function of mixture ratio, probably a result of momentum ratio dependent propellant mixing.
- Performance efficiency decreased at the 400 psia chamber pressure compared to test data obtained at chamber pressures of 200 and 300 psia, probably a result of reactive stream separation.
- Compared to the data from the EDM'd OFO triplet injector, the pre-atomized element unit yielded higher performance over the entire mixture ratio range with film-coolant and equal or lower performance without film-coolant, again a probable consequence of momentum ratio dependent propellant mixing differences.

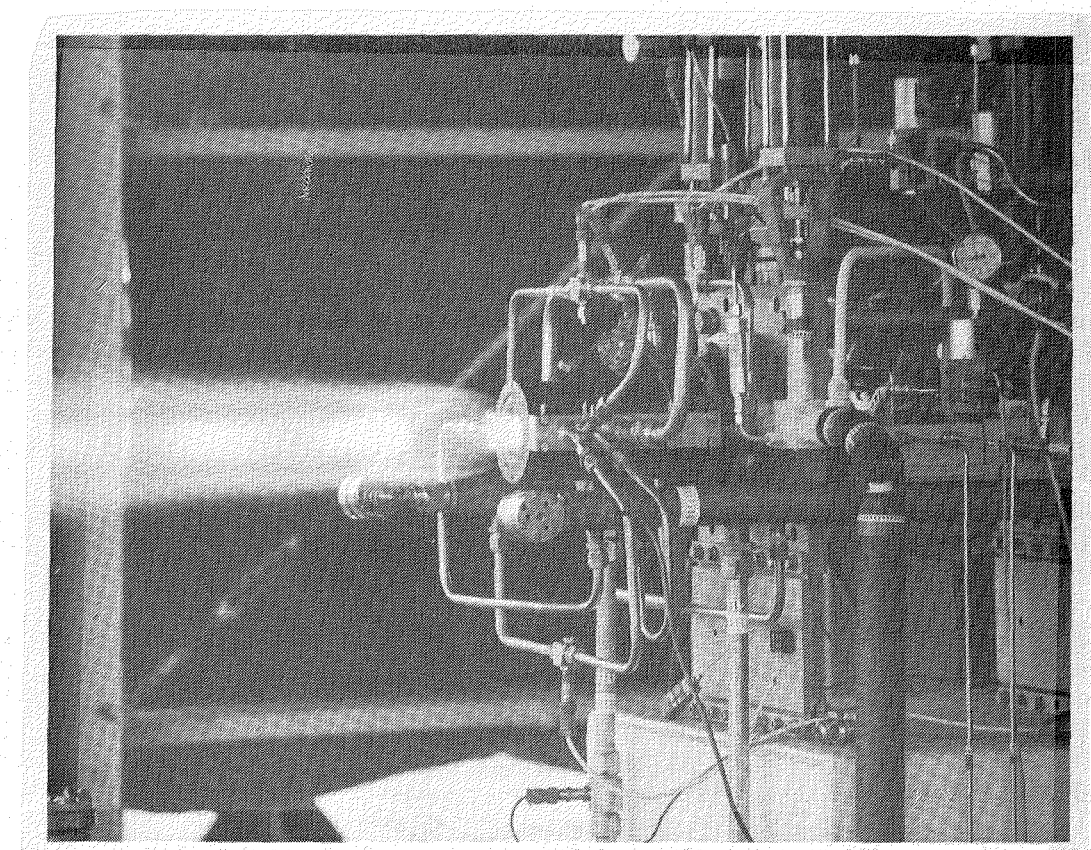

C 0282 164

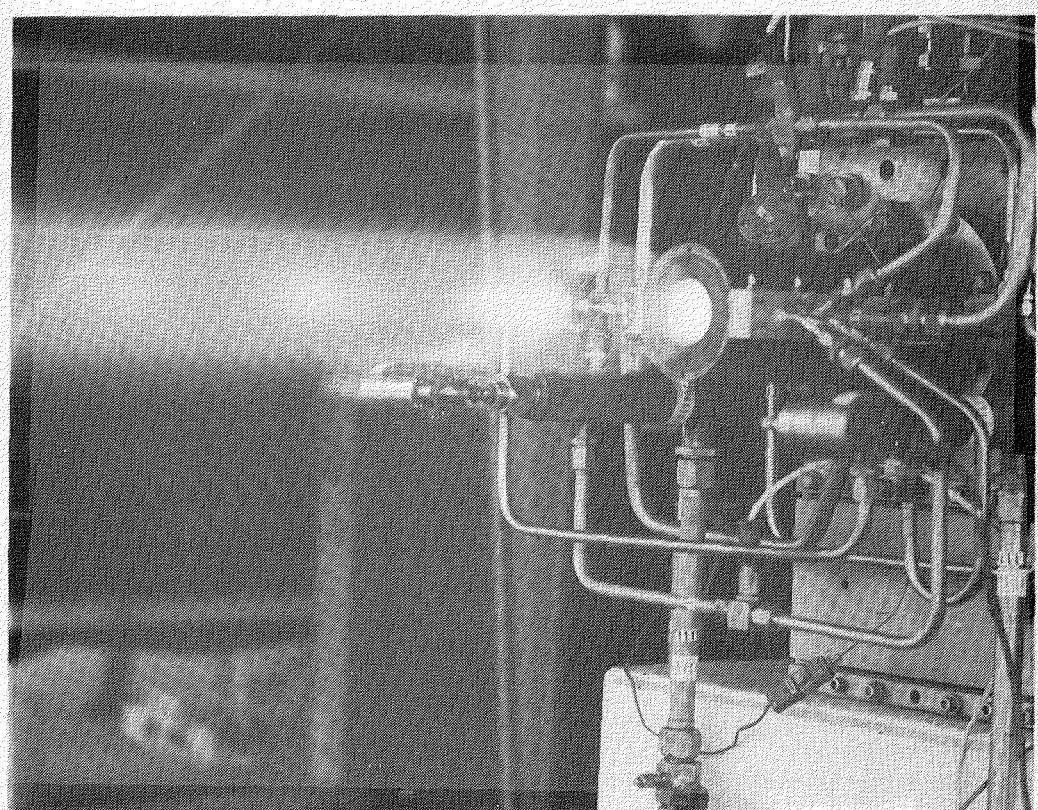

C 0882 049

Figure 121. LOX/Ethanol Combustion and Heat Transfer Test Exhaust Plumes, Conventional OFO Triplet Injector (Top Photo), and Preatomized Triplet Platelet Injector (Bottom Photo)

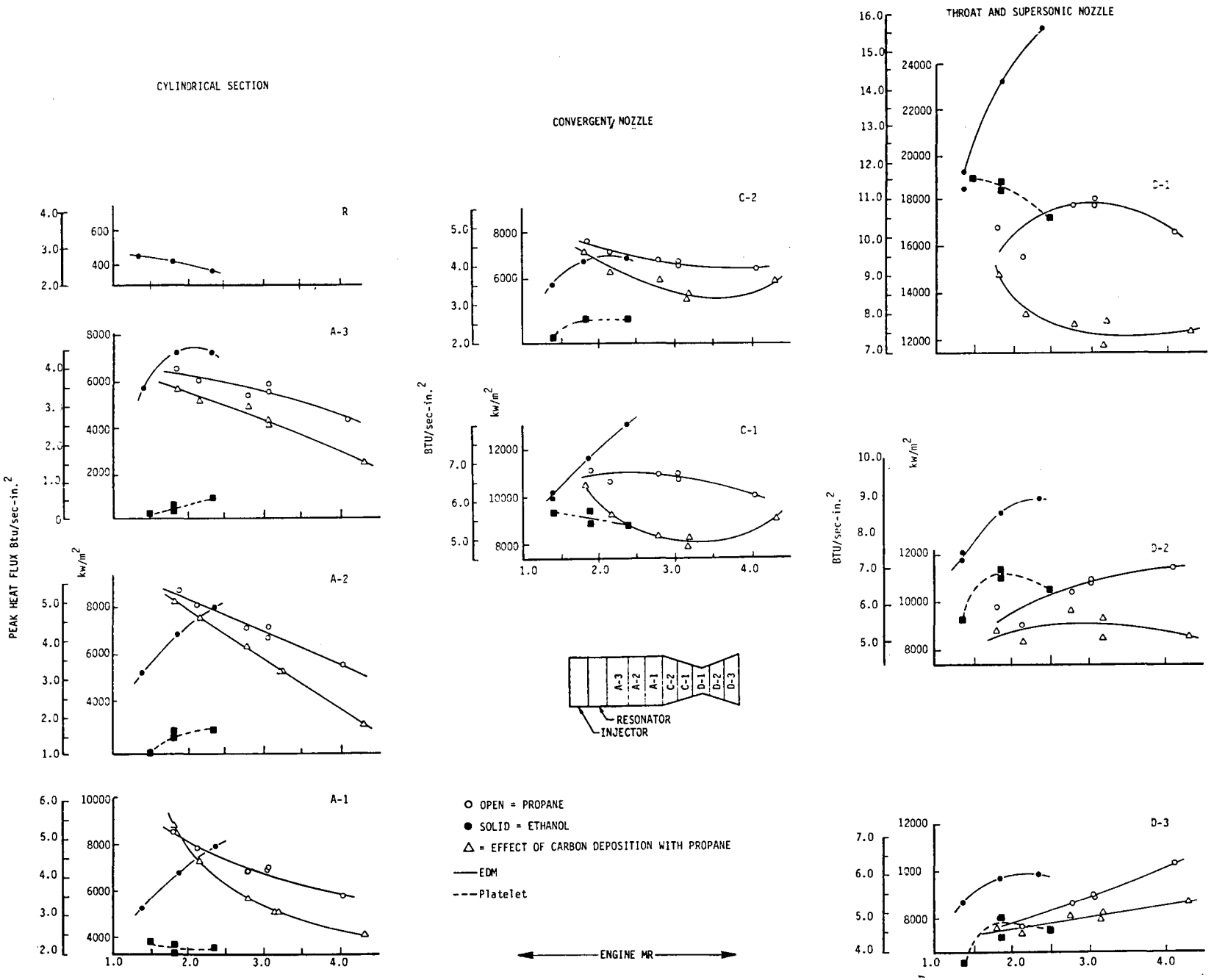

Figure 122. Maximum and Steady-State Heat Flux Versus Engine MR for a Chamber Pressure of 300 psia, No Fuel Film Cooling

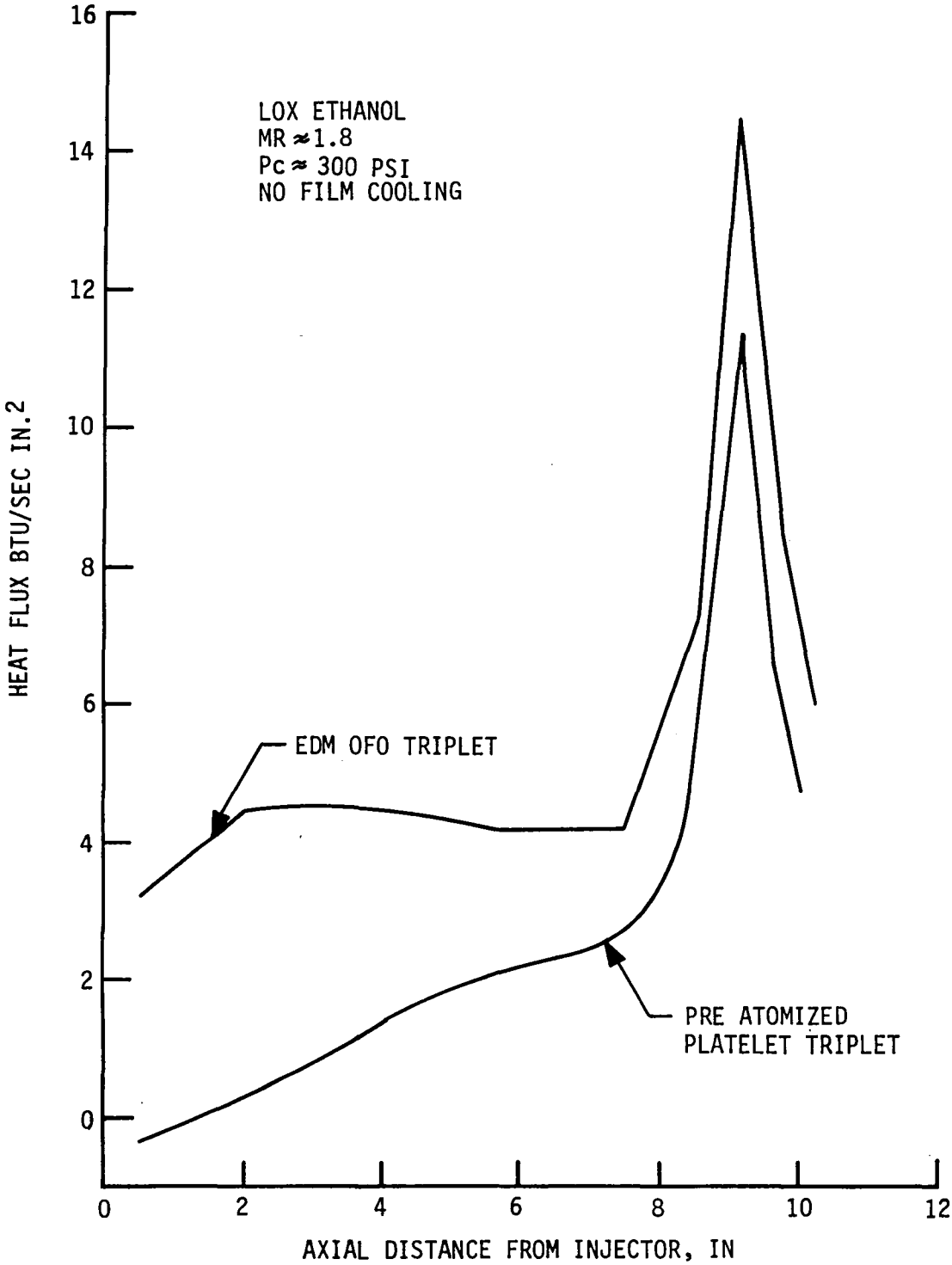

Figure 123. Comparison of EDM and Platelet Injector Heat Flux Profiles

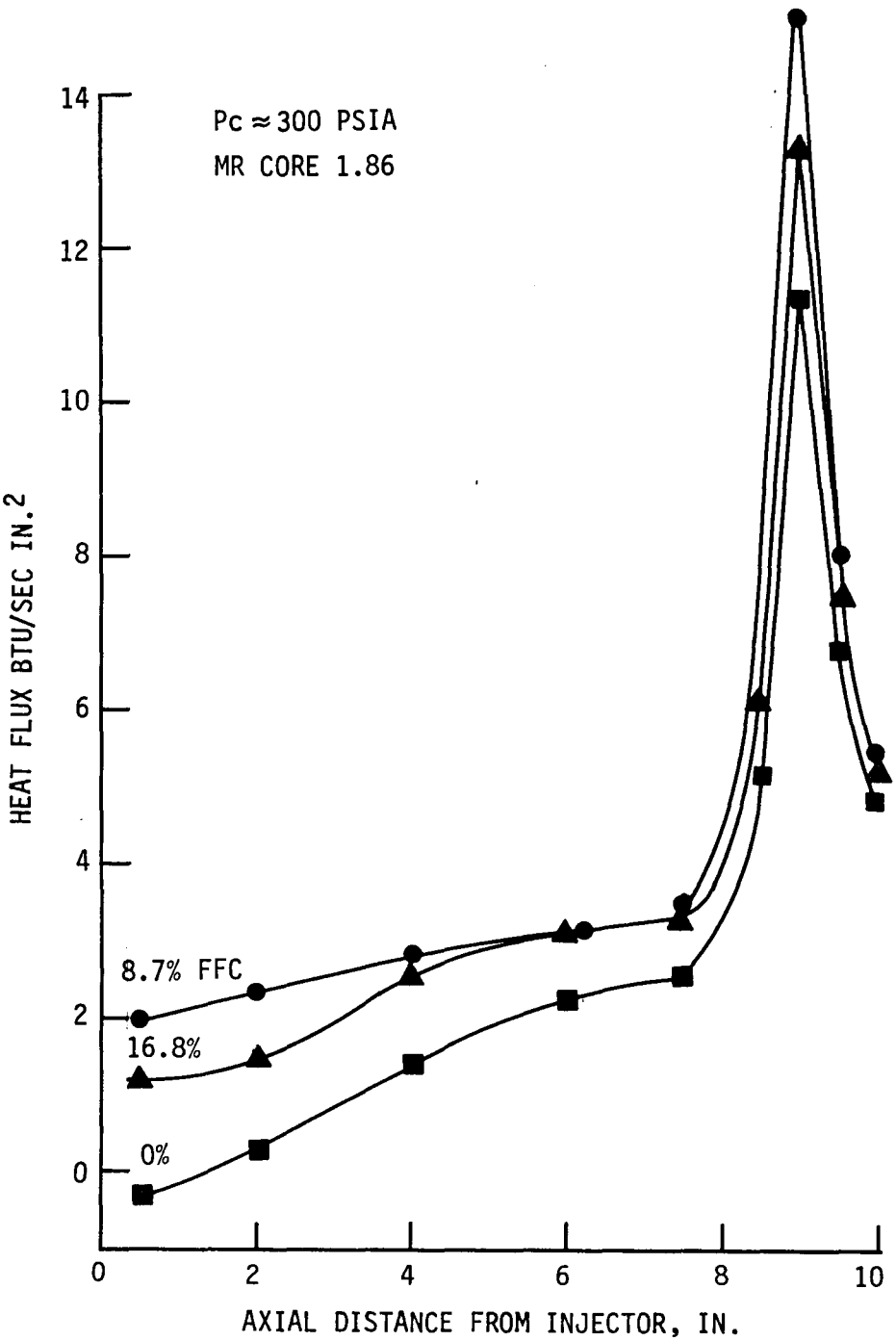

Figure 124. Heat Flux Versus Distance for Platelet Injector with LOX/Ethanol Propellants

TABLE XVIII

PAT INJECTOR PERFORMANCE DATA SUMMARY
LOX/ETHANOL PROPELLANTS

Test	Date	Data Summary (sec)	TOJ (°F)	TFJ (°F)	POJI (psia)	MR_{Eng}	$\dot{W}_{ox}$ (lbm/sec)	$\dot{W}_{FT}$ (lbm/sec)	MR_c	$\dot{W}_{FFC}$ (lbm/sec)	$\frac{\dot{W}_{FFC}}{\dot{W}_{FT}}$ (%)	POJ (psia)	PFJ (psia)	ΔPOJ (psi)	ΔPFJ (psi)	F_{vac} (lbf)	C*	Isp_{vac}	% Isp_{Vac}	η_{comb}	K_{WOJ}	k_{WFJ}
161	6-17-82	1.3-1.85	-257	81	283	1.24	2.1289	1.7125	1.61	.3870	22.6	414.8	586.7	131.8	303.7	886.7	5216	230.8	-		.17656	.08588
162		Early Shutdown (No Data)																				
163	6-17-82	20.3-20.85	-276	77	298	1.549	2.3990	1.5484	1.863	.2605	16.8	455.3	582.3	157.3	284.3	942.1	5345	238.7	93.0	97.1	.18092	.08617
		28.3-30.3	-277	76	285	1.867	2.5026	1.3401	-	-	0	451.8	588.7	166.8	303.7	898.1	5258	233.7	92.2	95.5	.18342	.08678
164	6-17-82	1.3-1.85	-256	86	299	1.992	2.6278	1.3192	2.399	.2237	17.0	507.9	506.1	208.9	207.1	946.8	5368	239.9	-	-	.17483	.08614
165	6-17-82	20.3-20.85	-263	78	296	2.070	2.6069	1.2592	2.491	.2129	16.9	491.9	482.0	195.9	186.0	934.4	5414	241.7	96.7	100.3	.17938	.08650
		28.3-30.3	-264	78	283	2.456	2.7040	1.1008	-	-	0	488.4	486.3	205.4	203.3	889.3	5266	233.7	96.2	99.8	.18192	.08711
166	6-18-82	20.3-20.85	-266	73	295	1.163	2.1713	1.8664	1.405	.3211	17.2	430.5	705.5	135.5	410.5	931.7	5180	230.8	93.7	99.3	.17911	.08596
		28.3-30.3	-267	73	281	1.431	2.2890	1.5991	-	-	0	427.2	714.2	146.2	433.2	883.8	5124	227.3	89.0	94.2	.18172	.08660
167	6-18-82	20.3-29.85	-265	73	201	1.546	1.6090	1.0407	1.852	.1717	16.5	274.8	325.1	73.8	124.1	632.8	5370	238.8	93.4	97.3	.17933	.08784
		28.3-30.30	-267	73	194	1.873	1.6920	.9031	-		0	272.8	326.6	78.8	132.6	607.1	5289	233.7	92.7	96.1	.18227	.08829
168	6-18-82	20.3-20.85	-267	75	396	1.562	3.2250	2.0642	1.890	.3579	17.3	684.7	898.7	288.7	502.7	1249	5301	236.2	91.7	95.6	.18203	.08578
		28.3-30.30	-267	75	377	1.878	3.3196	1.7681	-	-	0	680.0	909.8	303.0	532.8	1185	5252	232.9	91.6	94.7	.18309	.08637
169	6-18-82	20.3-20.85	-270	74	292	1.704	2.4515	1.4389	1.865	.1285	8.7	463.5	583.9	171.5	291.9	923.3	5324	237.3	92.8	96.5	.17890	.08677
		28.3-30.3	-270	74	288	1.880	2.5084	1.3345	-	-	0	461.0	587.3	173.0	299.3	902.9	5303	234.9	92.8	96.0	.18187	.08690

E, Tasks II and IV Subscale Injector Characterization (cont.)

Plots showing the performance trends with mixture ratio, % film-cooling and chamber pressure are shown on Figures 125 through 130.

The variation of specific impulse with engine mixture ratio is shown on Figure 125 for the nominal 300 psia chamber pressure tests. The peak PAT element Isp appears to occur at an engine mixture ratio of approximately 2.0 without fuel film-cooling and at a value of 2.0 when approximately 17% fuel film-cooling is utilized. An engine mixture ratio of 2.0 with 17% fuel film-cooling corresponds to a core mixture ratio of approximately 2.4. This peak O/F value was similar to that observed when testing the OFO EDM'd injector, as is indicated on the figure. Figure 125 shows an increase in specific impulse with the introduction of fuel film-coolant. This effect was also seen with the EDM'd triplet injector at low engine mixture ratio and probably is caused by an oxidizer-rich zone along the chamber wall which combusts at more nearly stoichiometric conditions when fuel film-coolant is added. A cross plot which shows the influence of fuel film-cooling on specific impulse is presented on Figure 126. For a constant core mixture ratio and chamber pressure, introducing 17% fuel film-coolant, increased specific impulse 8.1 seconds at an engine mixture ratio of 2.0 and 5.6 seconds at an engine mixture ratio of 1.70.

The influence of chamber pressure on specific impulse is shown by the data on Figure 127. For the preatomized OFO injector, the performance decreases as chamber pressure is increased from 300 to 400 psia. This may be indicative of Reactive Stream Separation. The test data from the LOX/ethanol tests with the EDM'd OFO triplet did not indicate this trend. Thus combustion zone mixing, whether caused by RSS or inadequate momentum ratio, appears more significant with the preatomized OFO design than with the coherent stream EDM'd OFO design.

The unusual influence of fuel film-cooling on engine performance, i.e., increased specific impulse as fuel film-cooling is added, led to an evaluation of the propellant mixing occurring within the combustion chamber. Based on propellant vaporization models, both propellants are predicted to be nearly completely vaporized at the chamber throat. Thus, it is assumed that the major combustion inefficiency is due to incomplete propellant mixing. This assumption is supported by the performance data trends with mixture ratio. Also, the thermal data indicate a cold wall in the near injector region which is probably due to an oxidizer-rich zone.

A simplified mixing model was formulated to further understand the performance data. The procedure used was as follows.

First, a mixing efficiency, E_M, was derived from the uncooled test data. This E_M defined the two stream tube mixture ratios and mass fractions which would yield the measured performance. Next the fuel film-coolant flow was added to the oxidizer-rich (outer) stream tube and performance was recalculated. A comparison of this performance modeling with the measured perfor-

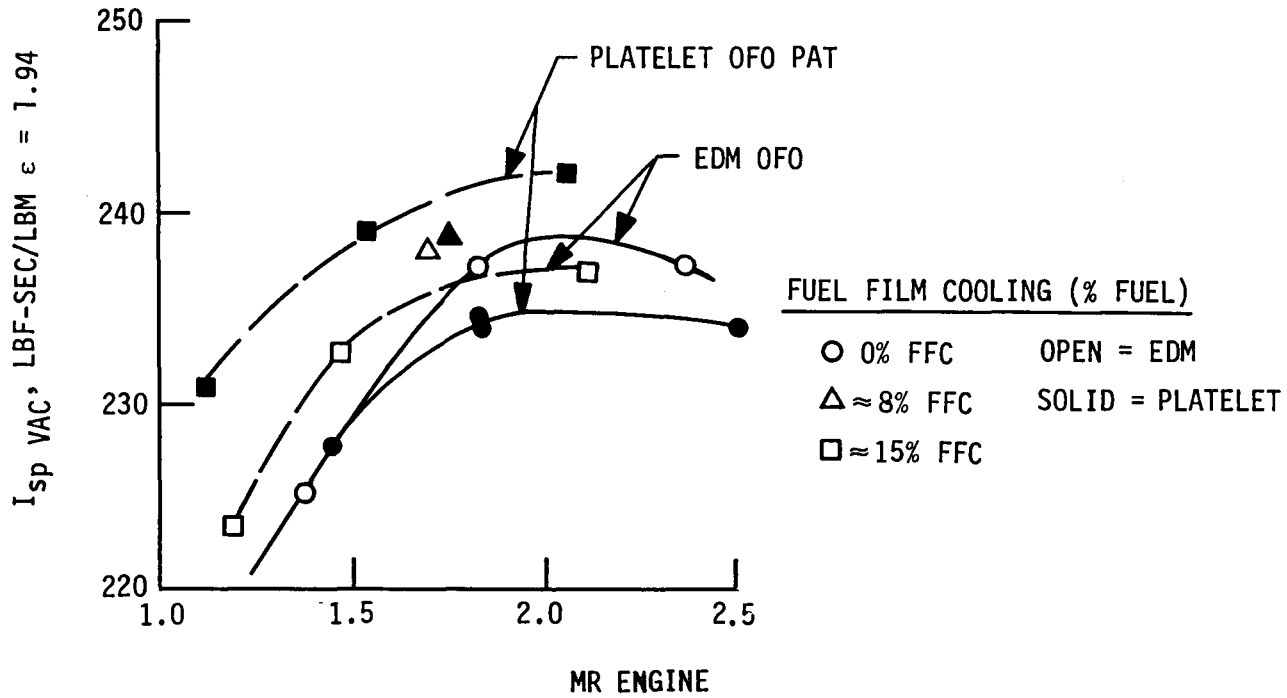

Figure 125. Comparison of Platelet and EDM Orifice Injector Performance with LOX/Ethanol

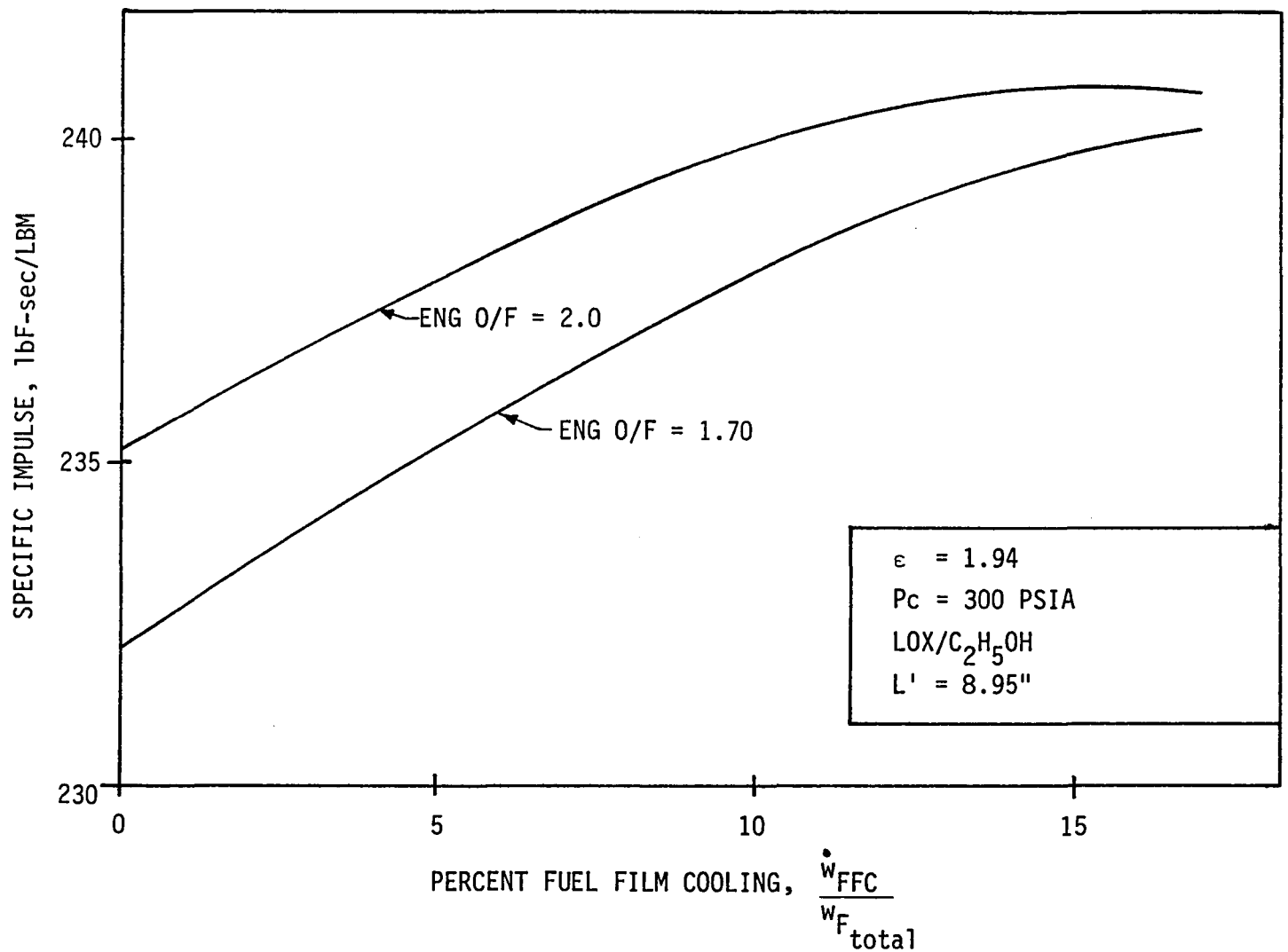

Figure 126. Influence of Percent Fuel Film Cooling and Mixture Ratio On Specific Impulse of PAT Injector

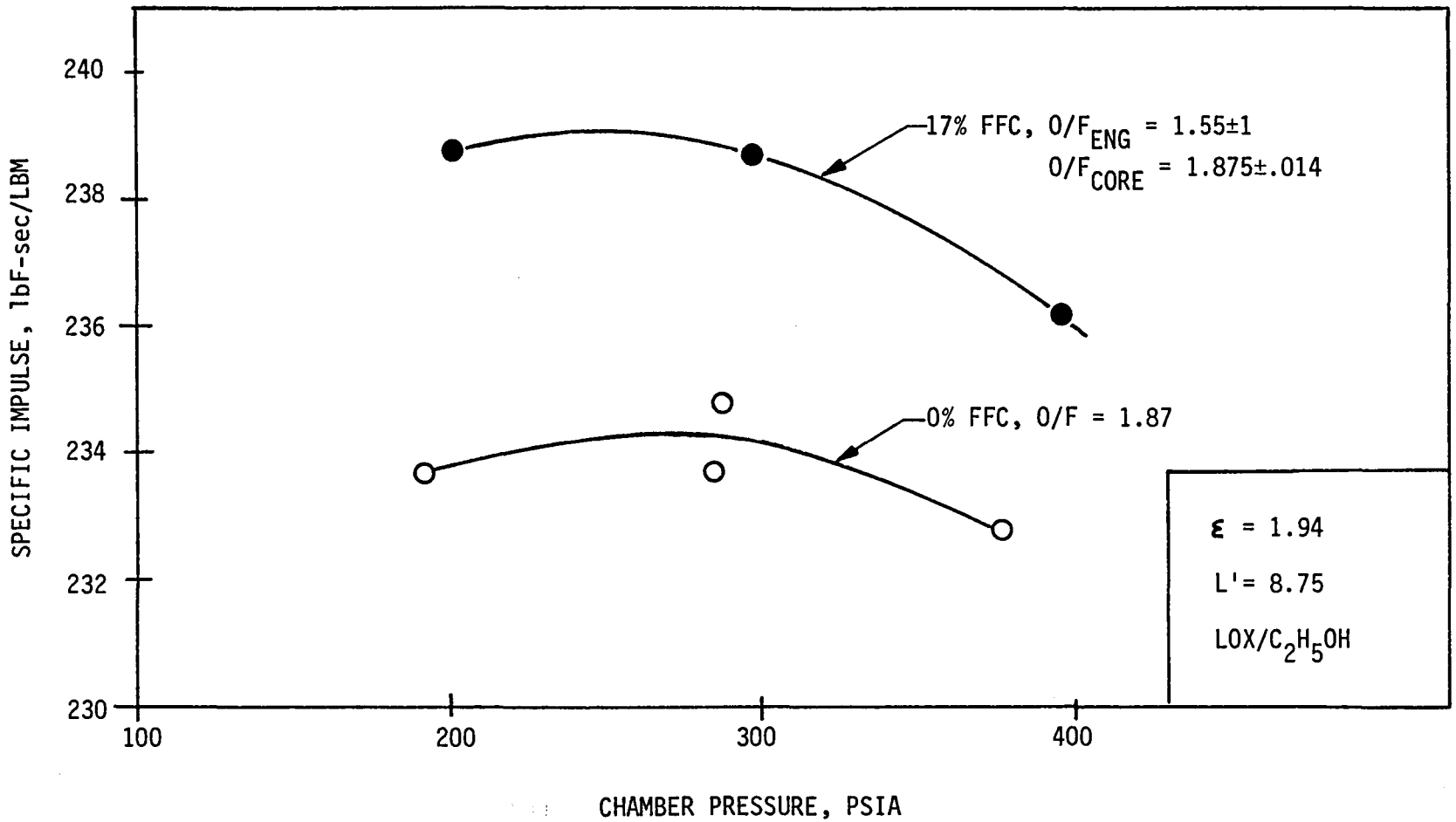

Figure 127. Influence of Chamber Pressure on Specific Impulse of PAT Injector

mance is shown on Figure 128. The predictions show fair agreement with the test data. Tests 165 and 166 showed the largest predictive errors, approximately 2 seconds, and were at the highest and lowest mixture ratios tested, respectively (2.07 and 1.16 with film-coolant). The E_M values needed to match the test data for the uncooled tests were in the range of 0.64 to 0.68, except for the 2.07 mixture ratio test (Test No. 165) which appeared to exhibit complete mixing, i.e., $E_M = 1.0$. For the film-cooled tests, in addition to the core and barrier stream tubes, a core mixing loss equivalent to an E_M of 0.85 was assumed. An increase in this core E_M would increase the predicted Isp for the cooled tests and decrease the slight bias of the prediction evident on the figure.

The test data are plotted on Figure 129 in terms of percent of One-Dimensional Equilibrium (ODE) specific impulse. These data show an increase in % Isp with increasing mixture ratio for the non film-cooled portion of the tests, probably due to better propellant mixing with increasing momentum ratio. The film-cooled performance data show a low efficiency of 92.8% at a mixture ratio of approximately 1.40 to 1.50 and a higher value of 96.7% at a mixture ratio of 2.07. The data displayed on Figure 130 use the percent combustion efficiency as the dependent parameter, where the combustion efficiency is defined as the specific impulse efficiency divided by the boundary layer, divergence and kinetic efficiencies. The combustion efficiencies are thus the geometric sum of the core mixing and vaporization efficiency (the energy release efficiency) and the mixing efficiency of the coolant and core stream tubes (the cooling efficiency). The combustion efficiency data show the same basic trends as the % Isp data of the previous figure. The major difference between the two figures is a result of a variation in the predicted kinetic loss with mixture ratio, which is implicit in Figure 130.

The experimental combustion efficiencies were 94% to 100% for the tests without film-cooling and 95% to 100% for the film-cooled tests.

g. Test Series VII - GOX/Ethanol, Ethanol Film-Cooling, 8.7-in. Water Cooled Calorimeter Chamber, Swirler Fuel and Doublet GOX Injector

(1) Test Objectives

The Task III (Ref. 1) engine system study identified the gaseous oxygen (GOX) and liquid ethanol propellant combination as being most desirable for use in a pulsing type reaction control engine (RCE) because it eliminated the need for maintaining cryogenic liquid-phase oxygen at the valves of the numerous RCE thrusters in the Space Shuttle. The selected flight system flow schematic is shown in Figure 131.

The objective of this test series was to experimentally investigate potential combustion and heat transfer problems associated with the use of GOX/ethanol propellants and to quantify the attainable specific impulse.

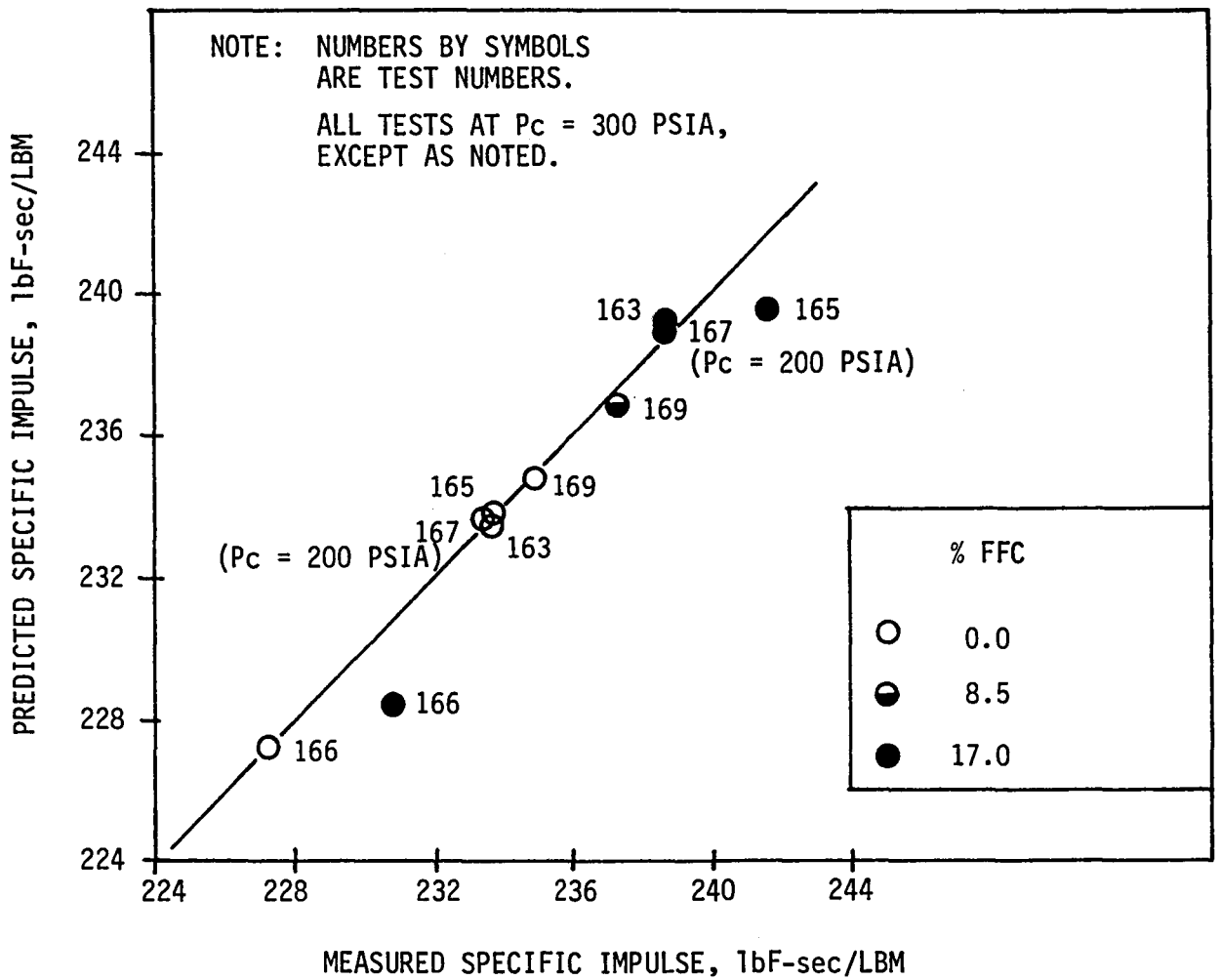

Figure 128. Comparison of Measured and Predicted Performances Using Two Stream Tube Mixing Model

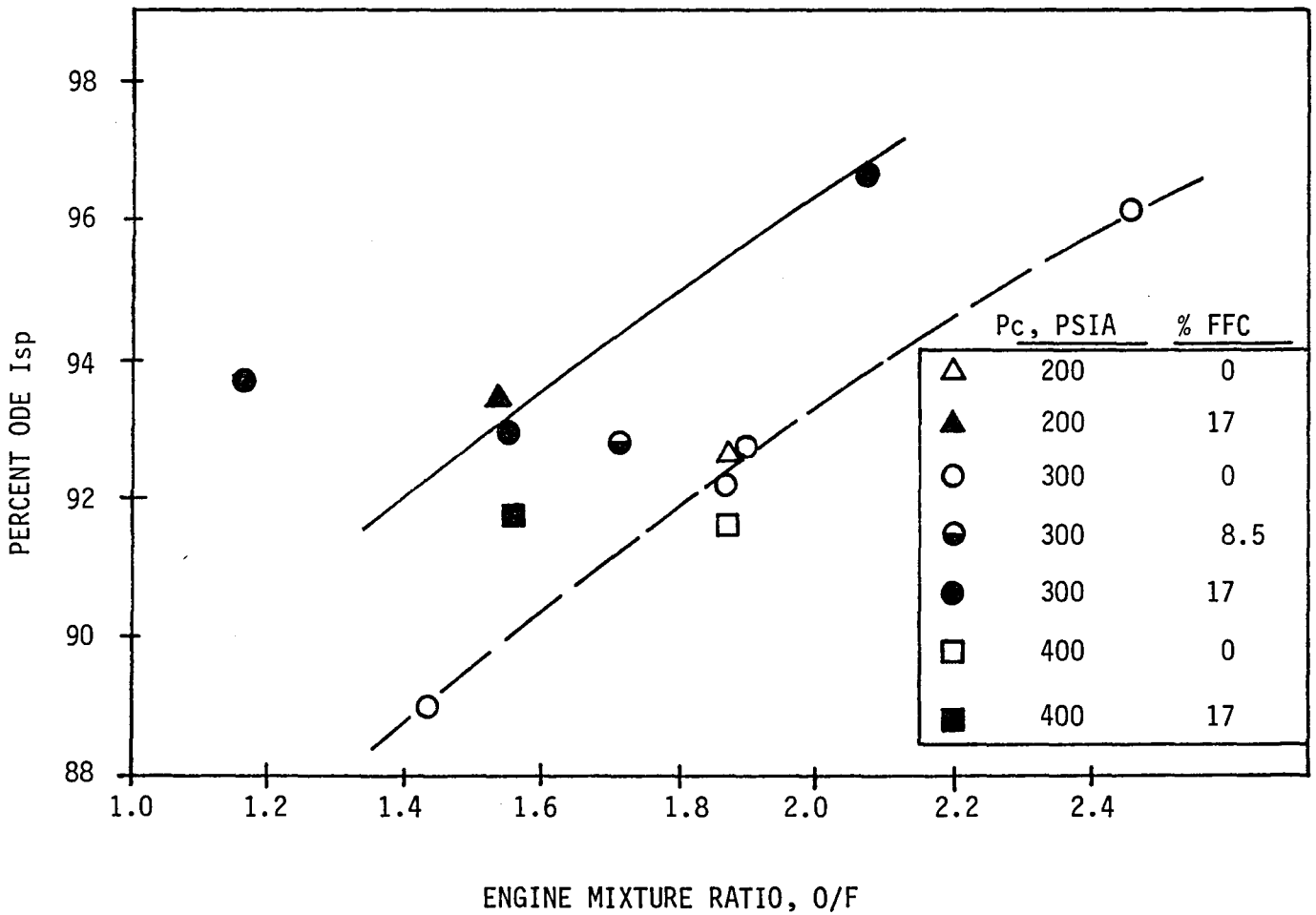

Figure 129. Influence of PAT Injector Operating Conditions on Percent Specific Impulse

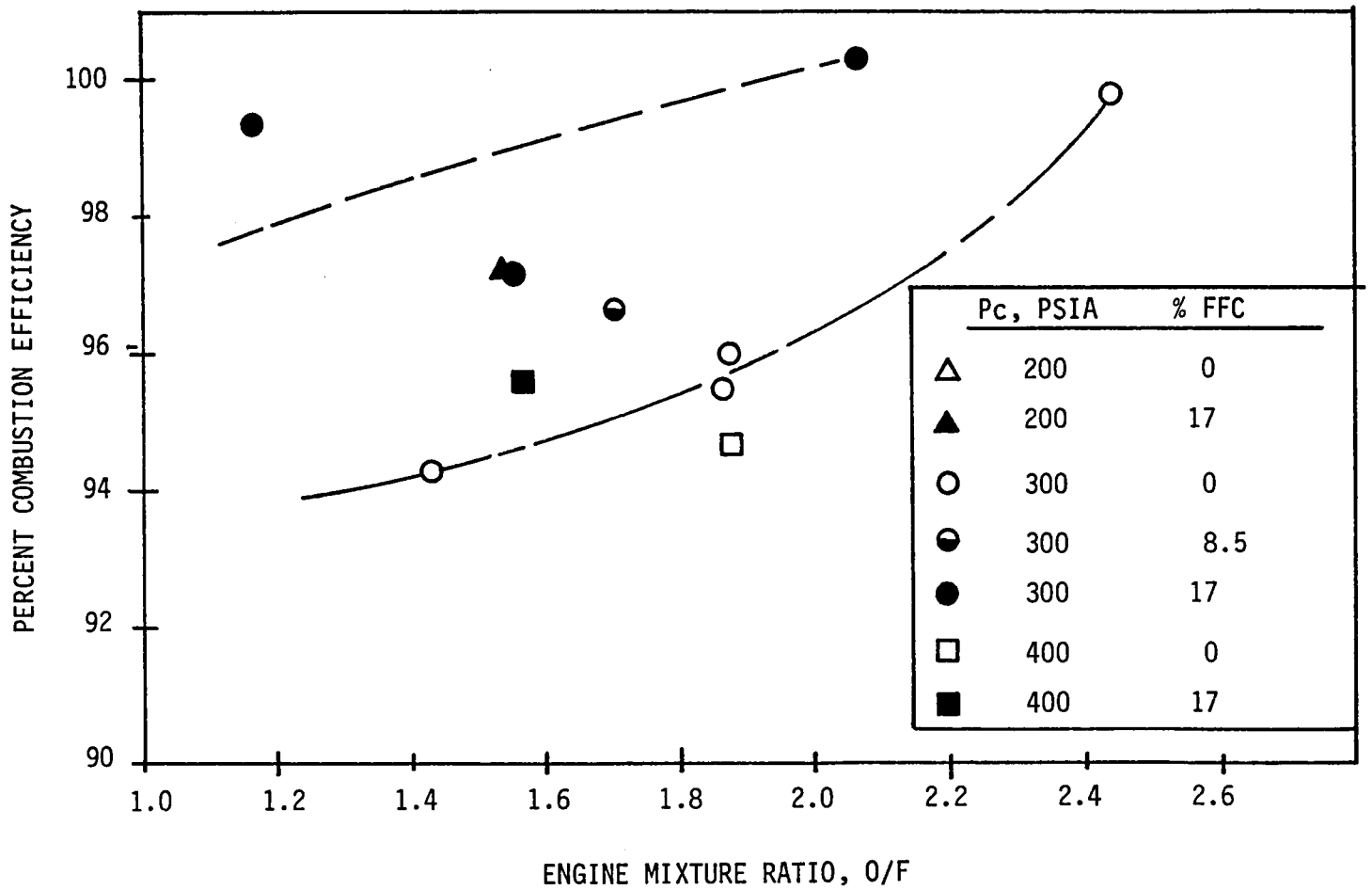

Figure 130. Influence of PAT Injector Operating Condition on Combustion Efficiency

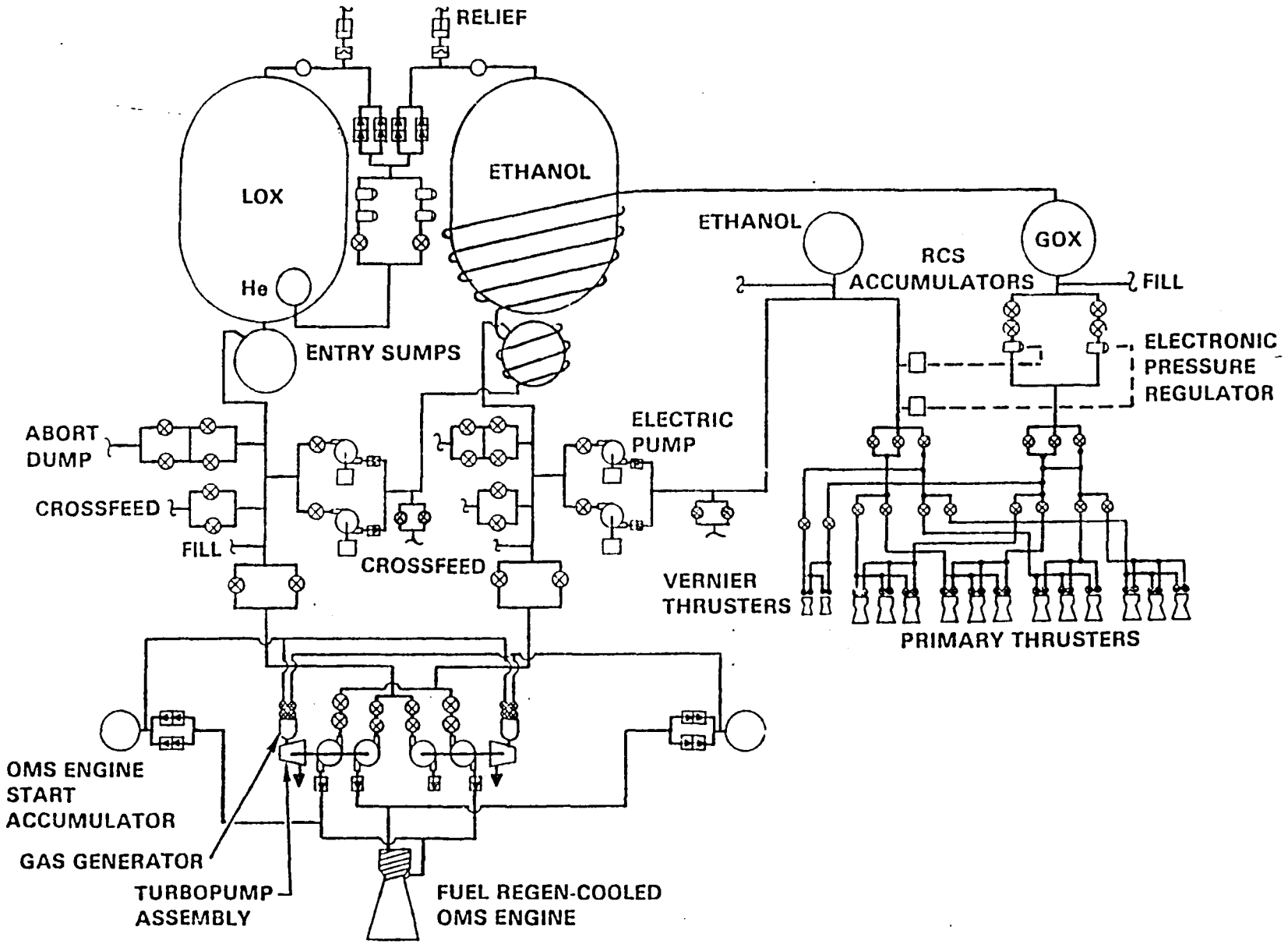

Figure 131. LOX/Hydrocarbon Auxiliary Propulsion System Flow Schematic

E, Tasks II and IV Subscale Injector Characterization (cont.)

The investigation of the effects of propellant supply temperature (-130°F to +70°F), chamber pressure (100 to 300 psia), film-coolant flow, and mixture ratio were included in this test series.

(2) Test Facility

The test facility employed to supply the GOX/ethanol propellants at those conditions is shown schematically in Figure 132 and photographically in Figure 133.

In the test system, oxygen is supplied from high pressure cylinders. A pebble bed heat exchanger is used to temperature-condition the oxygen delivered to the engine. It is positioned between the pressure-regulated oxygen supply and NBS-calibrated sonic flow control nozzle. When cold oxygen is required, the heat exchanger is precooled to the desired temperature by circulating a gas/liquid blend of nitrogen through the massive bed. The bed is vacuum-pumped and purged with GO_2 to remove the nitrogen prior to the test. The fuel is cooled by circulating the gas/liquid blend of nitrogen through a tube-and-shell heat exchanger until the desired liquid temperature is reached. The double-wall propellant lines are also temperature-conditioned by use of the nitrogen. Propellant is circulated or bled prior to each test to insure that the temperature conditions at the thrust chamber valves are the same as in the heat exchanger.

(3) Test Hardware

The engine components employed in this test series included the swirler fuel/doublet oxidizer platelet injector (Figures 134 and 135), water-cooled chamber, and fuel film-cooling injector. The injector is a 45 element OFO preatomized triplet type incorporating a pattern having a central fuel vortex and two EDM oxidizer orifices which form a doublet, having an impingement point on the axis of the swirler. The chamber length to the throat is 8.7 inch.

(4) Cold-Flow

Pattern cold-flow check of the injector shown in Figure 135 was accomplished using water to simulate the fuel and GN_2 to simulate the GOX. The test conditions, flowrates, and supply pressures, exhausting to atmosphere, are listed in Table XIX. Figure 136 shows a typical spray pattern of the fuel swirler. This excellent level of atomization was attained with only 15 psi pressure drop. Figure 136 also shows combined fuel and oxidizer simulant flow at conditions which are closer to normal operation.

(5) Test Summary

Hot fire testing of gaseous oxygen/ethanol was initiated on 16 December 1982. Analysis of the fuel prior to this test series indicated a water content of 0.08%.

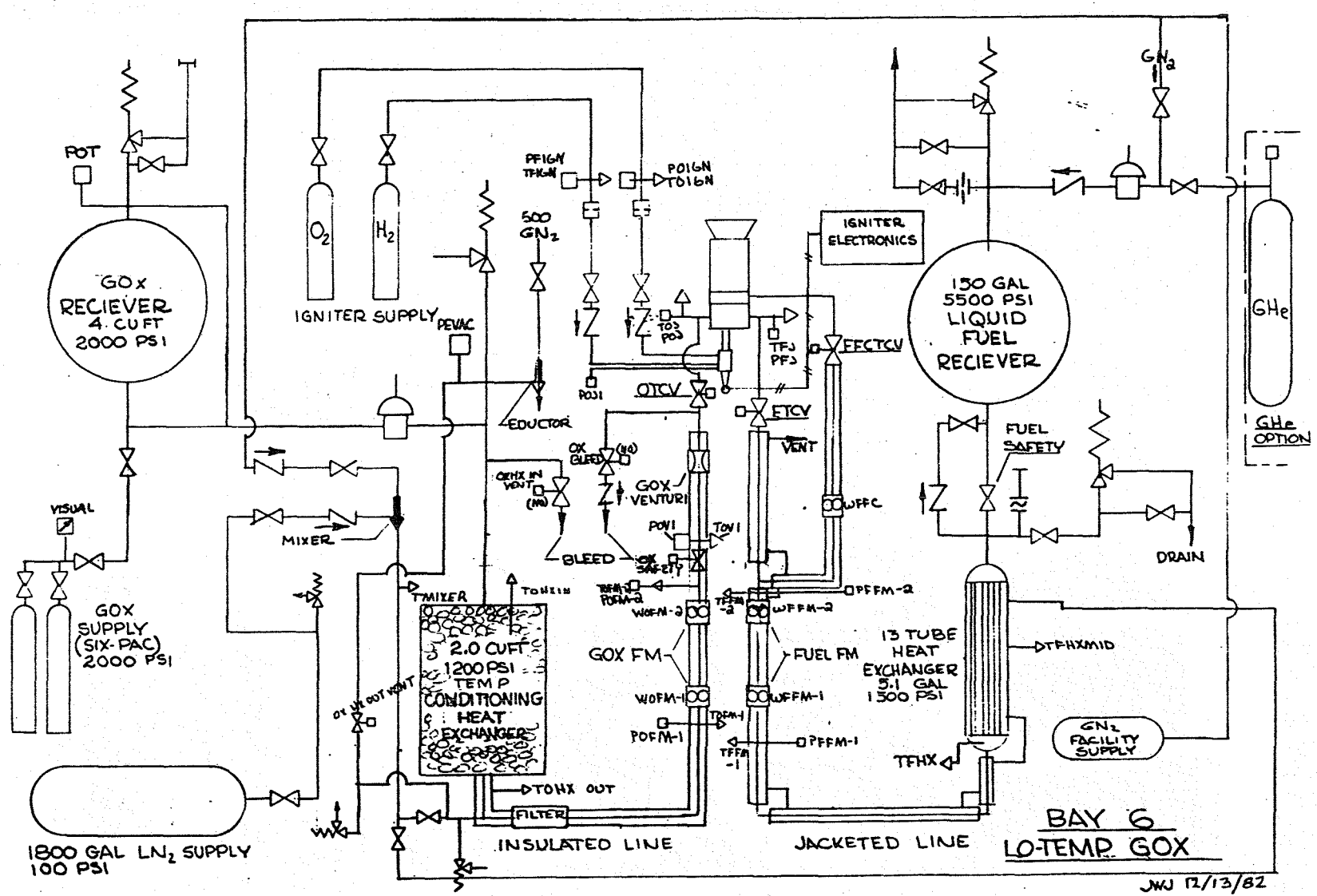

Figure 132. Bay 6 Test Facility Flow Schematic

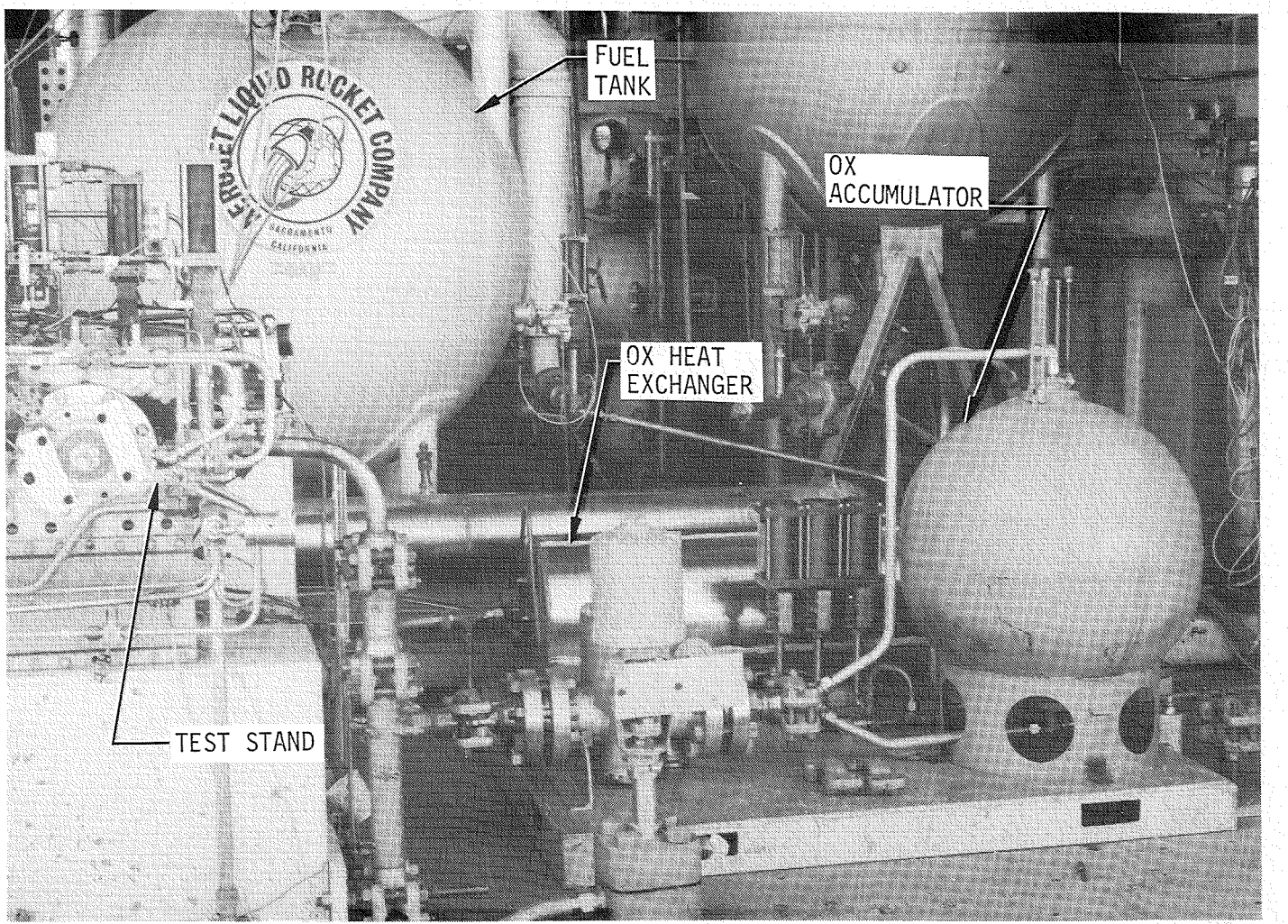

C1082057

Figure 133. Bay 6 Test Facility for GOX/Ethanol Testing

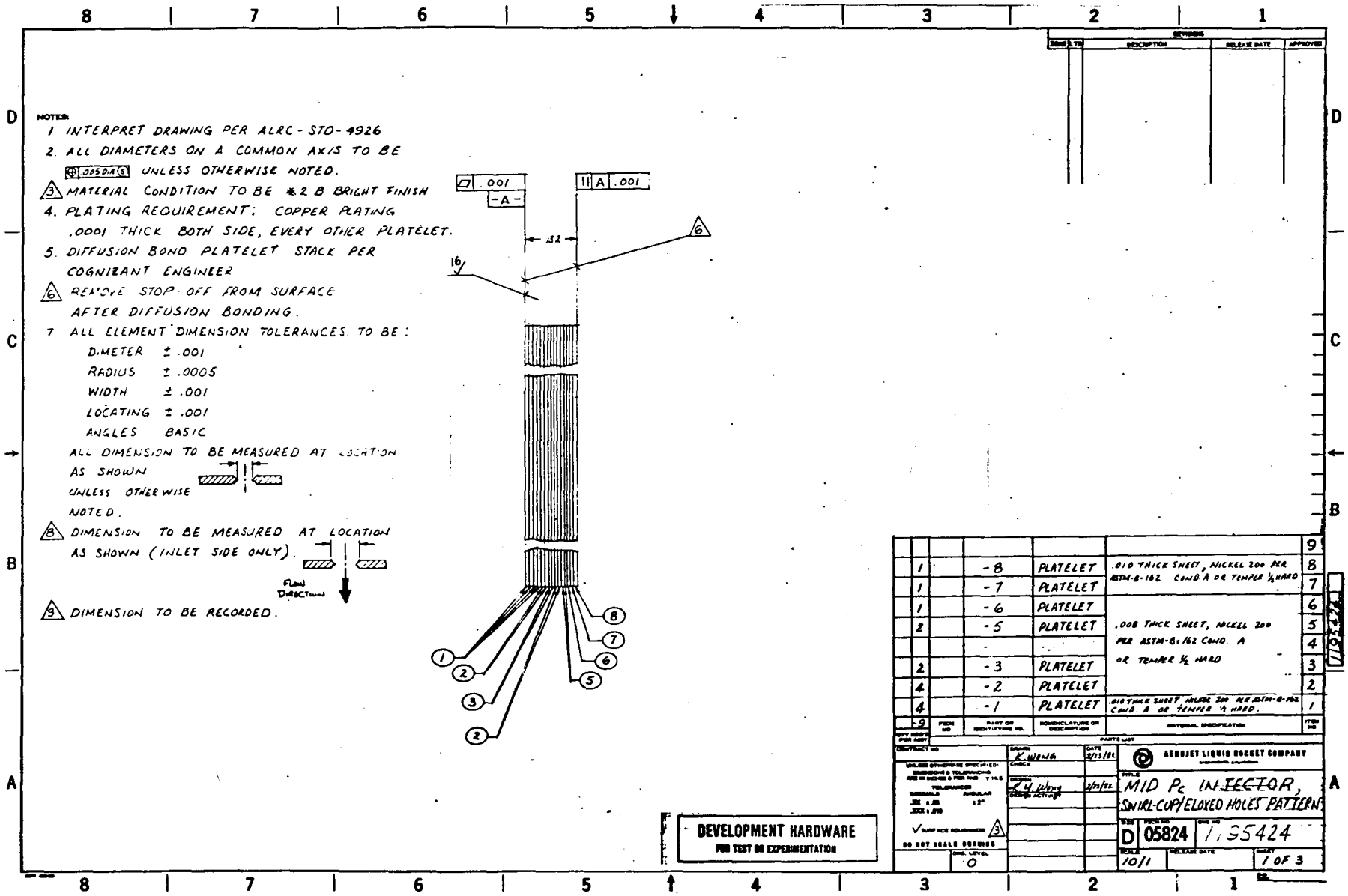

Figure 134. GOX/Ethanol Platelet Injector, Drawing 1195424 (1 of 3)

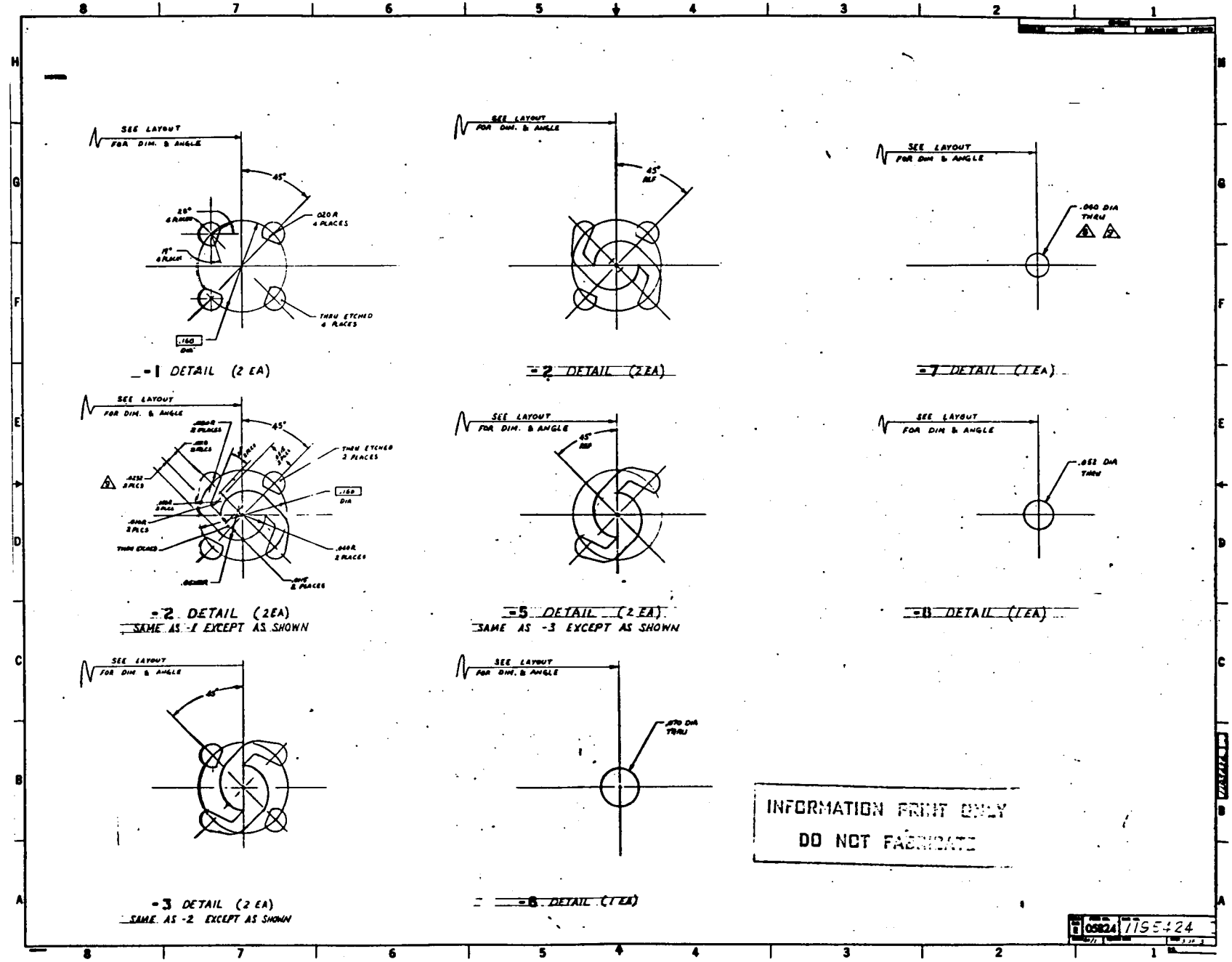

Figure 134. GOX/Ethanol Platelet Injector, Drawing 1195424 (2 of 3)

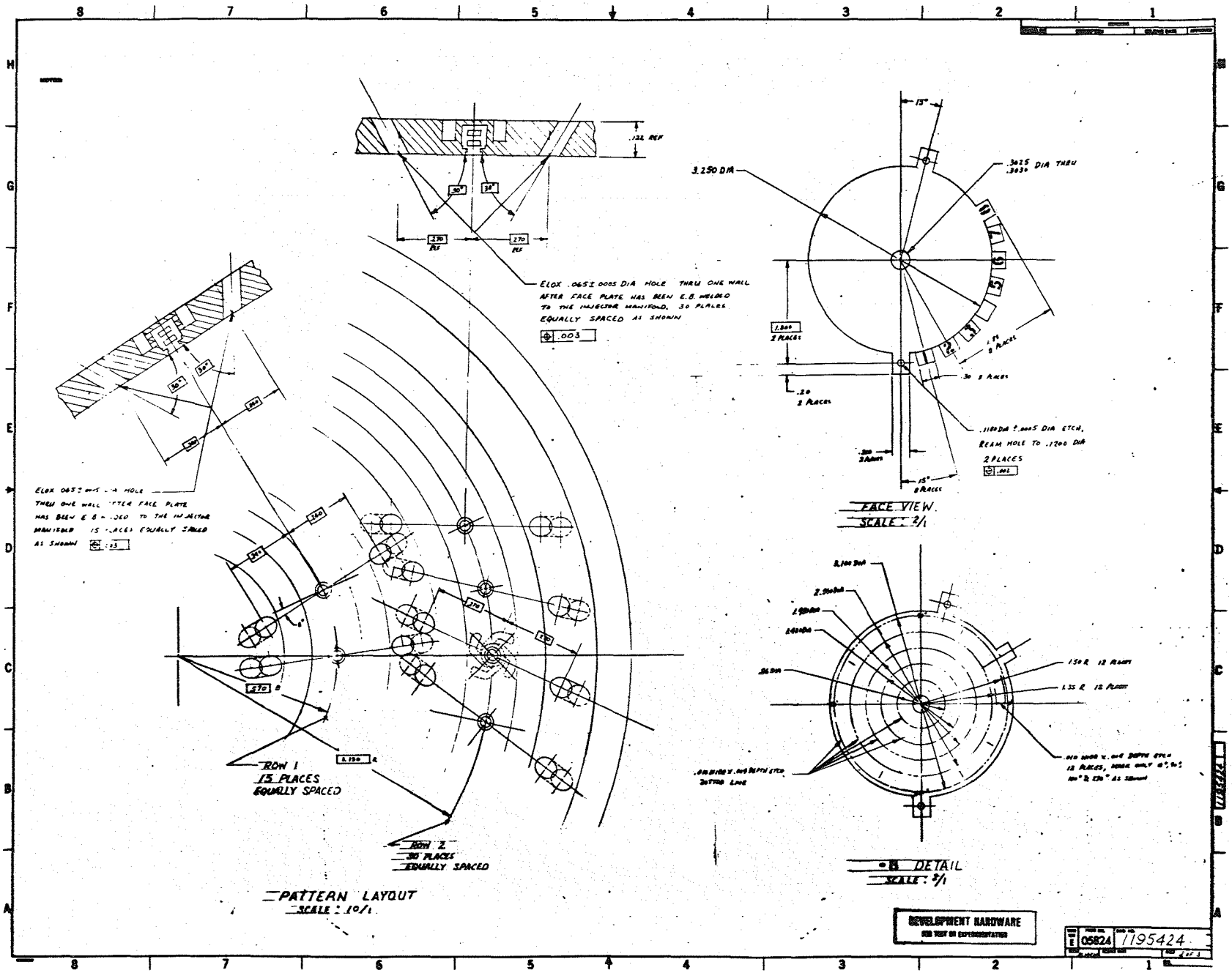

Figure 134. GOX/Ethanol Platelet Injector, Drawing 1195424 (3 of 3)

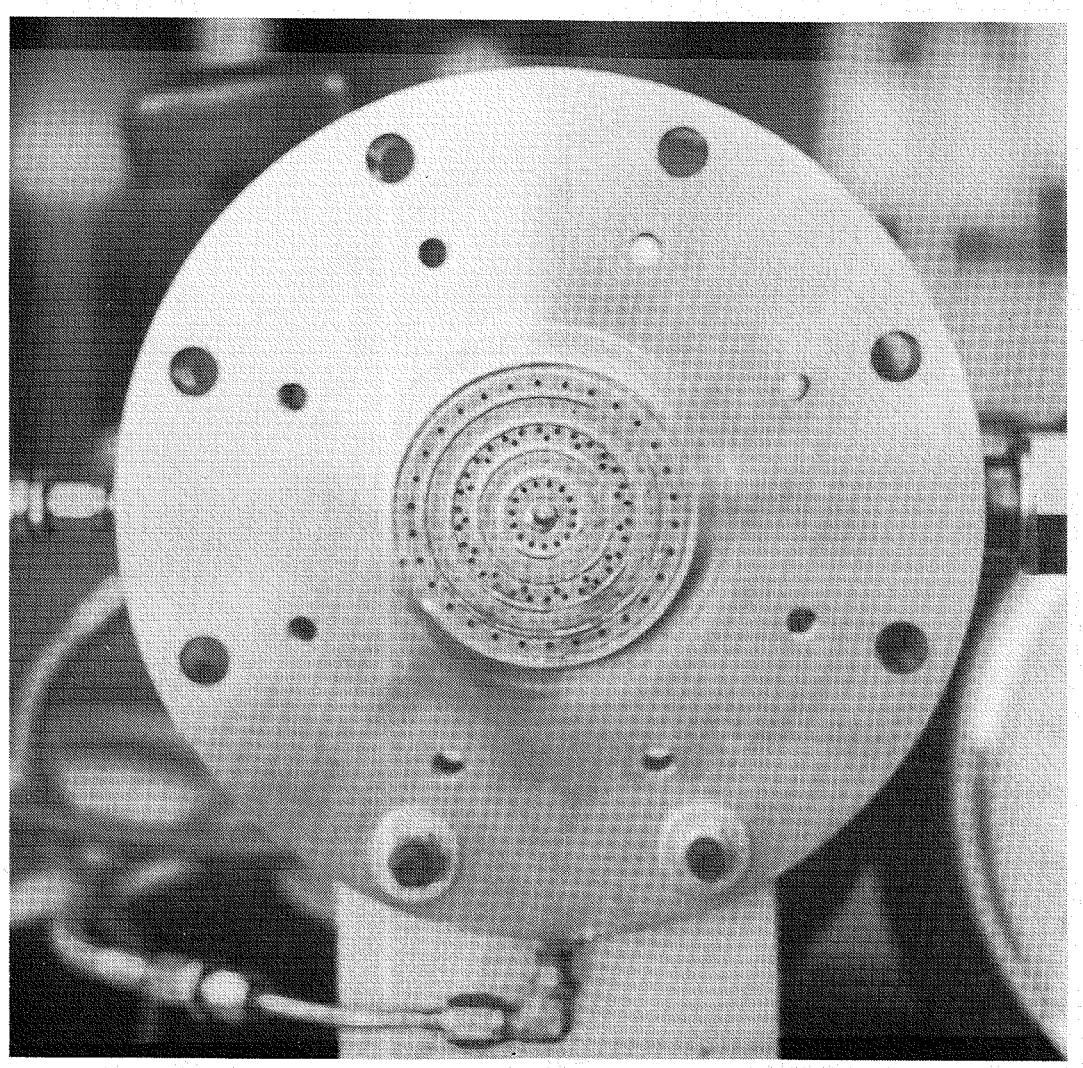

C 1082 056

Figure 135. GOX/Ethanol Platelet Injector

TABLE XIX

COLD FLOW TEST RESULTS

Fuel Circuit - Water Flow

Data Pt	Valve Inlet Pressure, psig	Manifold Pressure, psig	Flow, H_2O lb/sec	$Kw_{man.}$	Kw_{line}
1	276	262	1.70	.105	.102
2	200	192	1.45	.105	.103
3	160	155	1.28	.103	.101
4	100	95	1.00	.103	.100
5	14	-	.34	-	.094

Oxidizer Circuit - GN_2 Flow (Assumed Temperature 530°R)

Data Pt	NBS Venturi Inlet Pressure, psia	Oxidizer Manifold Pressure, psia	GN_2 Flow, lb/sec	Cd A, ($in.^2$)
1	280	130	.67	.229*
2	140	60	.34	.250*
3	155	70	.365	.230*
4	40	20	.09	.222**

*Sonic Flow

**Subsonic Flow

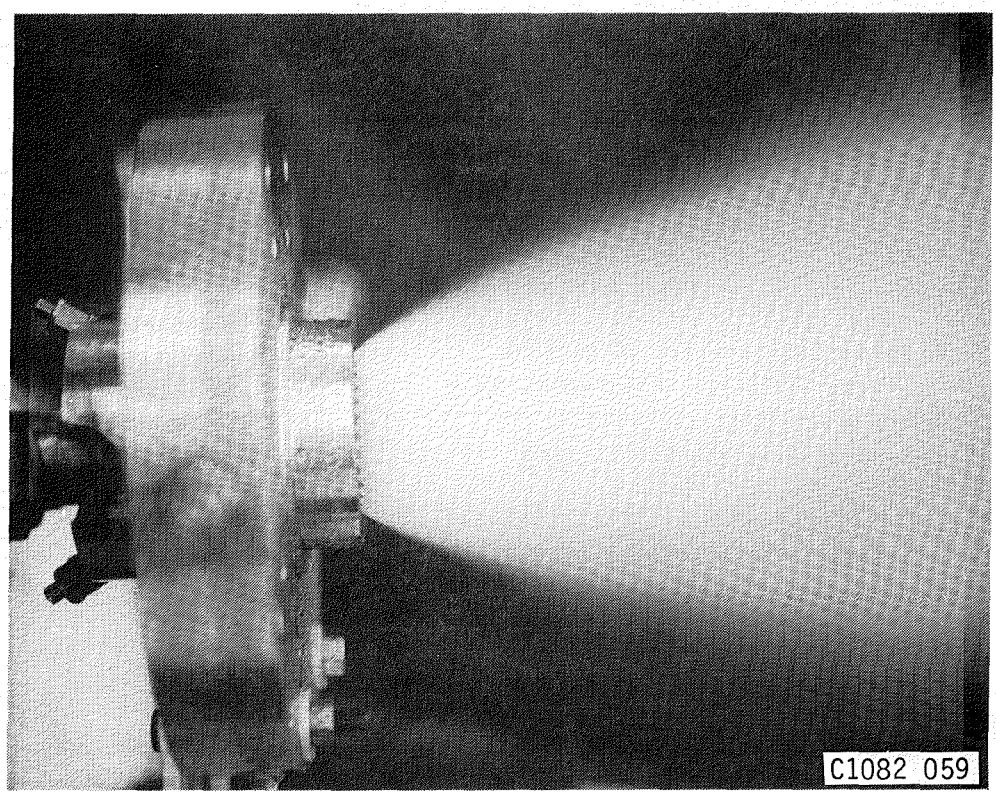

GOX ETHANOL INJECTOR COLD FLOW. FUEL SWIRLER ONLY ΔP = 15 PSI

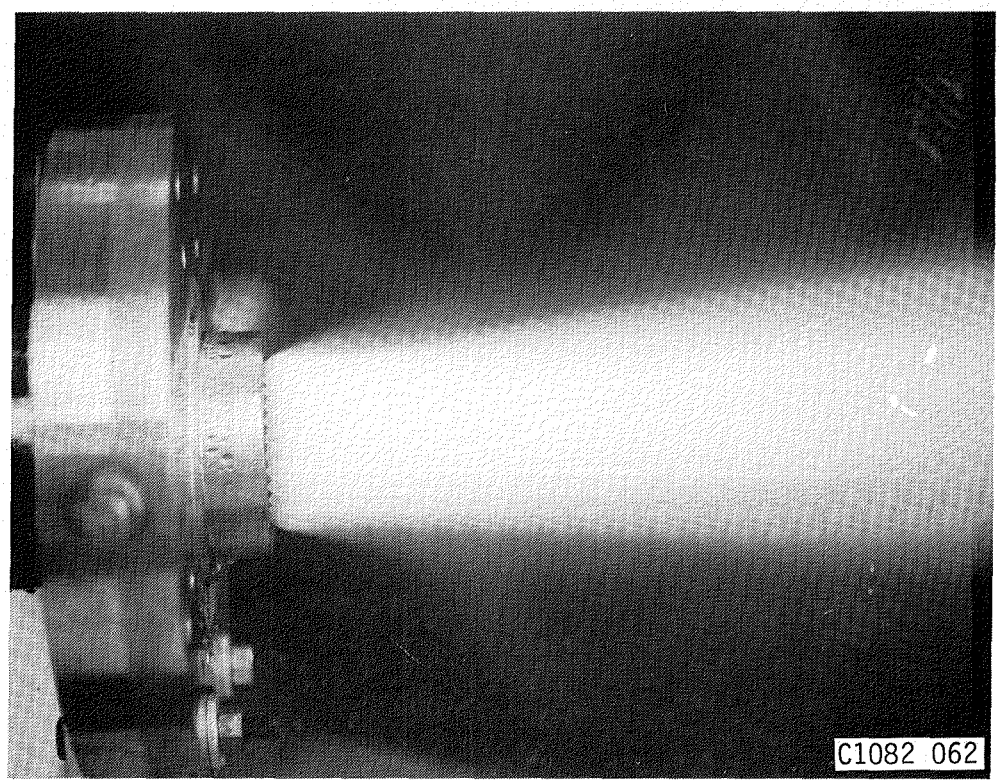

GOX/ETHANOL INJECTOR COLD FLOW. FUEL ΔP = 98 PSI OX ΔP = 55 PSI

Figure 136. GOX/Ethanol Injector Cold Flow

E, Tasks II and IV Subscale Injector Characterization (cont.)

The series was designated as RLB6-988 starting with Test 101. Tests 101 through 111 were accomplished with propellant temperatures near the projected upper limits of operation approximately 50°F. Tests 141 through 142 utilized propellants near the lower temperature limits (approximately -130°F). The nominal test duration except for checkout and aborts was 15 seconds with fuel film-cooling plus 5 additional seconds of operation with the valve to the film-cooling injector closed. Tables XX and XXI summarize the conditions for the 13 tests conducted and the performance and heat flux measurements.

Test 101 was a checkout of 1.3 sec duration at a nominal pressure of 300 psia and MR of 1.7. The ignition sequence was smooth and nominal. The engine was stable, and desired flow conditions were achieved.

Test 102 was 20 seconds duration with the first 15 seconds providing approximately 21% fuel film cooling and the last 5 seconds providing 0% fuel film-cooling.

Test 103 was to be a high MR, low pressure test (2.4, at 150 psia) but was aborted, after normal start, at 1.5 seconds the abort was due to the faulty setting of a kill parameter.

Test 104 repeated Test 103 conditions for the full duration of 20 seconds. Inspection of the injector and chamber after each test showed no carbon on either component and no heat-marking on the injector.

Test 105 was the first test on 17 December, with a duration of 1.5 seconds and chamber pressure of 300 psia. Testing was terminated after a normal ignition due to a faulty kill parameter.

Test 106 was a repeat of test 105 for the full duration of 20 seconds. The mixture ratio in this test started at the planned high end (2.4) but decayed throughout the test due to a fall-off in pressure at the flow control venturi inlet. The drop in pressure was due to low oxidizer cascade pressure aggravated by the internal propellant temperature decay due to the high blowdown rate from the gas bottles. No hardware damage was noted. A chamber oxidation pattern matching the six manifold down-comers (see Figure 20) was noted following this test.

Test 107 was a nominal 20 second duration test at 150 psia and MR of 1.7.

Test 108 was normal at 20 seconds but at a fuel- rich MR of 1.3. Data for film cooling flows of 20% and 0% were attained in both of the above tests.

Test 109 was a repeat of Test 107 with the film cooling flow set at 10%. This test was manually terminated at 6.5 seconds in order to avoid risk to the injector due to low fuel coolant flow resulting from the combination of low pressure and low coolant flow fraction. No hardware damage or overheating was observed on postfire inspections.

TABLE XX

GOX/ETHANOL PERFORMANCE DATA SUMMARY

Test No.	Date	Data Summary sec	P_{oj} I psia	MR Eng	MR Core	$\dot{w}_o$ lb/sec	$\dot{w}_{fT}$ lb/sec	% FFC	P_{oJ} psia	P_{fJ} psia	P_{fJC} psia	F_{VAC} lbF	T_{oJ} °F	T_{fJ} °F	C* FPS	Isp_{VAC} sec	Kw_f	Kw_o	% C*	% ERE
RLB6988-																				
101	12/16/83	1.2-1.38	293.2	1.32	1.66	2.291	1.728	20.5	431.9	513.9	414.8	870.7	49.3	56.9	5314	232.0	.103	.708	—	—
102		5.3-5.8	300.9	1.39	1.74	2.395	1.719	20.3	450.5	514.7	418.2	903.0	43.3	53.5	5328	234.7	.104	.695		
		10.3-10.8	299.9	1.40	1.76	2.389	1.702	20.4	447.7	511.3	415.8	898.6	42.1	52.6	5340	234.9	.104	.698		
		18.8-20.8	287.8	1.68	1.68	2.378	1.414	0.0	440.7	518.7	290.7	861.6	41.0	52.7	5530	243.7	.104	.685		
103		1.2-1.38	147.5	2.10	2.72	1.400	.664	22.6	251.4	192.8	174.1	413.1	48.2	55.3	5206	230.3	.085	.636		
104		5.3-5.8	155.7	1.85	2.36	1.413	.761	21.6	256.6	208.3	186.2	444.6	45.7	53.5	5217	233.1	.092	.648		
		10.3-10.8	155.5	1.89	2.41	1.415	.748	21.8	257.0	207.3	185.4	444.3	44.8	53.3	5238	234.2	.091	.647		
		18.8-20.8	147.9	2.31	2.31	1.417	.612	0.0	253.4	206.6	154.8	421.3	43.8	51.8	5310	238.3	.089	.635		
105	12/17/83	1.2-1.38	299.2	1.99	2.49	2.707	1.360	20.1	490.5	435.4	375.6	896.3	49.8	56.9	5360	235.8	.104	.653		
106		1.3-1.8	300.0	1.94	2.44	2.686	1.379	20.2	488.2	440.3	378.5	900.1	46.7	56.0	5375	236.8	.104	.653		
		5.3-5.8	288.4	1.76	2.20	2.485	1.410	20.2	456.3	435.2	370.2	868.6	43.1	55.4	5393	239.0	.104	.666		
		10.3-10.8	275.2	1.58	1.98	2.283	1.443	20.2	424.3	428.0	360.3	824.9	43.2	54.4	5382	238.2	.104	.681		
		18.8-70.8	251.7	1.64	1.64	2.057	1.248	0.0	384.9	431.7	255.9	751.4	43.6	54.1	5549	246.2	.104	.683		
107		5.3-5.8	148.8	1.30	1.61	1.177	.903	19.5	224.7	209.0	184.2	418.4	49.6	54.8	5212	231.4	.104	.681		
		10.3-10.8	148.4	1.31	1.63	1.177	.895	19.5	224.6	207.6	183.3	417.7	48.9	54.4	5219	232.0	.104	.680		
		18.8-20.8	143.3	1.58	1.58	1.178	.741	0.0	222.3	206.4	151.3	403.7	48.0	53.7	5437	243.1	.104	.668		
108		5.3-5.8	143.4	1.02	1.27	1.053	1.026	19.7	207.3	221.2	188.6	399.1	50.8	54.4	5025	222.4	.104	.698		
		10.3-10.8	143.4	1.03	1.29	1.056	1.017	19.7	207.5	219.8	187.9	399.6	50.2	54.2	5038	223.3	.104	.697		
		18.8-20.8	140.4	1.26	1.25	1.061	.842	0.0	206.5	221.5	148.4	392.1	49.3	53.9	5374	239.3	.104	.689		
109		5.3-5.8	145.8	1.46	1.63	1.166	.797	10.8	221.9	202.0	155.2	404.2	49.9	54.6	5409	237.8	.106	.676		
111		5.3-5.8	90.3	1.64	2.26	.768	.466	27.3	143.6	121.1	108.5	224.6	51.9	54.8	5329	233.1	.068	.654		
		10.3-10.8	90.3	1.64	2.26	.769	.466	27.1	143.6	120.9	108.5	225.5	51.3	54.3	5328	233.6	.068	.654		
		18.8-20.8	85.5	2.14	2.25	.768	.358	0.0	141.4	120.2	95.8	212.2	50.5	54.2	5529	244.2	.065	.639		

TABLE XXI

GOX/ETHANOL THERMAL DATA

Test	Time	Pc psia	MR_c	MR	$\dot{w}_T$ lb/sec	% FFC	Heat Flux R	Heat Flux A_3	A_2 Btu/sec	A_1 Btu/sec	C_2 $in.^2$	C_1	D_1	D_2	D_3	Total Heat EQ Btu/sec
102	10	299.7	1.76	1.39	4.07	20.3	3.18	1.89	2.63	2.78	2.74	5.51	9.99	6.08	4.43	277
	20	288.0	1.68	1.67	3.78	0	4.25	2.92	3.67	3.58	3.72	6.49	12.36	8.26	5.86	358
104	15	155.4	2.42	1.92	2.16	21.8	2.09	1.16	1.59	1.90	2.05	3.29	4.91	4.18	3.40	195
	20	148.0	2.32	2.32	2.04	0	2.70	1.84	2.25	2.41	2.70	3.96	5.59	4.86	4.09	247
106	5	289.9	2.20	1.79	3.92	20.2	3.31	1.90	2.70	2.99	3.08	5.90	11.50	7.17	5.15	301
	10	276.2	1.98	1.58	3.71	20.2	3.11	1.86	2.54	2.74	2.86	5.51	10.53	6.51	4.80	279
	15	267.4	1.7	1.45	3.61	20.2	3.07	1.77	2.39	2.62	2.69	5.22	9.77	5.98	4.39	262
	20	251.5	1.65	1.62	3.28	0	3.91	2.50	3.10	3.19	3.27	5.72	10.95	7.23	5.16	320
107	10	148.5	1.62	1.31	2.07	19.5	1.84	1.05	1.34	1.56	1.60	2.69	3.89	2.91	2.38	141
	20	143.3	1.59	1.59	1.92	0	2.36	1.53	1.79	1.91	2.04	3.03	4.63	3.88	3.02	181
108	10	143.5	1.29	1.05	2.08	19.7	1.73	.864	1.11	1.27	1.31	2.41	3.25	2.01	1.73	123
	20	140.3	1.26	1.27	1.91	0	2.17	1.17	1.51	1.63	1.61	2.69	3.89	2.83	2.22	156
109	6	145.8	1.64	1.47	1.97	10.8	2.02	1.22	1.48	1.70	1.77	2.75	4.00	3.17	2.56	156
111	10	90.5	2.26	1.69	1.24	27.1	1.15	.681	.977	1.02	1.27	2.09	2.58	1.93	1.71	94
	20	85.2	2.25	2.18	1.14	0	1.91	1.31	1.58	1.66	1.93	2.78	3.23	2.31	2.02	145
141	11	281	1.6		3.85	16	2.99	1.89	1.76	2.18	2.10	3.92	5.46	3.60	2.65	261
	20				3.67	0	3.60	2.35	2.18	2.38	2.46	4.31	6.97	4.82	3.39	
142	14	145	1.84		1.86	14	2.18	1.30	1.37	1.49	1.61	2.81	3.44	2.17	1.58	155
	25				1.78	0	2.41	1.64	1.71	1.59	1.85	3.04	3.68	2.59	1.96	170

E, Tasks II and IV Subscale Injector Characterization (cont.)

Test 110 was a low pressure chug stability test (100 psia). Testing was aborted by a programming error for a low Pc kill.

Test 111 was a repeat test for the planned 20 seconds. A low cycle (1 to 2 Hz) oscillation of the exhaust plume was noted on the TV camera during this test. This appeared to be due to the hydraulic characteristics of the fuel feed system. The ringing amplitude was decaying with time during the first 15 sec; it then increased when the fuel film-cooling valve was closed at 15 seconds.

The chamber was removed following Test 111. All hardware was found to be in good condition at the conclusion of the testing with ambient temperature propellants.

Following Test 111, the injector and film cooling injector were utilized in the conduct of 30 tests of approximately 5 seconds each. A 4.75 in. L' heat sink copper chamber was tested with ambient temperature and cold propellants, as a part of Contract NAS 9-16639, LOX/Hydrocarbon Propellant Ignition Studies.

Test 141 was a resumption of testing with the water cooled 8.7 in. L' chamber with cold propellants. The test duration was 12 seconds with 15.5% fuel film-cooling plus an additional 7 seconds without film-cooling. The chamber pressure was 280 psia and core mixture ratio 1.6. The propellant temperatures in the injector manifold were oxidizer = -155°F and fuel = -115°F. The engine was stable throughout the test.

Posttest chamber inspection revealed a bulge in the copper liner at the interface between cooling circuit R and cooling circuit A-3. The chamber also had water in the bottom. A pressure check of the chamber cooling circuits, at approximately 500 psi, revealed no water leakage into the chamber; however, the coolant flow data from Test 141 indicated water transfer from A-3 to R. A decision was made to continue testing at reduced pressure since valid performance and down stream thermal data could be expected.

Test 142 was a 25 second long test (15 seconds with 14% FFC, 10 seconds without coolant) at a pressure of 140 psia and a core MR of 1.6. The oxidizer temperature ToJ was -150°F and the fuel ToJ was -120°F. The engine ran stably at both test conditions.

Testing was terminated following this test because the copper liner separation had become significantly greater. Figure 136A provides a photograph of the chamber and injector following Test 142. An intercoolant channel leak check between the throat station (D-1) and the two adjacent cooling circuits D-2 and C-1 was conducted at a pressure differential of 225 psi. A leak rate of 3% of the water flow between D-1 and D-2 was noted. A 3% coolant leakage means that the throat heat flux could be overstated in the data reduction by up to 3% while the D-2 flux could be up to 3% higher than computed. A 3% deviation in this type of measurement is not considered significant.

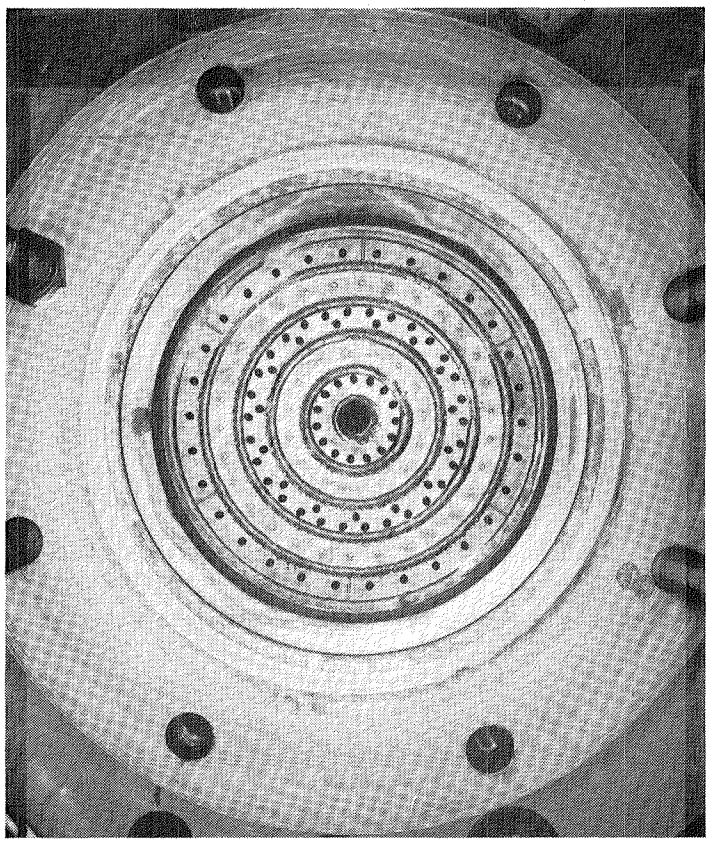

C383015

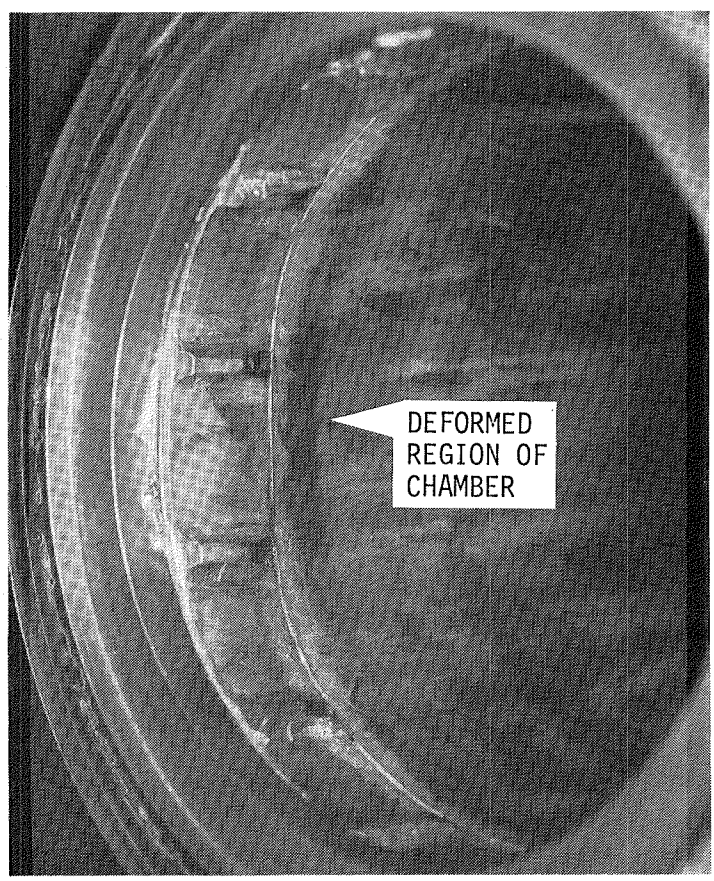

C383013

Figure 136A. Injector and Chamber Following Test 142.

E, Tasks II and IV Subscale Injector Characterization (cont.)

Figures 137 through 148 provide the measured heat flux versus time data for all tests in this series.

(6) Thermal Data Presentation

Figure 149 provides a cross plot of Test 102 data at two time periods; one at 12 seconds with 20.5% film-coolant and the second at 20 seconds with no film-coolant. In contrast to previous injectors, the addition of film-coolant reduces the chamber heat flux along the entire chamber length. The higher front end heat flux and then drop is probably due to recirculation of the hot combustor gas induced by the high OFO GOX injector velocity. An inward flow of air across the injector face was noted during the injector cold flow experiments shown in Figure 136. The drop in heat flux at 2 inches corresponds to the approximate region where the fuel swirler could be expected to impinge on the chamber wall.

Figure 150 displays the sensitivity of heat flux to both chamber pressure and mixture ratio from the time slices without film-cooling. The low throat heat flux at low pressure corresponds to the relaminarized condition predicted in the ALRC model. The increase in heat flux with increasing mixture ratio matches the predictions and suggests a well mixed combustion process, i.e., no blowapart.

Figure 151 shows the influence of film-cooling on heat flux at a selected pressure 145 psia and mixture ratio 1.6. The addition of 10.8 and 19.5% fuel, as coolant, reduces the heat flux along the entire length of the chamber by a small amount. This further indicates a well behaved combustion process and is in contrast to the dramatic flux reduction experienced with propane, and the rise with LOX/ethanol.

Figure 152 displays the influence of cold propellants on the heat flux profiles. Most significant is the reduction in throat heat flux. The reduction could be a result of the expected poor fuel vaporization and the impact of residual liquid fuel on the convergent nozzle. The possibility of a water leak in the chamber, however, cannot be ruled out. Since similar flux reductions were noted in testing with the 4.75 in. heat sink chamber, the effect is believed to be real.

(7) GOX/Ethanol Performance Data

The hot-fire test data from the GO_2/ethanol testing (Tables XXII, XXIII and Figure 153) indicated the following trends of engine performance.

Ambient Propellant Temperature Tests

8.7 Inch Chamber Length

° Combustion efficiencies in the range of 98.5-100% are indicated with the GOX/ethanol injector when fired without fuel film-cooling.

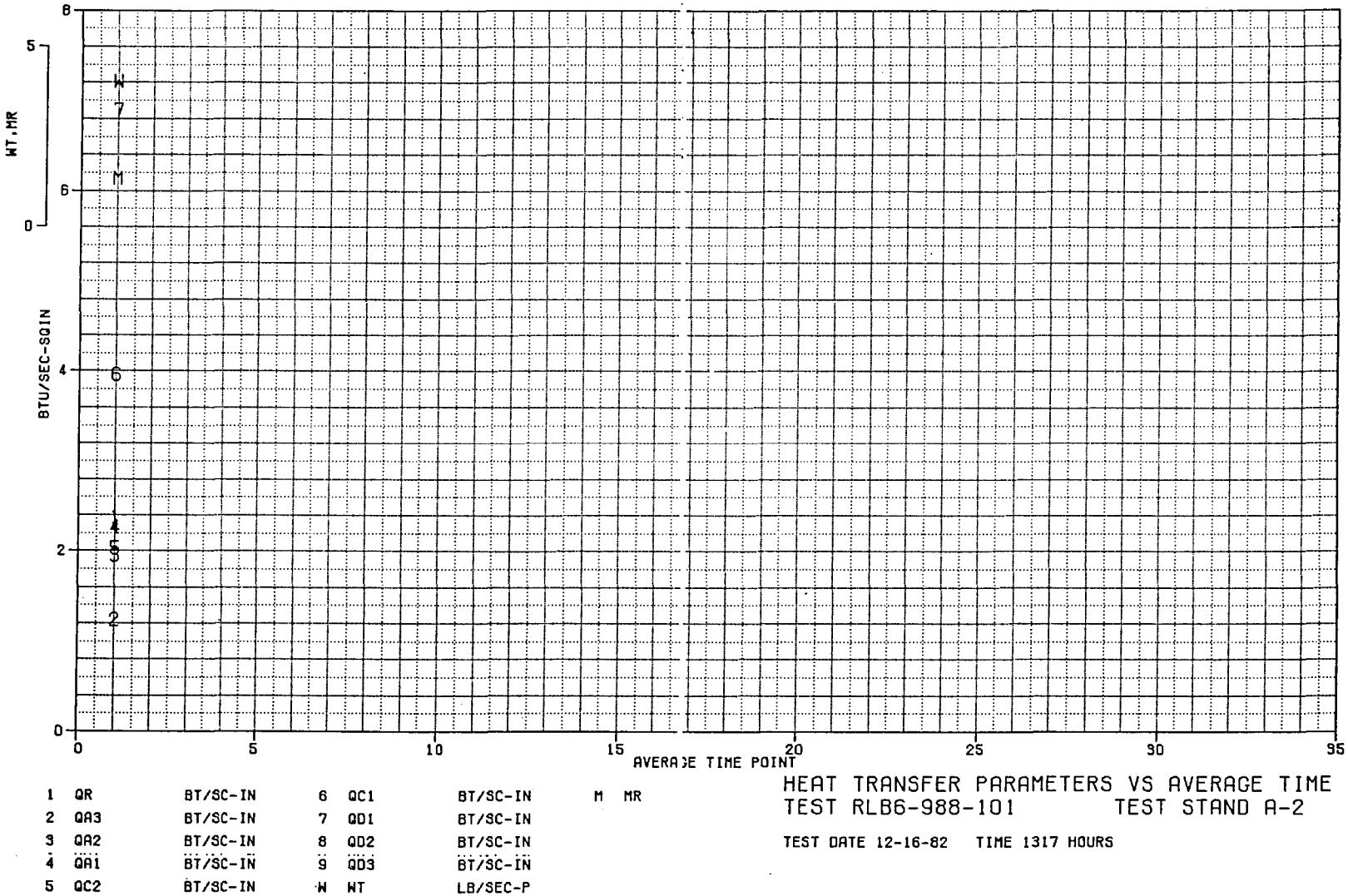

Figure 137. Heat Transfer Parameters Versus Average Time, Test RLB6-988-101

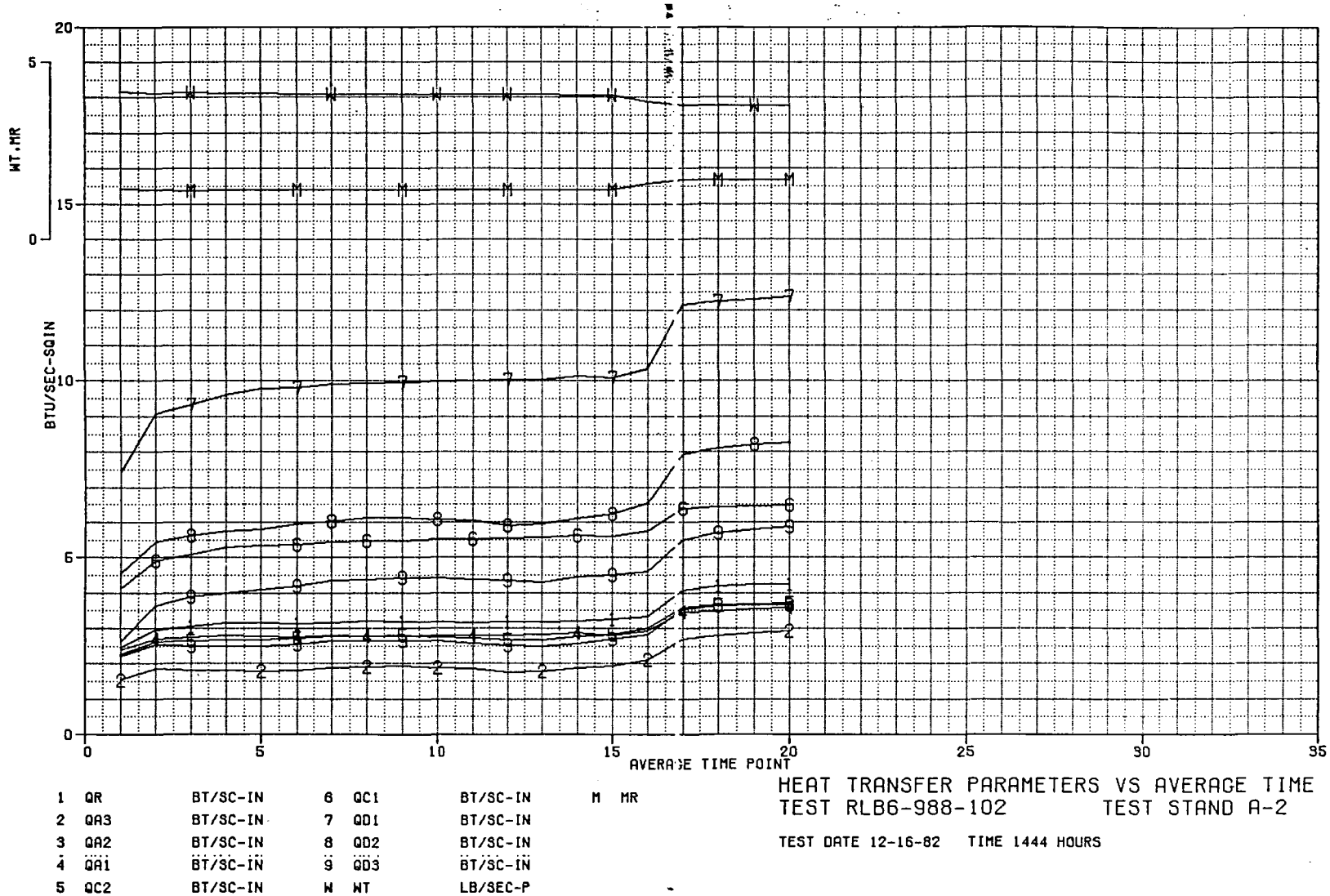

Figure 138. Heat Transfer Parameters Versus Average Time, Test RLB6-988-102

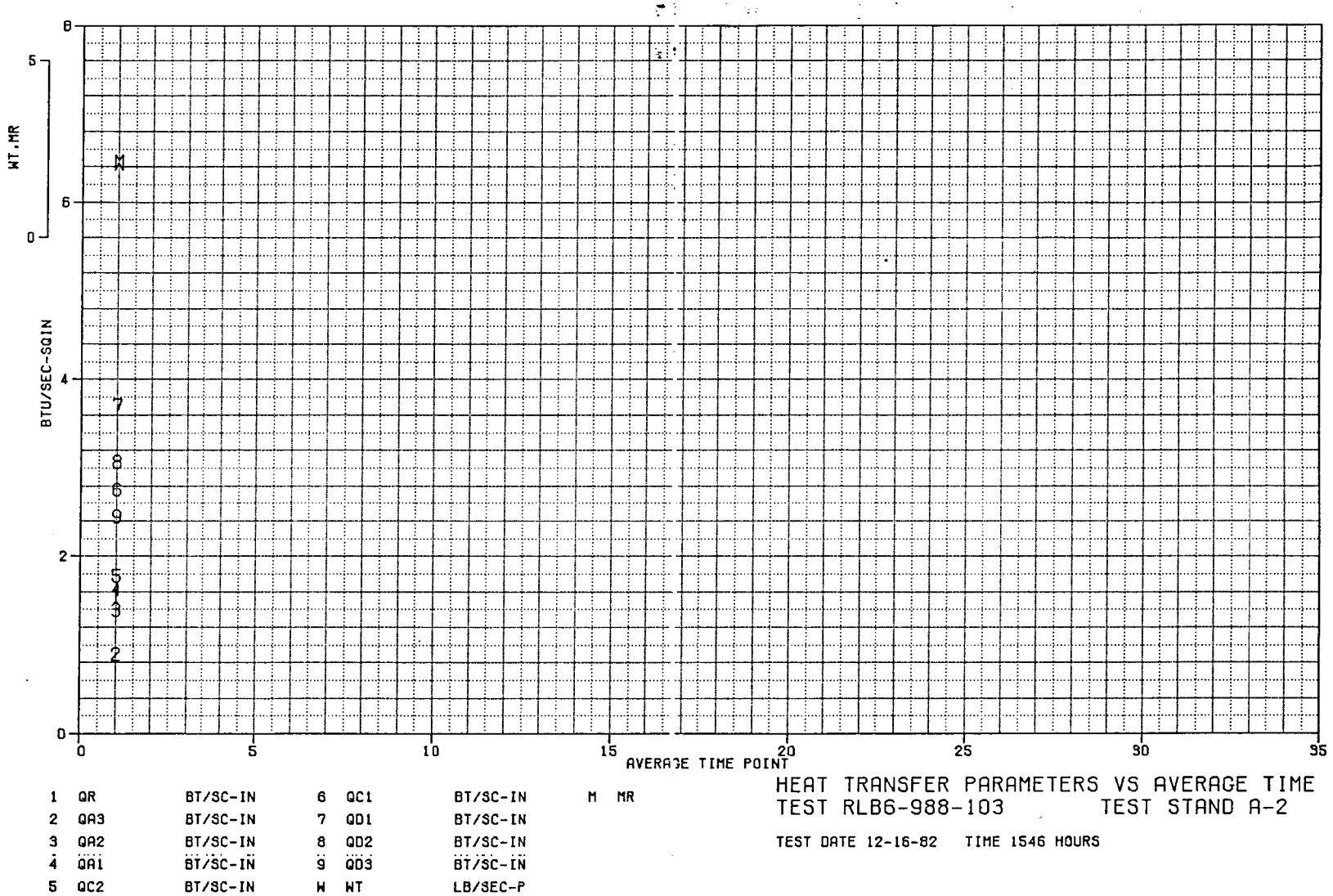

Figure 139. Heat Transfer Parameters Versus Average Time, Test RLB6-988-103

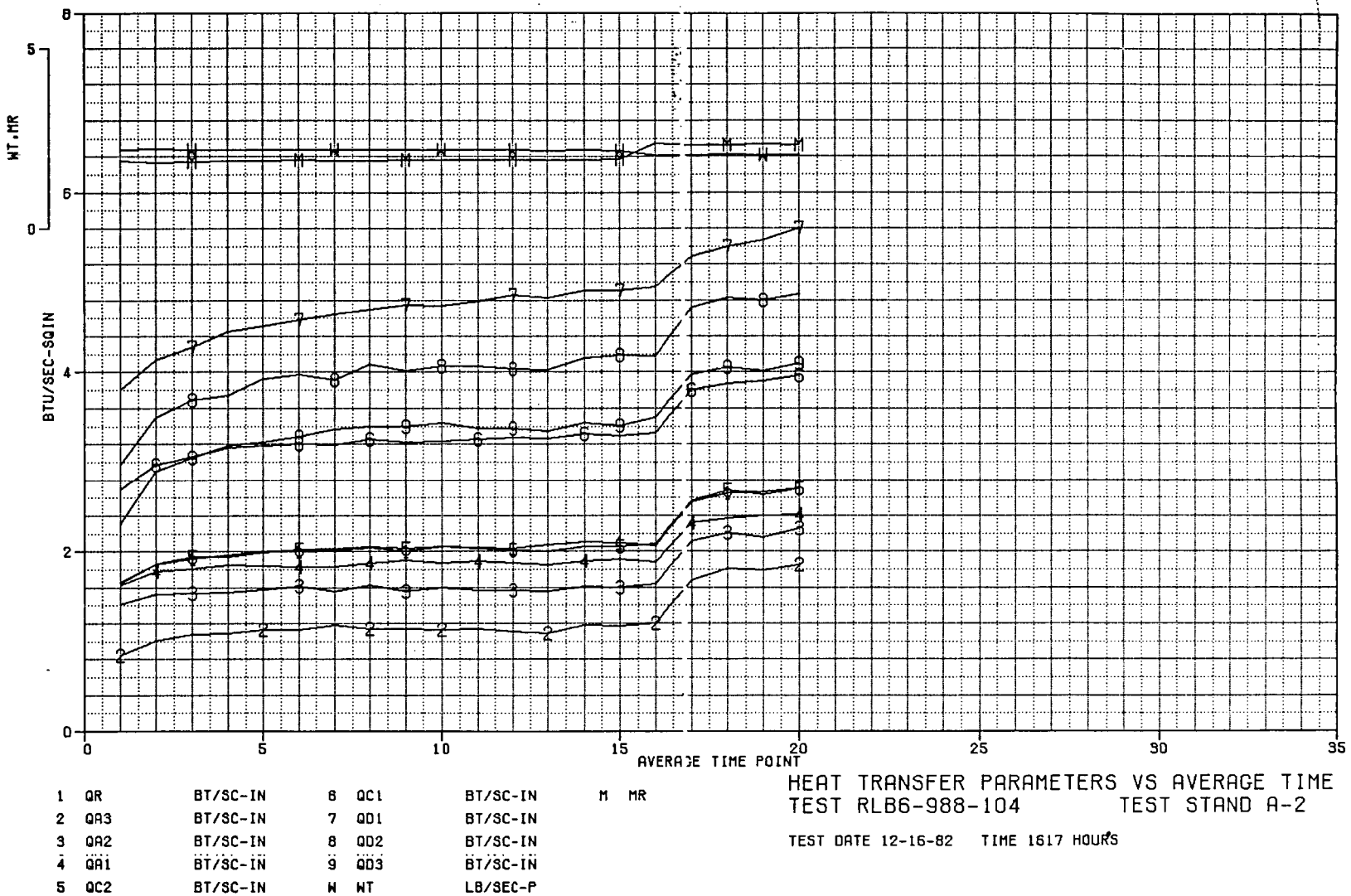

Figure 140. Heat Transfer Parameters Versus Average Time, Test RLB6-988-104

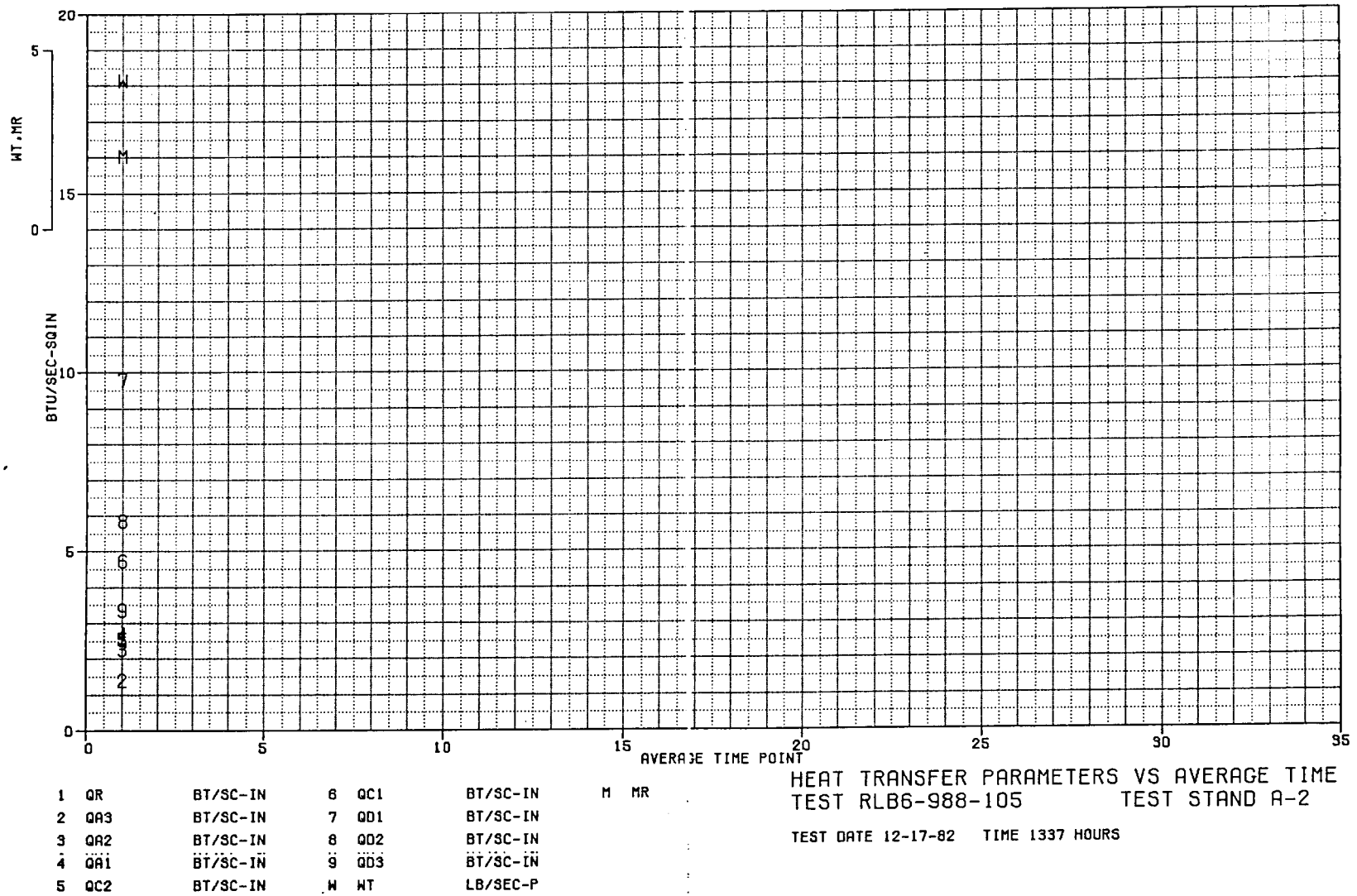

Figure 141. Heat Transfer Parameters Versus Average Time, Test RLB6-988-105

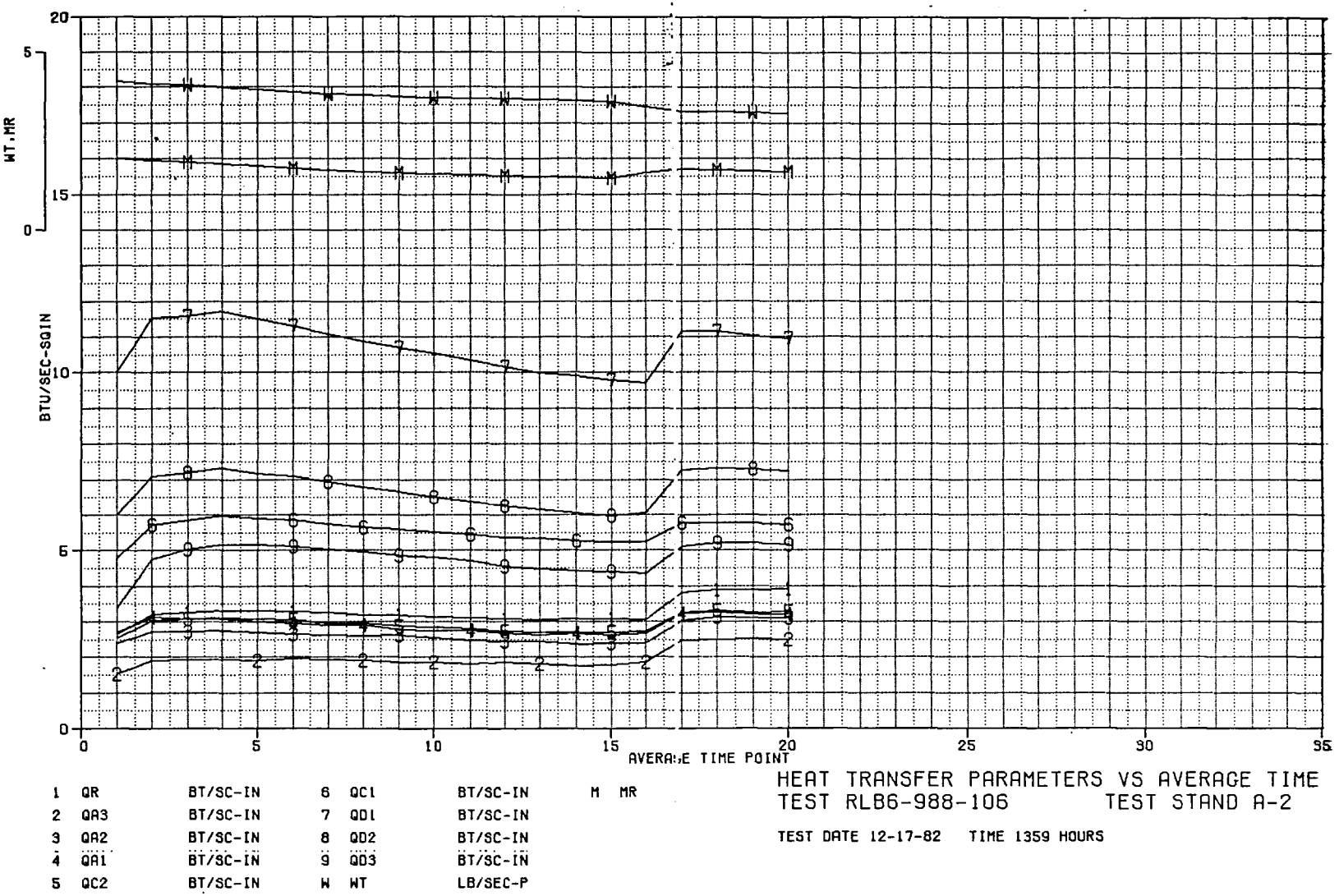

Figure 142. Heat Transfer Parameters Versus Average Time, Test RLB6-988-106

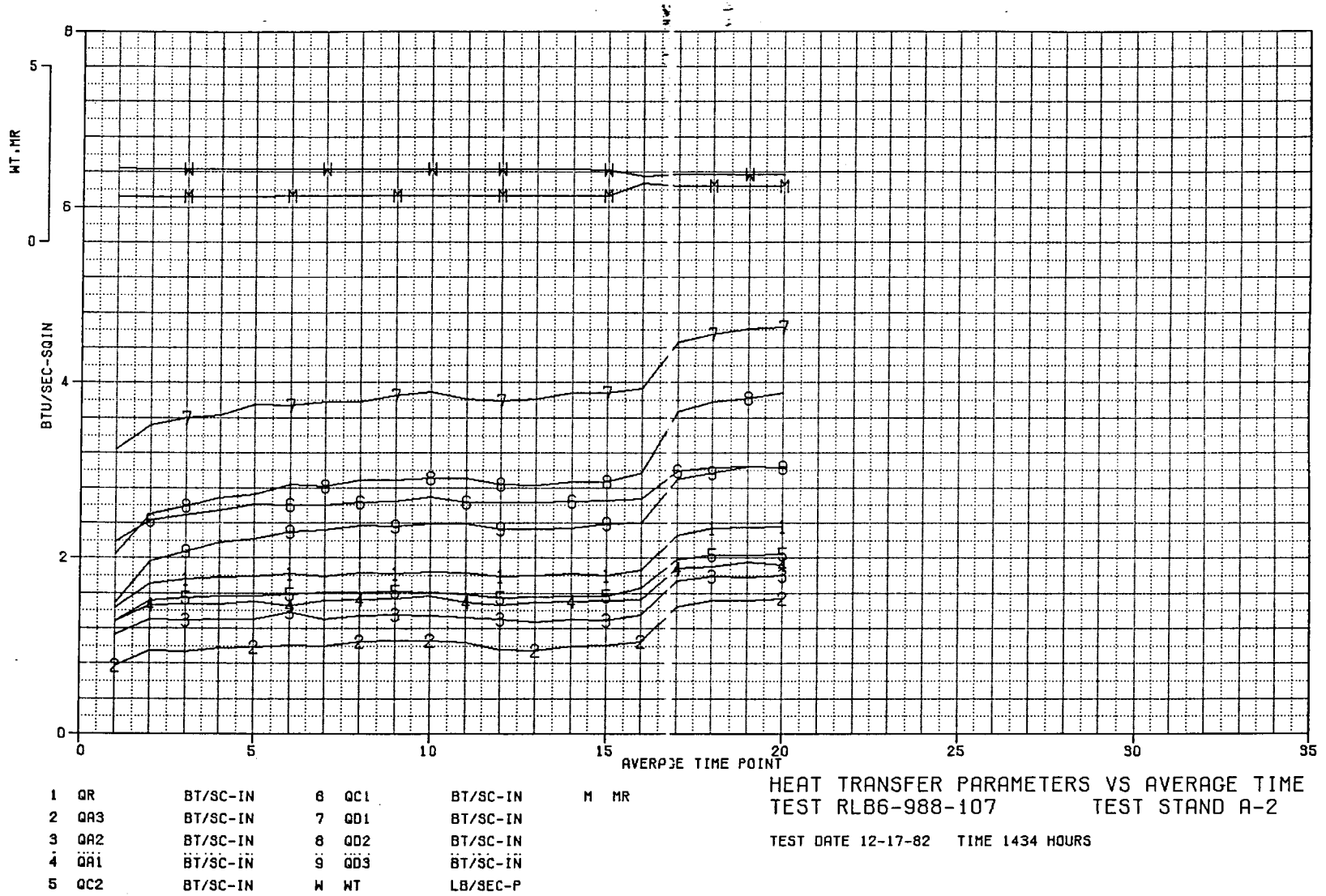

Figure 143. Heat Transfer Parameters Versus Average Time, Test RLB6-988-107

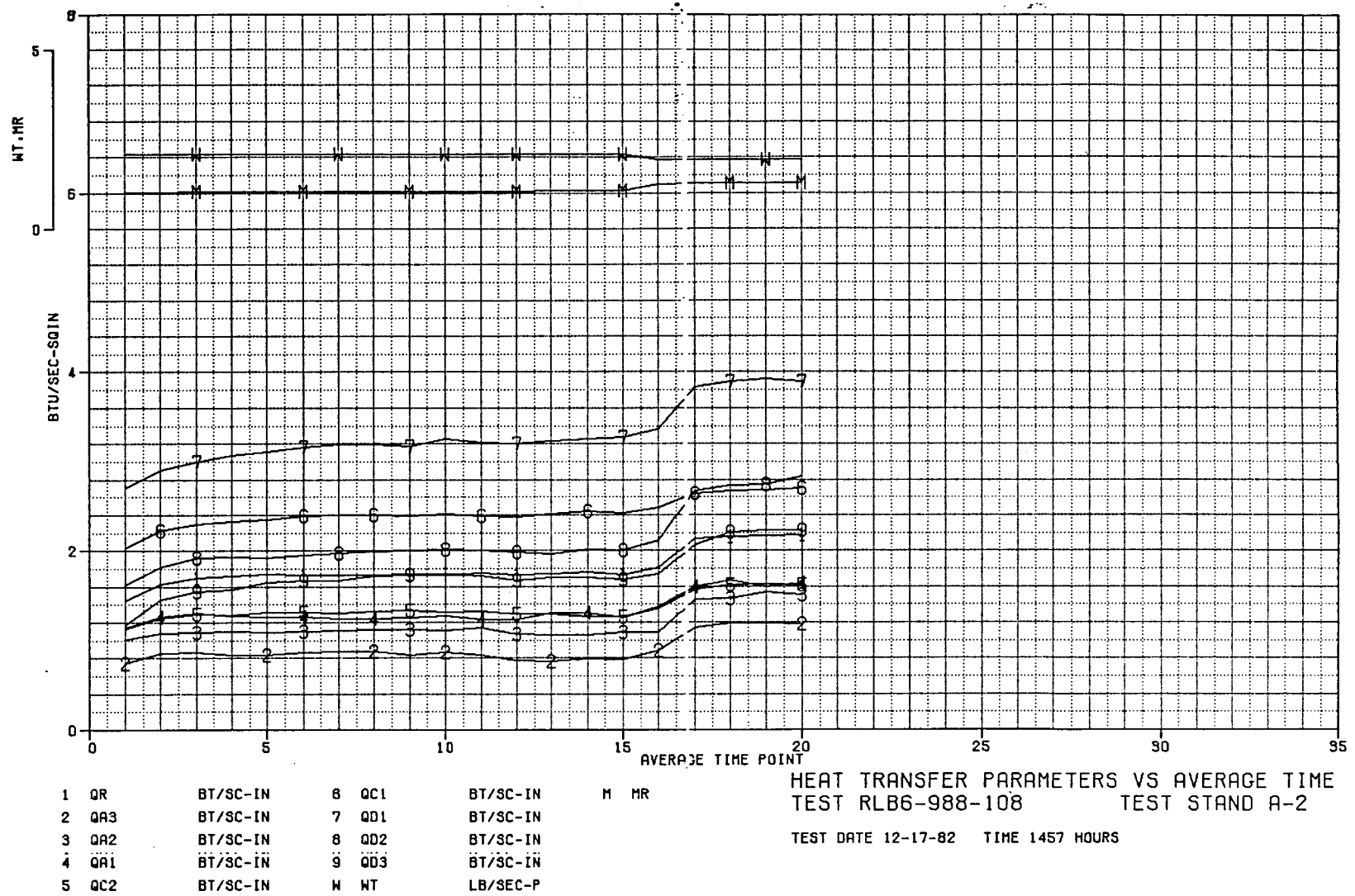

Figure 144. Heat Transfer Parameters Versus Average Time, Test RLB6-988-108

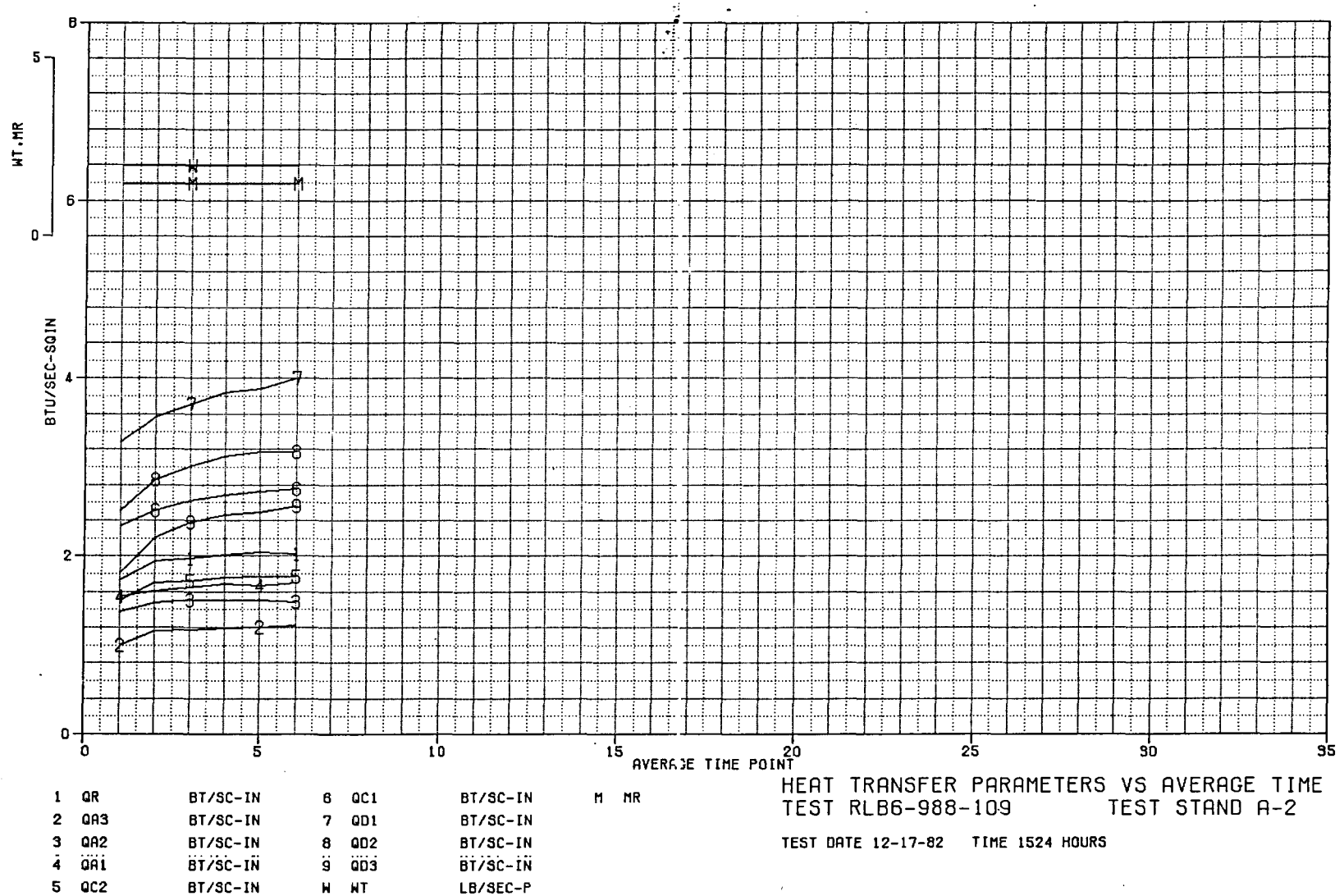

Figure 145. Heat Transfer Parameters Versus Average Time, Test RLB6-988-109

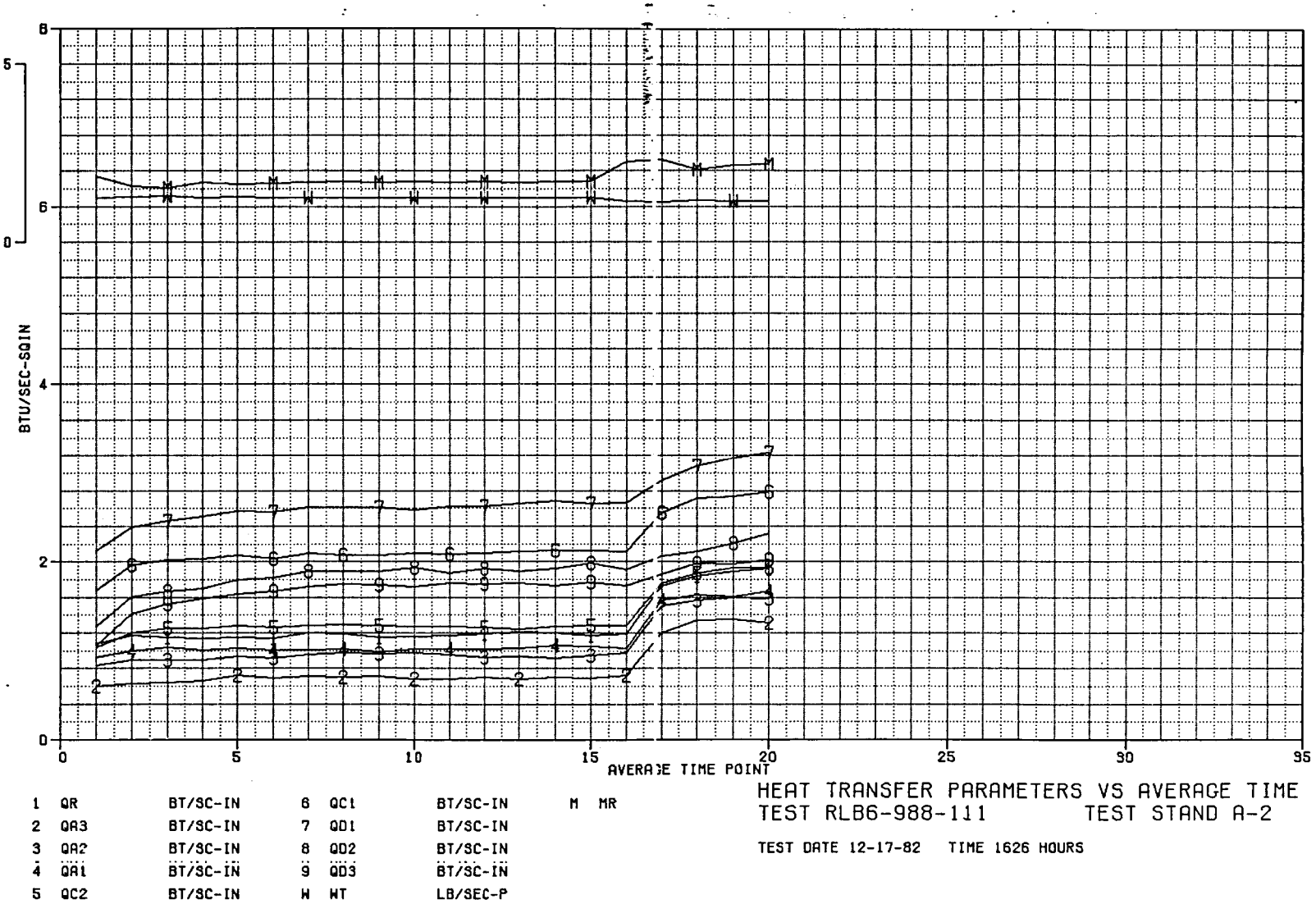

Figure 146. Heat Transfer Parameters Versus Average Time, Test RLB6-988-110

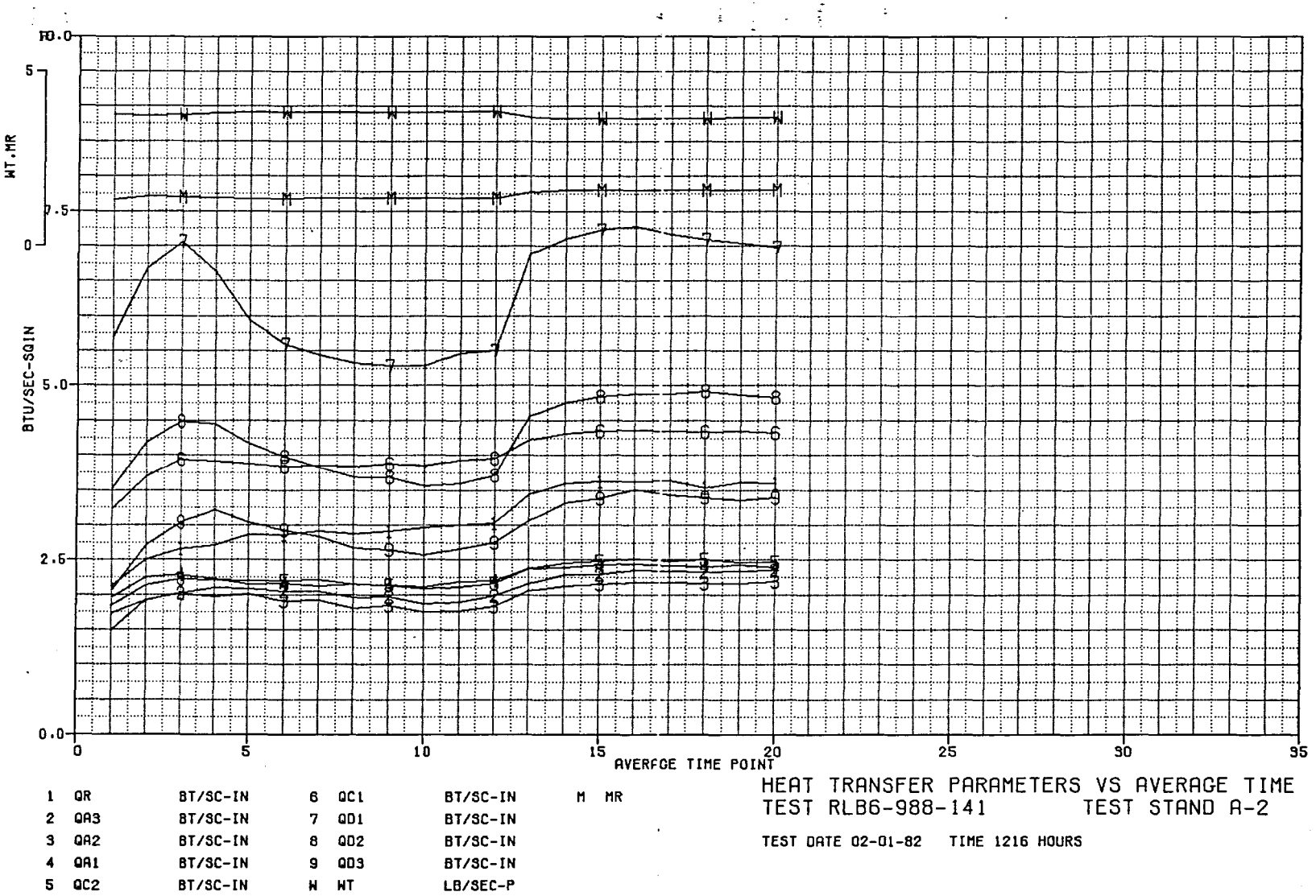

Figure 147. Heat Transfer Parameters Versus Average Time, Test RLB6-988-141

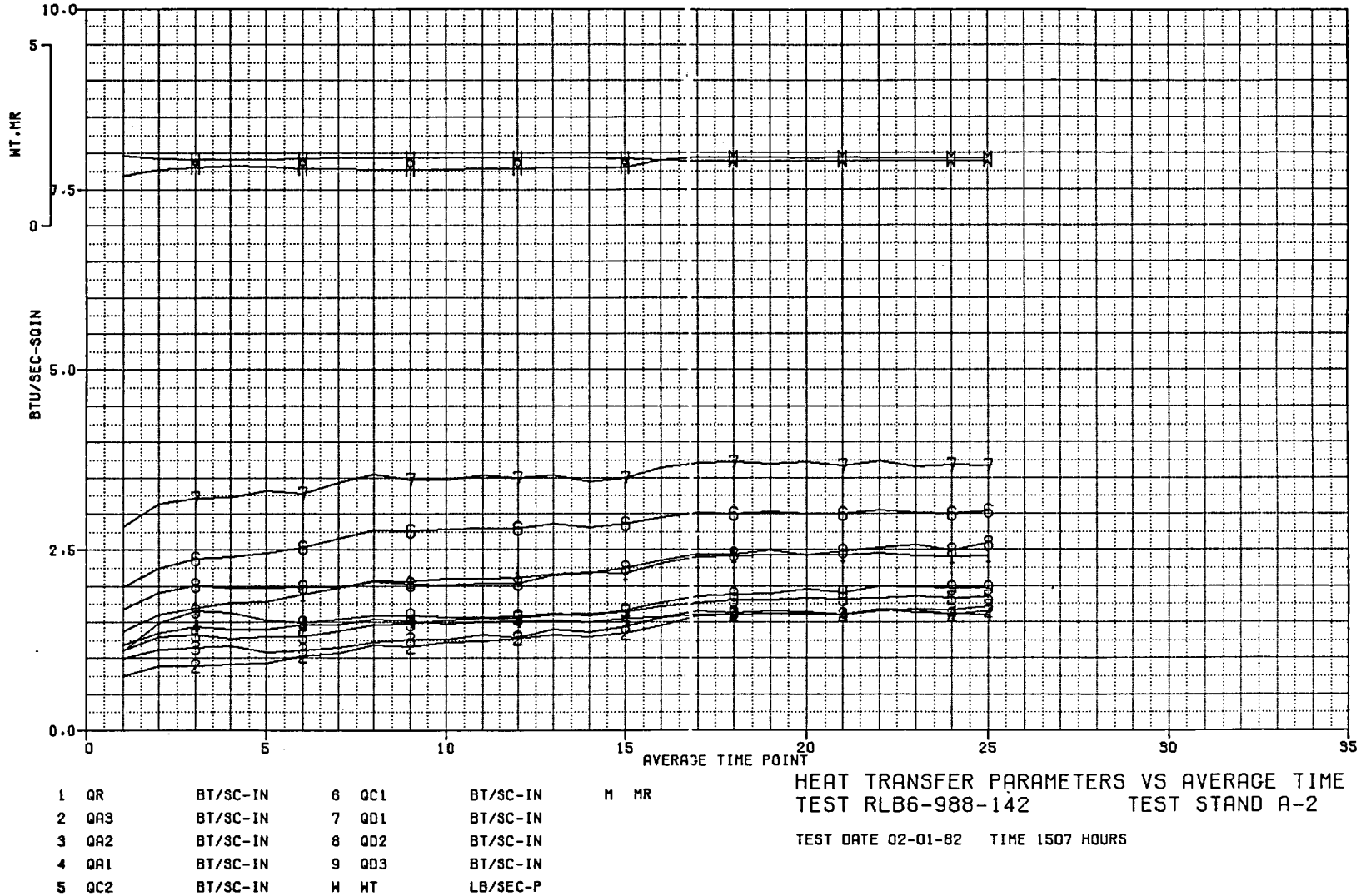

Figure 148. Heat Transfer Parameters Versus Average Time, Test RLB6-988-142

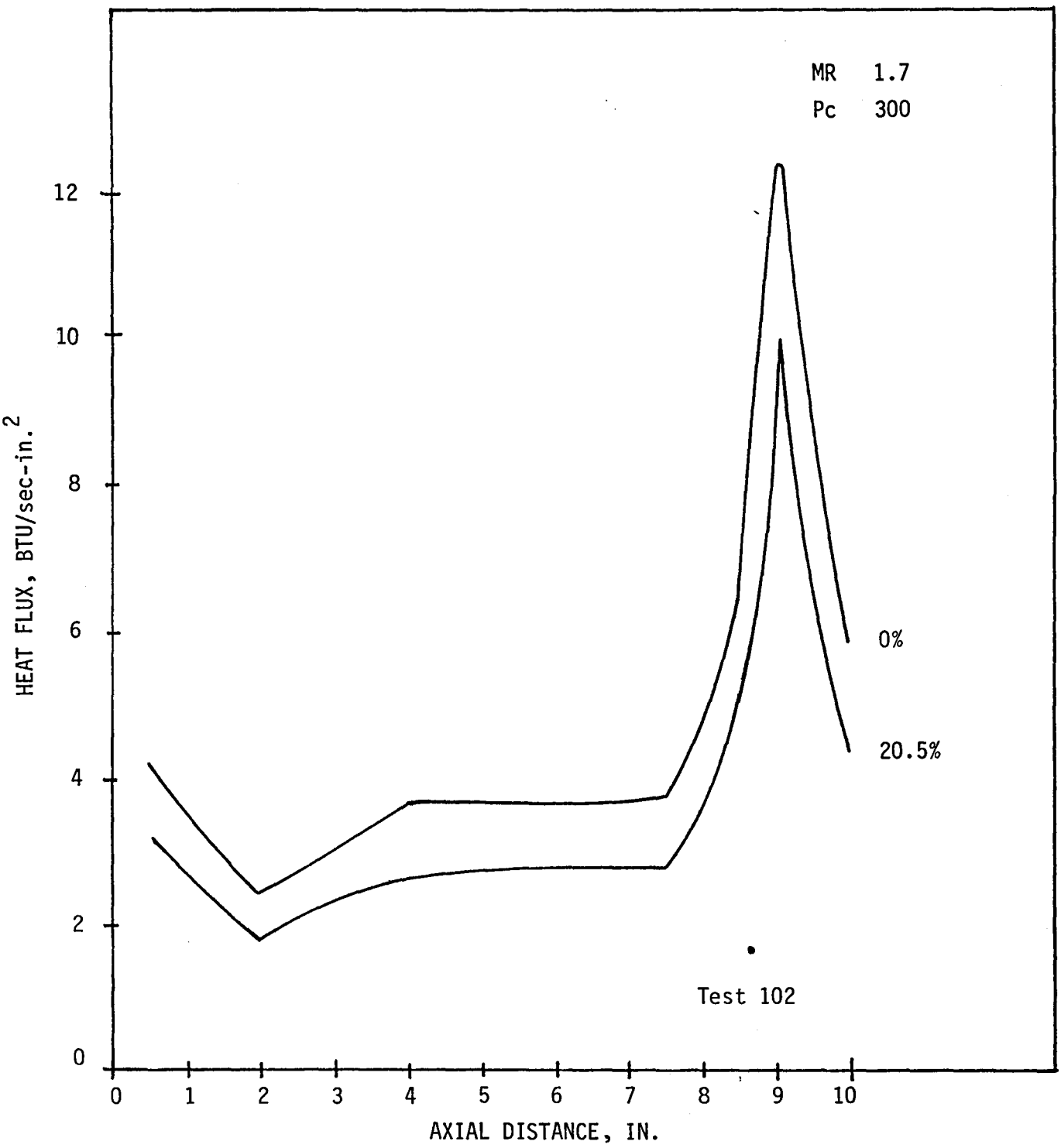

Figure 149. Heat Flux Profiles for GOX/Ethanol at 300 psi, MR = 1.7

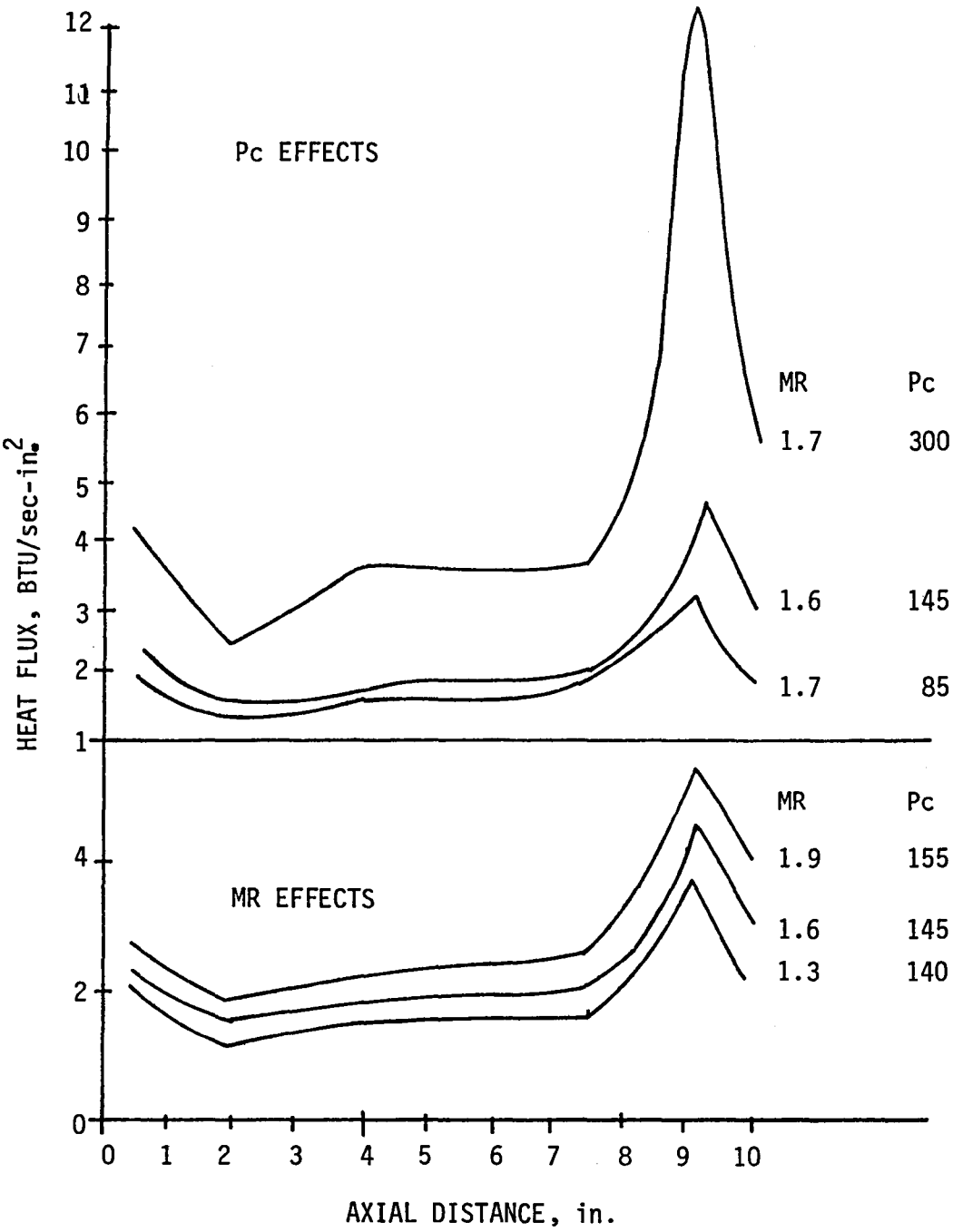

Figure 150. Pressure and Mixture Ratio Influence on Heat Flux Profiles for GOX/Ethanol Without FFC

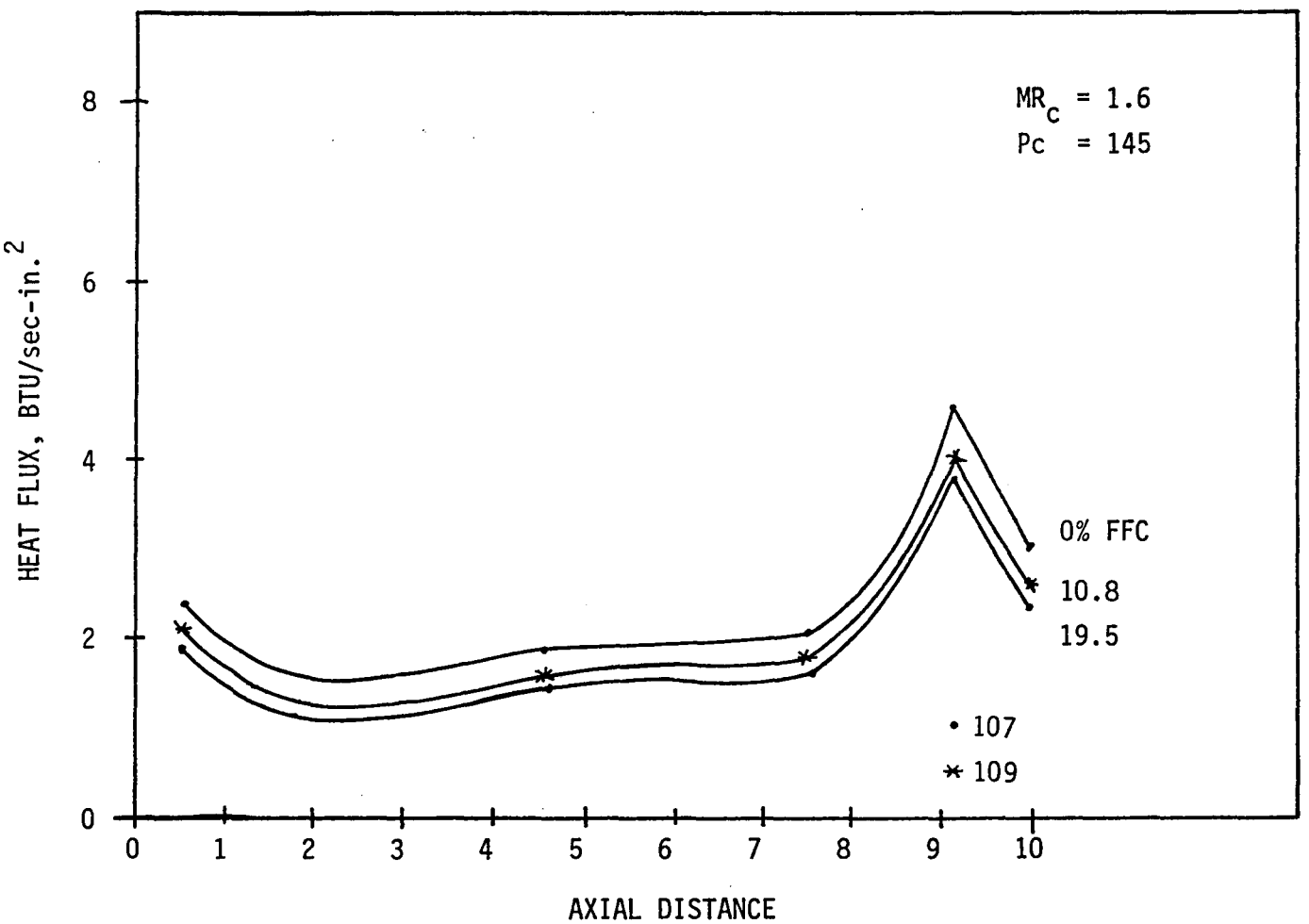

Figure 151. Effect of Fuel Film Cooling on Heat Flux Profiles for LOX/Ethanol

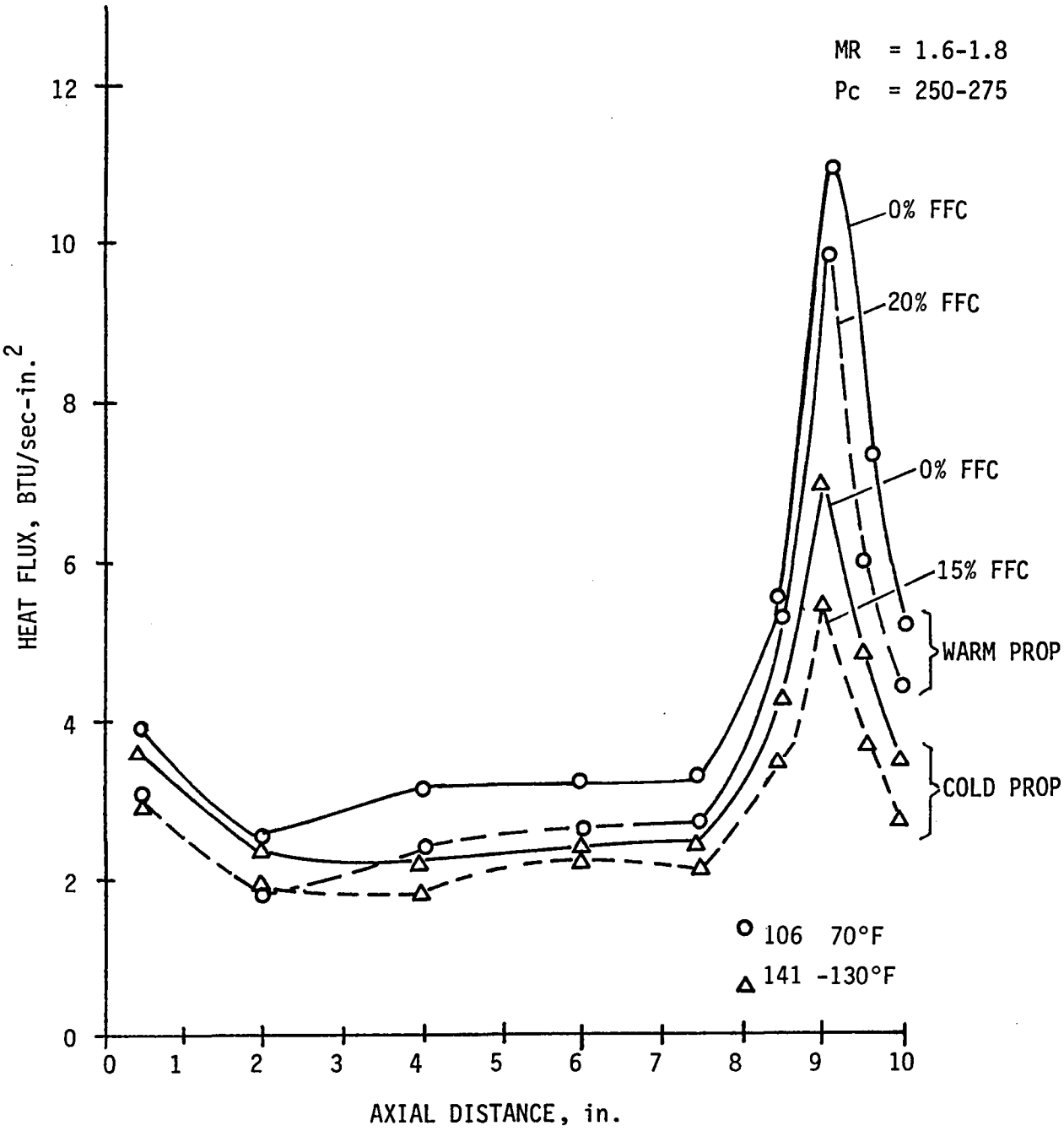

Figure 152. Comparison of Heat Flux Profiles

TABLE XXII

GOX/ETHANOL TEST PROGRAM WITH O-F-O INJECTOR

Test No. RL86-988-	Date	Dur	Sample Period	L'	% FFC	Pc	O/F eng	O/F core	T_{oJ}	T_{FJ}	P_{oJ}	P_{FJ}	W_o	W_f	K_{woj}	K_{wfj}	F_{vac}	C*	Isp_{vac}
101	12-16-82	1.38	1.2-1.38	8.75	20.5	293	1.326	1.668	49	57	432	513	2.292	1.7284	0.709	0.104	932.8	5314	232.0
102	12-16-82	20.8	1.3-1.85	8.75	20.5	304	1.398	1.758	47	56	451	523	2.415	1.7270	0.696	0.104	968.9	5343	233.9
			5.3-5.85	8.75	20.4	301	1.393	1.749	43	54	451	515	2.395	1.7200	0.696	0.105	965.9	5328	234.7
			10.3-10.35	8.75	20.4	300	1.404	1.764	42	53	448	511	2.390	1.7021	0.699	0.104	961.4	5341	235.0
			20.3-20.85	8.75	0	288	1.678	1.678	41	53	441	519	2.376	1.4156	0.685	0.104	924.3	5531	243.8
103	12-16-82	1.38	1.2-1.38	8.75	22.7	148	2.108	2.727	48	55	251	193	1.401	0.6643	0.637	0.085	475.7	5207	230.4
104	12-16-82	20.8	1.3-1.85	8.75	21.6	156	1.845	2.353	47	54	257	209	1.412	0.7652	0.650	0.092	504.6	5232	231.8
			5.3-5.85	8.75	21.7	156	1.856	2.369	46	54	257	208	1.413	0.7615	0.649	0.092	506.9	5217	233.1
			10.3-10.85	8.75	21.8	156	1.891	2.420	45	53	258	207	1.415	0.7483	0.647	0.091	506.8	5239	234.2
			20.3-20.85	8.75	0	148	2.315	2.315	44	52	254	206	1.418	0.6122	0.634	0.089	483.2	5307	238.1
105	12-17-82	1.38	1.2-1.38	8.75	20.2	299	1.991	2.494	50	57	491	435	2.707	1.3601	0.654	0.104	959.2	5361	235.8
106	12-17-82	20.8	1.3-1.85	8.75	20.2	300	1.948	2.441	47	56	488	440	2.687	1.3796	0.653	0.104	963.1	5376	236.8
			5.3-5.85	8.75	20.3	288	1.762	2.209	43	55	456	435	2.486	1.4108	0.667	0.104	931.5	5393	239.1
			10.3-10.85	8.75	20.2	226	1.582	1.984	43	54	424	428	2.283	1.4430	0.682	0.104	887.9	5382	238.3
			20.3-20.85	8.75	0	251	1.631	1.630	44	54	383	432	2.042	1.2522	0.685	0.104	811.1	5550	246.2
107	12-17-82	20.8	1.3-1.85	8.75	19.6	149	1.294	1.609	52	56	225	210	1.177	0.9096	0.682	0.105	479.8	5213	229.9
			5.3-5.85	8.75	19.6	149	1.303	1.620	50	55	225	209	1.177	0.9034	0.682	0.105	481.6	5212	231.5
			10.3-10.85	8.75	19.6	148	1.316	1.636	49	54	225	208	1.178	0.8951	0.681	0.105	480.9	5219	232.0
			20.3-20.85	8.75	0	143	1.590	1.590	48	54	222	206	1.179	0.7411	0.668	0.105	466.9	5439	243.2
108	12-17-82	20.8	1.3-1.85	8.75	19.8	143	1.010	1.258	52	55	206	222	1.046	1.0360	0.698	0.105	457.9	4994	219.9
			5.3-5.85	8.75	19.7	143	1.026	1.278	51	54	207	221	1.054	1.0265	0.699	0.105	462.8	5026	222.5
			10.3-10.85	8.75	19.7	143	1.038	1.292	50	54	208	220	1.056	1.0179	0.698	0.105	463.3	5039	223.4
			20.3-20.85	8.75	0	141	1.261	1.260	49	54	207	222	1.062	0.8422	0.689	0.105	456.0	5378	239.5
109	12-17-82	6.4	1.3-1.85	8.75	10.8	147	1.443	1.619	52	55	222	203	1.163	0.8054	0.679	0.107	464.0	5427	235.8
			5.3-5.85	8.75	10.8	146	1.461	1.639	50	55	222	202	1.166	0.7980	0.676	0.106	467.1	5410	237.8
110		MALF																	
111	12-17-82	20.8	1.3-1.85	8.75	28.4	90	1.752	2.448	54	56	144	119	0.774	0.4416	0.650	0.065	284.0	5366	233.6
			5.3-5.85	8.75	27.3	90	1.649	2.268	52	55	144	121	0.769	0.4662	0.654	0.065	287.9	5330	233.1
			10.3-10.85	8.75	27.2	90	1.647	2.262	51	54	144	121	0.769	0.4670	0.655	0.069	288.8	5328	233.7
			20.3-20.85	8.75	5.2	85	2.202	2.324	51	54	141	120	0.769	0.3491	0.637	0.063	274.5	5554	245.6
141	2-01-83	20.5	1.3-1.85	8.75	15.2	277	1.299	1.532	-152	-136	358	455	2.264	1.7434	0.734	0.118	881.5	5004	220.0
			5.3-5.85	8.75	16.4	282	1.357	1.623	-158	-113	360	456	2.306	1.6995	0.766	0.115	908.0	5107	226.7
			10.3-10.85	8.75	15.6	285	1.364	1.616	-159	-119	360	457	2.308	1.6917	0.784	0.117	918.0	5163	229.5
			18.5-20.5	8.75	0	280	1.579	1.579	-159	-91	356	472	2.297	1.4547	0.781	0.113	903.0	5403	240.7
142	2-01-83	25.5	1.3.1.85	8.75	15.4	141	1.325	1.566	-144	-111	188	184	1.164	0.8786	0.729	0.121	453.6	5009	222.1
			5.3-5.85	8.75	11.2	142	1.380	1.554	-150	-137	188	182	1.174	0.8509	0.746	0.128	463.8	5083	229.0
			10.3-10.85	8.75	13.1	145	1.433	1.650	-153	-114	188	183	1.178	0.8217	0.769	0.123	471.6	5247	235.9
			20.3-2.85	8.75	0	144	1.643	1.643	-156	-119	187	184	1.179	0.7173	0.773	0.122	472.0	5505	249.0
			23.5-25.5	8.75	0	144	1.638	1.639	-156	-116	187	184	1.179	0.7192	0.771	0.121	472.3	5477	248.9

TABLE XXIII

SUMMARY OF GOX/ETHANOL TESTING

Chamber Length, L', in.	Chamber Type	Propellant Temperature °F	% Fuel Film Coolant % FFC	Chamber Pressure Pc, psia	Combustion Efficiency/ % ER
8.7	H_2O Cooled	50	0	140-300	98.5-100
8.7	H_2O Cooled	50	20	140-300	95-97
4.7	Heat Sink	50	0	140-300	96-98
4.7	Heat Sink	50	16	140	92-93
4.7	Heat Sink	50	16	300	93-95
8.7	H_2O Cooled	-100	0	300	96.5
8.7	H_2O Cooled	-100	16	300	93.5
4.7	Heat Sink	-100	0	150	89-92
4.7	Heat Sink	-100	16	150-300	87-90

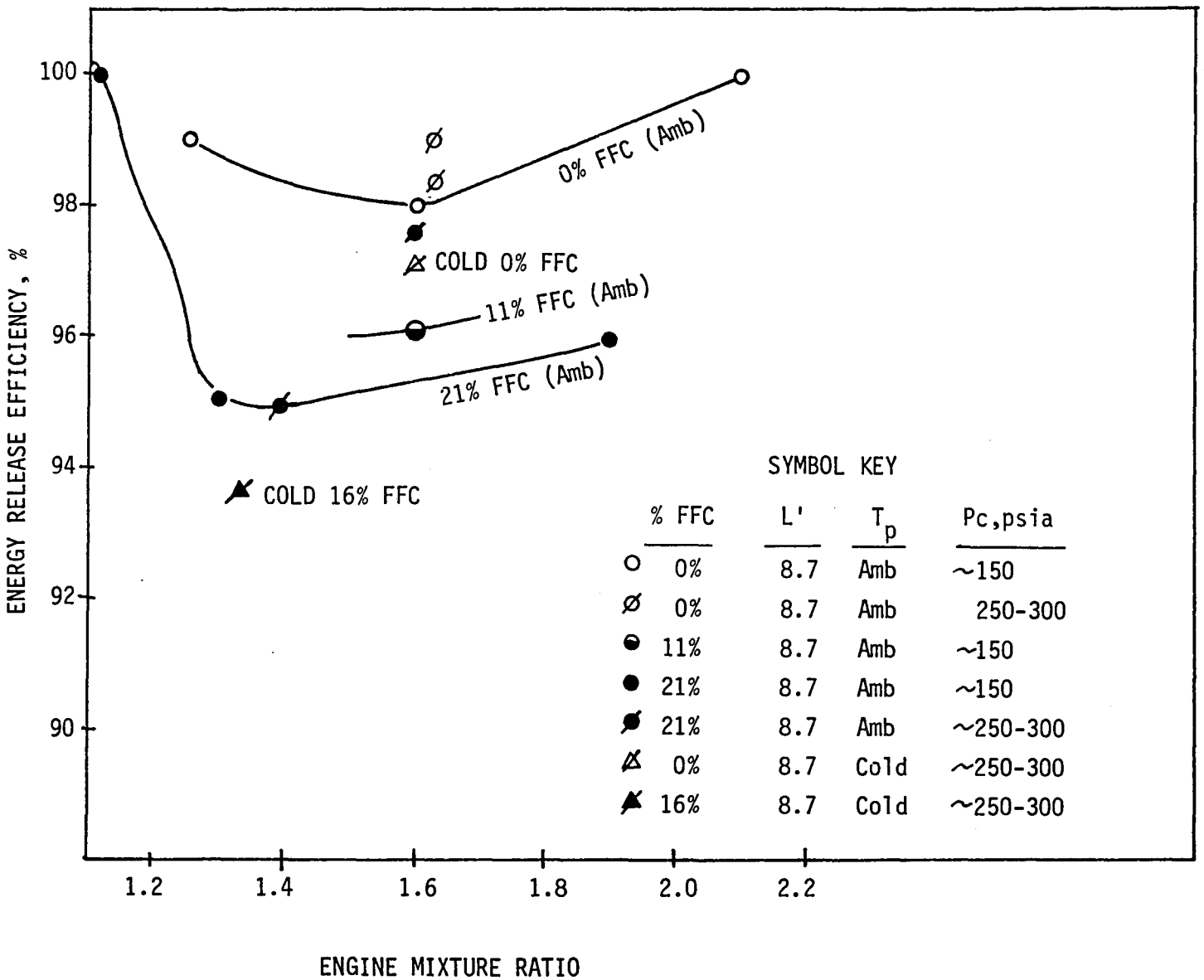

Figure 153. GOX/Ethanol Injector Energy Release Efficiency

E, Tasks II and IV Subscale Injector Characterization (cont.)

- 20% fuel film-cooling reduces performance approximately 3% compared to the 0% FFC case.
- The performance increases approximately 1% when chamber pressure is increased from 150 psia to 300 psia.
- The impact of engine mixture ratio on combustion efficiency is less than with previous OFO triplet injectors fired with LOX/ethanol.

4.7 Inch Chamber Length (Data from Contract NAS 9-16639)

- Performance is reduced by approximately 2% when the chamber length is reduced from 8.7 in. to 4.7 inch.
- 20% fuel film-cooling reduces performance approximately 2% compared to the 0% FFC base.
- The tests with the shorter chamber indicate adequate performance may be achieved within a Space Shuttle RCS envelope constraint.

Chilled Propellant Tests

Test data from the chilled propellant tests of the 4.7 inch long chamber indicates approximately a 6% reduction in performance compared to the ambient temperature cases. Performance data trends from the chilled propellant tests are difficult to establish for the film-cooled tests. Also, hydraulic data (fuel admittances and oxidizer injector orifice discharge coefficients) show significantly increased values with the chilled propellants compared to the ambient temperature cases. This may be due to transient flow and thermal influences caused by the short test durations (approximately 5 seconds). Two long duration tests (approximately 20 seconds) were conducted with chilled propellants. Data from both these tests (Tests 141 and 142) indicated a substantial (approximately 4%) increase in performance with time. Thus the data may not be valid (a chamber circuit water leak was observed after Test 142).

Comparison with Previous O_2/Ethanol OFO Triplet and PAT Element Injectors

As shown in Table XXIV, the OFO triplet designed for the GOX/ethanol testing yields improved performance compared to the previous injectors over the mixture ratio range tested with no fuel film-cooling. With fuel film-cooling, the GOX/ethanol performance is approximately equal to the performance of the LOX/ethanol platelet OFO injector but significantly better than the LOX/ethanol EDM'd triplet. (The three injectors were test fired with different nominal fuel film-cooling percentages, therefore precise performance differences are not available.) The performance reduction with the addition of film-coolant for the GOX/ethanol injector (coupled with the high combustion efficiency for the uncooled tests and the relative insensitivity of η_{comb}

TABLE XXIV

PERFORMANCE COMPARISON OF O_2/C_2H_5 OH TRIPLET INJECTORS

Injector Pattern	Film Cooling %	Combustion Efficiency η_{Cond}	Comments
EDM'd O-F-O LOX/Ethanol 40 Elements	0	92-100	η_{comb} increases with increasing O/F
	14	93.5-98.5	η_{comb} increases with increasing O/F, higher η_{comb} with FFC at low O/F
Platelet O-F-O (Splash Plate Oxidizer/Swirler Fuel) LOX/Ethanol 45 Elements	0	94-100	η_{comb} increases with O/F
	17	97-100	η_{comb} strong function of O/F, η_{comb} higher with FFC over O/F range 1.2 to 2.0
GOX/Ethanol O-F-O (EDM'd Oxidizer/ Swirler Fuel)	0	98.5-100	η_{comb} weak function of O/F
	20	95-97	η_{comb} weak function of O/F, η_{comb} reduction when FFC added

NOTE: L' = 0.75"
Pc = 300 psia
ε = 2:1

to mixture ratio) indicate improved injector core propellant mixing compared to the previous injectors. The improved mixing is probably a consequence of uniform GOX diffusion across the chamber cross section. It appears that fuel vaporization is the significant performance limitation with the GOX/ethanol injector for ambient temperature uncooled tests using both 4.7 and 8.7 inch chamber lengths.

6. Thermal Data Correlation and Summary - Test Series I-VII

Correlation of selected heat transfer data from all seven test series is provided in this section. Figure 154 displays a small portion (<5%) of the data available for this data correlation activity. The figure shows the influence of the following variables on the throat heat flux without film-cooling, propellant injector type, mixture ratio and chamber pressures.

This phase of the program correlated the heat flux data from nine axial chamber stations. Correlation of the test data generated with film-cooling is recommended as future work.

a. Summary

The heat transfer correlation coefficient (C_g) values were experimentally evaluated for LOX/propane and LOX/ethanol using a water-cooled calorimetric chamber. Nine tests with LOX/propane fired with an electrical-discharge-machined (EDM) OFO triplet injector without fuel film-cooling were analyzed. Four tests with LOX/ethanol fired with an EDM OFO triplet injector and six tests fired with a platelet preatomized OFO triplet injector with and without fuel film-cooling were also analyzed. The C_g values were evaluated using both frozen and shifting equilibrium properties.

The series 3 and 4 C_g values which were based on shifting equilibrium properties apparently provided better correlation of the experimental test data than those based on frozen equilibrium properties as illustrated in Figures 155 and 156. As a result, shifting C_g values were used for comparisons and demonstrating parameter effects.

The C_g values in the barrel for LOX/propane and LOX/ethanol fired with the EDM injector were approximately of the same magnitude. The C_g values for LOX/propane were significantly lower in the throat and nozzle than for LOX/ethanol fired with the EDM injector due to carbon deposition from propane.

The C_g values for LOX/ethanol fired with the platelet injector were significantly lower than the EDM injector throughout the entire chamber. Apparently the platelet injector produced an oxidizer-rich environment along its periphery due to blowapart effects. As a result, the addition of fuel film-cooling to LOX/ethanol fired with the platelet injector significantly increa-

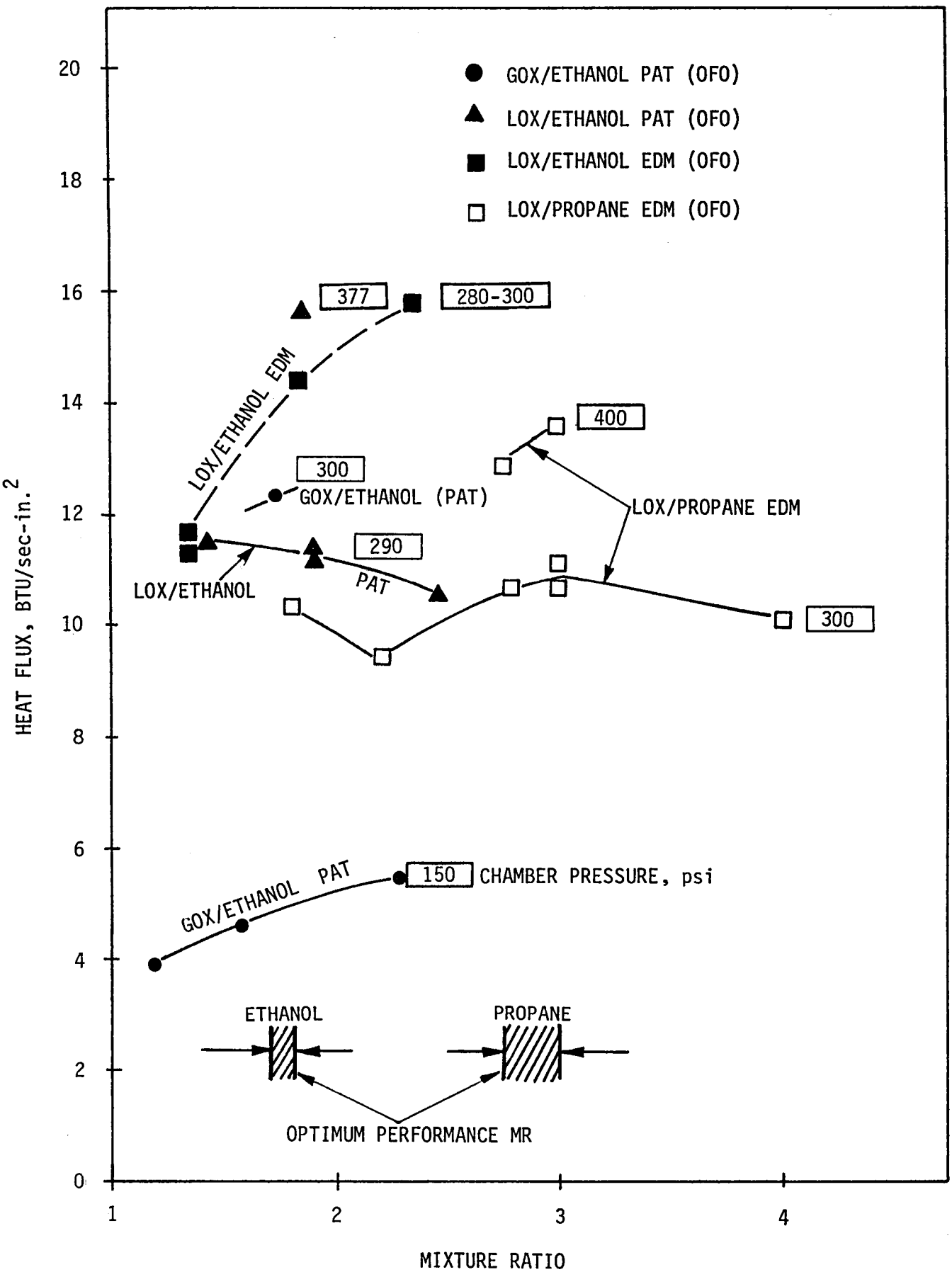

Figure 154. Sensitivity of Maximum Thrust Heat Flux to Mixture Ratio

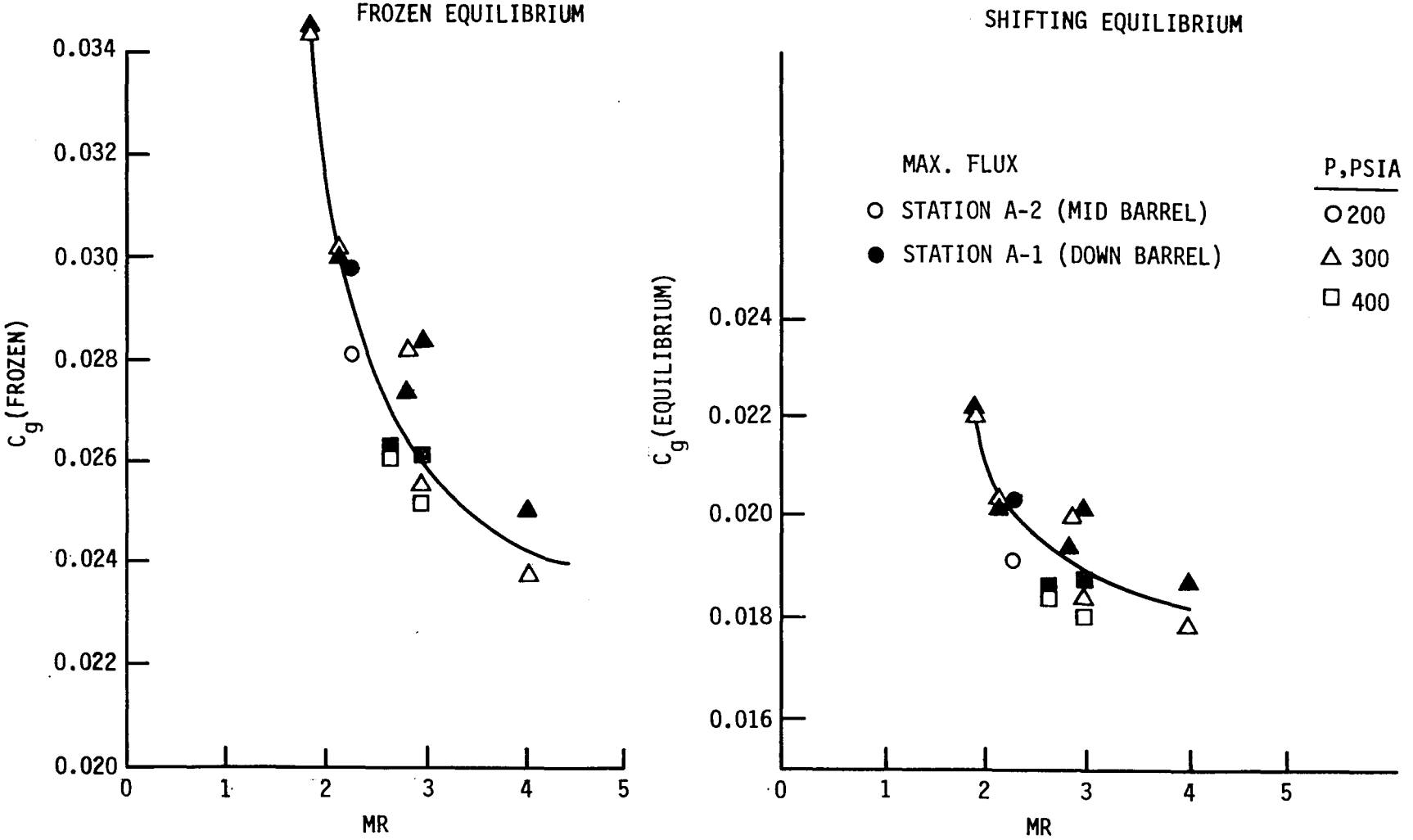

Figure 155. Chamber Region Cg Versus Mixture Ratio

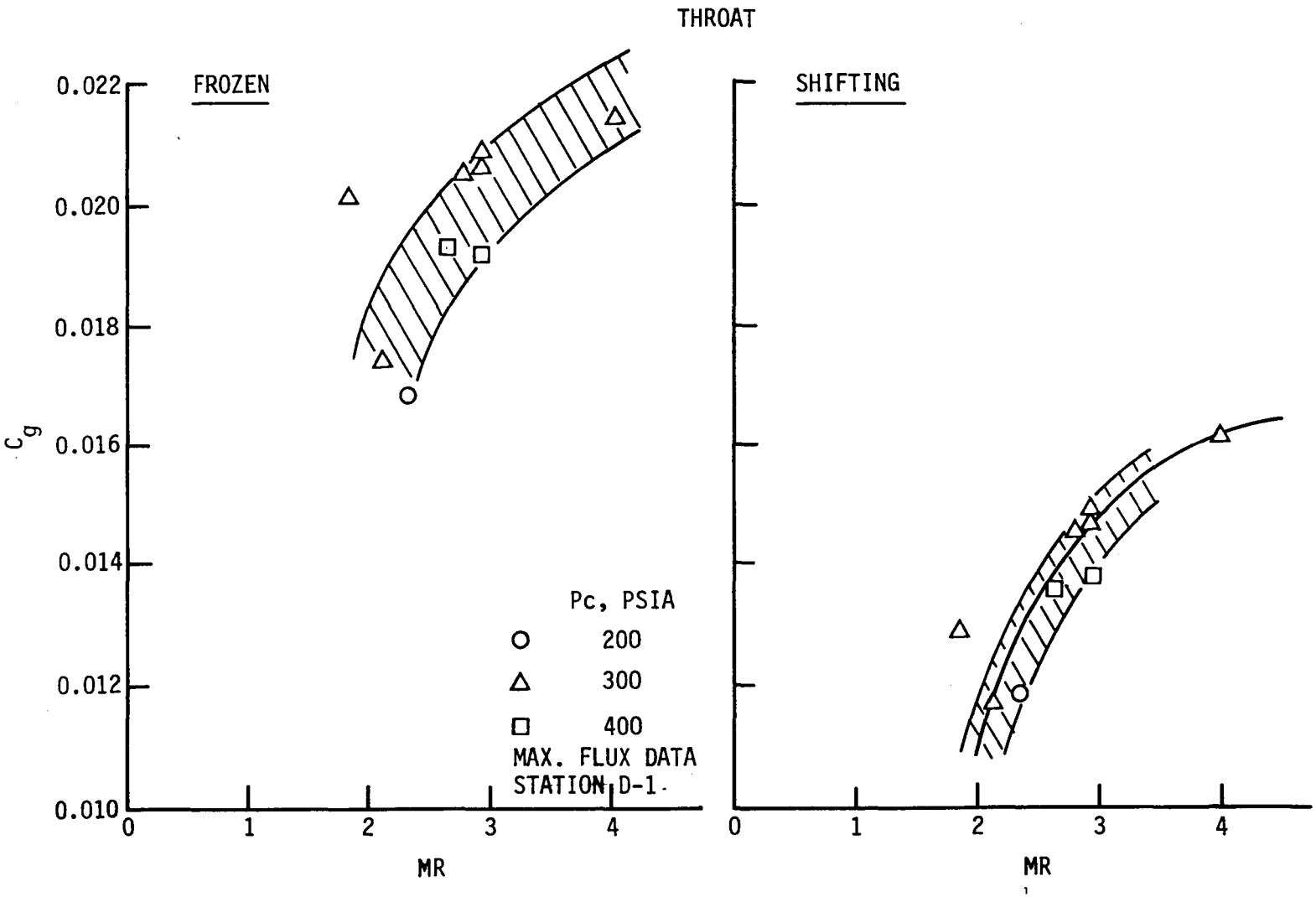

Figure 156. Throat Station Cg Versus Mixture Ratio

sed C_g values at the injector-end of the chamber. In contrast, the addition of fuel film-cooling to LOX/ethanol fired with the EDM injector significantly decreased the C_g values at the injector-end of the chamber.

The C_g values for LOX/ethanol fired with the EDM injector (highest experimental C_g values) were in close agreement with values used in preliminary designs at the throat and in the nozzle, but differed elsewhere.

b. Discussion

The experimental heat transfer correlation coefficient (C_g) value was evaluated for LOX/propane and LOX/ethanol with the equation shown in Figure 157 using both frozen and shifting equilibrium properties. The combustion gas temperatures and properties were evaluated using the ODE (TRAN72) computer program. The gas properties used to calculate the C_g values are given in Table IX for LOX/propane and Appendix C for LOX/ethanol. The C_{ps}/C_{pf} values as a function of mixture ratio for both LOX/propane and LOX/ethanol are given in Appendix C. The gas-side wall temperature was assumed to be 1000°R for LOX/ethanol and 1110°R for LOX/propane. The C_g values with fuel film-cooling were evaluated in the same manner as without fuel film cooling. The combustion gas temperatures and properties were evaluated at the overall engine mixture ratio. A proper evaluation of C_g values with fuel film-cooling would have required a characterization of the mixing occurring between the fuel film-coolant and the free stream gas, which was beyond the scope of this analysis.

Nine hot-firing tests (134-140, 142-143) using LOX/ propane were analyzed. The heat flux for LOX/propane peaked during the first 2-10 seconds of the firing and then steadily decreased thereafter as carbon deposits accumulated. The maximum heat flux values were used to calculate C_g values. The chamber wall condition, with respect to carbon deposits that these C_g values represented, was a major uncertainty in this analysis. Previous sections provide the measured heat flux and tabulations of the calculated C_g values. Figures 158 and 159 illustrate the frozen and shifting C_g profiles, respectively. The shifting C_g values appeared to provide better data correlation than the frozen C_g values. Peak C_g values occurred in the barrel. The C_g values increased with decreasing mixture ratio in the barrel and increased with increasing mixture ratio in the throat section and in the nozzle. The inversion of mixture ratio at the wall, starting at nozzle convergence, would explain the observed effects on C_g values. Thus the injector design plays a major role in the chamber heat transfer.

Four hot-firing tests (156 - 159) using LOX/ethanol and the same injector with an EDM OFO triplet injection pattern and a fuel film cooling ring were analyzed. The fuel film-cooling ring increased the L' of the calorimetric chamber to 8.7 inches and moved the resonator circuit into the barrel section of the chamber just downstream of the injector. These tests operated over a chamber pressure range of 270 to 400 psia, a mixture ratio range of 1.2 to

Frozen Equilibrium

$$Cg_f = \frac{Q/A\ D^{1.8}}{\dot{w}_t^{0.8}\ (Tr - Tw_g)\ (Te/Tf)^{0.8}\ (\frac{4}{\pi})^{0.8}\ Cp_f\ Pr_f^{-0.6}}$$

where Q/A = gas side heat flux, Btu/sec-in.^{2}

D = diameter, in.

$\dot{w}_t$ = total propellant flowrate, lbM/sec

Te = freestream combustion gas temperature, °R

Tw_g = gas-side wall temperature, °R

Tf = (film temperature = Tr + Tw_g)/2, °R

$Tr = Te + Pr_f^{1/3}\ (Tc - Te)$

μ_f = gas viscosity, evaluated at Tf, °R lbM/in.-sec

Cp_f = gas heat capacity frozen properties, evaluated at Tf Btu/lbM °R

Pr_f = gas Prandtl No., evaluated at Tf, °R

Shifting Equilbrium

$$Cg_s = \frac{Cg\ frozen}{Cp_s/Cp_f}$$

where $Cp_s = \frac{\Delta H}{\Delta T} = \frac{Hc - Hw}{Tc - Tw_g}$ Hc = H at Pc & Tc; Hw = H at Pc & Tw_g

Figure 157. Equations Used in Thermal Data Analysis

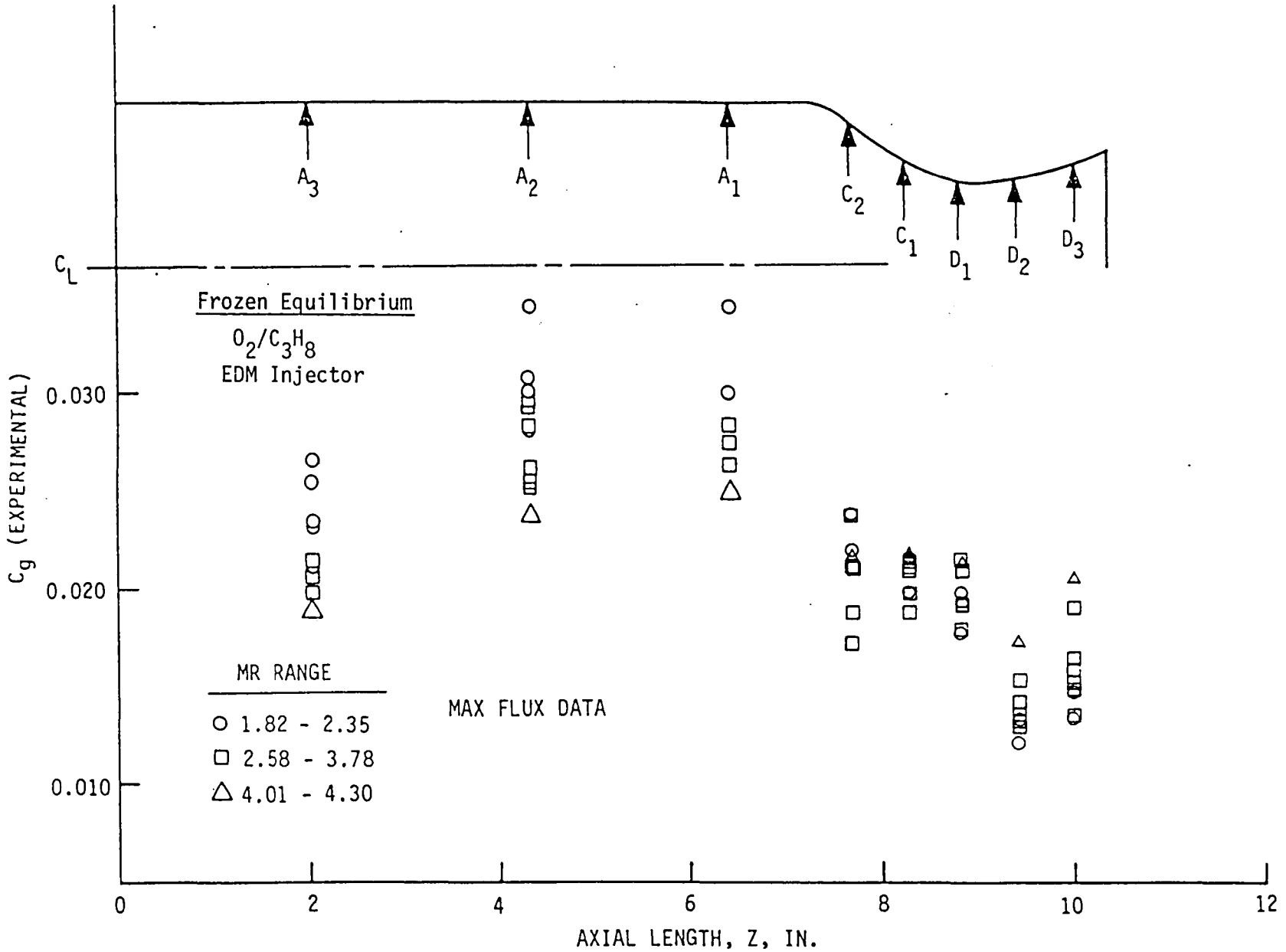

Figure 158. Cg Profiles for an OFO Triplet Injector Burning LOX/Propane and Assuming Frozen Equilibrium Chemistry

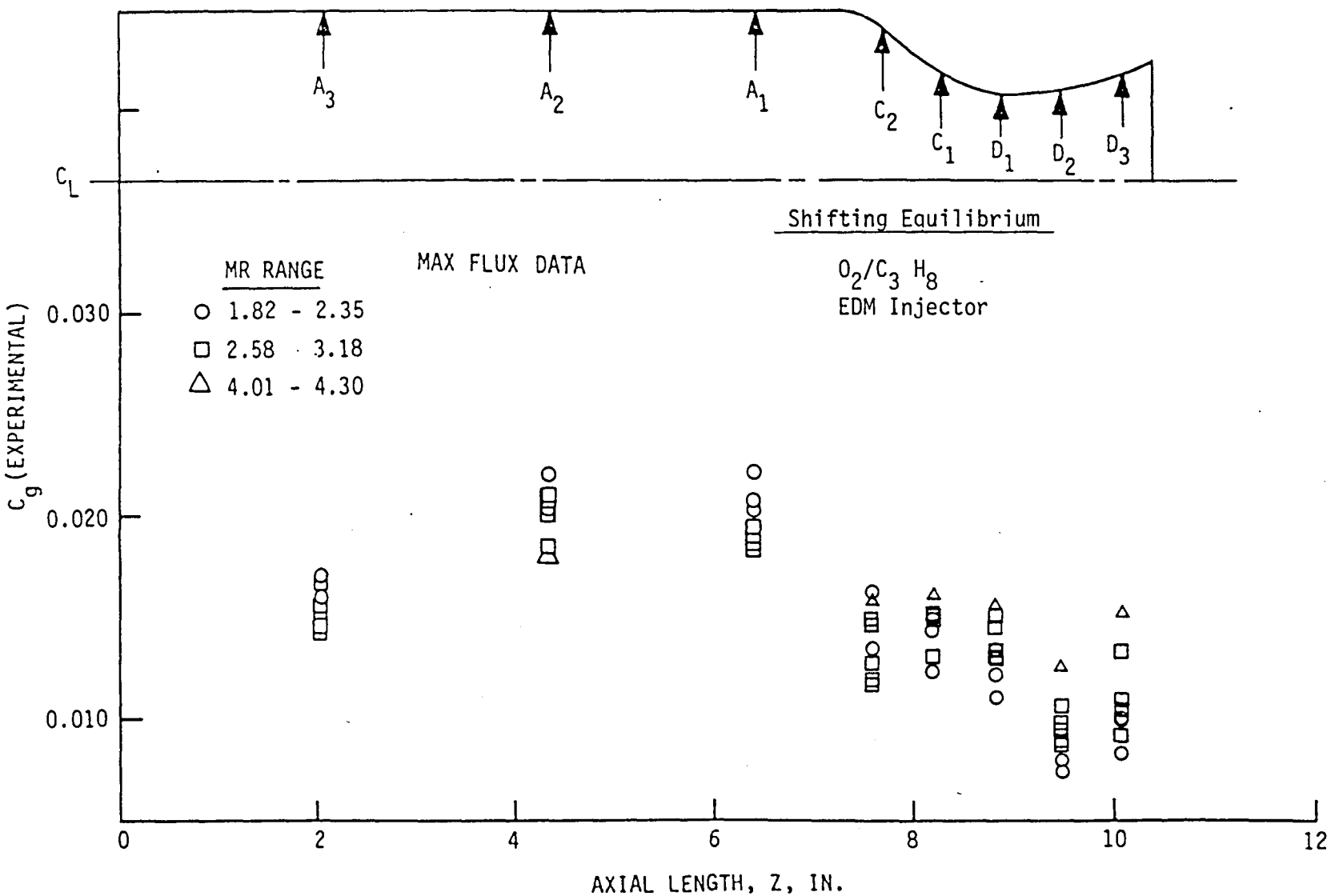

Figure 159. Cg Profiles for an OFO Triplet Injector Burning LOX/Propane and Assuming Equilibrium Chemistry

2.4, and at fuel film-cooling percentges of 0, 8, and 14%. The duration of each test was 30 seconds. The heat flux for LOX/ ethanol with fuel-film cooling reached steady-state in approximately 15 seconds and remained constant until the fuel film-cooling valve was shut off. The heat flux without fuel film-cooling reached steady-state in approximately 5 seconds. The maximum heat flux values were used to calculate C_g values with fuel film-cooling and the heat flux values at the end of each test were used to calculate C_g values without fuel film cooling. Previous sections provided the measured heat flux and calculated C_g values. Figures 160 and 161 illustrate the frozen and shifting C_g profiles, respectively. The data scatter appeared to be less for the shifting C_g values. Peak C_g values occurred at the throat and in the barrel. The C_g values increased with increasing mixture ratio throughout the entire chamber, except for the resonator where the trends reversed. In the absence of test data, a chamber C_g of 0.026 and throat C_g of 0.020 would be employed for design using frozen properties. It is obvious that the actual test conditions are more severe than would be estimated for normal design practice.

Six additional hot-firing tests (163, 165 - 169) using LOX/ethanol were analyzed. An injector with a platelet preatomized OFO triplet injection pattern and an 8.7 inch L' chamber were used. These tests operated over a chamber pressure range of 190 to 400 psia, a mixture ratio range of 1.2 to 2.5 and at fuel film-cooling percentages of 0, 9, and 17%. The duration of each test was 30 seconds. The heat flux for LOX/ethanol with fuel film cooling reached steady state in approximately 15 seconds and remained constant until the fuel film-cooling valve was shutoff. The heat flux without fuel film cooling reached steady state in approximately 5 seconds. The maximum heat flux values were used to calculate C_g values with fuel film-cooling and the heat flux values at the end of each test were used to calculate C_g values without fuel film-cooling. Tables in previous sections provide the measured heat flux and calculated C_g values. Figures 162 and 163 illustrate the frozen and shifting C_g values, respectively. The shifting C_g values again appeared to provide a better correlation of the data. Peak C_g values occurred in the throat and the values are much greater than those observed with storable and cryogenic propellants. The C_g values in the barrel decreased towards the injector and several were negative at the resonator indicating the impingement of LOX on the chamber wall. Figure 164 shows the influence of fuel film-cooling at fixed core mixture ratio and chamber pressure. The addition of 8.7% fuel film cooling along the periphery of the injector increased the injector end C_g values significantly. This indicated that the environment at the injector end of chamber wall was oxidizer rich without fuel film-cooling. Blowapart effects in the barrel were the probable cause since an oxidizer element was at the outermost row of the OFO triplet pattern. When the fuel film-cooling was increased to 16.8%, the injector end C_g values were not as great, indicating that the chamber wall environment had turned fuel rich. The effect of fuel film-cooling diminished away from the injector.

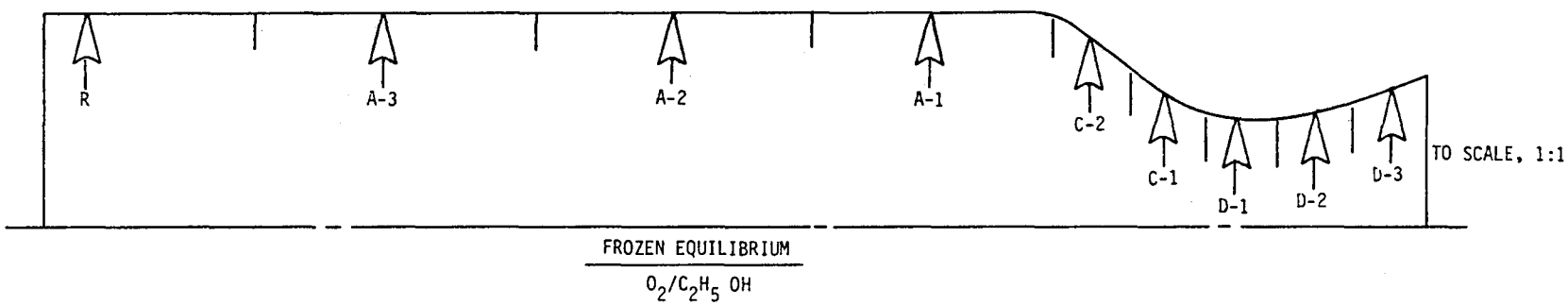

FROZEN EQUILIBRIUM

O_2/C_2H_5 OH

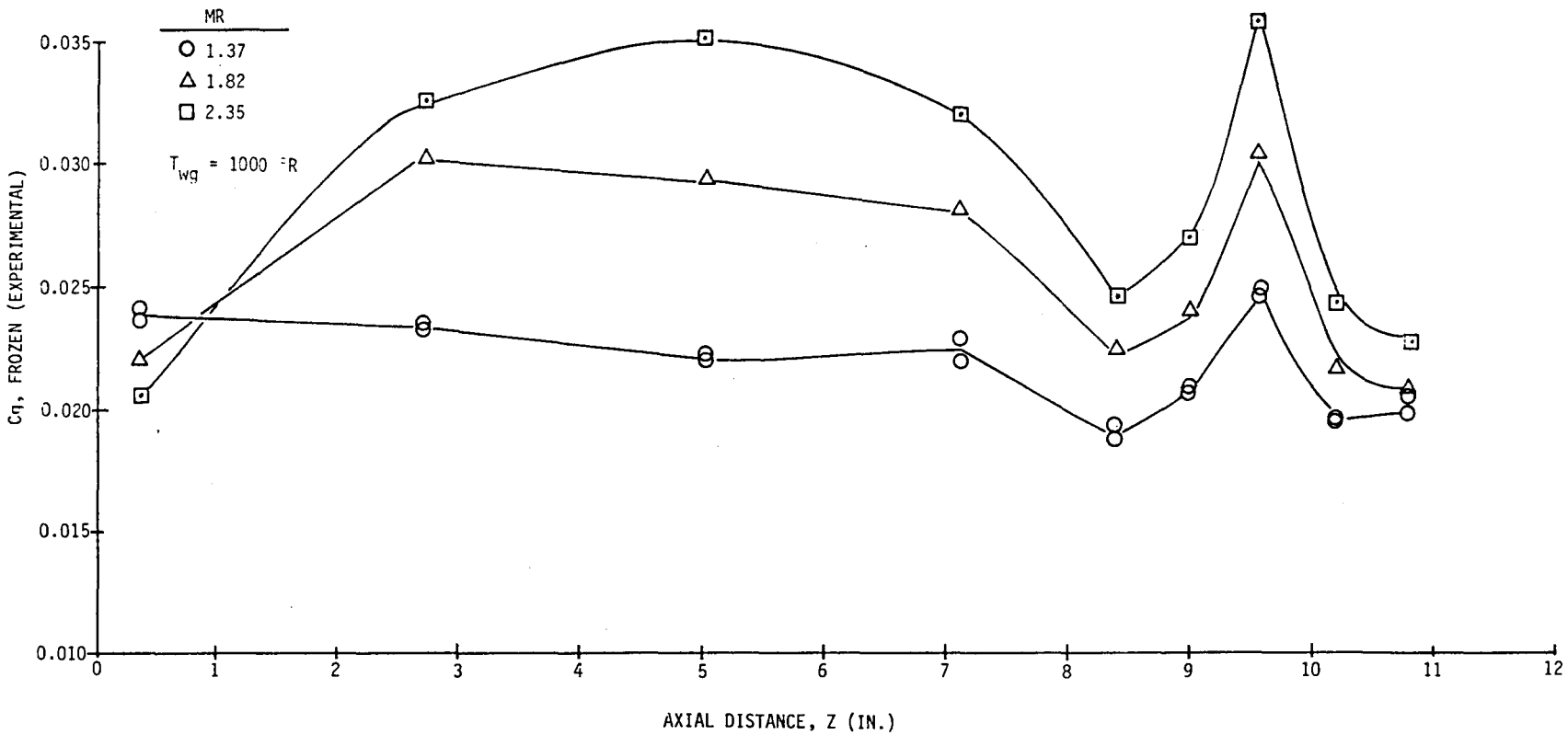

Figure 160. Experimental Cgs Profile for LOX/Ethanol with an OFO Triplet in 8.7-inch L' Chamber

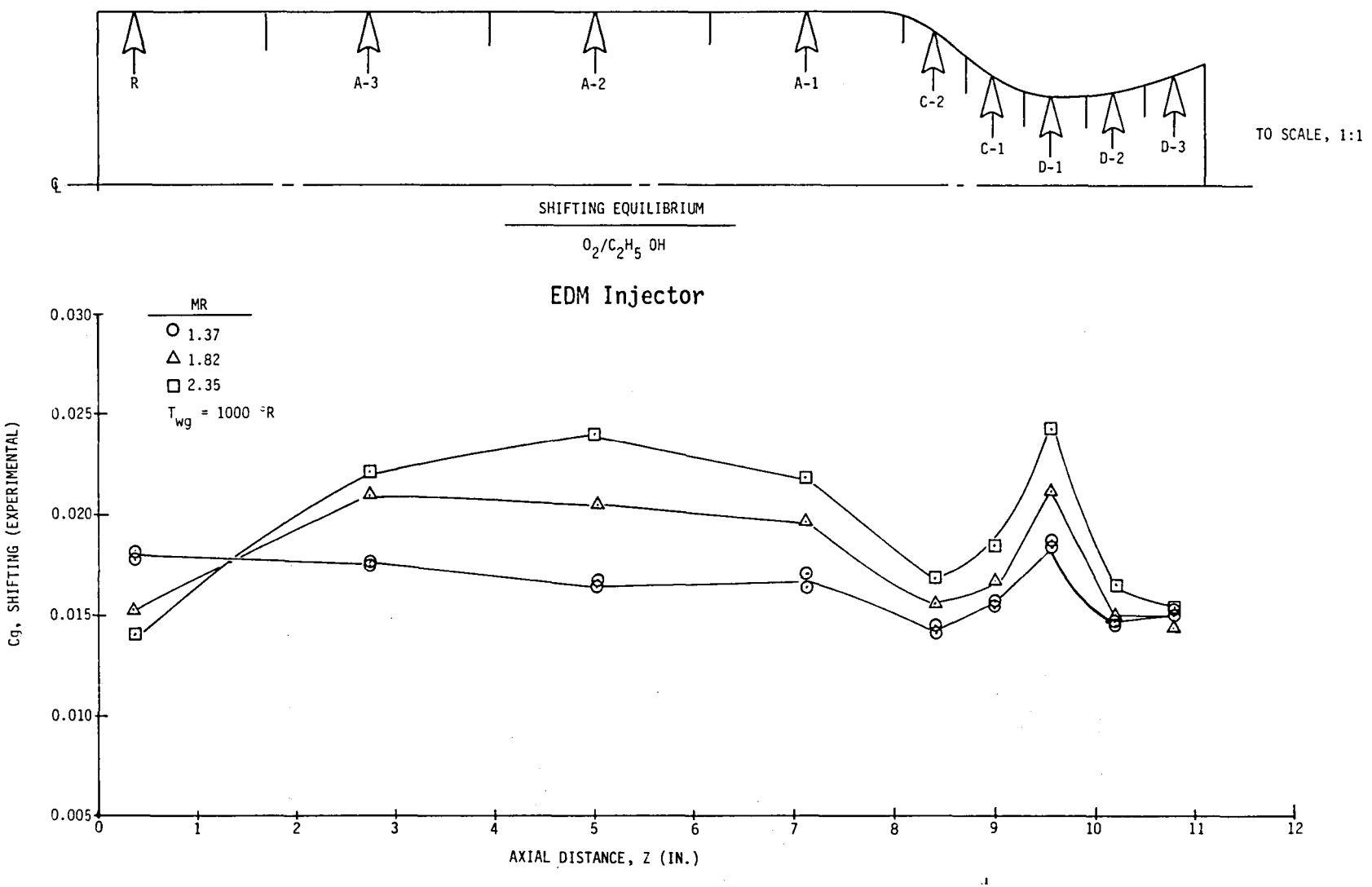

Figure 161. Experimental Cgs Profile for LOX/Ethanol with an OFO Triplet Injector in 8.7-inch L' Chamber

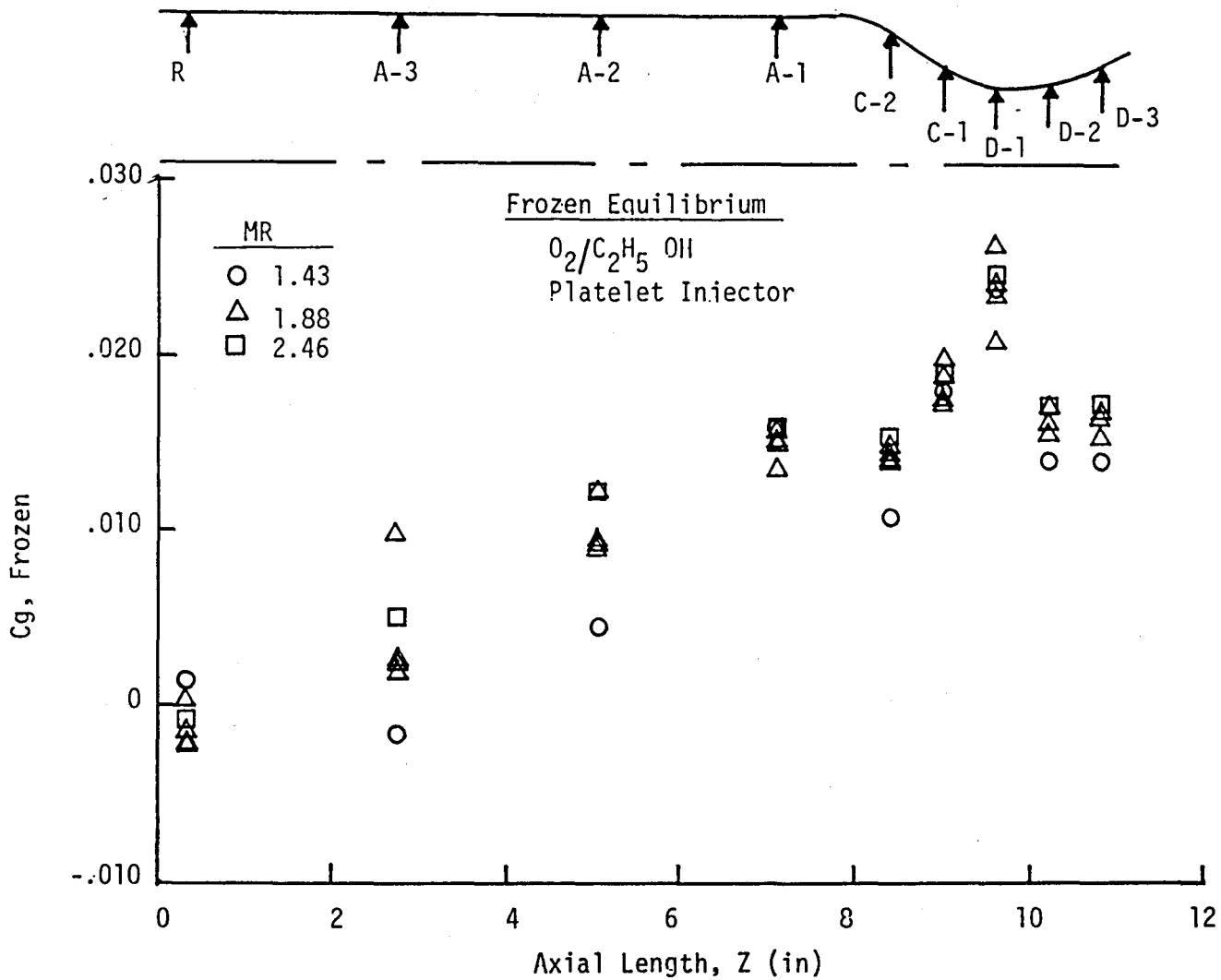

Figure 162. Experimental Frozen Cg Profile for LOX/Ethanol with a Platelet OFO Triplet in an 8.7-inch L' Chamber

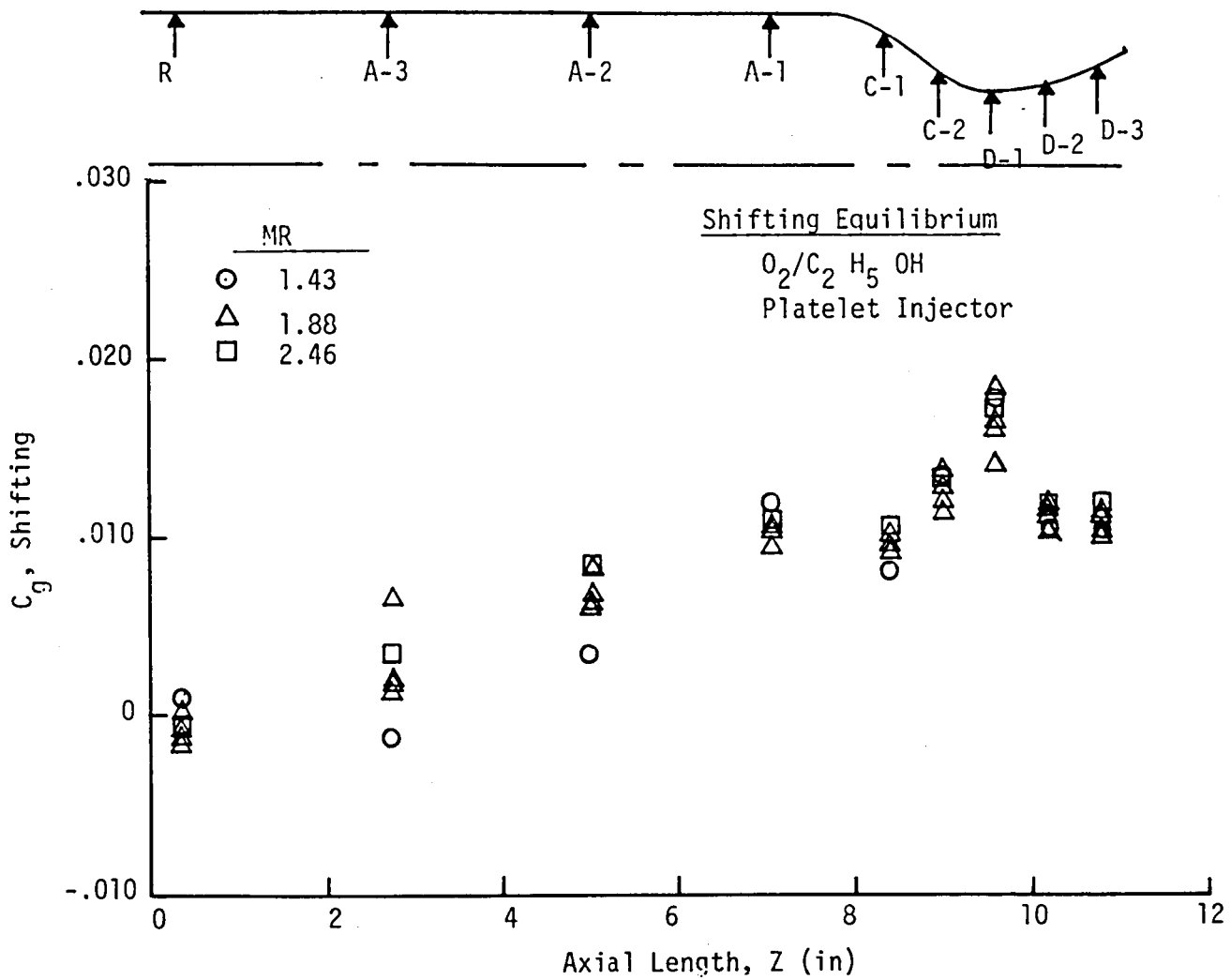

Figure 163. Experimental Shifting Cg Profile for LOX/Ethanol with a Platelet OFO Triplet in an 8.7-inch L' Chamber

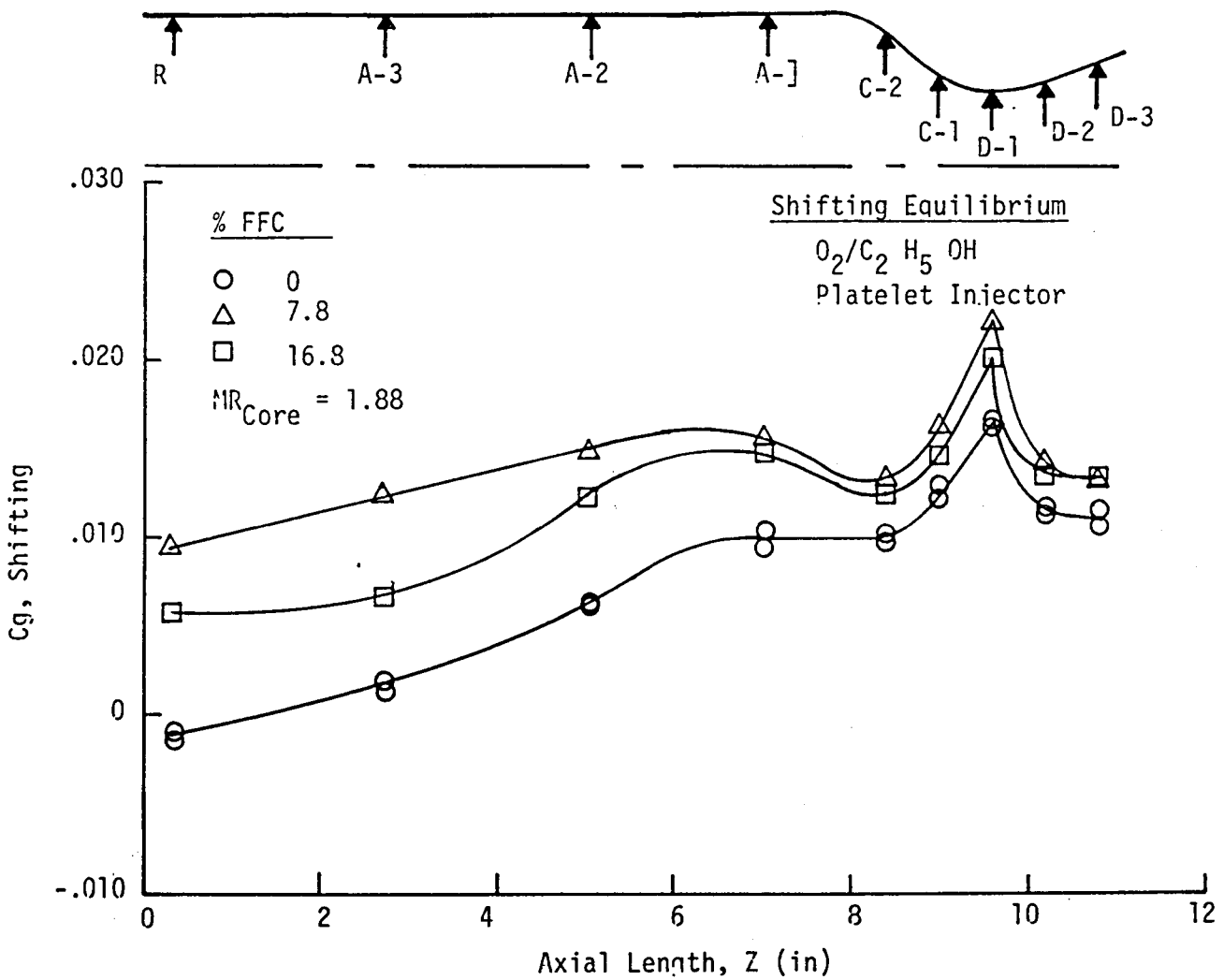

Figure 164. The Influence of Fuel Film Cooling on the Experimental Shifting Cg Profile for LOX/Ethanol with a Platelet OFO Triplet in an 8.7-inch L' Chamber

The effect of chamber pressure on C_g values is illustrated in Figure 165. The C_g values decreased with decreasing chamber pressure just upstream of the throat and at the throat due to reverse transition laminarization of the boundary layer. Throat Reynolds number calculations for LOX/ethanol (Appendix D) indicated that gas flow would be in reverse transition to laminar flow at chamber pressures below 300 psia and fully laminar at chamber pressures below 140 psia. Thus only the high Pc test in Figure 165 was fully turbulent in the throat region.

A comparison of the effect of propellant combination, injector design, and mixture ratio on shifting C_g values without fuel film-cooling at each chamber section is illustrated in Figure 166. The data from the first two long-duration tests (134 and 135) with LOX/propane are shown as half-shaded squares to indicate the degree of test-to-test carbon deposition carryover. The continuity of the first two tests with the rest of the data indicated no significant carryover of carbon deposits occurred. Therefore, each test started with a relatively clean chamber wall. The C_g values for LOX/propane increased with decreasing mixture ratio in the barrel. The trend reversed for the rest of the chamber with mixture ratio effects becoming more pronounced approaching the nozzle. Also the C_g values in the nozzle for LOX/propane were significantly lower than for LOX/ethanol fired with the same injector (EDM). The cause appeared to be carbon deposition in the throat section and nozzle, which increased with decreasing mixture ratio. Testing with propane revealed sooting of the chamber, in contrast to testing with ethanol which produced a clean chamber and a clear exhaust plume. The C_g values in the barrel for LOX/propane and LOX/ethanol fired with the same injector design (EDM) were about the same.

The C_g values for LOX/ethanol were significantly lower when fired with the platelet injector than with the EDM injector throughout the entire chamber. As previously discussed, the platelet injector apparently produced an oxidizer-rich environment along its periphery. As a result, the C_g values based on the engine mixture ratio were low and relatively insensitive to engine mixture ratio. In contrast, the C_g values for LOX/ethanol fired with the EDM injector increased significantly with increasing mixture ratio throughout the fuel chamber length. The wide variation in C_g values with mixture ratio and injector design demonstrated that the injector played a major role in controlling the chamber heat transfer profile.

A comparison of the C_g values of LOX/ethanol fired with the EDM injector with C_g values (Ref. 2) obtained in previous hydrocarbon propellant testing is shown in Figure 167. The C_g values at the throat and in the nozzle are in good agreement. The preliminary design C_g values used in the Task III trade studies were conservatively higher in the convergent section, but too low in the barrel. The addition of fuel film- cooling with LOX/ethanol reduced the C_g values at the injector end of the chamber, which more closely resembles the C_g values used in preliminary designs.

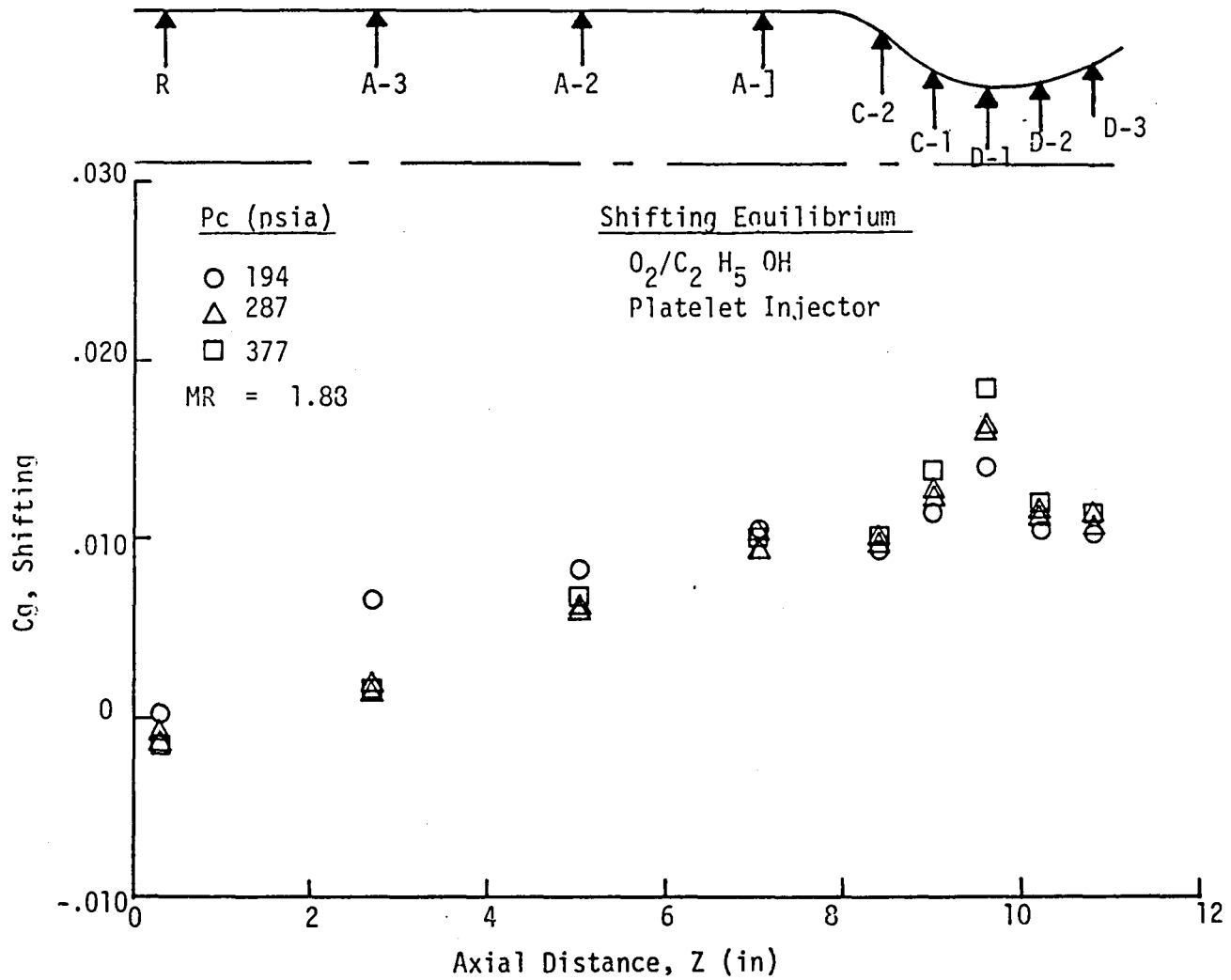

Figure 165. The Influence of Chamber Pressure on the Experimental Shifting Cg Profile for LOX/Ethanol with a Platelet OFO Triplet in an 8.7-inch L' Chamber

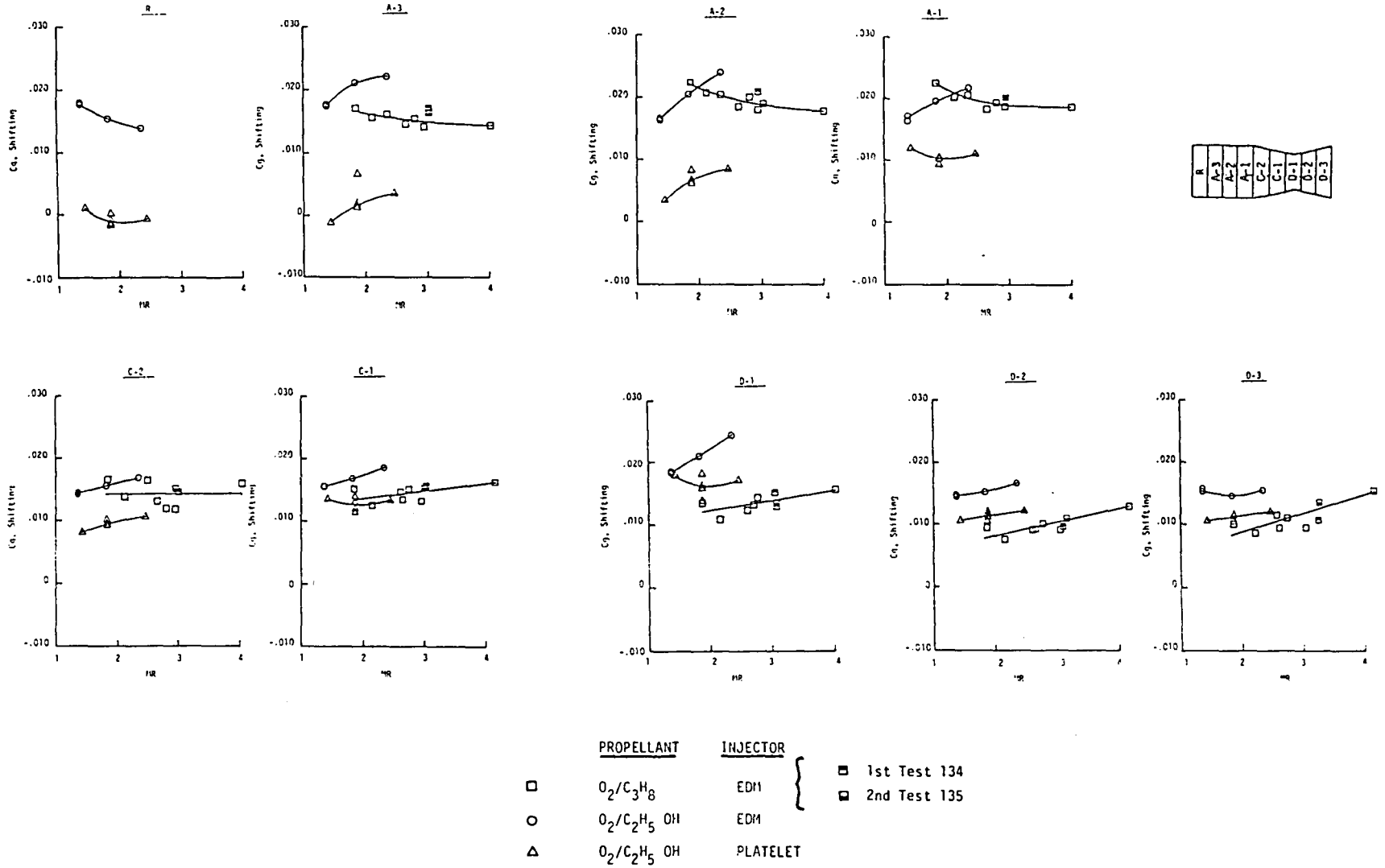

Figure 166. Experimental Shifting Cg Value Comparison by Station for LOX/Propane and LOX/Ethanol with an OFO Triplet

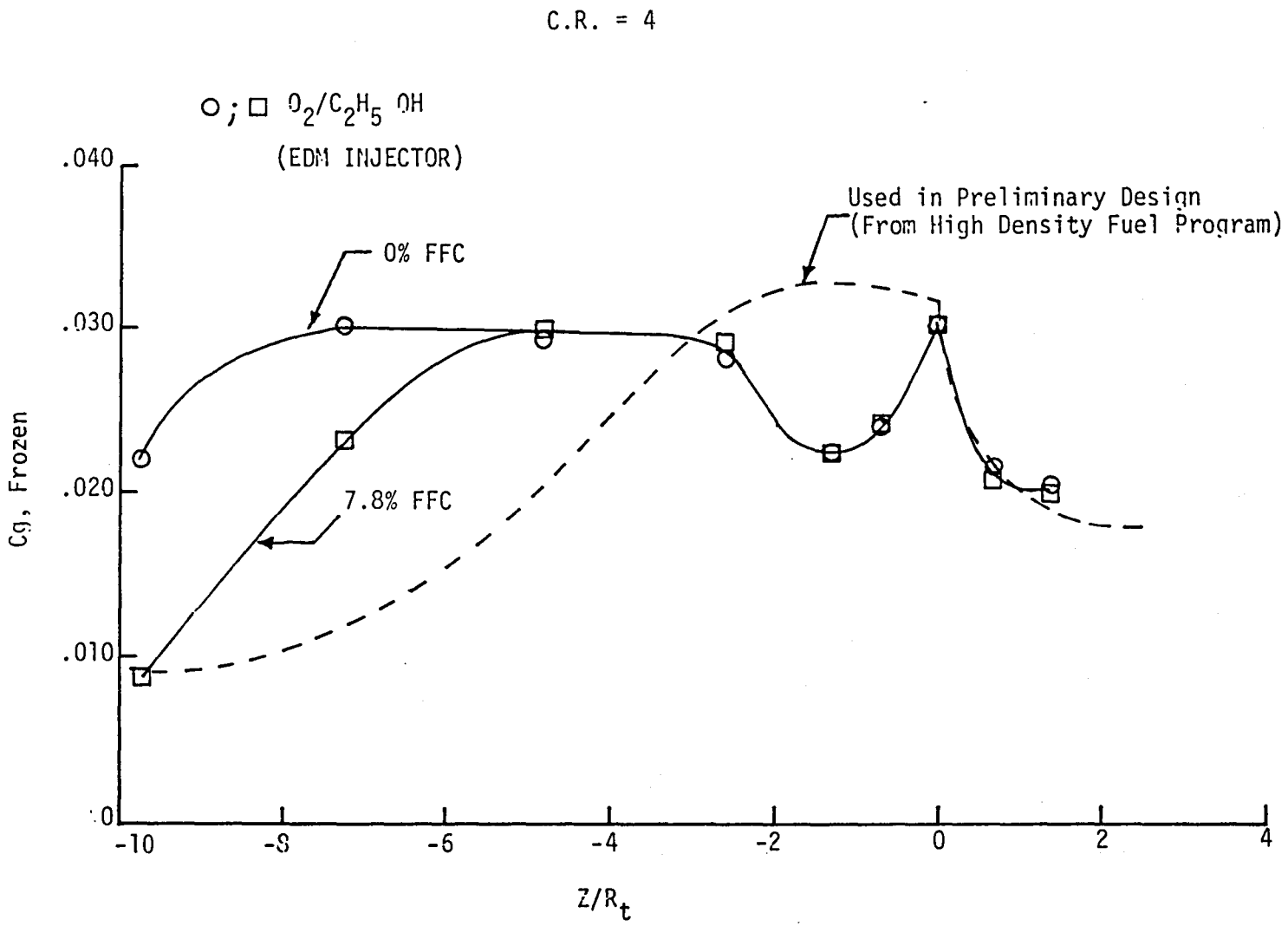

Figure 167. Comparison of Experimental Frozen Cg Profile with Preliminary Design Values

E, Tasks II and IV Subscale Injector Characterization (cont.)

It is of major significance that the same high throat C_g values were again observed (Ref. D-2) for a hydrocarbon fuel. In the past this effect has been apparently buried under a deposit of soot. With the development of improved higher performance clean burning injectors, this high throat C_g value may become a major cooling problem.

Effect of carbon deposition In LOX/Propane Tests Without FFC. An estimate of the resistance due to carbon deposition was made by comparing the maximum flux, $(Q/A)_{max}$, at the start of each test with the flux at 60 seconds into the firing. The resistance value, expressed as t/k, is calculated as follows:

$$t/k = (T_c - T_{sat}) \left[\frac{1}{(Q/A)_{60}} - \frac{1}{(Q/A)_{max}} \right]$$

where T_c = the theoretical combustion temperature, °R

T_{sat} = the coolant-side wall temperature, °R. This is assumed to be the saturation temperature of water in the cooling circuit.

$(Q/A)_{60}$ = local flux at 60 sec, Btu/sec-in.^{2}

$(Q/A)_{max}$ = maximum flux at same station, Btu/sec-in.^{2}

t/k = soot resistance $\frac{\text{sec-in.}^2\text{-°R}}{\text{Btu}}$

These data are shown in Figures 168, 169, and 170.

The increased deposition at higher mixture ratios could be from the condensation of heavy hydrocarbon vapors on the cooled chamber wall (600°F) rather than from a buildup of layers of solid carbon. The theory could be tested by operating at higher chamber wall temperatures of approximately 2000°F. If the theory is correct, the time-variance in heat flux would be diminished. Further analysis and testing are required in order to truly understand the physical phenomena causing these results.

No carbon deposition effects were noted in the ethanol testing.

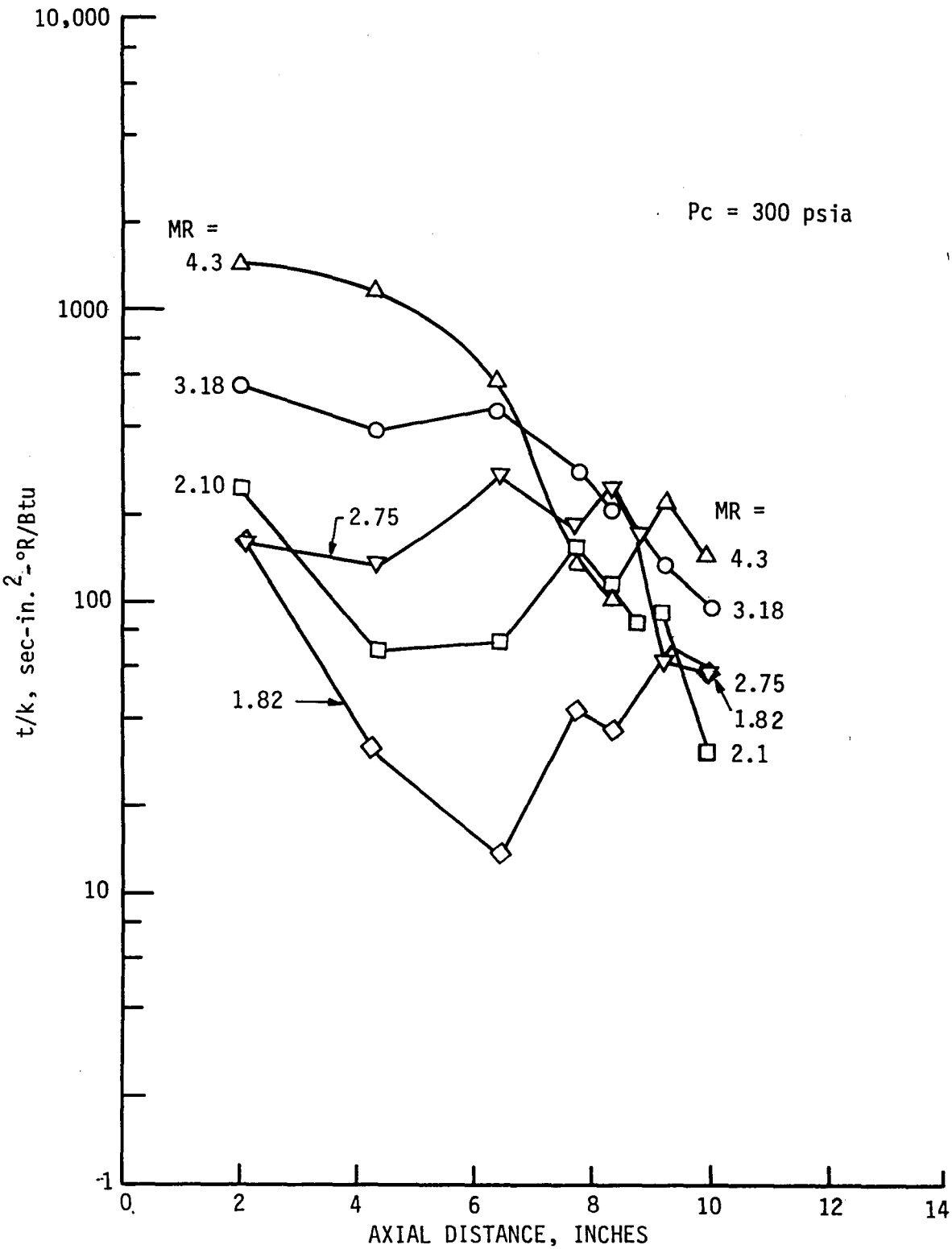

Figure 168. Effect of Location on Soot Resistance

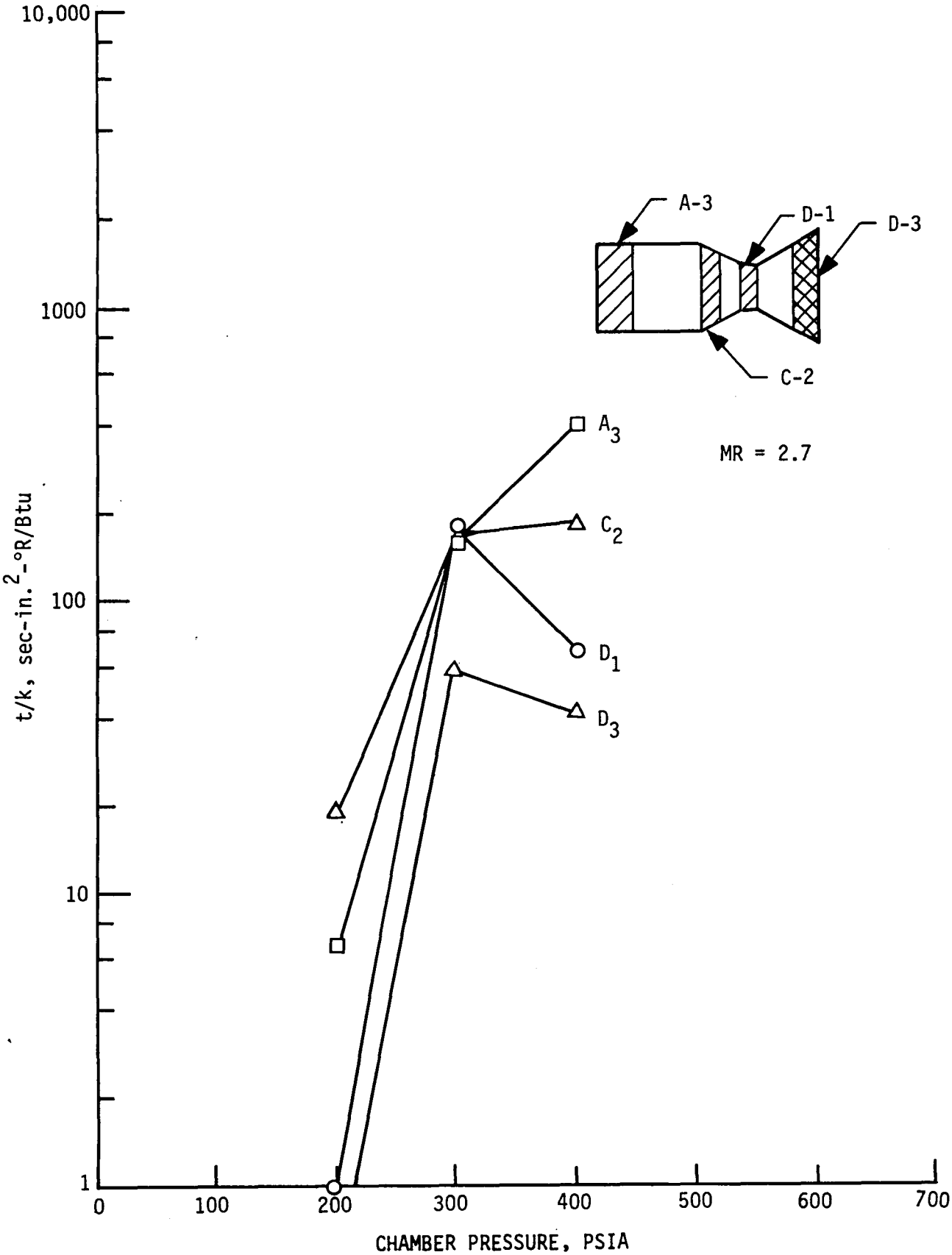

Figure 169. Effect of Pc on Soot Resistance

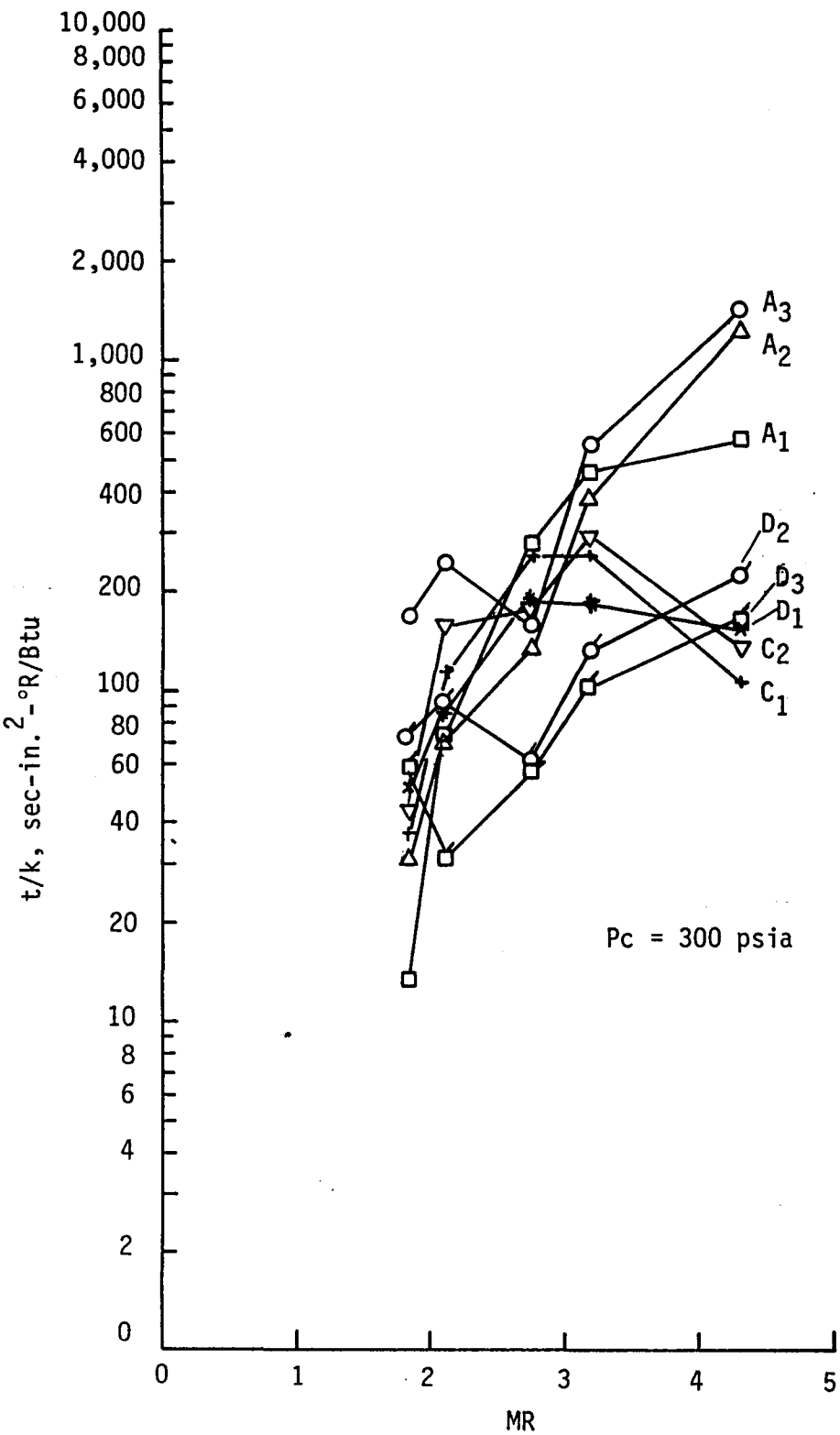

Figure 170. Effect of MR on Soot Resistance

REFERENCES

1. MDAC Report MDC E 2548, G. F. Orton, P. D. Mark, D. D. Weber, "LOX Hydrocarbon Auxiliary Propulsion System Study," Final Report NAS 9-16305.

2. Labotz, R. J., et al, - High Density Fuel Combustion and Cooling Investigation, NASA CR 165177, September 1980.

3. G. Elverum and T. Morey, "Criteria for Optimum Mixture Ratio Distribution Using Several Types of Impinging Stream Injector Elements," Memo 30-5, JPL, 25 February 1959.

4. R. M. McHale, "Noncircular Orifice Holes and Advanced Fabrication Techniques for Liquid Rocket Injectors," Phases III and IV, Contract Final Report, NAS 9-9528, May 1974.

APPENDIX A
TRIPLET INJECTOR ELEMENT
MIXING CHARACTERISTICS

APPENDIX A
TRIPLET INJECTOR ELEMENT MIXING CHARACTERISTICS

Propellant mixing of a triplet injector element is achieved through the momentum mixing of the propellant sprays, which are formed by the momentum exchange of the propellant jets upon impingement. The fan angles ($2\alpha_1$) of the sprays made by the two outer jets ("1") are equal due to the symmetry and they are dependent only on the impingement angle (θ). The fan angle ($2\alpha_2$) of the spray in the middle is controlled by the ratio of the vertical momentum of the outer jet to the ultimate axial momentum of the center jet. As a result, the fan angle of the center spray is determined by the momentum ratio of propellant 1 to propellant 2 for a fixed impingement angle.

From the point of view of the fan geometry, the mixing efficiency of a triplet injector element is mostly affected by the relative fan angles between the two propellants. The maximum mixing efficiency is attained as the fan angles of the two propellants become equal. The Rocketdyne uni-element cold-flow data as plotted in the attached figure uphold this argument.

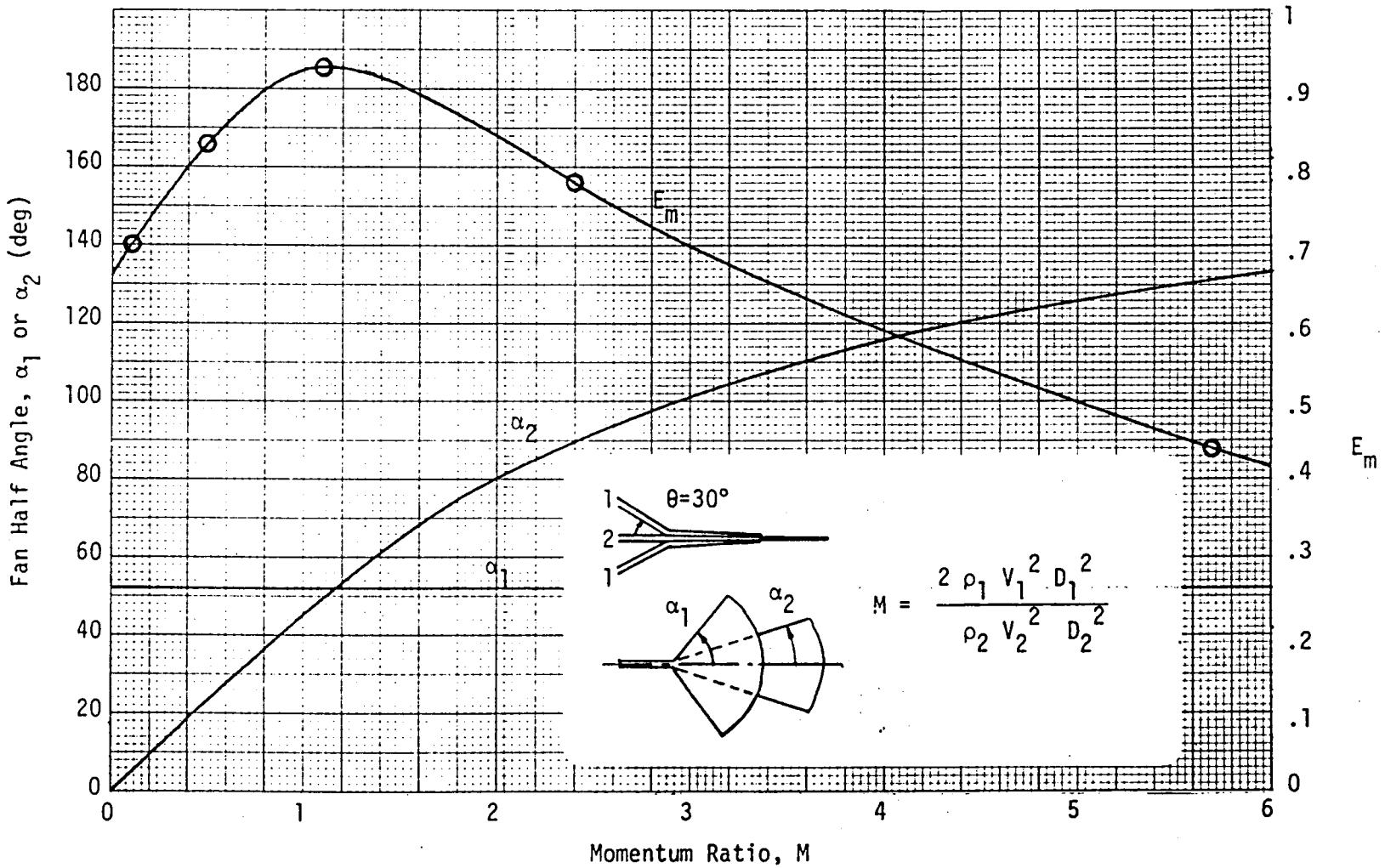

TRIPLET FAN ANGLE PREDICTED BY SIMPLIFIED SPRAY MODEL

APPENDIX B
CAVITATING ORIFICE

APPENDIX B

CAVITATING ORIFICE

I NONCAVITATING FLOW PHYSICAL SYSTEM

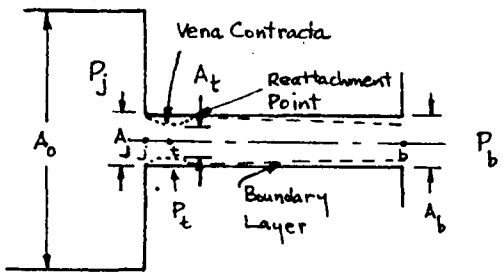

See Reference B1

II ASSUMPTIONS

1. No loss from j to t. Bernoulli Eq:

$$P_j - P_t = 1/2\ \rho\ V_t^2$$

$$\text{or} \quad V_t = \sqrt{\frac{2\ (P_j - P_t)}{\rho}} \tag{1}$$

2. Loss from t to b accounted for by C_D defined as:

$$C_D = \frac{\dot{W}}{\rho\ A_b\ V_{b,\ \text{no loss}}}$$

where:

$$V_{b,\ \text{no loss}} = \sqrt{\frac{2\ (P_j - P_b)}{\rho}}$$

Therefore

$$C_D = \frac{\dot{W}}{\rho\ A_b \sqrt{\frac{2\ (P_j - P_b)}{\rho}}} \tag{2}$$

III DERIVATION

$$\dot{W} = \rho V_t A_t$$

$$= \rho \frac{A_t}{A_b} A_b \sqrt{\frac{2 (P_j - P_t)}{\rho}}$$

$$= C_c \rho A_b \sqrt{\frac{2 (P_j - P_t)}{\rho}} \qquad (3)$$

Substitute (3) into (2):

$$C_D = C_c \left[\frac{P_j - P_t}{P_j - P_b} \right]^{1/2} \qquad (4)$$

IV DISCUSSION

1. At low P_j-P_b, the pressure of vena contracta (P_t) is greater than the fluid vapor pressure and the flow is noncavitating. C_D is dependent on Reynolds number and the orifice length/diameter ratio. See Reference C2.

2. As P_j-P_b increases, P_t decreases until it is equal to the fluid vapor pressure. At this point, the flow starts cavitating at a condition specified as follows.

$$\left(\frac{P_j - P_t}{P_j - P_b} \right)_{\text{critical}} = \frac{P_j - P_v}{P_j - P_b}$$

$$C_{D,\,\text{critical}} = C_c \left[\frac{P_j - P_v}{P_j - P_b} \right]^{1/2} \qquad (5)$$

IV Discussion (cont.)

3. If $P_j - P_b$ continues to increase without hydraulic flip, $(P_j - P_v)/(P_j - P_b)$ will approach unity, at which $C_D = C_c$ and can be calculated using the following correlation:

$$C_c = 0.611 + 0.38 \left(\frac{A_j}{A_o}\right)^3$$

4. The above orifice flow regimes can be summarized by the following figure.

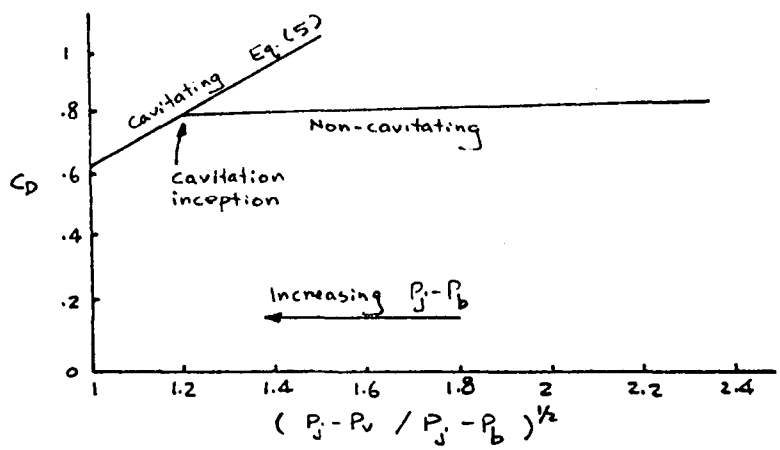

V REFERENCES

B1. W. H. Nurick, "Orifice Cavitation and Its Effect on Spray Mixing", J. Fluid Engineering, Dec. 1976

B2. J. I. Ito, "A General Model Describing Hydraulic Flip in Sharp Edge Orifices", 6th ICRPG

APPENDIX C
GAS PROPERTY VALUE FOR LOX/ETHANOL USED IN CG CALCULATIONS

O_2/C_2H_5OH (W/O FILM COOLING)

(EDM INJECTOR)

RUN	PC	MR	WT	SECTION	D	ϕ	Tc	Te	T_R	Tr	T_{wg}	Hc	Hw	$C_{p,s}$	$C_{p,F}$	DBF	$C_{g,F}$	$C_{D,F}$
56	2'12	1.36	3.79	R	3.40	3.54	5538	5538	5538	3269	1000	-198	-4183	.658	.494	.00172	.0241	.0151
				A-3	3.40	3.44		5538	5538	3269					.494	.00172	.0234	.0176
				A-2	3.40	3.21		5538	5538	3269					.494	.00172	.0219	.0164
				A-1	3.40	3.35		5538	5538	3269					.494	.00172	.0228	.0171
				C-2	2.998	3.55		5524	5535	3268					.494	.00172	.0193	.0145
				C-1	2.294	6.08		5489	5530	3265					.494	.00172	.0206	.0156
				D-1	1.740	11.30		5180	5481	3241					.493	.00172	.0245	.0184
				D-2	1.878	7.33		4818	5423	3212					.493	.00172	.0194	.0145
				D-3	2.206	5.30		4400	5357	3179					.492	.00171	.0204	.0153
157	276	1.37	3.85	R	3.40	3.54	5538	5538	5538	3269	1000	-1198	-4183	.658	.494	.00172	.0238	.0179
				A-3	3.110	3.47		5538	5538	3269					.494	.00172	.0233	.0175
				A-2	3.40	3.28		5538	5538	3269					.494	.00172	.0221	.0166
				A-1	3.40	3.26		5538	5538	3269					.494	.00172	.0219	.0164
				C-2	2.998	3.50		5524	5535	3268					.494	.00172	.0188	.0141
				C-1	2.294	6.23		5489	5530	3265					.494	.00172	.0208	.0156
				D-1	1.740	11.67		5180	5481	3241					.493	.00172	.0249	.0187
				D-2	1.878	7.45		4818	5423	3212					.493	.00172	.0195	.0146
				D-3	2.206	5.20		4400	5357	3179					.492	.00171	.0198	.0148
158	289	1.82	3.84	R	3.40	3.27	5930	5930	5930	3465	1000	-1033	-4353	.673	.469	.00157	.0220	.0153
				A-3	3.40	4.18		5930	5930	3465					.469	.00157	.0302	.0210
				A-2	3.40	4.36		5930	5930	3465					.469	.00157	.0294	.0205
				A-1	3.40	4.18		5930	5930	3465					.469	.00157	.0282	.0197
				C-2	2.998	4.16		5920	5929	3465					.469	.00157	.0224	.0156
				C-1	2.294	7.18		5893	5925	3463					.468	.00157	.0240	.0167
				D-1	1.740	14.43		5669	5895	3448					.468	.00156	.0305	.0212
				D-2	1.878	8.64		5430	5863	3432					.468	.00156	.0215	.0150
				D-3	2.206	5.92		5176	5829	3415					.467	.00155	.0207	.0144

O_2/C_2H_5OH (W/O FILM COOLING)
(EDM INJECTOR)

R:N	Pc	MR	W_T	SECTION	D	ϕ	T_c	T_e	T_R	T_F	T_{w_g}	H_c	H_w	$C_{P,s}$	$C_{P,F}$	DB_F	$C_{g,F}$	$C_{g,s}$
159	292	2.35	3.88	R	3.40	2.80	5903	5903	5903	3452	1000	-897	4073	.648	.442	.00144	.0205	.0140
				A-3	3.40	4.45		5903	5903	3452					.442	.00144	.0326	.0222
				A-2	3.40	4.80		5903	5903	3452					.442	.00144	.0352	.0240
				A-1	3.40	4.37		5903	5903	3452					.442	.00144	.0320	.0218
				C-2	2.998	4.20		5893	5902	3451					.442	.00144	.0246	.0168
				C-1	2.294	7.43		5867	5899	3450					.442	.00144	.0270	.0184
				D-1	1.740	15.68		5650	5872	3436					.441	.00144	.0358	.0244
				D-2	1.878	8.95		5417	5844	3422					.441	.00144	.0243	.0165
				D-3	2.206	6.02		5173	5815	3408					.441	.00144	.0227	.0154

O_2/C_2H_5OH (WITH 7.8% FFC) @ $t = 20$ sec

158	293	1.69 ENG 1.83 NOZ	3.88	R	3.40	1.31	5818	5818	5818	3409	1000	-1081	-4304	.669	.476	.00161	.0088	.0063
				A-3	3.40	3.46		5818	5818	3409					.476	.00161	.0231	.0164
				A-2	3.40	4.49		5818	5818	3409					.476	.00161	.0300	.0213
				A-1	3.40	4.36		5818	5818	3409					.476	.00161	.0292	.0208
				C-2	2.998	4.16		5808	5817	3409					.476	.00161	.0222	.0158
				C-1	2.294	7.31		5783	5814	3407					.476	.00161	.0242	.0172
				D-1	1.740	14.58		5569	5787	3394					.475	.00161	.0303	.0215
				D-2	1.878	8.33		5339	5760	3380					.475	.00161	.0206	.0146
				D-3	2.206	5.81		5099	5731	3366					.474	.00161	.0200	.0142

O_2/C_2H_5OH (WITH 14.2% FFC) @ $t = 5$ sec

155	294	1.76 ENG 1.91 NOZ	3.97	A-3	3.40	2.54	5616	5616	5616	3308	1000	-1165	-4217	.661	.489	.00169	.0166	.0123
				A-2	3.40	4.14		5616	5616	3308	1000	-1165	-4217	.661	.489	.00169	.0271	.0200

O_2/C_2H_5OH (W/O FILM COOLING)

(PLATELET INJECTOR)

RUN	PC	MR	WT	SECTION	D	FLUX	TC	TE	TR	TF	TWG	CPS	CPF	CPS/CPF	DBF	CGF	CGS
163	285.	1.87	3.85	R	3.400	-.31	5938.	5938.	5938.	3469.	1000.	.679	.466	1.46	.00155	-.0021	-.0014
				A-3	3.400	.28		5938.	5938.	3469.	1000.	.679	.466	1.46	.00155	.0019	.0013
				A-2	3.400	1.36		5938.	5938.	3469.	1000.	.679	.466	1.46	.00155	.0092	.0063
				A-1	3.400	2.23		5938.	5938.	3469.	1000.	.679	.466	1.46	.00155	.0152	.0104
				C-2	2.998	3.60		5937.	5937.	3468.	1000.	.679	.466	1.46	.00155	.0141	.0097
				C-1	2.294	5.34		5902.	5933.	3467.	1000.	.679	.466	1.46	.00155	.0176	.0121
				D-1	1.740	11.40		5680.	5904.	3452.	1000.	.679	.466	1.46	.00155	.0242	.0166
				D-2	1.878	6.78		5443.	5873.	3436.	1000.	.679	.465	1.46	.00155	.0171	.0117
				D-3	2.206	4.79		5192.	5840.	3420.	1000.	.679	.465	1.46	.00154	.0169	.0116

RUN	PC	MR	WT	SECTION	D	FLUX	TC	TE	TR	TF	TWG	CPS	CPF	CPS/CPF	DBF	CGF	CGS
165	293.	2.46	3.81	R	3.400	-.11	5882.	5882.	5882.	3441.	1000.	.628	.436	1.44	.00142	-.0008	-.0006
				A-3	3.400	.66		5882.	5882.	3441.	1000.	.628	.436	1.44	.00142	.0050	.0035
				A-2	3.400	1.62		5882.	5882.	3441.	1000.	.628	.436	1.44	.00142	.0122	.0085
				A-1	3.400	2.12		5882.	5882.	3441.	1000.	.628	.436	1.44	.00142	.0160	.0111
				C-2	2.998	2.56		5871.	5881.	3440.	1000.	.628	.436	1.44	.00142	.0154	.0107
				C-1	2.294	5.10		5846.	5878.	3439.	1000.	.628	.436	1.44	.00142	.0191	.0133
				D-1	1.740	10.51		5628.	5851.	3426.	1000.	.628	.436	1.44	.00142	.0247	.0172
				D-2	1.878	6.14		5396.	5824.	3412.	1000.	.628	.436	1.44	.00142	.0172	.0119
				D-3	2.206	4.42		5149.	5794.	3397.	1000.	.628	.435	1.44	.00142	.0173	.0120

RUN	PC	MR	WT	SECTION	D	FLUX	TC	TE	TR	TF	TWG	CPS	CPF	CPS/CPF	DBF	CGF	CGS
166	281.	1.43	3.89	R	3.400	.22	5657.	5657.	5657.	3328.	1000.	.653	.491	1.33	.00170	.0014	.0011
				A-3	3.400	-.25		5657.	5657.	3328.	1000.	.653	.491	1.33	.00170	-.0016	-.0012
				A-2	3.400	.69		5657.	5657.	3328.	1000.	.653	.491	1.33	.00170	.0045	.0034
				A-1	3.400	2.43		5657.	5657.	3328.	1000.	.653	.491	1.33	.00170	.0159	.0120
				C-2	2.998	2.07		5642.	5655.	3327.	1000.	.653	.491	1.33	.00170	.0108	.0081
				C-1	2.294	5.56		5612.	5650.	3325.	1000.	.653	.491	1.33	.00170	.0181	.0136
				D-1	1.740	11.52		5326.	5605.	3303.	1000.	.653	.490	1.33	.00170	.0239	.0179
				D-2	1.878	5.60		4994.	5554.	3277.	1000.	.653	.489	1.33	.00169	.0141	.0106
				D-3	2.206	3.86		4607.	5493.	3247.	1000.	.653	.489	1.34	.00169	.0140	.0105

O_2/C_2H_2 (W/O FILM COOLING)
(PLATELET INJECTOR)

RUN	PC	MR	WT	SECTION	D	FLUX	TC	TE	TR	TF	TWG	CPS	CPF	CPS/CPF	DBF	CGF	CGS
167	194.	1.87	2.59	R	3.400	.03	5857.	5857.	5857.	3428.	1000.	.691	.465	1.49	.00154	.0003	.0002
				A-3	3.400	1.04		5857.	5857.	3428.	1000.	.691	.465	1.49	.00154	.0099	.0067
				A-2	3.400	1.28		5857.	5857.	3428.	1000.	.691	.465	1.49	.00154	.0122	.0082
				A-1	3.400	1.66		5857.	5857.	3428.	1000.	.691	.465	1.49	.00154	.0158	.0107
				C-2	2.998	1.33		5846.	5854.	3428.	1000.	.691	.465	1.49	.00154	.0139	.0094
				C-1	2.294	3.63		5821.	5837.	3426.	1000.	.691	.465	1.49	.00154	.0172	.0115
				D-1	1.740	7.04		5608.	5819.	3412.	1000.	.691	.465	1.49	.00154	.0209	.0141
				D-2	1.878	4.43		5378.	5794.	3397.	1000.	.691	.464	1.49	.00154	.0157	.0105
				D-3	2.206	3.12		5138.	5766.	3381.	1000.	.691	.464	1.49	.00154	.0154	.0103

RUN	PC	MR	WT	SECTION	D	FLUX	TC	TE	TR	TF	TWG	CPS	CPF	CPS/CPF	DBF	CGF	CGS
168	377.	1.88	5.09	R	3.400	-.42	6002.	6002.	6002.	3501.	1000.	.671	.467	1.44	.00156	-.0022	-.0016
				A-3	3.400	.47		6002.	6002.	3501.	1000.	.671	.467	1.44	.00156	.0025	.0017
				A-2	3.400	1.82		6002.	6002.	3501.	1000.	.671	.467	1.44	.00156	.0097	.0068
				A-1	3.400	2.81		6002.	6002.	3501.	1000.	.671	.467	1.44	.00156	.0150	.0104
				C-2	2.998	3.43		5992.	6001.	3500.	1000.	.671	.467	1.44	.00156	.0146	.0102
				C-1	2.294	7.54		5965.	5997.	3499.	1000.	.671	.467	1.44	.00156	.0200	.0139
				D-1	1.740	15.88		5738.	5967.	3484.	1000.	.671	.466	1.44	.00155	.0265	.0184
				D-2	1.878	8.68		5495.	5935.	3468.	1000.	.671	.466	1.44	.00155	.0173	.0120
				D-3	2.206	5.94		5239.	5902.	3451.	1000.	.671	.466	1.44	.00155	.0165	.0114

RUN	PC	MR	WT	SECTION	D	FLUX	TC	TE	TR	TF	TWG	CPS	CPF	CPS/CPF	DBF	CGF	CGS
169	288.	1.88	3.85	R	3.400	-.20	5943.	5943.	5943.	3471.	1000.	.679	.466	1.46	.00155	-.0014	-.0009
				A-3	3.400	.41		5943.	5943.	3471.	1000.	.679	.466	1.46	.00155	.0028	.0019
				A-2	3.400	1.32		5943.	5943.	3471.	1000.	.679	.466	1.46	.00155	.0090	.0061
				A-1	3.400	2.01		5943.	5943.	3471.	1000.	.679	.466	1.46	.00155	.0136	.0094
				C-2	2.998	2.75		5932.	5942.	3471.	1000.	.679	.466	1.46	.00155	.0149	.0102
				C-1	2.294	5.58		5907.	5938.	3469.	1000.	.679	.466	1.46	.00155	.0188	.0129
				D-1	1.740	11.20		5686.	5909.	3455.	1000.	.679	.466	1.46	.00155	.0237	.0162
				D-2	1.878	6.46		5448.	5876.	3439.	1000.	.679	.465	1.46	.00155	.0163	.0112
				D-3	2.206	4.40		5198.	5841.	3423.	1000.	.679	.465	1.46	.00154	.0155	.0106

O_2/C_2H_5OH (WITH FILM COOLING)
(PLATELET INJECTOR)

RUN	PC	MR	WT	SECTION	D	FLUX	TC	TE	TR	TF	TWG	CPS	CPF	CPS/CPF	DBF	CGF	CGS
163	297.	1.55	3.95	R	3.400	1.19	5812.	5812.	5812.	3406.	1000.	.651	.484	1.35	.00166	.0076	.0057
				A-3	3.400	1.41		5812.	5812.	3406.	1000.	.651	.484	1.35	.00166	.0090	.0067
				A-2	3.400	2.57		5812.	5812.	3406.	1000.	.651	.484	1.35	.00166	.0165	.0122
				A-1	3.400	3.12		5812.	5812.	3406.	1000.	.651	.484	1.35	.00166	.0200	.0148
				C-2	2.998	3.27		5799.	5810.	3405.	1000.	.651	.484	1.35	.00166	.0167	.0124
				C-1	2.294	6.19		5770.	5806.	3403.	1000.	.651	.484	1.35	.00166	.0197	.0146
				D-1	1.740	13.38		5516.	5768.	3384.	1000.	.651	.483	1.35	.00166	.0269	.0200
				D-2	1.878	7.60		5232.	5726.	3363.	1000.	.651	.483	1.35	.00165	.0184	.0136
				D-3	2.206	5.32		4906.	5678.	3339.	1000.	.651	.482	1.35	.00165	.0182	.0135

RUN	PC	MR	WT	SECTION	D	FLUX	TC	TE	TR	TF	TWG	CPS	CPF	CPS/CPF	DBF	CGF	CGS
165	295.	2.08	3.87	R	3.400	1.38	5950.	5950.	5950.	3475.	1000.	.701	.456	1.54	.00149	.0097	.0063
				A-3	3.400	2.07		5950.	5950.	3475.	1000.	.701	.456	1.54	.00149	.0145	.0094
				A-2	3.400	3.22		5950.	5950.	3475.	1000.	.701	.456	1.54	.00149	.0226	.0147
				A-1	3.400	3.43		5950.	5950.	3475.	1000.	.701	.456	1.54	.00149	.0241	.0156
				C-2	2.998	3.67		5938.	5949.	3474.	1000.	.701	.456	1.54	.00149	.0206	.0134
				C-1	2.294	6.80		5912.	5945.	3473.	1000.	.701	.456	1.54	.00149	.0236	.0154
				D-1	1.740	15.16		5695.	5919.	3459.	1000.	.701	.456	1.54	.00149	.0331	.0215
				D-2	1.878	8.48		5461.	5890.	3445.	1000.	.701	.455	1.54	.00149	.0221	.0143
				D-3	2.206	5.89		5216.	5859.	3430.	1000.	.701	.455	1.54	.00149	.0213	.0138

RUN	PC	MR	WT	SECTION	D	FLUX	TC	TE	TR	TF	TWG	CPS	CPF	CPS/CPF	DBF	CGF	CGS
166	294.	1.17	4.04	R	3.400	1.53	4978.	4978.	4978.	2989.	1000.	.704	.506	1.39	.00179	.0110	.0079
				A-3	3.400	1.10		4978.	4978.	2989.	1000.	.704	.506	1.39	.00179	.0079	.0057
				A-2	3.400	1.79		4978.	4978.	2989.	1000.	.704	.506	1.39	.00179	.0128	.0092
				A-1	3.400	2.97		4978.	4978.	2989.	1000.	.704	.506	1.39	.00179	.0213	.0153
				C-2	2.998	2.68		4960.	4975.	2987.	1000.	.704	.506	1.39	.00179	.0154	.0111
				C-1	2.294	6.20		4917.	4967.	2984.	1000.	.704	.506	1.39	.00179	.0222	.0159
				D-1	1.740	12.56		4544.	4902.	2951.	1000.	.704	.505	1.39	.00179	.0294	.0211
				D-2	1.878	6.07		4127.	4828.	2914.	1000.	.704	.503	1.40	.00178	.0178	.0128
				D-3	2.206	4.08		3684.	4751.	2875.	1000.	.704	.502	1.40	.00177	.0178	.0127

O_2/C -OH (WITH HCM COOLING)

(PLATELET INJECTOR)

RUN	PC	MR	WT	SECTION	D	FLUX	TC	TE	TR	TF	TWG	CPS	CPF	CPS/CPF	DBF	CGF	CGS
167	201.	1.51	2.64	R	3.400	1.27	5732.	5732.	5732.	3366.	1000.	.660	.483	1.37	.00165	.0115	.0084
				A-3	3.400	1.55		5732.	5732.	3366.	1000.	.660	.483	1.37	.00165	.0140	.0102
				A-2	3.400	2.22		5732.	5732.	3366.	1000.	.660	.483	1.37	.00165	.0201	.0147
				A-1	3.400	2.60		5732.	5732.	3366.	1000.	.660	.483	1.37	.00165	.0235	.0172
				C-2	2.998	2.70		5720.	5730.	3365.	1000.	.660	.483	1.37	.00165	.0195	.0142
				C-1	2.294	4.72		5691.	5726.	3363.	1000.	.660	.483	1.37	.00165	.0211	.0155
				D-1	1.740	9.80		5448.	5690.	3345.	1000.	.660	.482	1.37	.00165	.0278	.0203
				D-2	1.878	5.95		5173.	5649.	3325.	1000.	.660	.482	1.37	.00165	.0203	.0148
				D-3	2.206	4.10		4859.	5603.	3301.	1000.	.660	.481	1.37	.00164	.0198	.0144

RUN	PC	MR	WT	SECTION	D	FLUX	TC	TE	TR	TF	TWG	CPS	CPF	CPS/CPF	DBF	CGF	CGS
168	394.	1.56	5.27	R	3.400	1.32	5855.	5855.	5855.	3427.	1000.	.644	.484	1.33	.00166	.0066	.0050
				A-3	3.400	1.89		5855.	5855.	3427.	1000.	.644	.484	1.33	.00166	.0095	.0071
				A-2	3.400	3.67		5855.	5855.	3427.	1000.	.644	.484	1.33	.00166	.0184	.0139
				A-1	3.400	4.13		5855.	5855.	3427.	1000.	.644	.484	1.33	.00166	.0208	.0156
				C-2	2.998	4.49		5840.	5853.	3426.	1000.	.644	.484	1.33	.00166	.0180	.0136
				C-1	2.294	9.70		5812.	5849.	3424.	1000.	.644	.484	1.33	.00166	.0242	.0182
				D-1	1.740	19.68		5547.	5809.	3405.	1000.	.644	.484	1.33	.00166	.0311	.0234
				D-2	1.878	9.82		5248.	5765.	3383.	1000.	.644	.483	1.33	.00166	.0187	.0141
				D-3	2.206	6.78		4904.	5714.	3357.	1000.	.644	.482	1.33	.00165	.0184	.0138

RUN	PC	MR	WT	SECTION	D	FLUX	TC	TE	TR	TF	TWG	CPS	CPF	CPS/CPF	DBF	CGF	CGS
169	293.	1.71	3.90	R	3.400	2.03	5911.	5911.	5911.	3455.	1000.	.661	.474	1.39	.00160	.0133	.0095
				A-3	3.400	2.63		5911.	5911.	3455.	1000.	.661	.474	1.39	.00160	.0172	.0124
				A-2	3.400	3.14		5911.	5911.	3455.	1000.	.661	.474	1.39	.00160	.0206	.0148
				A-1	3.400	3.31		5911.	5911.	3455.	1000.	.661	.474	1.39	.00160	.0217	.0156
				C-2	2.998	3.53		5898.	5909.	3455.	1000.	.661	.474	1.39	.00160	.0185	.0132
				C-1	2.294	6.97		5871.	5905.	3453.	1000.	.661	.474	1.39	.00160	.0226	.0162
				D-1	1.740	15.06		5641.	5873.	3437.	1000.	.661	.474	1.40	.00160	.0308	.0221
				D-2	1.878	8.08		5390.	5839.	3419.	1000.	.661	.474	1.40	.00160	.0198	.0142
				D-3	2.206	5.37		5119.	5801.	3400.	1000.	.661	.473	1.40	.00159	.0184	.0132

C_{PS}/C_{PF} VS. MR FOR LOX/PROPANE AND LOX/ETHANOL

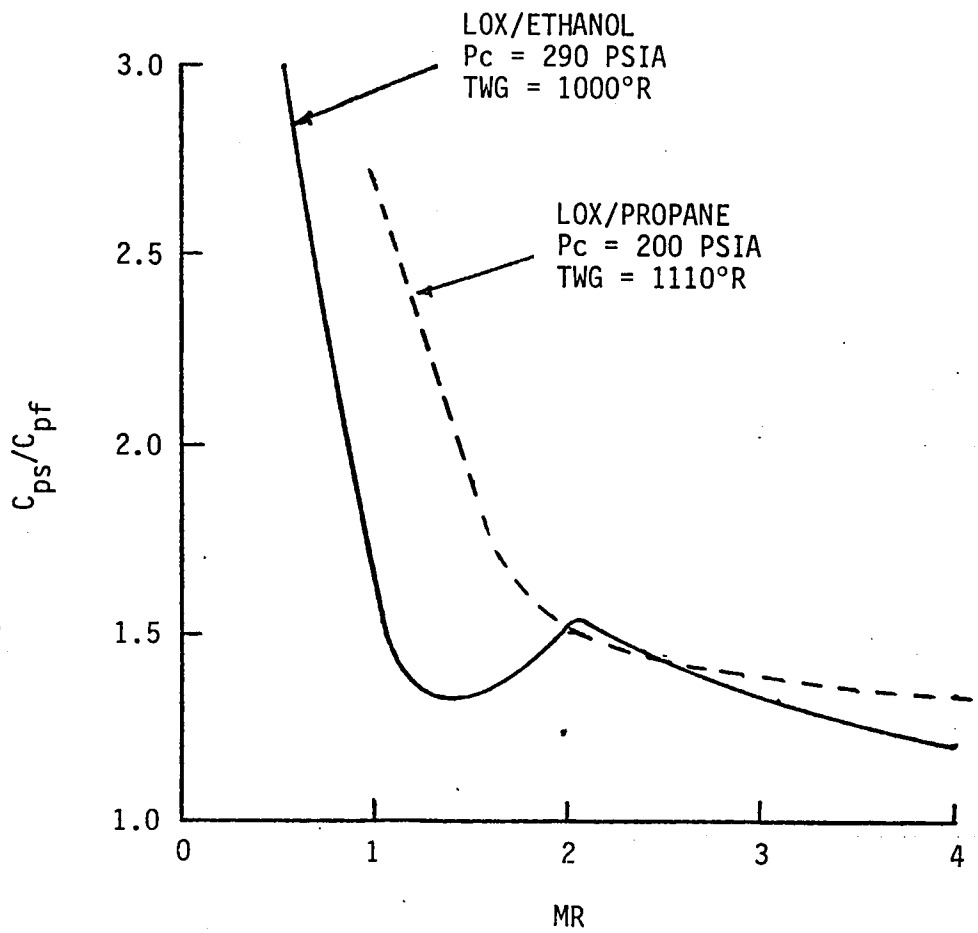

APPENDIX D
GAS FLOW REGIME CALCULATION FOR LOX/ETHANOL

APPENDIX D

GAS FLOW REGIME CALCULATION FOR LOX/ETHANOL

$$Re'_t = 20, \frac{T_e}{T_f}, \frac{W_T}{\pi \mu_f r_t}$$

$$St_F \, Pr_F^{0.6}$$

$D_t = 1.74$

(1) Laminar
(2) Reverse Transition
(3) Turbulent

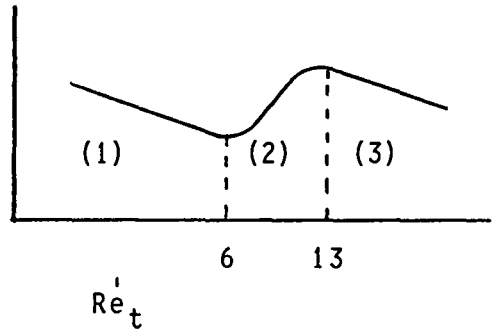

Pc	MR	W_T	Re'_t	Flow Regime
194	1.87	2.59	8.32	R.T.
285	1.87	3.85	12.4	R.T.
377	1.88	5.09	16.3	TURB

O/F = 1.89

$T_{^oR}$	μ
1000	1.254
2000	2.366
3000	3.301
4000	4.129
2496	2.844
3313	3.572
4305	4.370

$T_o = 6148$

$T_{e_t} = 5067 \quad Pr_t = .634$

$T_{wg} = 1000$ R

$T_r = 6100$

$T_f = 3550$

$\mu_f = 3.764$

$\therefore Re'_t = 3.212 \, W_T$

End of Document